2nd Hull Performance & Insight Conference

HullPIC'17

Ulrichshusen, 27-29 March 2017

Edited by Volker Bertram

Sponsored by

JOTUN

www.jotun.com

DNV·GL

www.dnvgl.com

ABS www.eagle.org | KYMA www.kyma.no | NAPA www.napa.fi | HOPPE MARINE MAIHAK www.hoppe-marine.com

MIROS www.miros.no | MMG Mecklenburger Metallguß www.mmg-propeller.de | PROPULSION DYNAMICS www.propulsiondynamics.com

eniram A WÄRTSILÄ COMPANY www.eniram.fi | HEMPEL www.hempel.com | VAF INSTRUMENTS www.vaf.nl

International. www.akzonobel.com | VEINLAND one source - multiple solutions www.veinland.net | ecosubsea www.ecosubsea.com

AMERICAN chemet CORPORATION www.chemet.com | enamor www.enamor.pl | MARORKA www.marorka.com

Index

Some Heretic Thoughts on ISO 19030

Volker Bertram, DNV GL, Hamburg/Germany, volker.bertram@dnvgl.com

Abstract

This paper addresses selected issues of hull performance monitoring. The intention is to raise awareness of some sources of inaccuracies in the standard procedure of ISO 19030. (1) Water temperature affects viscosity and thus resistance. Variations of 2-3% of calm-water resistance in design condition may result. (2) Wind force corrections are simple and cheap. In turn, they are suspected to have large errors. This should be investigated in more detail. (3) Current speed plays a role because it varies over depth. A filtering condition for significant current speed should be used, rather than a correction. (4) The performance indicators following ISO 19030 will still depend on speed. Users should at least be aware of this.

1. Introduction

ISO 19030 has been published in its first edition – finally, one may be tempted to say. After years of debate, detailed discussions, homework and HullPIC 2016, one is also tempted to close the matter and move on to something else. However, since HullPIC 2016 assorted colleagues and customers have come to me with questions on performance monitoring, as perplexing results were found or additional justification was sought. On such occasions, I scribbled down some keywords as a reminder to share these aspects with a wider audience at HullPIC 2017.

2. Selected aspects of ISO 19030 (and most performance monitoring systems)

2.1. Wind

The wind force correction in ISO 19030 follows closely the approach in ISO 15016. The only difference is that windage area and its center are variable in ISO 19030 to reflect variable draft, and constant in ISO 15016.

The influence of the wind on resistance is due to three factors:

1. Longitudinal wind force on the ship (= direct wind resistance)
2. Transverse wind force inducing a side drift which leads to an added hydrodynamic resistance
3. The yaw moment due to wind must be compensated by the rudder. This induces a higher rudder resistance, different side drift and thus hydrodynamic resistance.

In the ISO 19030 standard approach, the correction for wind forces considers only the first contribution. This is generally the case when wind correction uses force coefficients from wind tunnel tests or "ship-typical" force coefficients, such as the STA-JIP coefficients taken in ISO 15016 and ISO 19030, *Herradon de Grado and Bertram (2016)*. Also approaches using CFD (Computational Fluid Dynamics) will generally give longitudinal force, transverse force and yaw moment separately. The ship is generally considered to be fixed and hydrodynamic effects would require additional investigations. We investigated the effect of the indirect wind force in longitudinal direction due to transverse wind force and yaw moment for a containership (contributions from item 2 and 3 in the list above). For design conditions at Bft 5-6 and the most unfavorable wind direction (around 40° oblique from ahead), the direct wind force (item 1) was 4.5% of the calm-water resistance and indirect wind force (items 2 and 3) were 4.5% of the direct force, or 0.2% of the calm-water resistance, see Appendix 1. It thus seems acceptable to neglect these terms. However, side wind and resulting drift will induce asymmetric inflow to the propeller. Qualitatively, I would expect a reduced propeller efficiency and thus power increase, but I have no quantitative insight on the magnitude.

So how accurately do we capture the direct wind resistance? Let's look first at the design condition. In a joint industry project with Jotun and Norddeutsche Reederei H. Schuldt GmbH & Co (NRS), we looked at the possible errors from wind force estimates. Various approaches to estimate added resistance and side force were compared with wind tunnel tests for a typical containership, Fig.1. For this ship, we had dedicated wind tunnel tests from Force Technology. The approaches were:

- DNV GL (old) - Wind forces and moments are estimated following Blendermann in *Brix (1993)*, using the standard option given there (converted to the frontal area as reference area).
- Jotun (old) - Wind forces are estimated following *Blendermann (1986)*, where the curve in the original publication was approximated by a polynomial fit.
- SRA-JIP – given as curves in ISO 15016 and ISO 19030, and tables in *Herradon de Grado and Bertram (2015)*. Note that the angle of incidence in *Herradon de Grado and Bertram (2015)* is defined with 180° for head wind, 0° for following wind.

Fig.2 compares wind force coefficients for average (port/starboard) values of wind tunnel tests and the above three approaches. The JIP-SRA approach is closest to the wind tunnel tests, typically 27% off, while the other two approaches show typical errors of 40%. The current approaches of DNV GL and Jotun follow ISO 19030, i.e. the approach with the best results in the above study. However, for design conditions we still see ~30% error by employing the generic "ship-type" coefficients rather than the ship-specific conditions.

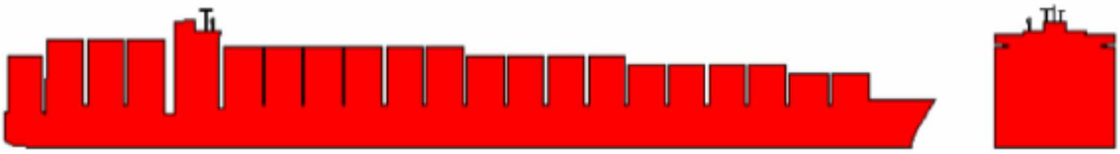

Fig. 1: Lateral plan of investigated containership (design condition)

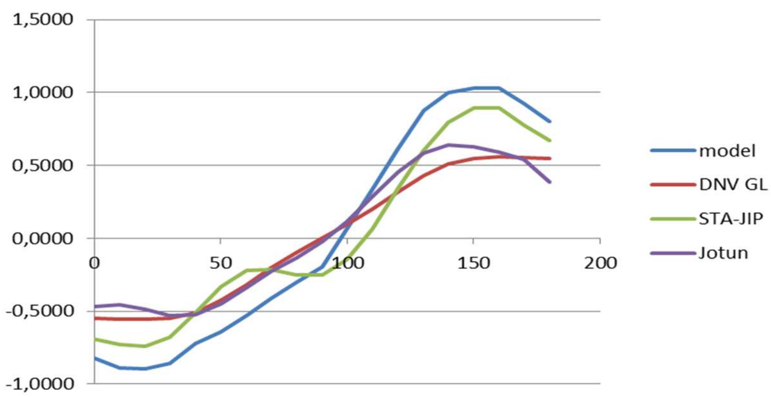

Fig.2: Wind force coefficients

We take a constant density of air in our standard formulae for wind resistance, typically 1.225 kg/m3, the value at sea level for 15°C. Variations of ±15°C give variations of ±5.5% in density and thus wind forces. Considering changes in humidity would lead to larger variations. The good – or depressing – news is that these variations are still small compared to other sources of errors in wind force estimates.

And then we have the ship in off-design condition. Published wind force coefficients generally depend on (relative) wind direction and ship type. For containerships, there may be different sets of coefficients between "deck load" and "no deck load"; but this 'step function' is rarely used in my experience. Wind force coefficients in ISO 19030 are assumed to be draft-independent; however, in reality they will change with draft (as for example ratios between lateral and frontal areas will change, air draft to length and width ratios will change, etc.). I am not aware of any investigation of the effect of draft on wind force coefficients. Such an investigation based on CFD could be an interesting master thesis and help us to get a feeling for the errors involved.

For lower ship speeds, the wind forces gain in relative importance. Filter criteria for wind (and other ambient conditions) should be related to the calm-water power at the actual condition (draft, trim, speed), respectively the induced speed loss at the actual conditions. If we assume errors of 50% in off-design condition wind force estimates, perhaps a reasonable filter condition would be excluding cases where estimated wind resistance exceeds 5% of estimated calm-water resistance.

2.2. Water temperature

The seawater temperature influences the resistance mostly through the kinematic viscosity. The influence due to changes in water density is much smaller, as changes in density affect similarly hull resistance and propeller thrust. The viscosity and the density of (surface) seawater as a function of temperature and salinity can be found in oceanographic handbooks in tabular form. For performance monitoring systems, it is more convenient to use (approximate) formulas. For the kinematic viscosity ν [m/s^2], *Bertram (2012)* gives:

$$\nu = 10^{-6} \cdot (0.0014 \cdot s + (0.000645 \cdot t - 0.0503) \cdot t + 1.75) \qquad (1)$$

and for seawater density ρ [kg/m^3]:

$$\rho = 1027 + [-0.15 \cdot (t - 10) + 0.78 \cdot (s - 35)] \qquad (2)$$

Here we specify the salinity *s* in ‰ and the seawater temperature *t* in °C. Default values are seawater temperature of 15°C and salinity of 35‰.

Changing viscosity directly affects the frictional resistance. Consider the percentage of frictional resistance in total resistance. For design conditions, this may vary between 50% (offshore supply vessel) and 80% (large oil tanker). However, we are generally not interested in design conditions. Various factors change the percentage in practice:

- Speed – For lower speeds, the wave making will decay, and the frictional resistance will take a higher percentage of overall resistance.
- Draft (and trim) – For lower draft, wetted surface and thus the frictional resistance decrease and the wave resistance typically increases. Thus the frictional resistance will take a lower percentage of overall resistance.
- Added resistance – Added resistance due to wind and waves increases the total resistance. Thus the (unchanged) frictional resistance will take a lower percentage of overall resistance.

In order to estimate the effect of water temperature quantitatively, I set up a simple Excel file. The frictional resistance coefficient is calculated following ITTC'57 (the standard approach used by towing tanks), *Bertram (2012)*. The viscosity is computed as function of water temperature folliwng Eq.(1). The wetted surface is simply estimated as 90% of the wetted surface of a box of same length, width and draft.

Fig.3 shows the result for a large oil tanker at design speed, where I assumed moderate added resistance (as typically found in performance monitoring, filtering for higher wind speed). I then input 70% as the percentage of frictional resistance in total resistance. The other resistance parts are assumed to be constant. The resistance (and thus in very good approximation also power) is 2.5% lower at 30°C water temperature than at the reference condition of 15°C. For 0°C, we would have 3.6% higher resistance. So a variation of 30°C (possibly for a winter journey from Rotterdam to the Persian Gulf) would mean >5% variation due to water temperature.

3,5	%	salinity		3,5	%			
15	°C	temperature		30	°C			
1,1896E-06	m^2/s	viscosity		8,705E-07	m^2/s			
1025	kg/m^3	density		1025	kg/m^3			
320,00	m	ship length L_{pp}		320,00	m			
19,00	m	draft T		19,00	m			
70,00	m	width B		70,00	m			
16,00	kn	ship speed		16,00	kn			
8,23	m/s	ship speed		8,23	m/s			
33498	m^2	wetted surface		33498	m^2			
2,21E+09		Reynolds number		3,03E+09				
0,00139014		coeff. Friction resist.		0,00134019				
1617	kN	Friction resistance		1559	kN			
70	%	R_F / R_T						
2309	kN	Total		2251	Total		-2,5%	difference
693	kN	Other Resistance		693	kN			

Fig.3: Excel estimate for effect of water temperature; input arrays marked in light blue

Bos (2016) gives power variations for the Mediterranean Sea of 2% due to temperature variations of 7% over the year. The differences are no doubt due to different assumptions mainly for the size of the vessel and the percentage of the frictional resistance in overall resistance.

In any case, the effect of water temperature is neither overwhelming nor negligible. It seems to be a pebble in our shoe which may be irritating enough over time to include a (simple) temperature correction in future editions of ISO 19030.

2.3. Current speed

ISO 19030 focusses on speed through water. The ship hydrodynamicist in me wholeheartedly agrees. It is the speed through water and the delivered power that need to be correlated to assess performance. But then how do we estimate speed through water? The speed log is notoriously inaccurate, e.g. *Wienke and Lampe (2016), Bos (2016)*. Perhaps using the much more accurate speed over ground as a proxy? But then, when we have significant current speed, we would also have (potentially very large) unaccountable errors in our performance indicators. Perhaps we should follow *Bos (2016)* and use measured speed over ground and estimated current speed (e.g. from metocean hindcast data). But *Bos (2016)* also reminded us that current speed decays over depth and actually also direction may change over depth. So if we have (significant) current speed, the very term “speed through water” does not make sense anymore. We would have, for example, the waterline moving with 12.5 kn through water and the bottom with 12 kn.

For me, the conclusion is that we should use only data sets where current speed is small, i.e. we need a filter for current speed, e.g. looking at speed over ground and speed through water. One option could be to look at long-term average differences between speed over ground and speed through water, taking the difference as a base error (bias) and then filtering for remaining differences.

In many cases, we do not want to avoid currents. They can help us in energy efficient operation. But we should be aware that currents are problematic for performance monitoring. Possibly CFD studies could shed more light into the effect of current velocity variations over depth on power requirements. With better quantification, filter criteria could be selected. But I fear that it is still a long way to a practicable and rational handling of the issues stemming from background currents.

2.4. Speed-dependent performance

In a nutshell, the basic idea of ISO 19030 (and all other performance monitoring approaches) is:

- Correct for different ambient conditions (wind, waves, current, temperature, …)
- Correct for different operational conditions (speed, draft, trim, rudder angle, …)

And you obtain a performance at a reference (or normal) condition. All other conditions are normalized to a comparable level field. Sounds good. But then we implement the performance monitoring theory with assorted corrections, maybe following ISO 19030, maybe claiming to be even better than ISO 19030 because we consider this or that feature on top. Dynamic, holistic, computer accurate.

Then we (or even worse a customer) take a closer look. The performance indicator seems to be speed dependent. Before we blame sensor accuracy (always a good villain) or suspect a bug in the performance monitoring software, let's revisit ship hydrodynamics. Fouling increases hull roughness. This will directly affect friction resistance, not affect wave and wind resistance, and somewhat affect the viscous pressure (or residual) resistance. As speed goes down, wave resistance will decay much more rapidly than friction resistance. Typically wave resistance may decay with speed to the 4^{th} power and friction resistance with speed to the 2^{nd} power. Then changes in hull roughness will lead to a higher increase in power at lower speed than at higher speed.

In addition, there are the corrections for ambient conditions. For example, the popular Kreitner formula for added resistance in waves does not contain speed as a variable. However, added resistance depends strongly on speed, *Bertram (2016)*. Then the correction will be sometimes too small and sometimes over-compensate depending among other things on ship type. A systematic speed-dependent error in the corrections for ambient condition can thus also contribute to a systematic error in the performance indicator.

So with the currently used hydrodynamic models, we must expect the performance indicator to be speed dependent. There are various options to process this information:

1. The time-honoured "everything will average out if only our operational profiles don't change". Unfortunately, most ship operators want to change operational profiles every now and then. And is closing our eyes and hoping for the best the best we can do?
2. We filter for speed. Say, we only take data sets in a range of speeds, e.g. 15-17 kn. That removes a strong dependency on speed. But it might also remove a lot of data sets. For many ships, we will be left with an insufficient number of data sets to track performance.
3. We set up the hydrodynamic model to end all hydrodynamic models. Rather than correcting back to a power or speed, we correct back to an average roughness. We would then need power as a function of speed, draft, trim, roughness, and ideally also wind and waves. Then we measure power, correct for ambient conditions and solve the corrected power for given speed, draft and trim for the existing roughness. This would mean a major change in the hydrodynamic model of ISO 19030. It would also mean extensive CFD simulations for all ships, more extensive than recommended already for containerships, *Ishiguro et al. (2016)*, *Dückert et al. (2016)*, as we have hull roughness as an additional parameter. And how trustworthy (= accurate) are changes in roughness captured in commercial CFD codes by varying a surface roughness parameter? I asked several marine CFD experts and most answered with a shrug or a wince.
4. We are aware of the problem; we don't like it, but we accept it and hope that over time a better alternative will become available.

3. Conclusion

ISO 19030 is like democracy. It is far from being ideal, but a lot better than what we had in the past. The standard was developed based on limited experience (even if we all pooled our knowledge) and with a conscious decision to sacrifice theoretical rigor on the altar of affordability and wider acceptance. Some of the current short-comings may be accepted but we should be aware of them. Others might be debated and eventually included in future revisions.

Acknowledgement

I am grateful to Mr. Björn Walther (NRS) and Dr. Andreas Krapp (Jotun) for the permission to show selective results for wind force computations.

References

BERTRAM, V. (2012), *Practical Ship Hydrodynamics*, Butterworth & Heinemann, Oxford

BERTRAM, V., *Added Power in Waves – Time to Stop Lying (to Ourselves)*, 1st HullPIC Conf., Pavone, pp.5-13

BLENDERMANN, W. (1986), *Die Windkräfte am Schiff*, IfS Report 467, Univ. Hamburg
https://tubdok.tub.tuhh.de/bitstream/11420/919/1/Bericht_Nr.467_W.Blendermann_Die_Windkrfte_am_Schiff.pdf

BOS, M. (2016), *How MetOcean Data Can Improve Accuracy and Reliability of Vessel Performance Estimates*,1st HullPIC Conf., Pavone, pp.106-114

BRIX, J. (1993) (Ed.), *Manoeuvring Technical Manual*, Seehafen-Verlag, Hamburg
DÜCKERT, T.; SCHMODE, D.; TULLBERG, M. (2016), *Computing Hull & Propeller Performance: Ship Model Alternatives and Data Acquisition Methods*, 1st HullPIC Conf., Pavone, pp.23-28

HERRADON DE GRADO, E.; BERTRAM, V. (2016), *Predicting added resistance in wind and waves employing artificial neural nets*, 1st HullPIC Conf., Pavone, pp.14-22

ISHIGURO, T.; ORIHARA, H.; YOSHIDA, H. (2016), *Verification of Full-Scale Vessel's Performance under Actual Sea by On-board Monitoring System: A Shipbuilder's View*, 1st HullPIC Conf., Pavone, pp.70-81

ITTC (1999), *CFD, Resistance and Flow Benchmark Database for CFD Validation for Resistance and Propulsion*, International Towing Tank Conference
http://ittc.info/downloads/Archive of recommended procedures/2011 Recommended Procedures/7.5-03-02-02.pdf

WIENKE, J.; LAMPE, J. (2016), *Energy Efficiency Design Index in View of Performance Monitoring*, 1st HullPIC Conf., Pavone, pp.137-144

WOLFF, K. (1981), *Ermittlung der Manövriereigenschaften fünf repräsentativer Schiffstypen mit Hilfe von CPMC-Modellversuchen (Determination of the manoeuvring properties of five representative ship types with the help of CPMC model tests)*, Report 412, Institut für Schiffbau, University of Hamburg
https://tubdok.tub.tuhh.de/bitstream/11420/843/1/Bericht_Nr.412_K.Wolff_Ermittlung_der_Manvriereigenschaften_fnf_reprsentativer_Schiffstypen_mit_Hilfe_von_CPMC_Modellversuchen.pdf

Appendix 1: Indirect wind force in longitudinal direction

The test case is the "Hamburg Test Case", a standard validation test case of the International Towing Tank Conference, *ITTC (1999)*. For this ship, resistance and propulsion data and geometry are public domain. The ship has L_{pp} = 156 m and design speed 21.3 kn (=10.954 m/s corresponding to F_n = 0.28). The calm-water resistance for this ship is taken to 1182 kN, based on simulations of Prof H. Söding (in personal communication in 2012).

We assume a wind of Beaufort 5 coming from an apparent direction of 35° oblique from ahead at the height of the center of the frontal area above water. This is a conservative case. At this angle, we typically have the maximum wind resistance and maximum yaw moment and Bft 5 is above the recommended filter for ISO 19030 of Bft 4.

- Direct wind force

  Following the approach of Blendermann in *Brix (1993)*, taking also the wind coefficients for the 'container ship' from there, and the reference frontal windage area for the 'Hamburg Test Case' of A_F = 645 m^2, we obtain a longitudinal wind force X_{wind} = -53 kN, side force Y_{wind} = 279.4 kN, and yaw moment N_{wind} = 6046 kNm. The direct wind resistance is then 53/1182 = 4.5% ≈ 5% of the calm-water resistance.

- Indirect wind force

  Since wind transverse force and yaw moment are small at Bft 5, we can use the simplified, linearized equations of maneuvering, *Bertram (2012)*, p.245. Considering the wind forces, we then write:

$$Y_v v + Y_\delta \delta + Y_{wind} = 0 \tag{A.1}$$

$$N_v v + N_\delta \delta + N_{wind} = 0 \tag{A.2}$$

Here, v is the drift velocity, δ the rudder angle, Y_v the transverse hydrodynamic force per drift velocity, Y_δ the transverse hydrodynamic force per rudder angle. The above system of equations requires the maneuvering coefficients to solve for v and δ. *Wolff (1981)* gives non-dimensional maneuvering coefficients based on large-scale model tests. The coefficients are also found in *Brix (1993)* and *Bertram (2012)*. For our estimate, we use the maneuvering coefficients of Wolff's containership, *Bertram (2012)*, pp.246-247: $Y'_v = -8470 \cdot 10^{-6}$, $Y'_\delta = 1660 \cdot 10^{-6}$, $N'_v = -3800 \cdot 10^{-6}$, $N'_\delta = -793 \cdot 10^{-6}$. The prime indicates nondimensional coefficients. These maneuvering coefficients were made nondimensional with suitable powers of L_{pp}, u (longitudinal speed through water) and $\rho/2$. For our test case, we then have (in suitable powers of t, m, s):

$$Y_v = Y'_v \cdot \frac{\rho}{2} \cdot L^2 \cdot u = -8470 \cdot 10^{-6} \cdot \frac{1.025}{2} \cdot 156^2 \cdot 10.954 = -1157 \tag{A.3}$$

$$Y_\delta = Y'_\delta \cdot \frac{\rho}{2} \cdot L^2 \cdot u^2 = 1660 \cdot 10^{-6} \cdot \frac{1.025}{2} \cdot 156^2 \cdot 10.954^2 = 2484 \tag{A.4}$$

$$N_v = N'_v \cdot \frac{\rho}{2} \cdot L^3 \cdot u = -3800 \cdot 10^{-6} \cdot \frac{1.025}{2} \cdot 156^3 \cdot 10.954 = -81000 \tag{A.5}$$

$$N_\delta = N'_\delta \cdot \frac{\rho}{2} \cdot L^3 \cdot u^2 = -793 \cdot 10^{-6} \cdot \frac{1.025}{2} \cdot 156^3 \cdot 10.954^2 = -185000 \tag{A.6}$$

With Y_{wind} = 279.4 kN and N_{wind} = 6046 kNm (see above), we then solve the linear system of equations (A.1.1) and (A.1.2).

$$-1157v + 2485\delta + 279.4 = 0 \tag{A.7}$$

$$-81000v - 185000\delta + 6046 = 0 \tag{A.8}$$

Thus we obtain: v = 0.161 m/s and δ = –0.0377 = –2.16°.

We can now compute the corresponding longitudinal force, using quadratic coefficients (as all linear coefficients are zero). Again, we use Wolff's non-dimensional maneuvering coefficients for a containership: $X'_{vv} = -1355 \cdot 10^{-6}$, $X'_{\delta\delta} = -696 \cdot 10^{-6}$, $X'_{v\delta} = 611 \cdot 10^{-6}$. This gives dimensional coefficients:

$$X_{vv} = X'_{vv} \cdot \frac{\rho}{2} \cdot L^2 = -1355 \cdot 10^{-6} \cdot \frac{1.025}{2} \cdot 156^2 = -16.9 \qquad \text{(A.9)}$$

$$X_{\delta\delta} = X'_{\delta\delta} \cdot \frac{\rho}{2} \cdot L^2 \cdot u^2 = -696 \cdot 10^{-6} \cdot \frac{1.025}{2} \cdot 156^2 \cdot 10.954^2 = -1042 \qquad \text{(A.10)}$$

$$X_{v\delta} = X'_{v\delta} \cdot \frac{\rho}{2} \cdot L^2 \cdot u = 611 \cdot 10^{-6} \cdot \frac{1.025}{2} \cdot 156^2 \cdot 10.954 = 83.5 \qquad \text{(A.11)}$$

We then get the indirect wind force in longitudinal direction as:

$$\begin{aligned} X &= X_{vv} \cdot v^2 + X_{\delta\delta} \cdot \delta^2 + X_{v\delta} \cdot v\delta \\ &= -16.9 \cdot 0.161^2 - 1042 \cdot (0.0377)^2 - 83.5 \cdot 0.161 \cdot 0.0377 \qquad \text{(A.12)} \\ &= -2.4\,\text{kN} \end{aligned}$$

The indirect wind force of 2.4 kN is 2.4/53 = 4.5% of the direct wind force or 0.2% of the calm-water resistance. This is negligibly small.

How are Monitoring Reporting Solutions Impacted by MRV?

Torsten Büssow, Jarle Blomhoff, DNV GL, Hamburg/Germany, torsten.buessow@dnvgl.com

Abstract

This paper describes how the mandatory MRV (monitoring, reporting, verification) requirements can be handled with minimum extra effort if good monitoring tools are already in place (e.g. for performance monitoring). Existing solutions, available support and recommended processes by DNV GL are described.

1. Introduction

Regional and global requirements will force ship operators to monitor and report fuel consumption (and indirectly performance) in the near future. The coming monitoring and reporting requirements are closely linked to performance monitoring and can be implemented with minimum hassle if appropriate performance monitoring systems are already in place.

1.1. EU MRV requirements

As a first step towards cutting greenhouse gas emissions from maritime transport, the EU (European Union) requires operators of ships ≥5000 GT to monitor and report carbon emissions and transport work on all voyages to, from and between EU ports. Cornerstones of MRV (Monitoring, Reporting and Verification) requirements are:

- Monitoring Plans (MP) must be submitted to an accredited verifier (e.g. DNV GL) by 31.8.2017 and must be successfully assessed by 31.12.2017 latest by the verifier.
- The first monitoring and reporting period starts 1.1.2018 and ends 31.12.2018.
- The final verified emission report must be submitted to the EU commission by 30.4.2019 latest.
- Starting from 30.6.2019, ships need to carry a Document of Compliance on-board.

The following data items reporting within this MRV scheme:

- Port of departure
- Amount and emission factor for each type of fuel consumed in total
- CO_2 emitted (split between "at sea" and "at berth")
- Distance travelled
- Time spent at sea
- Cargo carried (ship type specific)
- Transport work

More detailed guidelines are under development, clarifying e.g. issues of reporting and verification.

1.2. IMO DCS requirements

In 2016, IMO's Maritime Environmental Protection Committee (MEPC) adopted amendments to MARPOL (Maritime Pollution Convention) introducing a mandatory Data Collection System (DCS). The IMO requirements will become mandatory roughly one year delay mandatory on a global level. Cornerstones of this Data Collection System are:

- All ships ≥5000 GT need to report fuel consumption with data collection starting 1.1.2019.

- A plan for data collection must be included in the SEEMP (mandatory Ship Energy Efficiency Management Plan) by latest 31.12.2018 (SEEMP Part II).
- An annual fuel consumption report (covering 1.1. to 31.12. of the year) should be submitted and verified (by a recognized organization) within 1.6. of the subsequent year.
- A confirmation of compliance (CoC) will be provided after the SEEMP Part II is updated and a statement of compliance (SoC) after the annual report is verified and submitted to the flag state administration.

The Data Collection System requires the following data items to be reported:

- IMO Number
- Ship type
- GT (gross tons), NT (net tons), DWT (deadweight)
- Power output of engines (for engines ≥ 130 kW)
- EEDI (Energy Efficiency Design Index), if applicable
- Ice Class
- Fuel oil consumption, by fuel oil type
- Distance travelled
- Hours underway
- Method used for collecting fuel oil consumption data

1.3. MRV vs. DCS – Similarities and differences

The EU MRV system will become effective in 2018, IMO DCS system in 2019. Under both schemes, ships must collect and report voyage data, allowing monitoring, reporting and verification of CO_2 emissions and ship efficiency data.

There are similarities, but also significant differences between the two systems, with technical, commercial and legal implications. A harmonization of both systems is complicated political processes both in the EU and in IMO. Therefore, at least several years of both systems overlapping have to be expected. IT (information technology) tools for monitoring and reporting will become a practical necessity, creating documentation automatically based on a common database of monitored data.

The two main differences is that the EU has an interest in comparing emissions for the cargo import to and export from the member states, hence they require ships to report actually carried cargo. In addition, the EU wants to increase public pressure to reduce emissions and will make the reports publicly available for every vessel. IMO on the other hand wants to measure the efficiency of the fleet, not necessarily of the carried cargo. In addition, they have an interest in protecting crucial company business information on cargo carried. It therefor bases the cargo on design capacity and avoids making the results available to the public.

Overlapping systems will duplicate the effort for verification of both duplicate monitoring plans as well as reported emissions.

2. Closing the gap and be ready for MRV

The key tasks in preparing for the EU MRV regulation come with typical issues which have to be addressed:

1. Decide on IT system to support data acquisition, monitoring, and reporting
    - Is my internal solution good enough?
    - What will be the total cost of alternative vendor options?

2. Verify data input and quality
    - Do we gather all necessary data?
    - What is the efficiency index for my ship type?
    - Is the data quality good enough?
3. Implement (and if necessary adapt) system
    - Do we have enough IT resources?
    - Do we have backup and other procedures in place?
4. Prepare monitoring plans
    - How do I write the MRV plan?
5. Monitor, prepare report, and have it verified
    - How much work will it take to export data?
    - Will we pass the verification process?
    - Can I get any additional benefit from the MRV work?
    - How is my efficiency compared to my competition?

The most important question to consider now is whether to use an existing in-house system or buying (out-sourcing to a third party). The decision – as usually – depends on how mature the in-house system is (= cost for required software upgrade and maintenance) and how expensive third-party systems are per ship. The general trend of outsourcing is expected to increase further since the performance monitoring and reporting systems have become more mature and now offers significant economies of scale by combining multiple fleets. After all, the reporting and monitoring of a vessel is quite a generic task and does not need to be adapted to each individual company. Furthermore, few companies can compete with professional IT software development companies, and therefore will rather outsource this task to focus on their core business of operating and managing vessels.

Essentially DNV GL offers support at all stages of the process. If the complete process chain from initial assessment to verification of the MRV report is supported by DNV GL, special care has to be taken that independent units perform mutually exclusive tasks ("preparation of documents" and "verification of documents") to comply with internal and external process requirements. See https://www.dnvgl.com/maritime/mrv-regulation.html for more details on our services.

3. MRV Monitoring Plan

While preparing an MRV monitoring plan is not rocket science, it resembles in many ways preparing your tax return: it is tedious and fairly complex (the guideline by the EU commission has 21 pages of bureaucratic jargon…) and most people perceive it as a daunting task. Software can help to minimize the hassle and get it right the first time.

As with a tax declaration, there are (mostly) constant items (ship data, installed main and auxiliary engines, etc.) and yearly changing data (voyage data and fuel consumption data). As of 2017, a DNV GL app helps you in the actual task of preparing the MRV monitoring plan. The online tool uses fully automatic or fixed values where possible, Fig.1, and uses pull-down menus of standard options to select to minimize typing work, Fig. 2.

The tool checks automatically whether all necessary information has been supplied and points out missing fields with open information. Prefilled data (e.g. from regulations) and "mix & match" options make it easy to prepare the plan while options to amend text blocks offer the required flexibility to customize MRV plans. All input can be saved for later revisions. Once the MRV plan has been prepare it can be exported (downloaded) as pdf file.

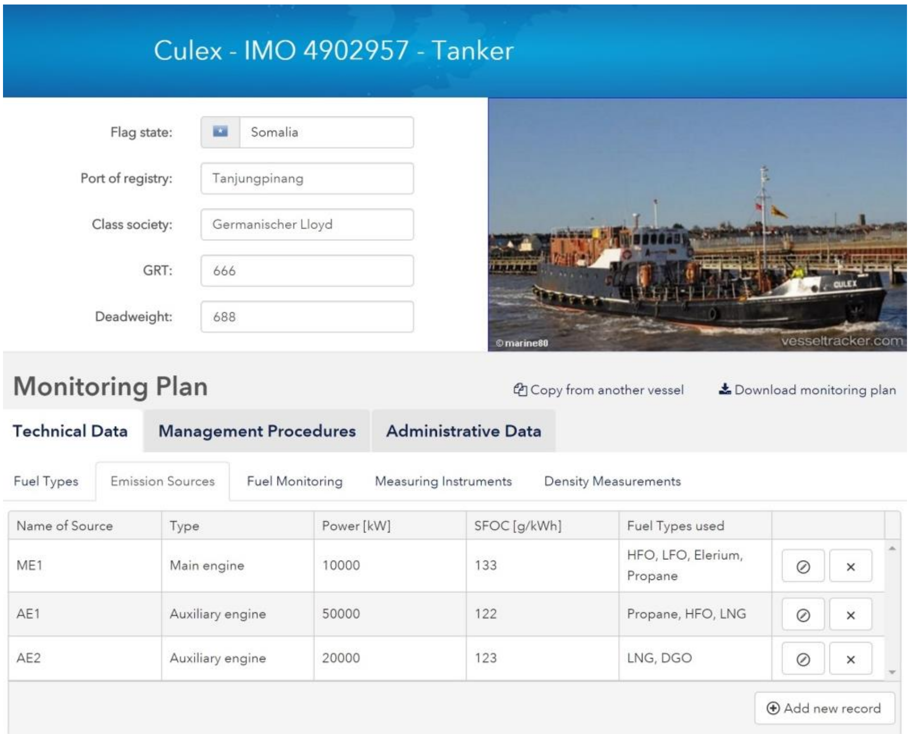

Fig. 1: Pre-filled technical data as default values are taken e.g. from databases (MRV app)

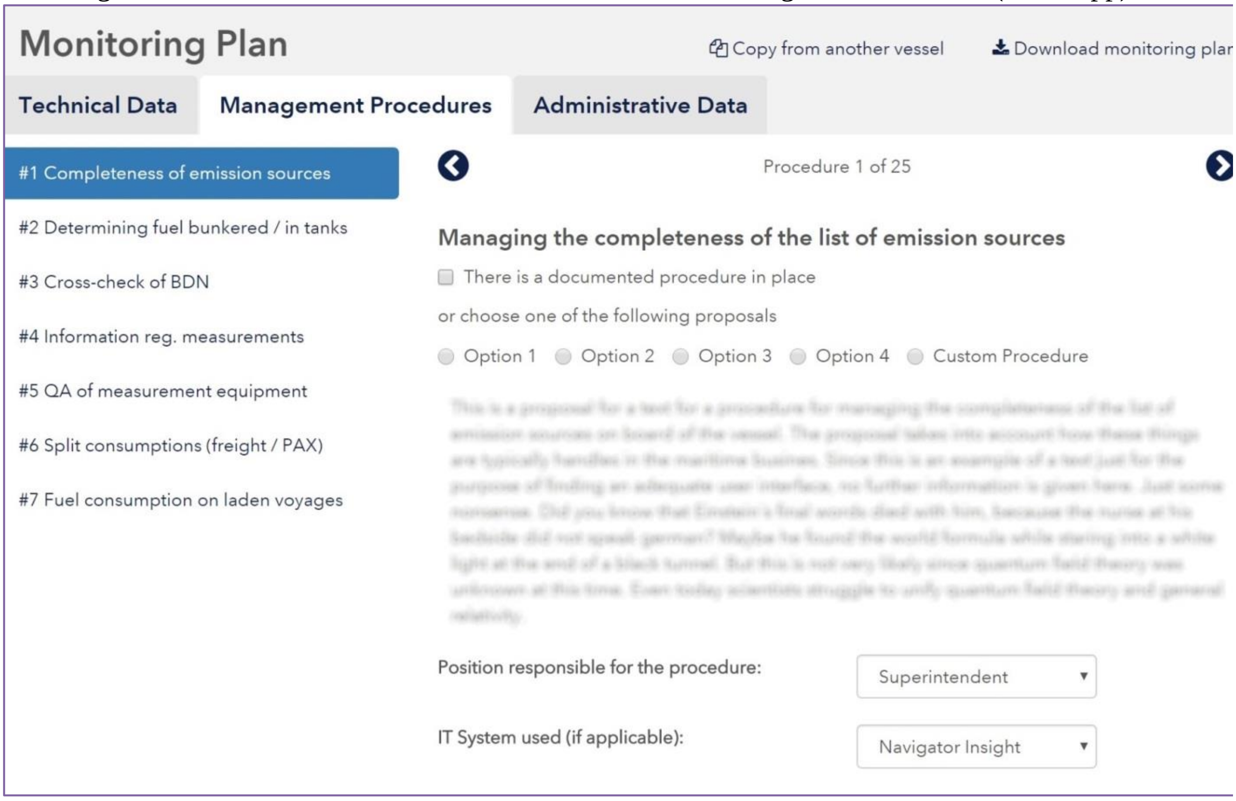

Fig. 2: Text blocks can be selected from standard options with a simple mouse click (MRV app)

4. Use of reporting tools for efficient compliance

The MRV and DCS schemes will require ship operators to deliver proper, verifiable voyage data. Most frequently in our observation, the biggest issue for ship operators with respect to MRV compliant systems is related to the quality of these data and the record keeping. Typical issues are:

- There is no voyage reporting or the reports are not stored
- Voyage reporting is based on plain e-mails with no further processing
- Data quality is not known or known to be insufficient

Minimum requirements for any reporting tool in terms of MRV and DCS compliance include:

- Collection of all relevant data
- Proper data quality with plausibility checks
- Automatic data processing for MRV and DCS output

However, collected data should be used for more than mere compliance. Ship and fleet performance management based on data monitoring and intelligent processing is a powerful tool for improving energy efficiency and generally business performance improvement, *Dückert et al. (2016)*. DNV GL supports this approach with its Navigator Insight tool, Appendix 1.

5. Conclusion

In 2017, EU regulations will require voyage data monitoring, recording and verification. A year later, similar, but not identical, reporting requirements will be imposed by IMO. The EU and IMO requirements can be handled with minimum extra effort if good monitoring tools are already in place (e.g. for performance monitoring). DNV GL offers support in all phases of preparation and implementation.

Acknowledgements

We thank our DNV GL colleagues for their valuable input (in alphabetical order): Volker Bertram, Jan Haul, Torsten Mundt, and Nils Wegener.

References

DÜCKERT, T.; SCHMODE, D.; TULLBERG, M. (2016), *Computing hull & propeller performance: ship model alternatives and data acquisition methods*, 1st Hull Performance & Insight Conf. (HullPIC), Pavone, pp.23-28

https://www.dnvgl.com/maritime/mrv-regulation.html

https://www.dnvgl.com/maritime/technical-regulatory-news/index.html

https://www.dnvgl.com/maritime/mrv-regulation-webinar.html

https://www.dnvgl.com/services/eco-insight-easy-fleet-performance-management-1175

https://www.dnvgl.com/services/fleet-performance-and-ship-performance-monitoring-system-navigator-insight-1452

Appendix 1 – "Navigator Insight" tool

For emission reporting and performance monitoring, the key is to collect and evaluate voyage and operational data in a structured way. This data is important for ship management, transparency, and for external reporting to charterers, cargo owners, non-governmental organizations such as the Clean Cargo Working Group (CCWG) (https://www.bsr.org/collaboration/groups/clean-cargo-working-group), the EU MRV scheme or IMO's DCS. The quality of data collected determines its usefulness for trending and analysis or in further internal and external reporting.

The Navigator Insight tool provides an onboard module for structured and harmonized data reporting that instantaneously alerts crew of potential reporting errors or implausible data. The event-based reports are logged on the onshore server, providing the base for ship or fleet voyage monitoring.

The data collected onboard in Navigator Insight feeds into DNV GL's performance management portal ECO Insight. ECO Insight provides comprehensive performance dashboards, benchmarks and industry data such as AIS (Automatic Identification System), fuel quality or weather data. Combined, this furnishes the information for industry best-practice performance management.

Navigator Insight user can:

- use current ship-to-shore reporting processes with existing information
- use integrated performance monitoring systems that allow the crew to report the typical voyage (e.g. arrival, departure, noon) and events
- structure information for re-use in any type of analysis or reporting
- get automatically generated log-abstracts in the office and onboard with customized content
- run a controlled e-mail push service with key event information
- ensure higher data quality and completeness by means of numerous plausibility checks in the
- system based on vessel-specific technical data
- substitute existing ship-to-shore reporting processes so the crew only has to fill out reports once
- create environment reports according to known standards for ESI (Environmental Ship Index), http://www.environmentalshipindex.org/Public/Home, CSI (Clean Shipping Index), http://www.cleanshippingindex.com/, and CCWG

Navigator Insight strikes the balance between completely manual reporting systems, which often suffer from data quality issues, and fully automated performance monitoring. It is intuitive to use without onboard training needs.

By late 2016, Navigator Insight had ~1000 vessels using the system, making it the most widely adopted solution worldwide. Being already MRV compliant, Fig.3, and with its proven record for data quality, *Dückert et al. (2016)*, certification of MRV compliance is straightforward if data monitoring and reporting is based on Navigator Insight (possibly combined with ECO Insight for performance assessment and business insight).

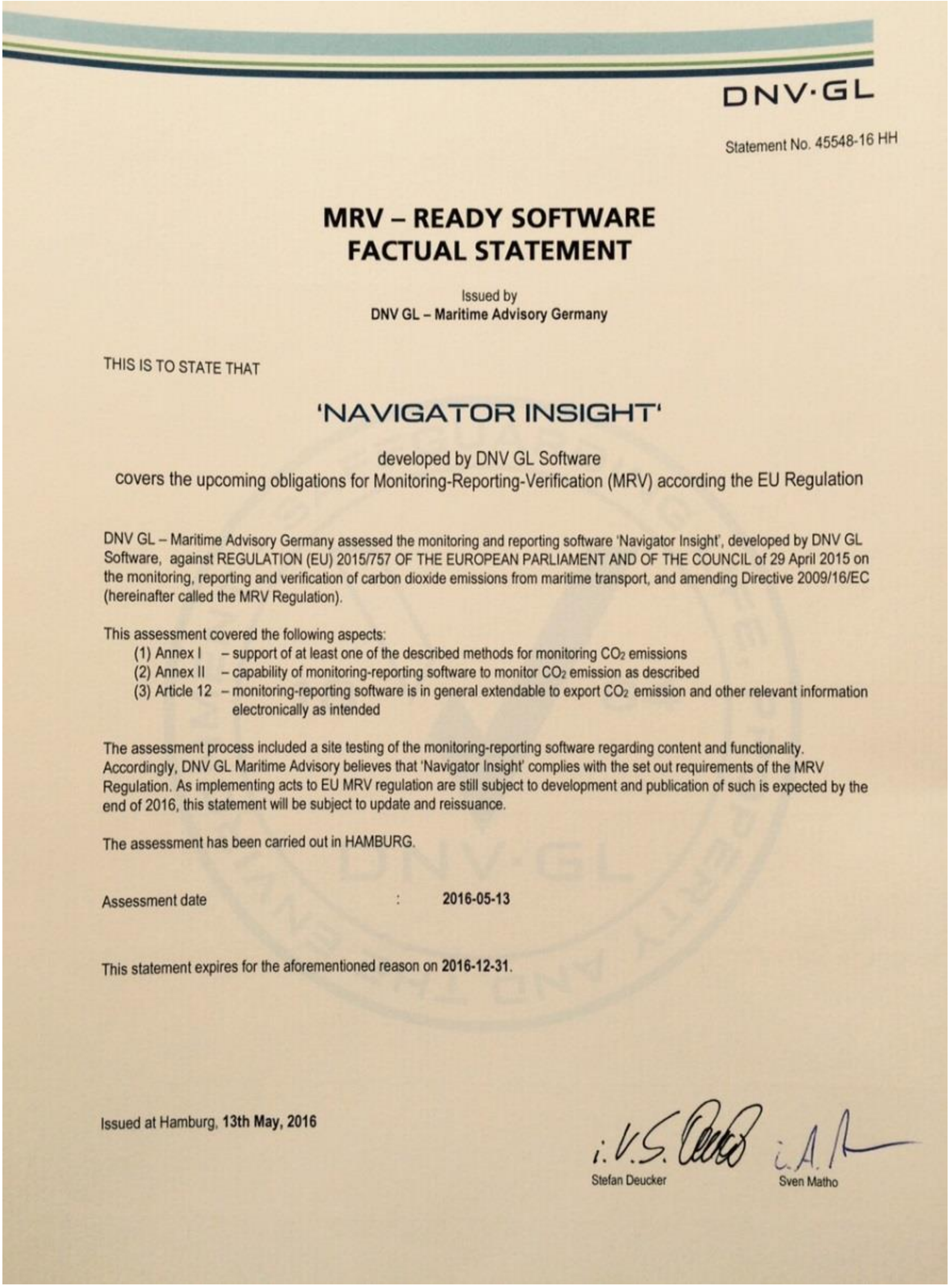

DNV·GL

Statement No. 45548-16 HH

MRV – READY SOFTWARE
FACTUAL STATEMENT

Issued by
DNV GL – Maritime Advisory Germany

THIS IS TO STATE THAT

'NAVIGATOR INSIGHT'

developed by DNV GL Software
covers the upcoming obligations for Monitoring-Reporting-Verification (MRV) according the EU Regulation

DNV GL – Maritime Advisory Germany assessed the monitoring and reporting software 'Navigator Insight', developed by DNV GL Software, against REGULATION (EU) 2015/757 OF THE EUROPEAN PARLIAMENT AND OF THE COUNCIL of 29 April 2015 on the monitoring, reporting and verification of carbon dioxide emissions from maritime transport, and amending Directive 2009/16/EC (hereinafter called the MRV Regulation).

This assessment covered the following aspects:
(1) Annex I – support of at least one of the described methods for monitoring CO_2 emissions
(2) Annex II – capability of monitoring-reporting software to monitor CO_2 emission as described
(3) Article 12 – monitoring-reporting software is in general extendable to export CO_2 emission and other relevant information electronically as intended

The assessment process included a site testing of the monitoring-reporting software regarding content and functionality. Accordingly, DNV GL Maritime Advisory believes that 'Navigator Insight' complies with the set out requirements of the MRV Regulation. As implementing acts to EU MRV regulation are still subject to development and publication of such is expected by the end of 2016, this statement will be subject to update and reissuance.

The assessment has been carried out in HAMBURG.

Assessment date : **2016-05-13**

This statement expires for the aforementioned reason on **2016-12-31**.

Issued at Hamburg, **13th May, 2016**

i.V. Stefan Deucker i.A. Sven Matho

Fig.3: Navigator Insight tool is ready for MRV reporting allowing fast accreditation if reports are based on the tool

Influence of Noise and Bias on the Uncertainty of Data-Based Hull Performance Prediction

Daniel Schmode, DNV GL, Hamburg/Germany, daniel.schmode@dnvgl.com

Abstract

The error in hull performance prediction is the difference between the true hull performance and the result of a hull performance measurement procedure. There are many sources of error, both in data acquisition and in fundamental models used in hull performance calculation. This paper discusses various uncertainty sources, distinguishing between random errors (noise) and systematic errors (bias). The paper shows exemplarily the progression of sensor errors through a standard hull performance calculation procedure to global uncertainty of the hull performance indicator.

1. Data-based hull performance prediction

Hull performance monitoring is based on data reported from ship operation. This data needs to be

- normalized (to a baseline), i.e. corrected for deviation from the baseline conditions
- filtered, e.g. for condition with known large errors
- averaged, reducing a scatter cloud to unique value or function

Key variables are shaft power and speed (through water), establishing a speed-power curve. Additional variables to monitor are needed for normalization and/or filter criteria, including:

- loading condition data (draft, trim)
- ambient condition data (wind direction and speed, wave direction, significant height, and spectrum, …)

Each of these variables comes with uncertainties. In addition, the performance calculation process has its own uncertainties, e.g. due to simplifications of underlying models, see e.g. *Bertram (2017)*. ISO 19030 gives uncertainties for some sensors. These are mostly based on supplier information, reflecting ideal, laboratory conditions. Most ships in service will have larger errors due to installation errors and wear-and-tear over time. *Freund (2013)* gives also uncertainties for assorted sensors on board, distinguishing between ideal conditions (vendor specification) and typical values encountered in industry.

ISO 19030 also gives a global uncertainty for the 'default' method as outlined in part 2 of the standard. This global uncertainty is based on a Monte Carlo simulation, i.e. a random variation of input variables within specified uncertainty intervals which reflects the error in measuring data and the impact on the final performance indicator, https://en.wikipedia.org/wiki/Monte_Carlo_method. The approach behind the calculation of this global uncertainty assumes that errors are independent of each other and the procedure of obtaining and processing the data. Reality again is more complex that this modeling approach, as data quality may depend also on sampling process, as discussed in *Dückert et al. (2016)*.

2. Uncertainties in data acquisition

Data acquisition is difficult, as discussed in HullPIC 2016 e.g. by *Bos (2016), Jonsson and Fridriksson (2016),* and *Baur (2016)*. Data may be logged in various forms and formats:

- Automatically or manually
- In simple tables or advanced voyage reporting software

Data quality depends on the approach, but also the sensors. Issues to consider include:

- Initial quality of sensors – vendors generally give uncertainties for norm conditions in a controlled environment, e.g. on a laboratory test bed. Installation on board may already introduce additional uncertainties (errors) which may or may not be compensated by initial calibration (if performed). For example, a speed log may be installed slightly askew and the resulting error for design speed compensated during sea trial calibration.
- Actual quality of sensors – over time, conditions of sensors may deteriorate, due to wear and tear or simple aging. The actual quality will be lower than the initial quality, and depends among others on the maintenance of the sensor. For example, speed logs may be affected by local fouling.
- Human factors – Humans may act as sensors (e.g. estimating sea state) or as recording device (reading data from a screen and entering it in a recording system, in the simplest form an email). Humans may introduce avoiding unintentional errors (misreading, mistyping) and intentional errors (deliberate lying for assorted reasons). Data quality then depends on care and goodwill.
- Robustness of automatic loggers – Connections between sensors and recording systems may have interface problems where data gets corrupted or lost; in the most trivial case a cable between sensor and logger gets disconnected.

3. Noise versus Bias

Errors can be random or systematic. We call random errors “noise” and systematic errors “bias”.

3.1. Noise

Noise has no preferred direction. So averaging over a large number of measurements will yield an error converging to zero as the number of datasets increases. The resulting performance indicator may be imprecise, but not inaccurate. The impact of random error depends on the number of measurements and the standard deviation of the distribution. Thus imprecision can be reduced by increasing the sample size or by decreasing the standard deviation (loosely speaking the inherent scatter). For example, various speed readings taking at exactly the same ship speed may still scatter due to air bubbles or ambient wave motion. Some readings will be too high, some too low. By taking enough measurement and averaging them we get the correct speed.

To illustrate the effect of noise in speed and power measurement we carried out a simple simulation. In Fig.1, a synthetic hull performance time history is plotted in green. The shown vessel was coated in 2014 and 2016 and is degrading with a rate of 10% per year in the first period and with 13% per year in the second period. These numbers are pure fiction. Now we assume the speed log produces noise with a standard deviation of 2% and the shaft power meter with a standard deviation of 1%. We simulate to take one measurement every second day. Since we know the “true” data, we apply a random noise on the speed and the power and compute the hull performance index. The resulting noisy data points are plotted in Fig.1 in light blue. As a last step in the simulation we apply regressions to the data for the two periods. These regressions are plotted in dark blue. As expected, the regression is quite close to the “truth”, but does not coincide exactly, due to the finite number of data sets.

Fig.2 shows the same simulation, but with fewer synthetic measurements points. Here only one measurement per week is simulated. Especially in the shorter period, the difference between the regression and the “truth” is apparent.

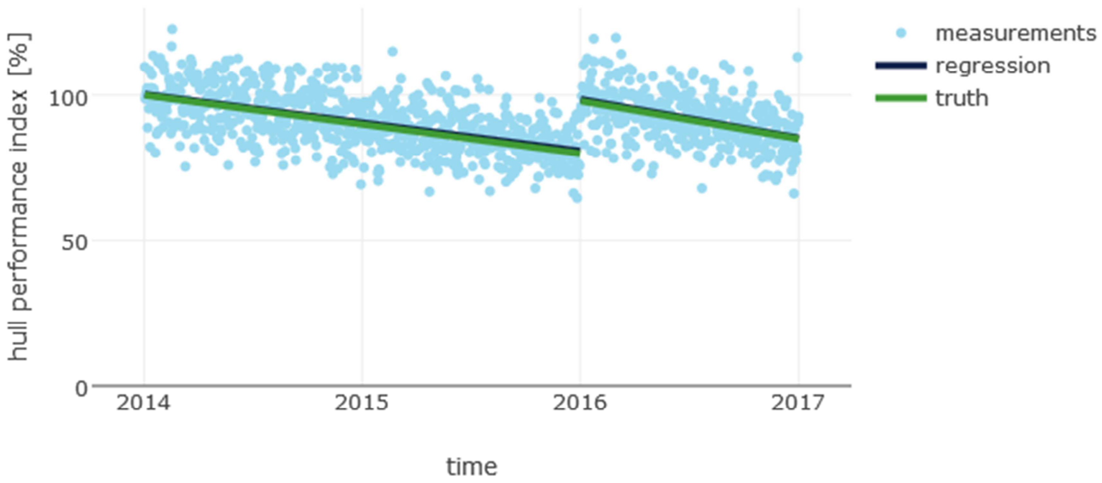

Fig.1: Simulation of hull performance regression (measurements every second day)

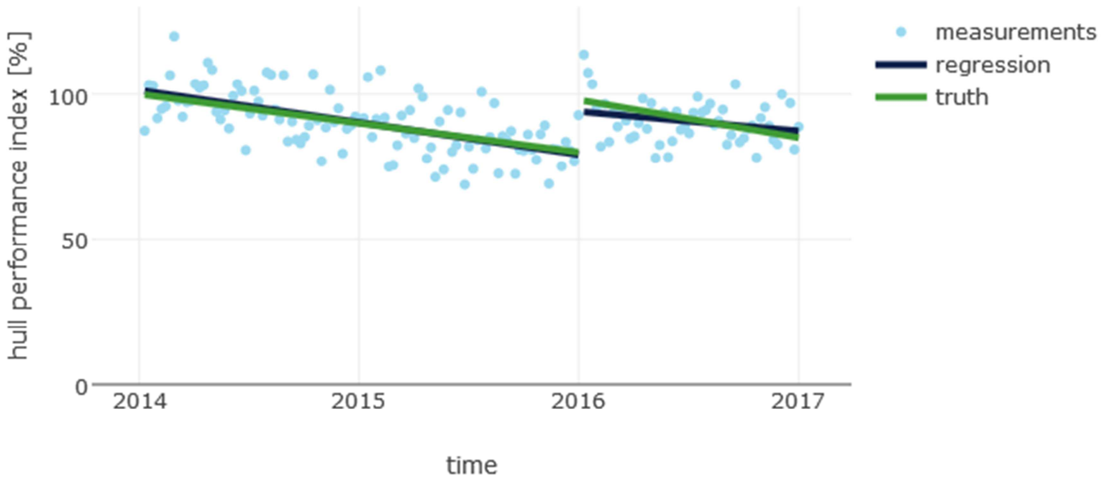

Fig.2: Simulation of hull performance regression (measurements once per week)

By taking new samples with the same standard deviations and measurement frequencies we will get different regression lines. Thus re-executing this numerical experiment will yield a variation of regression lines. Their slope and offset are again noisy. To illustrate how much the regression lines vary for repeated simulation, Fig.3 presents the "truth" and the regression lines for 100 random simulations for 1 measurement per week.

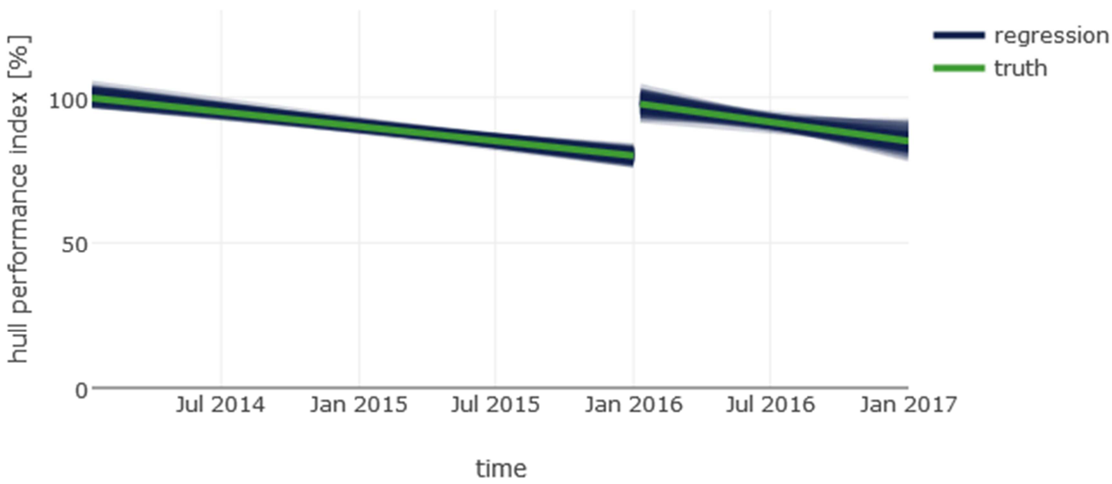

Fig.3: Variation of regression lines indicating noise in slope and offset for 1 measurement per week

We see that a relatively small measurement error can cause significant uncertainties in the trend lines (regression lines) for low measurement frequency. Since the synthetic errors follow a normal (Gaussian) distribution, uncertainty in the trend lines decreases with increasing frequency of measurement. Fig.4 shows the same 100 variations for a measurement frequency of one measurement per day. The resulting uncertainty in the trend curves is rather small.

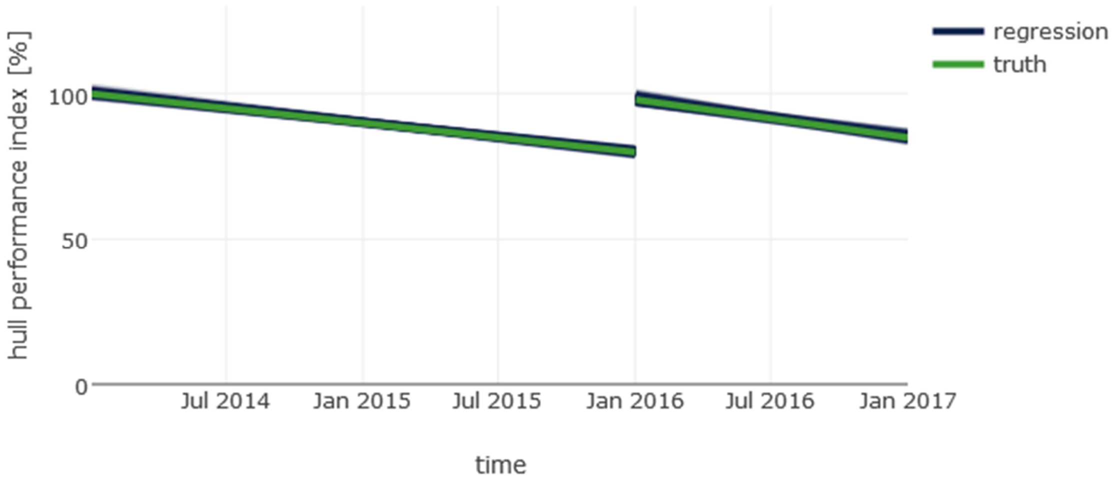

Fig.4: Variation of regression lines for 1 measurement per day

By further increasing the measurement frequency to one per hour, the uncertainty gets even smaller, Fig.5. However, such high measuring frequency would come with additional expenses as at this rate automatic data logger systems need to be employed.

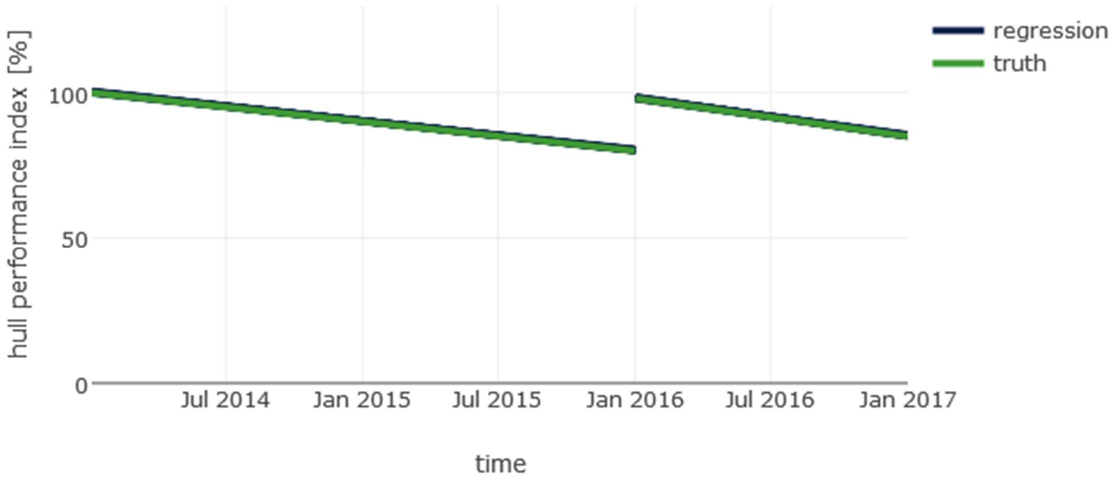

Fig.5: Variation of regression lines for 1 measurement per hour

So far, we assumed independent and identically distributed random variables. By applying the standard tools of statistics, confidence intervals can be computed. These confidence intervals reflect exactly what this simple simulation demonstrates. The conclusion is that at a certain point adding much more data does not significantly improve the accuracy (respectively reduce uncertainty in the trend lines). It is then smarter to focus on improving data quality.

3.2. Bias

Bias refers to deviations that are not due to chance alone. Examples are an improperly calibrated measuring device or a broken sensor. Bias may change over time, e.g. for shaft power measurements where the strain gauge material experiences fatigue. Or they may change with speed, sea state, draft or other variables. Errors in speed logs may show variability with sea state as increased ship motions changes local pressure measurements and in turn the derived speed. For bias, averaging over a large number of measurements does not lead to vanishing error. Constant bias can be eliminated by calibration, but bias depending on time (or other time-dependent variables) is not easily eliminated. Fig.6 illustrates the effect of a constant bias of 2% on the speed log. Here the hull performance is clearly over predicted. Neither repeating the experiment nor increasing the measurement frequency does cure the problem, Fig.7.

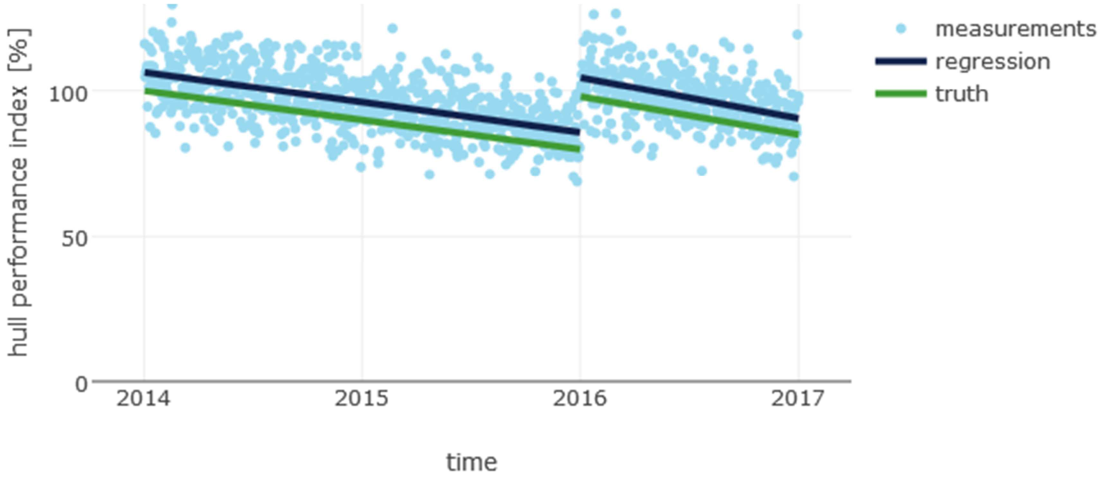

Fig.6: Example of effect of constant 2% bias in speed log on trend lines, 1 measurement per day

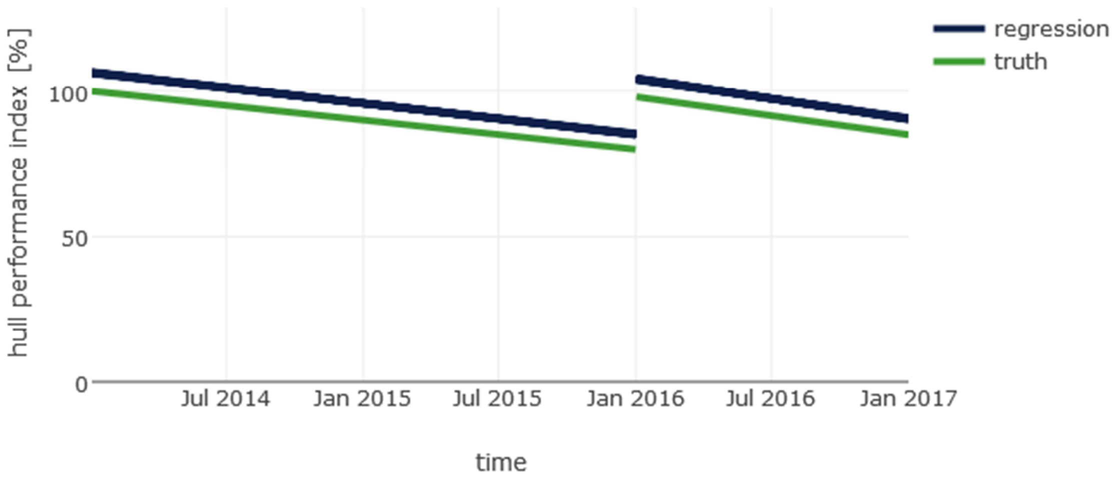

Fig.7: As Fig.6, but 100 simulations for measurement frequency of 1 measurement per hour

3. Conclusion

The shown simulations illustrate the effect of noise and bias on the hull performance indicator. The uncertainty due to noise (assumed to be random and following a normal distribution) can be cured by increasing measurement frequency. We recommend on average one measurement per day to get proper prediction for the hull performance development in a typical evaluation period.

The uncertainty due to bias is more problematic as it is independent from the measurement frequency. Here proper maintenance and monitoring of the sensors is essential. We recommend a smart voyage reporting software that applies ship specific plausibility checks during data recording. If sensor defects are quickly identified sensors can be replaced / restored restoring global uncertainty to (near)-ideal values. In our experience, data quality for hull performance purposes depends much more on the maintenance of the sensors that on the reporting regime.

References

BAUR, M.v. (2016), *Acquisition and integration of meaningful performance data on board challenges and experiences*, 1st HullPIC Conf., Pavone, pp.230-238
http://data.hullpic.info/HullPIC2016.pdf

BERTRAM, V. (2017), *Some heretic thoughts on ISO 19030*, 2nd HullPIC Conf., Ulrichshusen, pp.12-18
http://data.hullpic.info/HullPIC2017.pdf

BOS, M (2016), *How MetOcean data can improve accuracy and reliability of vessel performance estimates*, pp.106-115
http://data.hullpic.info/HullPIC2016.pdf

DÜCKERT, T.; SCHMODE, D.; TULLBERG, M. (2016), *Computing hull & propeller performance: ship model alternatives and data acquisition methods*, 1st HullPIC Conf., Pavone, pp.23-28
http://data.hullpic.info/HullPIC2016.pdf

FREUND, M. (2013), *Holistic analysis of onboard consumption and efficiency of the energy systems of ships*, PhD thesis, Helmut-Schmidt University, Hamburg
http://edoc.sub.uni-hamburg.de/hsu/volltexte/2013/3004/pdf/2012_Freund.pdf

JONSSON, S.; FRIDRIKSSON, H. (2016), *Continuous estimate of hull and propeller performance using auto-logged data*, 1st HullPIC Conf., Pavone, pp.332-338
http://data.hullpic.info/HullPIC2016.pdf

The Role of Accurate Now-Cast Data in Ship Efficiency Analysis

Michael Haranen, NAPA Ltd., Helsinki/Finland, michael.haranen@napa.fi
Sami Myöhänen, NAPA Ltd., Helsinki/Finland, sami.myohanen@napa.fi
Dragos Sebastian Cristea, NAPA Ltd., Helsinki/Finland, dragos.cristea@napa.fi

Abstract

This paper describes the results of statistical analysis of data collected from many vessels to discuss the problems which may occur during the data collection onboard, and the role of the now-cast data for technical performance evaluation. The research is focused on the quality of measurements of wind and speed through the water. The main goal of the research is to reveal the benefits of using now-cast data and its effect on the quality of statistical models which can be used for performance evaluation purposes. The results of the statistical analysis show that the now-cast data can be successfully used for validation of the on-board measurements and, in some cases, can substitute the onboard data without lack of analysis quality.

1 Introduction

An understanding of the factors that influence the ship resistance and their behavior is very important as they can be used for the technical performance evaluation. By technical performance, we understand here the relationship between the speed through the water and the corresponding energy consumption of the ship. This relationship may be described by using physical laws or can be estimated statistically by using machine learning and data mining techniques using sensor data collected onboard, *Haranen (2016)*. The most important goal of the technical performance evaluation is to quantify possible deterioration of the hull condition due to hull or propeller fouling, paint problems, aging, etc. The performance evaluation can be done by data correction, *ISO 19030*, or with the aid of statistical modeling.

Regardless of the methodological approach for the technical performance analysis and evaluation, it is important to assess and separate the effect of operational conditions and environmental factors. Therefore, it is extremely important to have accurate data for all variables which we use for the technical performance evaluation. Usually we use variables like propulsion power consumption, engine rpm, speed through water, draft, trim, wind speed and direction, wave and swell height, water temperature, water depth, etc.

This paper mostly concerns about the quality of the wind data and measurements of the speed through the water. It is known that data collected onboard ship may be inaccurate and biased. Many publications describe problems with onboard measurements of the speed through the water or wind. Unfortunately, the problems described in the publications are usually case specific and thus cannot be generalized. In our research, we analyzed the data collected from many ships and tried to assess the scope of the problems with the onboard data for the wind and the speed through the water.

In the paper, we elaborate on the role of now-cast data from the technical performance analysis point of view. The term now-casting is widely used in meteorology and is defined as the prediction for the present, near future and recent past weather conditions. Our research is focused on questions like:

- How can we use the now-cast data for validation of the data collected onboard?
- Can we prove that using the now-cast data will increase the accuracy and reliability of the analysis in general?
- Is it better to use wind measurements onboard or should we rely on now-cast data?
- Is it better to use speed log signals or should we calculate the ship speed through water from the speed over ground and now-cast ocean currents?

2 Data collection challenges

The main goal of this section is to discuss challenges related to data collection onboard ship and the role of the now-cast data, which is available from many independent weather providers. Nowadays, systems onboard the ship are capable to collect the environmental data for many sources. For example, it is common that every ship has an anemometer, thus collection of the wind speed and direction data seems to be a simple task. Echo sounders are standard devices on all ships, making it easy to collect information about water depth. With newest technology, it is also possible to measure and record the sea surface conditions, like wave and swell height and period. However, collection of the environmental data onboard the ship can be a challenging task and subject to errors.

While studying several scholars' research, we could identify plenty of issues that can appear for onboard weather and sea state related measurements. Referring to biased wind data, *Taylor et al. (1995)* emphasized that there are several possible sources of error for anemometer wind measurements. It is not known how well the deployed anemometers have been calibrated or what, if any, measures are taken to ensure that the instruments remain within calibration. In use, the anemometer is exposed to a turbulent flow, which fluctuates as the ship rolls and pitches and the anemometer may not be "vertical" with respect to the mean flow. The reported wind is an estimate of the average reading of a fluctuating analog dial made by the ship's officer and, thus, subject to errors. Errors are made also in converting to true wind velocity. According to *Moat et al. (2005)*, wind speed measurements obtained from ship-mounted anemometers are biased by the distortion of the airflow around the ship's hull and superstructure.

Depending on the ship type, location of the wind transducer, trim and wind direction, there can be big inaccuracies in certain wind directions in varying load conditions. For example, on a container ship with the deckhouse at the aft ship, the situation is very different depending on how high container stacks are in front of the deckhouse and when the relative wind is coming from the bow region. On the other hand, it is quite common for ferries and car carriers that the wind is measured at the bow, but there is huge ship behind it. At the following wind, it is very difficult to measure wind in such a condition and then the wind driven wave data prediction fails as well.

As for the sea state measurements, in *Stredulinsky and Thornhill (2009)* the authors state that wave or swell height measurements can be performed through different methods, like using x-band radars, Doppler radars or wave buoys. Still, all these technologies present issues and challenges. With x-band Radar, there is no direct measurement of the wave elevation. The sensor captures backscattered intensities of the reflected Radar magnetic waves on the ocean surface. These intensity images must be converted into wave images by relying on 3D Fourier analysis. According to *Nielsen (2008)*, wave buoys do have several drawbacks. The first is that they require a suitable crane onboard the ship for deployment and recovery, which can be a difficult operation in high sea states. Trial operations must remain in relatively close proximity to the wave buoys for data to be useful. This limits the length of straight track runs before the vessel must return to the buoy. If several buoys are deployed, they can drift away from each other. This requires the ship to do manual adjustments. Buoy data may contain errors and its quality must be checked. In *Simos et al. (2010)*, another method, used for wave measurements, is presented: an over-the-bow downward-looking Doppler radar. The radar gives the distance to the wave surface and, when combined with an accelerometer, can give the actual wave height. Many sea trials using this system have shown that it works reasonably well, but that there tends to be sensitivity in the wave height measurements to relative heading. It tends to work best in beam seas. Other drawbacks are that it does not give wave spectra (only wave height and characteristic encounter frequency are given), and it can be damaged in severe sea conditions.

On depth measurement issues, *Godin (1995)* states that sonars are complex and hard to calibrate. They include many sub-systems that possess their own configuration and calibration routines. There are several sources of error associated with depth measurements, and they must be detected and quantified by systematic testing procedures before being corrected or eliminated. For example, deep-water surveys (> 1000 m) involve much larger sonar footprints and thus, corresponding lower accuracy both in the positioning and in the depth measurements are usually acceptable. In addition, the accuracy requirements are much harder to meet in shallow waters (< 100m) where the calibration of the sounding systems becomes a critical issue, see *Hare and Tessier (1995)*.

As we can see from the numerous examples, onboard data collection is a challenging task. At the same time the importance of accurate environmental data, which we use for the ship technical performance evaluation, is pointed out in many research papers. Here are some notable examples: determining how ship navigation is affected by extreme weather conditions, *Xia (2006*b) identifying algorithms and models for the prediction of ship speed and power for different weather states, *Chen (2013), Soda et al. (2012*c) determining fuel savings algorithms, *Hellstrom (2003*d) researching new architectural ship designs, for example Flettner rotors design, *Traut et al. (2014*e) determining different ship routes based on weather and sea currents forecasts, *Padhy et al. (2008), Tsujimoto et al. (2006), Panigrahi et al. (2012), Zhang and Huang (2017), Cai (2014*f) analyzing characteristics of propulsion performance under various weather and sea conditions, *Sasaki (2009), Yokoi (2010), Tsujimoto (2000), Kayano (2013)*.

In this research, the accuracy of the wind data is under investigation. In the case of the ship's technical performance evaluation, the goal is to estimate the effect of wind speed/direction on ship performance. Usually, in slow winds, the ship will lose speed in headwinds and will gain speed in the case of following winds. If the wind speed is high, the speed will be reduced in both cases due to the increased wave actions and steering corrections. Having correct wind measures will highly increase the quality of the model and correspondingly will increase the quality of the research.

When we speak about technical performance evaluation there are two major sources of environmental data. We can collect data onboard, manually or by using sensors. On the other hand, there are numerous weather providers which make independent weather now-cast data available. We can identify two general benefits from the now-cast data. First, this data can be used for validation of the data that is collected onboard. Second, if for some reason we are not able to use the onboard sensor data or the data is erroneous, we can use the now-cast data instead.

2.1 Weather Interpolation Service

In Napa practice, now-cast data from several independent weather providers is used. They send data covering all important aspects related to sea conditions, like sea currents speed and direction, tidal currents speed and direction, air pressure, wave heights, wave direction, swell heights, water temperature, water salinity, wind speed, wind direction, ice concentration, salinity, etc.

The data files, containing environmental parameters, are built based on a grid with predefined resolution. Fig.1 shows the example for of grid data for the oceanic currents. To obtain exact environmental conditions for a certain ship, available weather now-cast data is interpolated according to the ship location and time. The important characteristic of the Napa platform is the ability to correctly approximate weather and sea conditions for specific coordinates in time (according to ship position and time of the measurement). Coordinate resolution can vary between providers or between parameters. As an example, sea current parameters are defined using a 0.25° resolution grid, while wind-related parameters are using a 0.5° resolution. For different providers/parameters the grid resolution can vary even more: 0.001°, 0.1°, 0.08°, 0.02°, 1.25°, etc. In this context, our interpolation functionality was developed to provide accurate weather data values for any reported ship position during the voyage of a ship.

For interpolation, we use the bilinear and trilinear interpolation procedure, which is an extension of the linear interpolation. The main idea of the trilinear interpolation is shown in Fig.2. In order to fulfill the interpolation procedure, the weather files should contain data for the necessary dates and time, determined from the timestamps when the ship sailed over certain coordinates. In addition, it is mandatory for the ships to send both latitude and longitude for their position and the reference time of the measurement, Fig.2.

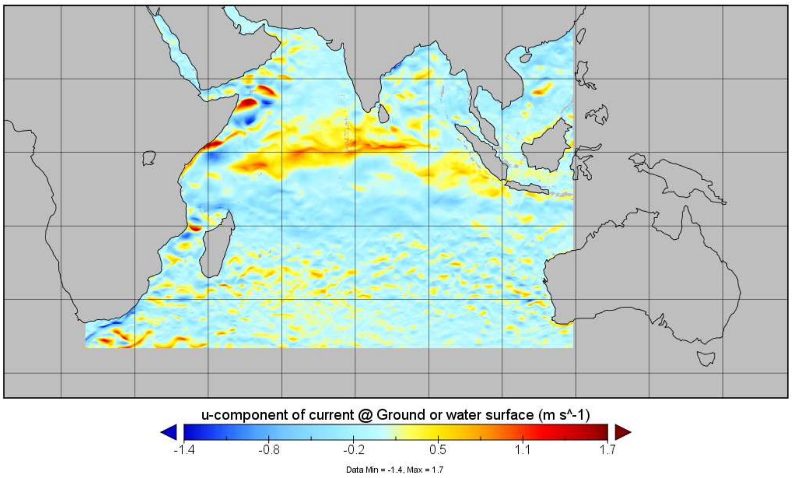

Fig.1: Current data for the Indian Ocean

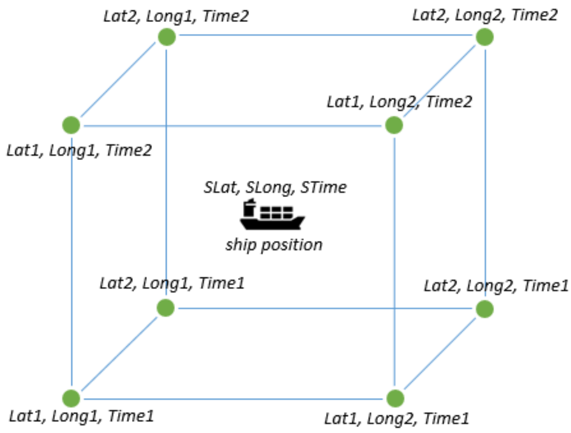

Fig.2: Ship position from the trilinear interpolation perspective

3 On-board wind versus now-cast wind

This section is devoted to a comparison of the now-cast wind and wind measured onboard. First, we investigate how often the problems related to the wind measurement onboard the ship may be faced in general. Then, we present the results of the modeling test. The goal of the modeling test is to elaborate on the quality and goodness of the wind data from different sources.

Before data analysis and modeling, the onboard wind measurements need to be adjusted so that they correspond to the same height as the now-cast wind. Now-cast data usually contains the wind measurements reported at the height of 10 meters. Thus, the onboard measurements are adjusted to the same height by using the power law of the wind profile as follows:

$$V = V_m \left(\frac{h}{h_m}\right)^{1/7},$$

V_m is the measured wind speed at the height h_m (depends on the anemometer location on-board), and $h = 10\ m$.

In Napa practice, for the sake of simplicity, the wind speed and direction are transformed into headwind and crosswind components. Fig.3 gives an example in which the time-series of the onboard and now-cast headwind are depicted demonstrating a good match between different sources for the wind data. Our onboard data represent 5-minute averages for the headwind. The now-cast wind is usually reported every 3 hours and it is interpolated to correspond to the same time resolution. As one can notice from Fig.3, the values are close to each other. In this example case, the linear correlation between now-cast and onboard headwind is about 95.5%, which suggests that there is no major problem with the onboard measured wind.

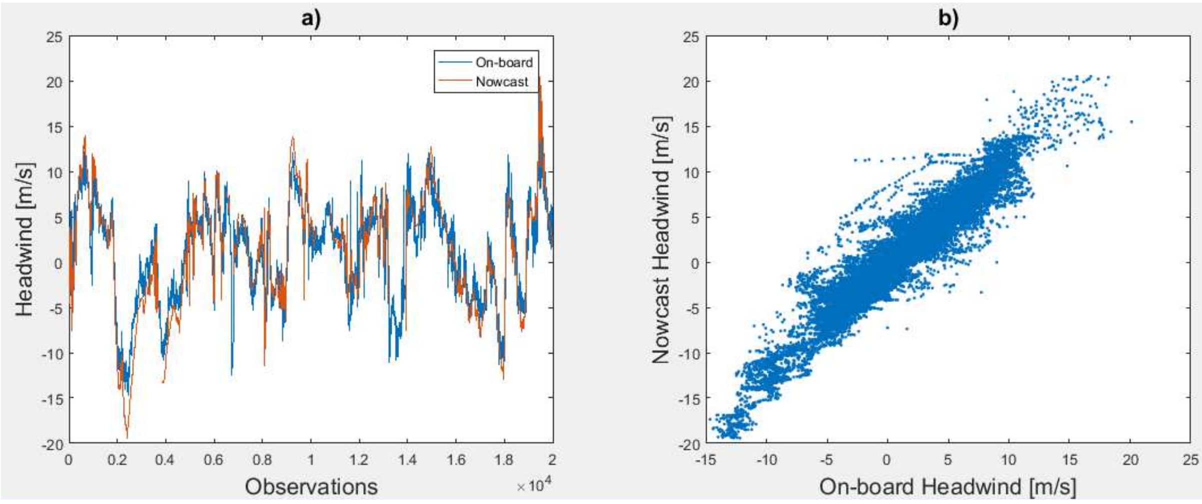

Fig.3: Now-cast vs. onboard headwind

In Fig.4 and Table I the result of the wind comparison based on the data of 150 randomly selected ships. For each vessel, the linear correlation between wind components from two different sources, now-cast vs. onboard wind, were calculated. Fig.4a shows the distribution of the correlation for the headwind, Fig.4b for the crosswind component. Table I helps to understand the situation in general. As one can see, in about 20%-25% of all tested cases the linear correlation between wind components from two different sources is less than 80%. The results of this random test show that we may face some kind of problem with the wind measurements onboard for every fifth ship. This means that the wind data, which is measured onboard, should be always checked and validated against the now-cast data, which can be obtained from independent weather providers.

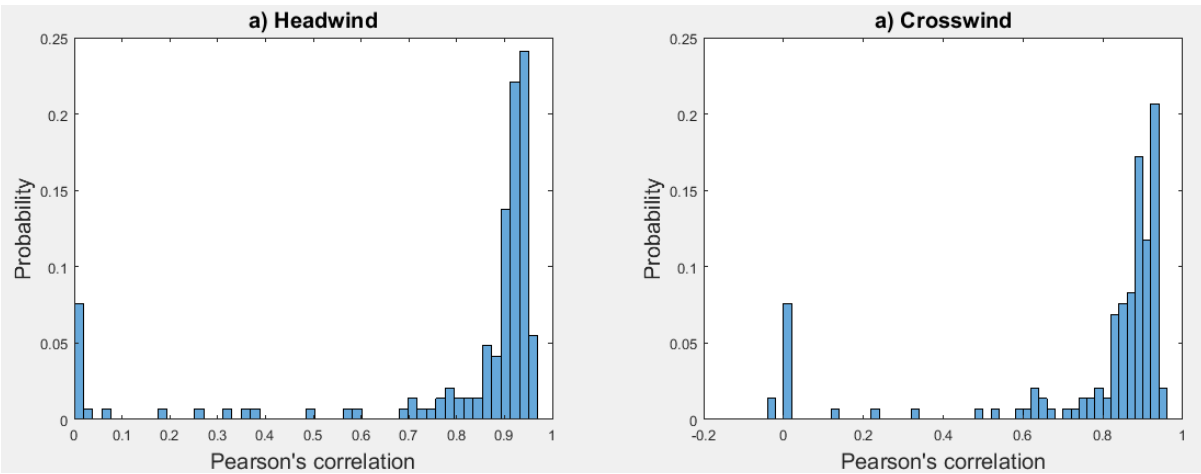

Fig.4: Distribution of the linear correlation between wind components from two different sources

Table I: Correlation vs. ship percentage

Now-cast vs. on-board headwind correlation		Now-cast vs. on-board crosswind correlation	
Pearson’s correlation	Percentage of vessels	Pearson’s correlation	Percentage of vessels
< 80%	21%	< 80%	23%
80%-90%	17%	80%-90%	42%
90%-95%	56%	90%-95%	34%
>95%	6%	>95%	1%

3.1 Model-based comparison

Let us now examine the cases without any problems with the wind measurements onboard.
The most interesting questions are:

- What is the difference between the onboard and now-cast wind from the modeling point of view?
- Can we achieve better results by using onboard or now-cast data?
- Can we substitute erroneous onboard wind data with now-cast data without lack of accuracy of the analysis?

To find the answers to these questions we have implemented a modeling test. The main idea of the test is to compare predicting errors of the ship specific statistical models in which we use the wind from different sources. During the experiment, the model responses and all other model inputs except the wind remain unchanged. We assume that the smaller the model prediction errors are the better the wind components reflect the variation of the model response and the better the quality of the wind data is. For example, if the ship specific model uses the now-cast wind data and its prediction error is smaller than the error of the model, which uses the measurements onboard, then the now-cast data is adequate and has a better quality from the modeling point of view.

In Napa practice, we use a statistical modeling approach while analyzing the ship technical performance. During the analysis, we model the ship propulsion power and the speed through water using separate statistical models. Those models use many input variables, which reflect the variation of the operation and environmental conditions of the ship. The wind is one of the most important inputs for the statistical model and quality of the wind speed readings significantly affect the model quality.

The modeling test procedure is simple. For each ship dataset, we create models which explain the variation of the propulsion power consumption and the speed through the water. Two rounds of modeling procedure are completed. During the first round, we use the onboard wind data while modeling and, during the second round, the now-cast wind data is used. All other model inputs and response values remain the same during the experiment.

For the test the model structure is selected to be a generalized additive model, *Hastie (1986)*, whose structure is:

$$\hat{Y} = \alpha + f_1(X_1) + \cdots + f_n(X_n) + f_{n+1}(t),$$

where $\hat{Y}$ is the model response, X_i, i = 1, … , n, is the set of the model inputs, like the engine rpm, draft, trim, wind speed and direction, swell, water temperature, etc.; t is the time variable, which stands for the time related deterioration of the hull condition. The f_j are smooth functions, which are specified for each ship separately.

To compare the modeling results we use the statistical descriptors, like mean absolute percent error (MAPE) which is define as follows:

$$MAPE = \frac{\sum_1^m \left|\frac{\hat{Y}_i - Y_i}{Y_i}\right|}{m} 100\%,$$

$\hat{Y}_i$, is the value estimated by the model, Y_i is the observed value of the response, i=1, … , m, is the number of all observations.

The experiment is done for 50 randomly selected ships with no observed problems in the wind measurements onboard. For each ship, we built the predictive models for the propulsion power and for the speed through the water. The main assumption is that the smaller the MAPE metric is the better the model is, the better the quality of the wind parameter source.

Additionally, we calculate the difference between the MAPE descriptors for each ship models. The MAPE difference for each ship is defined as:

$$MAPE_{difference} = MAPE_{nowcast} - MAPE_{onboard},$$

$MAPE_{nowcast}$ is the mean absolute percent error of the model which uses the now-cast wind, and $MAPE_{onboard}$ is the error of the model which uses the onboard wind data.

The results of the statistical experiment are shown in Figs.5 and 6. In Fig.5a the distribution of the MAPE is shown for the power model which uses the onboard and now-cast wind data. The distributions are almost similar so it is hard to assess which source of the wind data is better. The median of all observed MAPE metrics is about 2.1%, which describes the general level of the quality of the model for the propulsion power. In Fig.5b the distribution of the pairwise differences between MAPE descriptors for each ship is shown. The median of the distribution is +0.08%, which suggests that in general, statistical models that use the now-cast data have slightly higher errors compared to the models that use the onboard wind data.

In Fig.6a and b the same kind of results are shown for the speed model. Accordingly, the median of MAPE for all ship model is around 1.56% - see Fig.6a. The distribution of the MAPE differences is shown in Fig.6b. As in the case of the power model, the difference is positive, about +0.075%, suggesting that the models that use the now-cast wind measurements have slightly higher errors. Although the models that use now-cast wind data have slightly higher prediction errors, we can claim that the decrease in the model accuracy is not dramatic at all. According to results of the modeling test, if we use the now-cast wind measurements instead of onboard wind data, the model mean absolute percent errors will increase just about 0.1% in average.

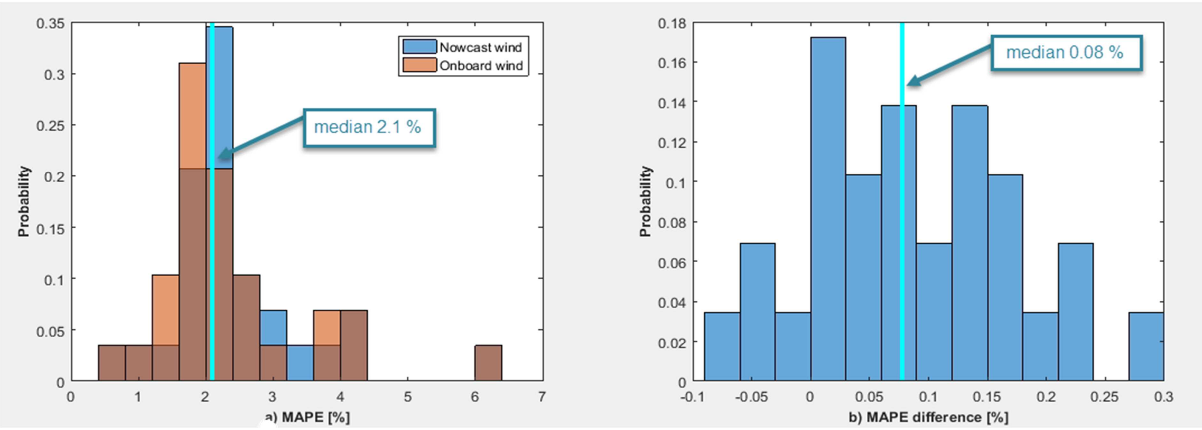

Fig.5: Comparison of errors for the power model; a) distribution of MAPE for models which use the now-cast and onboard wind, b) distribution of MAPE difference.

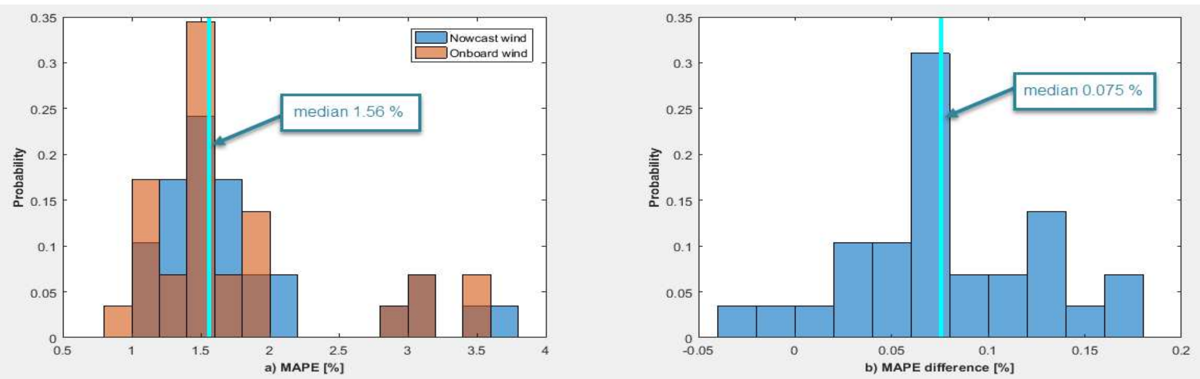

Fig. 6: Comparison of errors for the speed model; a) distribution of MAPE for models which use the now-cast and onboard wind, b) distribution of MAPE difference.

Based on the results of the experiment, we may conclude that in the cases without any problems with the onboard wind data it is preferable to use the onboard wind for the modeling and technical performance evaluation. If there are problems with the wind data collection or there is no data at all, we can substitute the wind data by the now-cast wind data without major decrease of the accuracy of the analysis.

4 Speed through water

The speed of the ship can be considered as one of the most important variables when we evaluate the technical performance of the ship. The most natural situation onboard is when the speed is measured in two different ways. The first way is to measure the speed through the water (STW) by using a speed log. The second way considers using the Global Positioning System (GPS) and obtains the speed over the ground (SOG). The speed over the ground measured by GPS is always considered to be the most accurate way for speed measuring. However, for ship technical performance evaluation, the speed through the water is what we need. Therefore, in a situation when the speed through the water is not available for some reason, it can be approximated by using the speed over the ground and the ocean currents. The ocean currents can be estimated by numerical modeling and the information about currents is usually a part of the now-cast data available from independent weather providers.

4.1 Quality of the speed measurements

It is a widely known fact that measurement of the speed through the water can be inaccurate. There are different types of devices for the ship speed measurement. Probably most widely used devices are based on the Doppler effect and electromagnetic property of water, *Babicz (2015)*. Nowadays the speed log devices are claimed to be accurate or at least manufacturers advertise them to be accurate. However, there are many different publications which describe the problems related to the measurements of the speed through water; see for example *Bos (2016)*. Bos describes the systematic and non-systematic errors related to the speed log.

Here are a couple of examples from Napa practice demonstrating problems which can be faced with the speed through water measurements. The time-series in Fig.7 describes the ratio between the speed over ground and the speed through the water for a RO-RO ship that operates in the Baltic Sea area. It is assumed that when the speed through the water is measured correctly, the ratio SOG/STW should follow the normal distribution with mean value equal to one. In Fig.7, we can clearly see the drift of the ratio, which appears a few months after the ship maintenance. At maximum, the ratio between SOG and STW achieves values about 1.3-1.4, which corresponds to a 30-40% average error in STW.

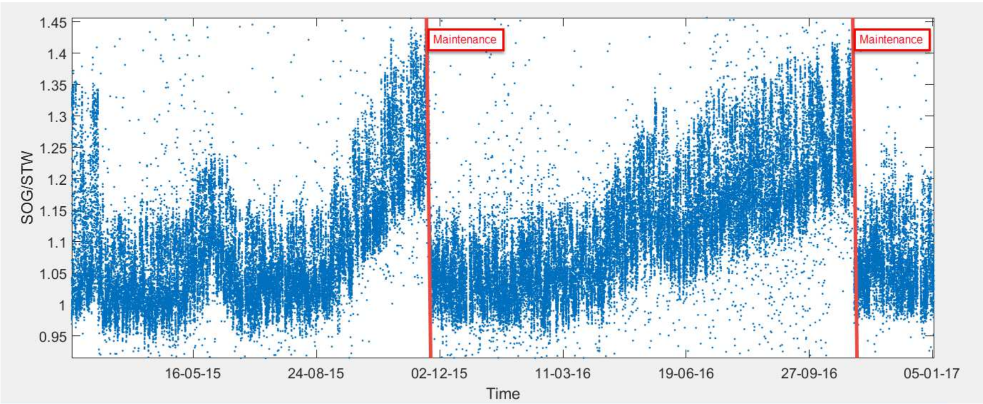

Fig.7: Ratio SOG/STW for RO-RO vessel indicating hard problems with STW measurements

The ratio between the speed over ground and the speed through water for the second ship is depicted in Fig.8. In this example case, we can see not only the systematic bias, which is about 5%, but also a seasonal variation of the ratio, about +/- 2.5%, which seems to be related to the variation of the water temperature.

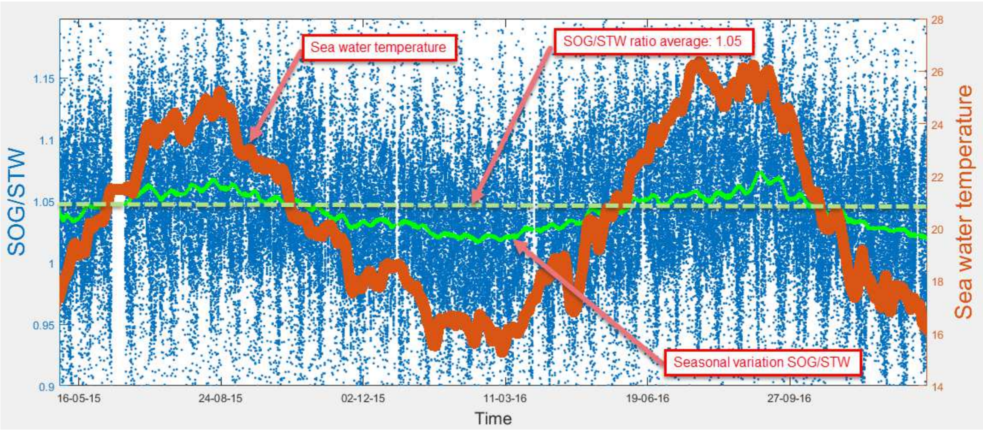

Fig.8: SOG/STW ratio for the RO-RO vessel indicating bias and seasonal variation in STW measurements.

Taking in account different publications and our own experience in Napa, we need to admit that the speed through the water must be always checked before doing any analysis concerning the ship technical performance. In our research, we tried to estimate statistically how often the problems with the speed log readings occur in general.

We have tested the speed log measurements from over 150 randomly selected ships. To describe the quality of the speed log measurements we are using statistical descriptor like the median of the absolute difference (*MAD*) between SOG and STW values, which is defined as follows:

$$MAD = median|V_i^{SOG} - V_i^{STW}|,\ i=1,\ \ldots,\ n,$$

where *n* is the number of all observation in the available data. This descriptor can be interpreted as the systematic bias of the speed log readings. We choose median instead of mean in order to avoid the outliers in the data, which may affect the mean value significantly.

We also estimate the possible linear drift in the speed log readings. This is done by fitting a linear model into the difference between SOG and STW, and estimating how much it is changed during the period of one year. Additionally, we calculate the standard deviation of the fitted linear model residuals, which describes the spread of the differences between SOG and STW.

In Fig.9, the main idea of the drift evaluation is described. In the example case we can see a small drift about 0.5 knots during the period of nine months. The standard deviation about 0.7 of the linear fit residuals indicates that there is no substantial problem with the speed log because the drift and deviation of the speed differences can be explained by the ocean currents.

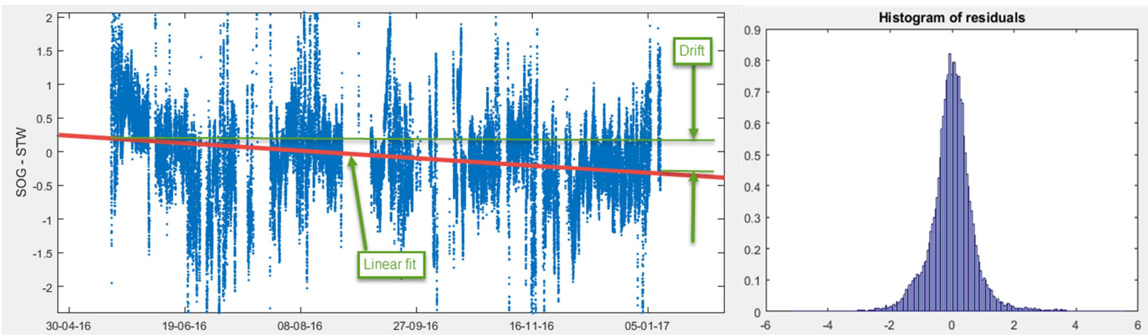

Fig.9: The linear model revealing the speed log drift about 0.5 knots during the period of 1 year, and the distribution of the model residuals with standard deviation about 0.7 knots.

In Fig.10 and Table II, statistics calculated from 150 randomly selected ships are shown. They reflect the general situation with the speed log quality. According to the statistical distribution, the bias over 2 knots in the measurement of the speed through the water was found in 3% of all tested ships, and 89% of the ships have STW bias of less than 1 knot. Annual drift of less than 1 knot was found in 82% of the cases, and in 84% of the cases, the standard deviation of the difference between SOG and STW was less than 2 knots.

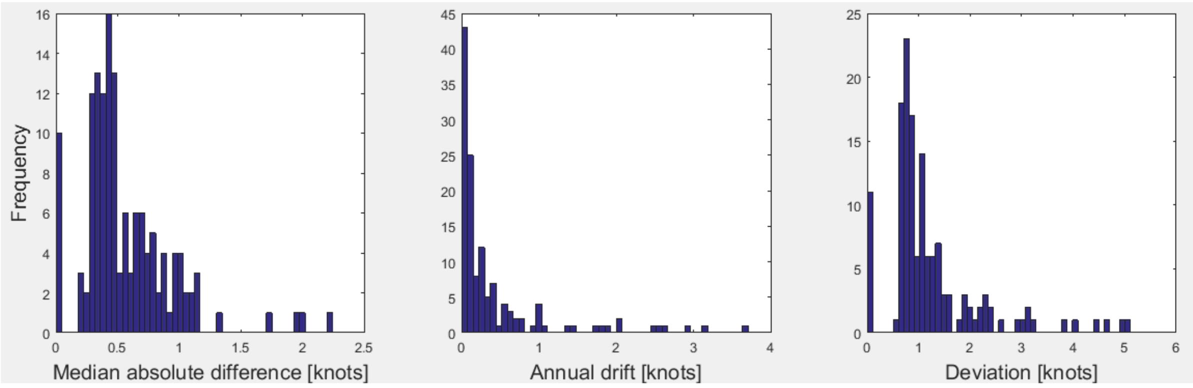

Fig.10: Distributions of statistics, which describe the quality of the speed, log reading

Table II: Percentage of statistics

MAD [knots]		Annual drift [knots]		Deviation [knots]	
less than 0.5	57%	less than 1	82%	less than 1	53%
0.5-1	32%	1-2	5%	1-2	31%
1-2	8%	2-4	6%	2-4	12%
over 2	3%	over 4	7%	over 4	4%

The statistics presented in Fig.10 and Table II suggest that, in general, we may expect that in 10-15% of all cases we will have some problems with the measurements of the speed through the water.

In the cases with erroneous data, different strategies can be applied during the data analysis. The first strategy concerns possible correction of the STW readings. The systematic bias can be a result of faulty device calibration and can be corrected in some cases. In certain cases, we can also correct the drift in the STW readings afterward. The second strategy concerns using the now-cast data for the ocean currents. The main idea of this strategy is to calculate the speed through the water from the speed over ground and the sea currents. In the next section, we will discuss the difference between using the speed from different sources.

4.2 Model comparison test

The modeling test for the comparison of the speed through the water from different sources is similar to the test conducted for the comparison of the wind data. The modeling test is conducted for the ships' datasets, which have no problems with the speed log data. In this case we inspect the error statistics for the model which predicts the speed through the water. For each ship dataset, the set of the model inputs and the model structure is fixed, and only the source of the model response are changed.

In the test the model responses are:

- speed measured by a speed log (STW),
- speed which is combined from the speed over the ground and the now-cast ocean currents (SOG+currents),
- speed over ground (SOG).

We assumed that the model that uses as the response the speed over the ground should have a higher prediction error comparing to the model that uses the speed log readings as the response. This happens because the model loses some information because it does not take into account the effect of ocean currents. However, we built the model for SOG just to have a baseline for the comparison.

The goal of the modeling test is to investigate what happens to the predictive accuracy of the statistical model if we change the data source of the speed. How much do we lose or gain in the model accuracy if we, for example, substitute the speed log readings with the speed, which is combined from the speed over the ground and the ocean currents from now-cast data.

Fig.11 represents the results of the modeling test. The normalized histograms of the mean absolute percent error (see definition of the MAPE in section 4.1) are shown for the models whose responses are taken from the different speed sources. The MAPE distribution of the SOG models has a median value about 3.25%. This is more than two times higher compared to the MAPE distribution of the STW models, which has a median of about 1.4%. This is the price of not taking in account the effect of the ocean currents. The MAPE distribution for the models, which use the speed through the water combined from SOG and the ocean currents now-cast, has the median about 2.9%. However, the improvement is not very dramatic comparing to the SOG models.

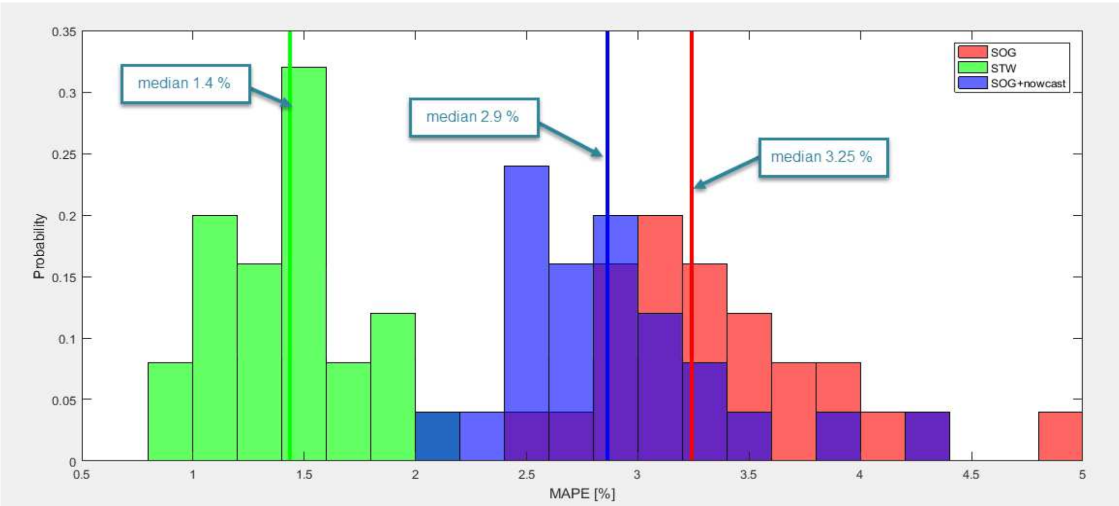

Fig.11: Distribution of MAPE for models with different responses

The results of the modeling test suggest that in the cases with no observed problems with the speed log readings we should always utilize the STW measured onboard in order to have the best model accuracy. However, in cases with erroneous speed log data we can substitute it by the speed through the water values, which are combined from the speed over the ground and the now-cast ocean currents.

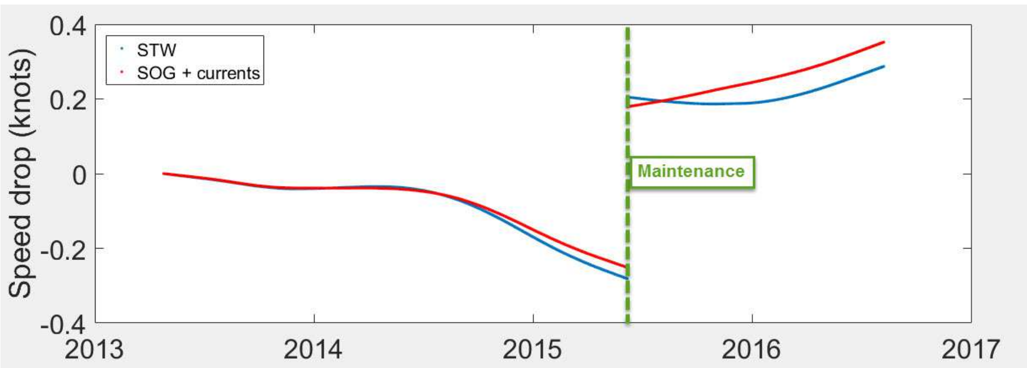

Fig.12: Speed drop estimated from the STW (blue) and speed that is combined from SOG and now-cast ocean currents (red).

In Fig.12, we present the example of the analysis case for technical performance evaluation. The speed drop due to the decreased hull condition is visualized for the period of more than three years. A negative speed drop indicates a decrease of the speed, a positive, in contrary, increase of the speed, for example after the ship maintenance. In the analysis we have used two different sources for the ship speed, the speed through the water that was measured by a speed log, and the speed that is combined from the speed over the ground and the now-cast ocean currents. The estimated speed drop is denoted in knots. As can be seen, the difference between the speed drop that is estimated with different speed is small.

In Fig.13, we visualize the result of comparison of the speed drop that was evaluated by the statistical models from different speed sources. For each ship data set the speed drop was estimated from the three different responses: STW, SOG and SOG combined with the now-cast ocean currents. For each ship we calculated the mean absolute error between the speed drop estimations done with different responses as follows:

$$MAE = \frac{|V_i^1 - V_i^2|}{n}, \; i=1, \ldots, n,$$

where V_i^1 is the speed drop estimated by the model 1, V_i^2 is the speed drop estimated by the model 2, and n is the number of observations. The MAE is calculated for two pairs of models: STW vs. SOG, and STW vs. SOG+currents.

The box-plots in Fig.13 describe the distribution of the mean absolute errors over all ships' datasets. As we can see, that difference between the speed drop (estimated by the statistical models, which are built from difference sources), is small. The median difference between the speed drop for the pair STW versus SOG+currents is about 0.06 knots, and for the pair STW versus SOG is 0.08 knots.

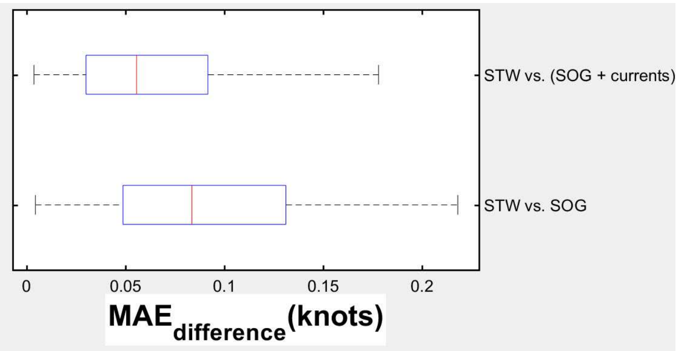

Fig.13: Distributions for difference between the speed drop: STW vs SOG, STW vs. SOG+currents

5 Conclusions

The accuracy and quality of the ship data, which we use for the technical performance evaluation, is essential. At the same time, data collection onboard the ship may be difficult and subject to errors. Therefore, the role of the independent now-cast data cannot be underestimated. We can use the now-cast data for validation of the onboard sensor data. We can also substitute the onboard data with the now-cast data in the case when we have some problems with the data collection onboard.

The current research was focused on the quality of the wind data and the data of the speed through the water. According to the statistical analysis and modeling tests, we may claim that:

- In 20% - 25% of all cases, we may face problems with the wind measurements onboard ship.
- We should always validate the quality of the onboard wind data by using the now-cast data from independent weather providers.
- In the case of the erroneous onboard wind data, it can be substituted by the now-cast wind data without major decrease of the accuracy of the analysis.

- In 10% - 15% of all cases, we may face problems with the measurements of the speed through water onboard the ship.
- The onboard data for the speed through the water should be always checked and validated before the technical analysis.
- In the case of the erroneous data for the speed through the water, we can replace it by the speed, which is combined from the speed over the ground and the now-cast ocean currents data.

References

BABICZ, J. (2015), *Encyclopedia of Ship Technology*, Wärtsilä Corporation, 2nd Ed.; ISBN 978-952-93-5536-5

BOS, M. (2016), *How metocean data can improve accuracy and reliability of vessel performance estimates*, 1st Hull Performance & Insight Conference, Pavone, pp.106-114

CAI, Y.; WEN, Y.; WU, L. (2014), *Ship route design for avoiding heavy weather and sea conditions*, J. Marine Navigation and Safety of Sea Transportation 8/4

CHEN, C.; SHIGEAKI, S.; KENJI, S. (2013), *Numerical ship navigation based on weather and ocean simulation*, Ocean Engineering 69, 44–53.

GODIN, A. (1996), *The calibration of shallow water multibeam echo sounding systems*, Canadian Hydrographic Conf.; Halifax, pp.25-31

HARANEN, M.; PAKKANEN, P.; KARIRANTA, R.; SALO, J. (2016), *White, grey and black-box modeling in ship performance evaluation*, 1st Hull Performance & Insight Conference, Pavone, pp.115-127

HARE, R.; TESSIER, B. (1995), *Water level accuracy estimation for real-time navigation in the St. Lawrence River*, Canadian Hydrographic Service, Internal Report, Laurentian region, 147 p.

HASTIE, T.; TIBSHIRANI, R. (1986), *Generalized additive models*, Statisti. Science 1/3, pp.297-318

HASTIE, T.; TIBSHIRANI, R.; FRIEDMAN, J. (2003), *The Elements of Statistical Learning*, Springer

HELLSTROM, T. (2003), *Three levels of fuel optimization at sea*, 2nd Conf. Computer Applications and Information Technology in the Marine Industries (COMPIT), Hamburg

ISO 15016, *Ships and marine technology - Guidelines for the assessment of speed and power performance by analysis of speed trial data*

ISO/CD 19030-1, *Ship and marine technology - Measurements of changes in hull and propeller performance, Part 1: General Principles* (2015)

ISO/CD 19030-2, *Ship and marine technology - Measurements of changes in hull and propeller performance, Part 2: Default method* (2015)

KAYANO, J.; YABUKI, H.; SASAKI, N.; HIWATASHI, R. (2013), *A Study on the Propulsion Performance in the Actual Sea by means of Full-scale Experiments*, Int. J. Marine Navigation and Safety of Sea Transportation 7/4

MOAT, B.; YELLAND, M.; MOLLAND, A. (2006), *Quantifying the airflow distortion over merchant ships: part II: application of model results*, J. Atmos. and Ocean. Tech. 23, pp.351-360

MOLLAND, A.F.; TURNOCK, S.R; HUDSON, D.A. (2011), *Ship Resistance and Propulsion*, Cambridge University Press

NIELSEN, U.D. (2008b), *The wave buoy analogy – Estimating high-frequency wave excitations*, Applied Ocean Research 30, pp.100-106

PADHY, C. P.; SEN, D.; BHASKARAN, P. K. (2008), *Application of wave model for weather routing of ships in the North Indian Ocean*, Natural Hazards 44/3, pp.373-385

PANIGRAHI, J.K.; PADHY, C.P.; SEN, D.; SWAIN, J.; LARSEN, O. (2012), *Optimal ship tracking on a navigation route between two ports: a hydrodynamics approach*, J. Marine Science and Technology 17/1, pp.59-67

SASAKI, N. (2009), *Development of ship performance index (10 modes at sea)*, Report of National Maritime Research Institute 9/4, pp.1-46

SIMOS, A.N.; TANNURI, E.A.; SPARANO, J.V.; MATOS, V.L.F. (2010), *Estimating wave spectra from the motions of moored vessels: Experimental validation*, Applied Ocean Research 32, pp.191-208

SODA, T.; SHIOTANI, S.; et al. (2012), *Research on ship navigation in numerical simulation of weather and ocean in a bay*, Int. J. Marine Navigation and Safety of Sea Transportation 6/1, pp.19–25

STREDULINSKY, D.C.; THORNHILL, E.M. (2009), *Shipboard Wave Measurement through Fusion of Wave Radar and Ship Motion Data*, Defence R&D Canada – Atlantic, TM

TRAUT, M.; GILBERT, P.; WALSH, C.; BOWS, A.; FILIPPONE, A.; STANSBY, P.; WOOD, R. (2014), *Propulsive power contribution of a kite and a Flettner rotor on selected shipping routes*, Applied Energy 113, pp.362–372

TSUJIMOTO, M.; TANIZAWA, K. (2006), *Development of a weather adaptive navigation system considering ship performance in actual seas*, 25th Conf. Offshore Mechanics and Arctic Engineering, Hamburg, pp.4-9

XIA, H.; SHIOTANI, S.; et al. (2006a), *A study of weather routing considering real-time data of weather and ocean for sailing ship in coastal area–basic simulation of ship positioning by ship maneuvering and experiment by a real ship*, J. Kansai Society of Naval Architects, Japan 234, pp.159–166

XIA, H.; SHIOTANI, S.; et al. (2006b), *Estimation of ship's course for sailing on route by navigation simulation in coastal water*, J. Japan Institute of Navigation 115, pp.51–57

YOKOI, T. (2010), *A mechanism on parallel processing to numerical weather prediction for weather routing – Accuracy evaluation and performance benchmark of the sea surface wind prediction*, Asia Navigation Conf., pp.33-40

ZHANG, J.; HUANG, L. (2007), *Optimal ship weather routing using isochrone method on the basis of weather changes*, Int. Conf. Transportation Engineering, ASCE, pp.2650-2655

ISO 19030 – Ideas for Further Improvement

Geir Axel Oftedahl, Jotun, Sandefjord/Norway, geir.axel.oftedahl@jotun.no

Abstract

The first revision in the ISO 19030 series was published in November 16. 2016. The purpose of this paper is to bring forward the ideas for further improvement generated during the work on the first revision of the standard. The paper also proposes a framework for organizing these and potentially additional ideas for improvement.

1. Background

The first revision in the ISO 19030 series was published in November 2016. The stated aim of the series is to "prescribe practical methods for measuring changes in ship specific hull and propeller performance and to define a set of relevant performance indicators for hull and propeller maintenance, repair and retrofit activities", ISO (2016), p.vi.

An implied purpose of any measurement standard is to facilitate general agreement on how to measure something. In the case of the ISO 19030 series, generally agreed upon methods for measuring hull and propeller performance are expected to make it easier for decision makers to learn from the past and thereby make better informed decisions for tomorrow. Also to provide much needed transparency for buyers and sellers of technologies and services intended to improve hull and propeller performance. And finally, to make it easier for the same buyers and sellers to enter into performance based-contracts and thereby better align incentives, Oftedahl and Søyland (2016).

The more than 50 experts who joined ISO TC8 SC2 WG7 (WG7) spent more than 12000 hours on drafting and editing the ISO 19030 series before reaching consensus that the drafts were sufficiently mature so as to merit publication of a first revision. Sufficiently mature does not mean perfect, however. As is probably always the case when working on a new standard, also WG7 needed to strike a balance between degree of perfection and time to completion. Many ideas for further improvement had to be left for future revisions.

The purpose of this paper is to bring forward the ideas for further improvement that were generated as a part of work on the first revision of the standard and that are relevant given the stated aim and / or implied purpose of the ISO 19030 series. In order to do so, the paper proposes a framework for organizing these ideas that may be useful also when adding new ideas.

2. Framework for organizing ideas for further work

Given the stated aim of the ISO 19030 series an obvious starting point for organizing ideas for further work should be the extent to which the prescribed measurement methods are practical and the extent to which the defined performance indicators are as relevant or useful. There are at least two ways in which the prescribed measurement methods can become more practical; applicability can be improved and / or barriers to application can be reduced. There are also at least two ways in which the relevance or usefulness of the standard can be enhanced; additional areas where the standard can be of use can be included and / or the usefulness within the areas already included can be further improved.

The extent to which the ISO 19030 series delivers on the stated aim is bound to drive the adoption of the standard and thereby delivery on its implied purpose. Increasing the awareness of the extent to which the standard delivers on its stated aim will do the same.

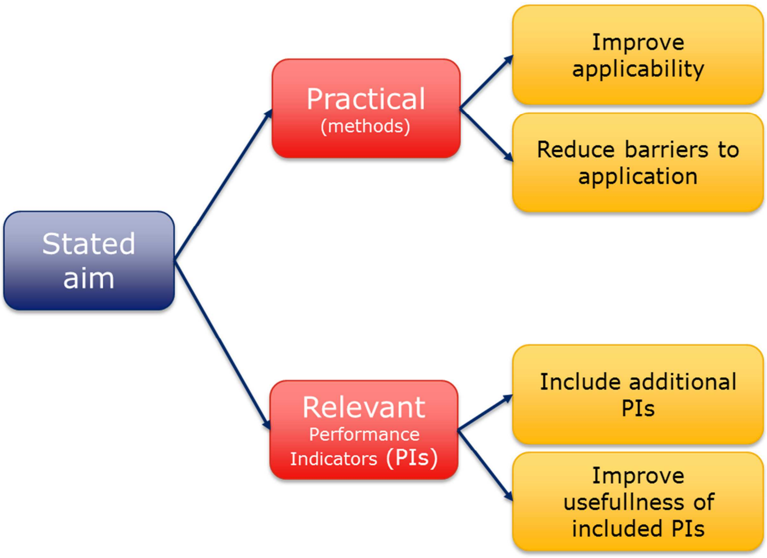

Fig. 1: Framework for organizing ideas flowing from stated aim

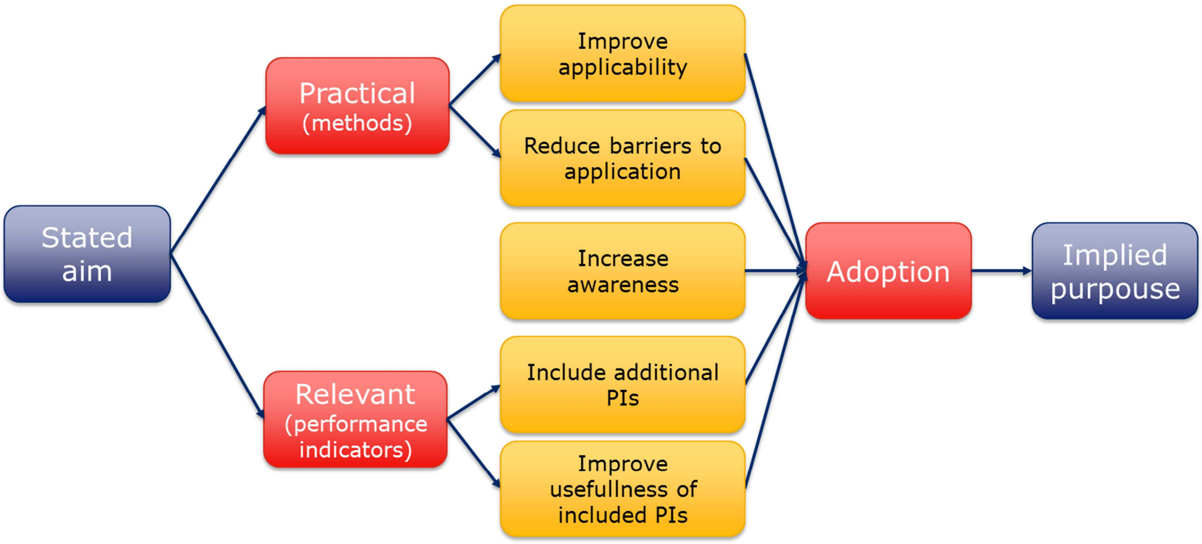

Fig. 2: Link between stated aim and implied purpose

As a side note, the obvious interrelationship between delivery on the stated aim of the ISO 19030 series and its implied (and generic) purpose, is an indication that the stated aim of the standard is well aligned with both users' interest and ISO's mandate.

3. Ideas for further work

3.1. Extend applicability

1. Include support for variable pitch propellers and podded propulsion units: The measurement methods prescribed in the first revision of the ISO 19030 series are not applicable for ships with variable pitch propellers or vessels with podded propulsion units such as Azipods. While methods for measuring hull and propeller performance on ships with variable pitch propellers or podded propulsion units will add some complexity, the working group proposed that this should be sought addressed in later revisions of the standard.

3.2. Reduce barriers to application

2. Reduce need for investments in additional sensors: The ISO 19030 series, and in particular the default method in Part 2 of the series, specifies sensors beyond what is typically available on ships in the world fleet today. Retrofit is possible (or it would not have been included in the standard) but for some prohibitively costly. The speed of innovation within sensors technologies has been accelerating and a number of new sensor technologies, including virtual sensors, are rapidly coming to market. The possibility of reducing the need for sensors should therefore be considered in future revisions of the standard.

3. Reduce need for investments in external ship specific speed-power-draught-trim model data: Part 2 of the ISO 19030 series also specifies ship specific speed-power-draught-trim model data beyond what is typically available. Additional model data can be generated by use of speed trials as per ISO 15016, towing tank tests and/or CFD modeling, but again this is often quite expensive. As a part of the work on the first revision of the standard the working group looked into the possibility of generating additional ship specific speed-power-draught-trim model data from logged data using e.g. "self-learning algorithms" and / or simplified speed trials. The working group found these areas to have a lot of promise but at the same time to be too immature to be included in the default method. The speed of innovation also within these areas has since accelerated and inclusion of additional sources of model data should be considered in future revisions.

4. (Further) improve clarity: It is fair to assume that many of the members in the working group involved in the drafting and editing the standard had an above average interest in, and understanding of, the subject at hand. As a result of this it is not unlikely that passages in the standard can be difficult to follow for the average user. Future revisions should seek to identify and address any such passages in need of clarification.

3.3. Include additional performance indicators

5. Separate performance indicators for hull and propeller performance: In the first revision of ISO 19030 it is not possible to independently measure hull and propeller performance. The four performance indicators defined in the standard are therefore based on measurements of changes in both. This complicates the determination of the effectiveness of individual hull or propeller maintenance, repair and retrofit activities. Accurately and reliably isolating hull from propeller performance would require accurate and reliable thrust measurements. At the time, the required sensor technologies were considered by the working group to be too immature. Thrust sensors are expected to continue to mature and independent measurements of hull and propeller performance, as well as independent sets of performance indicators for the two should be considered in future revisions.

3.4. Improve usefulness of included performance indicators

6. Increase "measurement resolution": Two of the four performance indicators in the first revision require both the reference period and the evaluation period to be of minimum 12 months' duration in order for the guidance provided on accuracy to be valid. This essentially in order to reduce the probability that environmental factors not corrected for, such as e.g. waves and side currents, are unequally distributed across the two periods – e.g. on account of seasonal changes. For the remaining two performance indicators, the Maintenance trigger and Maintenance effect, accuracy has been sacrificed in order enable timelier indication. The working group did consider adding additional corrections but found that, given the current state of the needed sensor technologies and/or underlying science, adding such corrections would serve to decrease rather than increase accuracy.

As relevant sensor technologies and the underlying science become more mature, it may be possible to significantly reduce the required length of reference and evaluation period. This would increase usefulness and should therefore be considered in future revisions.

7. Increase robustness to changes in operational and environmental conditions: The relative importance of the different resistance components varies with operational (e.g. speed and displacement) and environmental conditions (e.g. waves). In the first revision of the ISO 19030 series, operational and environmental conditions must be comparable over the reference and evaluation period in order for the guidance provided on accuracy to be valid. Future revisions should consider if more accurate correction formulae are available and can be used to reduce the dependence on comparable operational and environmental condition.

4. Summary

This paper has brought forward the ideas for further improvement that were generated as a part of work on the first revision of the standard and that are relevant given the stated aim and / or implied purpose of the ISO 19030 series. The paper has also proposed a framework for organizing these ideas that may be useful as new ideas are brought forward in the future.

References

ISO (2016), *Measurement of changes in hull and propeller performance — Part 1: General principles*, ISO 19030-1

OFTEDAHL, G.A.; SØYLAND, S. (2016), *ISO 19030 – Motivation, Scope and Development*, 1st HullPic Conf., Pavone

Ultrasound-Based Antifouling Solutions

Jan Kelling, HASYTEC, Schönkirchen/Germany, j.kelling@hasytec.com

Abstract

This paper gives an overview of upcoming new antifouling regulations, different ultrasound working principles, examples of applications and results, and benefits leading to a lower Total Cost Of Ownership.

1. Introduction

HASYTEC carries out maintenance and start-ups for military and civilian ships. When it comes to repairs and modernization measures regarding the whole electronic systems for cargo vessels or military vehicles we have always been the right partner. Mainly we perform repair works on ships for the German Navy. We've specialized in electronic systems and devices of submarines and benefit from more than 20 years' experience. However, our technical support is not limited to 'undersea'. We also provide support for mine warfare systems, tenders or combat support vessels when it comes to electronic systems or battery management solutions.

For some time, we have been dealing with ultrasound devices which we found on the market for antifouling solutions. On this base, we founded a research department which has provided us with serious knowledge and insight about this innovative antifouling solution.

2. Upcoming new Antifouling Regulations

In relation to the IMO convention "International Convention on the control of harmful Anti-Fouling Systems on Ships (2001)", the European Union finalized the EU Regulation No. 528/2012. This regulation on biocide containing products regulates the marketing and use of biocide containing products, which due to the activity of the active ingredients contained in them for the protection of humans, animals, materials or products against harmful organisms such as pests or bacteria, may be used. The aim of the Regulation is to ensure a better functioning of the biocide containing Products market in the EU, while ensuring a high level of protection for human health and for the environment. As an example, almost no copper based active substance will get permission to be used in the future. Every system has to be approved to be marketed and the environmentally harmful systems shall be sorted out. This leaves essentially two options:

- taking the risk of using less effective antifouling systems which leads to higher costs for maintenance and repair as well as to higher fuel expenses
- looking for alternatives to replace the currently used antifouling systems

3. Different Ultrasound Working Principles

3.1. Biofilm in general

The biofilms are formed when bacteria adhere to a solid surface and enclose themselves in a sticky polysaccharide. Once this polysaccharide is formed the bacteria can no longer leave the surface, and when new bacteria are produced they stay within the polysaccharide layer. This layer, which is the biofilm, is highly protective for the organisms within it. In fact, it is considered a fact that many bacteria could not survive in the environment outside of biofilms.

Biofilms are ubiquitous in the environment. They form on our teeth, inside our bodies, in our streams and oceans, on natural surfaces continually wetted by dripping water. They also are formed inside of all of our water pipes, toilets, and drains, and, in fact, everywhere where there is persistent water.

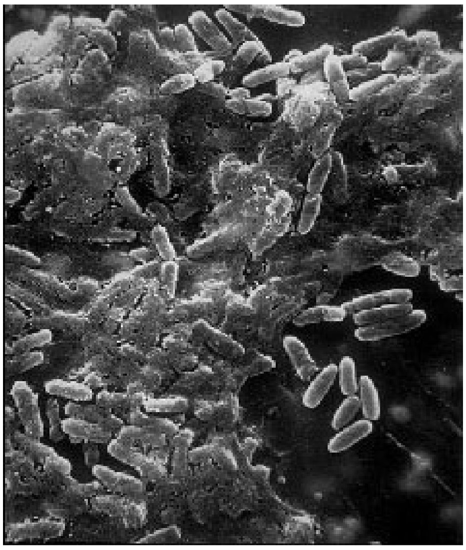

Fig.1 Biofilms under the microscope

In general, while a few fungi can form their own biofilms, and a few inhabit bacterial biofilms, the so-called "moulds" generally do not grow in or even on the surface of biofilms. This is because there is generally too much water. The majority of fungi will not grow under water, while biofilms are always under water at least most of the time. Biofilms will not go away on their own, and considerable effort is required to eliminate them. Biofilms on teeth, components of which contribute to plaque formation and tooth decay, are removed by diligent scrubbing with somewhat abrasive materials. Unfortunately, the biofilms return within hours, and teeth cleaning is an endless process.

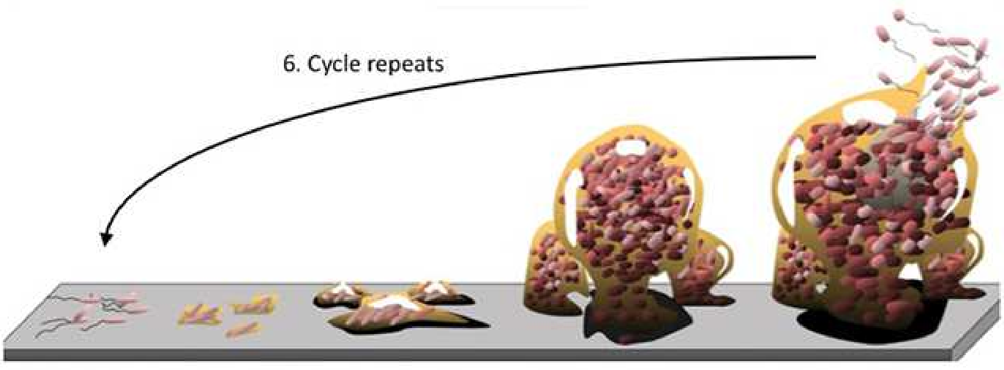

Fig.2: Biofilm growth cycle

Biofilms on other surfaces can be scrubbed away, or can be disrupted using very hot water (steam is best) and concentrated oxidizing agents. However, they will return quickly unless the water source is removed. Hence, there are always biofilms present where, by definition, water is always present (e.g., in the ocean, rivers, our mouths, and our water pipes).

3.2. High-powered ultrasound causing cavitation

Older ultrasound methods followed the idea of getting rid of hard growth which had already attached. Using hard cavitation, this working principle might work in certain situations but may also damage the vessel's steel itself. As a consequence, this approach was not accepted by the market.

3.3. Low-powered ultrasound not causing cavitation

Using low-powered ultrasound (which does not cause cavitation in a certain combination of frequencies, altitudes and power consumption) follows only one idea: avoiding biofilm on every liquid carrying surface. Avoiding biofilm means at the same time avoiding marine growth as barnacles, shells and algae. This working principle is relatively new and unknown on the market. But this new kind of antifouling system has a huge potential regarding protecting the environment, being sustainable and not harming either humans or animals.

4. Response of fish to low-powered ultrasound

Fig.3 shops the startle response of fish to the low-powered ultrasound. The fish that responded to the stimuli increased their swimming speed and often made tight turns. No startle response was ever seen during test periods apart from during signal presentation. In almost all cases when a startle response was seen, the fish swam away from the sound source. The fish always resumed normal swimming behaviour within a few seconds of the end of the 900 ms acoustic stimulus presentation.

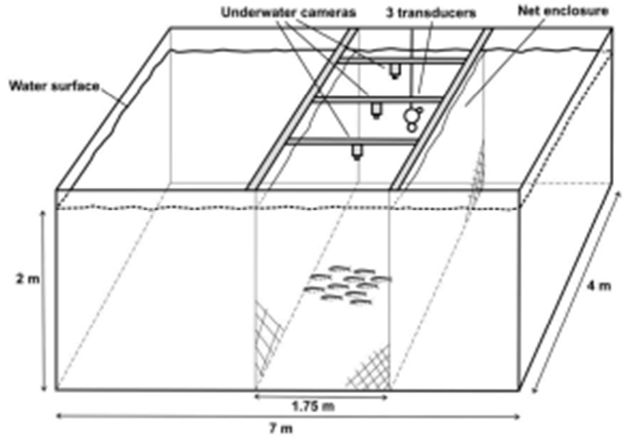

Fig.3: Startle response of captive North Sea fish species to underwater tones 0.1 to 64 kHz, source: Science Direct from 7.9.2008

For sea bass, 50% reaction threshold ranges were reached for signals between 0.1 and 0.7 kHz, Fig.4A. The sea bass did not react to the maximum received levels that could be produced for the higher frequency signals. For thicklip mullet, 50% reaction thresholds were reached for signals between 0.4 and 0.7 kHz, Fig.4B. The fish did not react to the maximum received levels that could be produced for the other frequencies. However, the mullet reacted to one of the twelve 0.1 kHz signal trials and two of the 0.125 kHz signal trials, which suggests that the 50% reaction threshold level for those frequencies was only a few dB above the maximum level that could be produced with the available equipment. For pout, 50% reaction thresholds were reached for signals between 0.1 and 0.250 kHz, Fig.4C. The pout did not react to the maximum received levels that could be produced for the higher frequency signals. For Atlantic cod and common eel, no 50% reaction thresholds could be reached with the maximum levels for the frequencies that could be produced with the available equipment, Fig.4D and E. For Pollack, no 50% reaction thresholds could be reached with the maximum levels for the frequencies that could be produced with the available equipment, Fig.4F. However, there was some reaction to the maximum levels that could be produced for signals of 0.1 kHz (reaction in 4 of the 15 trials), 0.125 kHz (4 trials), 0.250 kHz (2 trials) and 0.4 kHz (3 trials). For horse mackerel, 50% reaction thresholds were reached for signals between 0.1 and 2 kHz, Fig.4G. The horse mackerel did not react to the maximum received levels that could be produced for the higher frequency signals. Atlantic herring reacted to two frequencies. The 50% reaction threshold was reached only for the 4 kHz signal, Fig.4H. There was also some reaction to the 0.4 kHz signal (in 2 of the 12 trials). The herring did not react to the maximum received levels that could be produced for the other frequencies.

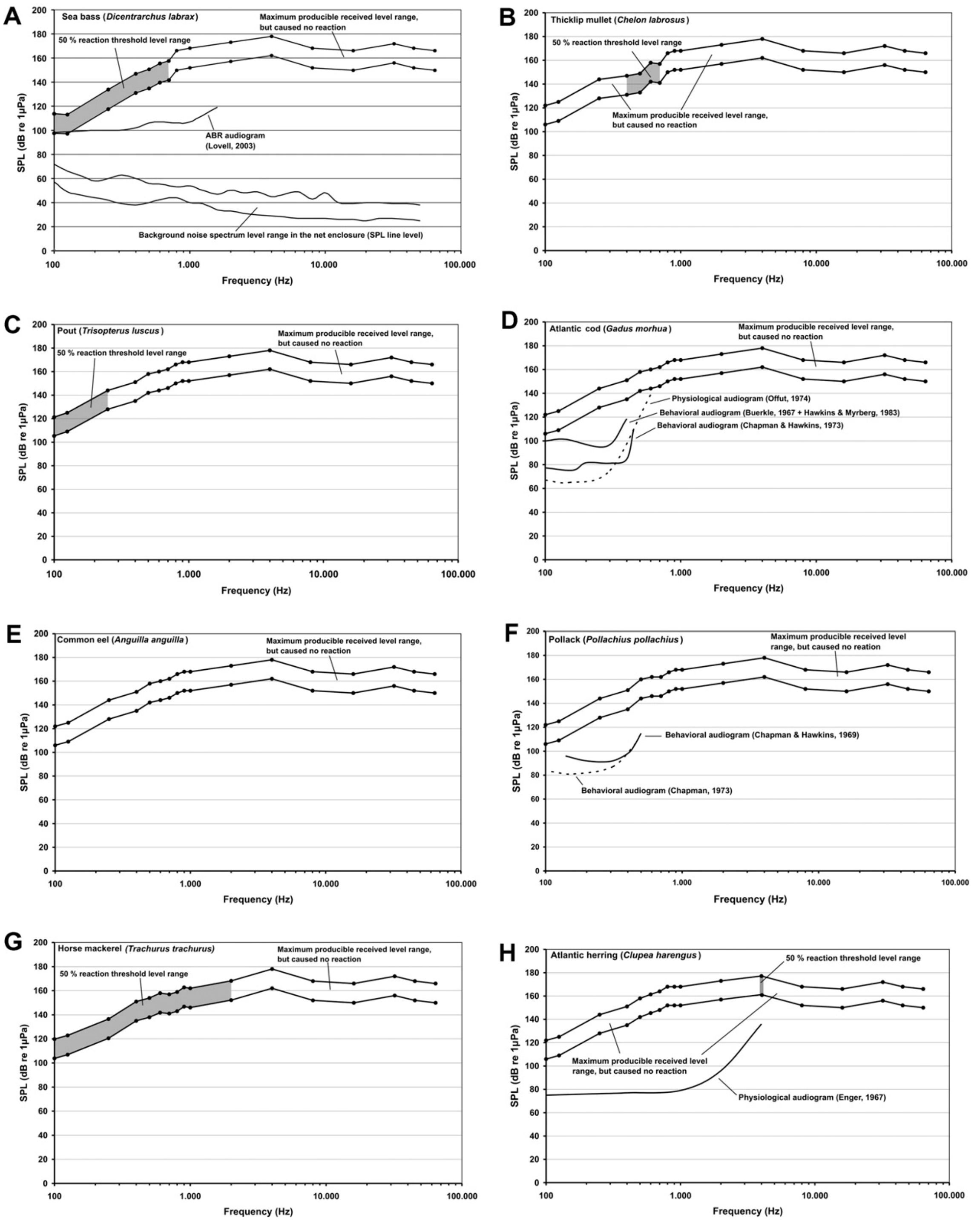

Fig.4: The maximum received level range that could be produced in the tank for the test frequencies causing no reactions, and, for some species, the 50% reaction SPL ranges (shaded areas represent ±8 dB of average received level).

(A) Sea bass (0.1-0.7 kHz; school size: 17 fish), and the background noise range in the net enclosure, which applies to all species. Also shown is the auditory brainstem response (ABR) audiogram of sea bass. (B) Thicklip mullet (0.4-0.7 kHz; school size: 11 fish). (C) Pout (0.1-0.250 kHz; school size: 9 fish). (D) Atlantic cod (school size: 5 fish). Also shown thresholds of Atlantic cod. (E) Common eel (school size: 10 fish). (F) Pollack (school size: 4 fish). There was some reaction (<50%) to the maximum levels that could be produced for signals of 0.1 kHz, 0.125 kHz, 0.250 kHz and 0.4 kHz. Also shown are two hearing thresholds of pollack. (G) Horse mackerel (0.1 2 kHz, school size: 13 fish). (H) Atlantic herring (4 kHz, school size: 4 fish). Also shown is the hearing threshold of Atlantic herring

We judged that the researchers used consistent criteria for classing a trial as a response trial or a non-response trial, because their classifications were always identical, and the startle response was very obvious (not a subtle increase in swimming speed or swimming depth as was observed in a previous study; *Kastelein et al. (2007)*.

The size of their tank influences the general swimming behaviour of many fish species. Before the fish were put in the test tank, they were kept in much smaller circular tanks, in which they swam very slowly or not at all. In the net enclosure in the large test tank, the fish were much more active; they behaved in the same way as fish in the previous study in this tank, which had the entire tank available to them, *Kastelein et al. (2007)*. So, although the test tank was far from a natural environment, it was a much better study area than the smaller tanks used in several previous studies on reactions of fish to sound.

The study fish had been housed, for at least part of their lives, in tanks at aquaria and fish farms. However, those facilities had water filtration systems that were relatively quiet, so the study animals had probably not been exposed to higher sound levels than wild conspecifics. As the location of the study site was selected because of its remote location and quiet environment, the tank was designed specifically for acoustic research, and the area around the tank was strictly controlled (nobody was present within 100 m of the tank, except the researchers who sat quietly), there was little background noise, and startle responses were not observed outside the signal presentations.

The reactions of the fish in the present study were probably dependent on the context in which the sounds were produced, and the fish probably responded differently than would wild fish. Even in the wild, animals behave differently depending on location, temperature, physiological state, age, body size, and school size. So, even if the present study had been conducted in the wild, the findings may not have been of universal value.

5. Examples of applications and results

Figs.5-7 demonstrate the effectiveness of the ultrasound solution.

Fig.5: Tugboat without (top) and with (bottom) ultrasound protection

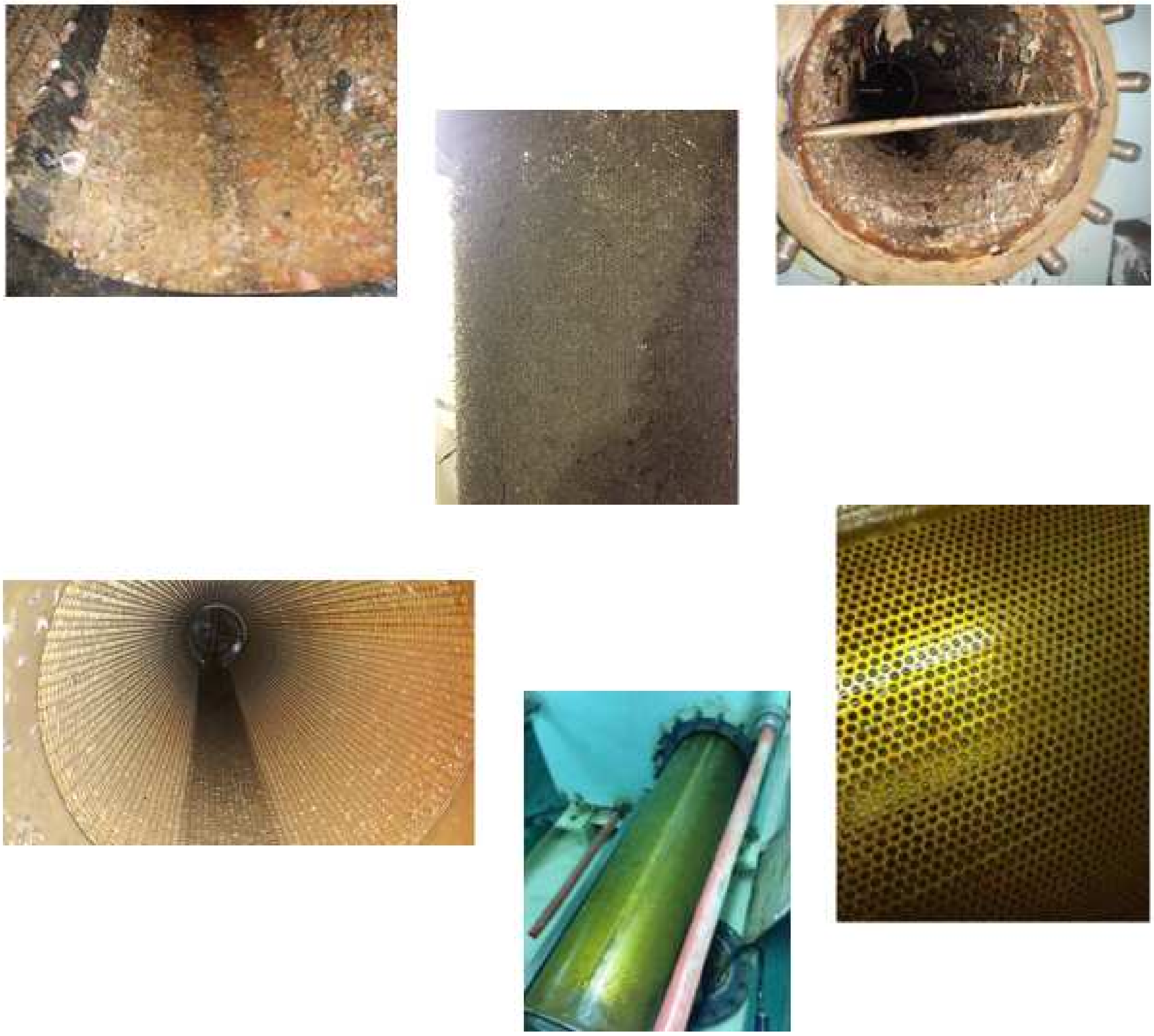

Fig.6: Low-temperature cooler on 13000 TEU containership without (top) and with (bottom) ultrasound protection after 13 months trading Europe / Fareast Asia

Fig.7: Boxcooler on anchor handling tug with ultrasound protection after 24 months trading West-Africa and Caribbean

6. Benefits leading to a lower Total Cost Of Ownership

There are clear advantages of using ultrasound for antifouling:

- ✓ Maintenance free
- ✓ Environmental friendly
- ✓ Sustainable
- ✓ One-time investment
- ✓ No running costs for consumptions or maintenance/repair

The following calculation example refers to the “MV Öland” of Reederei Danz & Tietjens, as given in private communication by the captain of the vessel. The difference in fuel consumption for the hull free of growth compared to the hull with a lot of growth was given as 2 t/day. For 220 days/year at sea this gives 440 t saved. At 500€/t fuel cost, this converts to 220.000 € saved per year.

The investment for the ultrasound system involving ~140 transducers (for hull, bow thruster, sea chests, coolers and inner vessel pipes, incl. installation) are ~183.000 €, leading to a return on investment of 10 months. This estimate ignores the advantages of savings in copper anodes and chemicals, but also the running of the system which leads to reliability.

In the future, the savings should be quantified more reliably using performance monitoring.

References

KASTELEIN, R.A.; HEUL, S.v.d.; VEEN, J.v.d.; VERBOOM, W.C.; JENNINGS, N.; REIJNDERS, P. (2007), *Effects of acoustic alarms, designed to reduce small cetacean bycatch, on the behaviour of North Sea fish species in a large tank*, Marine Environmental Research 64, pp.160-180

A Detailed Look at the Speed-Power Relation of Different Vessel Types at Different Loading Conditions

Andreas Krapp, Jotun A/S, Sandefjord/Norway, andreas.krapp@jotun.no
Daniel Schmode, DNV GL, Hamburg/Germany, daniel.schmode@dnvgl.com

Abstract

At HullPic 2016, the problems related to simple interpolation approaches for speed-power curves was discussed for container vessels. The present contribution extends this study to other ship types. Dense speed-power-draft-trim matrices based on CFD simulations are used as main data source in the exploration.

1. Introduction

Many hull and propeller performance analysis methods use speed-power reference curves in dealing with variations in speed and power, also the ISO 19030 default method, *ISO (2016)*. These curves depend on the loading condition of the vessel, most importantly the vessel's draft and trim. Using such dense speed-power curves reflecting trim and draft is a good way to deal with the variation of loading conditions in the analysis of hull and propeller performance. However, reference curves are often not available for all loading conditions or speed ranges a vessel encounters; then interpolation and extrapolation are often used to cover the blind spots. At the first HullPIC in 2016, the problems related to such approaches, mainly the non-linearity between draft changes and power requirements, was discussed for container vessels by *Krapp and Bertram (2016)*. Based on dense speed-power-draft-trim matrices from Computational Fluid Dynamics (CFD) simulations for three container vessel classes, it was concluded that there is no straightforward way to interpolate between speed-power curves for intermediate draft values. Only near design speed and draft, linear or quadratic interpolation becomes acceptable. However, where the region of acceptable interpolation starts depends on ship type and no obvious way has been identified to decide from the outset when linear interpolation can be used for a specific vessel.

The question then arises how the situation is for other vessel types with different speed ranges and hull shapes (particularly bow and stern characteristics). This paper extends the study of *Krapp and Bertram (2016)* to other ship types, namely bulk carriers and LNG carriers. Dense speed-power-draft-trim matrices based on CFD simulations are used as main data source in the exploration.

2. Methods used

For the current study, CFD simulations were performed. The RANS (Reynolds averaged Navier-Stokes) simulations considered full-scale conditions, free surface (=wave making), and dynamic trim and sinkage. Trims given in this paper refer to static trim (at zero speed). The propeller is modeled by a body-force approach. Propulsion efficiency is modeled by a semi-empirical method and correlated with available model tests. The speed-power matrix is generated using 8 speeds, 7 drafts and 7 trims. The computational approach is described in more detail in *Hansen and Hochkirch (2014)*. In the following discussions, speed means "speed through water", power "break power", and draft "static draft amidship". Trim is defined draft aft minus draft fore in [m], and divided by Lpp in [°]. Positive trim thus means a ship trimmed by the stern.

3. Impact of draft/trim variations for LNG carrier

We performed CFD simulations for an LNG carrier of length L_{pp} = 279 m, 45 m beam and 26 m depth, with a design draft T = 10 m and a design speed of 20.3 kn (corresponding to a Froude number of 0.20). The block coefficient at design draft was C_B = 0.75. These parameters are typical for conventional LNG carriers.

Fig.1 shows the speed-power curves for two loading conditions (laden with T = 12.3 m and even keel; ballast at T = 9.5 m and 1.0 m trim). These curves are typically available from model tests. One noticeable, “non-intuitive” characteristic in this case is the crossing of the ballast and laden curves at intermediate speed: it is more efficient to operate at higher draft than in ballast. We have observed this pattern in numerous speed trial/model test reports for different LNG vessels. The reason for this feature is probably the bulbous bow designed exclusively for design condition. The bulbous bow then pierces the free surface in ballast condition with significant wave breaking and consequently high resistance.

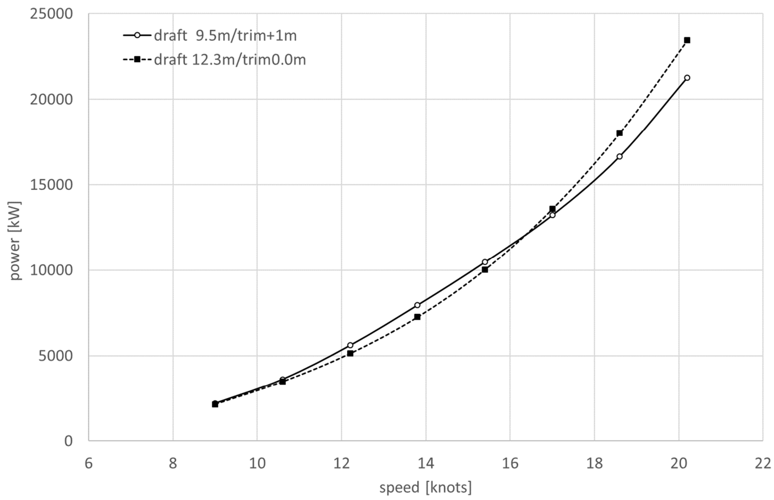

Fig.1: Speed-power curves for LNG vessel at ballast and laden condition

In order to shed more light onto the dependency of the speed-power curves on draft and trim, different “cuts” in the speed-power-draft-trim surfaces were made. Fig.2 (left) shows the speed-power curves at even keel, trim by stern and trim by bow for light, medium and full load. Fig.2 (right) shows the change in power by increase in draft for different vessel speeds.

The spread of the speed-power curves for different draft values is limited. This reflects the relatively moderate variation of drafts for LNG vessels. The curves for ballast, medium and full load diverge in the higher speed range. At even keel, the differences become relevant for speeds above 14 kn. When trimmed by stern, the curves of low and high draft cross and the lowest draft situation becomes the one with highest power for speeds below ~15 kn. When trimmed by bow, a more “intuitive” behavior is observed where lowest draft gives lowest power demand. The change in power demand over draft, Fig.2 (right) confirms above stated trends: low dependency on draft for lower speeds for even keel and trim by bow, lower draft gives lower power demands. However, for trim by stern, an increase in draft by 1 m decreases the power demand by up to ~500kW at 13.8 kn.

Clearly, it is a challenge to predict the differences in speed-power behavior of an LNG vessel for different draft and trim situations based on only the typical model test curves shown in Fig.1. As for containerships, *Krapp and Bertram (2016)*, non-linear effects are strong, especially for low draft and medium-to-low speed. However, the variations are less pronounced for the LNG vessel, because the differences in draft between ballast and laden are less pronounced. Furthermore, in the operational profile of an LNG vessel intermediate drafts are less often encountered.

Figs.3 and 4 show the operational profiles in terms of draft, trim and speed from automatic in-service performance monitoring for two LNG tankers with similar dimensions as CFD-investigated test vessel. The vessels represent two different operational scenarios. LNG vessel 2 serves in a regular trade between two destinations; LNG vessel 1 trades world-wide between many different destinations. However, the overall operational profile of the two vessels is comparable in terms of draft patterns. They exhibit two well defined draft peaks, one at ballast draft and one at laden draft. The trim profile of LNG vessel 2 is very narrow with only minor trimming by bow. LNG vessel 1 has a broader trim distribution, with a dominance of trimming by bow. The speed varies at lot more for LNG vessel 1 where speeds between 10 and 20 kn are almost equally populated. For LNG vessel 2 a much narrower distribution around one dominant speed is observed.

Given these operational profiles with two dominant drafts, the impact of having reliable speed-power curves for the intermediate draft range is less pronounced for LNG vessels than for containerships. Nevertheless, given the variability in trim in at least parts of the LNG fleet and the potential power penalties in operating under non-optimal trim, it is certainly advisable to refer to dense speed-power-draft-trim references also for LNG vessels.

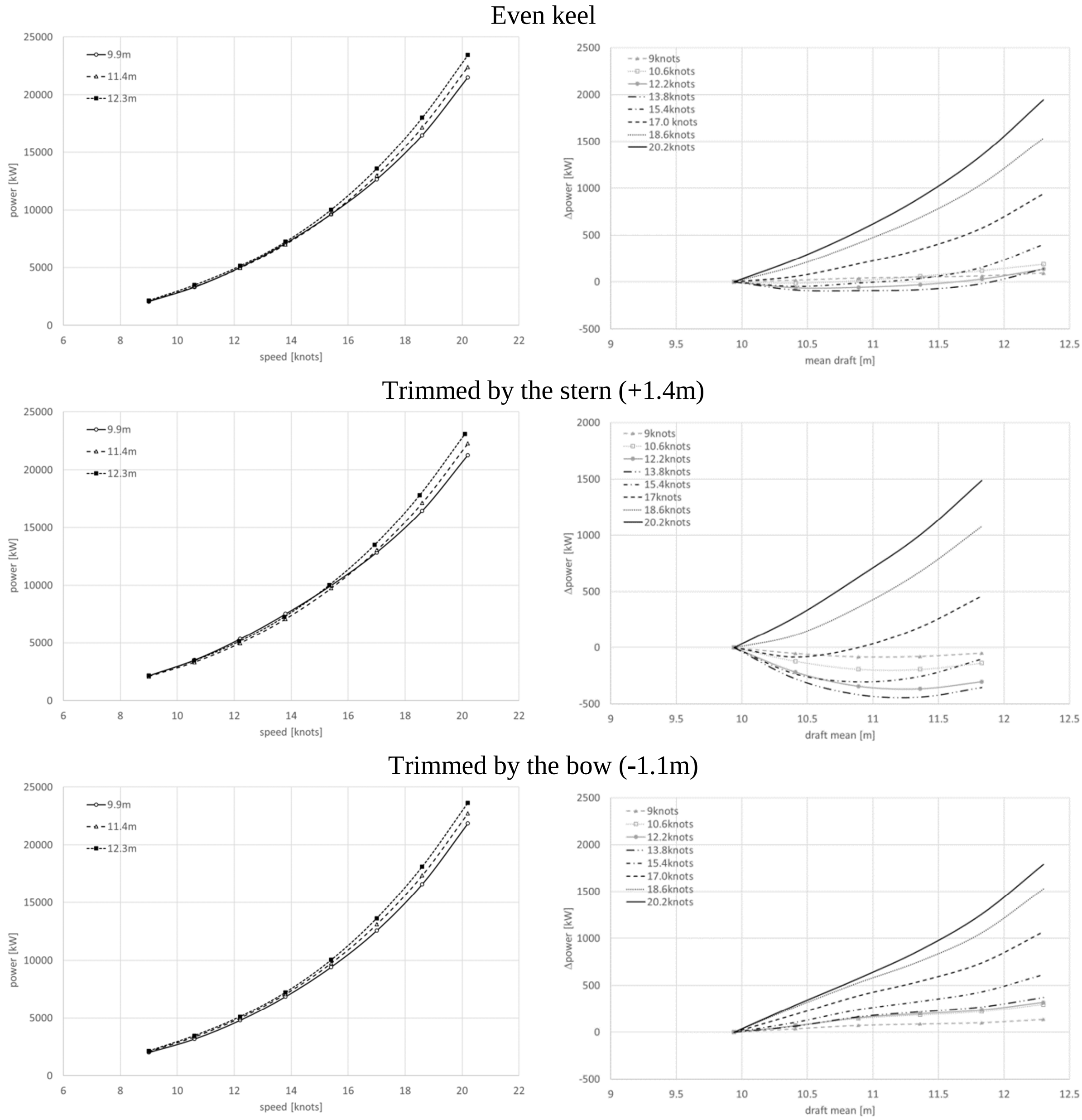

Fig.2: (left) Speed-power curve for LNG vessel for different draft values.
(right) Change in power by change in draft for LNG vessel for different speed values.

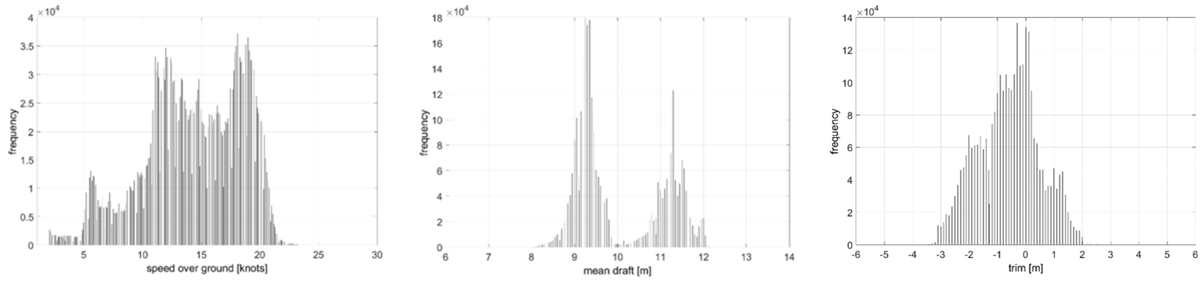

Fig.3: Speed, draft and trim profile of LNG vessel 1 in world-wide trade over 2.5 years

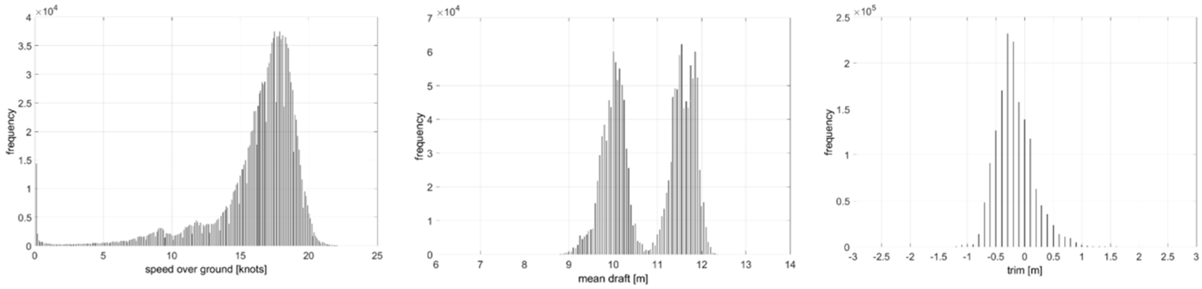

Fig.4: Speed, draft and trim profile of LNG vessel 2 in fixed trade over 1.5 years

4. Impact of draft/trim variations for Bulk carrier

We performed CFD simulations on a Handymax bulk carrier of 188 m length, 30 m beam, 21 m depth, block coefficient C_B = 0.567, design draft of 10 m, and design speed of 15.2 kn (Froude number 0.18). These parameters are typical for relatively slender Handymax bulk carriers. Fig.5 (left) shows speed-power curves at ballast, laden and two intermediate draft values. One observes a clear split between ballast and laden draft over the whole speed range for all three trim conditions. The ballast condition demands always less power than the laden condition. Interestingly, the intermediate draft curves are closer to the ballast curve than to the laden curve, even if the draft values of 9.8 m and 10.7 m are evenly distributed between ballast (8.0 m) and laden (12.4 m). Fig.5 (right) shows the change in power demand over draft for different speeds and trim situations. There is a clear change in gradient in these curves around 10 m draft. Below 10 m draft, a change in draft has only a minor impact on the power demand; above 10 m draft a steep increase is noted. A closer look, however, reveals that this step change in power demand on draft change applies only for higher speeds. At lower speeds the power changes rather linearly with draft.

In contrast to the studied container vessels, *Krapp and Bertram (2016)*, and the LNG tanker, the bulk carrier does not show the situation that a lower draft value corresponds to a higher power. There is no gain in power observed by an increase in draft (no negative values in Fig.5 (right)).

In order to estimate the relevance of the intermediate draft range and the variability in operationally realized trim, the in-service speed, draft and trim profile of a bulk carrier of a size comparable to the simulated one is shown in Fig.6. Given the variability in the bulker market, this profile is not considered representative for Handymax bulk carriers in general; it is just one possible example. The vessel is operated under a broad range of speeds, and most importantly under a very broad range of draft values where no draft dominates the distribution. The vessel is operated only modestly trimmed, mainly by the stern. It is obvious that reliable speed-power reference curves for intermediate draft ranges are needed for bulk carriers in trades comparable to the presented case.

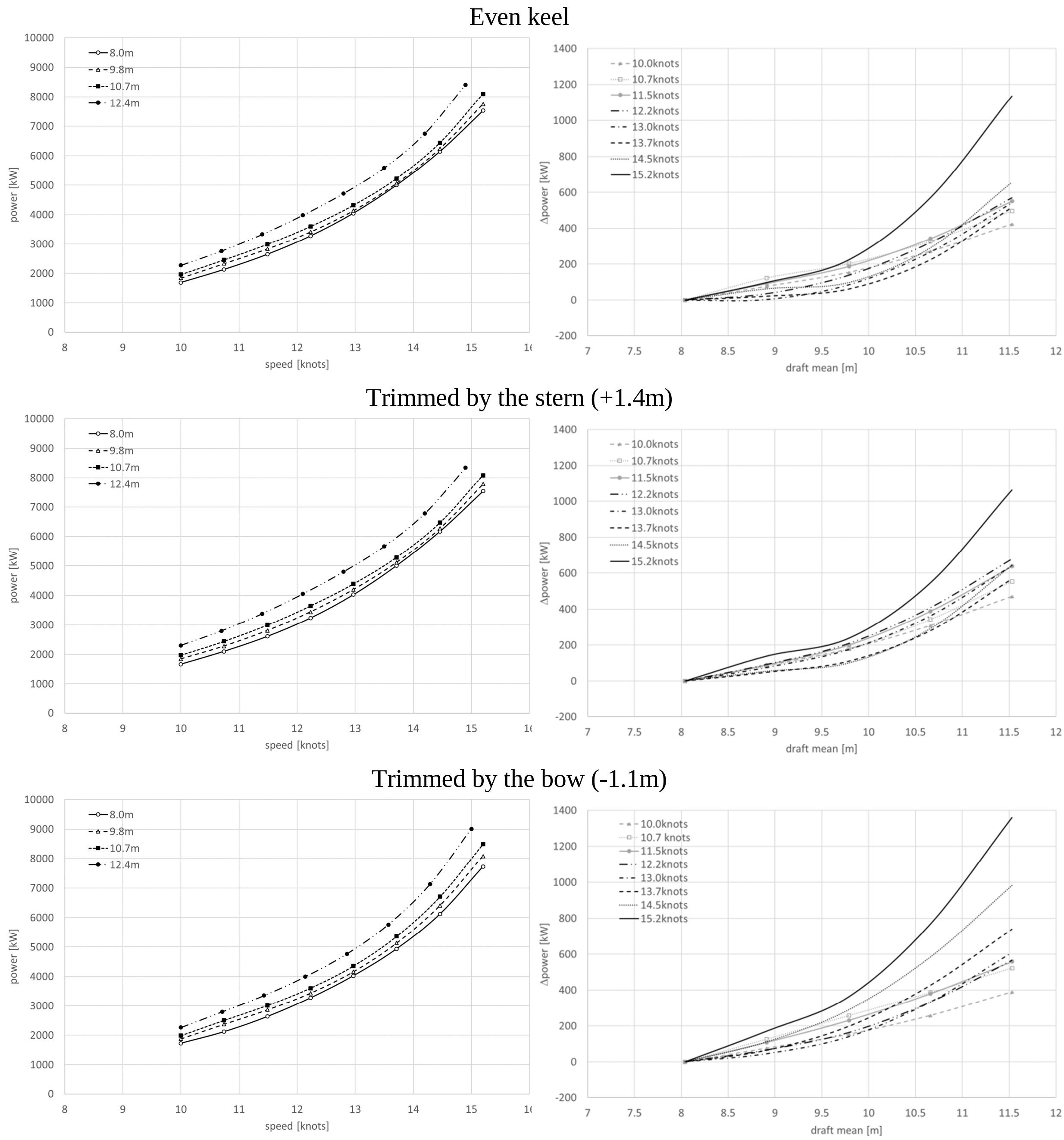

Fig.5: (left) Speed-power curve for bulk carrier for different draft values.
(right) Change in power by change in draft for bulk carrier for different speed values.

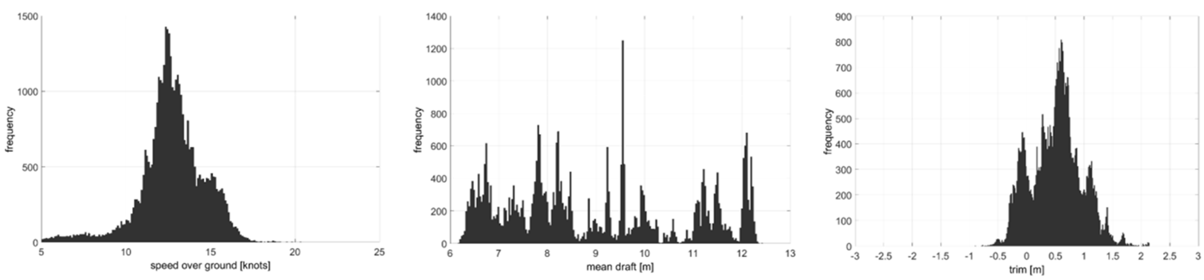

Fig.6: Speed, draft and trim profile of a bulk carrier in a world-wide trade over 2 years

5. Uncertainty of linear interpolation for draft changes

Without dense speed-power-draft-trim reference matrices, one has to find ways to estimate speed power curves. One commonly used approach is to interpolate linearly between the known curves for ballast and laden conditions. Looking at Figs. 2 (right) and 5 (right), such an approach can only be considered as a first approximation. Firstly, the dependency of power on draft change is nonlinear for most speed ranges, and secondly, the relation is different for different speeds. In order to estimate the importance of such an approximation, the interpolation error has been computed as follows for constant vessel speed:

$$P_{est} = P_{ballast} + \frac{P_{laden} - P_{ballast}}{T_{laden} - T_{ballast}} \cdot (T_{int} - T_{ballast})$$

$$error = \frac{P_{est} - P_{int}}{P_{int}} \cdot 100$$

where
- $T_{ballast}$ draft in ballast conditions in m
- T_{laden} draft in laden conditions in m
- T_{int} draft at intermediate conditions in m
- $P_{ballast}$ power in ballast conditions (from CFD) in kW
- P_{laden} power in laden conditions (from CFD) in kW
- P_{int} power at intermediate conditions (from CFD) in kW
- P_{est} estimated power at intermediate conditions in kW
- $error$ percentage error of the estimated power

Fig.7 shows the percentage error for interpolating between the laden and the ballast curve the LNG tanker, the bulk carrier and a container vessel (see *Krapp and Bertram (2016)* for details). The maximum interpolation error for the LNG tanker amounts to ~2.5%, for the bulk carrier to 4% and for the container vessel the error varies between –22% and +8%.

LNG tanker

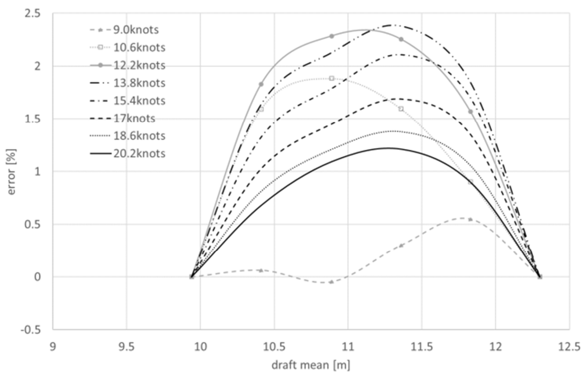

Bulk carrier

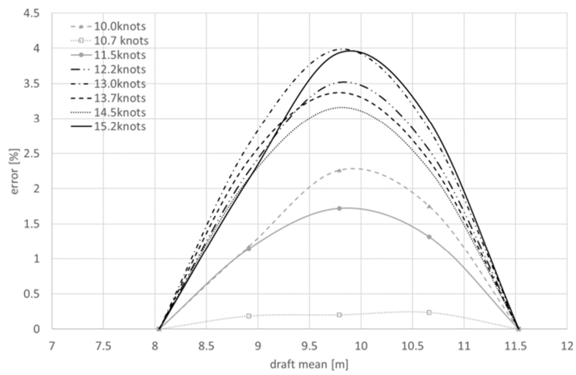

Container vessel

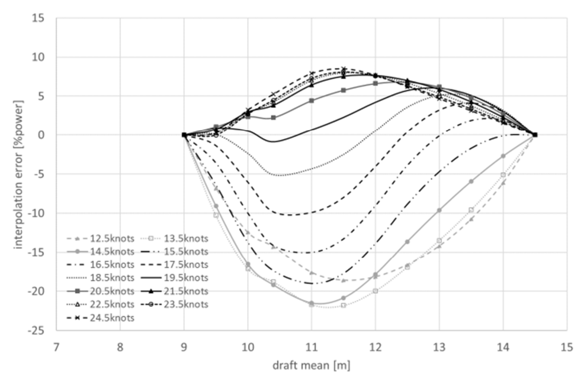

Fig.7: Speed, draft and trim profile of a bulk carrier in a world-wide trade over 2 years

7. Summary and conclusion

Speed-power curves are used as reference curves to correct for draft, trim and speed variations in vessel performance analysis.

The impact of draft and trim variations on speed-power curves has been studied for a LNG tanker and a Handymax bulk carrier and compared with the results of a previous study on container vessels. Based on dense CFD matrices it can be concluded that also for LNG tankers and bulk carriers, there is no straightforward way to interpolate between speed-power curves for intermediate draft values. It is noted, however, that the effect is less pronounced for the LNG tanker and the bulk carrier compared to the container vessels studied before.

The operational profile from two LNG vessels and one bulk carrier from in-service performance monitoring over several years of service were discussed. Intermediate draft values seem to be less important for LNG vessels, but very relevant for the bulk carrier in the study. On the other side, one of the LNG vessels was operated under a variety of trims. One can thus advice to use dense speed-power matrices for such cases as well to reduce uncertainty in vessel performance analysis.

The error made by linearly interpolating between the speed-power curves for different draft values has been estimated for the three vessel types. For the LNG vessel the maximum interpolation error amounts to 2.5% in power, for the bulk carrier 4% and for the container vessel the error ranges from -22% to 8%. These examples show that the choice of reference curves or the approach to generate new reference curves has a significant influence on the reliability of any vessel performance analysis.

Acknowledgements

The authors thank Prof. Volker Bertram for useful discussions and practical assistance in finalizing the paper.

References

HANSEN, H.; HOCHKIRCH, K. (2014), *Lean ECO-Assistant production for trim optimization*, 12th Conf. Computer and IT Applications in the Maritime Industries (COMPIT), Cortona, pp.76-84

ISO (2016), *Measurement of changes in hull and propeller performance - Part 1: General principles*, ISO 19030-1

KRAPP, A.; BERTRAM, V. (2016), *Hull performance analysis – Aspects of speed-power reference curves*, 1st HullPIC, Pavone, pp.41-48

Measurements and Prediction of Friction Drag of Hull Coatings

Bercelay Niebles Atencio, Valery Chernoray, Chalmers University of Technology, Gothenburg/Sweden, valery.chernoray@chalmers.se

Abstract

The prediction of the friction drag from surfaces with different types and shapes of roughness is still one of the major questions in fluid mechanics. The specific character of wall roughness may vary significantly from case to case. In this paper we show a method for obtaining the roughness function of an arbitrary rough surface by using resolved RANS simulations. This method is considerably cheaper in terms of resources and time than currently used experimental approaches. The drag characterization and roughness function determination is performed for marine coatings with different roughness size. The results are validated by experiments in a rotating disk rig and by data from a towing tank for same coatings. Furthermore, the roughness functions obtained are implemented in wall-function based CFD simulations and the computational results have demonstrated very satisfactory agreement with experiments.

1. Background

As is well known, two of the major contributors to the surface roughness of a ship hull are the hull coating and fouling. Antifouling coatings have been developed and used to counteract the effect of fouling on ship hulls, but a desirable characteristic of a good antifouling coating is of course a low contribution to drag.

The effect of hull roughness on vessel resistance has been studied by many researchers, but there is still no common agreement on the way the drag should be characterized, which implies finding the velocity decrement or roughness function, ΔU^{+}, or the equivalent roughness. Since the roughness drag depends largely on the actual roughness shape and distribution, there is no universal approach available for roughness characterisation.

The present study shows some indirect methods revised and used to validate a newly developed approach based on resolved RANS (Reynolds averaged Navier-Stokes) simulations to evaluate the drag of hull coatings. The new CFD (Computational Fluid Dynamics) based approach can be useful to replace expensive experiments for finding the roughness function. An approach for obtaining the roughness function for marine coatings from resolved RANS simulations is described and the results are validated by experimental data from rotating disk and towing tank methods. Finally, the validity of the roughness function is checked by implementing it in wall-function based RANS simulations.

2. Methodology

2.1. Test Surfaces

Three different types of rough surfaces were used that correspond to realistic surfaces of marine coatings. Models of flat plates and disks were prepared and scanned using 3D laser profilometry at Jotun A/S. These flat plates and disks were tested in experimental rigs at Chalmers and MARINTEK. The 3D profilometer surface scans were used as an input geometry for resolved CFD calculations.

The way to obtain coatings with different roughness values is explained in detail in *Savio et al. (2015)*. The coating applications were made by spraying the surfaces to give the three levels of roughness A, B and C. Level A of roughness simulates an optimal newly built ship or full blast dry docking paint application. The second level (B) of roughness represents a poorly applied coating, and roughness C represents a severe case of underlying roughness accumulated from many dry dockings and a very poor application.

The test disks and flat plates were scanned by Martin Axelsson, R&D Chemist from Jotun A/S using a 3D laser profilometer. For the flat plate, the scanning was performed at six locations on each plate. For the disk, the scanning was performed at four locations on each disk and two disks of each type were prepared. In addition, for the flat plates, the scanning was complemented by stylus measurements with the TQC DC9000 hull roughness analyser. The profilometer scanning resulted in data files with coordinates XYZ that were used in CFD. Fig.1 shows an example of the surface that resulted from the scanning process.

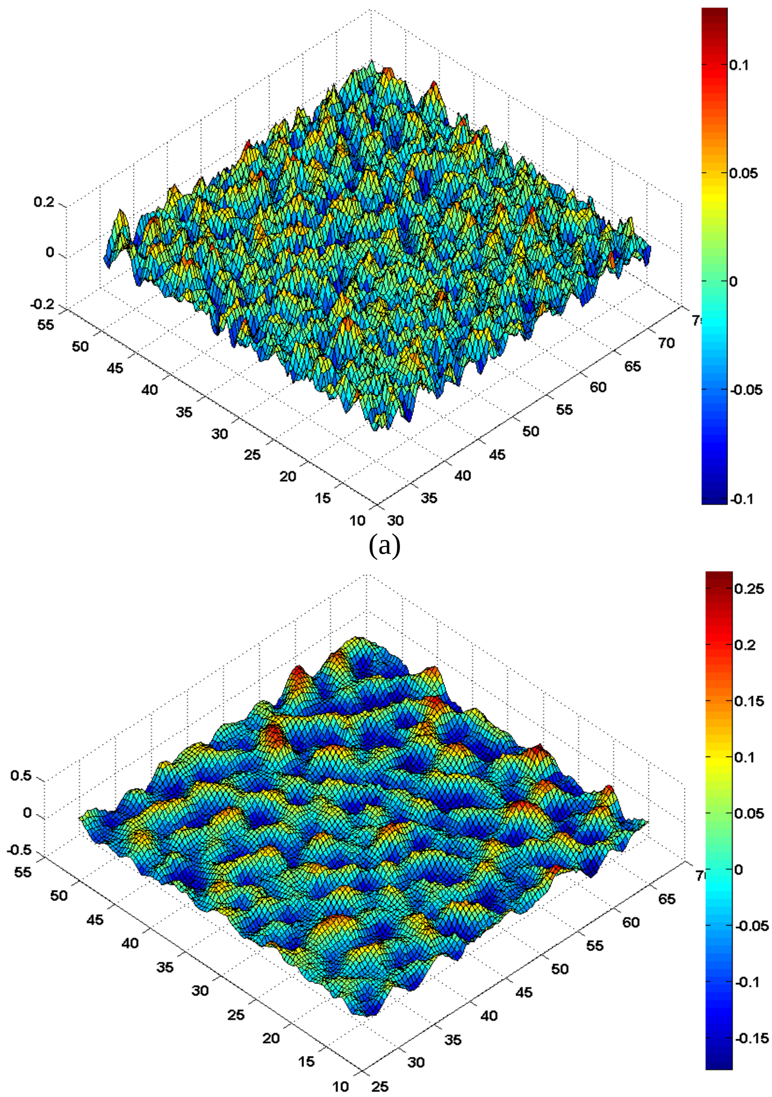

(a)

(b)

Fig.1: Surface scans showing roughness type B (a) and type C (b). Dimensions in mm.

2.2. Resolved CFD Approach

Using the entire disc or plate to create a domain and then simulating the flow in this domain would imply expensive computational resources. A representative area of the entire scan was selected to be simulated for this reason. The scanned areas are 40 mm × 40 mm, but an area of 5 mm × 20 mm was used for the simulations. This simulated area should exhibit characteristics of the roughness presented in the entire disc or plate.

The ICEM CFD V.17 software was used to create the meshes. In ICEM CFD, the surface scan data are imported as an STL file and the flow domain for CFD solver is created. The height of the simulated channel is $2h$ = 0.02 m and the height of the domain is h = 0.01 m. The number of cells for the different cases varied between 5 and 6 million. All meshes were refined near the wall of the domain, and a mesh dependency test was carried out by evaluating how the wall shear stress varied when the number of cells increased.

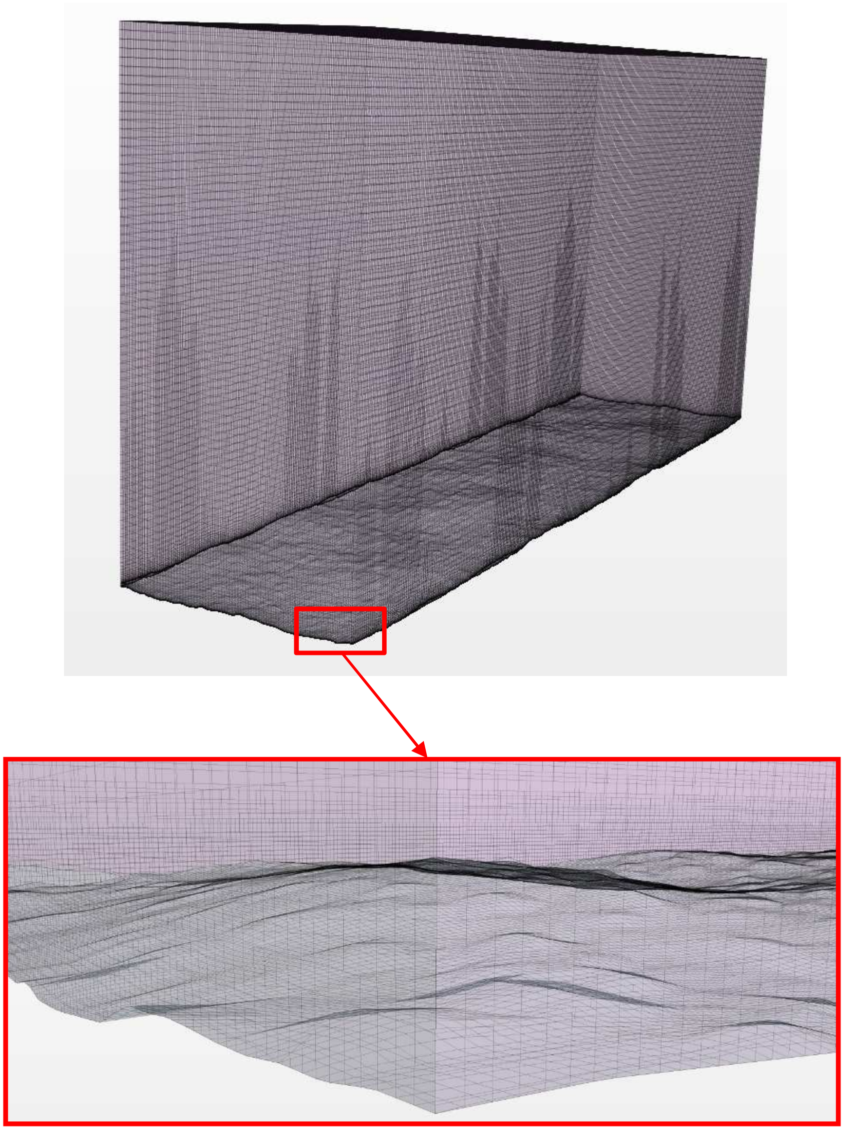

Fig.2: Meshed domain for case B with a zoomed area close to the wall.

2.3. Experiments

A rotating disk rig was designed and constructed for Micro-PIV and torque measurements. The disk is driven by an electric motor and rotates inside a 20-liter water tank. Fig.3 shows a schematic of the rig.

Different disks with different roughness value were used for the experiments. These include one smooth disk for reference, two cases with sandpaper, three cases of disks with different marine coating applications, A, B, C and one case with periodic roughness. Table I illustrates the different cases and their average roughness. The peak value of roughness is given for the periodic roughness.

Table I: Experimental cases of surface roughness for rotating disks with average heights in μm

Smooth	**A**	**B**	**C**	**80-G**	**400-G**	**Periodic**
0.55	13	33	55	201	35	500 (peak)

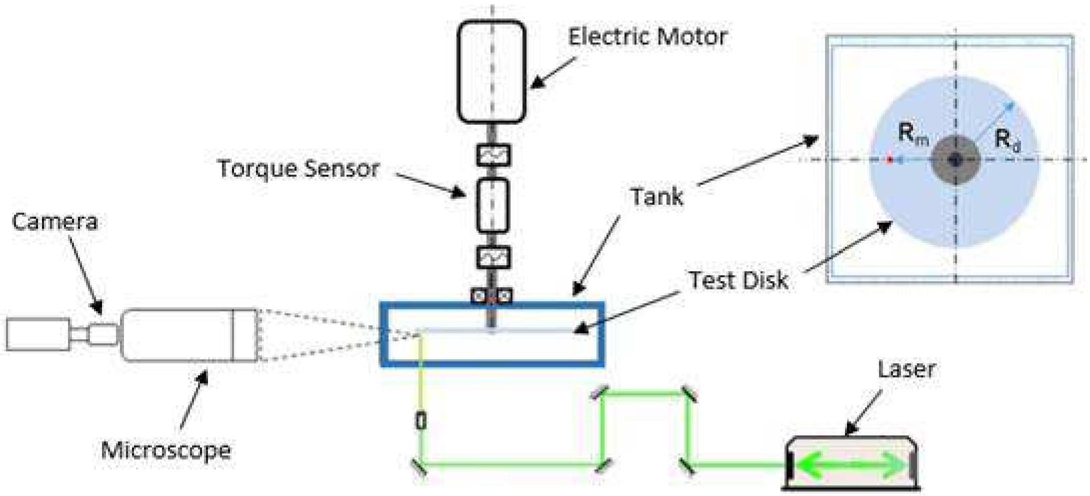

Fig. 3. Schematic of the rotating disk rig.

- Micro-PIV Measurements
  Measurement of boundary layer profiles on disks is a challenging task due to the very small thickness of the boundary layer (3–5 mm). To measure the azimuthal velocity component near the disk wall with the high spatial resolution and to capture the inner layer of the turbulent boundary layer, a microscopic optics was used with a magnification of 12 times. The seeding of the flow was done by using PMMA microparticles GmbH of 1 μm in diameter. The images were registered, magnified and transferred by a monochrome double-frame CCD camera with a resolution of 2048 × 2048 pixels. The recording of this camera was synchronized with the specific angle of rotation of the test disk through a hall sensor. Complete details and the set-up for these measurements are described in *Niebles Atencio et al. (2016).*

- Torque Measurements
  For the torque measurement test, a Kistler type 4503A torque meter was installed on the rotating disk rig connecting the electric motor and the rotating disk shaft, Fig.3. The torque sensor operates based on the strain gauge principle. The torque meter output was monitored by an analogue to digital converter (ADC) controlled by a PC. The torque was measured for rotational velocities from 0 to 1200 rpm. The measurement procedure included a warm up of the running rig and the measurement equipment for at least one hour before experiments.

- Towing Tank Tests
  Towing tank tests were performed by the Norwegian Marine Technology Research Institute (MARINTEK) and reported by *Savio et al. (2015).* In summary, test plates with different roughness values, A, B and C (previously mentioned), were towed in the wake of a leading (front) plate which was smooth. The Reynolds numbers during tests were based on the total length of plates and ranged between 3×10^7 and 9×10^7.

3. Results

Figs. 4-6 show results after post-processing the torque measurements, the data from the towed plates and the resolved CFD simulations. This post-processing was done according to *Granville (1982, 1987).* The plots are illustrating how the resistance caused by the roughness varies with the Reynolds number. Note that the Reynolds numbers are defined differently for the rotating disk, flat plate in a towing tank and channel. In this paper only results for marine coatings are presented (i.e., cases A, B and C). From these plots we can indirectly obtain the roughness function (ΔU^+) and, once it is determined, we are able to compare the resulting roughness functions in the three cases, Fig.7.

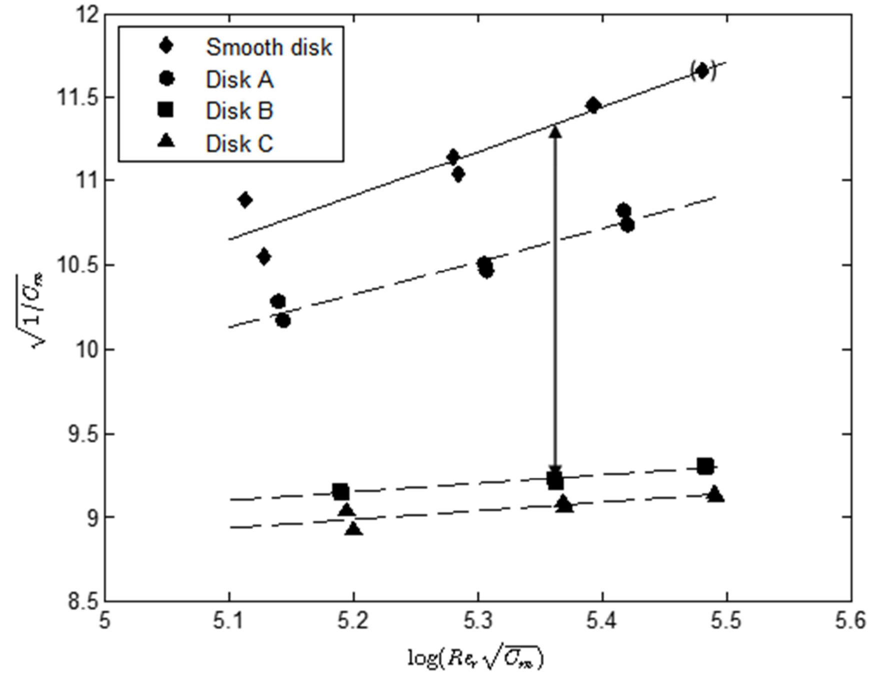

Fig.4: Experimental data for rotating disks in non-dimensional variables for ΔU^+ determination

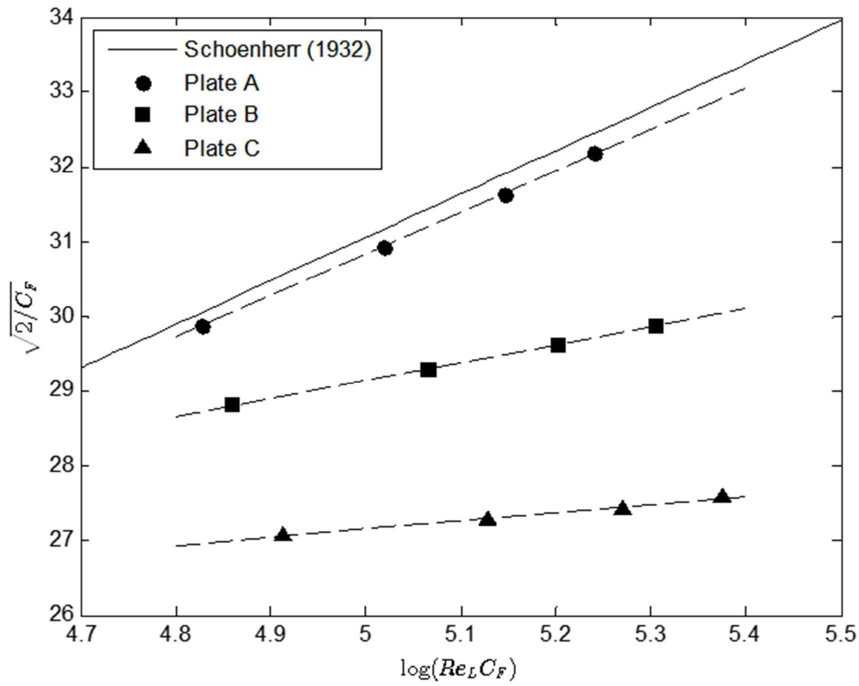

Fig.5. Experimental data for towed plates in non-dimensional variables for ΔU^+ determination

Resulting ΔU^+ values obtained are shown in Fig. 7 against the roughness Reynolds number. In this case, the roughness height is the root mean square of roughness (R_q) for cases A and B, while the equivalent roughness height of 43 μm is used for case C. The *Cebeci and Bradshaw (1977)* roughness function is also shown using two different values for the roughness constant, C_S. The results show that the roughness function by Cebeci and Bradshaw with C_S = 0.5 describes the data at a high Reynolds number, using R_q as the roughness height.

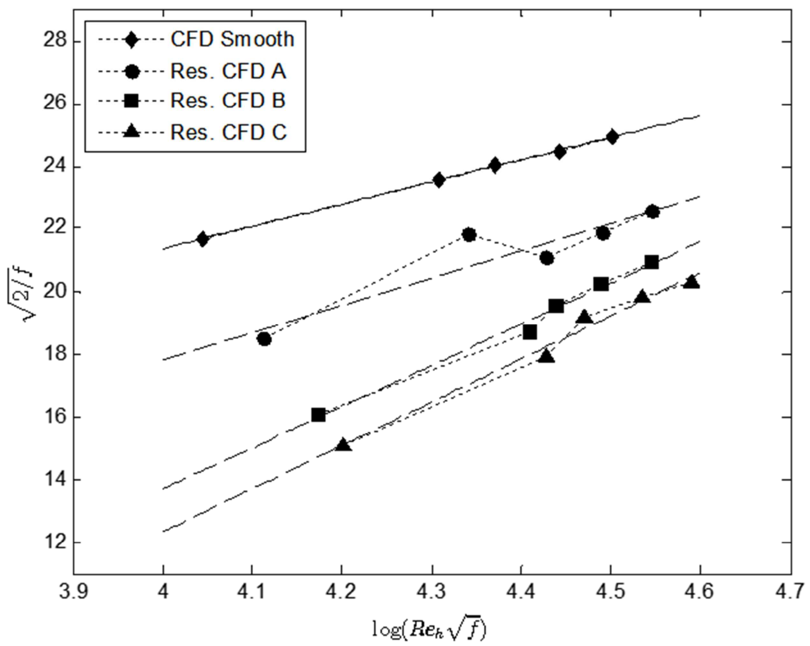

Fig.6: Resolved CFD data in non-dimensional variables for ΔU^+ determination

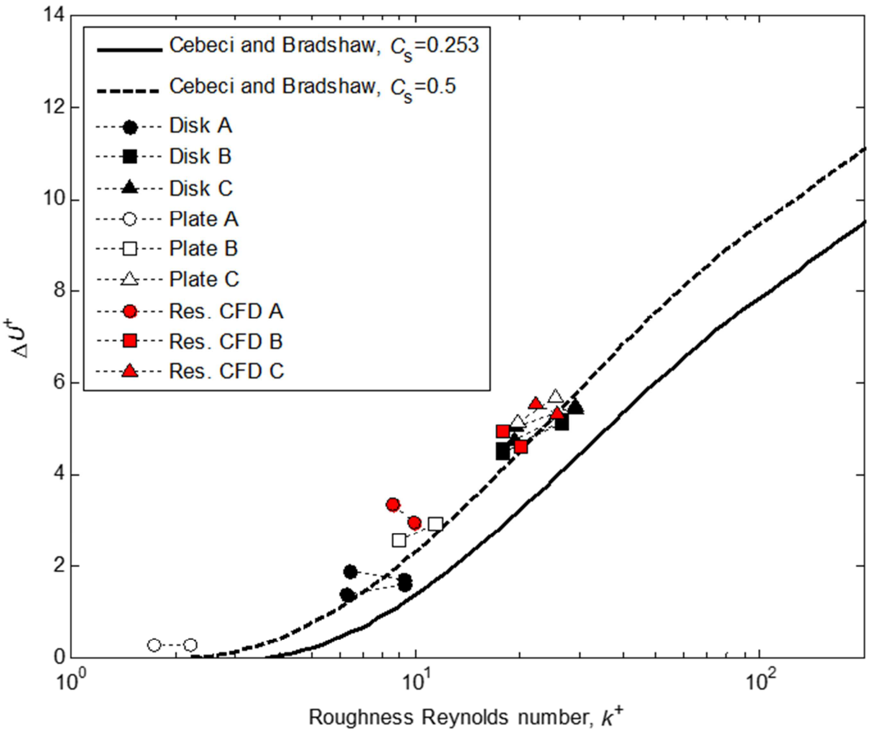

Fig.7: Comparison of results from rotary disks, towed plates and resolved CFD

4. Validation by a WFCFD simulation

The obtained wall functions were used in wall function based CFD (WFCFD) simulations to check the consistency in the results. According to our above findings, the Cebeci and Bradshaw roughness function, with C_s = 0.5 and R_q as the roughness height, was used in these CFD simulations. The flat plate in the simulations was similar to that in experiments by *Savio et al. (2015)* and consisted of a smooth front plate and a rough aft plate. The front plate length is 4 m and the aft plate is 6 m. The height of the domain is 0.5 m and contains 220000 mesh cells. The inlet boundary conditions are 9 m/s, 2% turbulence intensity and a 1-mm turbulence length scale. The resulting mesh y^+ for the front plate varied from 120 to 75 from nose to aft. For the aft plate, the mesh y^+ was in a range from 70 to 100 depending on the roughness case. The mesh independency was checked by modifying the mesh y^+ values. No checks were performed to vary the mesh density outside of the boundary layer since the mesh is already very dense for these types of calculations. The maximum cell size was 5 mm and the boundary layer thickness on the aft plate was 50-100 mm, so that 15-25 cells were present in the boundary layer. The flow equations were solved using a standard $k-\varepsilon$ turbulence model with standard wall functions in a segregated manner with second order accurate discretization schemes.

Since the CFD simulations were performed at exactly the same velocities as experiments, it was possible to use the increase in the drag coefficient due to the roughness for comparison rather than absolute values of the drag coefficient. The absolute values of the drag coefficient were slightly different in the CFD and experiments since the CFD over predicted the drag of smooth cases.

The results of this study are summarized in Table II. The wall-function CFD approach (WFCFD), in general gives very good predictions, which confirms the validity of the roughness function.

Table II: Comparison of towing tank experiments with WFCFD calculations

	MARINTECs Exp.		**WFCFD**	
	C_F	ΔC_F, %	C_F	ΔC_F, %
Smooth	0.00191	**-**	0.00202	**-**
Case A	0.00193	**1**	0.00202	**0**
Case B	0.00224	**18**	0.00240	**19**
Case C	0.00263	**38**	0.00292	**44**

5. Concluding remarks and discussion

A drag evaluation of marine coatings was made by two experimental methods that used to validate a newly developed approach based on resolved RANS simulations. This new CFD based approach potentially can replace expensive experiments and find, with acceptable reliability, the roughness function of arbitrary roughness. The small scale rig has shown itself to be a very practical and compact way to estimate the drag caused by marine coatings and can be used to replace more expensive large scale tests. Guidelines and standards are needed in order to establish reliable approaches for the drag characterisation of marine coatings.

Acknowledgements

This research is supported by the EU FP7 Project "Low-toxic cost-efficient environment-friendly antifouling materials" (BYEFOULING) under Grant Agreement no. 612717. We also thank Jotun A/S and their staff for all the support and help during the development of this project.

References

CEBECI, T.; BRADSHAW, P. (1977), *Momentum Transfer in Boundary Layers*, Hemisphere Publishing/McGraw-Hill, pp.176-180

GRANVILLE, P.S. (1982), *Drag-characterization method for arbitrarily rough surfaces by means of rotating disks*, J. Fluids Eng. 104, pp.373-377

GRANVILLE, P.S. (1987), *Three indirect methods for the drag characterization of arbitrarily rough surfaces on flat plates*, J. Ship Res. 31, pp.70-77

NIEBLES ATENCIO, B.; TOKAREV, M.; CHERNORAY, V. (2016), *Submicron Resolution Long-Distance Micro-PIV Measurements in a Rough-Wall Boundary Layer*, 18th Int. Symp. on the Application of Laser and Imaging Techniques to Fluid Mechanics

SAVIO, L.; OLA BERGE, B.; KOUSHAN, K.; AXELSSON, M. (2015), *Measurements of added resistance due to increased roughness on flat plates*, 4th Int. Conf. on Advanced Model Measurement Technology for the Maritime Industry (AMT'15)

SCHOENHERR, K.E. (1932), *Resistances of flat surfaces moving through a fluid*. Trans. SNAME 40, pp. 279-313

UNCTAD (2015), *Review of Maritime Transport*, United Nations Conference on Trade and Development (UNCTAD), p. X

Friction Measurements of Different Coatings in a Friction Tunnel

Reinhard Schulze, SVAtech, Potsdam/Germany, schulze@sva-potsdam.de
Rhena Klose, SVA Potsdam, Potsdam/Germany, klose@sva-potsdam.de

Abstract

In this paper the measurement procedure for friction measurements in the friction tunnel of the SVAtech are described. In the end, investigations made for different coatings and surface structures are presented by friction characteristic curves in comparison to the smooth plate.

1. Introduction

The frictional resistance of a ship is a substantial part of its total resistance. This is influenced, among other things, by the texture of the skin (e.g. type of coating, degree of fouling). To minimize the power consumption and thereby reduce costs and protect the environment, it is therefore sensible to hold frictional resistance as low as possible by special coatings or surface structures. Corresponding studies can be performed in the friction tunnel of the SVAtech. These experimental studies allow for more accurate conclusions then a mere roughness analysis of the surface. These studies are not limited to the shipbuilding industry only, but are also applicable in the aerospace and automotive industries. In this paper the measurement procedure and studies made for different coatings and surface structures are described.

2. Basics

The friction coefficient c_F can be expressed by the wall shear stress τ_W, the density ρ and the velocity V as follows, *Schlichting and Gersten (2006), Junglas (2009)*:

$$c_F = \frac{\tau_W}{0.5 \cdot \rho \cdot V^2} \quad . \tag{1}$$

The wall shear stress τ_W can be calculated for a channel with a rectangular cross-section (width a, height b) from the gradient of pressure differences at arbitrary points multiplied by the area of cross-section divided by channel perimeter. It follows:

$$\tau_W = \frac{(p_2 - p_1) \cdot (a \cdot b)}{2 \cdot x \cdot (a + b)} \tag{2}$$

with the frictional force $F = (p_2 - p_1) \cdot (a \cdot b)$ and the reference surface for the wall shear stress $A = 2 \cdot x \cdot (a + b)$.

For higher measuring accuracy a fitted gradient for a plurality of pressure measurement points is calculated (in SVAtech 12 pressure transducers are used with a distance of 0.08 m between them).

For a one-side wetted plate the following formulas based on semi-empirical methods are given, *Schlichting and Gersten (2006)*:

(*1*) Laminar boundary layer (Blasius) $\quad c_F = \dfrac{1.328}{\sqrt{Re}}$

(*2*) Purely turbulent, hydraulically smooth (Prandtl) $\quad c_F = \dfrac{0.074}{\sqrt[5]{Re}}$

(*3*) Friction characteristic by ITTC 1957 $\quad c_F = \dfrac{0.075}{(log(Re) - 2.0)^2}$

(*3a*) Transition zone laminar / turbulent $c_F = \frac{3.913}{(ln(Re))^{2.58}} - \frac{1700}{Re}$

Implicit representations for the friction coefficients can be easier derived from theoretical considerations. Although these representations do not allow closed explicit representations (such as (*1*) to (*3*)) they can relatively easily be treated by numerical algorithms for the solution of equations with one unknown. The friction coefficients can then be approximated as a function of the parameters (Reynolds number, roughness) with arbitrary precision. The most common representation is the Schönherr representation:

(*4*) Friction characteristic by Schönherr $\frac{1}{\sqrt{c_F}} = 4.13 \cdot \log(\mathrm{Re} \cdot c_F)$ (implicit)

A very good characterization of the surface properties (roughness) is possible by means of the implicit representation of the friction coefficient according to *Schlichting and Gersten (2006)*:

(*5*) Friction characteristic by Schlichting/Gersten

$$\sqrt{\frac{2}{c_F}} = \frac{1}{\kappa} \cdot \log(\frac{c_F}{2}\mathrm{Re}) + 5.0 - \frac{1}{\kappa} \cdot \log(3.4 + k^+_{tech}) \quad \text{(implicit)}$$

with an approximated representation of $k^+_{tech} = 0.001 \cdot \mathrm{Re} \cdot k/L$ and the Karman constant $\kappa = 0.41$. More precise is $k^+_{tech} = \frac{k_{tech}}{\delta_v}$, $k_{tech} \approx 4.2 \cdot Ra$, with the average surface roughness *Ra* defined by $Ra = \frac{1}{L} \cdot \int_0^L |y| \cdot dx$ ("Profilometer-roughness"). In this expression *y* is the local height of the surface over the mean height of the measured length *L*. The thickness of the sublayer can be expressed by:

$$\delta_v = \frac{\nu}{u_\tau} = \frac{50 \cdot x}{\mathrm{Re}_x \cdot \sqrt{\frac{c_f}{2}}} = \frac{50 \cdot x}{\frac{U \cdot x}{\nu} \cdot \sqrt{\frac{c_f}{2}}} = \frac{50 \cdot \nu}{U \cdot \sqrt{\frac{c_f}{2}}}.$$

With this formula it is also possible to approximate u_τ.

In Fig.1 the friction characteristics are presented. A summary of all described friction characteristics can be found in *Schlichting and Gersten (2006)*.

For all formulas and sizes SI units are used as basis. The friction characteristic (*3*) according to ITTC 1957 is used throughout for the estimation of the frictional resistance of ships and also the Reynolds number correction of propellers. Strictly speaking it contains a form factor but it has proven its practical application in different investigations.

By means of friction measurements SVAtech can determine the frictional resistance of flat plates. The methodology is based on studies in *Stinzing (1992)*. Two plates with the surface to be measured are located in test section MS2 (see Figs.2 and 3). Together they form a narrow rectangular channel. Test section MS1 is used as entrance region nowadays. The water flow with a definable speed is generated by means of an adjustable pump or an adjustable valve (see Fig.3, positions 1 and 2). From the pressure gradient at the pressure taps (see Fig.3, position 12) the wall shear stresses and hence the friction coefficients can be calculated as a function of velocity and Reynolds number, *Stinzing (1992)*.

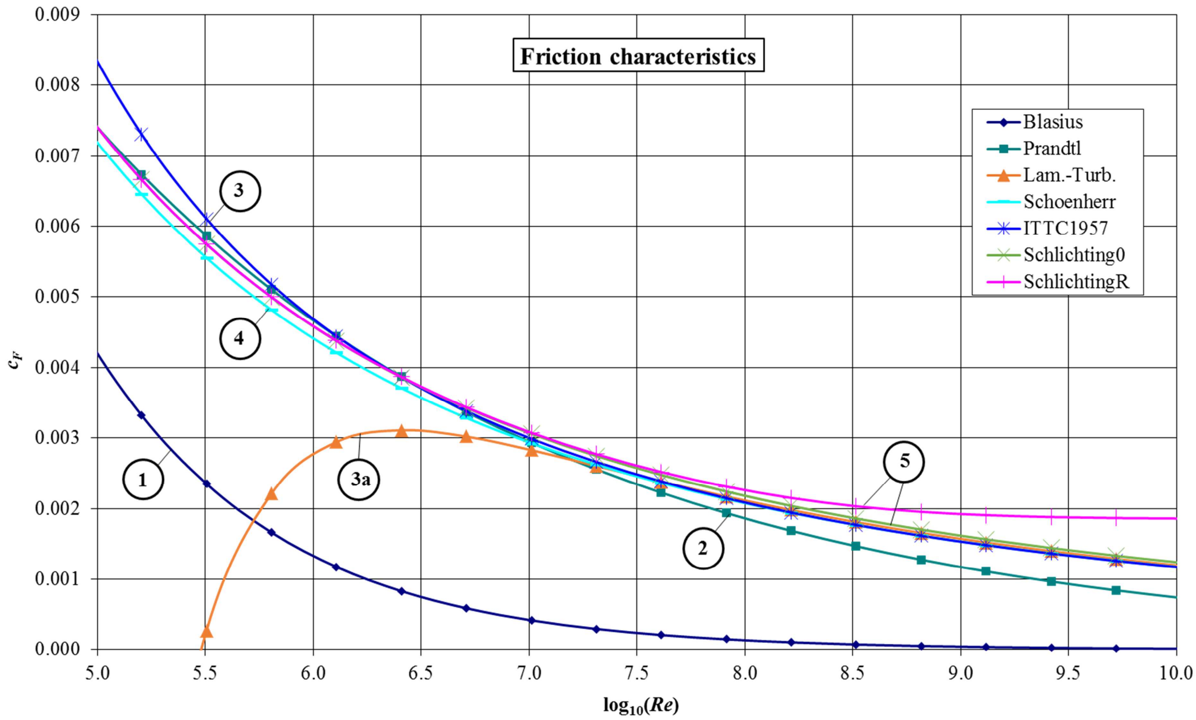

Fig.1: Frictional resistance coefficient characteristics c_F for different ranges and conditions (Schlichting0: technically smooth, SchlichtingR: technically rough with $k^+_{tech}/L = 10^{-6}$)

Fig.2: Friction tunnel of the SVAtech; test section MS1 is the first in flow direction and the second is test section MS2, which is used for the actual measurement

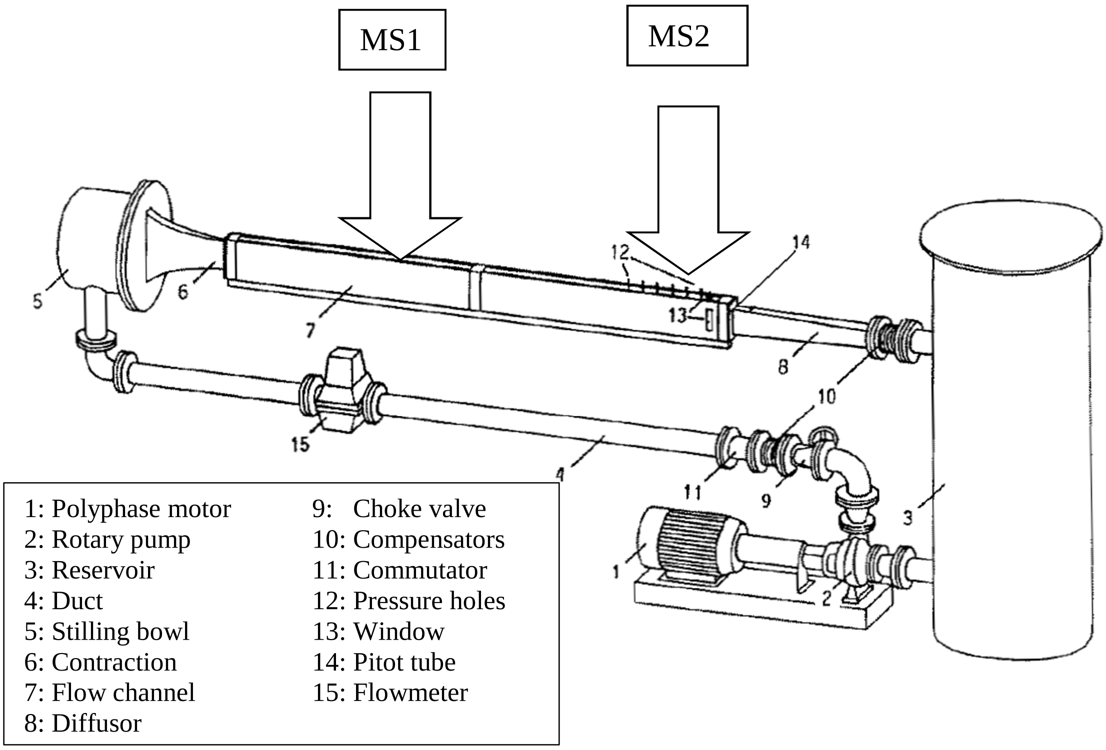

Fig.3: Schematic diagram of the friction tunnel

Test section MS2 has 12 pressure transducers with a distance of 80 mm to each other. These were connected to a venting system consisting of 12 valves. The pressure transducers measure the absolute pressure. The other parameters of the measurement section are defined with the notation of *Schulze (2010)*:

aba	= 0.012d0	! [m]	Distance of plates (might differ due to coating)
abb	= 0.1201d0	! [m]	Height of plates
f1	= 0.00144d0	! [m*m]	Cross section Area f1
f6	= 0.00144d0	! [m*m]	Cross section Area f6
dX	= 0.08d0	! [m]	Distance of bores

2.1 Microcontroller measurement board and engine control

The test device is completely controlled by a microcontroller board based on a Cortex M4 processor of type MK20DX256VLH7 with a rated speed of 96 MHz (see Fig.4). The data transfer to the host computer is realised by a blue tooth connection with 115000 baud.

12 pressure sensors, 2 temperature sensors and the speed meter are connected to the prozessor by 16 bit ADC’s. Futhermore, the processor organises the time schedule for 3 complete test cycles including the control of the pump. One test cycle includes up to 26 speed steps.

The firmware of the processor is written in a C similar programming language. The calculation of the friction coefficients are carried out directly by the firmware using Eq.(1). All measured original data (water speed, 12 pressure data and 2 temperatures) including the calculated c_F-value are transmitted by the processor to the PC- host and can be analyzed and possibly corrected there.

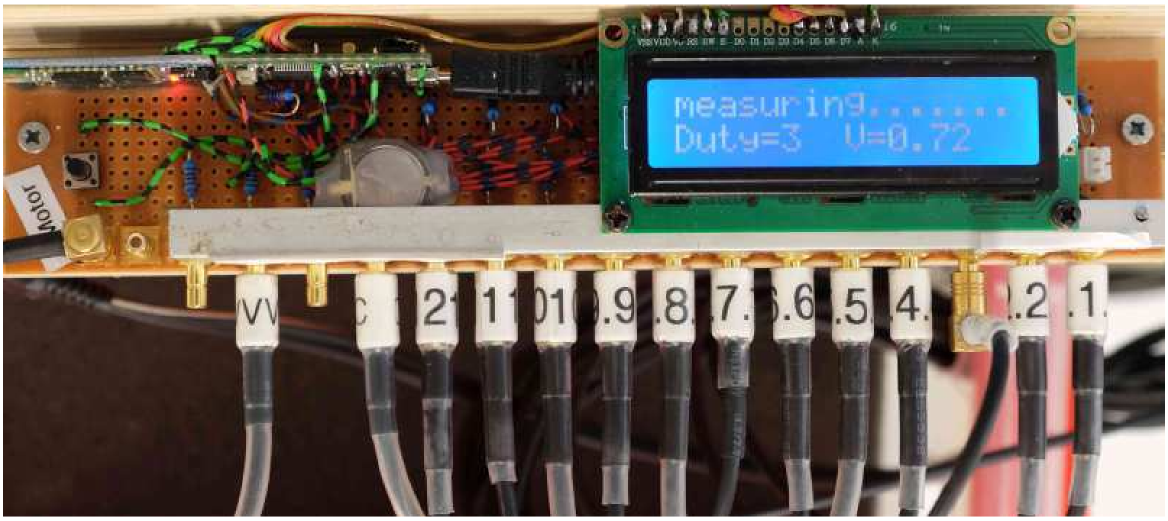

Fig.4: Microprocessor with LCD display (opened) and connectors

According to a cost-benefit analysis the decision was made for the pressure sensors from ‘freescale semiconductor’ type MPX4250DP CASE 867C (see Fig.5). The major advantage of these sensors is the integrated electronic amplification and pre-calibration. The sensors already have hose connections and are configured as differential pressure sensors. The power supply of the sensors must be a 5V stabilized input. The transfer function of these pressure transducers is presented in Fig.6.

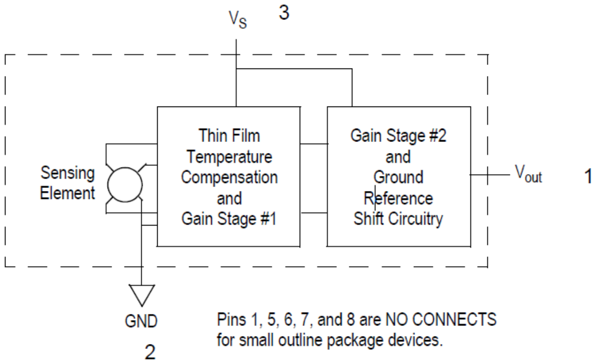

Fig.5: Principle of MPX4250 CASE 867C

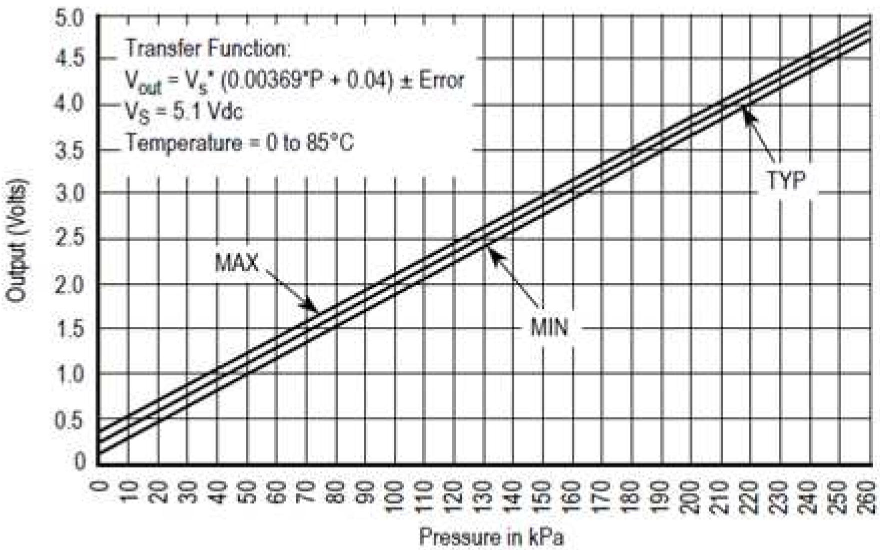

Fig.6: Transfer function of the sensor MPX4250

Because of Vout [V] = Vs [V] * (0.00369 ∗ p [Pa] + 0.04) it follows for the stabilised power supply of Vs = 5V: Vout [V] = 0.01845 * p [Pa] + 0.2 and hence for p: p [Pa] = (Vout [V] – 0.2) / 0.01845

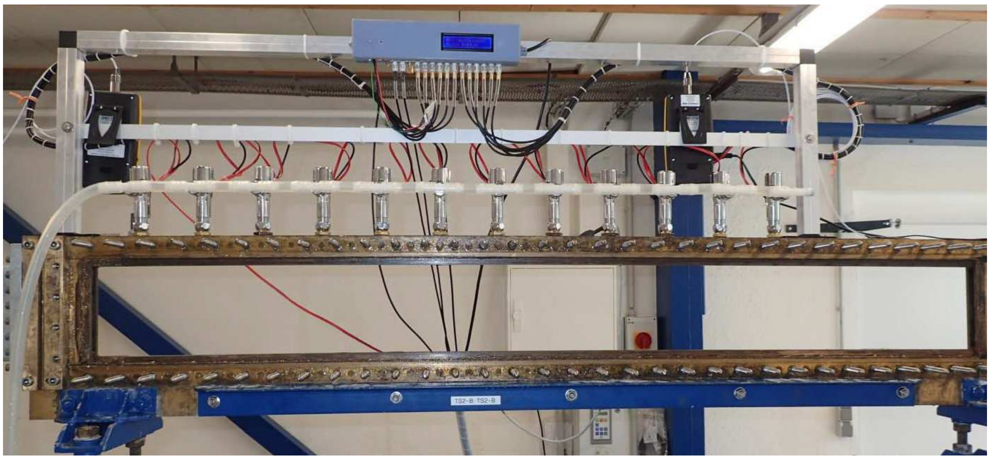

Fig.7: Pressure sensor bank (test section opened)

2.2 Flow meter

A magnetic inductive flow meter (see Fig.8) is used for the measurement of the volume flow, *Schulze (2010)*. By means of the equation of continuity the water velocity in the test section MS2 can be derived. The calculation of the velocity is described in chapter 2.3.

Fig.8: Flow meter PTB K7.2 - MAG 5100 W with MAG 5000

2.3 Velocity calculation in the test section

For the velocity in the test section MS2 is true:

$$V_{\mathrm{MS2}} = \frac{Q}{a \cdot b} = \frac{Q}{3600 \cdot 0.12\mathrm{m} \cdot 0.012\mathrm{m}} = \frac{Q}{5.184\mathrm{m}^2} = 0.192901234\mathrm{m}^{-2} \cdot Q \qquad (3)$$

with Q in [m^3/h] and V_{MS2} in [m/s].

For the velocity in the flow meter it follows for a flow meter diameter of D = 0.1 m (DN100):

$$V_{\mathrm{F}} = \frac{Q}{\pi D^2 / 4} = \frac{Q}{3600 \cdot 0.00785398\mathrm{m}^2} = 0.035677651\mathrm{m}^{-2} \cdot Q\,. \qquad (4)$$

Hence $V_{\mathrm{MS2}} = 5.454153912 \cdot V_{\mathrm{F}}\,.$ (5)

Following the factory calibration certificate "full scale" corresponds to 84.8 m^3/h, which is equivalent to 3 m/s in the flow meter.

On the other hand, 84.8 m^3/h correspond to U = 3.526 V (equivalent to I = 14.104 mA at a 250 Ohm resistor) by manually calibration. It follows that U = 5 V (I = 20 mA) is equivalent to 120 m^3/h.

Hence 1 V is equivalent to 24 m^3/h and the velocity in the test section is:

$$V_{\mathrm{MS2}} = 24 \cdot 0.192901234 \cdot U = 4.629629630 \cdot U \quad (6)$$

with V_{MS2} in [m/s] and U in [V].

2.4 Temperature

The temperature is measured at two positions by two semiconductor sensors LM35 which have been calibrated by a separate digital high accuracy pt100 temperature meter. One sensor is mounted directly above the test section and the other sensor inside the reservoir (see Fig.3, positions 3).

3. CFD calculations of the flow inside the friction tunnel

Numerical simulations were conducted to get insight of the flow in the friction tunnel and especially the test section. For the calculations a URANSE-solver was employed (Unsteady Reynolds-Averaged Navier-Stokes). In Fig.9 the streamlines for V_{MS} = 0.921 m/s are displayed in the duct after the flow meter, the stilling bowl and the test sections MS1 and MS2. The flow inside the test section is fully turbulent and not affected by the inlet or outlet geometry of the test sections.

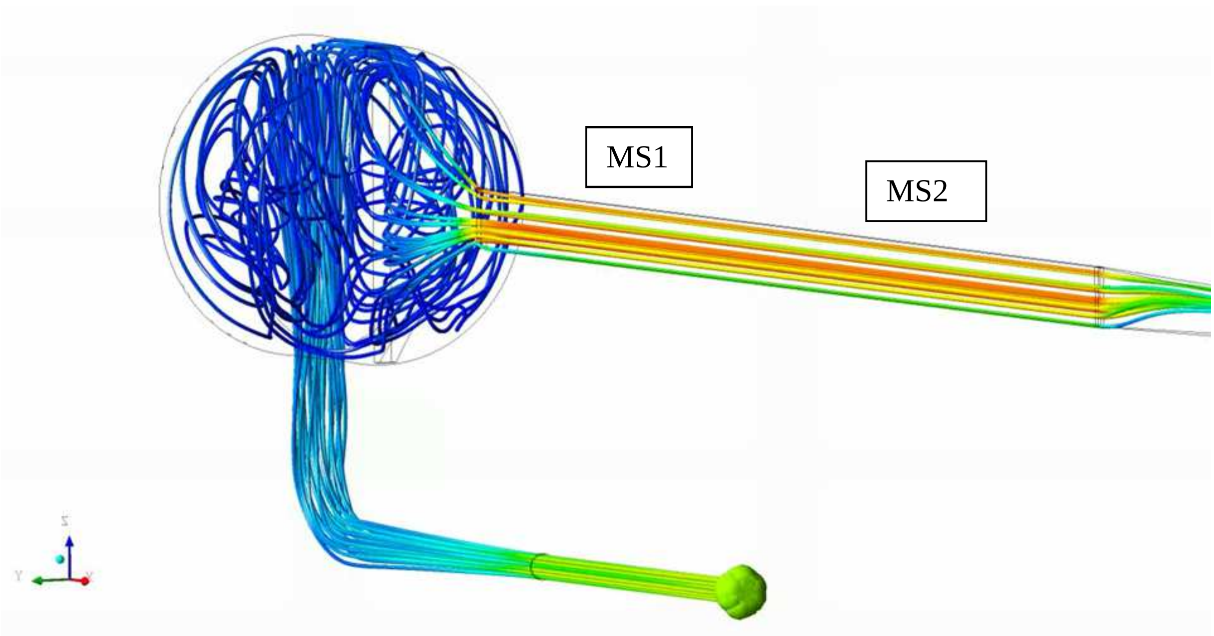

Fig.9: General flow field in the friction tunnel

The calculated pressure in the positions PP1 to PP12 (see Fig.10) gives a hint for the actual friction measurement of the smooth plate and the expected results. 20 additional control probes were applied to check for plausibility.

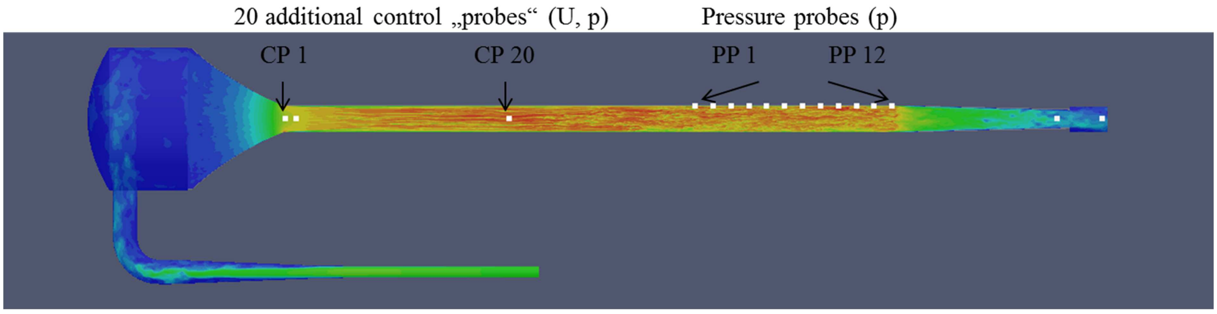

Fig.10: Pressure situation at the positions of probe points (PP1 to PP12 are located at the positions of the actual pressure sensors)

4. Friction presentation

Usually, the friction coefficient is presented over the Reynolds number. For the friction tunnel it is consequentially to present the friction coefficient over the Reynolds number of a pipe flow. In case of ship applications or other applications the Reynolds number of a flow around a body (e.g. plate) is of interest. The exact correspondence between the Reynolds number in a pipe flow and a flow around a body (e.g. flat plate) is generally unknown.

The SVA has experimentally determined a reference length for the determination of Reynolds number for an equivalent flow around a flat plate of 0.28 m. This was be done by extensive comparisons with measurements for a flat smooth plate. Another possibility consists for structured surfaces by a presentation over the S+ value, *Schlichting and Gersten (2006)*. The S+ value presents the dimensionless characteristic ‘length’ for one structure element (e.g. the riblet distance).

5. Examples of friction measurements with different surfaces

The test results for different surfaces are presented in Figs.11 to 14. The diagrams show the friction characteristics of the mean values of the three runs in dependency of the Reynolds number *Re*. Each diagram contains the measured friction characteristics together with the friction characteristic of the theoretical curves of smooth plates based on *Schlichting and Gersten (2006)* (green curve) and ITTC 1957 (blue curve).

Fig.11 presents the friction curve for a polished brass plate which can be assumed as technically smooth. Its friction characteristic is in line with the ITTC 1957 curve.

Fig.12 shows the friction characteristic of a plate on which a riblet structure was applied. For a certain Reynolds number range the friction is reduced in comparison to the smooth plate. For higher Reynolds numbers the friction is similar to that of a sand roughness of equivalent height. In chapter 4 it was remarked that for structured surfaces a presentation over the S+ value is more appropriate. An example is shown in Fig.16 for the same riblet structure as difference to the smooth plate determined by Schlichting/Gersten.

The friction characteristic of a ‘simple’ version of the before tested ‘perfect’ riblets are shown in Fig.13. It was realised by grinding a brass plate with sandpaper in flow direction. Microscopic photos of the surfaces show the differences between both structures (see Fig.15). Although the maximum drag reduction is not as high as for the ‘perfect’ riblets the ‘simple’ riblets have a lower friction than the smooth plate over a wider Reynolds number range than the ‘perfect’ riblets. A big advantage is its simple application in comparison to a ‘perfect’ riblet structure.

For the last example the antifouling spray ‘Biotard’ was investigated. Besides its antifouling properties which were proven in *Schulze and Barkmann (2010)* it also shows a slight drag reduction in comparison to the smooth plate over a wide Reynolds number range.

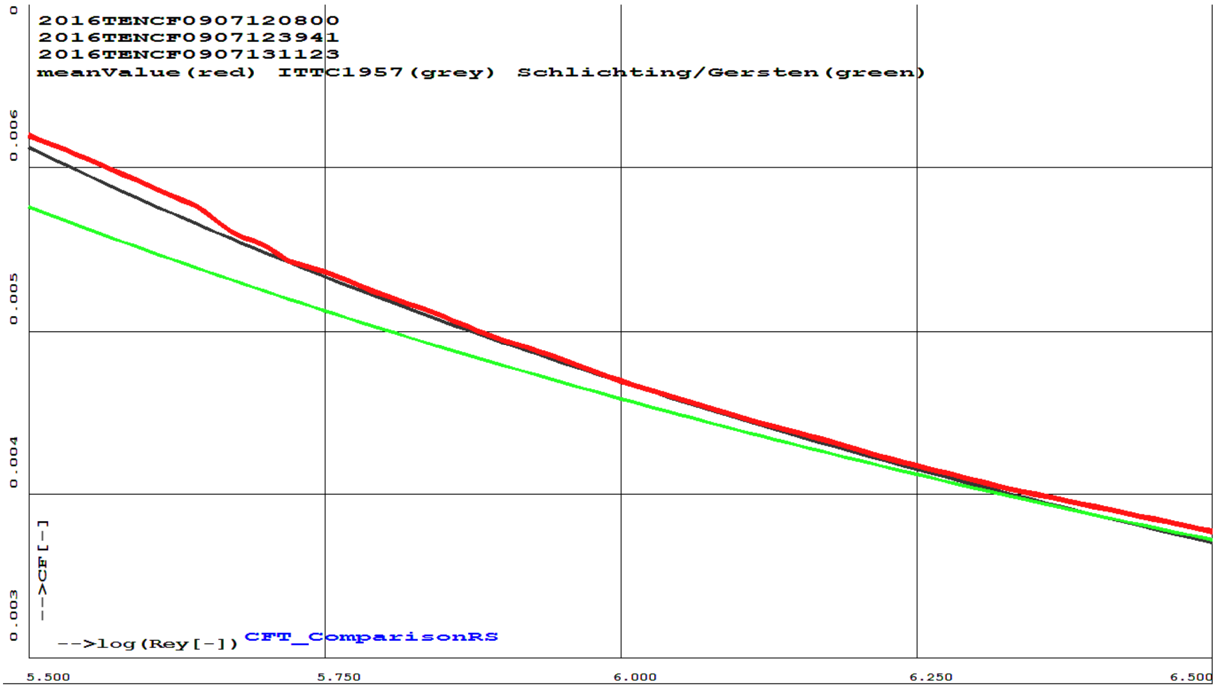

Fig.11: Friction characteristic of a technically smooth plate

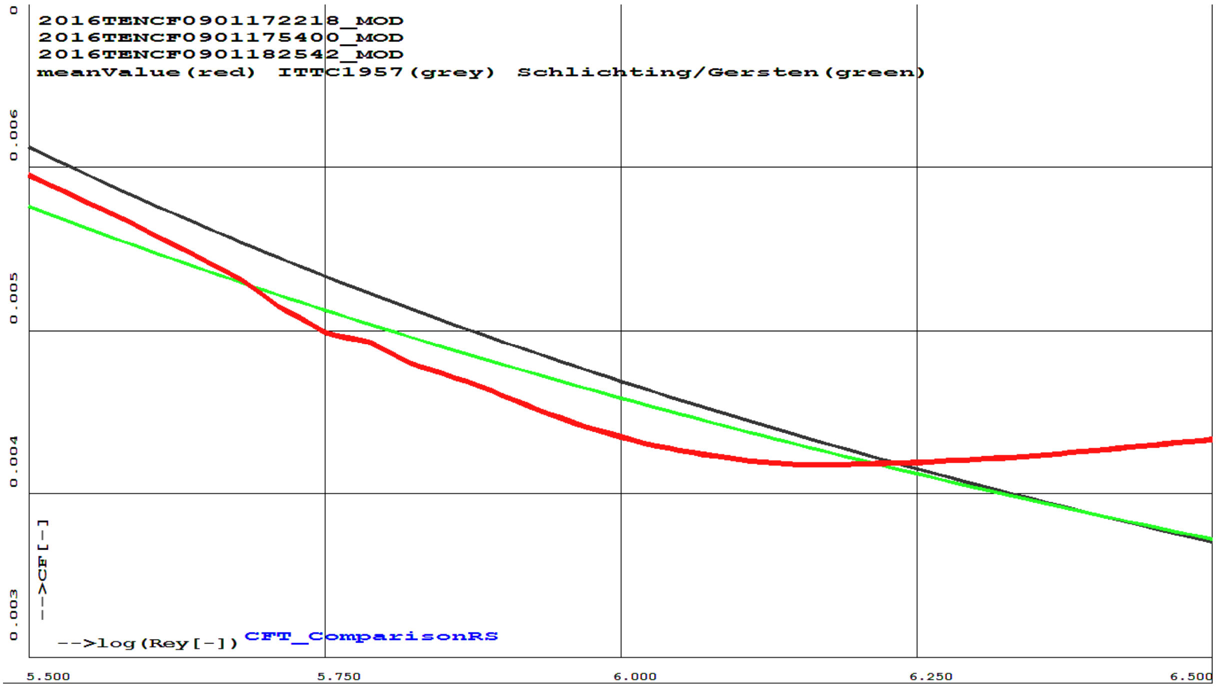

Fig.12: Friction characteristic of a plate with riblet structures

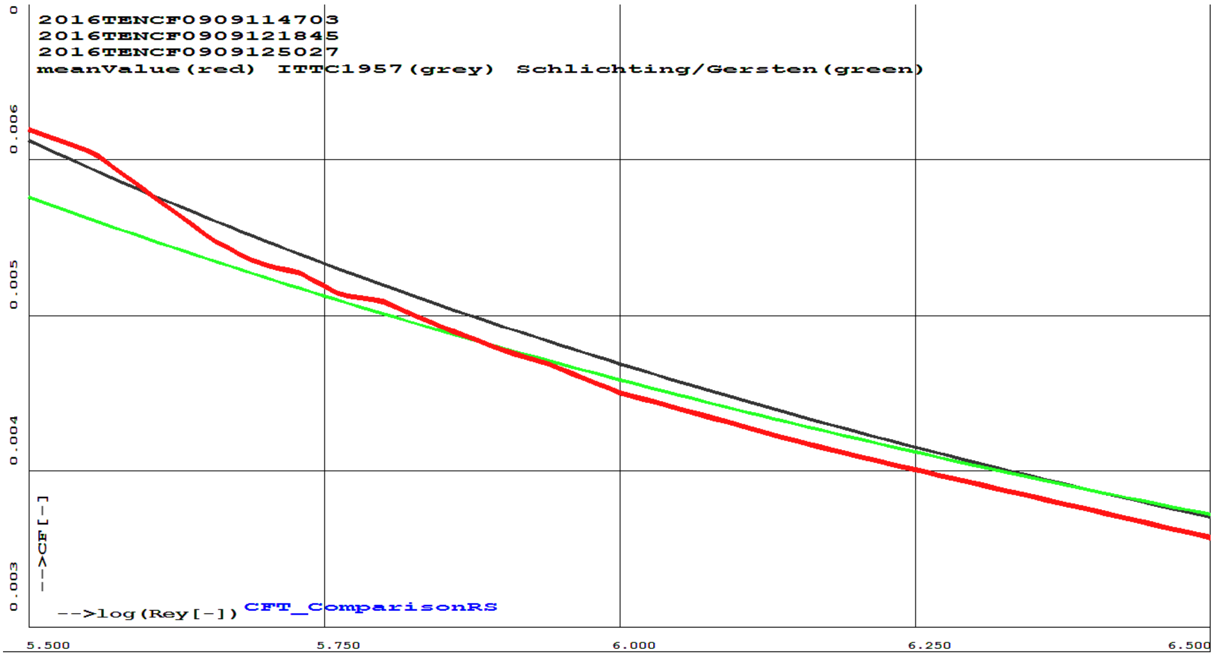

Fig.13: Friction characteristic of a plate grinded longitudinal sandpaper (‘simple’ riblets)

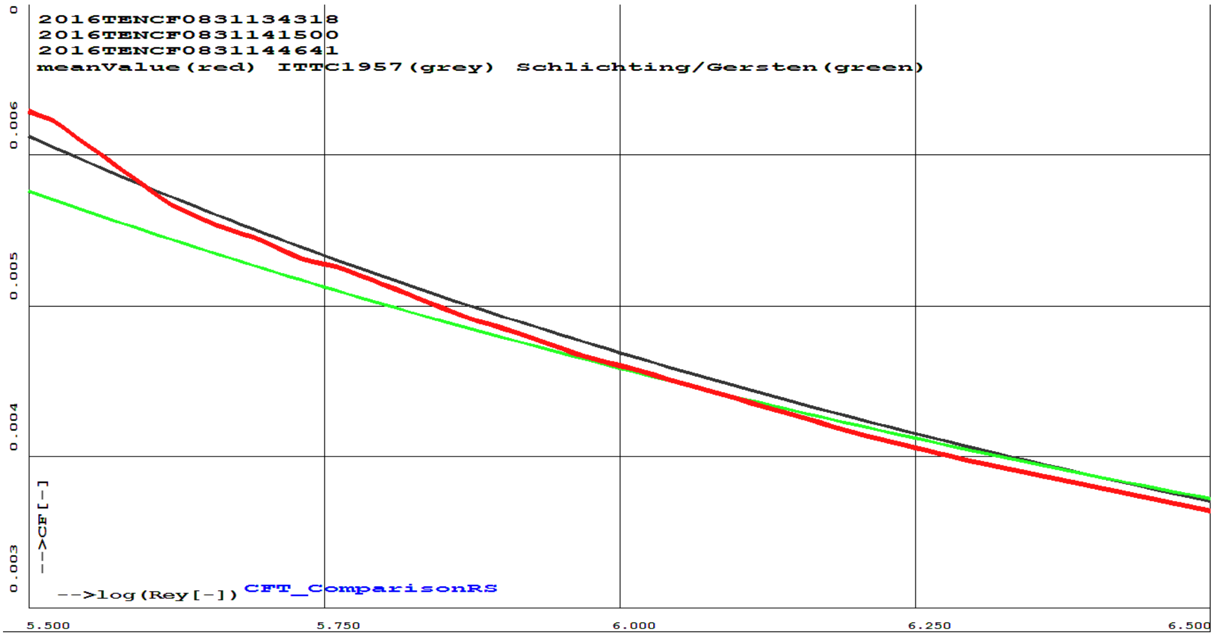

Fig.14: Friction characteristic of a plate coated with the antifouling spray ‘Biotard’

a) 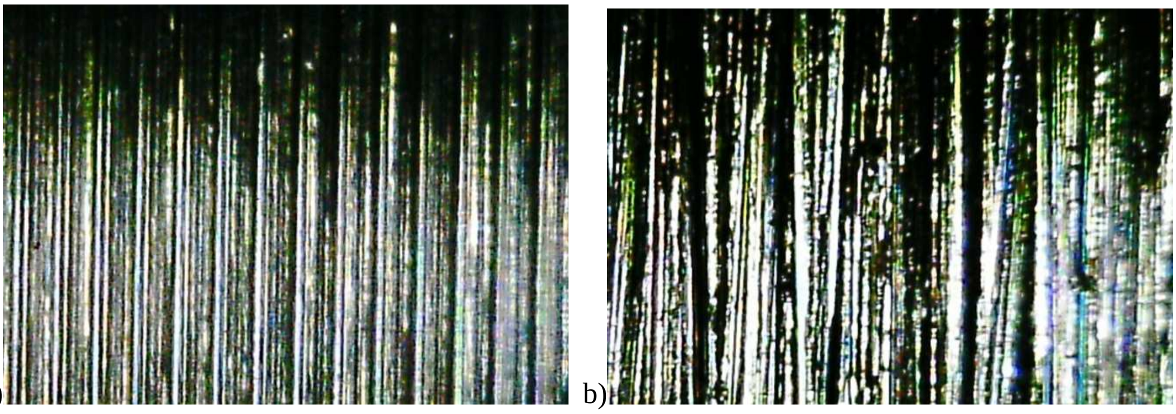 b)

Fig.15: Microscopic photos of the a) ‘perfect’ riblet structure and the b) ‘simple’ riblet structure made

by sandpaper and a belt grinder

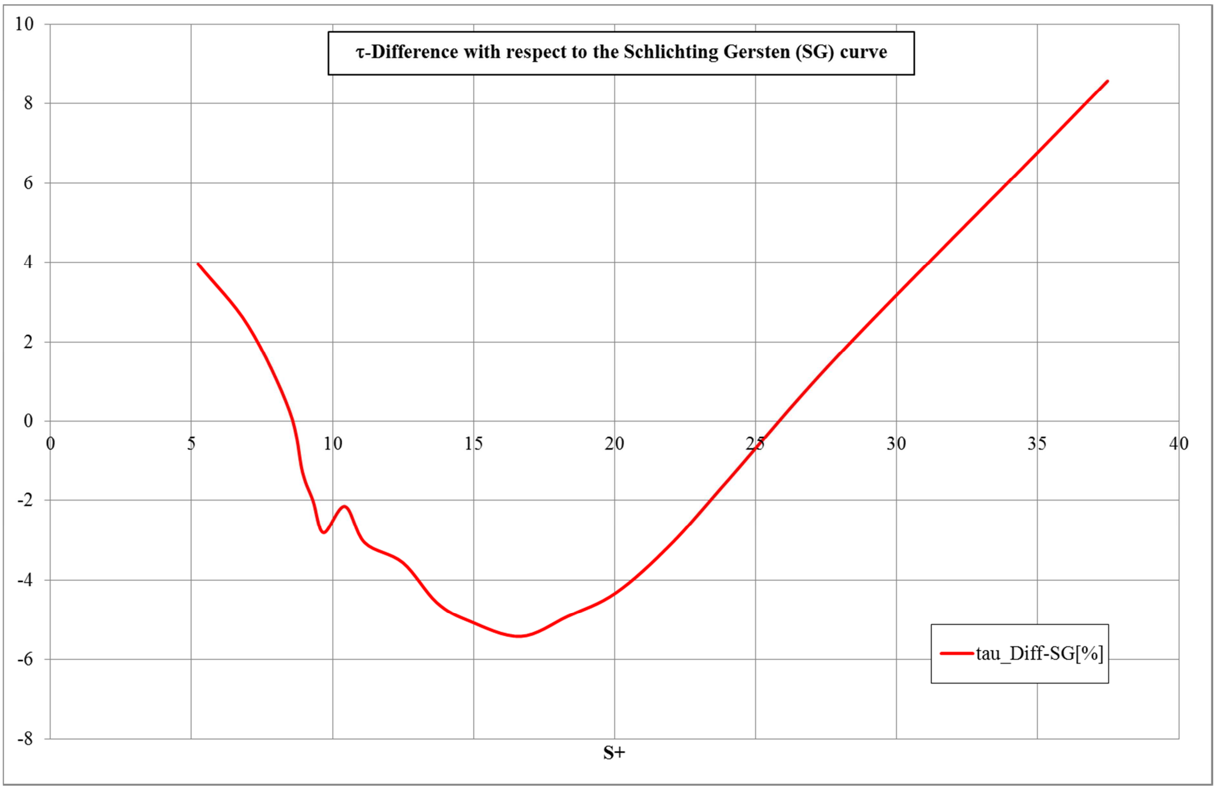

Fig.16: Friction reduction of the riblet structure displayed over S+ in comparison to the smooth plate determined by Schlichting/Gersten (corresponds to Fig.12)

6. Conclusion

The friction tunnel of the SVAtech provides reliable and quick friction measurements of different surfaces. Several coatings and surface structures were investigated and compared to the smooth plate. The field of application is wide.

References

SCHLICHTING, H.; GERSTEN, K. (2006), *Grenzschichttheorie*, Springer-Verlag

JUNGLAS, P. (2009), *Strömungslehre 2*, FHWT, Private Fachhochschule für Wirtschaft und Technik, http://peter-junglas.de/fh/vorlesungen/skripte/stroemungslehre2.pdf

STINZING, H.-D. (1992), *Entwicklung eines praktikablen Verfahrens zur Bestimmung des Rauhigkeitswiderstandes von Schiffen*, FDS-Bericht 240, Hamburg

SCHULZE, R. (2010), *Umrüstung des Rauhigkeitsmessstandes auf eine elektronische Messkette und Auswerteprogramm CFmeasRS zur Bestimmung des Reibungsbeiwertes von ebenen Platten*, Bericht 3649, SVA Potsdam

SCHULZE, R., BARKMANN, U. (2010), *Bestimmung der Reibungsbeiwerte für das Antifouling Produkt BIOTARD*, Bericht 3646, SVA Potsdam

The Big Data Concept in a Performance Monitoring Perspective

Bjarte Lund, Kyma a.s, Bergen/Norway**,** bl@kyma.no
Carlos Gonzalez, Kyma a.s, Bergen/Norway**,** cg@kyma.no

Abstract

The purpose of the ISO 19030 is to define a standardized and systematic method to measure and evaluate hull and propeller performance from a long-term perspective. One of the key factors when operating a modern fleet of vessels is tracking the marine growth. To maintain an optimum hydrodynamic hull and propeller performance requires that the ship owner establishes a system to continuously evaluate the status of the vessel's underwater surfaces and, whenever necessary, clean the hull and/or propeller. A fully automated Ship Performance Monitoring (SPM) system provides a very good foundation (or decision-making tool) for staying on top of this ongoing problem of marine growth. But once an effective system is in place and functioning well, the other factors that will contribute to increased efficiency must be considered. A SPM system meets all the requirements of the 19030 standard and has, at the same time, the additional features needed to use the concept of Big Data to further optimize overall performance, both at the vessel and fleet level. A SPM system is, in short, characterized by "high frequency" real-time data collection of as many logging parameters as possible. The challenge with the Big Data concept is, however, to convert this huge amount of real-time data into Smart Data. This paper will give some practical examples of how a fully automated SPM system can utilize the Big Data concept to further improve the overall vessel performance beyond the "normal" problems of keeping the hull fouling at a minimum. With a real-time data collection system, it is possible to continuously evaluate and analyse the Vessel performance and then take actions on-the-fly.

1. Introduction

The most common and cost-effective way of transporting goods between the continents are on the oceans with merchant vessels, but even though it seems to be the most cost effective way, it does not mean that it is still worthwhile and highly preferred to optimize the transportation process even further. Based on many different studies and research programs it has been shown that individual and sometimes independent details results in better fuel economy and a more optimized voyage.

This is a very interesting topic and it is highly relevant to investigate this field more closely, and especially in these times when the margins are becoming smaller.

By doing a quick search on the internet, you can easily find a lot of companies that advertise that they have a product with a good solution to reduce the fuel consumption, and hence lower the cost. This can for example be demonstrated by offering a new 'perfect' hull paint, a new hull design with bulbous bow, a better engine or propulsion system, or it can be simply software tools to optimize the voyage. It seems to be a potential in each of these products to save more fuel, and the obvious question would probably be how much fuel you could save altogether if you implement most of these solutions all together?

That is where Big Data analysis and a SPM system really comes together perfectly to give a whole new tool to analyze and evaluate the overall performance of a vessel. It is not before you join together all the possible parameters on a vessel into one big 'ocean/cloud' of data, it will be possible to put together all the pieces of the puzzle. With the help of statistical tools and technical knowledge, it is possible to connect data together which will give you answers you didn't even know how to ask for.
In some cases it could even be that by analyzing the online data it is possible to see connections

between the different data parameters which can explain why the vessel suddenly got a better performance. It could be that we did not even realize it gave a better efficiency, because we simply did not measure it, and therefore were unable to take advantage of this possible 'x-factor'.

Based on analysis of all relevant data it has been shown that for example one crew could run the vessel more efficient than the next. Or another example has clearly shown that the young Captain's used more fuel than the older and more experienced Captains. Empirical data have also shown that a certain draft/trim combination gave a much better speed than expected (even though this was not predicted through the design tests).

Big Data analysis seems to find new areas to be implemented in every day, and the concept seems even to have revolutionized the political election campaigns by being maybe the little extra advantage that tipped the voters in one direction. It is indications that this concept was used successfully both for the BREXIT campaign and the US elections. One analyzing company utilized the Big Data advantage by analyzing the internet behavior of the target groups and by that was able to give a much more precise information-package to this group and hence probably got a lot more voters to decide in favor of one side. The typical profile they made was to analyze for example the number of 'Likes' on Facebook, and combining this with the information for what kind of search words they used, *Grassegger and Krogerus (2017).*

In the last couple of years, it has become normal that the internet providers tailored the commercials based on your internet behavior. When you for example consider to buy a new refrigerator and you do a quick search on the net to see what's available, it is quite convenient that when you later check Facebook, you see, by coincidence, an ad for a new fancy refrigerator on your personal wall.

Technically speaking, this method could in theory be implemented to enhance the performance of the vessel. You could imagine that the behavior of the crew could be analyzed, and based on this they could get help/hints on how to improve their job. Going back to the case with the young Captain's which seems to be a little too hard on the power throttle, it could in theory pop up information on their computer that they should try to focus extra on fuel consumption, or it could be a good indication for the vessel managers to invite them to an extra training course, to teach them how to accelerate more optimized.

If you look to the nature, it can be shown that the overall propulsion efficiency of a dolphin seems to even defy the laws of nature with the impressive speed and super strength they possess. Many scientists have tried to find the answers to these superior capabilities of the dolphins. *Fish (2006)* concludes that the two most significant reasons for the super capabilities are the streamlined body shape and the specific behavioral mechanisms. The perfect hydrodynamic drop-shaped body together with a good L/B-ratio and the very efficient thruster, gives a propulsion efficiency which is far better than any conventional vessel is even close to achieve. The fact is that these very favorable skills have been designed by nature through an evolution over thousands of years, and unfortunately it still seems to be a while before scientists break the code and will be able to copy these skills perfectly. *Fish (2006)* predicted that the development of new hull designs, skin mechanics and propulsive systems may take advantage of some of the nature's best swimming mechanisms.

Finally, it is interesting to see that young dolphins often utilize drafting by swimming below the mid-section of the mother, taking advantage of the flow structure behind the mother and by that save up to 60% of the transport energy. Maybe it is a bit radical and probably not very practical to start with convoys again for merchant vessels, but it is a fact that the energy saving potential is quite high by following in the wake of another vessel.

It can of course be argued that a dolphin does not transport any goods (at least not yet, anyway), and that this is probably an unfair and unrealistic comparison, but it still shows that it seems to be a huge potential in optimizing the way we transport goods on the oceans.

Kyma believes that it will be considerable expectations towards the shipping industry to start incorporate Big Data analysis and start utilizing the potential that lies in optimizing all parts of the transportation chain at sea. And in this context it seems obvious that SPM systems have the necessary frequency and volume required to be used in a Big Data concept.

2. Applications of Big Data

There are several definitions for the concept of Big Data, Kyma will in this paper use the definition by *McKinsey (2011)*: 'datasets whose size is beyond the ability of typical database software tools to capture, store, manage, and analyze'.

The Big Data itself imply some challenges that must be considered carefully. Commonly, the challenges are grouped under the 5 V's, *https://en.wikipedia.org/wiki/Big_data*:

- Volume: The quantity of generated and stored data. The size of the data sets determines the value and potential insight- and whether it can actually be considered as Big Data or not.
- Variety: The type and nature of the data. This helps people who analyze the data sets to effectively use the resulting insights.
- Velocity: In this context, it is the speed at which the data is generated and processed (frequency) to meet the demands and challenges that lie in the path of growth and development.
- Variability: Inconsistency of the data sets can hamper the processes to handle and manage it.
- Veracity: The quality of captured data can vary greatly, affecting the possibility to accurate analysis.

It is obvious to understand that Big Data can be a useful and good decision-making tool if it is used correctly, but it is very important to understand that the huge amount of data needs to be handled efficiently to overcome the challenges presented previously.

A common way of presenting a method to utilize the Big Data concept is to use the term Smart Data. This implies that necessary steps are implemented to allow the shipping companies to filter the huge amount of data available, and extract only the significant and 'good data'.

The technical and operations staff needs to have good tools to evaluate, almost in real time, the vessel´s performance continuously and to be able to act on the given information to increase the efficiency continuously.

Focusing on the shipping industry, the Smart Data can be used to cut the operational costs of the vessels by means of further analysis on the most important parameters which will be crucial to increase the vessel performance and therefore, decrease the costs of running the vessels.

Some of these Smart Data analyzing methods that potentially can help the shipping companies to find solutions to increase their performance are for example:

- Vessel´s trim optimization
- Voyage planning
- Speed Optimization
- Emissions control (fuel optimization)
- Energy Management plan
- Charter Party monitoring

2.1 Vessel´s Trim optimization

The trim of a vessel is defined as the difference in draught fore and aft. The trimming of a vessel changes the water flow around the hull and therefore the hull resistance changes. The speed, and consequently the fuel consumption will be affected by the trim. Every vessel type has an optimum trim that differs based on the loading condition and vessel speed. The trim of the vessel can be changed either by shifting ballast water, or it can be optimized by loading the vessel accordingly, http://www.clipper-group.com/fleet-management/coach-performance-management/sustainability-efforts/optimal-trim. Trim optimization is one of the easiest and cheapest methods for vessel performance optimization and fuel consumption reduction.

Trim optimization is applicable for all vessel types and vessel ages. Some vessels have less flexibility regarding trim as, for example, cruise vessels which are designed for passenger comfort and facilities for the passengers. Furthermore, full-body vessels, where the resistance from viscous friction is higher than the wave friction (e.g. tank and bulk) will generally have a smaller potential for optimization by adjusting the trim and similarly the same effect is present for vessels with limited ballast capability and flexibility to store the cargo.

In order to be able to optimize the trim properly it is implied that the vessels needs sensors that can measure the draft and trim accurately. The traditional method for trim optimization has been with a loading computer and a specially dedicated trim optimization tool. This requires extra training in the use of such systems, http://glomeep.imo.org/technology/trim-and-draft-optimization/. There are commonly three ways to get the optimal vessel´s trim on a vessel: model tank tests, computational fluid dynamics (CFD), and sea trials. The accuracy of the above three methods will be affected by the number of samples forming the data sets to be analyzed. With a SPM system enabled, it is possible over time to collect data for all possible draft and trim conditions, and based on the analysis of the collected data, the most favorable conditions can be identified. This information is then presented to the crew in order to guide the crew to set the optimum trim. This database can also be shared and combined among any of the sister vessels, which results in a much quicker build-up of such a complete data set for the whole operational profile.

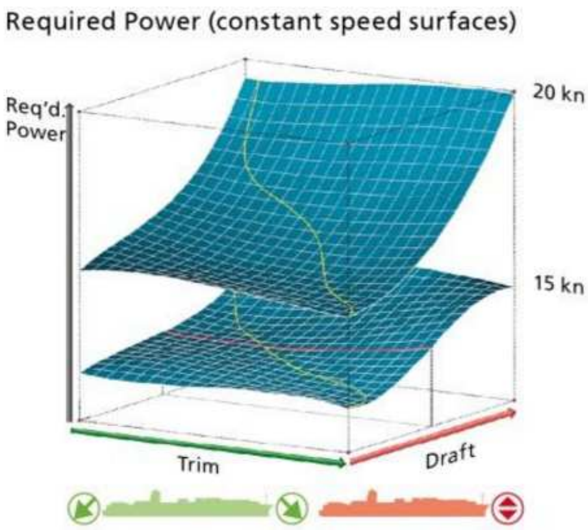

Fig.1: Output of a CFD-based trim software, source: DNV GL

The importance and benefit of the Smart Data to establish the optimal trim is very high. Logging continuously from the on board´s sensors like the: power delivered, vessel´s speed, mean draft, trim and wind, will create a huge database that by means of optimization algorithms will define the optimal trim for each of the different vessel conditions automatically.

2.2 Weather routing (Voyage planning)

Voyage planning is the procedure to develop a best possible route for the vessel. The plan includes the complete route from the start of the voyage when the vessel leaves the dock and harbor area, to the final destination of the voyage, such as approaching the destination, and mooring. This is generally called 'berth to berth'.

Efficient and sustainable sea transport is a key aspect to ensure cost competitive vessel operations. The constant need to increase economic feasibility, energy efficiency and safety while complying with emission regulations motivates further developments and improvements to the process of voyage optimization and weather routing systems.

These systems optimize a voyage based on the available meteorological and oceanographic information and models, taking into account also the vessels characteristics and the proposed routing plan. The quality of the optimum route depends highly on the quality of the model to be used and the algorithms used to find the best solution, *Walther et al. (2017)*..

The Big Data approach to this problem would be to integrate as much of this information as possible into one database, even storing all historical data from previous voyages, and then use this information to calculate the best route. With all of this information available, it will give the Captain the opportunity to extract information of previous voyages on the same route and by combining this with the current weather forecasts, the system can give the best theoretical route known. The vessel can even use the historical data to race against the best in class voyage, and by that try to always have an incentive to find ways of keeping up with the best practice. Any new approaches/events will immediately set a higher standard to reach for.

2.3 Speed Optimization

It is accepted as bad practice for a vessel to sail at full speed to the destination port if that results in the vessel have to wait for the on/off-loading. The RTA, required time of arrival is usually planned before the start of the voyage, but it can also be changed during the voyage, because of for example strikes, change in berth availability, weekend, labour cost, weather, etc. With this in mind, it would be very valuable information to get the latest status of the destination port sent on board as soon as possible. Any delays ashore could give the vessel the opportunity to either slow down or speed up to get to the port at the best possible time-spot. These factors should ideally be an input to the continuous updated voyage plan, so that speed can be adjusted accordingly. Slowing down will give the benefit that you save fuel and reduces emissions. To find the best possible solution to this complex situation, it needs to be a continuous data exchange between the ports and the vessels, and all this information needs to be analyzed and shared among the different roles in this process, *OCIMF (2017)*.

2.4 Emissions control (dual optimization: fuel consumption and vessel’s speed)

For vessels crossing in and out of an Emission Control Area (ECA), the common practice is to run on normal heavy fuel oil (HFO) when the vessel is in international waters, and then switch to a low-sulfur fuel such as marine gas oil (MGO) when running inside the ECA. As the prices of MGO is normally much higher, so it is an option for the vessel manager to order the vessel to go faster outside the ECA, when it is running on the cheaper fuel type, and then when entering the ECA, the vessel can slow down and focus on energy efficiency to save more of the expensive fuel type, *Fagerholt and Psaraftis (2017)*. The continuous data gathering on board the vessel of the position, vessel’s speed, fuel type used and fuel consumption, can also be used to give the crew a pre-warning before the vessel enters the ECA, telling the crew to commence the process to change over to the appropriate fuel type.

2.5 Energy Management action plan

Collecting and continuously evaluating the total energy consumption on board gives the vessel manager an opportunity to develop an operational plan to optimize energy usage on board of the vessels. The energy management plan should state a baseline hotel load, and continuously monitor the energy usage and give an alarm/warning if the total usage goes above this limit.

A G/E optimizing calculator can be used to always make sure that the generator sets are run at the optimum total specific fuel consumption and with the cheapest type of fuel. The plan should also state if it is only allowed to run on a specific maximum number of generator sets. Parameters such as running hours of the auxiliary engines, the power output from each individual generator set and total power output, and the number of generator sets running, will be important inputs in the energy management plan. With a better focus on the required hotel load, it will be possible for the vessel managers and the crews to detect potential areas of improvements to get a lower total required hotel load, and by that contribute to a better energy efficiency on the vessels.

2.6 Charter Party Benchmarking

Within the framework of a Charter Party contract we see quite clearly the differences between a noon report system and a SPM system. A Charter Party (CP) is a contract between the vessel owner and the charterer. The charterer takes over the vessel for either a certain amount of time (time charter) or for a given point-to-point voyage (voyage charter). The CP sets out all the terms upon which the deal is to be done and the freight rate, which is effectively the price of the hire. For a time charter, the charterer will pay for all the running costs of the vessel such as the fuel and insurance. The CP specifies among others a guaranteed fuel consumption (ton/day) for the Vessel. If the Vessel for some reason uses more fuel than the guaranteed fuel consumption, the Charterer is compensated for this. Following situations are just an example of some of the normal clauses used in a Charter Party contract to identify exclusion periods from the fuel warranty calculations:

- Time lost for stops at sea or any other time at sea which is considered a period of Off-Hire under this Charter
- Weather periods with wind more than Beaufort Force 5 for a continuous period of more than six (6) hrs
- Etc.

There are normally several more exclusion situations, but they have intentionally been left out in this case. To monitor continuously the performance status (fuel consumption) according to the Charter Party contract, it is common to have a separate system where the Charter Party allowed fuel consumption benchmark curve are monitored against the actual fuel consumption. A typical plot for a voyage could then look like shown in Fig.2. Fig.2 shows how the actual daily fuel consumption vs speed is compared against the allowed fuel consumption. Each dot indicates the daily fuel consumption in ton/day. The red benchmark curve shows the corresponding contractual conditions in the Charter Party.

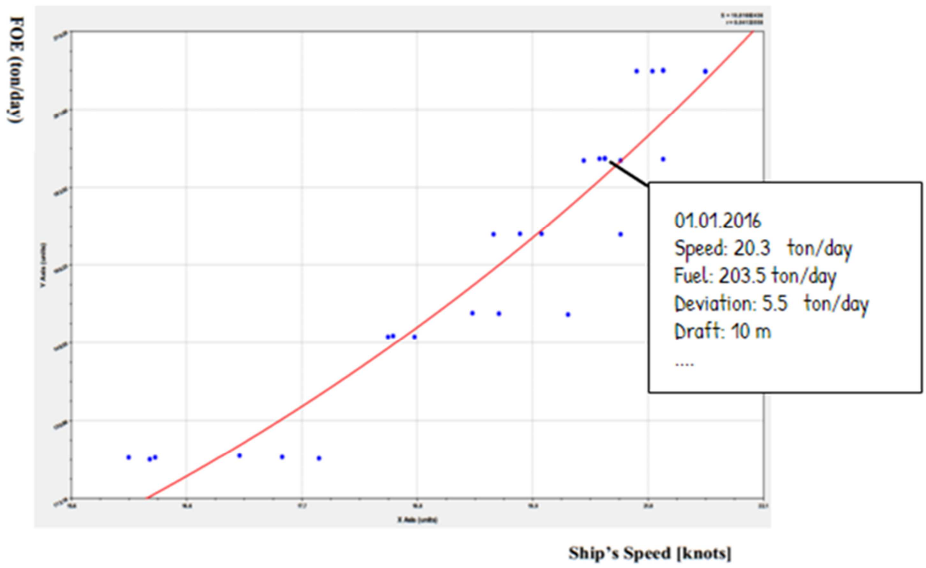

Fig.2: Charter Party benchmark curve, source: Kyma

2.7 Continuous emission measuring

Another area which will probably end up high on the agenda for vessel owners in the near future is the emissions from the vessel. Today it is up to each owner to decide if they want to reduce the emissions, but it seems quite clear that governments are on the verge to enforce taxes and/or emission limits that gives the vessel owners a good incentive to optimize the emissions of NOx, and SO2 and CO2. And that will force the vessel owners to take actions to both install emission cleaning systems and emission sensors to comply with a gradually more strict emissions taxes and reporting regime.

There seems to be established more and more emission controlled areas (ECA's), and Kyma believes that it will be a higher demand for monitoring and reporting of the actual emissions from a vessel, but especially when running inside these areas. With a map overlay in the SPM system it will be possible to give an alert to the chief engineer that the vessel is entering the ECA zone in an hour, and it is about time to start the preparations to change over to the correct type of fuel.

When the vessel enters the zone a emission report will start to be generated and will continue to monitor until the vessel is out of the zone again. The report will show the total emissions from the vessel as long as it has been inside the zone.

3. Practical examples

To give a practical example on how the use of Big Data and the SPM system data can be used to optimize the fuel efficiency, we can consider a vessel planning for a Ballast voyage from A to B.

3.1 Voyage planning

The agreed length of the voyage is set according to the Charter Party contract at for example 1460 nautical miles in this case. With an agreed vessel speed of 13,9 knots, the voyage is estimated to be approximately 105 hours and the required propulsion power is estimated to be ~ 9600 kW (see Fig.3, where the required speed is marked, giving the theoretic power necessary). The required shaft power will give an estimated fuel consumption per day of ~79.3 ton per day.

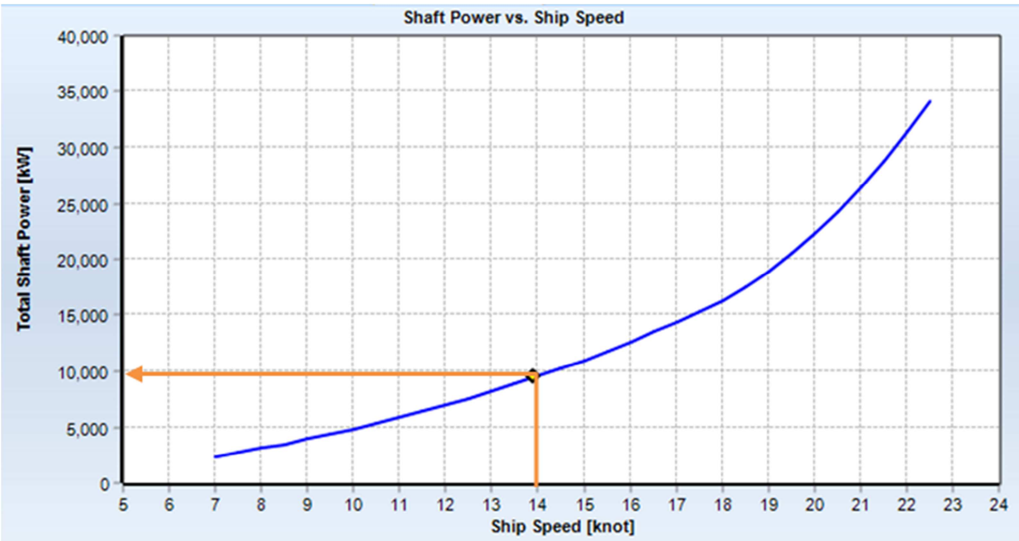

Fig.3: Shaft power vs vessel speed reference curve, source: Kyma

The best optimum route will of course be calculated before the voyage starts. Each way-point will be marked on the electronic chart, and will be used throughout the voyage to track the vessel and control that the vessel keeps the proposed voyage plan

3.2 G/E optimization

The Chief Engineer plans the voyage based on the required parameters from the Charterer. With the current energy management plan he knows how much hotel load he needs, and by entering the other required data for the voyage (like the required shaft power, and speed), he can calculate the optimum settings for the Generator sets. For this voyage, the recommended settings is to run two gen sets (as shown in Fig.4).

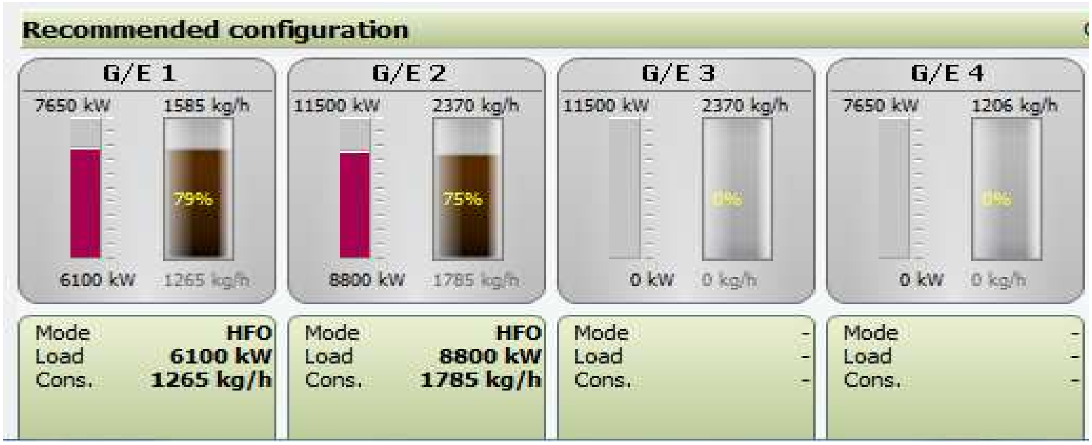

Fig.4: G/E Optimization, recommended configuration, source: Kyma

3.3 Speed optimized voyages

For this voyage it was decided to run the vessel with optimum speed. The ordered speed was set at 13.9 knots, and the Captain was supposed to keep this steady for the complete voyage. The vessel starts moving as instructed, and the following data is recorded for this voyage, Fig.5. The vessel started out a little bit too fast, but gradually adjusted the speed to be within the required speed. The recorded data shows however that the overall speed could have been optimized a bit more because of the variations in the speed. During the voyage, the RTA (Required Time of Arrival) was suddenly delayed, and the Charterer ordered therefore the Vessel to stop for bunkering near the end of the voyage to use the extra time for something useful. This extra bunkering resulted that the voyage took about 65 hours longer than initially planned.

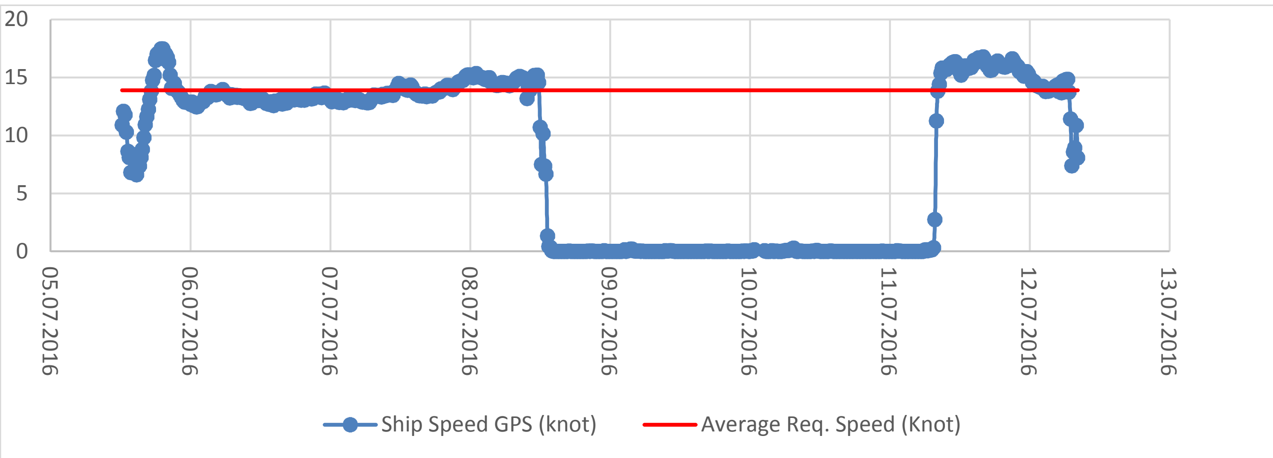

Fig.5: Vessel speed voyage profile, source: Kyma

Table I : Extract of Logbook data

Date	Distance		Port RPM	Stbd RPM	Speed	Port ME Slip	Stbd ME Slip	FO Cons MT	Remarks
	Logged	Obs'd			Knots	%	%	Total HFO	
06.07.2016	320	326	64.2	64.2	13.09	10.89	10.84	96.30	**Dep A 05/07/2016 1206LT**
07.07.2016	3	39	66.3	66.4	13.17	21.63	21.74	24	**64.1 ton, 277 nm**
08.07.2016	337	350	66.3	66.2	14.29	5.73	5.58	85.70	
09.07.2016	6	6	27.3	27.0	5.00	18.92	17.81	13.10	**08/07/2016 1312LT; Vessel anchored at X Anchorage**
10.07.2016	-	-	0.0	0.0	0.00			11.10	**Vessel anchored**
11.07.2016	86	85	65.9	65.9	14.66	-0.23	-0.12	27.00	**Dep anchorage 11/07/2016 06:12LT // 02:12UTC**
12.07.2016	274	273	67.1	67.3	14.92	-1.63	-1.37	62.80	**Arrival B 12/07/2016 0518LT // 0218UTC**
Summary	**1026**	**1079**	**51.0**	**51.0**	**10.7**	**9.2**	**9.1**	**320,0**	

Comments: Vessel adjusted the Speed to meet the ETA as per charterer's instructions. Vessel Bunkered in XX Anchorage.

Table I shows an extract of the collected data from the Logbook for this Voyage. Based on the data in this table, the total voyage time can be summarized as follows:

FAOP:
05/07/2016, 06:36 UTC-time, Local time: 12:06 (vessels clock on GMT + 5:30)
EOSP:
12/07/2016, 02:18 UTC-time, Local time: 05:18 (vessels clock on GMT + 3:00)
This gives a total voyage time of 163.7 hours.
During the voyage, the Captain also observed an exclusion period because of strong wind:
WIND FORCE > B.F. SCALE 5 (20 hours)
05/07/2016, 10:30 UTC-time
06/07/2016, 06:30 UTC-time
Fuel consumption in exclusion period:64.1 Ton, and distance travelled in period: 277 nm.

During the voyage, it was also identified the deviation period for the bunkering:
XX anchorage for Bunkering (65 hours)
08/07/2016, 09:12 UTC-time, Local time: 13:12.
11/07/2016, 02:12 UTC-time, Local time: 06:12.

The total summary of fuel and distance for the voyage from the automatic logging system looks like the data shown in Table II. Based on the Noon reporting and the SPM system we can summarize the two different monitoring methods in Table III, where the data is given according to total time at sea (no filters/exclusions):

Table II: Summary of fuel and distance per day, automatic logging system, source: Kyma

From date	To date	Actual consumption (ton)	Allowed consumption (ton)	Difference (ton)	Distance (nm)
05. Jul, 2016 12:06	06. Jul, 2016 12:00	95.87	73.65	22.22	307.44
06. Jul, 2016 12:00	07. Jul, 2016 12:00	90.33	74.99	15.33	316.52
07. Jul, 2016 12:00	08. Jul, 2016 12:00	83.42	83.30	0.12	345.20
08. Jul, 2016 12:00	09. Jul, 2016 12:00	13.62	15.64	-2.02	11.54
09. Jul, 2016 12:00	10. Jul, 2016 12:00	10.71	13.08	-2.37	0.54
10. Jul, 2016 12:00	11. Jul, 2016 12:00	21.61	27.02	-5.41	62.74
11. Jul, 2016 12:00	12. Jul, 2016 08:18	69.34	74.89	-5.55	303.70
Summary		384.90	362.57	22.33	1347.67

Table III: Comparison Noon report vs online SPM, no filters

	Noon report	SPM
Actual fuel consumption	384,1 ton	384,5 ton
Allowed consumption	346,85 ton	362,57 ton
Fuel saved (-)/excess (+)	37,25 ton	22,33 ton
Total distance travelled	1303 nm (Log), and 1357 nm (GPS)	1347,67 nm

As you can see from the two reporting systems, the overall data for total distance and fuel are quite similar, and definitely within the expected margin.

3.4 Charter Party Benchmarking

If we now analyse the current voyage show the same voyage as before, but this time we leave out the excluded periods, the differences gets bigger between the two methods. And this is the results for the plot for Fuel Consumption (Ton/day) against vessel Speed GPS (knots) for the current period when comparing against the charter party benchmark, included the exclusion and deviation period, Fig.6. Table IV is the corresponding summary table for each of the valid points marked on the plot.

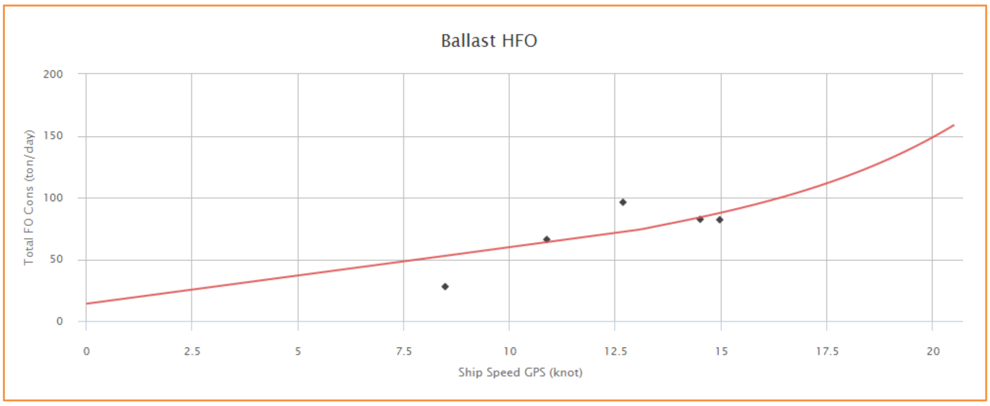

Fig.6: Charter Party benchmark results, source: Kyma

Table IV: Summary of the included time periods, source: Kyma

Summary | Charter party data

From date	To date	Total FO Cons Deviation (ton/day)	Ship Speed GPS (knot)	Total FO Cons (ton/day)	Slip Port (%)	Slip Stbd (%)	Wind Speed Abs. (knot)	Included time (hours)	Excluded time (hours)	Excluded data
05. Jul, 2016 12:06	06. Jul, 2016 12:00	**24.45**	12.69	96.20	28.46	28.48	22.58	18.50	5.50	⚠
06. Jul, 2016 12:00	07. Jul, 2016 12:00	**No data**	No data	No data	No data	No data	No data	0.00	24.00	⚠
07. Jul, 2016 12:00	08. Jul, 2016 12:00	**-1.69**	14.50	82.32	1.88	1.28	10.39	19.75	4.25	⚠
08. Jul, 2016 12:00	09. Jul, 2016 12:00	**-18.56**	8.47	27.92	-37.91	-24.20	4.14	1.25	22.75	⚠
09. Jul, 2016 12:00	10. Jul, 2016 12:00	**No data**	No data	No data	No data	No data	No data	0.00	22.50	⚠
10. Jul, 2016 12:00	11. Jul, 2016 12:00	**5.29**	10.90	66.13	2.45	-3.56	10.45	5.75	18.25	⚠
11. Jul, 2016 12:00	12. Jul, 2016 08:18	**-5.54**	14.96	81.98	-6.27	-12.88	14.97	20.30	0.00	
Summary								**65.55**	**97.25**	

And finally to calculate the overall difference in fuel consumption against the chartered benchmark level from the CP, we get the Table V summarizing per day and total.

Table 1: Summary of Charter Party results, with exclusion filters, source: Kyma

Summary | **Charter party data**

From date	To date	Actual consumption (ton)	Allowed consumption (ton)	Difference (ton)	Distance (nm)
05. Jul, 2016 12:06	06. Jul, 2016 12:00	74.15	56.41	17.75	234.69
06. Jul, 2016 12:00	07. Jul, 2016 12:00	0.00	0.00	0.00	0.00
07. Jul, 2016 12:00	08. Jul, 2016 12:00	67.74	69.23	-1.49	286.32
08. Jul, 2016 12:00	09. Jul, 2016 12:00	1.45	2.42	-0.97	10.59
09. Jul, 2016 12:00	10. Jul, 2016 12:00	0.00	0.00	0.00	0.00
10. Jul, 2016 12:00	11. Jul, 2016 12:00	15.84	16.38	-0.53	62.65
11. Jul, 2016 12:00	12. Jul, 2016 08:18	69.34	74.89	-5.55	303.70
Summary		**228.53**	**219.32**	**9.21**	**897.95**

Table 2: Comparison Noon report vs online SPM , with filters, source: Kyma a.s

	Noon report	SPM
Actual fuel consumption	320,00 ton	228,53 ton
Allowed consumption	259,97 ton	219,32 ton
Fuel saved (-)/excess (+)	60.03 ton	9,21 ton
Total "allowed" distance travelled	1026 nm	897,95 nm

Based on the Noon reporting and the SPM system we get therefore a new result, Table VI. The data from the Noon report and the data from the logging system show different results. With the Noon report we see that it is an overconsumption of ~60 ton and with the automatic logging system we get an overconsumption of only ~9 ton. So the difference of the two methods is around 51 ton of fuel for this short voyage. The difference between the two methods in this case is basically because of the difference in the exclusion period for the wind force.

It can be shown that the exclusion period recorded, when you set the filters according to the exact definition from the charter party (wind force above 21 knots continuous for at least 8 hours) the system records this to be around 34 hours, in comparison to the logbook which states "only" 20 hours.

It is of course very difficult for a person to evaluate just by observation if and when the wind is stronger than a specific wind condition. That is why the automatic logging will always give a much more accurate result than any human observation. Actually, the charter party conditions in this case seems in fact impossible to monitor with a conventional Noon reporting system, since the conditions are so specific (Wind Force > BF 5 for 8 hours continuously). The automatic logging system however shows quite clearly that the wind is very stable above the threshold value of 21 knots for complete exclusion period, and it doesn't fall below until the wind gradually decreases on Thursday the 7th July in the afternoon which gives a total exclusion period of 34 hours. See the actual logging history below of the wind speed in that period:

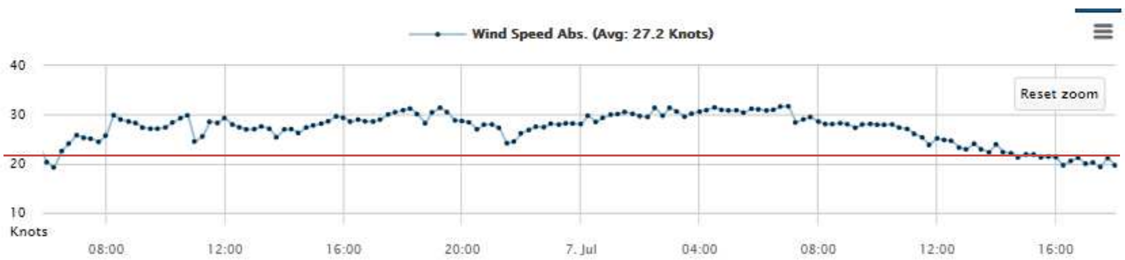

Wind limit @ BF 5

Fig.7: Wind force profile, source: Kyma

3.5 Automatic logging vs manually logged data

When observing the different methods of logging data (Noon reports vs SPM system), there are some important observations to be noted: The traditional way of settling the warranted fuel consumption for a voyage is to use the collected historical data from the Noon reports. Based on the total fuel consumption and an agreed distance, the key average results are calculated. The current case study of a specific voyage shows that the automatic data can be used as a good alternative to the traditional method, and in probably most cases the SPM system will give a much more accurate result than a manual Noon reporting system can provide. With a SPM system, it is possible to have a much closer day-to-day control of the performance against the Charter Party module.

4. Conclusion

This paper has tried to show how a SPM system can be used to evaluate the vessel performance status of a vessel from a Big Data perspective. The paper has identified a few areas where the Big Data concept will be a very useful tool. These situations are highlighted and it is shown how the practical use could be done.

There are a number of applications where Big Data can be used to optimize the performance of a vessel. The common challenge with Big Data sets for the shipping industry has traditionally been the limitations in transfer of data to shore, and vice versa. But in the last couple of years, the technology development on communication solution at sea have been significant, so today it doesn't seem that the file sizes are such a big issue anymore.

The identified applications in this paper are just a few examples of how it is possible to combine a SPM system with statistical analysis to optimize the vessel performance. The paper identifies for example trim optimization, weather routing, fuel consumption optimization, continuous Charter Party benchmarking, etc as areas where high frequency data can be used to draw conclusions on how to continuously optimize the vessel performance.

Kyma also foresee that especially with good sensors for emissions online monitoring, it will be possible to optimize the emission rate based on the input from the sensor.

The paper gives a few practical examples where the data from the SPM system are analyzed. It seems obvious in these situations that a high monitoring frequency is necessary. The SPM system is therefore the preferred solution for those applications because of the frequency and volume of available data.

The paper shows how the planning of and execution of a normal voyage can be optimized by monitoring and analyzing the data continuously. The voyage example shows a very normal situation for some vessels, where the arrival situation changes after the voyage have started. Then it is important to be able to re-calculate the route and come up with a new plan on the go.

The paper shows clearly the differences between a noon reporting system and the SPM when it comes to monitor the wind force. Actually, the normal charter party condition with wind above BF 5 for x hours is in fact impossible to monitor with a conventional Noon reporting system. The SPM system is superior to the noon reporting system when the frequency and density of data must be high. This is for example for applications to optimize the trim, weather routing, slip, emission monitoring and specific fuel rate. But in some cases, however, where the time horizon is large enough, it seems to be fairly good correlation between noon reporting and a SPM system.

The possibility to collect and analyze the data from the vessels continuously will be an important factor for evaluating how efficient the operation of the fleet can be. The investments in new technologies which allow the generation and analysis of Big Data will result in benefits to the companies, as it has been shown previously with several international studies, *McKinsey (2011)*.

References

FAGERHOLT, K.; PSARAFTIS, H. (2017), *On two speed optimization problems for ships that sail in and out of emission control areas*, Transportation Research Part D: Transport and Environment: http://www.sciencedirect.com/science/article/pii/S1361920915000802

FISH, F. E. (2006), *The myth and reality of Gray's paradox: Implication of dolphin drag reduction for technology*, Bioinspiration & Biomimetics 1(2), pp.17-25

GRASSEGGER, H.; KROGERUS, M. (2017), *The data that turned the world upside down*, https://motherboard.vice.com/en_us/article/how-our-likes-helped-trump-win

McKINSEY (2011), *Big Data: The next frontier for innovation, competition, and productivity*, http://www.mckinsey.com/business-functions/digital-mckinsey/our-insights/big-data-the-next-frontier-for-innovation

WALTHER, L.; RIZVANOLLI, A.; WENDEBOURG, M.; JAHN, C. (2017), *Modeling and optimization algorithms in ship weather routing*, Int. J. e-Navigation and Maritime Economy http://www.sciencedirect.com/science/article/pii/S2405535216300043

Development of an Online Ship Performance Monitoring System Dedicated for Biofouling and Anti-Fouling Coating Analysis

Alessandro Carchen, Newcastle University, Newcastle/UK, a.carchen@ncl.ac.uk
Kayvan Pazouki, Newcastle University, Newcastle/UK, kayvan.pazouki@ncl.ac.uk
Mehmet Atlar, Strathclyde University, Glasgow/UK, mehmet.atlar@strath.ac.uk

Abstract

The aim of this paper is to present the development of the first deterministic ship performance monitoring system dedicated to hull micro-fouling and coating analysis. The system aims to derive the impact of hull biofouling on the total powering of a vessel with a known and reasonable level of uncertainty. It uses a deterministic approach to calculate the contribution of every significant external disturbance (e.g. wind, waves). It then corrects the measured performance deriving the added contribution of the pure fouling as difference in powering requirement with that of clean hull condition. The Ship Performance Monitoring System is designed and installed on-board the Newcastle University (UNEW)'s R/V The Princess Royal as an automated platform. Field measurements and analysis results are presented and discussed.

1. Introduction

It is a long-accepted truth that as a ship's hull degrades and particularly because of biofouling growth on its surface, her performance is also subjected to a certain degree of decline, which is regrettably not directly measurable. Simultaneously, a major part of the natural phenomena occurring around a ship also contributes to affect her energy consumption to a certain extend. If therefore the impact of biofouling on a vessel's performance needs to be quantified with useful levels of accuracy, the problem becomes that of isolating it from all the other disturbances, which can be pursued if at least sufficient information is gathered periodically on the operative profile of the vessel, as summarised by the ISO 19030, *ISO (2016)*. The advent of automated high-frequency data logging and integrated ship performance monitoring systems has done nothing but improving this process, opening the path to diverse approaches and analysis methods. In the current framework, one based on the modelling of the physical forces acting on a vessel would be named a deterministic analysis method, which inherits the traditional Naval Architecture perspective.

Fig.1: Newcastle University's Research Vessel

This paper introduces the Ship Performance Monitoring System and deterministic analysis methodology under development at Newcastle University (UNEW), whose Research Vessel *The Princess Royal* is being used as a development platform and test bed. In an attempt to tie the many loose ends originating from the uncertainties within this topic, the performance monitoring method here presented exploits state of the art monitoring equipment and physical relations to specifically derive the effect that biofouling has on the performance of a vessel and the validating or invalidating uncertainty of such assessment. The prototype monitoring system and analysis method will be presented in detail. However, as the database is not completed as yet, the Uncertainty Analysis remains out of the scope of the present paper. These premises being set, the project stands the chance of being the meeting point between theoretical analysis, full-scale validation by means of a non-commercial proprietary vessel and state-of-the-art instrumentation.

2. Methodology

Being here the ultimate scope that of deriving the performance changes forced on a vessel by a fouled hull and propeller, hull resistance would be the target variable to observe. However, since it is not directly measurable, the power-speed relation stands as the closest means of assessment *(ISO (2016))*. If power and speed are measured under equal environmental and operational circumstances, an increase in power demand to move the ship at a same speed through water indicates an efficiency loss in either the propeller, the hull or even both. Unluckily enough, real environmental and operational circumstances alike, may vary even during the course of a single day and hence the performance analyst ought to ascertain that a clear perspective is gained on what the propulsive power in general is being used for, whether to overcome an environmental phenomenon or to match an operational change.

This fact has two major implications:

1. 1.The measured primary parameters of ship speed and power require a correction to some pre-defined standard conditions to exclude the implication of other factors but fouling in the analysis;
2. 2.To identify the state of these conditions, secondary parameters need to be measured as well ISO 19030, whose number is evidently a function of the targeted level of accuracy in the performance estimation.

An automated and reliable performance monitoring system therefore requires a discrete number of sensor for being able to identify the actual circumstances the ship is sailing into. A correction of the observed power-speed relation to a standard reference condition needs then to be fulfilled.

Not dissimilarly from other works of the like of *Orihara et al. (2016), Hasselaar (2007)* etc., the familiar expressions for propeller and hull behaviour are employed. For the sake of clarity of presentation, the method used within the project can be subdivided into the parallel threads and that identify four critical areas of study strictly interrelated one with another. In order of application:

1. Database of ship data (e.g. Propeller Open Water Diagrams, wind coefficients...)
2. Continuous full-scale measurements
3. Correction algorithm
4. Analysis methodology of hull and propeller performance

Although in principle the methodology to apply corrections dictates the number of the measurements to be taken, it allows us to follow the order established above for the sake of clarity.

3. Monitoring system

In 2011 UNEW launched the R/V *The Princess Royal*, a relatively high-speed catamaran, Fig.1, Table I. She was designed in-house with an innovative Deep-V hull form, anti-slamming bulbous bow and propeller stern tunnel to meet the needs driven by increasing marine research, teaching, offshore support and consultancy. This high reach scope compels a great adaptability to multi-purpose tasks ranging from conventional trawling to high-speeds full-scale cavitation observation as reported for example in *Aktas (2015), Atlar et al. (2013), Carchen et al. (2015)*. At present, *The Princess Royal* is committed to a testing campaign of novel antifouling coatings in the framework of the European Project SeaFRONT. Much in the same line as the variety of her tasks, the equipment range is also vast comprising both biology and technology oriented sensors, *Atlar et al. (2013)*.

Table I: R/V main dimensions

Length overall	L_{OA}	18.88 m	Design draft	T	1.80 m
Length b.p.	L_{PP}	16.45 m	Displacement	Δ	46 t
Breadth	B	7.30 m	Type of propellers		FPP

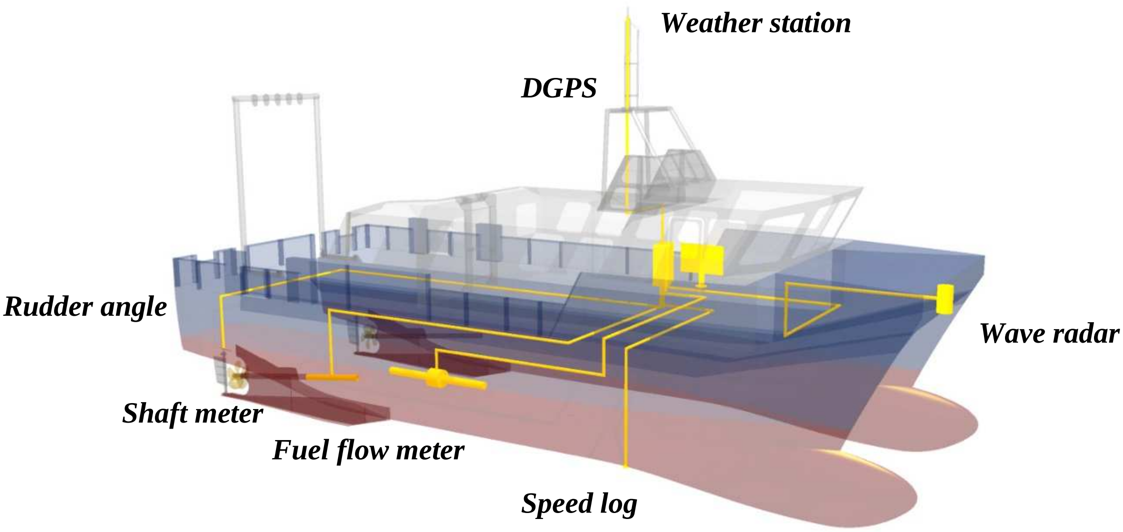

Fig.2: Layout of the Performance Monitoring System installed on the R/V

Fig.2 shows the sensors used for performance monitoring. The Ship Performance Monitoring System installed on *The Princess Royal* comprises:

- <u>DGPS</u>
  Function: Time, Position, Speed Over Ground (SOG), Course Over Ground (COG), Heading
  Location: Mast
  Sampling frequency: 1 Hz
- <u>Doppler Speed log</u>
  Installed during the 2015 Dry-Docking on the inner Portside demi-hull keel close to mid-ship. Doppler speed logs are naturally not affected by the changes in boundary layer, however, because of the Doppler principle on which they are based they are affected by heavy vessel motions, temperature and salinity of the water. The model installed onboard the R/V automatically corrects the measurement for temperature. Salt content is considered constant over the location of operation of the vessel, but clearly for long ranging vessels corrections have to be addressed. Ship motions have to be kept to a minimum

Fig. 3 Location of the Doppler

Fig.4: Locoation of EM speed logs

and generally this stays within the limitations imposed by the ITTC. To limit the motion of the sensor itself, its installation close to midship ensures that the least attainable heave is transferred.
Function: Speed Through Water (STW), Water Depth
Location: Inner Portside hull bottom plating close to midship, Fig.3
Sampling frequency: 1 Hz

- Electro-Magnetic (EM) speed log
  Unlike its counterpart, the EM log is not particularly affected by ship motions, temperature or salinity, but since it measures the speed through water on the hull surface, it is heavily affected by changes in boundary layer. For this reason, it is recommended their foremost installation on the hull, where the boundary layer is still to its minimum. In our experience, a constant drift from the true speed through water has been experienced across the sea trials conducted on the R/V from the dry-dock onwards. As such, the EM log is only used as a comparative measurement system.
  Function: standby Speed Through Water (STW)
  Location: Outer Starboard hull plating, Fig.4
  Sampling frequency: 1 Hz
- Instrumented shafts
  Two instrumented shafts are fitted on the vessel that were built, calibrated and installed by Design Unit of UNEW. They are designed to measure shaft torque, thrust and rate of revolution by means of rugged strain gauges and shaft marker. To increase the thrust measurement resolution, a reduced shaft section has been machined in way of the gauges. An axial parasitic load was observed on both shafts as caused by torsional strain and this is corrected in post processing operations.
  Function: Shaft RPM, Torque, Thrust
  Location: abaft the gearboxes
  Sampling frequency: 2 Hz
- Rudder potentiometer
  Function: Rudder angle
  Location: rudder stock
  Sampling frequency: 1 Hz
- Weather station
  The advanced weather station uses an ultrasonic anemometer on the top of the mast to measure the wind speed in the 3 axis system of the vessel.
  Function: Air speed, direction, temperature and pressure
  Location: Mast top
  Sampling frequency: 0.3 Hz
- Wave radar
  Function: Wave height, heave motion, apparent wave period
  Location: Bow
  Sampling frequency: 2.6 Hz
- Fuel flow meters
  Last generation volume flow meters for supply and return fuel lines provide the net engine fuel consumption over time. If the engines' SFOC is known, brake power can be reversed calculated and assessed against the one obtained from the shaft measurements. However, due confidentiality in the engine data has so far prevented from a complete and reliable comparison.
  Function: Fuel flow measurement (volume)
  Location: Engine rooms
  Sampling frequency: 0.02 Hz

Owing to the principles of the sensors, propeller RPM is generally the most reliable measurement on board together with shaft torque and SOG. Propeller thrust is conversely one of the least reliable measurements due to the structural phenomena related to the axial stress on the dedicated hollow intermediate shafts. Of the above, the only weather and wave data are collected on a separate platform, whilst all the others have been recently implemented in a single monitoring unit. As the wave data is the critical leading to a successful wave calculation, the simple wave radar is unsuited for the purpose. Hind-cast is used instead, considered to be a safer solution as exemplified by *Bos (2016)*.

4. Reference database

In addition to *in situ* measurements, reference data is needed regarding the separate response of the vessel and her propellers to different operating conditions.

- Propeller Open Water characteristics
  Depending on the adopted correction method, this can constitute the most important reference data at hand, as it is the case for the research here presented. Open Water characteristics were obtained by means of tests in the Emerson Cavitation Tunnel of Newcastle University, reported in *Carchen et al. (2015)*.
- Self-propulsion
  The main parameters here needed are the thrust deduction fraction t and the effects of trim and displacement change that may be estimated by means of experimental, computational or semi-empirical approaches. In the present case, t could be estimated by experimental self-propulsion tests conducted at Istanbul Technical University, *Atlar et al. (2013)*. The effect of trim and displacement is here neglected due to the restricted operations of the R/V.
- Direct wind resistance
  In a similar fashion to self-propulsion data, wind coefficients can also be obtained by various means. Nowadays, a large number of databases are published (see *ISO (2015)*), but owing to the unique profile of *The Princess Royal*, they have been obtained after a comparative study of Wind Tunnel Testing, Fig.6, and full-scale CFD simulations in Newcastle University, *Vranakis (2016), Axiotis (2016)*.
- Response function to regular waves
  Possibly one of the most critical issues in performance monitoring, the response to regular waves for a range of wave speeds and directions can be estimated within a reasonable degree of precision only by means of complicated model testing or CFD computations. At Newcastle University the commercial software StarCCM is employed to obtain the response function of the R/V together with conventional head seas model testing. In the very moment, the calculations are being carried out and for this reason the wave correction cannot be included in the analysis as yet.


Fig.5: Model tests in Emerson Cavitation Tunnel


Fig.6: Model tests in Wind Tunnel

5. Normalization to reference conditions

If the change in performance due to biofouling was evaluated directly on measured data, because of the numerous conditions a ship is sailing into the result would clearly be that of a widely scattered set of data. The purpose of a good correction or normalization algorithm at least embraces the reduction of the scatter to a minimum by means of filtering criteria and physical modelling. Conversely, the best normalization procedure equally produces scatter if misused. This implies that care has to be taken in the application of this delicate procedure and that the limits of the used methodology have to be thoroughly understood. Otherwise, no correction would generally be a safer choice. Generally, the principle "lighter correction-better correction" is applicable, the weight of a correction being an inverse function of the filtering limits. This is exemplified by ISO 19030's rather strict wind filtering. Nonetheless, this in return drastically reduces the useful sample size thus weakening the derived statistics. Evidently, the tuning of filtering criteria and applied correction is a balance between the two risks.

In the presented method, the reference condition is set to be that of calm weather, with no wind, no waves, steady state straight motion with rudder amidships and ISA conditions. Corrections are considered for a total resistance increase:

$$\Delta R = R_W + R_{AW} + R_\delta + R_\beta + R_{sal} + R_{dis}$$

- <u>Direct wind resistance</u> R_W
  It is here calculated by:
  $$R_W = 0.5\rho_A[C_X(\psi_{WR}) - C_X(180°)]L_{OA}^2 V_{WR}^2$$
  Where ρ_A is the air density, $C_X(\psi_{WR})$ a longitudinal wind coefficient function of the wind apparent direction, L_{OA} the ship's length overall and V_{WR} the relative wind velocity.
- <u>Added wave resistance</u> R_{AW}
  The calculation of added wave resistance is nothing less than a double-edged sword if ship performance is to be assessed. Discussion about the problematics related with its calculation are out of the scope of the present paper and *Bertram (2012,2016)* can be used as a reference. In general, a least wave correction is to be applied and significant filtering is required for both wave height and bearing. However, light corrections are often a due choice. Added wave resistance in irregular sea waves can be calculated by superposition of the directional wave spectrum and the response function of the added resistance in regular waves.
- The remaining steering resistance R_δ, resistance increase due to drift R_β, resistance increase due to salinity change R_{sal} and resistance increase due to change in displacement R_{dis} are treated where necessary according to the procedures used in the ISO 15016:2015.

The propeller Open Water characteristics form the basis of the normalization here presented, with it being part of the well-known *Taniguchi-Tamura (1966)* method earlier embraced by ITTC and the ISO 15016:2002. Its founding principles are ship speed and propeller torque identity. The reason for choosing this method stems from its being a relatively simple and direct method without sacrificing the accuracy of the calculation.

The familiar torque coefficient is calculated as follows to obtain the propeller working point by entering the Propeller Open Water diagram (torque identity):

$$K_Q = \frac{Q}{\rho n^2 D^5}$$

With Q being the measured torque, ρ the water density, n the propeller rate of revolutions in Hz and D the propeller diameter. The propeller advance coefficient can be expressed and calculated as the polynomial:

$$J = a_0 + a_1 K_Q + a_2 K_Q^2$$

J is defined as common practice by $J = V_A/nD$, V_A being the advance velocity $V_A = V_S(1-w)_Q$ with V_S and w being respectively the ship's speed and the measured effective wake fraction. Thence, the thrust coefficient is calculated:

$$K_{T,Q} = b_0 + b_1 J + b_2 J^2$$

With $K_{T,Q} = \frac{T}{\rho n^2 D^4}$. Note that the thrust coefficient is obtained from K_Q and not from direct calculation. From which the load factor and the total resistance are calculated respectively:

$$\tau = \frac{K_T}{J^2}$$

$$R_T = (1 - t) K_T \rho n^2 D^4$$

With t being the thrust deduction fraction. As the method assumes constant ship speed (or speed identity) the load factor increase caused by ΔR can be calculated as:

$$\Delta\tau = \tau \frac{\Delta R}{R_T}$$

With $\Delta\tau = \tau - \tau_{id}$, τ_{id} being the load factor corrected to reference conditions and from which:

$$J_{id} = \frac{-b_1 \pm \sqrt{b_1^2 - 4(b_1 - \tau_{id}) b_0}}{2b_2}$$

$$n_{id} = \frac{V_S (1 - w)_Q}{J_{id} D}$$

$K_{Q,id}$ is then reversely calculated and the corrected delivered power per shaft is finally expressed as:

$$P_{id} = 2\pi n_{id} Q_{id}$$

A few notes on the above:

1. Provided that the shaft's stern tube is maintained shaft losses are considered constant over time and thus are by necessity included in the relative comparison here under discussion;
2. The corrected power finally derived includes together hull and propeller fouling. Further discussion will be sustained in the next chapter.
3. The effective wake fraction is considered constant between measured and a calm water situation under the condition of small ship motions, drift and manoeuvring.

To keep within the domain of applicability of the aforementioned corrections, a range of filters are applied keeping into account recommendations for sea trials conditions given by *ITTC (2012)*:

1. Trim and displacement should be within 1% and 2% difference from the reference values. This is particularly true for bulbous bow ships where the emergence of the bulb may result in a larger difference than expected. In the case of *The Princess Royal*, the trim and displacement varies but slightly during her normal operation;
2. To avoid the application of shallow water corrections, a minimum water depth below the keel of 20 m is assumed according to ITTC suggestion;
3. Because of the unique motion response that the R/V has to waves, experience taught that a maximum wave height of 0.55 m is allowable, that is well below the ITTC restrictive ranges.
4. Wind limitations are restricted by the above condition roughly corresponding to Beaufort 3 for even a partially developed sea state.

The advantage of using a proprietary research vessel is partly that of being able to dispose of it at leisure or almost. This is permitting a considerable amount of parameters to be checked and kept under control during the development of the system through dedicated sea trials that took place periodically. Many filtering parameters are in such way applied *a priori* through the choice of time, location and course of the trials.

Fig.7 show the results of the calibration trials carried out in June 2015 with measured averages plotted against the normalized values. It should be noted that only wind correction had here to be applied, being a calm sea day with all the other conditions having satisfied. Yet, because of the large frontal area exposed to wind, corrections can be significant. Fig.8 shows instead the operating range of the propeller as visualized on the propeller Open Water Diagram.

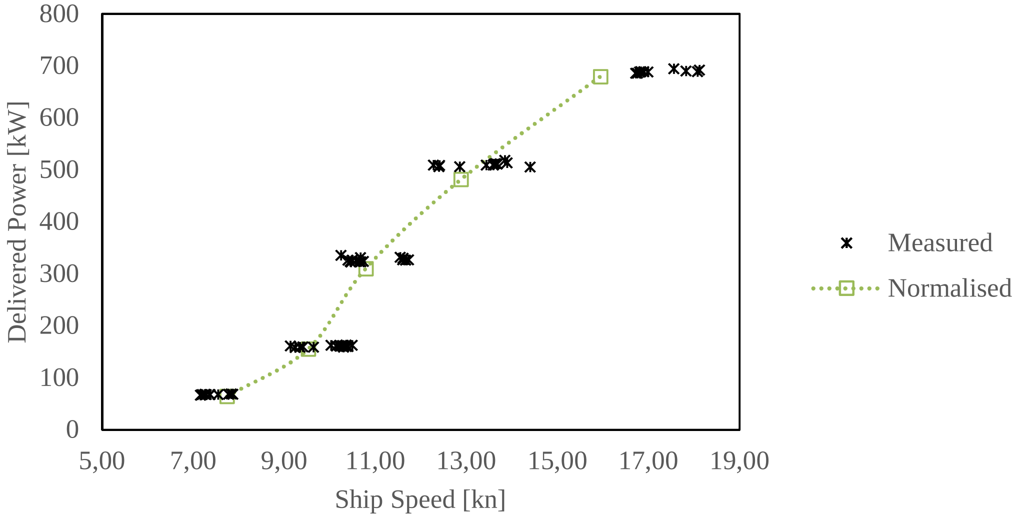

Fig.7: Power-Speed relation of the reference performance

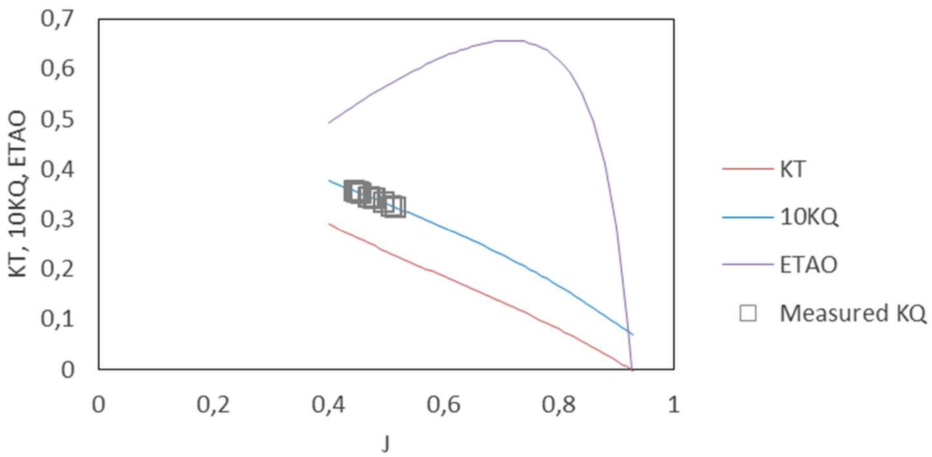

Fig.8: Operating point of the Princess Royal propellers during trials

Due to unfortunate circumstances, uncommonly harsh weather of 2016 winter/spring season first and a drastic change in trim and displacement render such data unsuited for biofouling assessment with subsequent trials, whose new reference is yet to be set. This new challenge is doing nothing but rendering the analysis more inherent with real world application, where by necessity or *force majeur* the operating conditions change and new reference data must be acquired.

6. Analysis method

Depending on the information sought and provided that the normalization procedure is sufficiently correct, the Delivered Power $P_{D,id}$ calculated above can be used in various ways to provide valuable information about its usage. Generally, two of them may be identified as the main ones, the first being related to the mapping of the actual, "instantaneous" power usage, the second to track its change over a long-term period. Clearly, whilst the earlier may be of limited interest to the ship operator, the latter can be used to assess the eventual periodicity of environmental effects and, among them, to track the impact that fouling build-up has. This may be simply done by tracking the timely change of:

$$\Delta P_{D,id} = \frac{P_{D,id}(t) - P_{D,id}(ref)}{P_{D,id}(ref)}$$

Where the normalised power $P_{D,id}(t)$ is at ship life-time t and $P_{D,id}(ref)$ at the reference time, e.g. just after a dry-docking.

However, as power analysis can be at times spurious, the calculated propeller wake fraction can be used alongside to provide further insight. Wake indicators are in use to monitor the hull's condition since as far as 1926, when *Telfer (1926)* devised his service performance method. A ship's wake is generally a "mild" function of ship speed, with this meaning that small changes occur for increasing speeds. At the same time, a change of the inflow would offset the function keeping the trend similar, being it for different ship loading, motions or changes in the boundary layer caused by hull fouling. Fig.9 shows how the measured wake fraction is lower than towing tank test data because of the full-scale heavy loaded condition against the light loaded of the self-propulsion test and the difficulty to scale the wake due to its Reynolds number dependence.

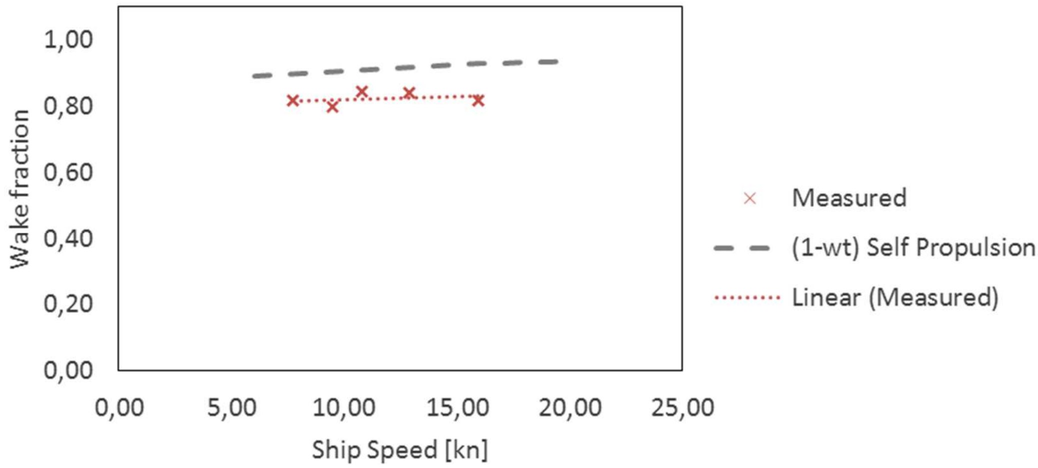

Fig.9: Measured wake fraction from reference speed trials

If the conditions described in Section 5 are met, one could be tempted to assume that a change in wake is directly related to hull fouling. Nevertheless, the wake is calculated based on the propeller OW curves and the measured torque Q (see Section 5), which is regarded as the only propeller parameter affected by propeller fouling, *Mosaad (1986)* - it increases with increased fouling. The wake thus calculated is therefore an apparent effective wake comprising both hull and propeller fouling. Although this combined effect is of the utmost interest to the ship operator, distinguishing hull and propeller fouling can be useful notwithstanding its great challenges. The measured wake can be thus considered as:

$$w_{app} = w_t + \Delta w$$

w_t is the true effective wake and Δw the increment due to propeller fouling. In case no propeller thrust is measured, Δw is by necessity estimated by means of propeller inspections and semi-empirical formulas. When propeller thrust is measured, the method here introduced may be used to evaluate the fouling state of the propeller.

Assuming a fouled propeller, an increase in torque is expected, i.e. an offset in the K_Q curve of the OW diagram. Therefore, an apparent advance coefficient is calculated as:

$$J_{app} = a_0 + a_1 K_Q + a_2 K_Q^2$$

As thrust is affected but negligibly by fouling, the relative advance coefficient can be assumed very close to the true working point of the propeller. Thus,

$$J_t = c_0 + c_1 K_T + c_2 K_T^2$$

Since the ship and propeller speed are constants,

$$\Delta w = \frac{J_t - J_{app}}{J_t} = \frac{(1-w)_t - (1-w)_{app}}{(1-w)_t}$$

The larger Δw, the more the propeller alone is fouled. However, because thrust measurement is not completely reliable, caution needs to be used and it is recommended that observations are made before attempting to draw conclusions. Δw here calculated from a sea trial (13.6.2015) of *The Princess Royal* is quite scattered, Fig.10, and no conclusion seem to be acceptable. Thrust here is the likely culprit and a certain trend can be spotted that may well be due to the parasitic axial load induced by the torsional strain and not captured accurately by the simple linear correction applied in post-processing. When compared to another trial conducted few days earlier (7.6.2015), Δw closely matches, inducing the consideration that the error is inherent in the measurement system. Because both sea trials took place soon after dry-docking, this can be set as the Reference Performance and hence the obtained Δw can be considered the baseline function irrespective of its values.

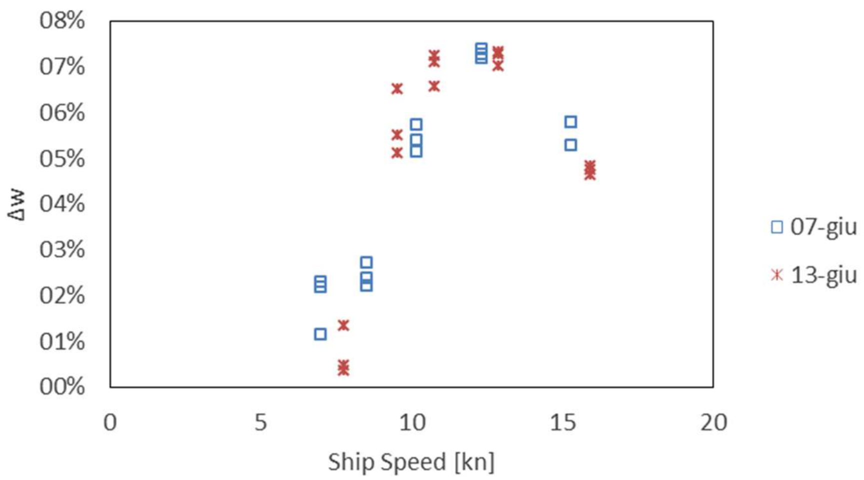

Fig.10: Δw plotted for two different sea trials against ship speed

When assessed over a longer term, Δw and $\Delta w_t = \frac{w_t(t) - w_t(ref)}{w_t(ref)}$ are clearly a more stable way of evaluating and telling apart the fouling state of hull and propeller and more confident conclusion can be drawn. Hopefully, future field measurements will allow this to be better proved.

7. Conclusions

A deterministic approach to Ship Performance Monitoring has been here introduced as being developed on-board Newcastle University's Research Vessel.

- The state-of-the-art equipment and the possibility to complete dedicated sea trials allow a clearer perspective on the implementation of the corrections and better understanding of the needed filtering criteria.
- A reference database is a corner stone in the use of a deterministic approach and this can be at times a challenge particularly when hull and propeller characteristics are not readily available. Quicker and cheaper methods to evaluate the ship response are also sought and future work will explore the possibility of different applications.
- A deterministic normalization has been used and suitable for Service Performance Monitoring

applications. Simple power and wake analysis principles are employed that give a more detailed perspective on hull and propeller fouling state. Uncertainty Analysis is needed to assess the limits of applicability and accuracy of the method, which is object of the future work.

- The greatest advantage of Service Performance Monitoring over conventional Speed Trials is that whilst the latter's aim is to derive absolute results matching with the predicted values, the earlier looks rather at a relative comparison between a reference baseline and an actual measurement. This in turn allows, with the big data we are entrusted nowadays, to generate multiple reference baselines, drastically reducing the need for heavy filtering or corrections for big differences in ship loading condition.

Acknowledgements

This research is sponsored by Stone Marine Propulsion Ltd. The Authors thank SMP Ltd for financial support and supply of NPT propellers for *The Princess Royal*. We would also thank International Paint for their support throughout the SeaFRONT project and supply of measuring equipment.

References

AKTAS, B.; LEIVADAROS, S.; ATLAR, M.; FITZIMMONS, P.; SASAKI, N. (2015) *An experimental approach to measure propeller cavitation noise onboard a research vessel,* 4th Int. Conf. Advanced Model Measurement Technology for the Maritime Industry (AMT'15), Istanbul

ATLAR, M.; AKTAS, B.; SAMPSON, R.; SEO, K.-C.; VIOLA, I.M.; FITZSIMMONS, P.; FETHERSTONHAUGH, C. (2013), *A multi-purpose marine science & technology Research Vessel for full-scale observations and measurements,* 3rd Int. Conf. Advanced Model Measurement Technology for the Maritime Industry (AMT'13)

ATLAR, M.; BASHIR, M.; TURKMEN, S.; YEGINBAYEVA, I.; CARCHEN, A.; POLITIS, G. (2015), *Design, manufacture and operation of a strut system deployed on a research catamaran to collect samples of dynamically grown biofilms in-service,* 4th Int. Conf. Advanced Model Measurement Technology for the Maritime Industry (AMT'15), Istanbul

AXIOTIS, D. (2016), *A CFD analysis for the calculation of wind loading on Newcastle University research vessel,* MSc Theses, Newcastle University

BERTRAM, V. (2012), *Practical Ship Hydrodynamics,* Butterworth & Heinemann, Oxford

BERTRAM, V. (2016), *Added power in waves – Time to stop lying (to ourselves),* 1st HullPIC Conf., Pavone

BOS, M. (2016), *How metocean data can improve accuracy and reliability of vessel performance estimates,* 1st HullPIC Conf., Pavone

CARCHEN, A.; SASAKI, N.; AKTAS, A.; TURKMEN, A.; ATLAR, A. (2015) *Design and review of the new NPT propeller for The Princess Royal,* 4th Int. Conf. Advanced Model Measurement Technology for the Maritime Industry (AMT'15), Istanbul

HASSELAAR, T.W.F. (2007) *An investigation into the development of an advanced ship performance monitoring and analysis system,* PhD Thesis, Newcastle University

ITTC, (2012), *Speed and Power Trials: Part 1-Preparation and Conduct,* Recommended procedure 7.5-04-01-01

ISO (2002), *Ships and marine technology – Guidelines for the assessment of speed and power* *performance by analysis of speed trial data.* ISO15016:2002

ISO (2015), *Ships and marine technology – Guidelines for the assessment of speed and power performance by analysis of speed trial data.* ISO15016:2015

ISO (2016), *Ships and marine technology – Measurement of changes in hull and propeller performance,* ISO 19030:2016 parts 1 to 3

MOSAAD, M.A. (1986), *Marine propeller roughness penalties,* PhD Thesis, Newcastle University

ORIHARA, H.; YOSHIDA, H.; AMAYA, I. (2016), *Evaluation of Full-Scale performance of large merchant ships by means of onboard performance monitoring,* 26th Int. Ocean and Polar Eng. Conf., Rhodes

TANIGUCHI, K.; TAMURA, K., (1966), *On a new method of correction for wind resistance relating to the analysis of speed trial results,* 11th ITTC

TELFER, E.V. (1926), *The practical analysis of merchant ship trials and service performance,* Trans. NECIES 43

VRANAKIS, M. (2016), *An investigation into the wind loadings applied to a Deep-V catamaran using model testing,* MSc Thesis, Newcastle University

Verification of the Effectiveness of Energy Saving Devices

Jan Wienke, DNV GL, Hamburg/Germany, jan.wienke@dnvgl.com

Abstract

This paper gives four examples for the verification of the effectiveness of energy saving devices. In each case the power saving is predicted by model tests. Sometimes, these model tests are already regarded as verification of the gains. Nevertheless, usually sea trials are performed to investigate the prognosis in full-scale. For the given examples the author has performed the measurements during the S/P trials. Analysis of the sea trial results and comparison with the model test results are presented.

1. Introduction

There are three different ways to verify the effectiveness of energy saving devices: Model tests, S/P trials prior and after installation of the Energy Saving Device (ESD) and performance monitoring for a specific period prior and after conversion.

The application of model tests provides results prior the decision to install the ESD. Besides, the comparison of configurations with and without ESD can easily be realized and different drafts can be investigated. Model tests are convenient to optimize the configuration of the ESD.

The performance of S/P trials delivers the most accurate and reliable results when the trials are performed in accordance with relevant standards and for good weather conditions. All measured values have to be taken by a controlled measuring system including measurements of the environmental conditions. In this way corrections for the environmental conditions can be determined; the S/P curve for ideal conditions can be determined and compared for the prior and after installation performance.

The S/P trials prior and after conversion provide results immediately after installation of the ESD. That might be relevant if the decision for a whole series of sister vessels is required. Partly, manufacturer of ESDs offer to install the first device for free if the installation on a series of ships is contracted for the case of a successful proof of the power savings for the first installation.

With a performance monitoring system on board the effectiveness of the ESD can be checked by continuous recording of data during service of the vessel; but the investigated intervals have to contain a sufficient duration to show the effect of the ESD and to average other effects as for example hull fouling or seasonal ship operation conditions. The duration of each interval should be one year, meaning that operational data of the year prior installation and the year after installation have to be analyzed. Hence, results are available not until one year has passed after installation of the ESD.

2. First example: Product tanker with duct

The particulars of the ship are given in Table I. It is a product tanker of 50,000 DWT with a relatively small main engine. Model tests for the ship were performed with and without duct in front of the propeller for a speed range between 11 knots and 16 knots. The tests were performed for design and scantling draft. A constant form factor was applied and the correlation allowance was the same for all tests. For the wake a small additional component was introduced for the tests with the duct to compensate for the thinner boundary layer of the duct. The model tests showed gains in power of around 4% when the duct was installed. Fig.1 gives the S/P curves for both drafts for the tests with duct.

Table I: Ship's characteristics

Type	50,000 DWT Class Product/Chemical Tanker
Length / Breadth	174 m / 32.2 m
MCR	8200 kW @ 99 rpm
Propeller	FPP / 4 blades / diameter 6.6 m
Design draft	
Draft fwd/aft	11.0 m / 11.0 m
Displacement	48748 m³
Block coefficient	0.773
Scantling draft	
Draft fwd/aft	13.0 m / 13.0 m
Displacement	58752 m³
Block coefficient	0.789

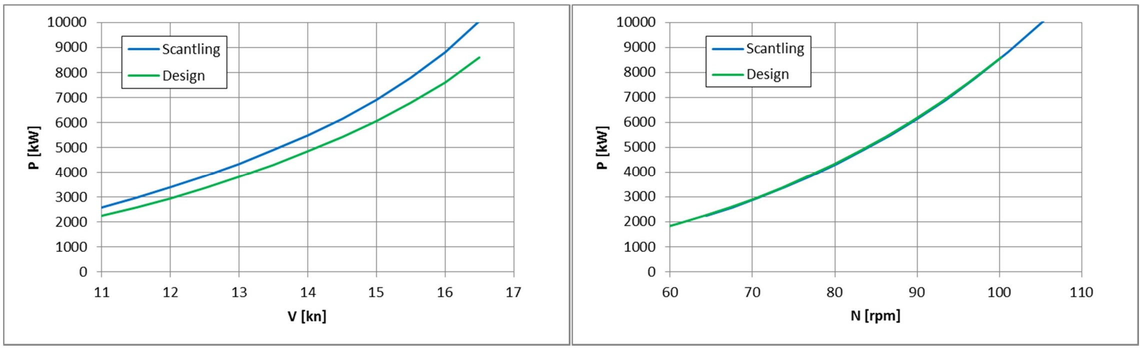

Fig.1: Model test results

Sea trials were performed before delivery of the newbuilding. With regard to contract the S/P tests were carried out in design draft. The weather conditions as given in Table II were good. The wind speed was measured continuously during each speed run and the wave height was measured prior the first speed run with a wave buoy, *Wienke (2016)*.

Table II: Sea trial conditions

Weather conditions	
Wind force	4 Bft from 100°
Sea state	wind waves neglectable, swell of 1 m to 295°
Water temperature	17°C
Water density	1025 kg/m³
Air temperature	26.5°C
Air pressure	1010 hPa
Hull conditions	
Draft fwd/aft	11.0 m / 11.0 m
Displacement	50008 t
Water depth	> 500 m

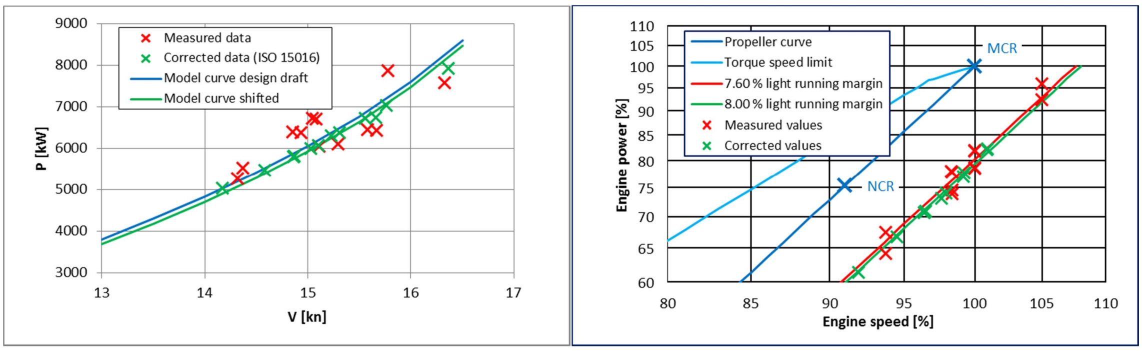

Fig.2: Sea trial results

The results of the S/P test are shown in Fig.2. For the runs against wind and waves the measured values are above the model curve (more power required); for the runs with the reciprocal heading the dots are below. After correction of the measured values the resulting values of the single runs are in good agreement with the model curve shifted by 125 kW; meaning that the sea trial results are little better than the model test prediction. The expectations were fulfilled so the duct seems to work as expected. The propeller light running margin was 8% according to the sea trial results.

3. Second example: VLCC with duct

Model tests are always performed for different drafts; normally for ballast, design and scantling draft. Sea trials are most often carried out only for ballast draft and the model test results are applied to transfer the sea trial results to the other drafts.

Sometimes, especially for tankers, there is the opportunity to perform the S/P trials for two different drafts. The ship of this example is a very large crude oil carrier with characteristics given in Table III.

Table 3: Ship's characteristics

Type	300,000 DWT Class Crude Oil Carrier
Length / Breadth	322 m / 60 m
MCR	24020 kW @ 65.7 rpm
Propeller	FPP / 4 blades / diameter 10.6 m
Ballast draft	
Draft fwd/aft	7.4 m / 11.0 m
Displacement	128090 m³
Block coefficient	0.719
Design draft	
Draft fwd/aft	20.5 m / 20.5 m
Displacement	314505 m³
Block coefficient	0.794
Scantling draft	
Draft fwd/aft	21.6 m / 21.6 m
Displacement	333410 m³
Block coefficient	0.799

The model tests were performed for three different drafts with a duct in front of the propeller. Different form factors were applied for each draft. The full-scale prognosis based on the model tests is in accordance with ITTC 1978, but for the tests with the duct a modification of the wake was included based on the assumption that the difference in wake after installation of the duct is the same in model and in full-scale (ITTC 1999 method). The results of the model tests with duct are shown in Fig.3.

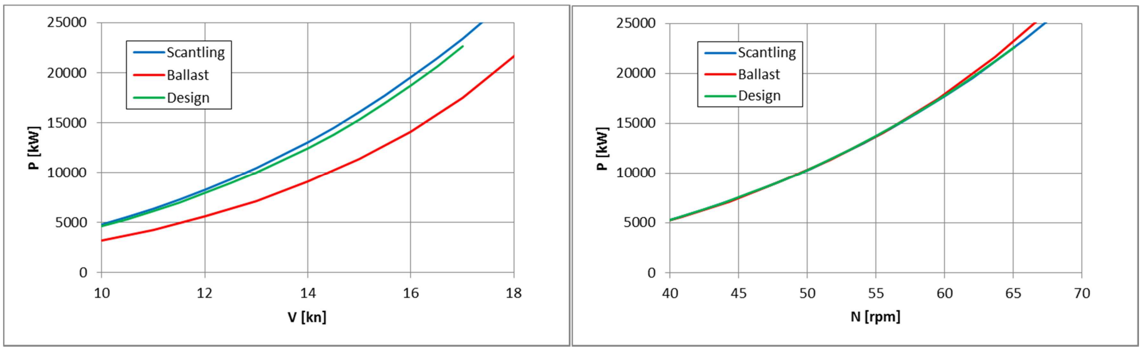

Fig.3: Model test results

The environmental conditions during the sea trials with scantling draft were fair, for ballast draft the conditions were good, see Table IV. Both S/P trials were carried out in water depths little above the limit to consider a shallow water correction. A strong impact on the measured values is due to the current in the sea trials area. During the tests on scantling draft the absolute variation in current was around 2 kn and for the tests on ballast draft it was 0.8 kn due to the tidal current. The period of the current is ~12 h; each single run took 2 hours due to the large mass of the ship and the requirements on the approach to get stable conditions during the speed runs. Each S/P trials took 16 h in total, meaning more than one period of the tidal current.

Table IV: Sea trial conditions

Speed test	1^{st} trials	2^{nd} trials
Condition	Scantling draft	Ballast draft
Weather conditions		
Wind force	4 Bft from 90°	4 Bft from 50°
Sea state	1.3 m to 200°	0.7 m to 200°
Water temperature	24.9°C	24.5°C
Water density	1022 kg/m³	1022 kg/m³
Air temperature	23°C	23°C
Air pressure	1007 hPa	1011 hPa
Hull conditions		
Draft fwd/aft	21.6 m / 21.6 m	7.45 m / 11.05 m
Displacement	341682 t	131622 t
Water depth	110 m	82 m

The measured values show a large scatter due to the current. After correction the model curve can be fitted to all points with good agreement. The adjustment of the model curve to the corrected data is done by vertical shifting of the model curve. It can be seen in Fig.4 that for scantling draft the model curve has to be shifted by more than 3000 kW, meaning that the result is distinctly worse than the model prognosis. For ballast draft the difference between sea trials and model curve is less. The difference is ~1000 kW.

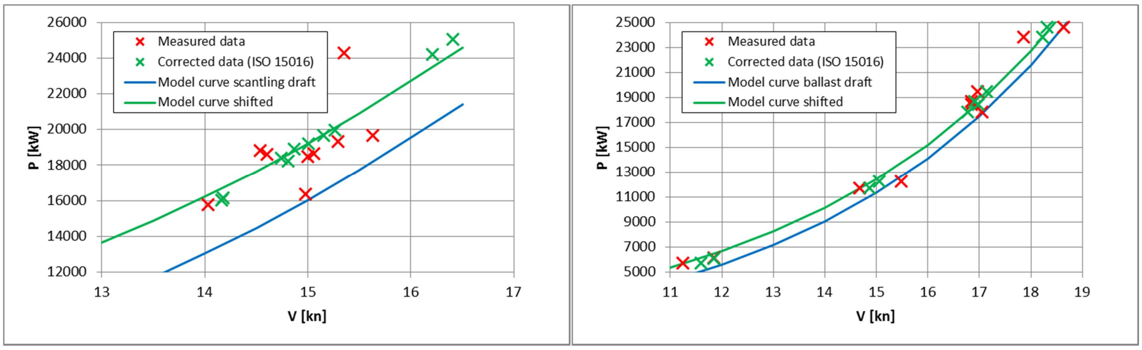

Fig.4: Sea trial results for scantling and ballast draft

In this case the sea trials showed that the model prognosis was too optimistic and in particular that the performance for scantling draft was distinctly overestimated. The different agreement for the different drafts indicates that the conversion from model to full-scale is not fully reliable here.

The light running margin of the propeller was slightly different for the two drafts. For scantling draft a light running margin of 2.9% was determined from S/P trials data; the corresponding value for ballast draft is 4.2%, Fig.5.

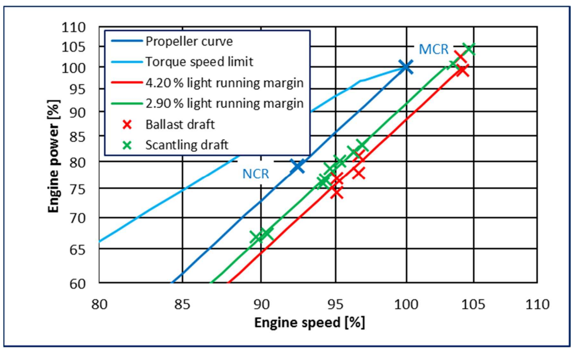

Fig.5: Sea trial results for scantling and ballast draft

4. Third example: Suezmax with duct

For retrofits with ducts in front of the propeller the power gain is a matter of particular interest for an economic evaluation of the conversion. In this example, tests were performed without duct (prior conversion) and with duct (after conversion) to determine the gain by the difference of the results. The ship of this example is a Suezmax tanker with characteristics given in Table V.

Table V: Ship's characteristics

Type	158,000 DWT Class Suezmax Tanker
Length / Breadth	264 m / 48 m
MCR	18660 kW @ 91 rpm
Propeller	FPP / 4 blades / diameter 8.35 m
Ballast draft	
Draft fwd/aft	7.65 m / 8.70 m
Displacement	79063 m³
Block coefficient	0.773

Model tests were performed for ballast and design draft in a speed range between 13 knots and 18 knots. Resistance and self-propulsion tests were carried out for both arrangements, namely without and with duct in front of the propeller. The model test results were extrapolated to full-scale in accordance with ITTC 1957 method, no form factor was applied. The model test results showed power savings of 5% for the design draft and even 6% in the ballast draft condition, Fig.6. At the same time a slight reduction of the propeller light running margin was predicted.

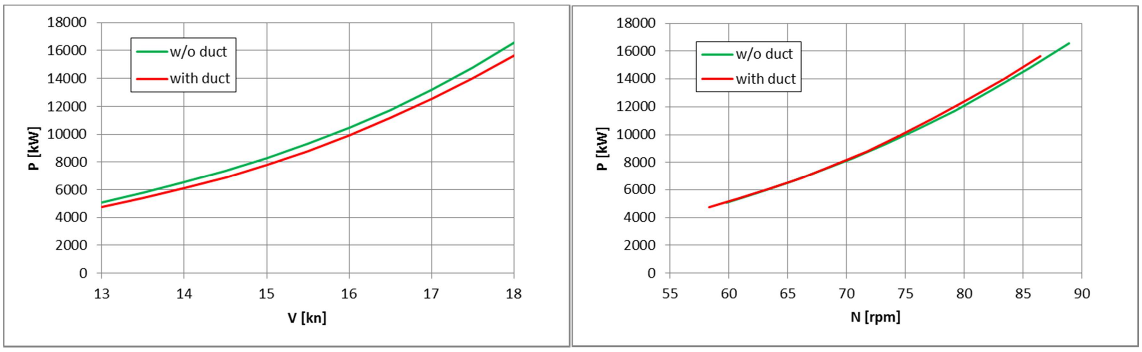

Fig.6: Model test results for ballast draft

Sea trials were performed two times, once prior modification and immediately after the yard stay. To avoid impact of different hull roughness on the results, the S/P trials prior modification were carried out after hull cleaning and painting. This means that the vessel went into the dock, standard maintenance work was carried out, the vessel left the dock for S/P trials, went back to dock again to install the duct and finally the vessel left the yard and the second S/P trials were performed. The environmental conditions for both S/P trials were very good and comparable (see Table VI). The tidal current during the sea trials changed by 0.6 kn and 0.8 kn, respectively.

Table VI: Sea trial conditions

Speed test	1st trials	2nd trials
Condition	w/o duct	with duct
Weather conditions		
Wind force	2-3 Bft from 0°, turning to 120°	3 Bft from 150°
Sea state	0.5 m to 180°	0.5 m to 295°
Water temperature	32°C	29°C
Water density	1026 kg/m³	1026 kg/m³
Air temperature	30.5°C	28.7°C
Air pressure	1008.5 hPa	1011.1 hPa
Hull conditions		
Draft fwd/aft	6.4 m / 9.1 m	6.4 m / 9.1 m
Displacement	75991 t	75857 t
Water depth	70 m	70 m

The sea trials were performed in the same area and with ballast draft. The results showed a worse performance than predicted by the model tests. For both S/P trials the corresponding model curve was fitted to the sea trial results with a shift along the vertical axis by around 100 kW, Fig.7.

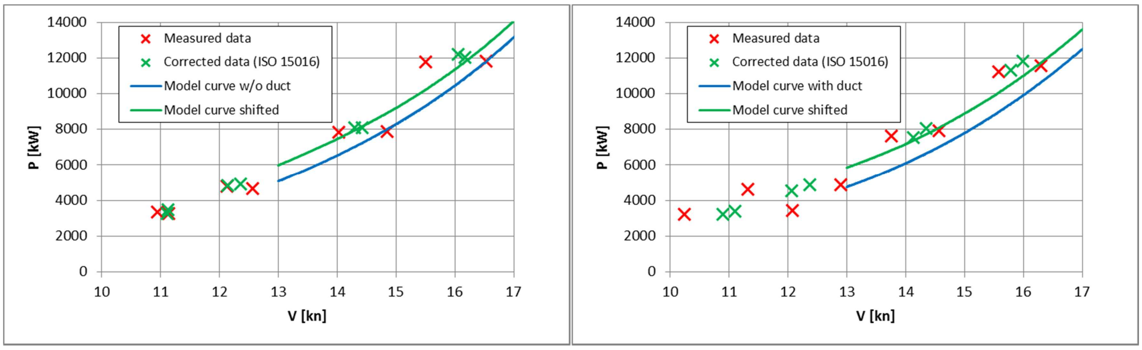

Fig.7: Sea trial results for ballast draft without and with duct

The direct comparison of both S/P trials illustrates that the shape of the model curve for the arrangement with duct is not in good agreement with the slope of the curve through the sea trial results, Fig.8 (left). Therefore a spline curve was fitted to the results of each S/P trials, Fig.8 (left). Both curves showed an amazing agreement, meaning that the S/P trials indicate that there is no power saving after installation of the duct in this case.

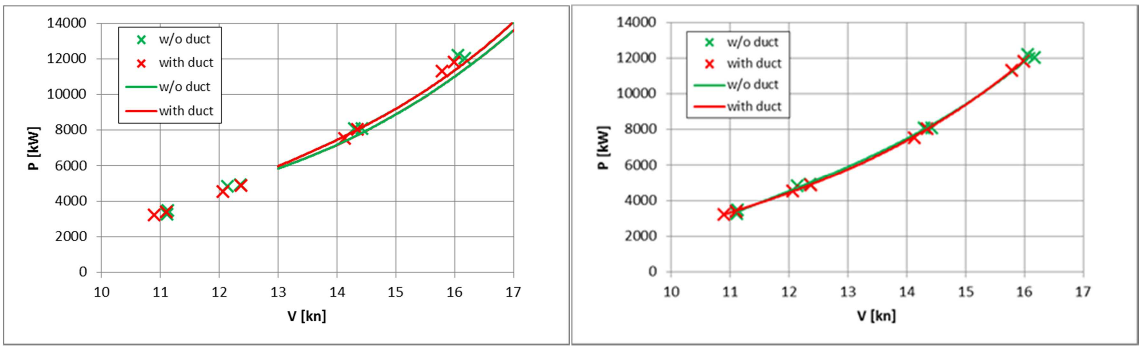

Fig.8: Comparison of sea trial results for ballast draft without and with duct

At the same time the sea trials confirmed the influence on the propeller light running margin. A reduction of the light running margin from 3% to 2% was determined from the S/P trials, Fig.9.

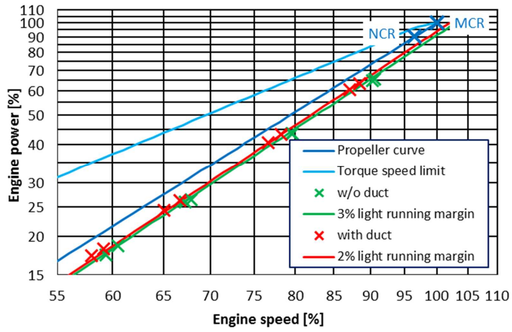

Fig.9: Sea trial results for scantling and ballast draft

A detailed error estimation was performed for the results of the S/P trials. The inaccuracy related to the measurement equipment was only ±0.2% since the identical devices were used for both trials. With regard to the environmental conditions an inaccuracy of ±0.8% was identified. The very good wind and wave conditions have only minor impact; the inaccuracy is mainly due to the current curve. In total, an accuracy of ±0.8% was determined for the power savings including measurement and evaluation errors. It was proven for this individual case that the power savings were distinctly lower than predicted by model tests or even absent.

5. Fourth example: VLCC with PBCF

The last example refers to the same series of ships as the second example, Table III. In addition to the duct in front of the propeller a propeller boss cap fin was installed on one of the sister vessels. Before, model tests were carried out to estimate the power gain of this measure. The model tests were performed for scantling draft only. The evaluation and extrapolation to full-scale are in accordance to ITTC 1999 method. The model tests predict a power saving of 1.2%, Fig.10.

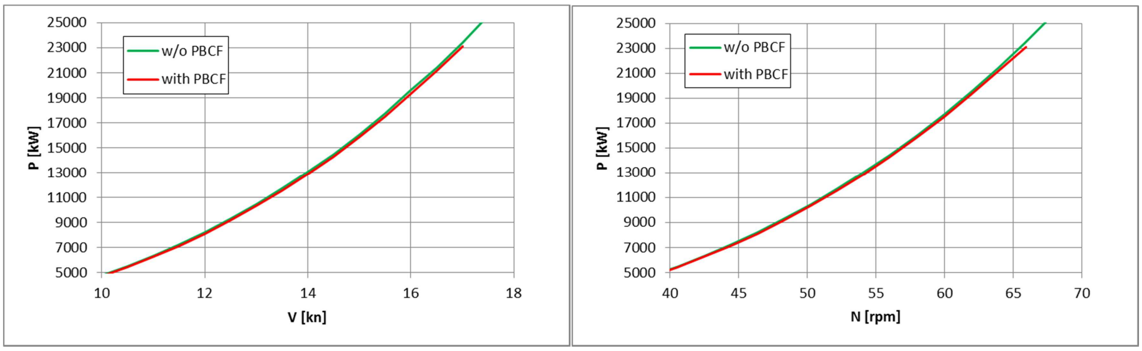

Fig.10: Model test results for scantling draft

S/P trials were performed for the vessel with the propeller boss cap fin and the results were compared to the sea trial results of two sister vessels. The environmental conditions for all sea trials are listed in Table VII. The maximum wind speed was 4 Bft and the maximum wave height was 1.0 m for the three different sea trials.

Table VII: Sea trial conditions

Speed test	1st ship	2nd ship	3rd ship
Condition	Scantling draft	Scantling draft	Scantling draft
Weather conditions			
Wind force	3 - 4 Bft from 340°	1-3 Bft from 160°	2 - 4 Bft from 260°
Sea state	0.7 m to 160°	1.0 m to 340°	1.0 m to 150°
Water temperature	16.5°C	9°C	15.7°C
Water density	1025.5 kg/m³	1022 kg/m³	1025 kg/m³
Air temperature	10.6°C	15.2°C	12°C
Air pressure	1024 hPa	1020 hPa	1015 hPa
Hull conditions			
Displacement	342568 t	342103 t	342414 t
Water depth	102 m	105 m	104 m

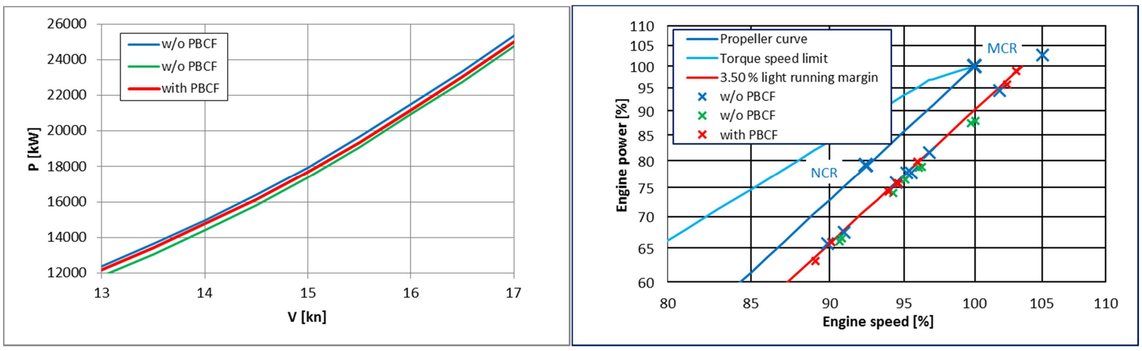

Fig.11: Sea trial results for 3 sister vessels in scantling draft

The S/P curves of the three sister vessels are combined in Fig.11. In this presentation no difference between the vessels without and with propeller boss cap fin appears. Due to the fluctuation of performance results within a series of sister vessels the verification of a small power saving of 1.2%

was not expectable for this comparison. *Wienke and Lampe (2016)* presented a series of sister vessels with a standard deviation of 3.7% for the determined power which will mask small power savings due to modifications.

A power saving of 1.2% can hardly be verified by sea trials. With tests prior and after installation in the same way as described for example 3 the verification of such a small difference is only possible for good and comparable environmental conditions.

6. Conclusions

The presented examples show partly distinct differences between the results from model tests and sea trials. The accuracy of the model test prognosis is mainly dependent on the extrapolation method from model to full-scale. Besides, different methods are applied to describe the wake.

The accuracy of S/P trials depends strongly on the weather conditions during the tests. A subjective observation and measurement of the environmental conditions is required for reliable test results. With an accurate procedure and good and comparable environmental conditions an accuracy of ±0.8% can be achieved for the S/P trials.

For retrofits it is important to separate between the impact of reduced hull roughness due to hull cleaning and painting and the effect of the ESD. An interruption of the docking time for S/P trials prior the installation of the ESD might be a solution for this requirement; for sure a costly and time-consuming but very accurate one.

References

WIENKE (2016), *Sea trial results impacted by sea state*, HANSA J. 153/9, pp.70-73

WIENKE, J.; LAMPE, J. (2016), *Energy efficiency design index in view of performance monitoring*, 1st Hull Performance & Insight Conference (HullPIC), Pavone, pp.137-144

A Study on the Principle and Energy Saving Effect of Multi ALV-Fin

Tomofumi Inoue, Japan Marine United Co., Tokyo/Japan, inoue-tomofumi@jmuc.co.jp
Yuki Saito, Japan Marine United Co., Tokyo/Japan, saitoh-yuhki@jmuc.co.jp

Abstract

Development of Energy Saving Device (ESD) is one of the most important missions for ship hydrodynamics engineer. Japan Marine United Co. (JMU) has developed Multi ALV-Fin (MALV-Fin) that is the new fin type of ESD having different concept and arrangement from existing fin type of ESDs. This paper describes the working principle and the energy saving effect of MALV-Fin based on CFD and model test. MALV-Fin contributes to the reduction of the axial velocity on the propeller plane and improves the hull efficiency, thereby demonstrating up to around 3% more energy saving effect by being incorporated with our ESDs system, Super Stream Duct and SURF-BULB.

1. Introduction

According to the worldwide demand for environmental protection inspired by global warming, development of eco-friendly vessels which applied an advanced technologies of hull form, propeller, rudder and Energy Saving Device (ESD), is one of the most important missions for ship hydrodynamics engineer. Among these technologies, ESD is highly cost-effective alternatives.

Japan Marine United Co. (JMU) has conducted the research and development of various types of ESDs for a long time. Among them, Super Stream Duct (SSD), LV-Fin (LV) and SURF-BULB (SB) greatly contribute to the fuel economy of the existing vessel. JMU has also been working on the optimization of these existing ESDs. As a next step, in order to enhance the ship hydrodynamics performance furthermore, it is indispensable to devise the new type of ESD having different concept from existing ESDs.

To meet this requirement, JMU developed a new ESD which control the flow field at the far upstream of the propeller and reduce the velocity on the propeller plane, resulting in a wake gain. This new type ESD, Multi ALV-Fin (MALV-Fin) consists of multi horizontal fins mounted above the bilge part right after side flat of the stern hull.

MALV-Fin is expected to have the synergistic effect by being incorporated with SSD and SB, thereby demonstrating up to around 3% more energy saving effect. This paper presents the working principle and the energy saving effect of MALV-Fin based on CFD and model test results.

2. Review of Existing Fin Type of ESDs

JMU has already developed pre-swirl and post-swirl type ESD, SSD, LV and SB, Fig.1a, b, *Yamamori et al. (2001), Masuko et al. (1998), Shiraki et al. (2007),* together with the high efficient contra-rotating propeller (CRP). Further, advanced hull shapes such as Ax-Bow, LEADGE-Bow and Low wind resistance accommodation are developed to reduce the sea margin under actual voyage, *Hirota et al. (2005), Matsumoto et al. (2005).*

SSD and LV, which is positioned in front of propeller, straightens complex stern flow caused by bilge vortices. SB, which is positioned behind propeller, recovers propeller rotational energy and reduce hub vortex between rudder and propeller. As a consequence, the above existing JMU's ESD has a future to recover the loss of energy that exists around propeller.

Focusing on stern fins type ESD mounted far from propeller, *Gougoulidis and Vasileiadis (2015), Hollenbach and Reinholz (2011)* summarized their configurations. In this literature, it is introduced that STF,Fig.1c, and SAVER-Fin, Fig.1d, *Lee et al. (2015),* weaken bilge vortices to promote surface pressure recovery. Vortex Generators, Fig.1e, *Hollenbach and Reinholz (2011)* accelerate the inflow to the propeller, resulting in reducing pressure pulse and vibration.

These existing fins, mounted around a bilge part near the bottom, mainly contribute to reduce the viscous resistance or the hull vibration, whereas MALV-Fin improves self-propulsive factor, e.g., hull efficiency by reducing the velocity on the propeller plane.

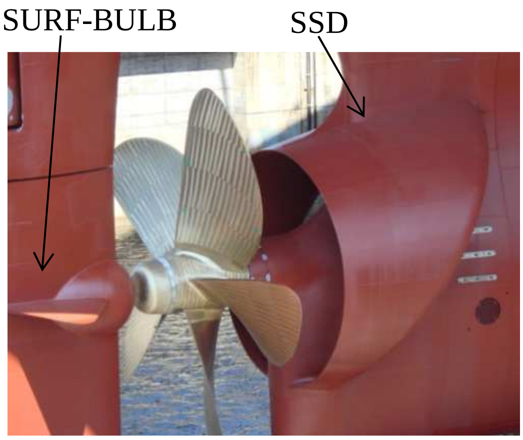

(a): SSD and SURF-BULB


(b): LV-Fin


(c): STF
http://www.sanoyas.co.jp/shipbuilding/news/2006/0731.html

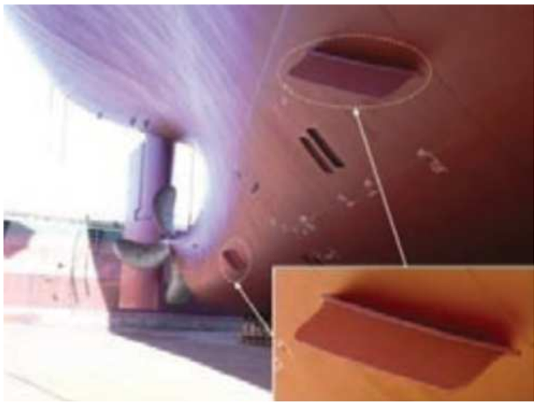
(d): SAVER-Fin

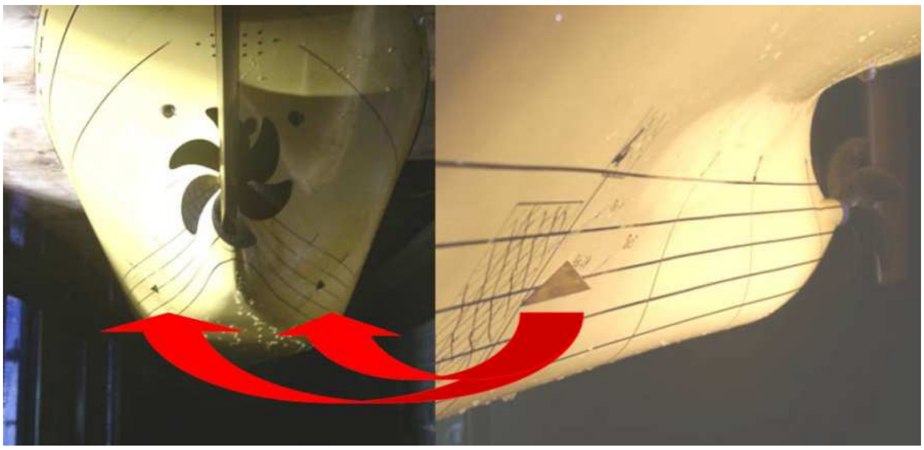
(e): Vortex Generator
Fig.1: Existing fin types of ESDs

3. Configuration of Objective Vessel and MALV-Fin

300,000DWT oil tanker is selected as an objective vessel in this study. Fig.2 shows the geometry of the hull and MALV-Fin which consists of two horizontal fins here. Those fins are fixed above bilge part right after side flat of the stern hull far from propeller.

Length b.p. (m)	320.3
Breadth (m)	60
Draught (m)	19.85

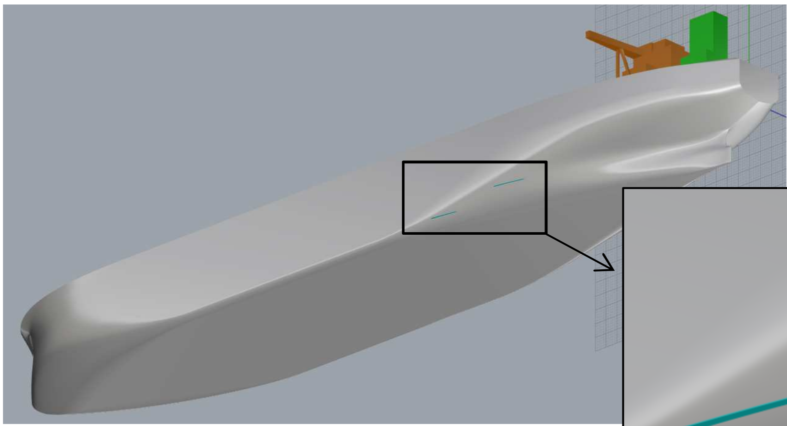

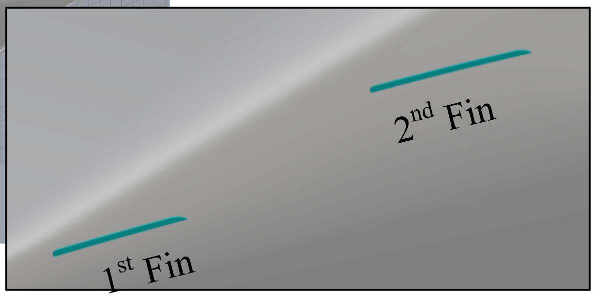

Fig.2: Configuration of objective vessel and MALV-Fin

4. CFD Setting and Validation

4.1. Mesh and Solver

Fig.3 shows the computational mesh prepared for this study. It has about 10 million unstructured, hexahedral meshes in a half side. Some parts of mesh are refined locally. The smallest spacing normal to the wall is set so that the non-dimensional viscous length, Y^+, is around 1. RANS steady computation using FLUENT v17.0 is applied. The turbulence model is Reynolds Stress Model since this model is superior to the others for the prediction of wake distribution including bilge vortices, *ITTC (2011)*. The free surface, dynamic trim and sinkage of the hull was not taken into account, assuming that the influence of free surface is negligible.

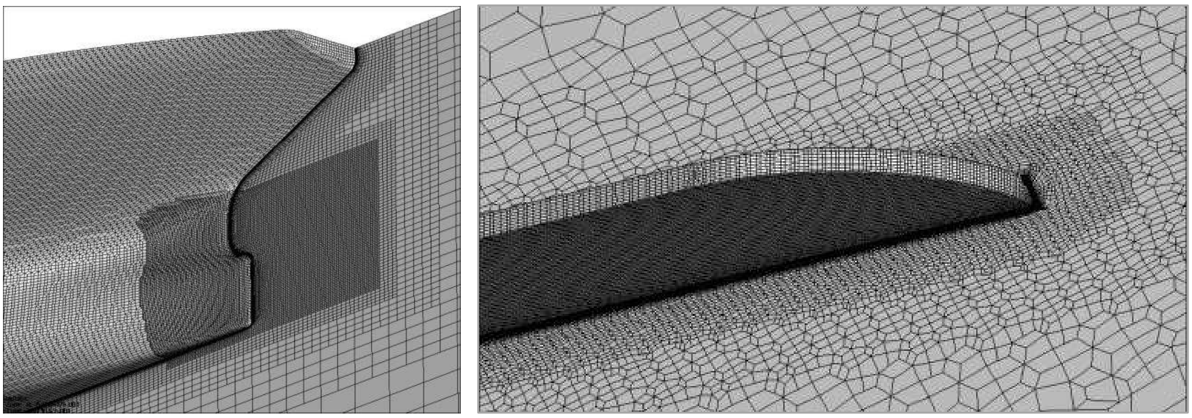

Fig.3: Computational mesh

4.2. Validation

In order to validate the reliability of the present computational model, the axial velocity distribution, that is, wake distribution on the propeller plane for bare hull is compared between model test and CFD beforehand as shown in Fig.4. Overall, the presented computational model estimates the wake distribution accurately including the hook characteristics caused by bilge vortices.

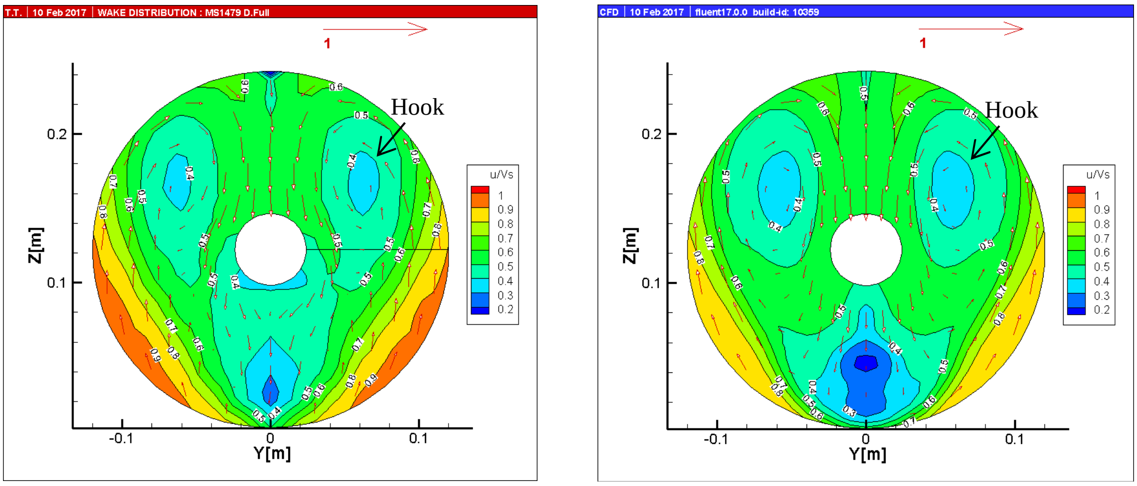

Fig.4: Axial velocity distribution on propeller plane (left: model test, right: CFD)

5. Working Principle and Energy Saving Effect of MALV-Fin

5.1. Influence on Flow Field by MALV-Fin Based on CFD Analysis

MALV-Fin contributes to the reduction of the axial velocity on the propeller plane, resulting in the around 4% of nominal wake gain based on CFD simulation, Table I. Fig.5 compares axial velocity distribution at the propeller plane: On the left, the axial velocity distribution with contour line in black represents for w/o-fins, and that in red is for with-fins; on the right, the difference of the axial velocity obtained as with-fins minus w/o-fins. The fins reduce the axial velocity on the propeller plane, whereas the axial velocity near the water surface is accelerated. A streamline plot, Fig.6, shows that MALV-Fin gathers more extensive flow field in the vicinity of the hull surface into the propeller plane along the streamlines. Consequently, MALV-Fin contributes to the reduction of the axial velocity on the propeller plane, resulting in the wake gain.

Table I: Average axial velocities on propeller plane and nominal wake gain

	w/o Fin (bare)	with 1st Fin	with 2nd Fin	with both Fin
Average Axial Velocity (normalized by w/o Fin)	1.000	0.983	0.982	0.961
Nominal Wake Gain (%)	base	1.7%	1.8%	3.9%

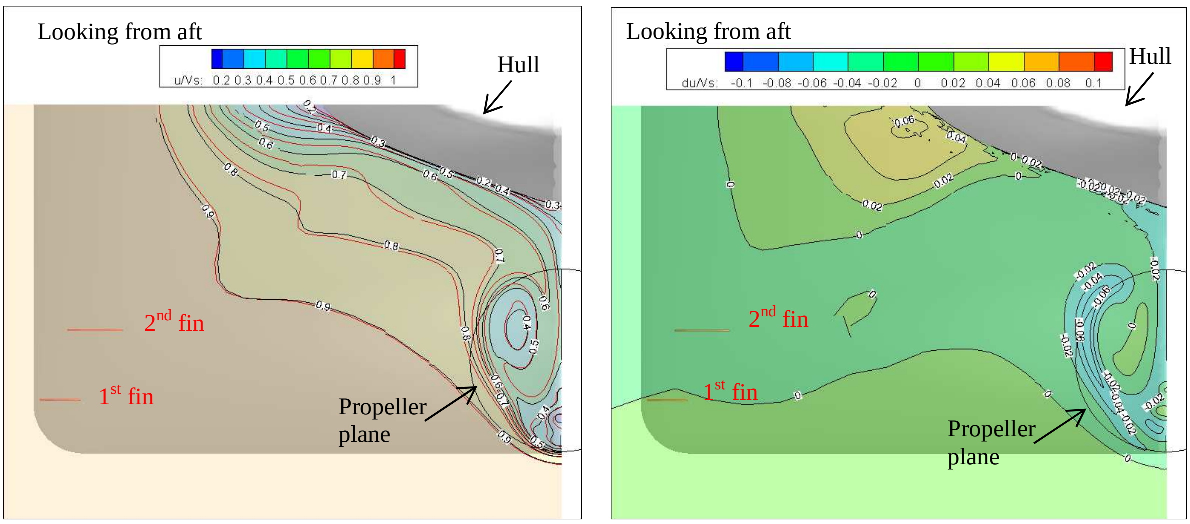

Fig.5: Comparison of axial velocity distribution at propeller plane
(left - black: w/o-fins, red: with-fins, right - difference of axial velocity)

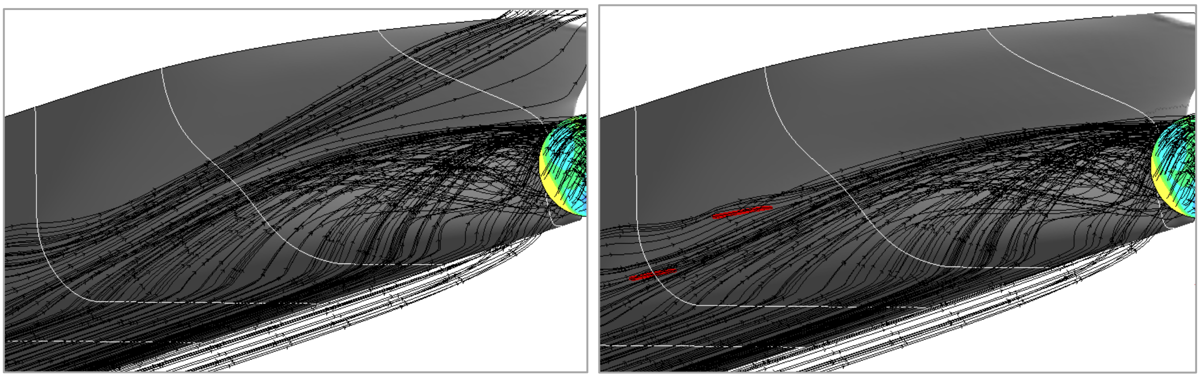

Fig.6: Streamlines analysis led into propeller plane (left: w/o-fins, right: with-fins)

To obtain the wake gain, it is extremely important to set MALV-Fin in the area of high incident flow angle. Fig.7 shows the flow angle contour and the local streamlines on the hull surface. MALV-Fin works to change the flow direction by being fitted in the area of high incident flow angle. This effect can be enhanced by increasing number of fin from single to pair.

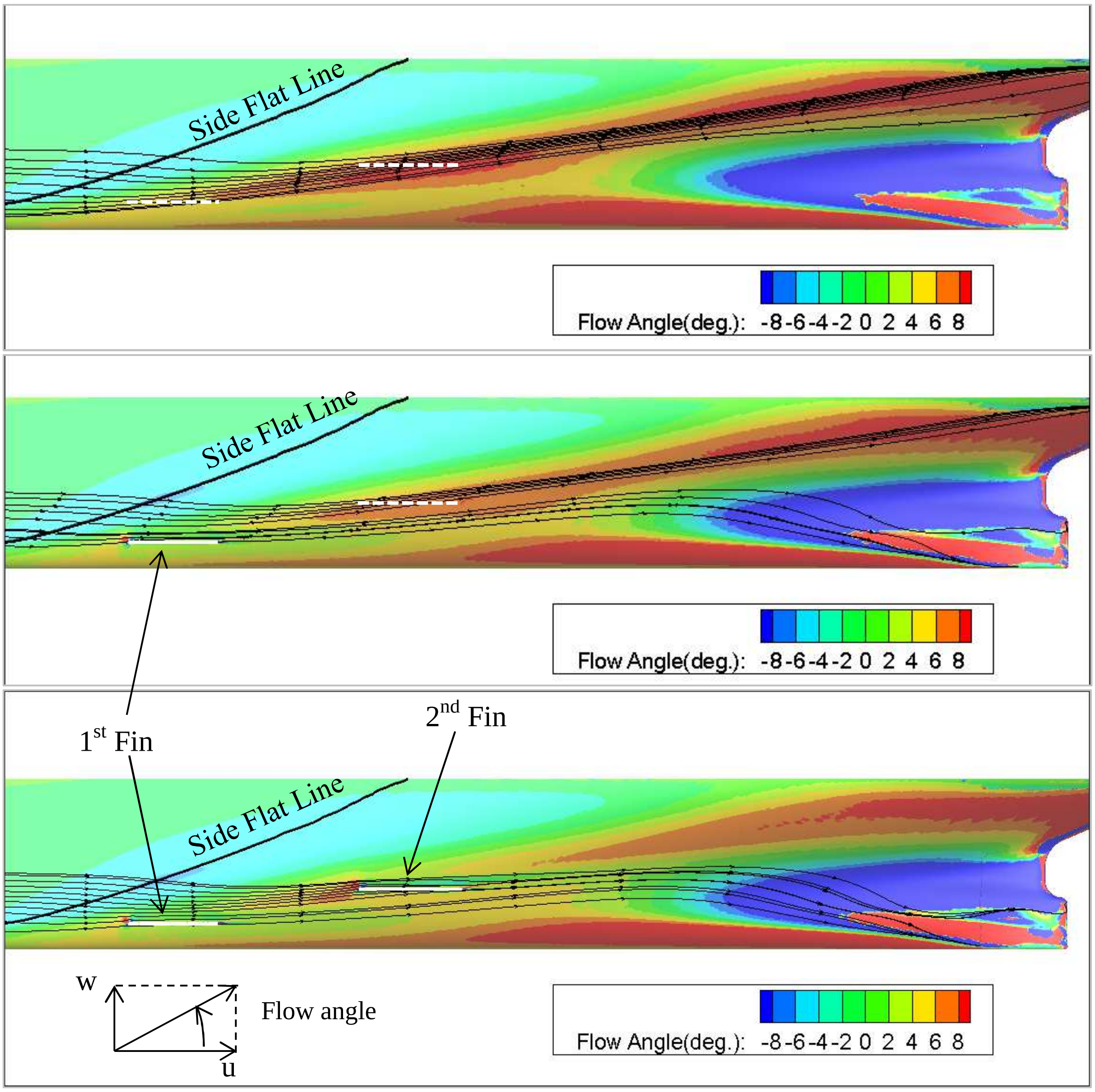

Fig.7: Flow angle contour and Streamlines on the hull surface
(upper: w/o-fin, middle: with-1st fin, lower: with-1st &2nd fins)

5.2. Model Test Results

The required power P_B can be estimated by Eq.(1). The factors except η_t can be obtained from model tests.

$$P_B = \frac{R_t \cdot V_s}{\eta_t \cdot \eta_h \cdot \eta_R \cdot \eta_o} \tag{1}$$

R_t: *Total Resistance*
V_s: *Ship Speed*
η_t: *Transmission Efficiency*
η_h: *Hull Efficiency*
η_R: *Relative Rotative Efficiency*
η_o: *Propeller Open Water Efficiency*

To quantify the effect of MALV-Fin in relation to each factor, their differences Δ relative to the variable of the basis are calculated by Eq.(2) and are summarized in Fig.8.

$$\Delta = \frac{[with\ Fin] - [basis]}{[basis]} \tag{2}$$

From Fig.8, some notices are as follows:

- MALV-Fin effect without existing ESDs (bare hull)
  MALV-Fin itself demonstrates around 1% more energy saving effect. The fins mainly improve hull efficiency η_h defined by the ratio of thrust deduction coefficient, 1-t, and effective wake coefficient, 1-w_m as follows.

$$\eta_h = \frac{1 - t}{1 - w_m} \tag{3}$$

  In general, 1-w_m decreases when the velocity on the propeller plane decreases. As mentioned in section 5.1, MALV-Fin contributes to the wake gain, resulting in improvement in η_h. η_o just responds to the variation of propeller loading caused by the change of η_h and hull resistance.

- MALV-Fin effect with existing ESDs
  Most remarkably, MALV-Fin enhances the propulsive performance when being incorporated with SSD and SB compared to that in case only MALV-Fin exists. This synergistic effect is around 2%. Since MALV-Fin is located far ahead of SSD and SB, it can be assumed that the performance of the existing ESDs is improved. As a result, we obtained up to around 3% more energy saving effect by fitting MALV-Fin to the objective vessel with SSD and SB. As for the synergistic effect, one possibility is that MALV-Fin increases the attack angle of the inflow to SSD, which is strongly related to the efficiency of the duct, *Inukai et al. (2011*), due to the reduction of the axial velocity. Fig.9 compares the attack angle of the inflow to the upper part of SSD between w/o and with MALV-Fin based on CFD simulation under the self-propulsion condition. The attack angle of SSD is increased qualitatively by the presence of MALV-Fin which could lead the increase of thrusting force generated by SSD. However, it is necessary to measure the force acting on SSD during self-propulsion test for more detailed quantitative evaluation in the future research.

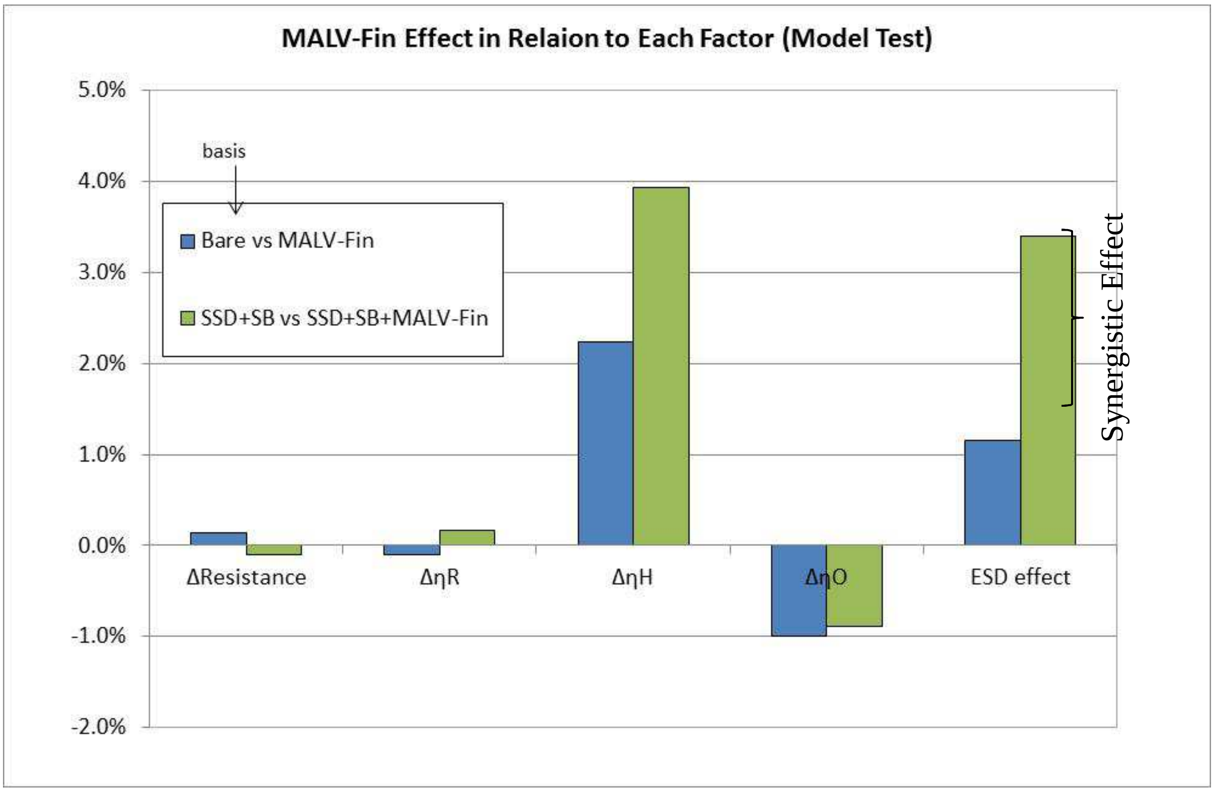

Fig.8: MALV-Fin effect in relation to each factor.

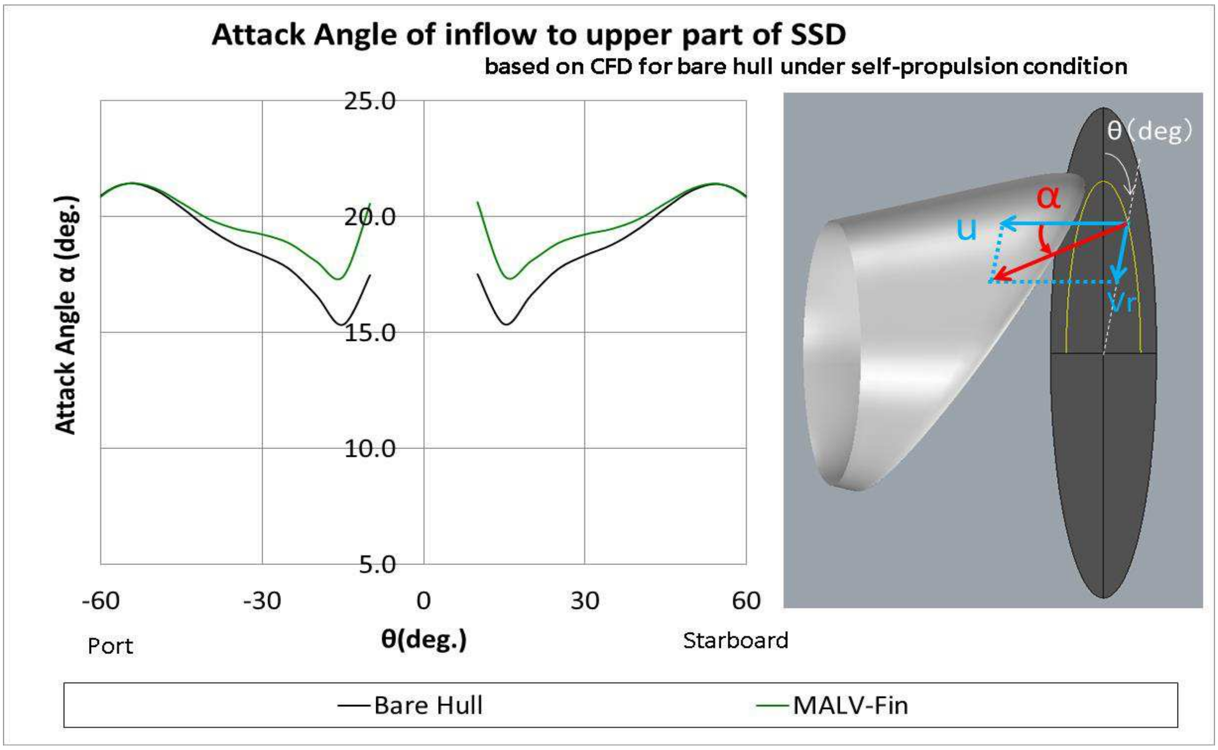

Fig.9: Attack angle of inflow to upper part of SSD from CFD simulation

Finally, model test results with ALV single fin mounted and MALV-Fin for various kinds of vessels are summarized in Fig.10. Overviewing this result, ALV and MALV-Fin has demonstrated the energy saving effect from 1 to 3% by being incorporating with the existing ESDs. In the case of hull L, M and N where both ALV and MALV-Fin were applied, it is show that the energy saving effect is enhanced by increasing number of fin from single to pair in every case. Further, series model test for hull N indicates that more synergistic effect is attainable when MALV-Fin with triple fin configuration is applied. JMU will continue the study to improve the performance of MALV-Fin furthermore in the future.

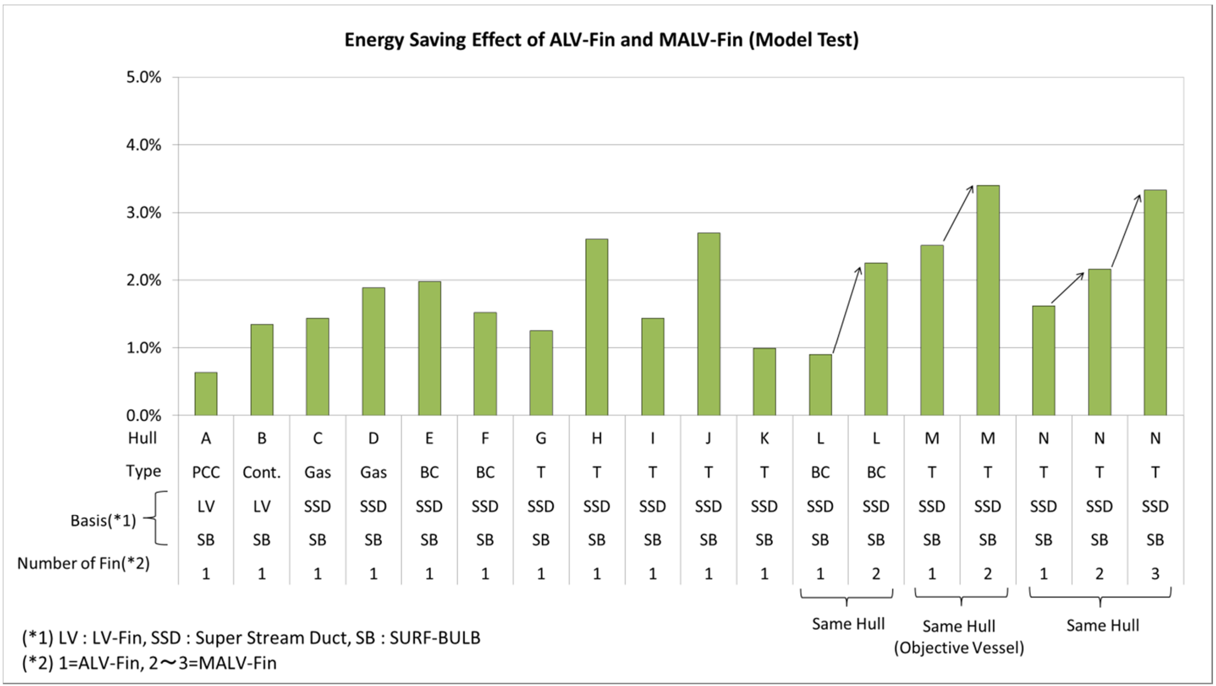

Fig.10: All the model tests for ALV and MALV-Fin

6. Conclusion

This paper presents the working principle and the energy saving effect of the new device, Multi ALV-Fin (MALV-Fin), by means of CFD and model test. Concluded remarks are summarized as follows.

(1) MALV-Fin consists of multi horizontal fins mounted above the bilge part right after side flat of the stern hull. This device contributes to the reduction of the axial velocity on the propeller plane, resulting in improvement of hull efficiency.
(2) MALV-Fin has the synergistic effect against the existing ESDs. MALV-Fin works to increase the attack angle of the inflow to Super Stream Duct (SSD) which would improve the efficiency of SSD more.
(3) MALV-Fin has the different concept and arrangement in contrast to the existing fin type ESDs. Around 3% more energy saving effect is attainable by fitting MALV-Fin to the objective vessel with SSD and SURF-BULB. On the other hand, MALV-Fin demonstrated around 1% energy saving effect by itself.

MALV-Fin, which is a patent-pending technology, has already applied to number of actual vessels. As a future work, we plan to extend more detailed research on the mechanism of the synergistic effect for the further improvement of this new energy saving device.

(*)ALV-Fin, SSD, Super Stream Duct, SURF-BULB, Ax-Bow and LEADGE-Bow are registered trademarks of Japan Marine United Co..

References

GOUGOULIDIS, G.; VASILEIADIS, N. (2015), *An Overview of Hydrodynamics Energy Efficiency Improvement Measures*, 5th Int. Symp. Ship Operations, Management & Economics

HIROTA, K.; MATSUMOTO, K.; TAKAGISHI, K.; YAMASAKI, K.; ORIHARA, H.; YOSHIDA, H. (2005*), Development of Bow Shape to Reduce the Added Resistance due to Waves and Verification on Full Scale Measurement*, Int. Conf. Marine Research and Transportation 2005

HOLLENBACH, U.; REINHOLZ, O. (2011*), Hydrodynamic Trends in Optimizing Propulsion*, 2nd Int. Symp. Marine Propulsors (SMP'11)

INUKAI, Y.; KANEKO, T.; NAGAYA, S.; OCHI, F. (2011*), Energy-saving principle of the IHIMU semicircular duct and its application to the flow field around full scale ships.*, Ishikawajima-Harima Engineering Review 44(1)

ITTC (2011*), The Specialist Committee on Scaling of Wake Field*, Final report and recommendations to the 26th ITTC

LEE, H. D.; HONG, C. B.; KIM, H. T.; CHOI, S. H.; HAN, J.M.; KIM, B.; LEE, J.H. (2015*), Development and Application of Energy Saving Devices to Improve Resistance and Propulsion Performance*, 25th Int. Ocean and Polar Engineering Conf.

MASUKO, A.; KOSHIBA, Y.; ISHIGURO, T. (1998*), Energy Saving Device for Ships IHI – L.V. Fin.*, Ishikawajima-Harima Engineering Review 38(6)

MATSUMOTO, K.; TANAKA, Y.; HIROTA, K.; AMAKAWA, M.; TAKAGISHI, K. (2005*), Reduction of Wind Force Acting on Ship*, ICMRT'05

SHIRAKI, A.; TORIUMI, M.; MATSUMOTO, K. (2007*), An application of energy-saving device "SURF-BULB" to an existing ship*, J. Japan Society of Naval Architects and Ocean Eng. 4 (in Japanese)

YAMAMORI, T.; FUJIMOTO, T.; MIYAMOTO, M.; NAGAHAMA, M. (2001*), Application of Overlaid Grid Method to Nemerical Simulation of Flow around Ship Equipped with Super Stream Duct (SSD)*, J. Kansai Society of Naval Architects 235 (in Japanese)

The Art of Scarcity:
Combining High-Frequency Data with Noon Reports in Ship Modeling

Matti Antola, Antti Solonen, Stratos Staboulis, Eniram Ltd, Helsinki/Finland
{matti.antola,antti.solonen,stratos.staboulis}@eniram.fi

Abstract

Traditional high-fidelity data acquisition techniques are typically expensive since they require integration to the vessel's automation and bridge systems. Especially on small to moderately sized or chartered vessels, the high cost makes such solutions unfeasible. We propose a new solution to the data acquisition problem based on a portable battery-powered on-board sensor. The high-frequency measurement data is combined with weather forecasts and noon-reports containing efficiency related quantities such as bunker fuel readings. The solution overcomes problems, such as crew over-reporting weather conditions and other inaccuracies, characteristic to a traditional fully noon-report reliant approach. This paper presents a proof-of-concept study of the proposed technique. Analyses and examples based on data collected by the Eniram Solutions and SkyLight platforms, respectively, are presented.

1. Introduction

In traditional vessel performance modeling techniques, vessel data is collected through interfacing an on-board PC with the vessel automation and navigation systems, and custom sensors. Such integration provides access to high-frequency measurements of various quantities, like propulsion power, fuel mass flow, and speed through water (STW), directly applicable to vessel performance monitoring. With the on-board computer, the data can be processed in real time and turned into intelligent money-saving operational decisions.

Unfortunately, exhaustive on-board integration requires considerable financial investment from the ship owner or charterer. Therefore, although such solutions enable fuel savings, they are not a feasible option for a significant proportion of the industry. For example, on numerous cargo or tanker vessels the fuel costs are not a liability of the ship owner because the ships and crew are hired by a charterer which may change from time to time. Hence, it may happen that neither the ship owner nor the charterer has the incentive to invest on an expensive automation integration-based fuel savings solution. As a consequence, there is need for a lightweight device that tracks, for instance, ship fuel consumption and thus aids the charterer in, i.e., validating the vessel performance compared to the values in the charter-party agreement; see e.g. *Rehmatulla and Smith (2015).*

Without access to vessel automation system, measurements of many quantities, such as speed through water (STW), propeller revolution rate or fuel flow, pivotal to performance tracking are not directly available. However, we claim that useful information on the vessel efficiency can be indirectly obtained. To this end, Eniram has developed a framework where an artificial measurement of the STW is formed by combining a GPS-based speed over ground (SOG) estimate with available ocean current forecasts. Using the forecast-STW and other meteorological data together with a suitable propulsion power model, instantaneous fuel flow rate can be estimated based on the daily total fuel consumption readings reported by the crew. The main advantage of the indirect estimation technique is that it drastically reduces the cost of the performance analysis instrument. Moreover, with a suitable embedded system for data processing and a wireless transmitter, the proposed technique provides marine vessels a robust interface to the internet of things. In particular, all actual data analysis computations can be carried out on a cloud server.

Compared to the traditional high-fidelity techniques, the proposed framework induces three main challenges: (i) increased level of measurement error due to noisy high-frequency data sources and aggregating, (ii) systematic modeling error implied by the scarcity of measurable quantities, and (iii) uncertainty caused by reliance on human input. More precisely, although the GPS-based SOG estimate is fairly accurate, the forecasts are often not (they have low bias, but momentary errors can be high). Since fuel flow is roughly proportional to the cube of STW, any error in STW estimation is magnified in fuel flow predictions. The resulting error is further boosted by the fact that the reported fuel consumption readings, with which the model is calibrated, are sums over lengthy time periods. The systematic error arises from the fact that a full-scale propulsion model relies on quantities, such as propeller revolution rate and draft among others, that are not available. Furthermore, the crew-fed noon-reports often contain crude errors and occasionally are completely lacking.

In this paper we present a general mathematical modeling framework that can be adapted to different applications. The leading idea is to formulate a model between the SOG, forecast data, and average fuel flow. We also present a proof-of-concept numerical study which deals with data collected by Eniram Skylight platform on a single anonymous vessel. Reference measurements are obtained from the full Eniram platform also present on the same vessel. The results indicate that the proposed technique can yield speed-fuel models that correlate well with the high-fidelity reference data. Moreover, the method gives a significantly more accurate view on the vessel's performance compared to an analysis that solely rely on the crew-reported aggregates.

2. Hydrodynamic measurement model

In this section we describe a generic mathematical model for predicting the required propulsion power using the available measurement data, i.e., speed through water and external meteorological conditions. Let us denote the velocity over ground by $\mathbf{u}_t$, and the water and air (wind) current velocities by $\mathbf{u}_t^{\mathrm{w}}, \mathbf{u}_t^{\mathrm{a}}$, respectively. We write the model in form

$$\begin{aligned} \mathbf{v}_t &= \mathbf{u}_t + \mathbf{u}_t^{\mathrm{w}}, \\ P_t &= R(\mathbf{v}_t, \mathbf{u}_t^{\mathrm{w}}, \mathbf{u}_t^{\mathrm{a}}, \boldsymbol{\theta}) v_t \end{aligned} \tag{1}$$

$\mathbf{v}_t$ is the velocity through water, and the bottom formula expresses the time-dependent power P_t consumed by the ship when moving at $\mathbf{v}_t$ in the presence of the current and wind speed $\mathbf{u}_t^{\mathrm{w}}, \mathbf{u}_t^{\mathrm{a}}$. The power is given by the resistance coefficient R multiplied by the STW v_t, that is, the magnitude of $\mathbf{v}_t$. Moreover, we have introduced an additional multidimensional resistance parameter $\boldsymbol{\theta}$ which depends on the object geometry and the properties of media. Let us emphasize that in our application P_t is not directly observable whereas measurements of $\mathbf{u}_t, \mathbf{u}_t^{\mathrm{a}}, \mathbf{u}_t^{\mathrm{w}}$ are assumed available. In what follows, we define an indirect fuel flow observation model dependent on the total fuel flow. Subsequently, it is possible to formulate an explicit optimization problem applicable for estimating the drag parameters.

Remark: Conventionally speed is defined as the magnitude of velocity. However, in the rest of the paper, the terms are used interchangeably since the rigorous meaning is always clear by the context.

2.1 Combining high-frequency data with low-frequency data

The fuel flow ϕ_t needed for producing a power P_t at time t is modeled through

$$\phi_t = g(P_t, \boldsymbol{\alpha}) \tag{2}$$

g is a mapping that characterizes the specific fuel oil consumption (SFOC) as a function of the power and an additional (time-independent) set of parameters $\boldsymbol{\alpha}$. As stated above, without integration to vessel automation system real-time monitoring of ϕ_t is unfeasible. Instead, we assume that – via communication with the crew – sums of ϕ_t over certain time periods ΔT of variable duration (e.g. a day) can be obtained. Summing the fuel flow over the time period and using (1) and (2) yields a total fuel flow formula

$$\Phi_{\Delta T} = \int_{\Delta T} \phi_t \, dt = \int_{\Delta T} g(P_t, \boldsymbol{\alpha}) \, dt = \int_{\Delta T} g(R(\mathbf{v}_t, \mathbf{u}_t^{\mathrm{w}}, \mathbf{u}_t^{\mathrm{a}}, \boldsymbol{\theta}) v_t, \boldsymbol{\alpha}) \, dt. \tag{3}$$

The exact mathematical formulations of the dependencies depend on the extent of the available measurement data. In any case, the arising numerical problem is to estimate the parameters $\boldsymbol{\alpha}, \boldsymbol{\theta}$ using (3) given noisy observations of the involving velocities and total fuel flows over a collection of different time periods. Depending on the selected model, the resulting (possibly non-linear) parameter estimation problem can be tackled, e.g., with Bayesian regression techniques; see e.g., *Gelman (2014)*. In addition, allowing the parameters to change in time would enable accounting for temporal changes in hull performance, for instance. The following worked-out example presents a case where the selected model yields a linear parameter estimation problem.

2.2 Example: Explicit equations in a simplified power model

This subsection illustrates what type of formulas the proposed technique brings up in practice. We consider a simple model where the resistance coefficient only depends on drags induced by air and water. More precisely, we impose

$$\begin{aligned} \mathbf{v}_t &= \mathbf{u}_t + \mathbf{u}_t^{\mathrm{w}}, \\ P_t &= \theta_1 v_t^3 + \theta_2 |\mathbf{u}_t^{\mathrm{a}} - \mathbf{u}_t|^2 v_t \cos\gamma_t, \\ \phi_t &= \alpha_1 P_t + \alpha_2 \end{aligned} \tag{4}$$

$\mathbf{u}_t^{\mathrm{a}}$ and $\mathbf{u}_t^{\mathrm{w}}$ are the air (wind) and water current velocities, respectively. Moreover, γ_t denotes the angle between the relative wind $\mathbf{u}_t^{\mathrm{a}} - \mathbf{u}_t$ and the ship heading. The parameters θ_1, θ_2 model the (unknown) resistance scalars. Consequently, (3) reduces to the form

$$\Phi_{\Delta T} = \alpha\theta_1 \int_{\Delta T} v_t^3 \, dt + \alpha\theta_2 \int_{\Delta T} |\mathbf{u}_t^{\mathrm{a}} - \mathbf{u}_t|^2 v_t \cos\gamma_t \, dt + |\Delta T|\alpha_2. \tag{5}$$

All the summands in (5) are available in the high-frequency input data. The scalar multipliers are unknown and are to be estimated using measured data. In particular, the SFOC and drag constants $\alpha_1, \alpha_2, \theta_1, \theta_2$ cannot be separately estimated. Sufficient amount of noon-reports enables the estimation of the weight parameters

$$\beta_1 = \alpha_1\theta_1, \quad \beta_2 = \alpha_1\theta_2, \quad \beta_2 = \alpha_2|\Delta T|. \tag{6}$$

Plugging the estimates of these parameters into (4) yields a predictive model for instantaneous fuel flow which is, in this case, proportional to the instantaneous power consumption with an unknown proportionality constant. With suitable post-processing, the estimated model can be turned into useful diagnostics such as speed-fuel curves and fuel consumption tracking as shown by the numerical examples given in Section 3.

2.3 Caveats and extensions

Since the forecast-STW estimates are noisy, one may ask if noon-reported STW or propeller revolution rates could also be of use in the proposed method. However, problems arise due to the fact that (4) includes an average of the cube of STW but not the cube of the average. Interchanging these quantities in general yields an error of order $|\Delta T| \times \sigma^2_{\Delta T}(v_t)$, that is, the length of the interval times the temporal variance of the observed STW. Hence, ignoring this non-symmetry can introduce significant proportions of extra noise. Moreover, communicating averages of powers of speeds through noon-reporting has not been evaluated yet but it seems impractical due to the induced extra reliance on human input. Let us also stress that the power model of (4) is obviously restricted. In practice, the list of explanatory quantities is larger than merely the water and air induced drags. For example, the effects of draft and ocean waves could be (and are in practice) included in the analysis. Careful elaborations of more complicated models are left for future studies.

3. Comparative numerical evaluation

In this section we present computational examples of the proposed technique based on measurement data collected by Eniram products. The leading idea is to attempt validating the noon-report-based estimation by comparing it to available high-frequency on-board measurements gathered by the full Eniram platform. We proceed with three examples all concerning a data collected about an anonymous cargo vessel equipped with both Eniram Skylight and the full platforms. In the first example, we visualize the obtained forecast-STW and, for comparison, the corresponding STW obtained from the full platform. The second example presents the estimated instantaneous fuel flow time-series and the last example illustrates estimated speed-fuel curves from the two sources.

Unfortunately, perfectly accurate high-fidelity fuel flow data are not available in the present case. However, both propulsion power and settling tanks' masses time series are available through Eniram. Based on these data, we estimate the specific fuel consumption profile of the vessel. The result is then used to construct an estimate of the reference fuel flow data against which the proposed method is evaluated. We emphasize that this study does not comprise an exhaustive validation of the method but instead a proof-of-concept numerical investigation.

3.1. Speed through water from SOG and forecasts

In practice, the SOG can be directly obtained from a GPS tracker which has an inbuilt method for speed estimation. As described in (1), the forecast-STW estimate is formed by adding the sea current forecast to the SOG time series. All forecast data are obtained from the National Oceanic and Atmospheric Administration (NOAA) weather service. As the reference speed we take the virtual-STW introduced in *Antola (2017)*. The virtual-STW is calculated by blending data from multiple sources, and according to *Antola (2017)*, it is systematically more reliable than the vessel's speed log.

The obtained SOG, forecast-STW and virtual-STW are mapped in Fig.1. We observe that, in the presence of significant currents (e.g. between Sep 08–10), the forecast-STW is more in accordance with the virtual-STW than what the mere SOG is. On the other hand the increased uncertainty induced by the forecasts is clearly visible on both charts. The discrepancy between the two STW estimates over a period of around two months (5 min sampling) is depicted on the right in Fig.1; the mean magnitude of discrepancy is 0.35 knots.

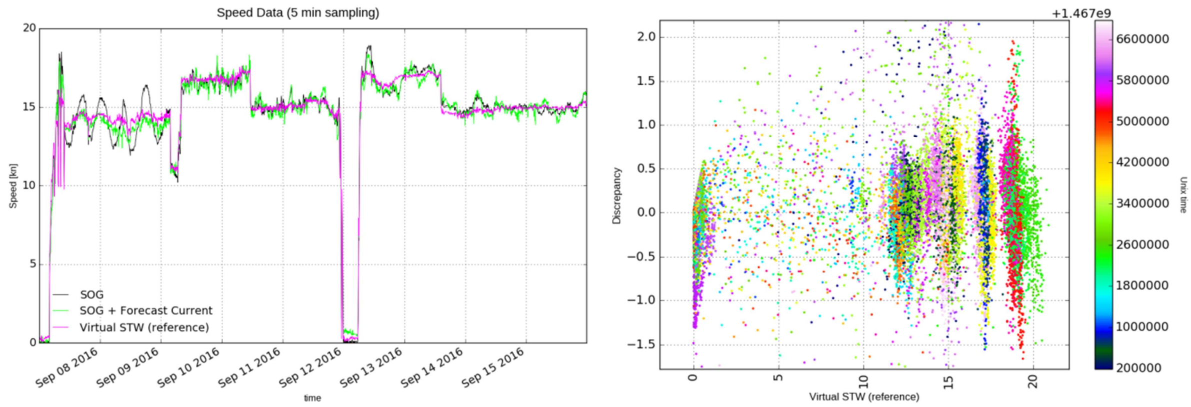

Fig.1: Left: SOG obtained via GPS (red), virtual-STW calculated using high-fidelity measurement data from Eniram Platform (green), and SOG plus current forecasts, i.e., the forecast-STW (blue). Right: Discrepancy between the forecast-STW and virtual-STW as a function of the latter.

3.2. Instantaneous fuel flow estimates

We proceed to applying (4) and (5) in estimating instantaneous fuel flow using the forecast-STW and meteorological data presented in 3.1. Actually, the model used in the fit is a generalization of (4) taking also draft effects and ocean waves into account. To avoid unnecessary complexifications, we leave further details for future studies. Values of the time-independent weight parameters β_1, β_2 as in (6) are estimated by Bayesian linear regression using the whole data. However, it should be noted that time-dependent generalizations can be straightforwardly implemented using e.g. Kalman-filter with a suitable evolution model highlighting the prior knowledge on the nature of the fouling effects.

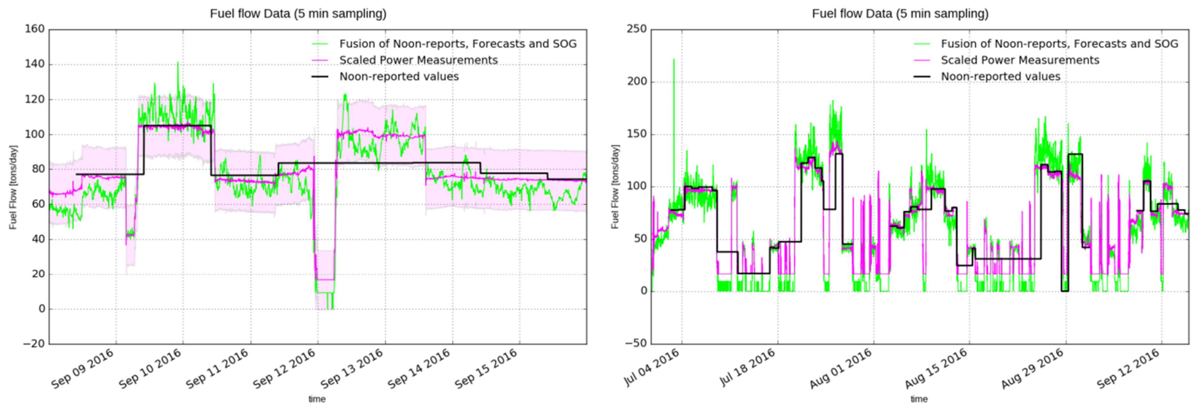

Fig. 2: Comparison of fuel flow histories of two different durations. The curves comprise (black) manually reported fuel mass flow daily averages, (magenta) reference measurements from Eniram Solutions Platform, and (green) estimates calculated using the proposed technique. The 95% confidence intervals are visualized in the left subfigure.

The results are mapped in Fig.2 including the reference fuel flow as well as the daily average fuel flows communicated by the crew. The reference fuel flow is estimated using the high-fidelity propulsion power and settling tanks' mass measurements available through the full Eniram platform on board. The 95% confidence interval in the (estimated) reference fuel flow is also visualized in the left-hand chart as a transparent magenta envelope. We observe that the fuel flow estimated with the proposed method – although containing larger random fluctuations than the reference measurement – is clearly more informative than the mere noon-report data. On the right we also present a subfigure containing estimates over the whole duration of the present data set but, for clarity, plotting the confidence interval is omitted. Interestingly, although the available average fuel flow measurements fall off range, the estimated (green) fuel flow captures properties of the reference data.

3.3 Projections onto the speed-fuel plane

As stated in 3.2, the employed fuel flow model depends on the STW together with external meteorological quantities. Therefore, fitting a cubic curve to the data in the speed-fuel plane gives a visual impression of the STW-dependent fuel consumption of the vessel in average weather conditions. Note that this differs from the curve that would be obtained with zero weather parameters corresponding to calm sea conditions.

The results are visualized in Fig.3. The left subfigure shows both types of fuel flow data plotted against their respective STW values, as well as the speed-fuel regression curve corresponding to the forecast-STW. Apart from the low-speed region, the speed-fuel point sets overlap nicely. On the right subfigure the two different fuel flows are plotted against each other together with a linear fit. The Pearson-correlation between the data sets is 0.98 indicating that the estimated fuel flow is qualitatively close to the high-fidelity power measurement.

Finally, a visual inspection reveals that the discrepancy grows along speed (colored dimension) which can be expected since, by (4), the forecast-STW noise is cubically amplified.

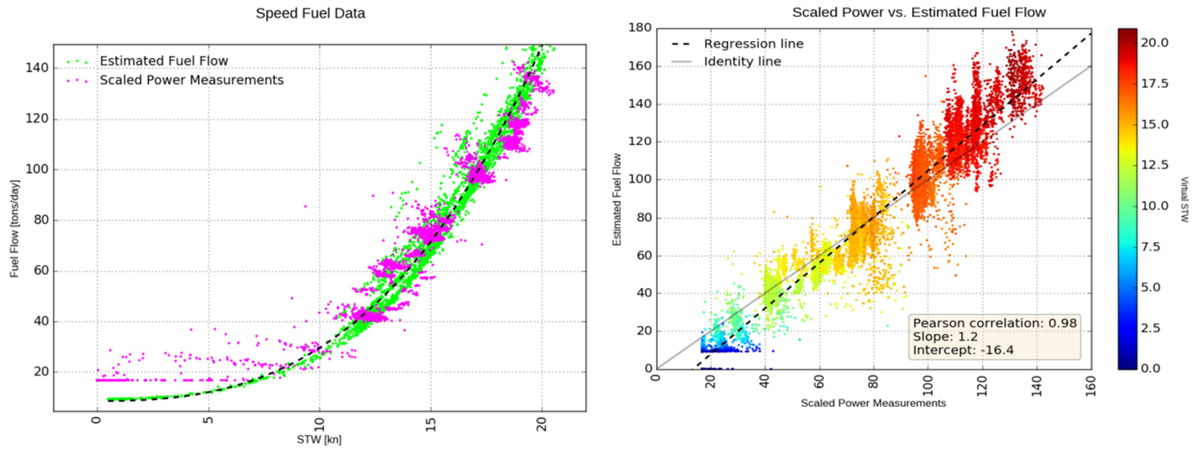

Fig. 3: Data mapped onto the speed-fuel plane. Left: The magenta and green scatter plots are the reference and estimated data, respectively. The dashed third order polynomial is fitted over the estimated data by linear regression. Right: Scatter plot of the estimated and reference data with the regression line.

4. Discussion

We have presented a computationally lightweight novel method for estimating instantaneous fuel consumption of a marine vessel when the speed over ground, water and wind, and (daily) aggregated fuel flow observations are available. The technique is based on a straightforward propulsion power model. The results indicate that the proposed method is capable of producing instantaneous fuel flow estimates which are qualitatively in accordance with high-frequency propulsion power consumption measurements. On the other hand, compared to high-fidelity measurement, the temporal resolution of the fuel flow estimate is considerably lower as expected.

References

ANTOLA, M. (2017), *The notorious speed through water*, 2nd Hull Performance & Insight Conference (HullPIC), Ulrichshusen

BERTRAM, V. (2012), *Practical Ship Hydrodynamics*, Butterworth & Heinemann, Oxford

COSTARELLI, D.; SPIGLER, R. (2015), *How sharp is the Jensen inequality?*, J. Inequalities and Applications 2015:69

GELMAN, A. (2014), *Bayesian Data Analysis*, Chapman & Hall/CRC

REHMATULLA, N.; SMITH, T. (2015), *Barriers to energy efficiency in shipping: A triangulated approach to investigate the principal agent problem*, Energy Policy 84, pp.44-57

Uncertainty of Ship Speed Determination when Sailing in Waves

Thijs W.F. Hasselaar, MARIN, Wageningen/Netherlands, t.hasselaar@marin.nl
Jeroen den Hollander, MARIN, Wageningen/Netherlands

Abstract

The validation ships designed for service conditions (lower speed, part load, representative sea state) cannot be done using traditional trials. Instead, single course runs must be performed in carefully quantified and monitored environmental conditions, such that the measurement can be compared with predictions. The irregular behaviour of the sea and atmosphere results in a constant surge motion of the vessel. Using time domain simulations the effect of these external forces on the ship speed has been quantified for a general cargo vessel and ferry in different sea states. Full-scale data of a container vessel and RoRo ship sailing in similar sea states has been used to validate the calculations including sensor uncertainties. Conclusions are made with respect to trial duration and achievable accuracy.

1. Introduction

Formulating the performance requirements for building contracts is a complicated task. Ideally a ship is designed and optimized for its service conditions; an average sea state, service speed and service loading conditions. Yet, the contractual performance is often stated in ballast trial conditions, which for cargo vessels often represent the speed corresponding to 100% MCR power of the engine, calm weather, ballast displacement with corresponding trim. The delivery trial has therefore little resemblance with the design specifications, and is more a random chosen condition to allow some kind of validation of the building process. The charterer however will have to state performance guarantees and requires knowledge of the capabilities and efficiency of their ship in service.

Traditional speed trials are done by sailing double runs in calm weather, correcting the measured power of each leg using empirical correction methods for wind and wave resistance, and averaging the speed over ground to cancel out the effect of current. The average speed and power represents the performance of the vessel in calm, no-wind, no-wave and no-current conditions, *ITTC (2014)*. The accuracy of the calculated performance highly depends on the environmental conditions at the time of trials and the corresponding calculation methods for added wind and wave resistance. When a vessel is however optimized for e.g. head seas BF4 in laden conditions, only a single leg speed run can be used for performance determination. This means the ship speed cannot be determined using solely the GPS, as the effects of current may be larger than the speed drop caused by wind and waves. The speed log must therefore be used to determine ship speed through water. The uncertainty of speed logs can however be large, depending on type, installation and sailing conditions, *Hasselaar (2015)*. Apart from the requirements of the instrumentation, the steadiness of the environment during single-leg speed runs is important to monitor. The sea and atmosphere are often irregular and unsteady, and a minimum measurement duration must be considered to statistically describe the environment and obtain repeatable measurements. The longer the measurement time, the higher the repeatability of the mean speed, but the more likely it is that the environmental conditions change.

Dallinga (2013) evaluated the effect of run duration on the mean and RMS values of a frigate sailing and manoeuvring in waves. Windage effects were not included in this research. Results showed an important contribution of low frequency excitation forces to the uncertainty of the mean speed determination. In this paper the sensitivity of the run duration will be discussed for other ship types. Service performance data collected onboard 3 vessels is used to evaluate the minimum run duration including the uncertainty from instrumentation. Conclusions will be made on minimum test duration, measurement uncertainty and best practice for performance measurement onboard ships in service.

2. Speed measurement uncertainty from single course runs

For single course trials the uncertainty in performance determination is dependent on the uncertainty in the speed log, shaft power measurement system and the variability of the environmental conditions. A ship sailing in waves experiences time-varying exciting from sources like:

- The chaotic character of a turbulent boundary layer and large scale eddy shedding, which affects propeller thrust and course keeping
- Low frequent variations in the wind speed and direction and wind driven current
- Low frequent variations in the magnitude of the excitation from waves, affecting added resistance and transverse forces and yaw moment
- Random elements in the autopilot hardware, such as dead band and delays.

The above factors not only affect the resistance and speed but also introduce low frequency course deviations. They have a direct effect on the uncertainty in ship speed measurements for single course speed trials, and dictate the minimum run duration to get sufficient accurate results. The effect of run duration on uncertainty of the mean of a run can be obtained directly from full-scale data. The speed through water signal from a ship is however affected by measurement uncertainties. Furthermore the environmental conditions will vary during the course over a day. To separate the speed variations caused by the variability of the environment, instrumentation errors and periodic fluctuations in wind and waves, time domain simulations are made for a 12.000 DWT general cargo vessel and a 9.700 DWT ferry. The particulars of the modeled vessel are presented in Table I.

Table I: Particulars vessel used for simulations

Parameter	General cargo	Ferry
L.O.A.	134 m	152 m
Beam	16.5 m	25.2 m
Design draught	7.1 m	5.7 m
Displacement	12.000 dwt	9.700 dwt
Design speed	16 kn	21.4kn
propulsion	Single CPP, 4.3m diameter	Double CPP, 4.2m diameter

3. Calculation of wave and wind resistance

To obtain a first impression of the uncertainties in stationary conditions, time domain simulations are made. 24-Hour time series of the general cargo and ferry sailing at design speed at four wave heights and wind speeds are made. From these time series sections of 10, 30, 60 and 180 minutes are taken. Only head sea conditions are considered. Variations in the average trial speed from the time sections are used to demonstrate the impact of the spectral characteristics on the vessel performance measurement. In the present work the effect of course keeping and the effect of the temporal and spatial variations in the incident flow are neglected. The sources of variations were limited to the natural variation of the added resistance in waves and the natural variations in the wind speed.

To calculate the speed variations from wind and wave resistance, the added resistance is separately calculated. To calculate time series of wave resistance, first the quadratic transfer functions (QTF) were calculated. Using the *Newman (1974)* approximation these were used to generate time histories for particular wave spectra. The QTF's were calculated with the Rankine source code FATIMA, *Dallinga (2015)*. Next, 24h time histories were generated by using a JONSWAP wave spectrum. Wave resistance time traces are made for significant wave heights of 0.5, 1.4, 2.15 and 3.75 m with a peak period of 6.2, 7.6, 8.4 and 10.1 s, respectively. This corresponds roughly to a sea state Douglas scale 2, 3, 4 and 5.

Low frequency induced wind forces can exceed 10% of the total ship resistance. Variability in the wind can therefore have significant impact to ship speed variations. To model the wind fluctuations a

Frøya wind spectrum was used. Combined with representative wind drag coefficients, 24 h time traces of wind resistance were made. The Frøya spectrum is defined by:

$$S(f) = 320\left(\frac{U_r}{10}\right)^2 \left(\frac{z}{10}\right)^{0.45} \left(1 + X^{0.468}\right)^{-\frac{5}{3 \cdot 0.468}}$$

With $X = 172\left(\frac{U_r}{10}\right)^{-0.75} \left(\frac{z}{10}\right)^{2/3} f$

z is the height above the sea level [m] and $U(z)$ the reference 1 hour speed at a height z and $U_r = U\,(10\,m)$, and f the frequency.

Wind speeds corresponding to Beaufort scale 2, 4, 5, and 6 were used (3, 6, 9 and 12 m/s at a reference height of 10 m). As the vessel forward speed increases the apparent wind speed, the vessel speed is added to the selected wind speeds.

4. Calculation of ship speed in wind and waves

To calculate the speed variations caused by added wind and wave resistance components, the propeller open water diagram was used to calculate the operating point of the propeller and consequently the power fluctuations. The analysis was made using a fixed pitch propeller to ease the calculation. This simplification has practically no influence on the results.

The ship's resistance is defined as:

$$R_{tot} = R_{Calm} + R_{wind} + R_{waves}$$

To calculate the initial propeller speed at this resistance, the required thrust is intersected with the open water diagram. By dividing K_T by J^2 the initially unknown propeller speed N is taken out of the equation:

$$\tau = \frac{K_T'}{J^2} = \frac{\dfrac{T}{\rho n_1^2 D^4}}{\left(\dfrac{V_a}{n_1 D}\right)^2} = \frac{R_{tot}}{\rho(1-thdf)\left[V_s(1-w)\right]^2 D^2}$$

This value can then be intersected with the thrust coefficient K_T of the propeller in open water conditions. The intersection gives the advance coefficient J, which is used to calculate the new propeller speed, shaft torque and power:

$$n_1 = \frac{V_s(1-w)}{J_1 D}$$

$$Q_1 = K_{Q1}\rho n_1^2 D^5$$

The time domain simulations follow by changing R_{wind} and R_{wave} according to their calculated spectra in time, and calculating the change in ship speed. As long as the propeller load remains within normal operating conditions the engine governor will keep the propeller speed constant regardless the load.

$$a(t) = \frac{T(1 - thdf) - R_{calm}(t) - R_{wave}(t) - R_{wind}(t)}{m}$$

$$\Delta Vs(t) = \frac{T(1 - thdf) - R_{calm}(t) - R_{wave}(t) - R_{wind}(t)}{m}\Delta t$$

$$Vs(t+1) = Vs(t) + \Delta Vs(t)$$

With $a(t)$ the ship's acceleration / deceleration due to wind and wave resistance
$thdf$ thrust deduction fraction
m Displacement of the vessel, including added mass (assumed 10% of displacement)
Vs Ship speed
t time step

The characteristics of the turbo charger affect the dynamic behaviour of the ship. In moderate sea states it is assumed however that the dynamics of the turbo charger affect the mass-spring characteristics of the vessel only little. Furthermore it is assumed that the engine layout is chosen such that during the tested wave and wind conditions the engine does not reach over-load conditions. In other words it is assumed that the engine can respond to the load changes by the propeller directly.

Fig.1 shows an example of a 24 time series of the simulated ship speed, shaft power, thrust and resistance. Large, non-periodic variations in ship speed can be observed. The time series of the power shows that the variations in power are maximum 10% of the mean and have periodic variations with a low period, which suggest that the diesel engine should be well capable of following the torque demand. The impact of not having modelled the dynamic behaviour of the diesel engine is therefore not relevant. The simplified model suffices.

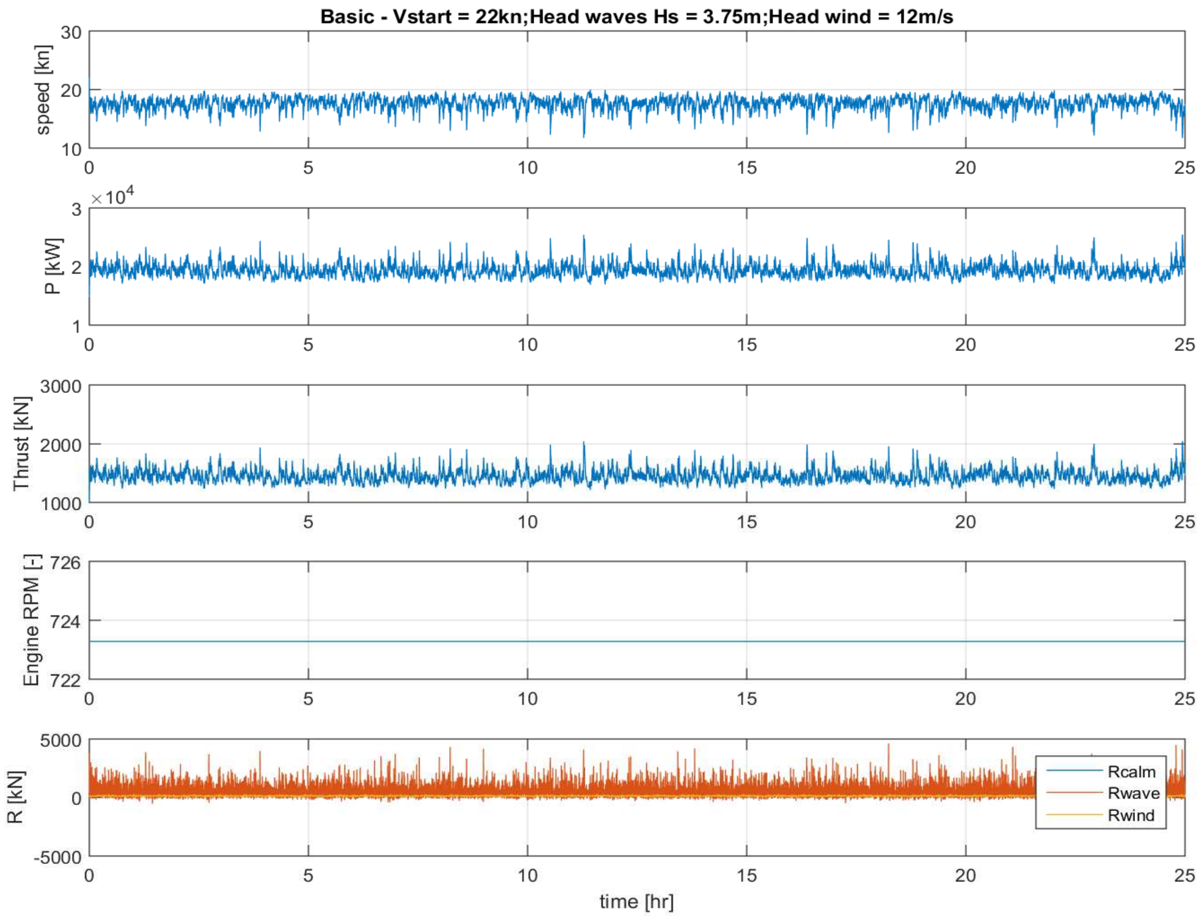

Fig.1: Simulated 24-h time series of a ferry sailing in 3.7 m waves and 12 m/s wind

5. Speed variations from simulated ship performance data in seas

The 24h time traces of ship speed are split up into smaller time windows (speed runs). For each run the mean is calculated. Using the available 24h data, there are 144 x 10-minute periods, 48 x 30-min periods, 24 x 60-min periods and 7 x 180-min periods. The standard deviation of the means is used to express the uncertainty in the ship speed determination when performing a single course trial run on a ship in service. In the simulations the measurement uncertainty from the speed log and the uncertainty in sea spectrum and natural weather variations are excluded.

Figs.2 and 3 shows 2x the standard deviation of the mean ship speed for the different weather conditions when each mean is calculated over various durations. It represents the theoretical 95% confidence interval that when the ship speed is measured over a period of *x* minutes, the same mean will be obtained if under the same conditions the speed is determined again *x* minutes later. The spread in mean speed for the different run durations show that the mean speed of a run is affected by low frequent variations that occur in seas described by a JONSWAP spectrum and wind of a Frøya spectrum. The longer the run duration, the more low-frequency components are captured within a run duration, and the lower the standard deviation of the calculated mean ship speed.

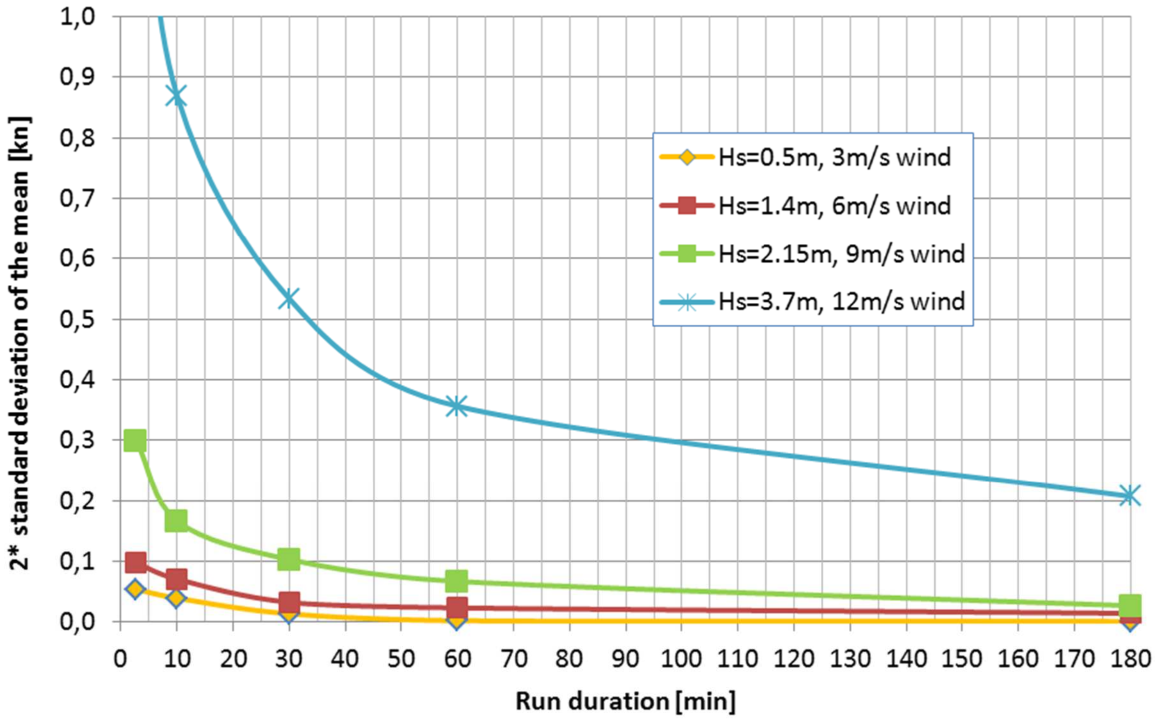

Fig.2: Uncertainty of the mean speed calculated using different run durations for a ferry at 22 kn

Fig.2 shows that in order to measure ship speed on the ferry at 22 kn with an uncertainty of ±0.12 kn (corresponding to 1.5% uncertainty in power), it is possible to measure the ship performance in waves up to 2.15m height over a single 20 minute measurement period. When the performance of the vessel is to be validated in higher sea states, the low-frequent variations in ship speed will become too long to measure ship speed with sufficient accuracy even with a run duration of 1-3 h. When the speed reduces, and the relative contribution of wind and wave resistance compared to the calm water resistance increases, the uncertainty increases rapidly. More importantly, less low-frequent waves are encountered in a set time period. Therefore the higher the speed, the more waves are encountered, and the less the deviation in the mean speeds. Fig.3 shows similar results for a general cargo vessel at much lower speeds. The relation between run duration and standard deviation in the mean speed approximates a squareroot decay. Low-frequent variations, that are not captured in a single measurement period, cause small deviations from this relationship. Based on these calculations it can be concluded that for the general cargo vessel the performance can be measured with 0.1 kn accuracy using a 15 minute run at 13 kn in SS3, whereas a 3 h run duration is required to get the same uncertainty in sea state 4. Higher sea states require unpractical long measurement durations, where there is a high chance of changes in the environmental conditions.

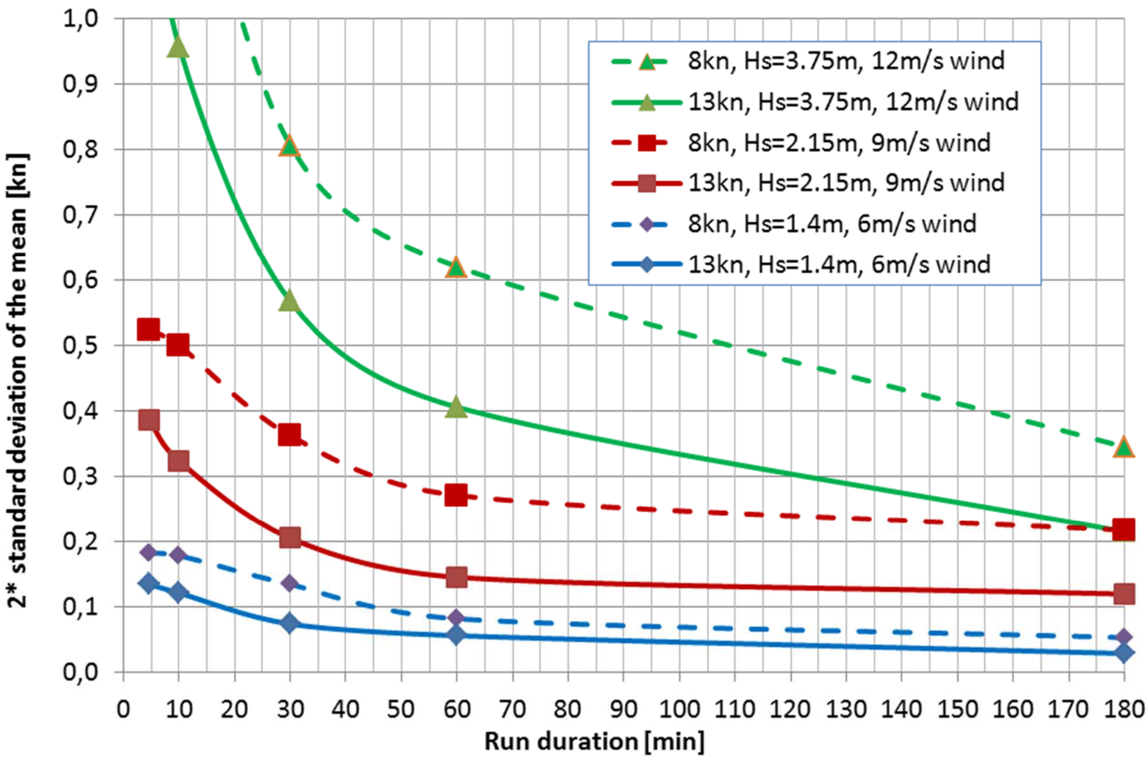

Fig.3: Uncertainty of the mean speed calculated using different run durations for a general cargo freighter at 8 and 13kn

6. Speed measurement uncertainty from actual service performance data

The uncertainty in the previous analysis considers only the irregular environmental conditions. In reality other uncertainties also play a role:

- Measurement uncertainty of the speed log; stratified current layers underneath the ship, effect of the ship's boundary layer on measurement volume
- Uncertainty in the definition of the environmental conditions. Ship speed is directly affected by wind, waves, drift, shallow water, stratified current etc. Ideally these conditions are constant and can be monitored accurately. However, the measurement of environmental conditions is practically difficult, as it requires advanced instruments such as a wave buoy or wave radar, and/or is affected by the ship, such as wind distortion at the anemometer site
- Uncertainty in performance estimations due the effects of low-frequent drift motion, varying propeller-hull interaction, rudder forces

To determine the uncertainty in performance measurement including these uncertainty sources requires in-service performance data from a ship in constant environmental conditions. For this case study, data from three ships has been used:

- 3.600 DWT general cargo vessel
- 26.000 DWT container vessel, design speed 20.6 kn
- 15.000 DWT RoRo car carrier, design speed 21.5 kn

The challenge hereby is to find conditions whereby the environmental conditions and ship performance can be considered constant. The time domain simulations indicate that performance monitoring should focus on fair weather conditions for merchant ships (assuming these vessels sail at moderate speeds). Periods with low relative wind speed and little ship motions have therefore been searched in a 2 year database of performance data. Figs.4 and 5 show the uncertainty for the container vessel and RoRo vessel respectively. Each line represents the uncertainty data taken from a continuous data set from a different day. There appears to be a large variation in speed uncertainty regardless careful selection of similar environmental conditions.

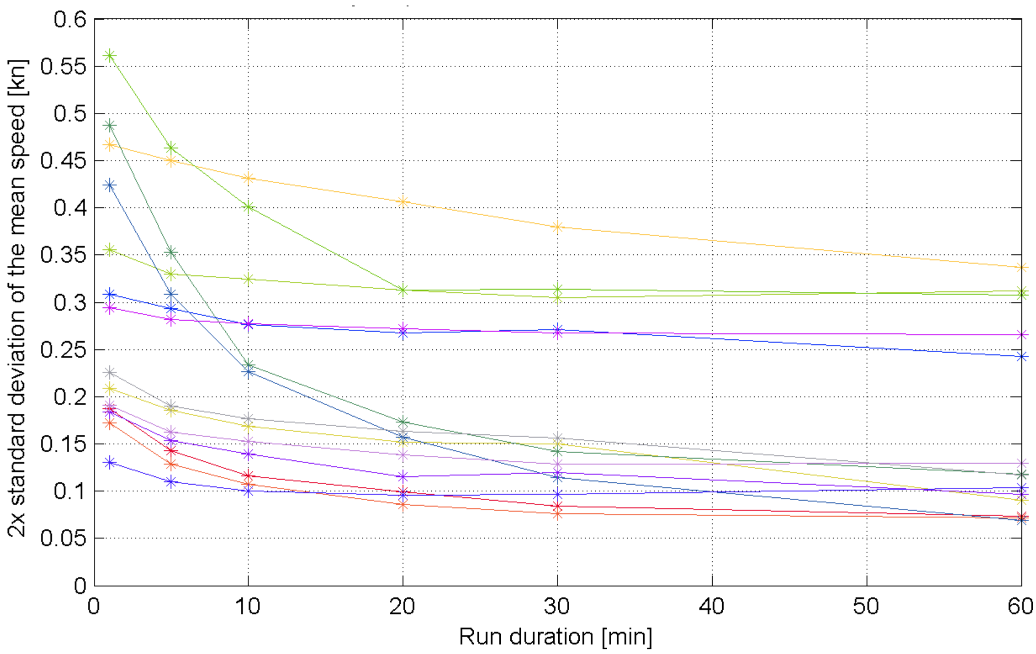

Fig. 4: Speed uncertainty of 180 m container vessel sailing at 16 kn in SS3-4. Each line represents data from a different day, but similar ship response

For both figures, most results are grouped close together, but that there are clear 'outliers' from days where there is a higher uncertainty. These periods could be flagged in the data as speed measurement 'errors' through post-processing. The propeller operating point (K_q), in combination with the propeller open water diagram provides hereby a useful parameter to validate the ship speed through water. Only when these data periods of inconsistent speed measurement can be identified, can single course speed runs be used to validate ship performance with an uncertainty in the order of ±0.15 kn.

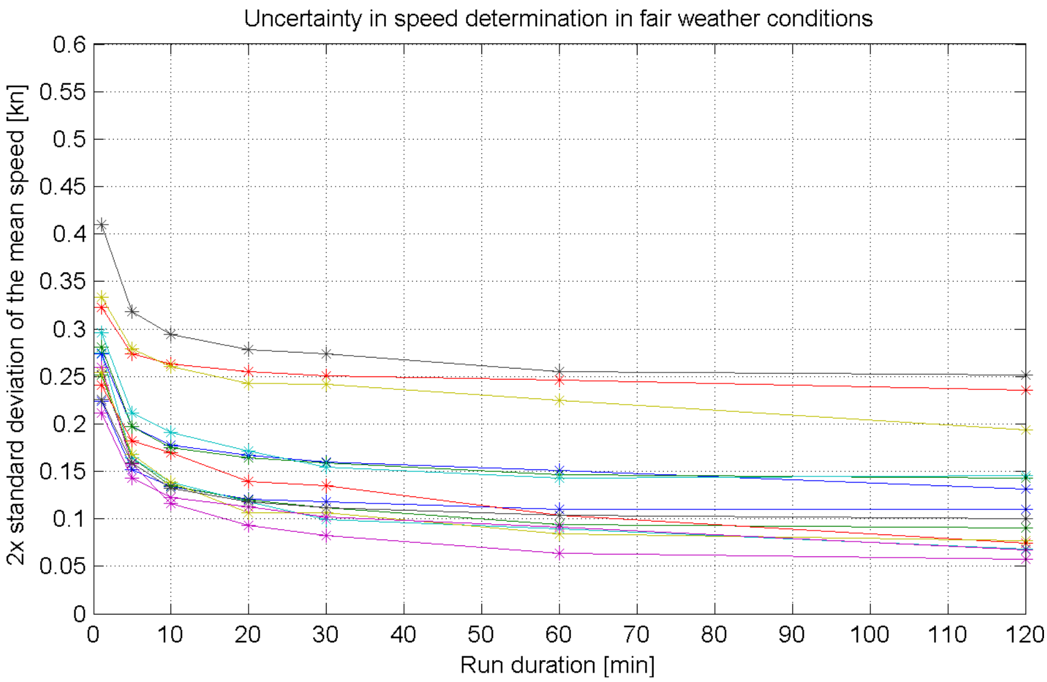

Fig.5: Speed uncertainty of 180m Car Carrier sailing at 17.4 kn in fair weather. Each line represents data from a different day, but similar ship response

For the much smaller and slower general cargo vessel the service data contained less periods of steady state performance in fair weather; the vessel responses were more pronounced, and due to the coastal routes the vessel changed heading frequently. Yet, some 9 data periods of more than 5 h could be identified to calculate the statistics for different test durations. For a 10 minute period maximum found uncertainty (2σ) in the mean speed was ±0.24 kn, with the 30 minute averaging period it was 0.15 kn at 10 kn.

7. Conclusions

The validation of ship performance in other than calm weather conditions with accuracy levels in the order of 1-2% requires a careful prepared trial procedure. Single course runs must be performed in carefully quantified and monitored environmental conditions, such that the measurement can be compared with predictions. A speed log must be used to determine ship speed. The irregular behaviour of the sea and atmosphere results in a constant surge motion of the vessel. Using time domain simulations the effect of these external forces on the ship speed have been quantified for a general cargo vessel and ferry in different sea states. Full-scale data of a container vessel and RoRo ship sailing in similar sea states has been used to validate the calculations including sensor uncertainties. It shows that, as long as sensor errors can be identified, ship performance can be estimated only at speeds higher than approx. 13 kn and a sea state equal or lower than Douglas 4 using a single trial run. Uncertainties in the quantification and measurement of environmental conditions result in uncertainty levels in the order of ±0.15 kn. For high speeds (22kn) a trial duration of 20 minutes provides an uncertainty level of ±0.10 kn for a ferry; for a general cargo vessel at 13 kn a 60 minute run duration is required.

The results further indicate that when the simple parameters wave height, wave direction, wind speed and direction are used to calculate the added wave and wind resistance, it may not be possible to fully correct measured ship performance to ideal trial conditions. The irregular marine environment requires long measurement periods in order to account for low-frequent surge motions of the ship. Statistical methods (e.g. averaging) are necessary account for these variations in order to derive performance trends. This clarifies a part of the large scatter in performance indicators found in ship performance monitoring schemes, where regardless best practices, statistical methods remain important to derive trends.

Acknowledgements

This research is partly funded by the Dutch Ministry of Economic Affairs and the European Union's 7th framework research and innovation programme under grant agreement No 605190.'

References

DALLINGA, R. (2015), *FATIMA takes on more prominent role in seakeeping assessments*, MARIN Report, December, www.marin.nl

HASSELAAR, T. (2015), *Speed measurements for ships in service*, Green Ship Technology Conf., Copenhagen

ITTC (2014), *Recommended Procedures and Guidelines - Speed and Power Trials, Part 2: Analysis of Speed/Power Trial data*, Pub. L. No. ITTC 7.5-04-01-01.2 (2014)

NEWMAN, J N. (1974), *Second-order, slowly-varying forces on vessels in irregular waves*, Int. Symp. Dynamics of Marine Vehicles and Structures in Waves, London

Measuring the Full-Scale Performance of a Propeller and Bulbous Bow Retrofit via Propeller Thrust Measurements

Erik van Ballegooijen, VAF Instruments, Dordrecht/Netherlands, evballegooijen@vaf.nl
Tiberiu Muntean, VAF Instruments, Dordrecht/Netherlands, tmuntean@vaf.nl
Marc Timmer, VAF Instruments, Dordrecht/Netherlands, mtimmer@vaf.nl

Abstract

This paper presents the possibilities offered by full-scale measurements of propeller thrust (and torque), for fuel saving potentials and emission reductions due to the retrofit of a new propeller design and a new bulbous bow design on a large TEU container vessel. It explains how via full-scale measurements of propeller thrust, in relation to other parameters like ship speed, the change in propeller efficiency and the hull resistance can separately be measured. This enables to evaluate the effects of the retrofit on reducing fuel consumption and emissions. An example is shown of the measurement results of propeller thrust and torque on a large TEU container vessel in service, before and after the vessel has been retrofitted with a new propeller design, and a new bulbous bow design.

1. Introduction

In general there is a large interest in the maritime world for ship propulsion efficiency. This has several reasons related to either cost savings, legislation, and/or environmental concern. In this respect also the upcoming MRV and IMO regulations on respectively CO_2 emissions and fuel consumption play an important role. Next to legislation the focus on fuel consumption has also a direct operational (fuel) cost reduction benefit. In view of the above fuel consumption reduction, the concept of slow steaming has been introduced on for instance container vessels. This in general resulted in significant fuel savings. But since the earlier container vessels have mainly been designed for higher ship speeds and therewith engine powers, the propeller and hull designs might not be optimum any more for the new operational conditions when applying slow steaming. In order to further benefit from the slow steaming, applying a retrofit to the vessel is considered as an option. The retrofit could exist of several modifications such as:

1. A new propeller design which is optimized for the new slow steaming operational condition of lower power and RPM. This might increase the propeller efficiency.
2. A new bulbous bow design which is optimized for the new slow steaming operational condition of lower ship speed, and possible lower draught, and there with an improved wave pattern of the ship's bow. This might reduce the hull resistance.

As both modifications imply a considerable amount of investment costs, the expected to be achieved fuel savings via increased propeller efficiency and/or reduced hull resistance need to be verified after the retrofit in order to verify if the predicted improvements are really achieved.

To determine the increase in propeller efficiency, and the reduction in hull resistance, before the actual retrofit, use can be made of calculations (like CFD), and/or model tests in a model basin. For determining the improvements of propeller and hull after the retrofit on the actual ship, full-scale measurements need to be performed. In order to be able to identify the improvement of the propeller separate from the improvement of the ship's hull, next to shaft power and RPM, also propeller thrust should be measured. If one is only relying on measurements of propeller shaft power or even only engine fuel consumption, the distinction between propeller and hull improvement cannot be made. This hampers a proper comparison of the actual improvements against the predicted improvements based on CFD and/or model tests. This paper provides a more detailed description on the full-scale propeller and hull performance measurements, and an example of the measurement results achieved on a large TEU container vessel in service prior and after it has been retrofitted with a new propeller and bulbous bow designs.

2. Theoretical approach for propeller and ship hull performance measurement

When looking at the performance of the propeller and ship hull retrofits, it is important to be able to separately measure the propeller performance from the hull resistance. In order to be able to do this it is needed to measure next to propeller power, also the propeller thrust.

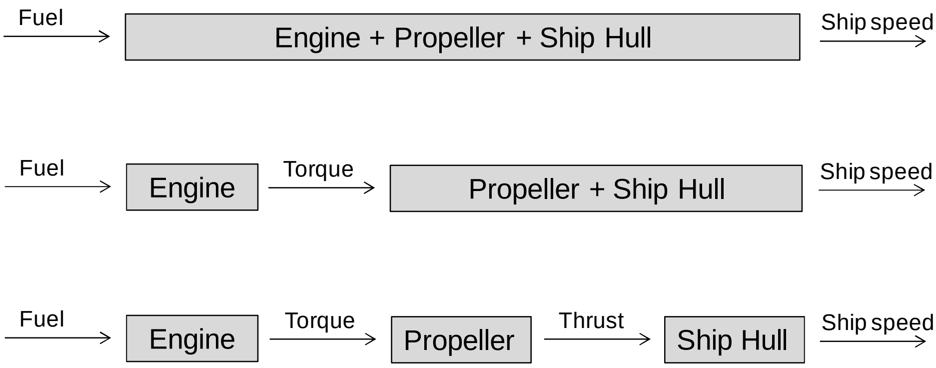

Fig.1: Three ways to monitor the ship propulsion performance and the involved detailed efficiencies

In order to measure the performance of the propeller and the ship hull (resistance), in practice several ways are used as are shown in Fig.1, based on either:

- Engine Fuel consumption (1st route in Fig.1)
- Torque (2nd route in Fig.1)
- Thrust (3rd route in Fig.1)

As can be seen, the 3rd route, where propeller thrust is measured (next to torque), is the only way at which the propeller performance can be separately measured from the hull performance (resistance). If in addition the fuel consumption of the propulsion engine is measured, also the efficiency of the engine can be determined separately.

2.1. Propeller performance determination

When looking at propeller theory the propeller efficiency (Eta-0) is clearly defined as the ratio between dimensionless propeller thrust (Kt) and dimensionless propeller torque (Kq), where J is the advance ratio of the propeller through the water:

$$Eta\text{-}0 = J\ Kt / 2\ \pi\ Kq$$

This formula is valid for both Fixed Pitch Propellers (FPP) as well as Controllable Pitch Propellers (CPP), and indicates that both thrust and torque needs to be measured in order to measure the propeller efficiency. As such the only proper way to measure the performance of the propeller separately from the performance / resistance of the hull, is via measuring thrust.

2.2. Hull resistance determination

A direct measurement of the hull performance is the amount of propeller thrust (*Tprop*) needed to overcome the hull resistance (*Rhull*) at a certain ship speed. For this the following function applies:

$$Tprop = f(Rhull)$$

If for instance only the propeller power is used to “measure” hull resistance (2nd route in Fig.1), there is an underlying assumption that the conversion of power to the propeller into thrust from the propeller is always a non changing constant. This is not the case in reality, as the propeller conversion from power to thrust is clearly related to the efficiency of the propeller, which changes over time and also per sailing condition like for instance for a fixed RPM CPP.

3. Full-scale measurement lay out used

In order to determine the propeller and ship hull condition via measurements, several parameters need to be taken into account and measured. In addition the measured data need to be enriched in order to be able to subtract the relevant data points for a proper comparison of the propulsion performance. In the next paragraph a general overview of the used measurement parameters and data enrichment is shown. Special attention is paid to the propeller thrust measurement via the TT-Sense® sensor, and the used data enrichment via the IVY® Propulsion Performance Management solution.

3.1. Parameters to be measured

In order to determine the propeller and ship hull condition, several parameters need to be taken into account and measured. A typical list of to be measured parameters consists of:

- Propeller thrust
- Propeller torque
- Propeller RPM
- Speedlog (STW)
- GPS location
- Ship draught
- Seastate
- Wind

The majority of these parameters are already measured and available on board of a ship via dedicated sensors, and / or log reports. Propeller power, via torque and RPM, is nowadays a rather common measurement on board of a ship. But in order to be able to separate the propeller performance from the ship hull performance, the propeller thrust needs to be measured as well. This asks for an additional propeller thrust sensor.

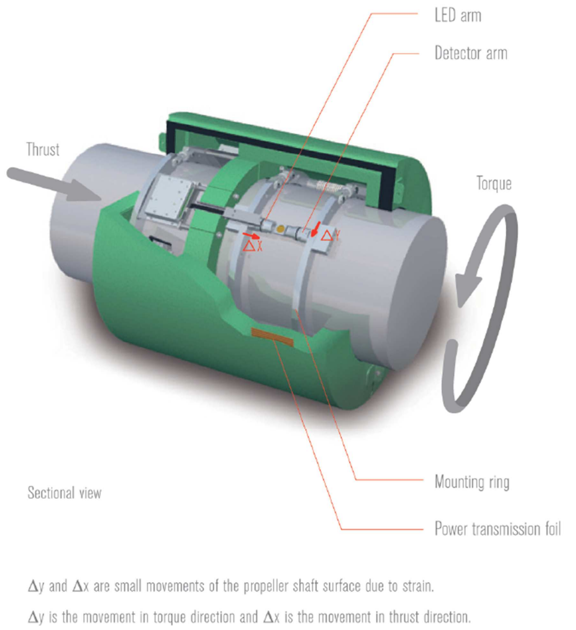

Fig.2: General working principle of the TT-Sense® Thrust and Torque sensor

For this, VAF Instruments (the Netherlands), a supplier of measurement systems for the maritime market, has developed the TT-Sense® thrust and torque sensor, as is shown in Fig.2. The sensor, which is already on the market for more than four years, has been used by VAF Instruments R&D department to quantify vessel performance and to track the changes in vessel performance over time. Until now experience is gained on many types of vessels from small cargo vessels towards 14000 TEU container vessels, as well as on navy vessel shaft lines. The working principle of the TT-Sense® sensor is based on, separately measure the torsion (torque) and compression (thrust) of the propeller shaft via very accurate optical sensors.

With the TT-Sense® sensor it is possible to separately measure the propeller efficiency of the actual propeller at full scale behind the vessel, next to the actual resistance of the vessels hull. See *Ballegooijen et al. (2016)* for more details.

3.2. Handling of measured data

VAF Instruments developed in addition the IVY® Propulsion Performance Management solution. This is a dedicated software solution that among others enriches the data from the TT-Sense® and translates it into easy to access dashboards with KPIs and graphs, showing the actual performance of the propeller and the ship hull separate. A typical example of the IVY® dashboard can be seen in Fig.3, where the measured performance over time of the propeller and the ship hull are shown.

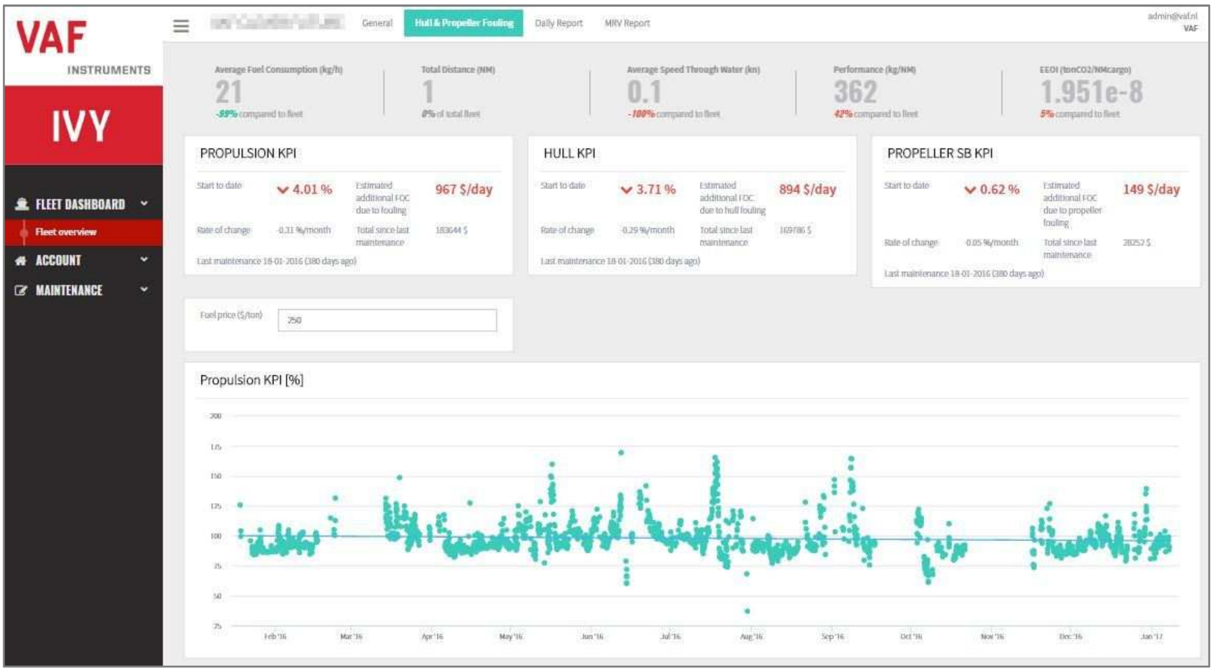

Fig.3: A typical example of the IVY® Propulsion Performance Management solution where the TT-Sense® measured propeller and hull performance is shown over time.

4. Full-scale measurements on a large TEU container vessel

The full-scale measurement results for a Large TEU container vessel which has been retrofitted with both a new propeller design and a new bulbous bow design, are presented in this paper. Measurements of the separate propeller performance and the hull resistance are performed via the use of the VAF Instruments TT-Sense® sensor, and the IVY® Propulsion Performance Management solution.

The following measurements are performed based on the TT-Sense® thrust measurements:

	Light draught	Design draught
Original propeller design	X	X
Original bulbous bow design	X	X
New propeller design	X	X
New bulbous bow design	X	X

Fig.4: Full-scale conditions for measurements performed with the TT-Sense® thrust sensor

The full-scale measurements with the VAF Instruments TT-Sense® thrust sensor on board of this large TEU container vessel comprise a period of more than 2 ½ years. About the first 1 ½ years are with the original propeller and original bulbous bow design. After the actual retrofit of the vessel when the vessel was equipped with the new propeller design and the new bulbous bow design, the full-scale measurements with the TT-Sense® thrust sensor continued for about ½ a year.

4.1 Full-scale propeller performance based on thrust measurements with the TT-Sense®

For predicting the possible performance improvements of the new propeller design, which will be applied at the retrofit of the vessel, model tests have been performed at a model test basin with both the original propeller and the new design propeller. The model tests predicted significant performance improvements for the new propeller design at the various ship speeds and for both light draught and design draught conditions. The new propeller performance improvements are rather insensitive to draught conditions and ship speed.

From the model tests, the propeller open water curves are available of both the original and the new propeller design. In addition there is 1 ½ year of full-scale propeller efficiency (thrust and torque) measurements done via the VAF Instruments TT-Sense® sensor for the original propeller design. Next to that there is for ½ a year of full-scale propeller efficiency (thrust and torque) measurements done via the TT-Sense® sensor for the new propeller design. Measurements are split into light draught and design draught conditions.

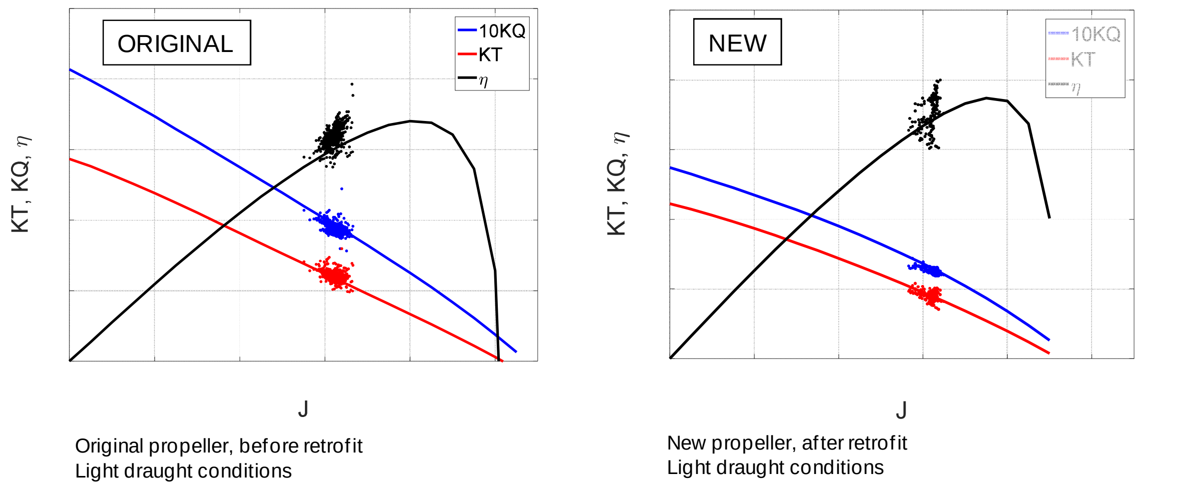

Fig. 5: Light draught: full-scale measurements with TT-Sense® sensor (dots) of the original propeller (left) versus new propeller (right), compared to model-test open-water curves (lines)

In Fig.5, full-scale TT-Sense® measurement results of the original propeller design and the new propeller design for the light draught condition of the vessel are shown. In the graphs a good comparison is seen between the full-scale measurements via the TT-Sense® thrust and torque sensor (dots), and the model test predicted open water curves (lines). This good comparison applies for both propeller designs (original and new). Herewith a good indication of the accuracy and the long term stability of the thrust and torque measurements is shown.

In Fig.6, the results of the full-scale propeller performance measurements via TT-Sense® sensor (dots) for the design draught conditions of the vessel are compared to the model test predicted open water curves (lines) of both the original propeller design and the new propeller design.

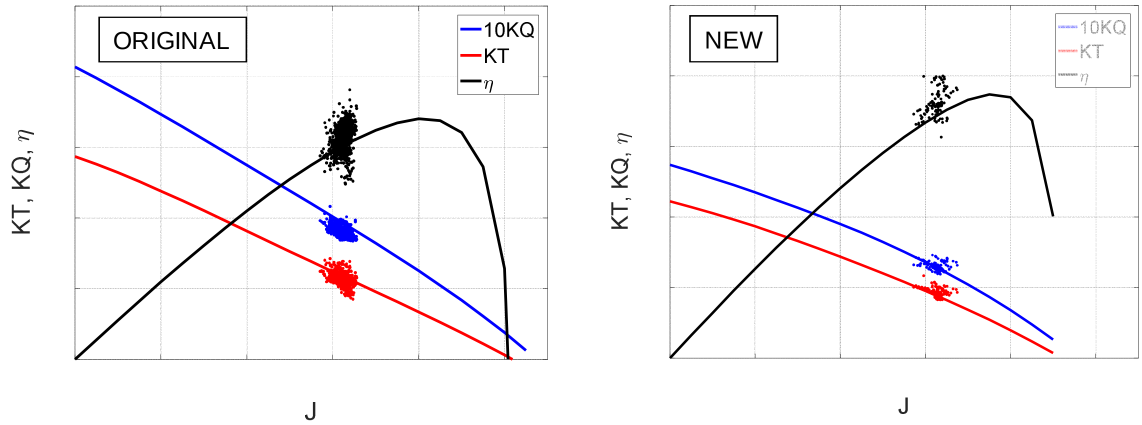

Original propeller, before retrofit
Design draught conditions

New propeller, after retrofit
Design draught conditions

Fig.6: Design draught: full-scale measurements with TT-Sense® sensor (dots) of the original propeller (left) versus new propeller (right), compared to model-test open-water curves (lines)

Fig.6 shows that also for design draught conditions a good comparison between the model test predicted propeller performance, and the full-scale measured propeller performance, is found. In addition herewith a good indication of the accuracy and the long term stability of the thrust and torque measurements via TT-Sense® is shown. As can be seen from Figs.5 and 6, the model test predicted performance improvement of the new propeller design correlates fairly well with the full-scale measurements of the new propeller. Next to the model tests, also the full-scale measurements point towards an improvement in efficiency by retrofitting the new propeller, as is shown in Fig. 7. Here the relative performance improvement in %, of the new propeller design compared to the original design, is plotted against 3 different slow steaming ship speeds. The ship speed (Vs) is shown as a fraction of the original vessel design speed (Vdesign).

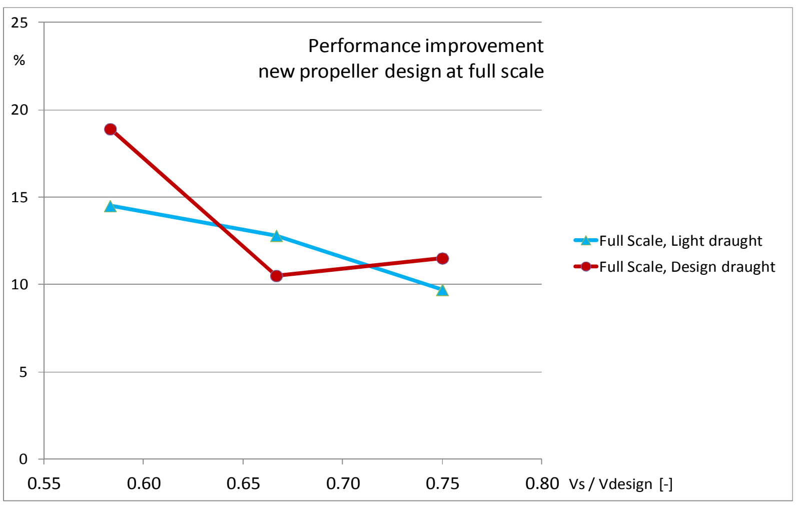

Fig.7: Full-scale new propeller design performance improvement compared to original design, based on thrust measurements via the TT-Sense® sensor

4.2. Full-scale bulbous bow performance improvements via TT-Sense® thrust measurements

Since at the vessel the propeller thrust is measured via the TT-Sense® thrust sensor, herewith also the total hull resistance is measured. Based on these measurements the possible resistance improvement of the new bulbous bow design can be measured. In Fig.8, the full-scale measured improvement in resistance due to the new bulbous bow design (compared to the original design) is shown for the various ship speeds and the 2 draughts.

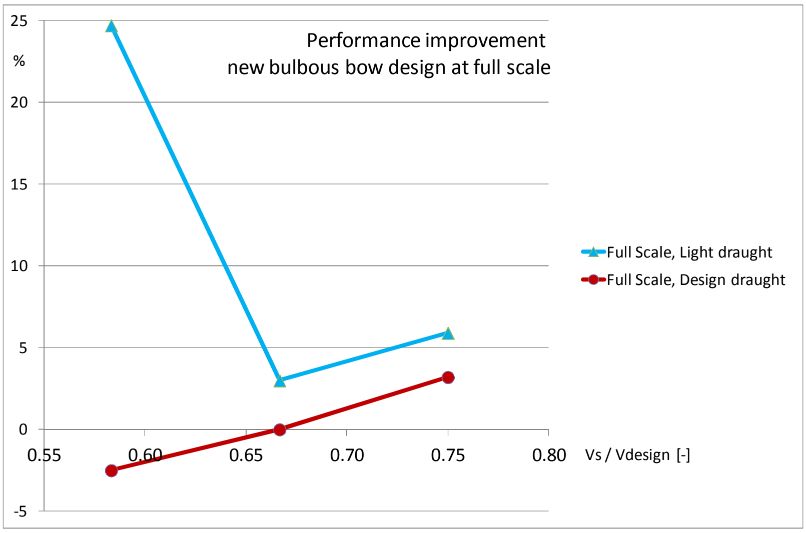

Fig.8: Full-scale new bulbous bow design performance improvements compared to original design, based on thrust measurements via the TT-Sense® thrust sensor.

Fig.8 shows that the improvement in full-scale hull resistance due to the new bulbous bow design is highly depending on the ship speed and the draught of the vessel. Especially at the design draught, the improvement in hull resistance compared to the original design, is measured to be limited.

4.3. Full-scale propeller + bulbous bow performance improvement measured by thrust

When combining the measured full-scale performance improvements of the new propeller design, with the performance improvements of the new bulbous bow design, the total performance improvement of the retrofit can be determined. Since the individual performance improvements of the new propeller design and the new bulbous bow design can be measured only via the full-scale thrust measurements, the full-scale measured performance improvements of both, as shown in paragraph 4.1. and 4.2. are combined. The total full-scale measured performance improvement of the retrofit, based on the TT-Sense® thrust measurements, are shown in Fig.9. As can be seen from Fig.9, the full-scale measurements indicate towards a total performance improvement due to the retrofit.

As indicated these full-scale measurements are based on thrust measurements. In order to further investigate the measured performance improvements, in the next paragraph the measurements are compared to full-scale measurements based on torque (power), and on fuel consumption of the main engine. As is shown in Fig.1, only via thrust measurements a distinction between propeller performance and hull resistance can be measured. When measuring the performance improvement of the retrofit via torque (power), the individual performances of the propeller and the hull are summed and cannot be measured separately (the 2nd route in Fig.1).

Finally when measuring the performance improvement of the retrofit via measuring the propulsion engine fuel consumption also the propulsion engine performance is summed together with the propeller and hull performance (the 1st route in Fig.1), and no distinction between engine, propeller, and hull performance can be made.

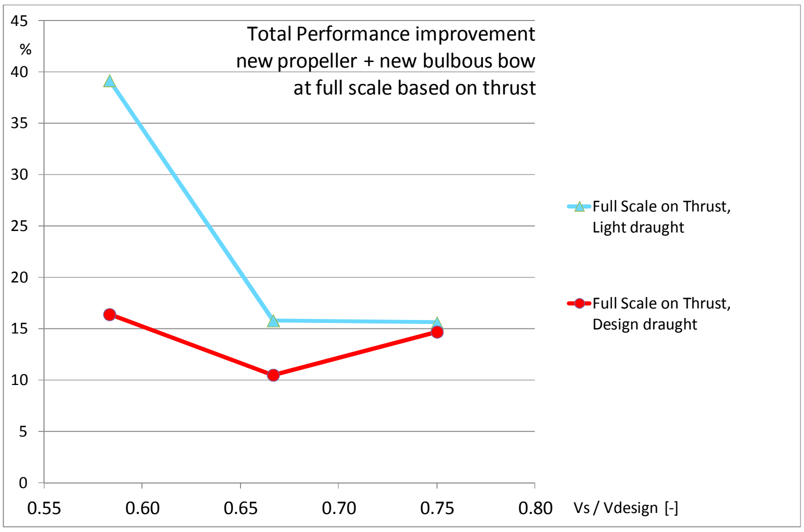

Fig. 9: Total full-scale retrofit performance improvement measured via TT-Sense®

Nevertheless, next to the thrust measurement route, a comparison is made with the torque (power) measuring route and the propulsion engine fuel consumption route, in the next paragraphs. This shall provide insight in the correlation and accuracy of the thrust measurements. Especially since the measurement of thrust, torque and fuel consumption are 3 independent measurements.

4.4. Full-scale propeller + bulbous bow performance improvement measured by torque (power)

In this paragraph the full-scale measurements based on torque (power) are shown. Fig.10 shows the total full-scale performance improvement due to the retrofit as measured via the propulsion power. The full-scale total performance improvement based on the torque (power) measurements is nearly identical to the total performance improvement based on thrust, which provides an indication of the value of both (independent) measurements.

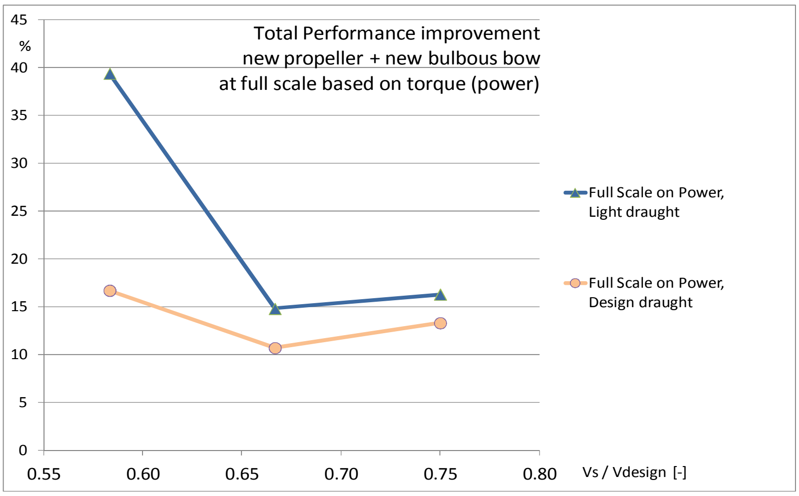

Fig.10: Total full-scale retrofit performance improvement based on torque (power) measurements

4.5. Full-scale propeller + bulbous bow performance improvement measured by engine fuel consumption

The third way to compare the full-scale propulsion improvements of the retrofit is via measurements of the actual fuel consumption of the propulsion engine. When measuring the fuel consumption of the engine, not only the change in performance of the new propeller design and the new bulbous bow design is summed, but now also the engine efficiency is incorporated as well. This as is shown in the 1st route of Fig.1.

Based on earlier investigations the engine efficiency is changing over time due to for instance engine deterioration, changes in caloric value of the fuels used, and operational conditions of the engine like the RPM dependability of the efficiency of the engine. Variations in engine efficiency of several percent are seen from past data. As such the measurements of the propulsion engine fuel consumption provides just an indication of the overall performance improvement of the propeller and bulbous bow retrofit. In addition, when measuring only engine fuel consumption, no split in efficiency improvements between engine, propeller and hull can be made, in contrary to when measuring thrust.

The full-scale measured propulsion engine fuel consumption is shown in Fig.11. The trend in the fuel consumption measurements, are comparable to the trends as seen in the full-scale thrust and power measurements as shown in the previous paragraphs. The differences seen between the full-scale performance improvements based on engine fuel consumption, compared to thrust or torque, are expected to be highly related to variations in the engine performance and fuel quality as described above. As such the measurements of the performance improvement of the retrofit via the engine fuel consumption measurements is less accurate when compared to the torque or thrust measurements (where the thrust measurements provide the most detailed insights via the split in propeller and hull performance).

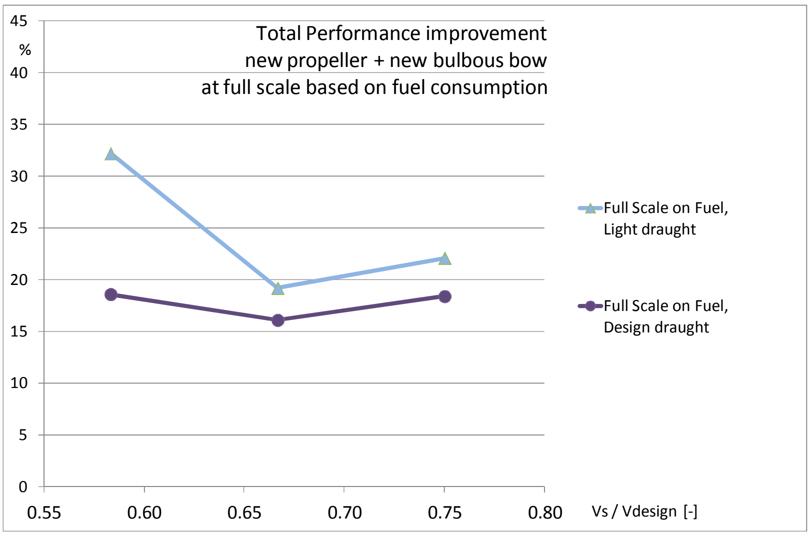

Fig.11: Total full-scale retrofit performance improvement based on engine fuel consumption measurements

5. Conclusions of the full-scale propeller + bulbous bow retrofit performance improvement measurements on a large TEU container vessel

The full-scale performance improvements by the retrofitting of a new propeller design and a new bulbous bow design are measured via 3 different routes (as is shown in Fig.1). First via the thrust measurements with the TT-Sense® sensor, secondly via torque (power) measurements, and third via the engine fuel consumption measurements.

Only via measuring the propeller thrust, the separate performance improvements by the new propeller design and the new bulbous bow design, can be determined. Also a comparison is made with the full-scale measurements based on torque (power), in order to verify the full-scale results based on thrust. Disadvantage of the measurements based on torque is that there can be made no distinction between the individual performance improvements of the new propeller design and the new bulbous bow design.

Also the engine fuel consumption improvement is measured and compared to the torque and thrust results. This is the least accurate way of measuring the propulsion performance improvement by the retrofit, as next to the improvements by the new propeller design and the new bulbous bow design, also the changes in engine performance (SFOC, fuel quality, etcetera) are measured. No distinction between the engine performance, propeller performance and hull performance can be made, when measuring engine fuel consumption.

The results of the full-scale measurements via thrust, torque and fuel consumption are split for the light draught conditions and the design draught conditions. In Fig.12, the total results of the full-scale performance improvements for the light draught conditions are shown. In Fig.13, the total results of the full-scale performance improvements for the design draught conditions are shown.

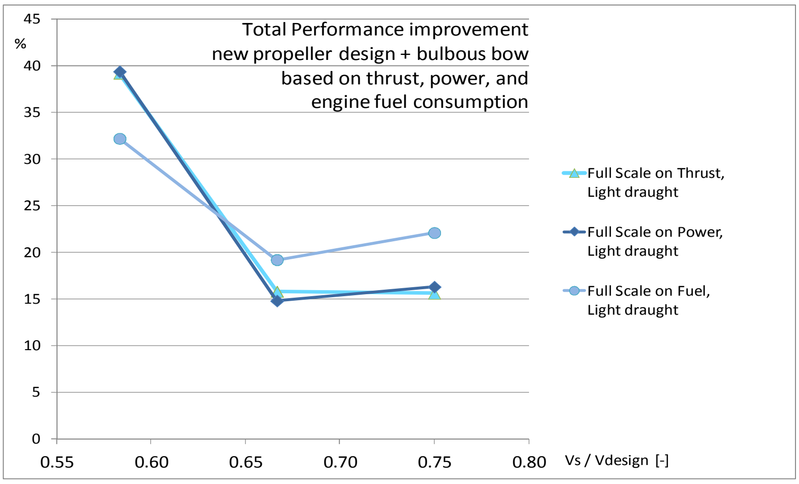

Fig.12: Total full-scale performance improvements based on thrust, torque (power), and engine fuel consumption measurements, for light draught conditions

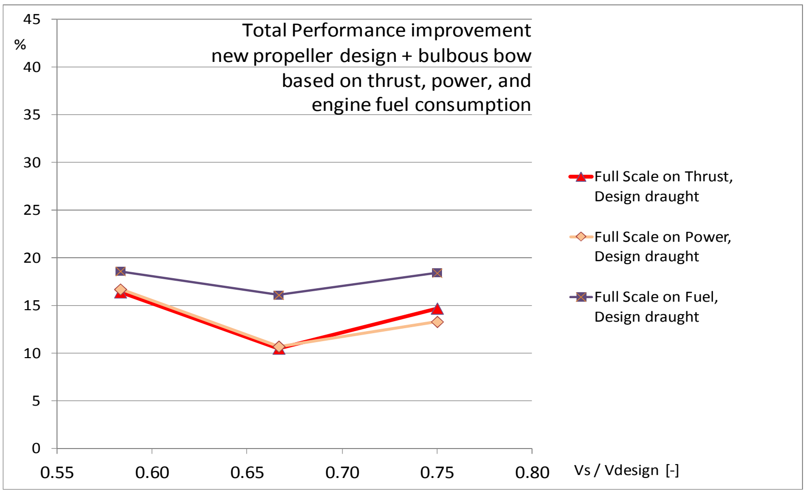

Fig.13: Total full-scale performance improvements based on thrust, torque (power), and engine fuel consumption measurements, for design draught conditions

The total retrofit full-scale measurement results of thrust and torque are very similar. In addition also the improvements based on fuel consumption show a comparable trend with the thrust and torque measurements. Given the fact that the full-scale measurement results are based on three different (independent) measurement principles, that provide comparable values (thrust and torque), and comparable trend (fuel consumption), provide a good indication of the final accuracy of the full-scale measured propulsion performance improvements via the thrust measurements.

From the investigation as described in this paper, it can be concluded that the full-scale retrofit performance measurements based on the TT-Sense® measurements, provide the most detailed insights into the performance improvements by the new propeller design, and separately by the new bulbous bow design.

References

AAS-HANSEN, M. (2010), *Monitoring of hull conditions of ships*, MSc thesis, NTNU, Trondheim

BALLEGOOIJEN, van, W.G.E.; MUNTEAN, T.V. (2016), *Fuel saving potentials via measuring propeller thrust and hull resistance at full scale: experience with ships in service*, 1st HullPIC, Pavone

BOOM, van den, H.J.J.; HASSELAAR, T.W.F. (2014), *Ship Speed-Power Performance Assessment*, SNAME 2014 Annual Meeting

LOGAN, K.P. (2011), *Using a ship's propeller for hull condition monitoring,* ASNE Intelligent Ships Symp. IX, Philadelphia

MUNTEAN, T.V. (2011), *Propeller efficiency at full scale*, PhD thesis, TU Eindhoven

PAERELI, S.; KRAPP, A.; BERTRAM, V. (2016), *Splitting propeller performance from hull performance – A challenge*, 1st HullPIC, Pavone

Numerical Investigation on Hull Roughness Effects on Propulsion Performance

Tom Goedicke, Mecklenburger Metallguss GmbH, Waren/Germany, goedicke@mmg-propeller.de

Abstract

This paper shows an investigation on hull roughness effects of a sea going ship using RANSE CFD. As surface roughness is closely related to frictional problems calculations are carried out in full scale in order to get rid of scaling issues. Resistance and propulsion simulations are performed applying sand grain roughness to a wall function model in Ansys CFX.

1. Surface Roughness

There are several sources categorizing fouling of ship hulls and investigating in resistance increase due to certain roughness heights. For this study mainly two former investigations were taken as reference. DEMIREL describes a similar numerical approaches to consider rough walls in RANSE CFD simulations. Categories of different surfaces are described in a more general way, but well connected to sand roughness which is the input variable in this investigation. One of the mostly referenced sources when it comes to marine roughness is the Naval Ships Technical Manual (NSTM), which gives very detailed description of existing types of fouling and suggests following table to relate fouling and sand roughness. Expected relations between the fouling types and additional power demand in ship operation are described by *Bertram (2012)*.

Table I: Roughness heights and corresponding sand-grain roughness according to NSTM

Description of Condition	NSTM Rating*	k_s (µm)	Rt_{50} (µm)
hydraulically smooth surface	0	0	0
typical as applied AF coating	0	30	150
deteriorated coating or light slime	10 - 20	100	300
heavy slime	30	300	600
small calcareous fouling or weed	40 - 60	1000	1000
medium calcareous fouling	70 - 80	3000	3000
heavy calcareous fouling	90 - 100	10000	10000

2. CFD Modelling

In general the commercial RANSE Code Ansys CFX is used in this study. For volume discretization tetrahedrical meshing is used in combination with prism layers for the wall resolution. The wall functions approach is used rather than the resolution of the boundary layer with respect to the computational effort. This also combines well with the model implemented for the surface roughness effect in Ansys CFX. Turbulence modelling is done using k-Omega SST turbulence model.

Meshes used for this investigation are divided in to ship and propeller mesh depending on the flow problem calculated. For resistance calculations meshing was done for half ship including free surface. For propulsion meshes for the full ship and propeller needed to be generated in order to capture to rotating propeller behind the ship. In order to save computational effort free surface is not taken into account in propulsion calculations. Mesh parameters are shown in Table II.

Table 2: Mesh Sizes

	Resistance	Propulsion Ship Domain	Propulsion Propeller Domain
Mesh size	18000000	12000000	7000000
average y^+	2000	2000	500

For taking roughness effects into account a numerical solution was used. The physical effect of a rough surface can be described as an increase of turbulence production near the wall, which leads to an increase of wall shear stress and influences the viscous sublayer in turbulent flows. In order to numerically taking care of this effect the velocity profile close to the wall is changed according to Fig.1.

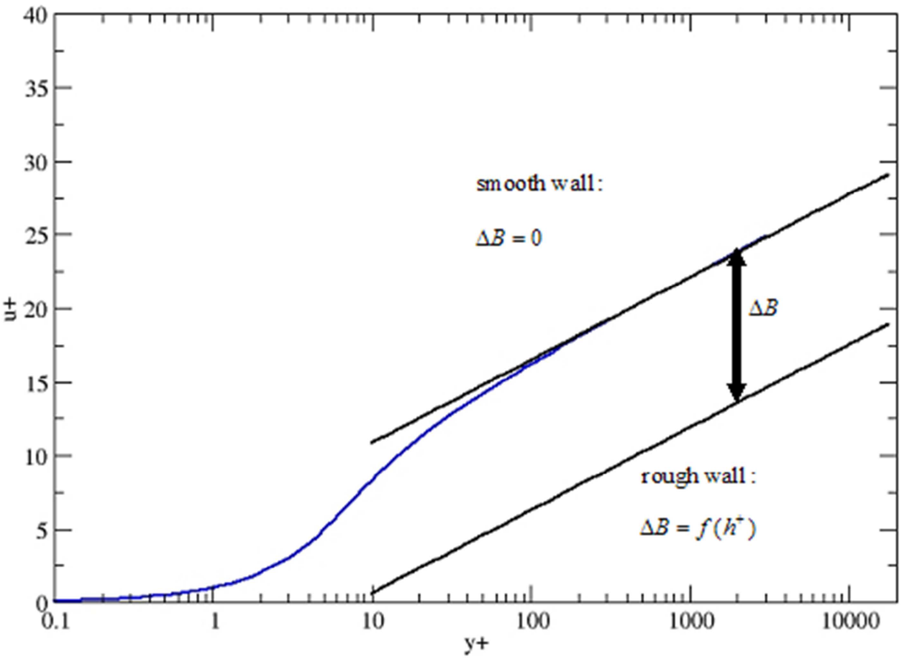

Fig.1: Shift in velocity profile close to the wall

The quantity of the down shift ΔB can be expressed by a sand-grain roughness, which can be described as sphere cover at the wall, with the spheres diameter equals roughness height h_S as shown in Fig.2. The surface roughness model implemented in Ansys CFX is using this assumption. Therefore the surface roughness is given to the numerics by a sand-grain roughness of h_S.

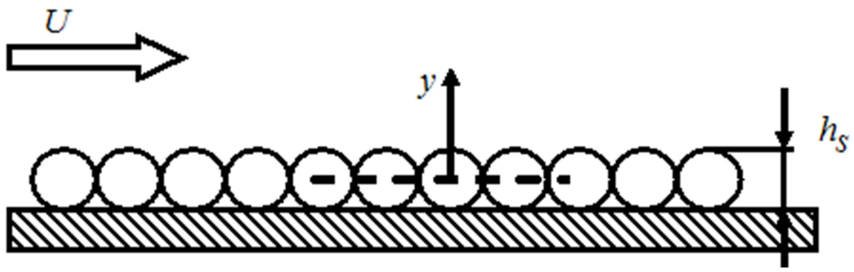

Fig.2: model of sand-grain roughness [ANSYS]

4. Case Study

This study is carried out for a 4000 TEU container ship, Table III, equipped with a fixed pitch propeller, Figs.3 and 4. Calculations were performed in draught 9.5m at 17 kn ship speed.

Table III: Test case particulars

L_{wl}	235.39 m
B_{wl}	32.25 m
T_{Design}	9.50 m
D_{prop}	7.75 m
z	6

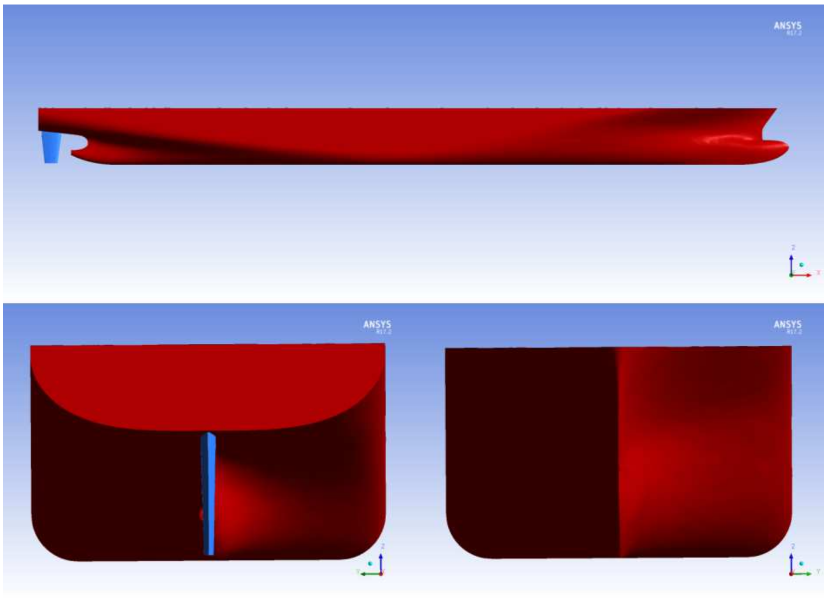

Fig.3: 4000TEU container vessel

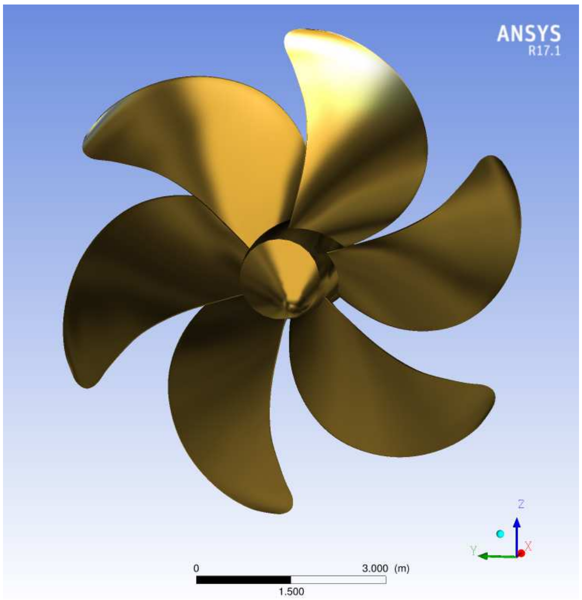

Fig.4: Propeller geometry of Test Case

3. Calculations and procedures

Three different tasks need to be solved when investigating in propulsion performance in detail.

A) Resistance of the hull
B) Propulsion performance of hull + propeller
C) Propeller without hull

The basic workflow of the propulsion performance analysis is explained by the flow chart in Fig.5. First the ship is towed at a fixed speed in order to get the resistance of the hull. Then the propeller is analyzed in a homogenous inflow in order to get the propeller characteristics. Finally both hull and propeller are simulated in a merged condition, which represents the propulsion condition.

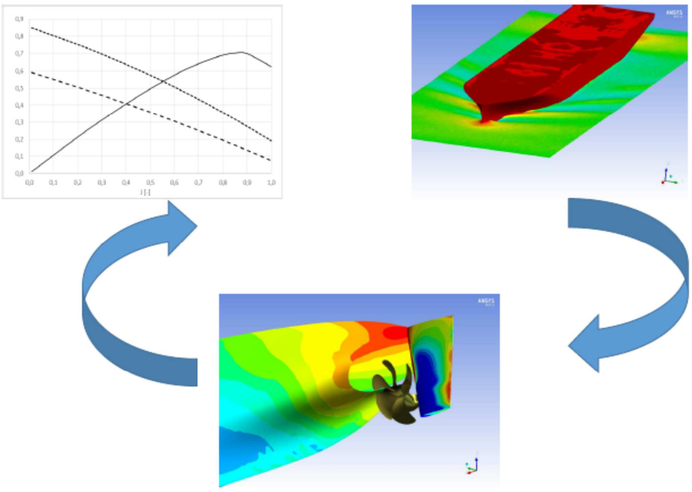

Fig.5: Analysis of propulsion performance

As the investigation is looking into hull roughness mainly, part B of performance analyses is neglected in the following discussion and the main focus lies in Part A and C.

It is expected that the resistance part of the vessels performance plays the biggest role when it comes to fouling. That is why resistance calculations will be starting point for the numerical investigation. Calculations in model scale 30.42 without roughness applied were performed in order to simulate a model test and using ITTC ’78 scaling procedure to gain a full scale resistance and propulsion figures as from model test. After that, full scale resistance with different sand-grain roughness values were performed in order to get information about the development of the nominal wake field and added resistance due to fouling.

Once finding a reasonable roughness value in the resistance study, this value will be taken into account for the propulsion investigation and being evaluated against smooth condition propulsion to gain information about hull propeller interaction in fouled conditions.

In order to divide propulsion efficiency into its parts the propeller open water test needs to be simulated. This study only takes hull roughness into account, so propeller surface in all simulations is taken as hydraulic smooth surface.

4. Results

4.1. Resistance of the hull

Table IV shows absolute resistance values comparing from model scale extrapolated smooth surface values with full scale values developing from smooth to rough hull surface. Increase of the integral values due to roughness is considered to be in the range of reported experiences in literature and experiences of real vessel operation.

Table IV: Absolute resistance

ModelScale extrapolated			k=0.3mm		k=0.15mm		K=0.075	
smooth	smooth		rough01		rough02		rough03	
RTS	RTS	Rel. Error	RTS	Rel. increase	RTS	Rel. increase	RTS	Rel. increase
713 kN	715 kN	0.31%	1010 kN	41.3%	934.2 kN	31.0%	879 kN	22.9%

For the target of finding influence of fouling effects on the flow around the propeller it is furthermore important to look into propeller inflow. Even if the nominal wake field cannot be considered as the propeller inflow, it will give a rough measure of the situation the propeller is going to work in. Especially the development of the nominal wake fields between the different roughness heights can give an insight of how the wake fraction in propulsion is going to behave.

Fig.6 shows the comparison of wake fraction in the propeller plane between the smooth wall configuration and rough wall configuration. As expected with the numerical model used, there is a more or less constant offset between the two configurations, with the rough configuration showing higher wake fraction distribution than the smooth configuration. Following the idea of wake fraction being an integral of relative velocity in the propeller plane is shown in Fig.7 it is possible to calculate w for the different calculation cases, as shown in Table III.

Table III: Nominal axial wake fractions as integral value

	smooth	rough01	rough02	rough03
w	0.275	0.331	0.305	0.299

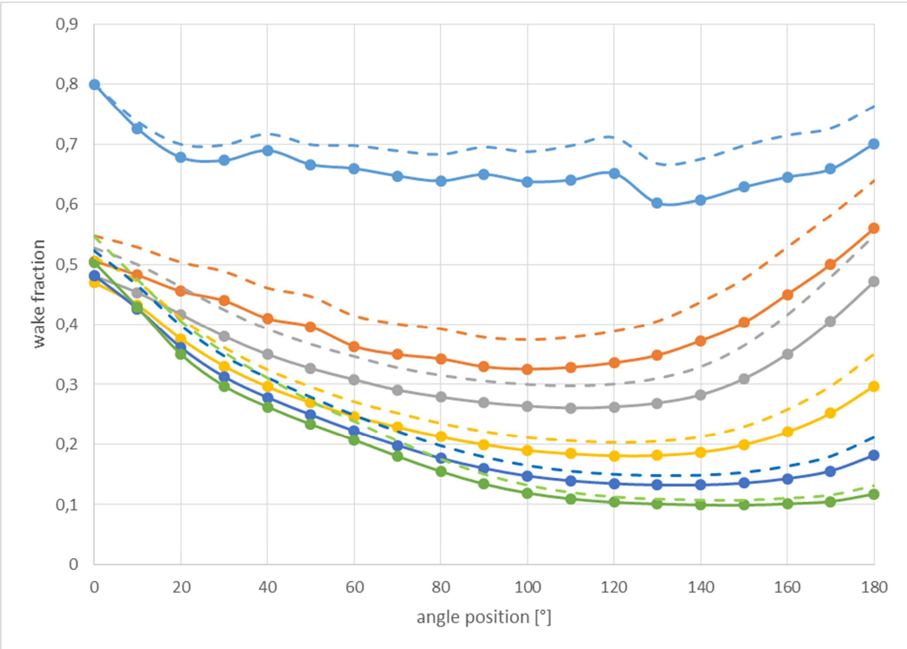

Fig.6: Wake fraction distribution smooth vs. rough02 wall

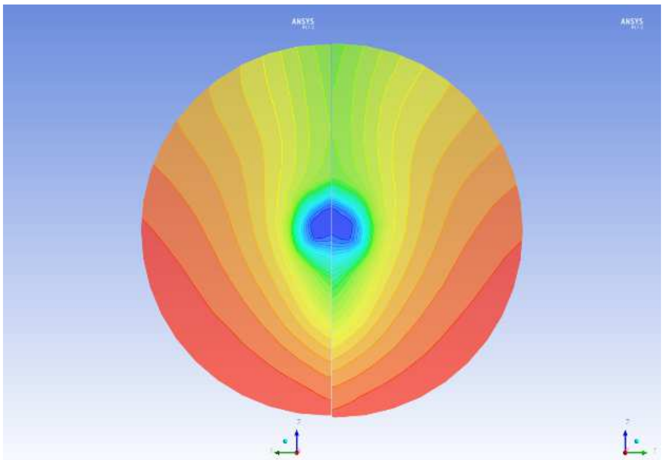

Fig.7: Nominal wake field comparison, left smooth, right rough

4.2. Propulsion performance of hull + propeller

Once it is shown that the wake of the rough hull looks different than the wake of the smooth hull the matter of interest is the response of the propeller. The most obvious response is closely related to the increase of resistance, because it leads to an increase of the propeller load and in most of the cases to reduction of the propeller efficiency η_O as shown in Fig.5.

This effect does not describe the change of propeller inflow, which could possibly change positively and in general procedures is not taken into account. Analyzing the propeller + hull interaction following the principle of thrust identity following results could be obtained.

Table IV: Propulsion elements

	Full Scale Trial Prediction			Hull efficiency elements						
	Vs [knots]	n [rpm]	PB [kW]	t [-]	ws [-]	PE [kW]	etaH [-]	etaR [-]	eta0 [-]	etaD [-]
Smooth modelscale	17.0	66.1	7995	0.161	0.209	6234	1.060	1.012	0.712	0.764
smooth	17.0	66.5	7849	0.106	0.187	6166	1.099	0.956	0.718	0.754
rough02	17.0	69.9	10833	0.149	0.229	8170	1.104	0.959	0.684	0.724

Resulting figures are considered to be in plausible range. Also the development looks as expected. There is a considerably high increase in wake fraction, but also in thrust deduction fraction. This leads to almost no change in hull efficiency η_H. Relative rotative efficiency η_R does not change with increased roughness and propeller open water efficiency η_O shows the expected decrease due to higher propeller load basically implemented by the higher ship resistance. To put the results in a more practical point of view following diagrams show speed-power and rpm-power relations, also in relation to the operational data of the vessel.

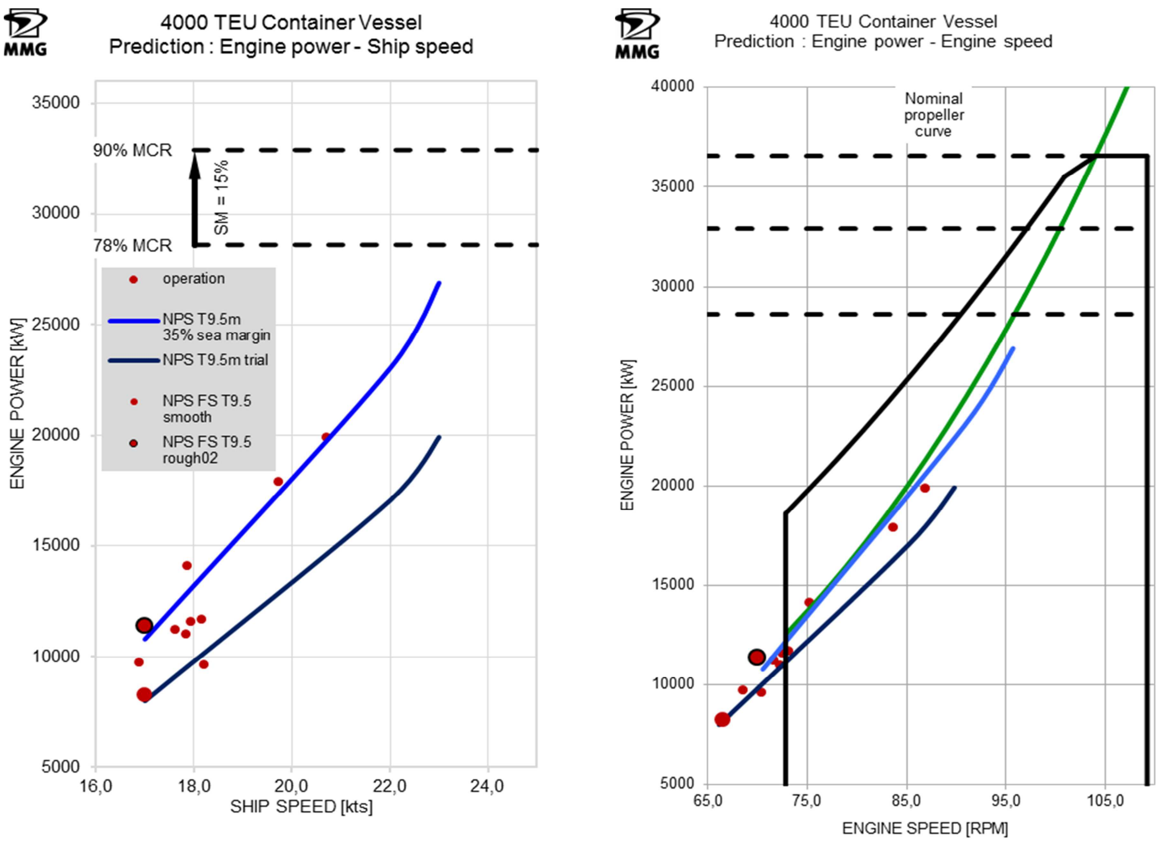

Fig.8: Speed Power, Power RPM relation

5. Conclusions

Finally it can be stated that the numerical model used in the study lead to plausible results in both resistance and propulsion situation. The efficiency drop can be separated into resistance increase and propulsion efficiency decrease. The influence of surface roughness on resistance is clearly the main part of the overall efficiency drop. Main interest of the investigation was the influence on the hull efficiency elements and propulsion performance. The results in propulsion situation show there is a rather small influence of the widened wake field on the propeller. The biggest effect on propulsion efficiency can be identified as a result of increased resistance as well, whereas relative rotative efficiency and hull efficiency are not significantly affected by the application of roughness on the hull. Still there is an effect on the resulting RPM from the increased wake fraction.

It can be concluded that it is worth looking into propulsion simulations including wall roughness. Even though the biggest part of the effects can be obtained from resistance increase only, there are significant changes in thrust deduction and wake fraction influencing the resulting RPM of the propeller. Furthermore this investigation can be seen as starting point for further studies in roughness on propeller surface also.

References

BERTRAM, V. (2012), *Practical Ship Hydrodynamics,* Butterworth & Heinemann, Oxford

DEMIREL, Y.K.; KHORASANCHI, M.; TURAN, O.; INCECIK, A.; SCHULTZ, M.P. (2014), *A CFD model for the frictional resistance prediction of antifouling coatings*, Ocean Engineering 89, pp.21-31

DEMIREL, Y.K.; TUIRAN, O.; INCECIK, A. (2016), *Predicting the effect of biofouling on ship resistance using CFD*, Applied Ocean Research 62, pp. 100-118

SCHULTZ, P. (2007), *Assessing the Hydrodynamic Performance of Fouling-Release Surfaces*, Naval Acadamy, Annapolis

Naval Ships Technical Manual, (2005), *Waterborne underwater hull cleaning of Navy ships*, US Navy

Experience in Applying ISO19030 to Field Data

Beom Jin Park, KRISO, Daejeon/Republic of Korea, baracude@netopia.re.kr
Myung-Soo Shin, KRISO, Daejeon/Republic of Korea, msshin@kriso.re.kr
Min-Suk Ki, KRISO, Daejeon/Republic of Korea, mski@kriso.re.kr
Gyeong Joong Lee, KRISO, Daejeon/Republic of Korea, gjlee@kriso.re.kr
Sang Bong Lee, LAB021, Busan/Republic of Korea, sblee@lab021.co.kr

Abstract

This paper describes study results of three bulk carrier data sets to investigate practical applicability of ISO19030. Changes in performance using operational data from three vessels of the same series are calculated in conformance with ISO19030 part 2 and part 3. The results show issues of filtering and reference condition removing too much of data which makes performance indicator results unreliable. More similar study should carry out to investigate these issues and amendments to ISO190d30.

1. Introduction

Since the beginning of the ISO19030 development, many shipping companies and operators have taken interest in the standard as they are faced with continuous pressure to reduce fuel and energy consumption. Now, the first version of the standard is published, many are curious on the practical applicability of the standard. To this end, a study was conducted to investigate the usefulness of the standard using operational data acquired from three bulk carriers.

ISO19030, since its inception, aimed at a practical standard to be used in operation environment. For example, wave correction was not included in the standard, as having no practical means to measure wave. Therefore, validation with operational data is very important for the purpose of ISO19030

2. Operational data used in the study

For this study, operational data from three vessels are used. They are all 178K bulk carriers carrying coal and ores between South Korea and Australia. They are of the same series, so their designs are identical. Table I**:** shows main dimensions of the vessels. Since all vessels are bulk carriers, they usually travel in either ballast or laden condition and hardly ever in other load conditions.

Table I: Main dimensions of the vessels

Length between perpendiculars	282.00 m
Breadth, moulded	45.00 m
Depth, moulded	24.75 m
Mean draught, Laden	18.25 m
Mean draught, Ballast	7.90 m

One vessel, designated as Vessel A, has older data gathering system with frequency of once in every 2 minutes. Vessel A is the only vessel with more than two years of operational data, and also equipped with shaft power meter. Vessel A is also only vessel that has undergone dry-docking, when new anti-foul paint and energy saving device (propeller boss fin cap) are applied. Therefore, both before and after dry-docking data is available. The other two vessels, designated as Vessel B and Vessel C have newer data gathering system with frequency of once in every 10 seconds. However, their operational data only include time span of about one year, and no dry-docking has been performed. Also, shaft power meter has not been installed yet, so only power values calculated from SFOC curve can be used. Table II shows characteristics of each vessel's operational data.

Table II: Operational data characteristics of each vessel

	Vessel A	Vessel B	Vessel C
Data begins at	2014-10-17	2015-10-29	2016-05-17
Data ends at	2016-10-12	2017-02-06	2017-02-06
Timespan of data	726 days	466 days	265 days
Dry-docking at	2015-11-12	none	none
Data interval	2 min.	10 s	10 s
Power measurements	Shaft power meter Calculated from SFOC	Calculated from SFOC	Calculated from SFOC
Speed measurements	Speed log	Speed log	Speed log

3. Vessel A calculation results

For vessel A, changes in performance before and after dry-docking are calculated in accordance with current ISO 19030 standard. This result will conform with part 3 of ISO 19030 due to low frequency of data. Reference period are set as before dry-docking and evaluation period is set as after dry-docking. About 13 months of data is available for reference period and 11 months of data for evaluation period.

For all analysis in this study, ISO 19030 validation software, developed by KRISO, was used. This software was developed while ISO 19030 was being developed and is freely for non-commercial use. The initial analysis results are shown in Table III**:**.

During dry-docking anti-fouling paint and PBCF were applied to Vessel A. The result shows that hull cleaning effect, new paint and PBCF jointly have improved the performance of Vessel A as much as almost 10%, which seems reasonable value.

However, from original 370,122 records, less 10% is used for actual performance calculation. About half of records are eliminated during filtering and about 85% of records are eliminated because they are out of reference condition. Further detailed analysis of filtering and reference condition is shown in Tables IV and V.

Table III: Vessel A calculation results using shaft power values

No. of data records	370,122
No. of data records after filtering	190,642
No. of data records after validation	161,790
No. of data records in reference condition	24,776
Average PV of reference period	-13.07%
Average PV of evaluation period	-3.12%
PI	9.95%

Table IV: Detailed analysis of filtering results for Vessel A

Parameters	No. of records filtered out	% of records filtered out
Speed through water	32,844	8.87%
Power	33,052	8.93%
Shaft revolution speed	30,607	8.27%
Relative wind velocity	32,617	8.81%
Relative wind Direction	32,907	8.89%
Speed over ground	24,213	6.54%
Heading	31,718	8.57%
Rudder angle	33,082	8.94%

Table V: Detailed analysis of reference condition results for Vessel A

Criteria	No. of records out of reference condition	% of records out of reference condition
Wind speed	42,855	58.40%
Water depth	7,290	9.94%
Power not within range of speed-power curve	11,217	15.29%
Rudder angle	4,864	6.63%

In ISO19030, filtering is based on Chauvenet's criteria for outlier detection. During filtering, no one parameter stands out as the main reason why so much data is filtered out. However, in reference condition, about 60% of data is out of reference condition due to wind speeds higher than 7.9 m/s. Since Vessel A had shaft power meter installed, performance analysis using shaft power meter values and using brake power values calculated by SFOC curve was also compared to find out if there are any noticeable difference between them. Table VI**:** shows the results using brake power values calculated from SFOC curve. Comparing Table III**:** and Table VI**:**, there is negligible difference between using shaft power values and using brake power values calculated from SFOC curve.

Table VI: Vessel A calculation results using SFOC curve

No. of data records	370,122
No. of data records after filtering	190,187
No. of data records after validation	161,120
No. of data records in reference condition	20,301
Average PV of reference period	-14.45%
Average PV of evaluation period	-5.20%
PI	9.25%

4. Vessel B calculation results

For Vessel B, since it did not undergo dry-docking, data is split in half and the performance change between first and second half is calculated. These results confirm with part 2 of current ISO 19030 standard. Table VII**:** shows calculation results. While less than 7% of data was filtered out, still 99% of data was being eliminated due to out of reference condition. The change in performance is almost negligible (<1%). Further analysis in reference condition, Table VIII, shows the same tendencies as Vessel A, as wind speed is the main reason most data outside of reference condition. Compared to Vessel A, number or records with power values not within range of speed-power curve was unusually high.

Table VII: Vessel B calculation results

No. of data records	2,412,691
No. of data records after filtering	2,248,998
No. of data records after validation	1,623,716
No. of data records in reference condition	55,961
Average PV of reference period	-13.81%
Average PV of evaluation period	-14.34%
PI	-0.54%

Table VIII: Detailed analysis of reference condition results for Vessel B

Criteria	No. of records out of reference condition	% of records out of reference condition
Wind speed	583,817	71.10%
Water depth	100,159	12.20%
Power not within range of speed-power curve	554,240	67.50%
Rudder angle	23,516	2.86%

Since changes in performance seems to be very small, maintenance trigger was calculated to investigate whether it can show general decrease in performance over time. First three months is used as reference period and evaluation periods are set by splitting the rest of data into three-months blocks. Table IX**:** shows that maintenance trigger does not show reliable results as we expect general decline in performance when no dry-docking or maintenance are done.

Table IX: Maintenance trigger of Vessel B

	Begin at	End at	Avg. PV	Difference from reference	Difference from previous
Reference	2015-11-01	2016-01-31	-13.94%	-	-
Evaluation	2016-02-01	2016-04-30	-13.14%	0.80%	0.80%
	2016-05-01	2016-07-31	-8.36%	5.58%	4.78%
	2016-08-01	2016-10-31	-11.67%	2.27%	-3.31%
	2016-11-01	2017-01-31	-16.22%	-2.29%	-4.55%

5. Vessel C calculation results

For Vessel C, the same as Vessel B, data is split in half and the performance change between first and second half is calculated. These results confirm with part 2 of current ISO 19030 standard.

Table X: Vessel C calculation results

No. of data records	1,542,991
No. of data records after filtering	1,419,220
No. of data records after validation	1,049,521
No. of data records in reference condition	127,269
Average PV of reference period	0.23%
Average PV of evaluation period	-3.26%
PI	-3.49%

Table XI: Detailed analysis of reference condition results for Vessel B

Criteria	No. of records out of reference condition	% of records out of reference condition
Wind speed	247,165	65.04%
Water depth	5,481	1.44%
Power not within range of speed-power curve	7,076	1.86%
Rudder angle	2,218	0.58%

Table X shows calculation results. The results show the same tendencies as Vessel B. Only 8% of data was filtered out, but 88% of data was being eliminated due to out of reference condition. However, it shows small decrease in performance. Further analysis in reference condition, Table XI**:**, shows, the same as Vessel A and Vessel B, wind speed is the main reason for most of data being outside of reference condition. Also, unlike Vessel B and similar to Vessel A, number or records with power values not within range of speed-power curve was very small.

6. Discussions

6.1. Effects of data frequency

ISO19030 part 2 requires data frequency higher than once in 15 seconds, but part 3 can be applied for lower frequency data. Further analysis by sampling from Vessel B and Vessel C data set shows that data frequency has higher impact on analysis results than expected, as shown in Table XII**:**.

Table XII: Effects of data frequency

Data interval	10 s	30 s	1 min.	2 min.
No. of data records	2,412,691	804,230	402,115	201,057
% of data filtered out	6.78%	15.15%	26.64%	46.02%
% of data invalidated	27.80%	24.58%	20.20%	12.57%
% of data out of reference condition	96.55%	96.27%	95.83%	95.35%
Average PV of reference period	-13.81%	-14.28%	-15.10%	-15.98%
Average PV of evaluation period	-14.34%	-14.49%	-14.63%	-14.46%
PI	-0.53%	-0.21%	0.47%	1.52%

Since filtering criteria is based on the standard error of mean and lower frequency data has higher variance for parameters with rapidly changing values, lower frequency data will lead to more data to be filtered out. However, 50% of data being filtered for being outlier does not conform with the intention of filtering. In ISO19030 part 3, clause 5.3, filtering and validation are required for data frequency higher than once in 10 minutes. Results in Table XII**:** shows that effects of data frequency in filtering should be further studied and new filtering criteria to be developed for more stable filtering performance.

Also, performance indicator value seems to be very sensitive to data frequency, but this is believed to be due to too small amount of data remaining for performance value calculation. If enough data is available, performance indicator should give stable values regardless of data frequency.

6.2. Reference wind condition

Table XIII**:** shows how much data is eliminated due to wind speed being too high and it shows too much data is being eliminated. The purpose of reference condition is to exclude data from infrequent and bad weather condition. However, results in Table XIII**:** shows that normal operating weather is being eliminated and further study is needed to decide whether reference condition is to stringent. This can also be the reason for unreliable maintenance trigger results in Table IX**:**.

Table XIII: % of data out of reference condition due to wind speed

Vessel A	Vessel B	Vessel C
58.40%	71.10%	65.04%

6.3. Speed-power reference curve

All three vessels were cursing in slower speed than design cruising speed. Therefore, using speed-power reference curve acquired during design, centred around design cruising speed does not cover much of power range measured in operational data. It was fortunate that new model tests were done for research purpose and they were used in the study, but this generally not the case. Therefore, most of ships may not have speed-power reference curve covering all operating power ranges.

From ship operator’s view, only practical solution included in both ISO19030 part 2 and 3 is passive monitoring approach as in ISO19030 part 3 clause 5.3.1.2.2. However, conditions outlined in clause 5.3.1.2.3 requires the same filtering, validation and reference conditions as in part 2. Therefore, previous discussion issues will also arise when acquiring data for passive monitoring approach.

Also, for vessels in same series having identical design, they all have same model test results. However, even with the same design, their actual speed-power performance may slightly differ. This can be identified if speed-power reference curve from sea trial is available, but many are found to be without sea trial results. One way to accommodate this, in the similar fashion as in sea trial analysis, is to use model test results and shift it in power axis to obtain new speed-power curve, thus covering all operating power ranges of each vessel. It can be possibly more accurate than fitting data to a new curve as in ISO19030 part 3 clause 5.3.1.2.4.

7. Conclusions

In this paper, study results of applying ISO19030 to three sets of bulk carrier data is described. The results show that ISO19030 can capture changes due to dry-docking, where anti-fouling paint and PBCF were applied. Performance indicators calculated using shaft power measurements and brake power calculated from SFOC curve are in good agreement.

However, there are a few issues unresolved. The first one is that filtering criteria is too stringent to exclude too much of data, especially when data frequency is low. The other one is wind speed reference condition is not appropriate for normal operation environment. These issues led to too much data being eliminated and thus making performance indicator unreliable.

More study on these issues should be carried out and from study results, general conclusion as to how ISO19030 should be amended should be drawn and applied in order to improve practical applicability of ISO19030 standard.

Notorious Speed Through Water

Matti Antola, Eniram, Helsinki/Finland, matti.antola@eniram.fi
Antti Solonen, Eniram, Helsinki/Finland, antti.solonen@eniram.fi
Jussi Pyörre, Eniram, Helsinki/Finland, jussi.pyorre@eniram.fi

Abstract

Speed Through Water (STW) is a critical variable when determining a vessel's performance. For example, any inaccuracies in speed are exacerbated in the admiralty coefficient, because it is proportional to the third power of STW. Eniram has developed a Virtual Log to accurately estimate STW using various data sources such as speed logs, Speed Over Ground (SOG), current forecasts, and propulsion related data. The Virtual STW can be used to quantify data quality issues in speed logs. In this paper we perform a study using data from one year and hundreds of vessels and find two main categories of quality issues. First, the speed logs are often miscalibrated, i.e. the measured STW is systematically too large or two small in certain speed ranges. Second, sometimes speed logs provide noisy and clearly erroneous measurements. We quantify how prevalent both issues are in the Eniram installation base depending on ship type.

1. Introduction

Marine transportation vessels have increasingly complex data systems capable of producing large amounts of information about vessel performance. The purpose of these data systems is the growing need to quantify and optimize vessel performance. Critical measurements for vessel performance include those pertaining to vessel speed and consumption. To quantify consumption, it is common to track either power used at propeller or fuel used at main engines. To quantify speed, the speed through water (STW) can be measured with an onboard device called the speed log. Because the ship can be traveling with or against currents, this reading can differ from the speed over ground (SOG) measured by a GPS system.

The importance of an accurate STW measurement is elucidated by three examples. First, varying currents change the distance needed to travel through water between two ports. Aiming for just-in-time arrivals increases your fuel efficiency, but requires a fine-tuned STW measurement. Second, a marine vessel's performance depends on the hull and propeller condition, which can deteriorate due to biological fouling (organisms accumulating on the hull surface), paint degradation and other factors, or improve due to a dry docking or cleaning of the hull, for instance. Even small changes in STW have a significant impact on propulsion power demand – this is obvious by just looking at the speed-power curve of any vessel. Since the relationship between propulsion power and vessel speed is roughly cubic, increasing the speed from 10 knots to 10.3 knots would already have roughly 10 % increase in propulsion power demand. The cubic relationship implies an amplification of noise in the STW and hence an accurate STW is required distinguish the slowly evolving fouling signal from the noisy background. Third, when assessing the onboard efficiency of any navigational operation (ballast operations, course change, etc…), the key is to know how much you gained or lost speed if you kept the rpm or power constant.

Even though STW is the most important measurement in terms of energy efficiency, it is often unreliable. Before the current trend of energy efficiency monitoring, the speed log was considered mainly as a backup system for GPS and thus the accuracy and reliability were secondary. A widely-used method for measuring STW is an instrument called Doppler Log that transmits ultrasound pulses from the vessel, and measures the backscatter echo from bubbles, biological material, and turbidity in water. The frequency shift (Doppler shift) can be utilized to calculate the speed of the vessel through water. Another common method is an electromagnetic log in which an electromagnetic field is created in the water. A water flow through the field induces a voltage on the sensor. The amplitude of the voltage depends on the STW.

Measuring STW using the aforementioned methods is a delicate task and prone to errors. What if there aren't enough impurities in the water for the Doppler log pulses to echo from? Could the hull of the ship alter the measured water flow such that measurements are inconsistent (and depend on draught and trim)? Does the measured STW correspond to the hydrodynamically relevant STW experienced by the ship, i.e. is the STW measurement done at a relevant depth? Are the sensors calibrated well, or is there a calibration mismatch depending on e.g. temperature? Is there an internal logic in the speed log, e.g. switching to bottom-tracking when in shallow waters? All these questions cause concerns. See *Bos (2016)* for a more detailed discussion.

When examining speed log data, two separate issues stand out. First, due to, e.g., the aforementioned difficulties, the speed logs can sometimes behave in a very erratic manner. Secondly, the speed logs experience calibration issues. Thus the long-term average difference between SOG and the measured STW differs from zero. A common way to assess the speed log quality is to compare the speed log readings to SOG obtained from GPS. This type of analysis can reveal potential calibration issues, and one can even derive a correction for STW readings based on the long-term differences, see, e.g., *vom Baur (2016)*. However, this method does not fix the erratic behavior of the speed log, nor does it account for possible changes in the calibration factor.

Meteorologists and oceanographers have developed sophisticated numerical models for predicting ocean currents. These forecasted currents along with measured SOG on board can be used to determine an estimated STW. This measurement has low bias in the sense that the long term averages are roughly correct, but, as it is based on forecasts generated by numerical models, momentary errors can be high. These forecasts are widely used in the shipping industry; for instance, *Bos (2016)* discusses how current forecasts can be used to assess the reliability of speed logs.

Another, less widely adopted technique is to build a hydrodynamic model of the ship, possibly taking into account such effects as wind, shallow waters, etc., see *Pyörre (2012), Solonen (2016)* for some discussion. The problem with this approach is that ships experience changes in hull and propeller performance (e.g. due to fouling of the hull), which is often neglected in such approaches. Also this framework depends on many data sources, e.g. wind sensors, which leads to missing or incorrect values if one of the data sources breaks or is missing.

2. Eniram Virtual Speed Log

The Virtual Speed Log, Fig.1, is a virtual sensing application that combines propeller data, SOG, speed log data, and current forecasts with modeling to produce a high-quality and correctly calibrated STW, denoted Virtual STW. The Virtual Speed Log can operate with real-time data and continuously updates itself to account for the current conditions, fouling or other hydrodynamic changes. The model can also operate with a reduced set of inputs, if e.g. the current forecasts or speed log data is unavailable.

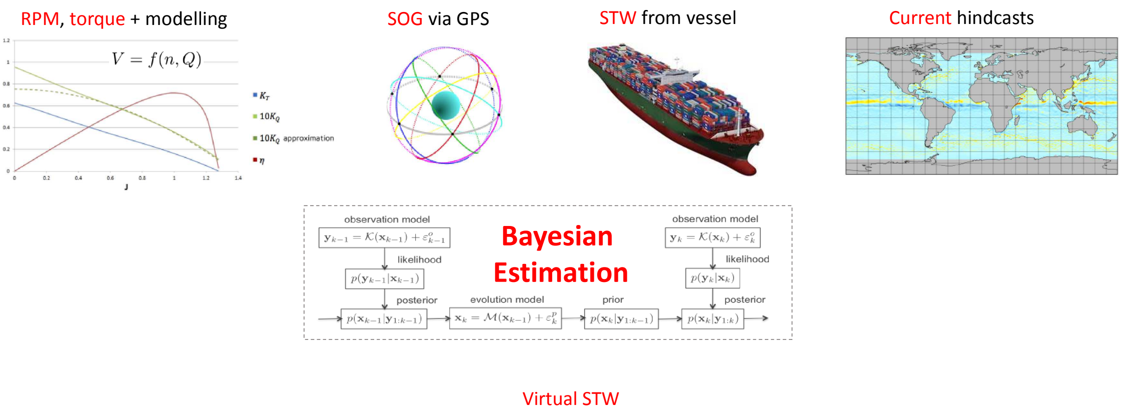

Fig.1: Schematic of the Virtual Speed Log

2.1. Hydrodynamic Model

The performance of a propeller at a given speed of water flow and rotation speed can be described, in the open water, deep-sea approximation, with two dimensionless functions called the torque and thrust coefficients:

$$K_Q(J,\bar{\alpha}) = \frac{Q}{\rho D^5 n^2}$$
$$K_T(J,\bar{\beta}) = \frac{T}{\rho D^4 n^2}.$$

This parametrization is derived from dimensional analysis. Here Q denotes torque, T denotes thrust, ρ is water density, D is diameter of the propeller, and n is revolution speed. The functions are tuned for a given propeller with a set of dimensionless parameters $\bar{\alpha}$ and $\bar{\beta}$[1], and they depend the dimensionless advance ratio $J = {}^{v_A}/_{nD}$, where v_A is the water speed at the propeller. When the propeller is placed near the ship hull, the wake field of the hull changes the water speed at the propeller, and hence v_A is less than the STW v_w. For simplicity of this analysis, we now set $v_A = v_w$. For a more detailed introduction, *Bertram (2012)*.

The functions K_Q and K_T are often expanded around a typical operating point $J = J_0$ to first or second order in J. For the purposes of data-based modeling, this results several unknown coefficients that can be fitted to the data. We note that the equation for K_Q already provides a method to estimate STW based on RPM and torque. However, here the target is to write a statistical state-space model with an observation function of the form $\bar{F}(\bar{s}_t) = \bar{z}_t + \bar{\varepsilon}_t$, where $\bar{s}_t$ corresponds to the modeled state of the ship at time t, $\bar{F}$ is the observation function, $\bar{z}_t$ is the set of observations at that time, and $\bar{\varepsilon}_t$ is the observation noise. The benefit of this kind of formulation is that it is easy to account for missing data and to combine different data sources with various levels of reliability. Hence, we take a slightly different approach, where we do not expand around the typical operating point J_0 but around a calm-sea point.

The hydrodynamic and aerodynamic resistance experienced by a ship is commonly divided into several additive terms. We write the total resistance as $R(v_w,\bar{u};\bar{\gamma})$, where there is a dependence on the STW, and $\bar{u}$, whose components contain relative wind and information on waves, squat, stabilizers, etc. The resistance function is tuned for a given ship with the parameters $\bar{\gamma}$, commonly called resistance coefficients. Next, we divide the total resistance into two terms. The first term gives the expected resistance at a certain speed and in otherwise calm-sea conditions, while the second term encodes the resistance caused by external conditions differing from calm-sea:

$$R(v_w,\bar{u}_R;\bar{\gamma}) = R_{cs}(v_w;\bar{\gamma}) + R_\Delta(v_w,\bar{u}_R;\bar{\gamma})$$
$$R_{cs}(v_w;\bar{\gamma}) \equiv R(v_w,\bar{u}_{cs}(v_w);\bar{\gamma}).$$

Here $\bar{u}_{cs}(v_w)$ defines the calm sea conditions as a function of STW; for example, the relative wind speed is taken equal to STW[2], and waves are set to zero. Now, if there is no acceleration, we can equate thrust and resistance, and write:

$$K_Q\left(\frac{v_w}{n},\bar{\alpha}\right) = \frac{Q}{\rho D^5 n^2}$$
$$K_T\left(\frac{v_w}{n},\bar{\beta}\right) = \frac{R_{cs}(v_w;\bar{\gamma}) + R_\Delta}{\rho D^4 n^2}.$$

[1] Vector-valued variables are distinguished by a bar over the name.
[2] Hence the calm sea resistance contains wind resistance experienced when true wind is zero.

It is worth noting that in an approximation, $R_{cs}(v_w;\bar{\gamma}) \sim v_w^2$, and hence

$$\frac{R_{cs}(v_w;\bar{\gamma})}{\rho D^4 n^2} \sim J^2.$$

This curve will always cross the K_T curve (which his decreasing as a function of J) at a crossing point corresponding to the calm-sea advance ratio J_{cs}. This value is numerically at the larger end of the operating range of the vessel, i.e. $J_{cs} > J_0$. In other terms, on average, the extra resistance $R_\Delta > 0$.

Given a certain form of the torque and thrust coefficients, and the calm-sea resistance, a possibly nonlinear solution for the Q and n can be derived in terms of v_w and R_Δ. For an analytic approach, it is useful to note that R_Δ is usually small compared to R_{cs}. Hence the equations can be solved as a perturbation series[3] in R_Δ/R_{cs}. As a result, we have two equations, where the parameters have been collected into a new vector $\bar{\lambda}$:

$$Q = f\left(v_w, R_\Delta; \bar{\lambda}\right) \# (1)$$
$$n = g\left(v_w, R_\Delta; \bar{\lambda}\right). \# (2)$$

2.2. Statistical Model

Using (1) and (2) requires a decision on how to model R_Δ, with several options available:

1. Model R_Δ as a time-dependent unknown. At high data frequencies, R_Δ should evolve relatively slowly, hence providing a constraint on the behavior of Q, n and v_w (locally in time).
2. Model R_Δ by using data on winds, and waves, and other resistance sources. This has the downside that the model becomes more complex (the resistance coefficients have to be learned from data) and also dependent on additional data sources, which can break or go missing.
3. Model R_Δ partially using wind and wave data, and partially as a time-dependent unknown.

The Virtual STW approach is based on a time-dependent R_Δ. In addition, the $\bar{\lambda}$ parameters cannot be taken constant as they change if the ship develops fouling, or if other changes happen in the calm-sea behavior (e.g. draft changes if it is not modeled). Hence $\bar{\lambda}$ is assumed to be a slowly evolving time-dependent parameter.

In addition to Q and n, the model uses observations of SOG (v_g)[4], the current forecast (c), and the speed log reading (v_w). The observation for SOG is written as estimated STW plus estimated current, where the estimated current changes slowly. The observation for STW is modeled by introducing a multiplicative *calibration factor*[5] (x). Hence the observation functions used to link the observations Q, n, v_g, v_w, and c to the estimated variables (specified with a hat) at a time t can be written

$$Q_t = f\left(\hat{v}_{w,t}, \hat{R}_{\Delta,t}; \hat{\bar{\lambda}}_t\right) + \varepsilon_{1,t}$$

[3] This is similar to solving as perturbation series in $J - J_0$.

[4] The label g refers to Ground; v_g is the speed of the ship relative to ground (earth's reference frame), while v_w is the speed of the ship relative to Water.

[5] Some speed logs have a table of speed offsets, so a more accurate approach would require that the calibration factor is an arbitrary function of STW. However, the calibration factor can change due to crew recalibrating the speed log device or due to calibration depending on circumstances, such as sea temperature. These facts add another layer of difficulty to the estimation task and hence we decide to use the simplest possible model.

$$
\begin{aligned}
n &= g\left(\hat{v}_{w,t}, \hat{R}_{\Delta,t}; \hat{\hat{\lambda}}_t\right) + \varepsilon_{2,t} \\
v_{g,t} &= \hat{v}_{w,t} + \hat{c}_t + \varepsilon_{3,t} \\
v_{w,t} &= \hat{x}_t^{-1}\hat{v}_{w,t} + \varepsilon_{4,t} \\
c_t &= \hat{c}_t + \varepsilon_{5,t} \\
R_{\Delta avg} &= \hat{R}_{\Delta,t} + \varepsilon_{6,t}.
\end{aligned}
$$

The last equation is necessary to calibrate the hydrodynamic model. The extra resistance should be centered around some typical positive value controlled by $R_{\Delta avg}$, a parameter of the model. In the absence of a current forecast (c), an observation of the form $0 = \hat{c}_t + \varepsilon_{5,t}$ is necessary to calibrate the speed log (i.e. to determine $\hat{x}_t$).

The evolution equation for the state variables is set to a random walk, i.e. for the estimated variables (collectively denoted $\hat{\hat{s}}$) we have:

$$\hat{\hat{s}}_t = \hat{\hat{s}}_{t-1} + \bar{\eta}_t.$$

We have introduced two random variables ($\bar{\varepsilon}$, $\bar{\eta}$), where the first controls the measurement noise, and the second controls the evolution speed of the state. If $\bar{\varepsilon}$, $\bar{\eta}$ are distributed according to a multivariate Gaussian distribution, uncorrelated in time, then the model can be calibrated with the Kalman filtering method. There is a hierarchy in the evolution speeds controlled by $\bar{\eta}$. The state variables $\hat{R}_\Delta$ and $\hat{c}$ can evolve relatively fast compared to $\hat{\hat{\lambda}}$ and $\hat{x}$.

2.3. Virtual STW Examples

To validate the Virtual STW model, we can compare to a simple minimum-bias robust STW model: the STW calculated from SOG and forecasts, i.e. Forecast STW. In equations[6],

$$\tilde{v}_{w,t} = v_{g,t} - c_t$$

Fig.2: Speed log with calibration error

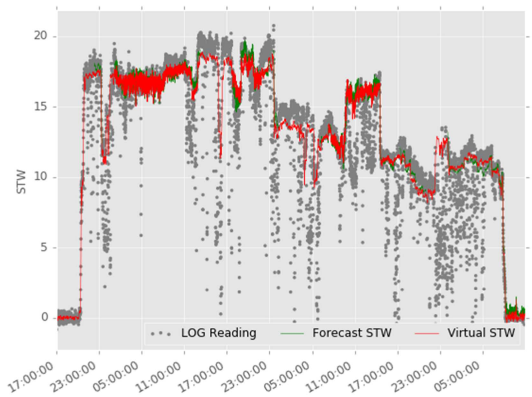

Fig.3: Speed log with erratic behavior

In Fig.2 we present a time-series figure of a typical miscalibrated speed log. Comparing the Forecast STW to the speed log reading, it is evident that the speed log is miscalibrated. Virtual STW follows the qualitative behavior of the speed log accurately, but is more centered around the Forecast STW. In Fig.3, we show an example time-series of a very erratic speed log. The speed log readings are extremely unstable, but Virtual STW displays a reasonable behavior.

[6] The vector nature of these equations is omitted here.

Fig.4 shows a scatterplot of Virtual STW vs Forecast STW, and speed log vs Forecast STW. The data is selected from hundreds of ships. Different vessels are given a different color. In the plot with speed log, certain vessels cluster in areas where either the Speed log reading is too large or too small. These ships have miscalibrated speed logs. In addition, there are many data points for which the speed log reading is 5-15knots below that of the Forecast STW. These correspond to the erratic behavior of the speed log. In the Virtual STW plot, such behaviors are absent, and the points cluster nicely around the diagonal.

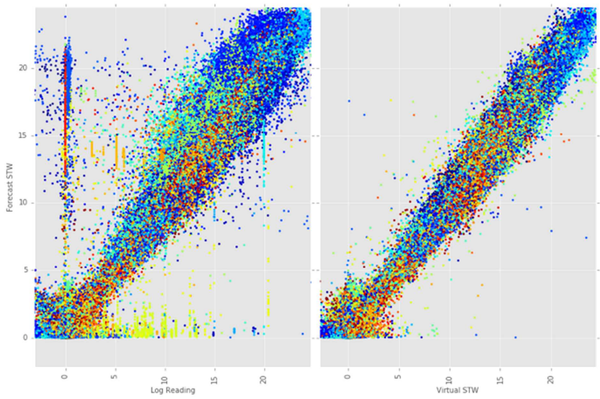

Fig.4: Speed log reading and Virtual STW vs Forecast STW. Color indicates vessel.

3. Quantifying Speed Log Quality

3.1. Data

The study is based on the Eniram database. The total number of vessels selected for the study is 186, Table I. Each ship is labeled either ‘cruise’ or ‘cargo’. Data is selected from the full year 2016. The analysed dataset contains the first 30-second sample of each hour. The data is further filtered to times where the current forecast was available, and SOG is above 6 kn. The total number of data points for the study is 784133. Mainly we are interested in comparing the speed log reading to Virtual STW[7]. However, to validate the results based on Virtual STW, we will also compare to Forecast STW.

Table I: Overall description of data

Ship Type	Number of Vessels	Total number of datapoints	Number of valid datapoints
Cruise	99	809827	445394
Cargo	86	627551	336546
Total	186	1445515	784133

3.2. Method

The first quality indicator will be the calibration factor found by the Virtual Speed log, i.e. $\hat{x}_t$, which should be equal to one for a correctly calibrated speed log. To compare to the Forecast STW, another calibration factor, denoted $\tilde{x}$, is taken constant for the whole year for each vessel, and is calculated as median$(\tilde{v}_{w,t}/v_{w,t})$ over data filtered with the condition that SOG > 6kn. Since the miscalibration of a speed log will produce a bias in the measured STW, the resulting residual (STW – Virtual STW) will not be zero-centered for some vessels. Hence the residual does not necessarily correlate with erratic speed log behavior. Instead, we will look at the distribution of the residual of the calibrated STW, which should be centered around zero:

[7] Obviously Virtual STW is not completely correct either. It is still robust against the erratic behaviour and will be better calibrated than the speed logs in general.

$$r_t = \hat{x}_t v_{w,t} - \hat{v}_{w,t} \#(2)$$
$$\tilde{r}_t = \tilde{x} v_{w,t} - \tilde{v}_{w,t}$$

The indicators $(r_t, \hat{x}_t, \tilde{r}_t, \tilde{x})$ will be aggregated and visualized for both the cargo and cruise segments. In addition to the distribution of both indicators, we also show the percentage of data points with errors less than some value:

$$ecdf_r(R) = \frac{1}{N}\sum_t^N (r_t < R) \#(3)$$
$$ecdf_{\hat{x}}(X) = \frac{1}{N}\sum_t^N (|1 - \hat{x}_t| < X) \#(4)$$

3.3. Results on Calibration Factor

In Fig.5 we present the results of the analysis on the calibration errors. Surprisingly, in general the cargo vessels outperform the cruise vessels: nearly 80% of vessels have calibration error less than 2% compared to the 55% of cruise vessels at the same mark. This is explained by the fact that the distribution for cargo vessels is better centered around the expected value of one, while cruise vessels seem to have slight bias towards the negative side. At extreme calibration errors, the amount of vessels is more even, and some vessels display calibration errors up to 15%. The results are similar for both the Virtual STW and the Forecast STW.

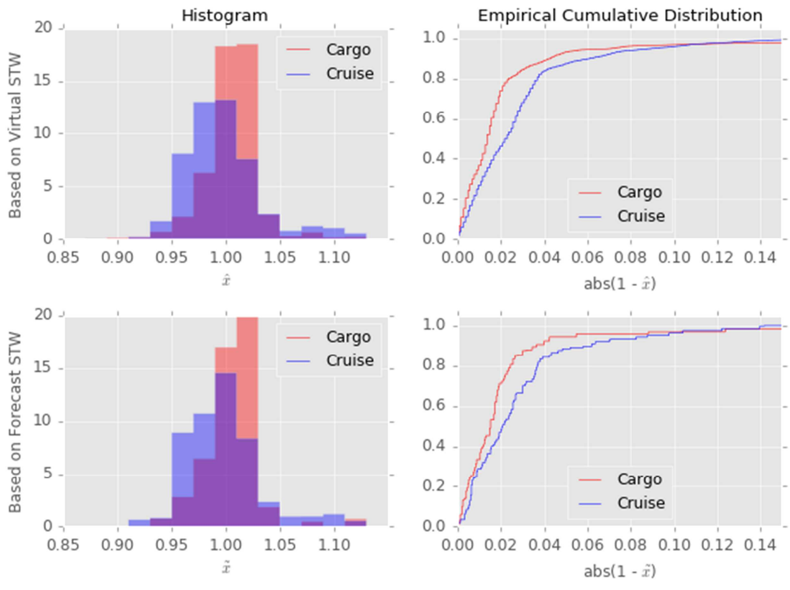

Fig.5: Speed log calibration factor statistics. On the left, we show the distribution of x and $\tilde{x}$, while on the right, we plot $ecdf_x$ and $ecdf_{\tilde{x}}$, see Eqs.(3) and (4).

In Fig.6 we quantify the amount of change in the calibration factor $\hat{x}_t$ by calculating the standard deviation over the year for each ship. In this plot, it is seen that the calibration factor has changed much more for the cruise vessels than for the cargo vessels. There are some possible explanations for this difference. First, it could be that the cruise customers typically care more about the speed log calibration and hence tend to recalibrate more often. However, calibrating the speed log is difficult and it is possible that these recalibrations result in a further need to recalibrate again. Second, the speed logs might be more prone to e.g. temperature effects. Third, the study dataset contains the STW reading which was displayed onboard, so if there are multiple speed logs with differing calibration errors and the crew is switching between them, the modeled calibration factor will also vary.

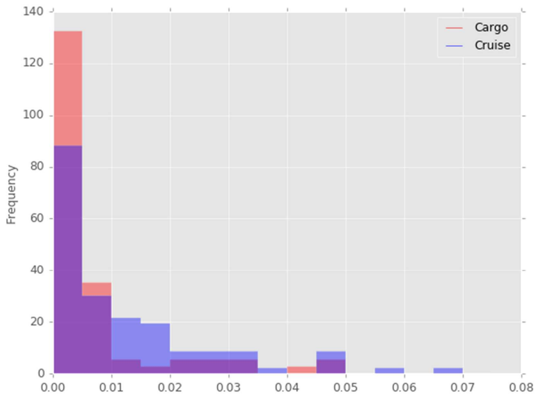

Fig.6: Standard deviation of calibration factor for each ship

3.4. Results on Residual

In Fig.7, we show the results on the speed log noise. Surprisingly again, the speed logs on cargo vessels outperform those on cruise vessels. From cargo vessels, about 85% of data points have a noise level of less than 0.2 knots, while for cruise, less than 70% of data has similar quality[8]. Comparing to the results using the forecast STW, it is clear the forecast STW contains more noise.

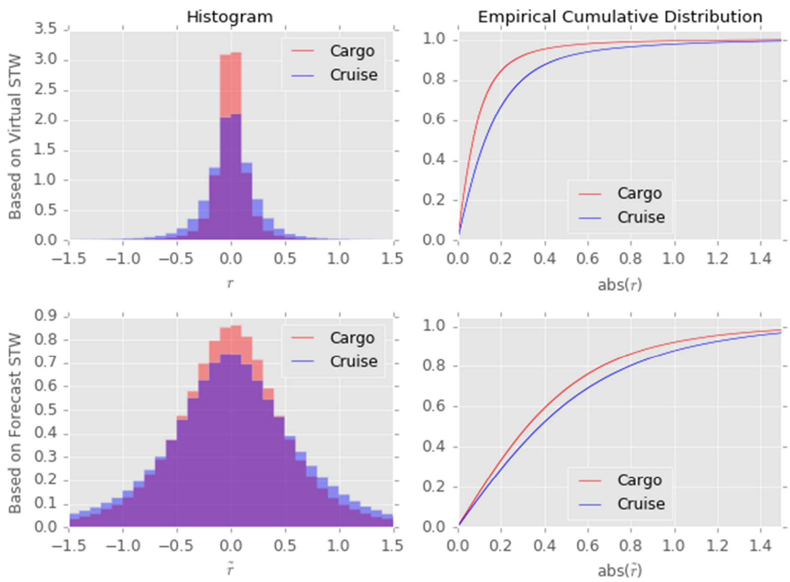

Fig.7: Speed log noise statistics. On the left, we show the distribution of r and $\tilde{r}$, while on the right, we plot $ecdf_r$ and $ecdf_{\tilde{r}}$, see Eqs.(3) and (4).

3.5. Implications for Performance Assessment

It is interesting to interpret the results in terms of their effect on estimates of vessel efficiency. Since the admiralty coefficient (ignoring draft variations)

$$Ad \sim \frac{\hat{v}_w^3}{P} \sim \hat{x}^3 \frac{v_w^3}{P},$$

[8] In unpresented results, we find support for the hypothesis that speed log data is noisier in shallow waters. Although cruise vessels sail more often in shallow waters, the presented results would be largely unaffected by filtering data based on the deep-water condition.

the third power of the calibration factor is an estimate of the ratio of the "correct" admiralty factor to the one calculated with the speed log reading. Fig.8 shows the distributions of the third power of the calibration factor. Now the distributions look drastically wider than before, and for the majority of the vessels, the true performance is over 5% off from the measured one. Thus vessel performance estimation is particularly sensitive to calibration errors.

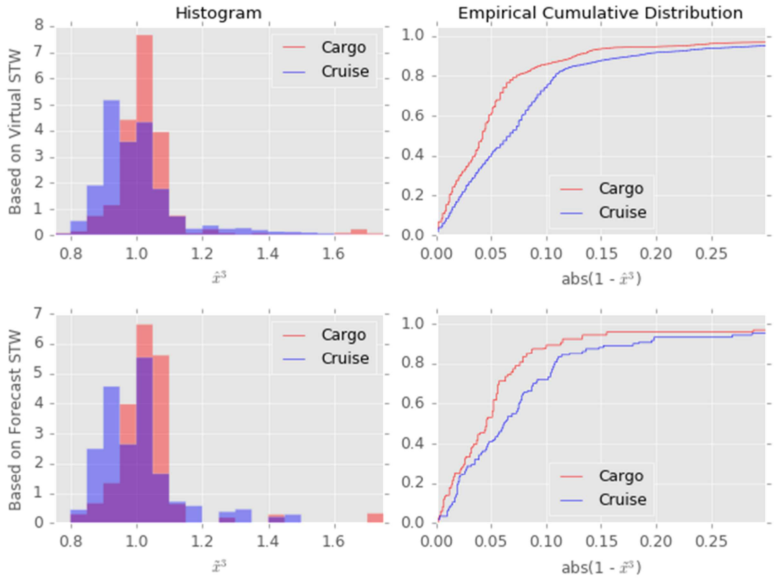

Fig.8: Implication of calibration on admiralty factor. On the left, we show the distribution of x^3 and $\tilde{x}^3$, while on the right, we plot $ecdf_{x^3}$ and $ecdf_{\tilde{x}^3}$, see Equations (3) and (4). The top row is based on Virtual STW as the reference STW and the bottom row is based on Forecast STW.

The amount of noise in the speed log mainly effects the resolution of detectable performance changes e.g. in the event of installation of a propeller energy saving device. In Fig.9, we show a comparison of admiralty calculated based on a relatively high-quality speed log to that based on Virtual STW. The noise-level in the admiralty calculated with Virtual STW is visibly smaller.

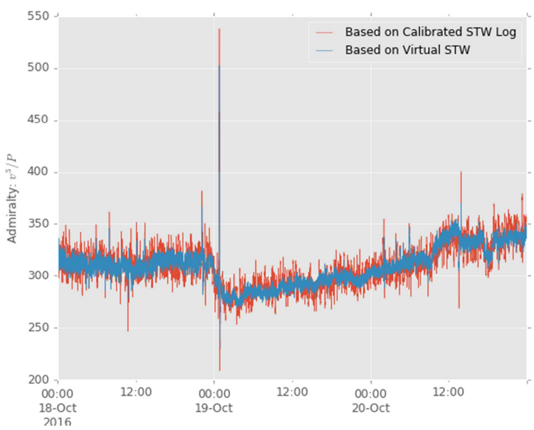

Fig.9: Admiralty time-series

4. **Conclusions**

We introduced the Eniram Virtual Speed Log, which is a virtual sensor application that models the ship hydrodynamics and uses propulsion related data together with speed data (SOG, STW, current forecasts) to estimate the most likely STW, called Virtual STW. By validating against a STW calculated from SOG and current forecasts, it was shown that the accuracy of Virtual STW is superior compared to speed log data. We then used the Virtual STW to evaluate and quantify vessel speed log quality. We find that calibration errors are relatively common and have a significant impact on vessel propulsion efficiency estimation. Moreover, calibration errors can change in time and hence greatly impact performance monitoring solutions.

References

BOS, M. (2016), *How metocean data can improve accuracy and reliability of vessel performance estimates*, HullPIC, Pavone, http://data.hullpic.info/HullPIC2016.pdf

PYÖRRE, J. (2012), *Getting up to speed*, Maritime IT & Electronics, June/July

SOLONEN, A. (2016), *Experiences with ISO 19030 – And beyond*, HullPIC, Pavone
http://data.hullpic.info/HullPIC2016.pdf

VOM BAUR, M. (2016), *Acquisition and integration of meaningful performance data on board challenges and experiences*, HullPIC, Pavone, http://data.hullpic.info/HullPIC2016.pdf

BERTRAM, V. (2012), *Practical Ship Hydrodynamics*, Butterworth & Heinemann, Oxford

Automatic MRV Reporting with Use of On-Board Performance Management Systems

Wojciech Gorski, Enamor, Gdynia/Poland, wojciech.gorski@enamor.pl

Abstract

European Parliament and the Council of European Union adopted on 29 of April 2015 regulation (EU) 2015/757 on the Monitoring, Reporting and Verification of carbon dioxide emissions from maritime transport (further referred to as MRV). This regulation was recently amended with detailed methods for determination of cargo quantity, fuel consumption, travelled distance and CO_2 emissions. Set of amendments published on 16 of December 2016 establishes the base for unified approach to MRV. Regulation will concern all ships over 5000 gross tonnes visiting EU ports after 1 January 2018. However already by 31 of August 2017 the monitoring plan for compliance with MRV must be prepared for each concerned vessel and submitted to verifier for acceptance. Adoption of MRV regulation will require significant bureaucratic efforts in data collection, verification and post-processing both for ship crew and owner office. This workload may be substantially reduced with use of performance management systems. Paper presents the approach to MRV data collection and reporting in simple, amiable manner. Special attention is paid to minimise crew involvement, automate data collection, smoothing post-processing and assure data integrity.

1. Overview of MRV regulation

According to *IMO (2014)* international maritime shipping is responsible 2.5% of global greenhouse gas (GHG) emissions. What is more worrying shipping emissions are predicted to rise by 50% to 250% by 2050 depending on the economic and energy consumption development scenario. This perspective is in drastic dissonance with ambitious goals of preventing climate change.

Although EU supports global actions led by IMO it also notices lack of agreement on market-based measures applicable for whole maritime shipping sector including existing ships. Monitoring, Reporting and Verification of carbon dioxide emissions from maritime transport (MRV) is therefore an element of global EU strategy to reduce GHG emissions from shipping. This strategy comprise also setting up GHG emissions reduction targets and defining mid to long term market-based measures implying GHG reductions.

EU Parliament and the Council of European Union adopted on 29 of April 2015 regulation (EU) 2015/757 on MRV, *EU (2015)*. This regulation was recently amended with detailed methods for determination of cargo quantity, fuel consumption, travelled distance and CO_2 emissions published on 16 of December 2016. It establishes the base for unified approach to MRV. Regulation will concern all ships over 5000 gross tonnes visiting EU ports after 1 January 2018. Starting 31 of August 2017 the monitoring plan for compliance with MRV must be prepared for each concerned vessel and submitted to verifier for acceptance. Adoption of MRV regulation will require significant bureaucratic efforts in data collection, verification and post-processing both for ship crew and owner office. This workload may be substantially reduced with use of performance management systems. Furthermore use of performance prediction models (being integral part of performance management systems) build based on data collected during ship's operation has the highest potential for effective reduction of emissions.

2. Data collection

Data collection constitutes the essential part of the carbon dioxide monitoring process. It must be carried out during all voyages which starts or ends in ports of a member state. Selected method of data collection must be provided in monitoring plan and must assure data accuracy and integrity. Although MRV regulation allows, in certain cases, for yearly reporting it is insufficient to collect data totals for such a long time period. In certain conditions voyage based reporting is required but even for such case additional division is mandatory. Due to the fact that carbon dioxide emissions should be attributed separately to periods of voyage and port stay data shall be aggregated at minimum for those periods. In general any of following changes if not recorded in continuous manner shall result in data collection:

- Fuel switchover,
- Port arrival and departure if combined with cargo/passenger operations,
- Anchorage.

If a ship is not equipped with data collection system allowing for continuous recording MRV related parameters (i.e. fuel consumption of each type, distance sailed and amount of cargo) fulfilling the EU regulation will result in additional crew duties. Crew will have to determine necessary data in timely manner which may interfere with its routine work. Furthermore processing of collected data in order to prepare required reports creates an additional bureaucratic burden.

Use of the ship performance management systems on-board may tremendously simplify monitoring and reporting of carbon dioxide emissions. Systems based on automatic data collection used for the purpose of ship performance management usually register information required for MRV. Therefore it is natural to develop appropriate interface for the purpose of MRV.

Enamor offers ship performance management system ESOS which is installed on over 100 ships. Since beginning of 2016 system undergoes major upgrade in a course of R&D project sponsored by The National Centre for Research and Development (agency of Minister of Science and Higher Education in Poland). ESOS successor, named SeaPerformer™, will optimize operation of the vessels in various ways including reduction of pollutants. Implementation of new European MRV regulations is included in the scope of research works.

SeaPerformer™ (as well as ESOS) allows continuous monitoring and registration of vital performance parameters provided by ship systems and sensors. There is variety of interfaces provided including NMEA, Modbus, CanOpen, TCP. It is also open for manual entries making the system independent of specific ship configuration and interfaces.

Manual data entry is used in case specific data cannot be measured (missing sensor e.g. wave sensor) or existing sensor does not provide data output (e.g. mechanical flow meter). SeaPerformer™ offers common interface for the purpose of performance analyses, EEOI and MRV. This unified approach makes data collection more efficient especially in case the same data are collected for different purposes (EEOI and MRV).

Interface is intended to be used on regular basis e.g. every 24 hours or at any time when important parameter, which is not monitored continuously, changes. It serves two purposes. Firstly it aggregates data (travelled distance and consumed fuel in case of MRV) and stores it for report preparation. Furthermore it supplements on-board database with parameters which are not continuously monitored. In such case SeaPerformer™ maintain the same value for subsequent database records until next manual entry is provided (e.g. cargo quantity). Typical data collection scheme during a single voyage is presented on Fig.1. Numbers in grey circle denotes the moment in time when data entry with use of the interface is prepared. Entries describe the following:

1. End of voyage first stage following departure (usually after first 24 hours),
2. End of voyage following stage (usually each 24 hours, always on port arrival and on beginning of anchorage),
3. End of cargo operations in port,
4. End of port stay (departure),
5. End of anchorage.

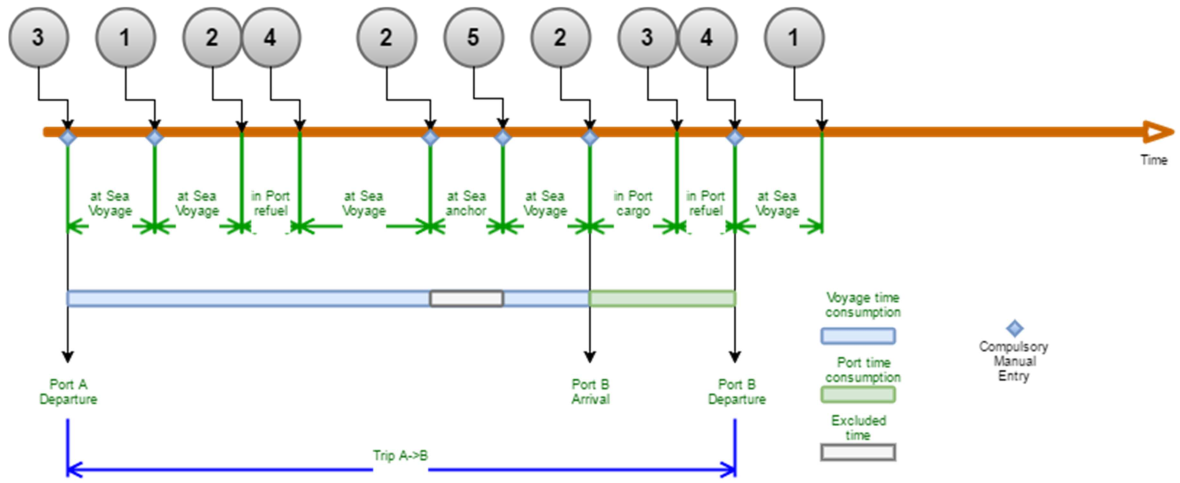

Fig.1: Scheme of MRV data collection during single trip

Manual data interface consists of collection of cards. Each card allows for gathering information of similar nature e.g. separate card for consumption of each fuel type and another for amount of cargo. Cards in general consist of two sections. First section contains aggregated values of continuously monitored parameters. Second section allows for manual entry. In case certain parameter is not monitored, first section remains empty or (for selected parameters) contains value provided in previous session. Operator may accept automatically aggregated value or may provide different value e.g. in case of sensor malfunction. Both values are stored and clearly indicated in data entry. Deviations from automatically aggregated values must be explained which is also stored in a database.

Manual data collection is a critical task. It is time consuming and prone to human error. Therefore appropriate interface must simplify this task and minimise the possibility of entering incorrect data. Taking into account these principles SeaPerformer^{TM} offers unified, contextual and conductive manual entry interface. Each of these properties requires deeper explanation.

Unification of manual entry interface allows using the same data collection scheme irrespectively of the purpose. No matter if data collection serves performance analyses, EEOI or MRV reporting the same interface is used. User familiarisation process is therefore much quicker and what is more important the same data used for different purposes are collected only once.

Contextual interface takes into account information provided by user at current data entry session and information collected in previous sessions. This way, interface adjusts its content to minimise data entry requests. Collection of destination port information serves as an example of contextual approach. This information is requested only in specific condition i.e. after first voyage segment following port departure. During subsequent segments data entries arrival port information is not requested. Contextual interface greatly simplifies the data acquisition process.

Conductive approach shall be understood as machine guided process of data gathering. In a combination with context sensitivity it allows quick and effortless information acquisition. User interaction is minimised to those entries which cannot be determined by a system itself. It is a great advantage in case of (at least partially) automated data collection systems where appropriate data pre-processing can be done in a background (e.g. aggregation of fuel consumption) minimising time-consuming user data manipulations.

2.1. Required data

Execution of MRV implies the following set of data to be recorded:

- Date and time of port departure and arrival,

- Amount of carbon dioxide emission,
- Travelled distance,
- Time spend at sea and in ports,
- Transport work,

In case any of the above parameters cannot be determined directly also its components must be recorded in order to allow verification.

2.2. Data sources

In general all MRV related signals can be registered by means of data collection system being a part of SeaPerformer™. Following section describes data sources required for automated data gathering. Date and time of port departure and arrival is determined based on GPS time signal in case data entry is done at the time of event. It can be also provided retrospectively by manual date selection. Selection of event time defines the aggregation period which lasts from previous data entry. Port names can be selected from drop-down table using name initials, port codes or country name. EU ports are specially indicated on the port list therefore voyages selection for the purpose of MRV can be done automatically.

Amount of carbon dioxide emission is determined by indirect method using the formula

$$CO_2\ Emission = Fuel\ consumption\ \times Emission\ factor$$

Since the *Emission factor* is fuel specific, consumption of each fuel type must be recorded separately. Consumption is determined by aggregation of fuel flow. Fuel flow data are generated by the fuel consumption monitoring (EFCM) subsystem. It is used for the purpose of interfacing fuel flow meters (volumetric or mass). In case of volumetric flow meters temperature correction is applied. EFCM provides fuel flow with respect to consumers (ME, AE, Boilers etc.) and fuel type. The latter is used for the purpose of MRV. *Emission factors* are defined for each fuel type in the interface settings.

Distance travelled is determined from the ship geographical positions provided by GPS system. Distance is calculated by integration of minute differences in ship's locations.

Time spend at sea and in ports are calculated from respective date and time of port departure and arrival. Anchorage time is deducted from port stay.
Transport work is calculates as:

$$Transport\ work = Traveled\ distance\ \times\ Cargo\ transported$$

Transported cargo is obtained by interfacing ship's loading computer.

2.3 Data integrity

Integrity of data used for MRV reporting is a prime requirement. Time gaps or incomplete data makes the MRV report unreliable and consequently may result in fail of the verification process. SeaPerformer™ assures data integrity both with respect to elimination of time gaps and data completeness.

Time integrity is secured by automatic selection of manual entry period. New entry always starts with closing date of previous entry. User cannot modify this date and therefore gaps are avoided. Existing entries may be modified (e.g. in case data sources malfunctions were detected after completion of data entry) and this process may also jeopardise time integrity. Modification of the data entry is done by complete removal of data entry and creation of one or more substituting entries. Interface remains in data entry mode until whole gap is covered.

Interface supports data completeness by used of redundancy and regeneration methods. Data redundancy is maintained by use of multiple data sources of the same type e.g. registration of additional GPS receivers. Multiple sources are arranged in order (usually according to their accuracy) and in case of primary signal failure it is substituted by secondary (or following) one. In order to cope with possible signals shifts primary signal is reconstructed based on the redundant signal trend as illustrated on Fig.2.

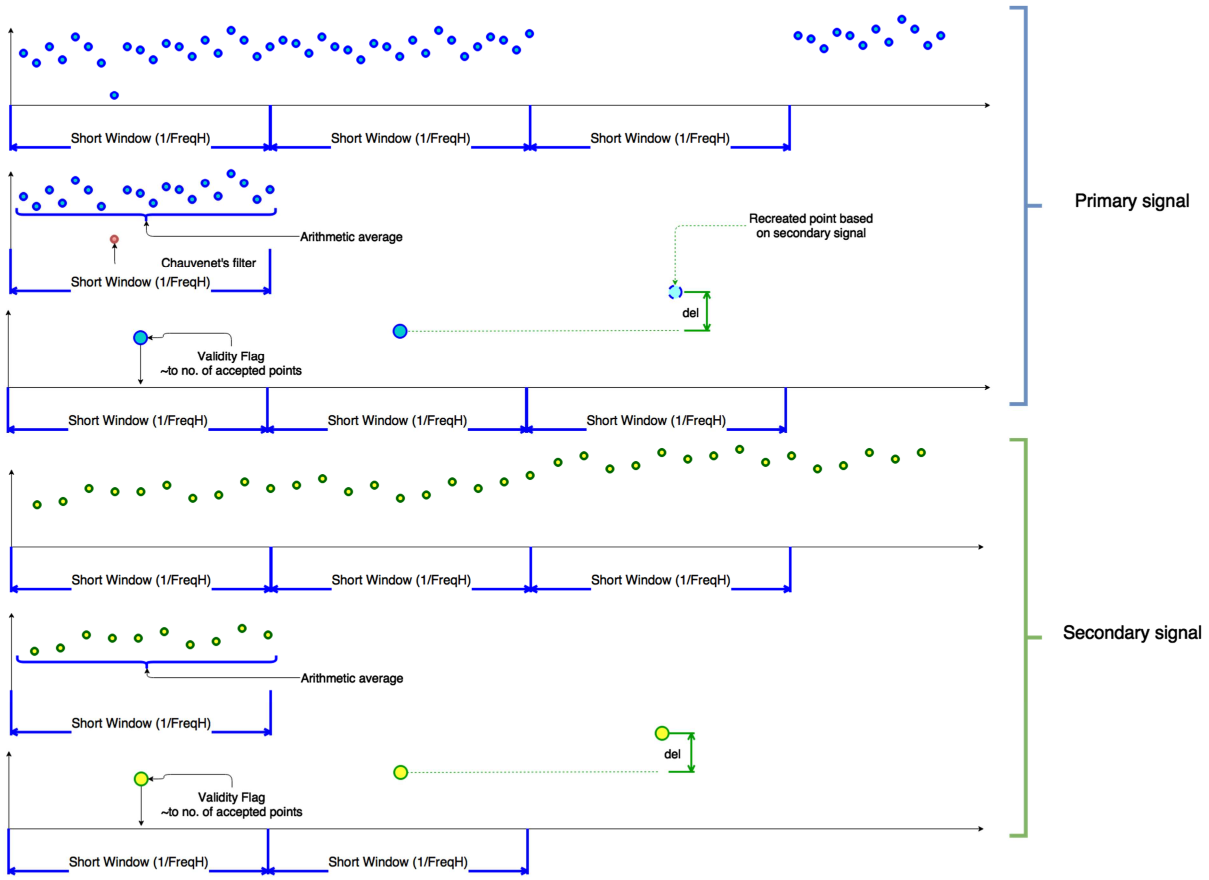

Fig.2: Signal redundancy

Another method used in order to maintain data completeness is signal regeneration. Twofold approach to this task can be realised. Somewhat simpler approach is regeneration based on another signal correlated with the missing one. As an example missing ME fuel consumption can regenerated based on shaft power meter. Power signal registered by stable and well calibrated device may be recalculated to fuel consumption using SFOC curve. Difference between estimated and real fuel consumption is sufficient for the purpose of substituting in case of primary system failure. Fig.3 illustrates such case. Green line denotes ME fuel consumption measured with pulse flow meter installed in fuel treatment system. Due to incorrect settings overflow valve allowed periodical recirculation to day tank (scattered signal between 0h and 17h) which was measured as additional fuel consumption. Proper fuel consumption was regenerated with use of calculated fuel consumption based on power meter signal (red line).

More advanced method of signal regeneration is based on utilisation of performance model. Multidimensional model tuned based on long term data collection may be successfully used not only for performance prediction as described by *Górski* (2016) but for missing signal regeneration as well. This approach may be especially interesting in case of general failure of data collection when most MRV related signals are missing. Performance model may efficiently predict e.g. fuel consumption based on minimum set of data (ship speed and loading condition) kept in ship logbook and weather conditions (available through weather services).

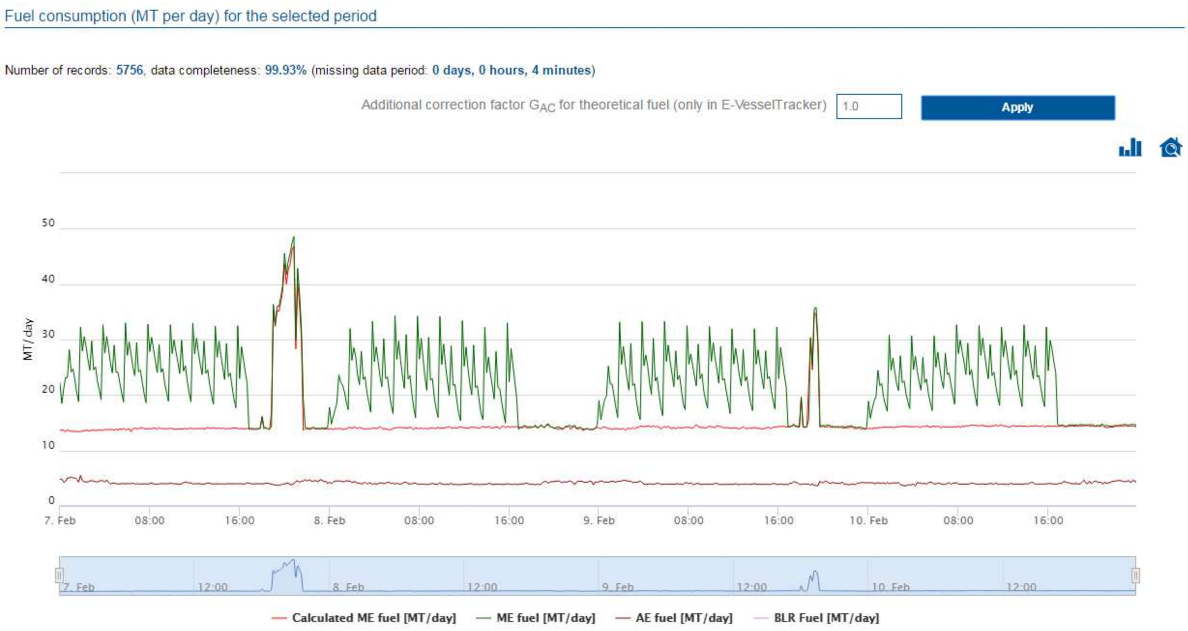

Fig.3: Regeneration based on correlated signal (calculated ME fuel consumption based on power meter signal)

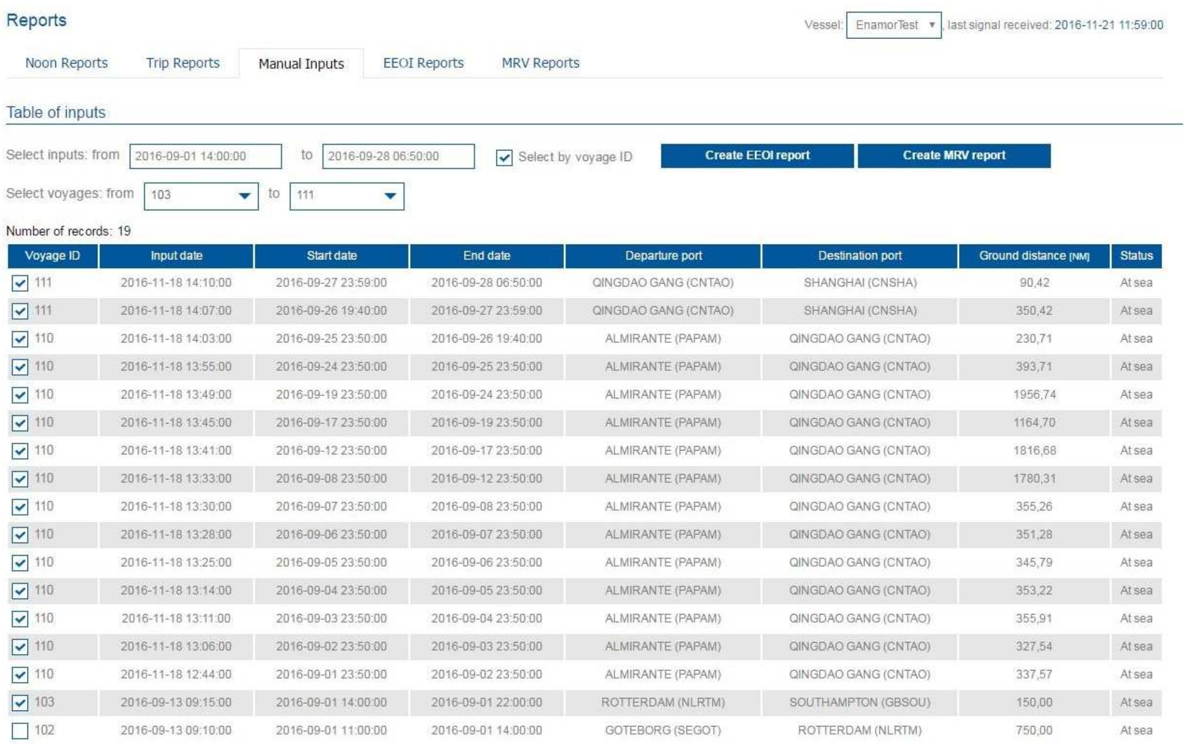

Voyage ID	Input date	Start date	End date	Departure port	Destination port	Ground distance [NM]	Status
111	2016-11-18 14:10:00	2016-09-27 23:59:00	2016-09-28 06:50:00	QINGDAO GANG (CNTAO)	SHANGHAI (CNSHA)	90,42	At sea
111	2016-11-18 14:07:00	2016-09-26 19:40:00	2016-09-27 23:59:00	QINGDAO GANG (CNTAO)	SHANGHAI (CNSHA)	350,42	At sea
110	2016-11-18 14:03:00	2016-09-25 23:50:00	2016-09-26 19:40:00	ALMIRANTE (PAPAM)	QINGDAO GANG (CNTAO)	230,71	At sea
110	2016-11-18 13:55:00	2016-09-24 23:50:00	2016-09-25 23:50:00	ALMIRANTE (PAPAM)	QINGDAO GANG (CNTAO)	393,71	At sea
110	2016-11-18 13:49:00	2016-09-19 23:50:00	2016-09-24 23:50:00	ALMIRANTE (PAPAM)	QINGDAO GANG (CNTAO)	1956,74	At sea
110	2016-11-18 13:45:00	2016-09-17 23:50:00	2016-09-19 23:50:00	ALMIRANTE (PAPAM)	QINGDAO GANG (CNTAO)	1164,70	At sea
110	2016-11-18 13:41:00	2016-09-12 23:50:00	2016-09-17 23:50:00	ALMIRANTE (PAPAM)	QINGDAO GANG (CNTAO)	1816,68	At sea
110	2016-11-18 13:33:00	2016-09-08 23:50:00	2016-09-12 23:50:00	ALMIRANTE (PAPAM)	QINGDAO GANG (CNTAO)	1780,31	At sea
110	2016-11-18 13:30:00	2016-09-07 23:50:00	2016-09-08 23:50:00	ALMIRANTE (PAPAM)	QINGDAO GANG (CNTAO)	355,26	At sea
110	2016-11-18 13:28:00	2016-09-06 23:50:00	2016-09-07 23:50:00	ALMIRANTE (PAPAM)	QINGDAO GANG (CNTAO)	351,28	At sea
110	2016-11-18 13:25:00	2016-09-05 23:50:00	2016-09-06 23:50:00	ALMIRANTE (PAPAM)	QINGDAO GANG (CNTAO)	345,79	At sea
110	2016-11-18 13:14:00	2016-09-04 23:50:00	2016-09-05 23:50:00	ALMIRANTE (PAPAM)	QINGDAO GANG (CNTAO)	353,22	At sea
110	2016-11-18 13:11:00	2016-09-03 23:50:00	2016-09-04 23:50:00	ALMIRANTE (PAPAM)	QINGDAO GANG (CNTAO)	355,91	At sea
110	2016-11-18 13:06:00	2016-09-02 23:50:00	2016-09-03 23:50:00	ALMIRANTE (PAPAM)	QINGDAO GANG (CNTAO)	327,54	At sea
110	2016-11-18 12:44:00	2016-09-01 23:50:00	2016-09-02 23:50:00	ALMIRANTE (PAPAM)	QINGDAO GANG (CNTAO)	337,57	At sea
103	2016-09-13 09:15:00	2016-09-01 14:00:00	2016-09-01 22:00:00	ROTTERDAM (NLRTM)	SOUTHAMPTON (GBSOU)	150,00	At sea
102	2016-09-13 09:10:00	2016-09-01 11:00:00	2016-09-01 14:00:00	GOTEBORG (SEGOT)	ROTTERDAM (NLRTM)	750,00	At sea

Fig.4: Selection of data range for MRV report

3. Reporting

MRV reporting, depending on the frequency of EU ports calls, shall be done either on voyage bases or yearly. Report shall be prepared in accordance with a template provided by *EU (2016)*. In order to simplify report preparation and minimise crew involvement SeaPerformer^{TM} enables report preparation through web server. Data entries prepared on-board are sent to the cloud server on regular basis (along with other monitored parameters). This way report can be prepared with use of any terminal with internet access e.g. at operator office. User (e.g. superintendent) can select required data either by voyage identifier or by date range and request appropriate report preparation, Fig.4. The same mechanism is used for MRV, EEOI and performance reporting. Created report is also stored in a cloud server for easy access.

4. Strategy of emission control

Practical approach to GHG emission reduction must be forwarded from global perspective to local conditions of each specific ship operation. Both ship level and fleet level GHG assessment tools must be provided since the ability to evaluate different operational strategies (e.g. trim, speed and route selection) allows for choosing the most efficient one in terms of economic and environmental goals. Research and development undertaken within SeaPerformer™ project aims on building consistent, ship level performance model and its application for GHG and economic optimisation both on ship and fleet levels. Application of such ship performance management systems in daily operation is essential in realisation of emission control strategy.

5. Summary

Implementation of European MRV requirements will result in additional obligations performed by ship crew and operator onshore officers. Data collection assuring its correctness and integrity may be time consuming and in some cases difficult. Reporting will require compilation of collected data for each vessel in a fleet and may result in bureaucratic burden.

Tasks imposed by EU regulations may be significantly simplified by use of ship performance management systems but the following requirements must be fulfilled:

- System must collect essential MRV data automatically in continuous manner,
- Automatic data collection should be supplemented by manual entries,
- System must assure data integrity and in case of data gaps must provide methods of missing data regeneration,
- Reporting shall be automated in accordance with EU template.

References

GÓRSKI, W. (2016), *Role of reference model in ship performance management*, HullPIC, Pavone

EU, (2015), *Regulation (EU) 2015/757 of 29 April 2015*, http://eur-lex.europa.eu/legal-content/EN/TXT/?qid=1487543648641&uri=CELEX:32015R0757

EU, (2016), *Regulation (EU) 2016/1927 of 4 November 2016*, http://eur-lex.europa.eu/legal-content/EN/ALL/?uri=uriserv:OJ.L_.2016.299.01.0001.01.ENG

IMO, (2014), *Third IMO Greenhouse Gas Study 2014*, IMO, London

Speed Loss Analysis of High-Speed Ro-Ro Vessels Coated with New Antifoulıng Technologies

Hasan Goler, U.N. Ro-Ro Isletmeleri, Istanbul/Turkey, hasang@unroro.com.tr
Kemal Bozkurt, U.N. Ro-Ro Isletmeleri, Istanbul/Turkey, kemal@unroro.com.tr

Abstract

This study reviews results of alternative hull coatings for high-speed Ro-Ro vessels and analyzes the potential to decrease fuel consumption and greenhouse gases (GHG). Field data of high-speed Ro-Ro vessels was studied according to ISO 19030 Part 3 for reference and evaluation periods. All vessels are sister vessels built in the same shipyard. Self-polishing and foul release coatings are tested against previous conventional coatings. Results indicate that the foul release silicone coatings create significant fuel savings.

1. Introduction

Increased hull roughness leads to increased frictional resistance, causing higher fuel consumption and GHG (Greenhouse Gas) emissions. The best method to reduce roughness is to apply a treatment to a ship's hull, to minimize its physical and biological roughness. Antifouling coatings are the most effective solutions to avoid fouling. New products aim to not just reduce fouling but make the hull surface as smooth as possible, and might lead to 60 billion of fuel saving, 384 million tons reduction in CO_2 and 3.6 million tons in SO_2 emissions, *Demirel et al. (2013)*.

Despite many available products and methods in the market, why is hull and propeller performance still relatively poor? Which coating is best for which ship type and operational profile? Or is there a coating which performs well under all conditions? These valid questions are still without clear answer. Efforts to develop “the ultimate” antifouling technology continue.

From the ship operator’s perspective, the problem is to decide which antifouling technology to select, an issue which repeats at each dry-docking when new coating is applied. So how does the ship operator make the decision? Ship operators approach this subject from two perspectives, price of coating and their experience. Most operators have an idea about the technologies in the market. They follow performance of coatings in their own fleet and what they hear from other operators. According to *Soyland and Oftedahl (2016)* the problem has been a lack of measurability. You cannot manage what you cannot measure is an old management adage that is still accurate today. A confusing multitude of measurement methods has been streamlined with the advent of ISO 19030. This standard is intended for all stakeholders who need to measure the changes in hull and propeller performance, including ship owners and operators, companies offering performance monitoring, shipbuilders and companies offering hull and propeller maintenance and coatings. ISO 19030 will make it easier for decision makers to learn from experience and thereby make better informed decisions. It will also provide much needed transparency for buyers and sellers of technologies and services intended to improve hull and propeller performance.

Many studies determined the impact of antifouling coatings by laboratory tests of coated cylindrical or flat panels, CFD simulations, coated rotor tests, chemical comparisons or adhesions tests. *Corbett et al. (2010*) study the benefits of Fluoropolymer Foul Release (FFR) hull coating technology regarding fuel cost savings, GHG reductions and other emissions that may be achieved by this technology. They examined fuel consumption data of three vessel types pre- and post-FFR application. The first vessel type is a tanker represented by a ship called Prem Divya; the second vessel type is a bulk cargo vessel represented by a ship called the Ikuna; the third vessel type is a container vessel where we compare the fuel oil consumption of three new builds coated with a tributyltin-free self-polishing copolymer (TBT-free SPC) to two new builds coated with FFR; all five container vessels are sister vessels. Results indicate that the application of FFR reduced speed-adjusted fuel oil consumption by 10% for the Prem Divya, 22% for the Ikuna, and no change in consumption for container vessels when carrying approximately 10,000 t of extra cargo. If similar fuel efficiency results were realized by all tanker and bulk cargo in the international fleet, annual fuel oil consumption could be reduced by roughly 16 million metric tons (MMT) per year, fuel expenditures by $4.4 to $8.8 billion, and CO_2 emissions by 49 MMT. Furthermore, analysis showed that reductions in CO_2 emissions are achieved at a negative cost, i.e. avoided emissions are coupled with cost savings for the ship owner. Additionally, they tried to explore the potential fuel oil consumption reductions for other vessel types including ferries, Roll-on/Roll-off (Ro-Ro) vessels, very-large crude carriers (VLCCs), and liquid natural gas (LNG) vessels. But the limited data set for other vessel types coated with FFR prevented confident use of statistical analysis methods to compare performance. They created a table by speed adjusted fuel consumptions for other type vessels and found 8.1% fuel consumption reduction for Ro-Ro vessels.

Lejars et al. (2012) published a detailed chemical review explaining fouling organisms, recent anti-fouling technologies with chemical background, working mechanism and surface structures.

Søyland and Oftedahl (2016) present ISO 19030, its motivation, scope and development. They described the history of ISO 19030 for hull and propeller performance assessment for ships in service. It outlines initial motivation, purpose and implementation of the standard. The standard is intended to support ship operators and suppliers in better business practice.

So far, most ships did not have required measurement tools like torque meters and sensors, data logging system, etc. Data uncertainty was high due to human error and equipment errors. It was needed to apply first test coating to same ship for one docking cycle and another one for next docking cycle to compare results with no major changes for the operation to analyze differences. Or you needed sister ships under same operational conditions to observe results with different coatings. Although some operators have valuable data, very little is published. To the best of our knowledge, only *Corbett et al. (2010)* worked on real data from ships. They compared results of SPC coating and FFR coating which were applied to 7 new builds (1 tanker, 1 bulker, 5 sister container vessels). *Meng et al. (2015)* study shipping log data based container ship fuel efficiency modeling.

The literature needs more studies regarding antifouling coating performances with field data despite the higher uncertainties compared with laboratory tests. We believe ISO 19030 will lead to more such real life studies. As a contribution, we studied a high-speed Ro-Ro fleet of 11 sister vessels. Our company wanted to improve efficiency using new hull coating technologies and to define the best antifouling coating technology for our vessels. Therefore, we decided to apply different coating technologies to each sister vessels and measure results of reference and evaluation periods.

2. Data and Methodology

Field data of 8 sister vessels used in the study. The oldest vessel was built in 2001 and the last one in 2008. The main idea of this study was to identify if there is any significant improvement on hull / propeller performance in respect to speed-loss and fuel consumption through new hull coating technologies. Reason for selecting these 8 vessels were:

- All vessels were built in same shipyard with same technical properties (albeit with some changes with built date).
- All vessels had same technology SPC antifouling coating at the beginning.
- All vessels used same fuel oil from same supplier during test period.
- All vessels were loaded with same type of cargo (trucks and trailers).
- All vessels were operated by same technical management with same planned maintenance system.
- All vessels were maintained with only genuine spare parts during their engine overhauls and routine maintenance activities.
- All vessels traded between the same routes and same waters in Mediterranean Sea.

2.1. Limitations and Assumptions

The methodology explained in ISO 19030 Part 3 was tried to use in this study as far as practicably possible. The vessels operate between Istanbul-Trieste, Istanbul-Toulon and Mersin-Trieste ports since 2000 and it takes a week for each vessel to complete one trip. Therefore, each leg of the trip was used as a sample instead of collecting daily data from noon reports. Speed over ground was approximated as each leg of the trip divided by duration of the trip. The vessels did not have torque meters; delivered power was approximated by fuel consumption, model test results of the ship and engine acceptance test result. The SFOC curve created in factory acceptance test of the engine was done with a fuel of 42274 kJ/kg. The actual LCV of the fuel which all vessels in question are consuming is 40200 kJ/kg. Therefore, the SFOC curve was corrected according to Lower Calorific Value of the fuel which vessels are consuming. As all vessels were sisters with same technical properties and working under same operational conditions and due to data of high number of voyages has been observed which is covering nearly all seasons of the year, it is assumed that, all vessels had same weather conditions as wind and sea states. Therefore, secondary measurement parameters as wind and water depth were not included in this study. The vessels were not fitted with draught sensors, but displacement for each sampling rate was available from stability reports issued by vessel for each sampling rate. Stability character of test vessels is almost same and they are using same stability software. Stability software on board has online gauging ability from every tank and only cargo weights and positions needs to be entered manually by crew. Cargo weight data provided for each voyage from the port authority. Product description explanations given in product data sheet of tested antifouling coatings were used as name/description of the coating.

2.2. Methodology

Application and test of new coatings to fleet started in 2013. 10 vessels docked until July 2014; 8 of them completed their first docking cycle with test application and docked again in 2015 and 2016 yielding performance of complete docking cycle for these vessels. Tables I and II give details and dry-docking history of test vessels.

In order to see if there is any significant improvement of speed loss and fuel consumption reduction by using new technology hull coatings, the procedure described below was used, Fig.1.

Table I: Details of test vessels

VESSEL NO	VESSEL 1	VESSEL 2	VESSEL 3	VESSEL 4	VESSEL 5	VESSEL 6	VESSEL 7	VESSEL 8
BUILT YEAR	2001	2002	2005	2005	2005	2006	2008	2008
GROSS TONNAGE	26469	26469	29004	29004	29004	29004	29004	29004
NET TONNAGE	7941	7941	8702	8702	8702	8702	8702	8702
DWT SUMMER LOAD	9865	9865	11636	11636	11636	11636	11523	11523
DWT DESIGN DRAUGHT	7092	7092	9481	9481	9481	9481	9481	9481
LIGHT SHIP	8663	8663	9041	9041	9041	9041	9152	9152
BREADTH	26 mtrs	26 mtrs	26 mtrs	26 mtrs	26 mtrs	26 mtrs	26 mtrs	26 mtrs
LENGTH OVER ALL	193 mtrs	193 mtrs	193 mtrs	193 mtrs	193 mtrs	193 mtrs	193 mtrs	193 mtrs
LENGTH BETWEEN PERP.	182,39 mtrs	182,39 mtrs	182,39 mtrs	182,39 mtrs	182,39 mtrs	182,39 mtrs	182,39 mtrs	182,39 mtrs
DEPTH TO MAIN DECK	8.6 mtrs	8.6 mtrs	8.6 mtrs	8.6 mtrs	8.6 mtrs	8.6 mtrs	8.6 mtrs	8.6 mtrs
DEPTH TO UPPER DECK	16.7 mtrs	16.7 mtrs	16.7 mtrs	16.7 mtrs	16.7 mtrs	16.7 mtrs	16.7 mtrs	16.7 mtrs
DRAUGHT(SUMMER LOAD)	6.45 mtrs	6.45 mtrs	7,00 mtrs	7,00 mtrs	7,00 mtrs	7,00 mtrs	7,00 mtrs	7,00 mtrs
DRAUGHT(DESIGNED)	5.7 mtrs	5.7 mtrs	6,45 mtrs	6,45 mtrs	6,45 mtrs	6,45 mtrs	6,45 mtrs	6,45 mtrs
SERVICE SPEED	21.6KN	21.6KN	21.6KN	21,5 KN	21,5 KN	21,5 KN	21,5 KN	21,5 KN
MAIN ENGINES	MCR 16200 KW	MCR 16200 KW	MCR 16200 KW	MCR 16200 KW	MCR 16200 KW	MCR 16200 KW	MCR 16800 KW	MCR 16800 KW
LANE METERS	3214	3214	3735	3735	3735	3735	3735	3735
CLASSIFICATION	DNV + 1 A1 GENERAL CARGO CARRIER RO-RO	DNV + 1 A1 GENERAL CARGO CARRIER RO-RO	DNV + 1 A1 GENERAL CARGO CARRIER RO-RO	DNV + 1 A1 GENERAL CARGO CARRIER RO-RO	DNV + 1 A1 GENERAL CARGO CARRIER RO-RO	DNV + 1 A1 GENERAL CARGO CARRIER RO-RO	DNV + 1 A1 GENERAL CARGO CARRIER RO-RO	DNV + 1 A1 GENERAL CARGO CARRIER RO-RO
BOW THRUSTER	1400KW(1900 HP)	1400KW(1900 HP)	1400KW(1900 HP)	1400KW(1900 HP)	1400KW(1900 HP)	1400KW(1900 HP)	1400KW(1900 HP)	1400KW(1900 HP)

Table II: Dry-docking history of test vessels

Vessel Name		DDn-1	DDn	DDn+1
VESSEL 1	Date of Drydock	4.05.2011	11.11.2013	13.08.2016
	Shipyard	BESIKTAS	BESIKTAS	SEFINE
	Blasting	SA 2 max %30	SA 2 %100	%10 sweep blasting
	Hull Coating	Self Polishing Coating - hydrolysing silyl acrylate	Foul Release Coating - advanced hydrogel silicone	Foul Release Coating - advanced hydrogel silicone
	Engine Overhaul	NO	NO	Both Engine 90.000 Hours overhaul Completed
VESSEL 2	Date of Drydock	17.08.2011	10.06.2014	17.01.2017
	Shipyard	BESIKTAS	BESIKTAS	SEFINE
	Blasting	SA 2 max %30	SA 2 %100	%10 sweep blasting
	Hull Coating	Self Polishing Coating - hydrolysing silyl acrylate	Foul Release Coating - advanced hydrogel silicone	Foul Release Coating - advanced hydrogel silicone
	Engine Overhaul	NO	NO	Both Engine 90.000 Hours overhaul Completed
VESSEL 3	Date of Drydock	8.04.2010	22.01.2013	29.03.2015
	Shipyard	BESIKTAS	GEMAK	GEMAK
	Blasting	SA 2 max %30	SA 2 max %25	SA 2 %100
	Hull Coating	Self Polishing Coating - hydrolysing silyl acrylate	Self Polishing Coating - hydrolysing silyl acrylate	Foul Release Coating - Advanced fluoropolymer technology
	Engine Overhaul	NO	NO	NO
VESSEL 4	Date of Drydock	29.06.2010	5.05.2013	16.05.2015
	Shipyard	BESIKTAS	GEMAK	BESIKTAS
	Blasting	SA 2 max %30	SA 2 %100	SA 2 %100
	Hull Coating	Self Polishing Coating - hydrolysing silyl acrylate	Self Polishing Coating - Biomimetic super-low-friction technology	Foul Release Coating - advanced hydrogel silicone
	Engine Overhaul	NO	NO	NO
VESSEL 5	Date of Drydock	30.08.2010	27.07.2013	2.06.2015
	Shipyard	BESIKTAS	BESIKTAS	BESIKTAS
	Blasting	SA 2 max %30	SA2 Full for flat bottom , SA1 5% for vertical sides	SA 2 %100
	Hull Coating	Self Polishing Coating - hydrolysing silyl acrylate	Self Polishing Coating - hydrolysing silyl methacrylate copolymers	Foul Release Coating - Advanced fluoropolymer technology
	Engine Overhaul	NO	NO	NO
VESSEL 6	Date of Drydock	22.04.2010	8.03.2013	9.10.2015
	Shipyard	BESIKTAS	GEMAK	BESIKTAS
	Blasting	SA 2 max %30	SA 2 max %25	SA 2 %100
	Hull Coating	Self Polishing Coating - hydrolysing silyl acrylate	Self Polishing Coating - hydrolysing silyl acrylate	Foul Release Coating - advanced hydrogel silicone
	Engine Overhaul	NO	NO	NO
	Other			MAN ALPHA KAPPEL PROPELLER MODIFICATION
VESSEL 7	Date of Drydock	4.02.2012	31.05.2013	28.04.2016
	Shipyard	BESIKTAS	BESIKTAS	SEFINE
	Blasting	SA 2 max %30	SA 2 max %25	SA 2 Max %15
	Hull Coating	Self Polishing Coating - hydrolysing silyl acrylate	Self Polishing Coating - hydrolysing silyl acrylate	Self Polishing Coating hydrolysing antifouling based on Nano acrylate Technology
	Engine Overhaul	NO	NO	NO
VESSEL 8	Date of Drydock	17.08.2011	28.08.2013	31.03.2016
	Shipyard	GEMAK	BESIKTAS	BESIKTAS
	Blasting	SA 2 max %30	SA 1 %10	SA 2 %100
	Hull Coating	Self Polishing Coating - hydrolysing silyl acrylate	Self Polishing Coating - linear polishing polymer (LPP)	Foul Release Coating - advanced hydrogel silicone
	Engine Overhaul	NO	NO	Both Engine 45.000 hours overhaul completed.
	Other			SCHOTTEL CLT PROPELLER MODIFICATION

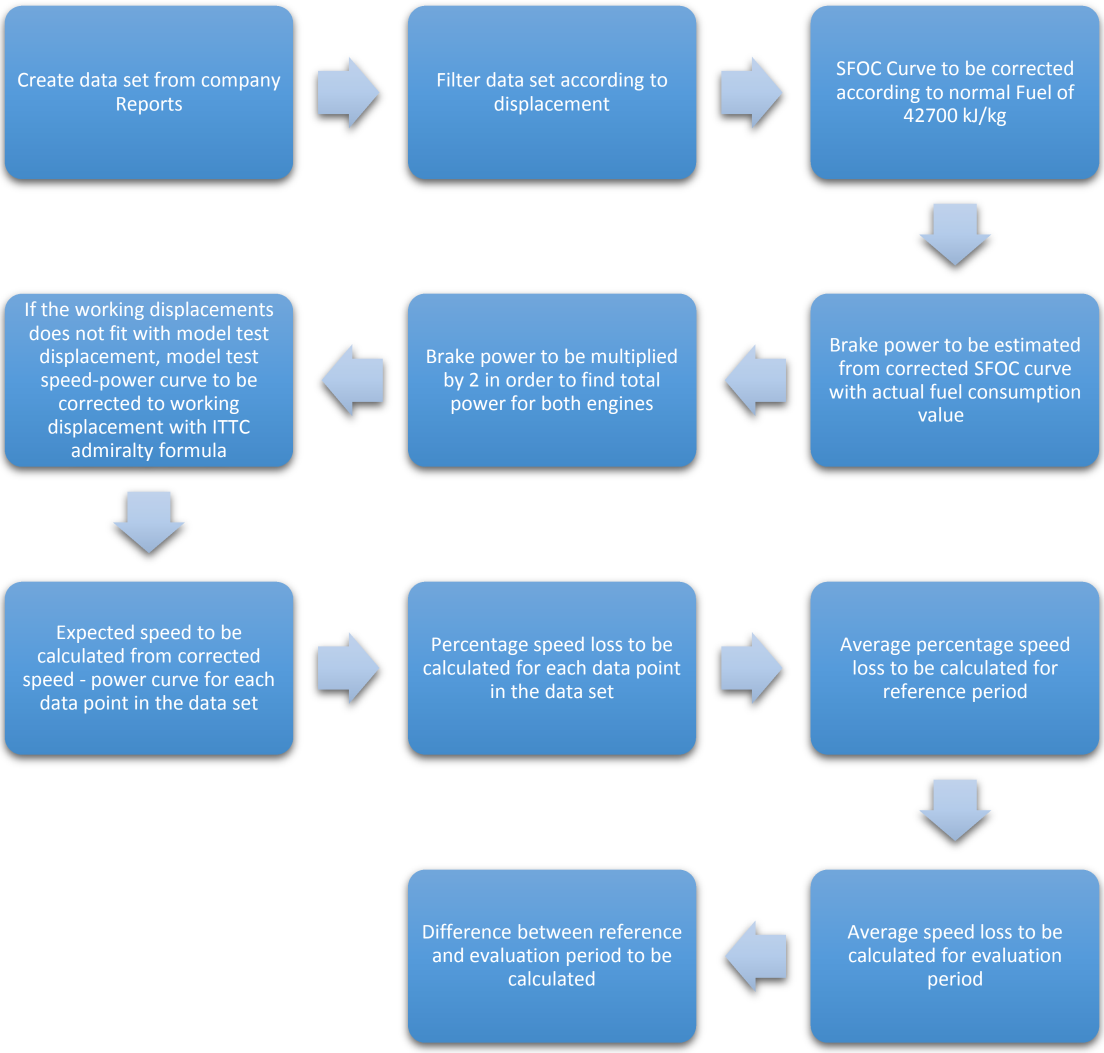

Fig.1: Methodology overview

1. Detailed tables were created as raw data for all test vessels from official arrival, departure, noon and Energy Efficiency Operational Index reports. Only data of the voyages completed in normal conditions were included in the analysis. Raw data included:

- Vessel Name
- Voyage Number
- Docking Cycle - Identification of voyage data refers to dry-docking period (e.g. DDN refers the dry-dock where test coating was applied, DDN-1 refers to previous dry-dock and DDN+1 refers to the next dry-dock after test application)
- Voyage between Ports - in order to identify sailed distance.
- Displacement
- Total fuel Consumption for each leg of the voyage
- Total Duration of Voyage for each leg
- Average Fuel Consumption per Hour for each leg - Calculated as total consumption divided by duration of voyage
- Total sailed distance in nm: Routes of each vessels collected from each test vessel to calculate correctly sailed distance
- Average Speed for the Voyage – in kn calculated by dividing sailed distance to duration, converted to m/s by 1 kn = 0.5144 m/s as a conversion factor.
- Average Fuel Consumption per mile for the voyage - dividing total consumption by sailed distance in nm

- Average Consumption Per engine in Kg - All test vessels have 2 main engines and average consumption per hour divided by 2 approximated each engine's consumption. Consumption in kg was corrected to normal fuel of 42700 kJ/kg due to actual fuel's Lower Calorific Value of 40200 kJ/kg.

2. Table filtered with ±5% for displacement of model test or working displacement according actual data of test vessel if model test displacement did not fit.

3. The SFOC reference curve based on shop tests was corrected in shop test report for environmental factors as per ISO 3046-1:2002. It was again corrected for normal fuel of 42700 kJ/kg with below formulation and new corrected SFOC curve issued.

$$SFOC_{LCVCorrcted} = \left(\frac{SFOC x LCV_{Normalfuel}}{LCV_{TestBed}} \right)$$

$SFOC_{LCVCorrcted}$: Corrected SFOC according to Normal fuel of 42700 kJ/kg

$SFOC$: SFOC value given is shop test report of the relevant engine

$LCV_{Normalfuel}$: 42.7 mJ/kg

$LCV_{TestBed}$: 42.274 mJ/kg

4. Delivered power of one engine approximated for each data point based on calculations of brake power P_B from an engine specific SFOC reference curve defined in Annex D of Part 2 of the standard:

$$P_B = f\left(M_{FOC} x \frac{LCV}{42{,}7} \right)$$

M_{FOC} : Mass of consumed fuel oil by main engine (kg/h)
LCV: Lower calorific value of fuel oil (mJ/kg)
f : SFOC reference curve (Corrected with ISO and normal fuel of 42.7 mJ/kg

5. Delivered power multiplied by 2 to find total power of both engines

6. Model test predictions were available for 18557.6 t displacement. For all vessels, a correction factor $(\Delta Voyage/\Delta ModelTest)^{2/3}$ was applied to the Speed-Power curve according to the ITTC displacement correction methodology.

7. Expected speed calculated for each data point from a speed-power reference curve at the corrected delivered power of both engines.

$$V_e = f x P_b$$

V_e : Expected Speed

f : Speed-Power Curve

P_b : Delivered power of both engine

8. Percentage speed loss, defined as Performance Value in the ISO19030 calculated for each data point in the corrected data set:

$$V_d = 100 x \left(\frac{V_m - V_e}{V_e} \right)$$

V_d : Percentage speed loss

V_m : Measured Speed

V_e : Expected Speed

9. Average percentage speed loss over reference period(s), calculated as:

$$V_{d,ref} = \frac{1}{k}\sum_{j}^{k}\frac{1}{n}\sum_{i}^{n} V_{d,j,i}$$

k number of reference periods
j reference period counter
n number of data points in the processed data set under reference conditions in the reference period j
i counter of data points in reference period j
$V_{d,j,i}$ percentage speed loss for data point i in reference period j
$V_{d,ref}$ average percentage speed loss over the reference period(s)

10. Average percentage speed loss over the evaluation period calculated as:

$$V_{d,eval} = \frac{1}{k}\sum_{i}^{j}\frac{1}{n}\sum_{i}^{n} V_{d,eval,i}$$

n number of data points in the processed data set under reference conditions of the evaluation period
$V_{d,eval,i}$ percentage speed loss for data point i in a data set of the evaluation period
$V_{d,eval}$ average percentage speed loss in data set of the evaluation period

11. Difference between average percentage speed loss in reference period and evaluation period:
$k_{HP} = V_{d,eval} - V_{d,ref}$
$V_{d,eval}$ average percentage speed loss in data set of the evaluation period
$V_{d,ref}$ average percentage speed loss over the reference period(s)
$k_{HP} = V_{d,eval} - V_{d,ref}$ Performance Indicator, PI

12. Average fuel consumption per hour value of reference and evaluation periods calculated from the data set.

13. New table created for each indicator from the data set in order to make fuel consumption comparisons between reference and evaluation period.

Table III: Sample result table

	Unit	Reference	Evaluation
Sample Size	pcs	36	66
disp total	t	544789.50	1000287.30
disp avr.	t	15133.04	15155.87
fuel total	t	5128.90	9469.72
fuel avr	t	142.,47	143.48
mile total	nm	42806.50	84690.80
hours total	h	2210.40	4302.90
speed avr	kn	19.38	19.71
Av.cons	t/h	2.32	2.20

14. Due to Fuel consumption being effected by speed, fuel consumption of evaluation period normalized based on average speed of reference period. This was achieved by substituting the below equation for the Fuel Oil Consumption (FOC) of evaluation period which was also used by Corbett's study to correct fuel consumption by speed:

$$FOC Normalized = FOC\ Evaluation \times \left(\frac{(AverageSpeed\ ReferencePeriod)}{AverageSpeed\ EvaluationPeriod} \right)^3$$

This equation converts the main engine fuel oil consumption for data entry of evaluation period to a normalized value according the reference period's average speed.

15. Analyze if the difference was significant between the average fuel consumption per hour value of reference period and corrected-normalized average fuel consumption per hour value of evaluation period. Below equation was used to test the difference among 2 means for the samples:

$$t = \frac{(\overline{X}_1 - \overline{X}_2) - (\mu_1 - \mu_2)}{\sqrt{\frac{s_1^2}{n_1} + \frac{s_2^2}{n_2}}}$$

Results to be displayed at the confidence level of 95%.

3. Findings and Conclusion

Data of reference periods and evaluation periods described in ISO 19030 compared to measure and evaluate hull performance. In order to prove results statistically, paired samples t-test was used for fuel consumption and speed parameters, Tables IV and V.

Vessel 1 was built in 2001. She was dry-docked in 2011 and conventional Self Polishing Hydrolyzing Silyl Acrylate hull coating was applied with spot blasting. Then she dry-docked again in 2013. As her hull was not fully blasted at any dry-docking after 2001, the hull condition was poor, Fig.2. Her hull was fully blasted, an Advanced Hydrogel Silicone Foul Release Coating applied. The average fuel oil consumption was 2.32 t/h for the reference period (previous year's data before entering dry-dock in 2013) and 2.20 t/h for the evaluation period (first year's data after dry-docking), i.e. by 5.04%. Speed increased to 19.71 kn from 19.38 kn. Had the vessel kept speed at 19.38 kn, consumption would have decreased to 2.06 t/h, i.e. by 11.27%. The speed loss was -9.70% for the reference period and -7.03% with the application of new coating, i.e. improved by 2.67% improvement.

Table IV: Results of Self Polishing Applications

		SELF POLISHING					
		Dry-docking Performance			In-service Performance		
		Referans Period	Evaluation Period	Difference	Referans Period	Evaluation Period	Difference
VESSEL 3	*Speed Loss %*	-8,807	-9,642	-0,84%	-9,642	-12,514	-2,87%
	Fuel Consumption mt/hr	2,438	2,525	3,57%	2,333	2,655	13,80%
VESSEL 6	*Speed Loss %*	-9,303	-7,972	1,33%	-7,972	-11,676	-3,70%
	Fuel Consumption mt/hr	2,391	2,252	-5,82%	2,306	2,718	17,88%
VESSEL 7	*Speed Loss %*	-6,960	-6,839	0,12%	-6,839	-9,944	-3,10%
	Fuel Consumption mt/hr	2,260	2,247	-0,54%	2,191	2,522	15,13%
VESSEL 8	*Speed Loss %*	-7,387	-8,813	-1,43%	-8,813	-11,467	-2,65%
	Fuel Consumption mt/hr	2,347	2,497	6,38%	2,191	2,479	13,13%
VESSEL 5	*Speed Loss %*	-8,280	-8,181	0,10%	-8,181	-10,432	-2,25%
	Fuel Consumption mt/hr	2,423	2,404	-0,75%	2,279	2,523	10,70%
VESSEL 7	*Speed Loss %*	-10,753	-9,351	1,40%			
	Fuel Consumption mt/hr	2,499	2,339	-6,41%			
VESSEL 4	*Speed Loss %*	-10,093	-9,163	0,93%	-9,163	-9,872	-0,71%
	Fuel Consumption mt/hr	2,482	2,378	-4,16%	2,385	2,456	2,98%

Table V: Results of Foul Release Applications

		FOUL RELEASE					
		Dry-docking Performance			In-service Performance		
		Referans Period	Evaluation Period	Difference	Referans Period	Evaluation Period	Difference
VESSEL 1	*Speed Loss %*	-9,709	-7,039	2,67%	-7,039	-8,811	-1,77%
	Fuel Consumption mt/hr	2,321	2,059	-11,27%	2,204	2,381	8,06%
VESSEL 2	*Speed Loss %*	-11,573	-7,089	4,48%	-7,089	-7,905	-0,82%
	Fuel Consumption mt/hr	2,270	1,858	-18,14%	2,110	2,186	3,60%
VESSEL 3	*Speed Loss %*	-12,428	-6,639	5,79%	-6,639	-6,360	0,28%
	Fuel Consumption mt/hr	2,264	1,753	-22,60%	2,301	2,272	-1,26%
VESSEL 4	*Speed Loss %*	-9,889	-6,958	2,93%			
	Fuel Consumption mt/hr	2,289	2,012	-12,07%			
VESSEL 5	*Speed Loss %*	-10,408	-6,237	4,17%	-6,237	-8,783	-2,55%
	Fuel Consumption mt/hr	2,306	1,920	-16,73%	2,345	2,620	11,73%
VESSEL 6	*Speed Loss %*	-12,169	-7,487	4,68%			
	Fuel Consumption mt/hr	2,345	1,903	-18,85%			
VESSEL 8	*Speed Loss %*	-11,726	-7,391	4,33%			
	Fuel Consumption mt/hr	2,438	2,003	-17,82%			

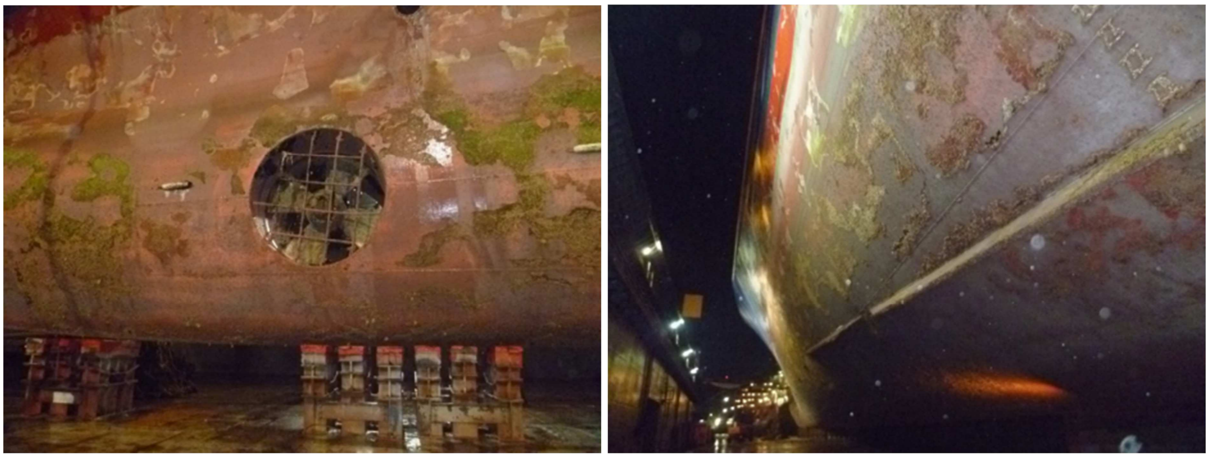

Fig.2: VESSEL 1, 2013 Dry-dock, Picture of hull condition, after first wash, Condition before Hydrogel Silicone Application

The difference in average fuel consumptions between reference period (2.32 t/h) and evaluation period (2.20 t/h) was statistically significant in the 95% confidence level. (In order to perform paired samples t-test, it is required to compare equal sample sizes for each period. As sample sizes of each period were not same, equal quantity of samples taken from each period which resulted minor differences on values e.g. 2.20 t/h reduced to 2.1969 t/h during statistical calculations. Same condition also valid for other vessels statistical analysis.) According to the In-Service Performance indicator, speed decreased to 19.33 kn from 19.71 kn, but fuel consumption remained same. Average consumption in the reference period was 2.20 t/h and 2.21 t/h in the evaluation period. Even for reduced speed in the evaluation period, fuel consumption remained same. Had the vessel kept speed as 19.71 kn in the evaluation period, fuel consumption would have been 2.39 t/h, i.e. increased by 8.06%. Vessel 1 dry-docked again in 2016. Hull and coating condition were checked visually. The hull was clean and coating condition was good. Only a bit of slime was observed on the vertical sides with a 0.5 m width on the loaded draft area where exposed to sunshine. Flat bottom was completely clean and no slime was observed, Fig.3. One layer of hydrogel silicone foul release coating was applied again to observe performance of vessel for the next 5 years, Fig.4. The vessel used to be dry-docked every 2.5 years. With the performance of advanced hydrogel silicone technology, our company decided to dry-dock the vessel every 5 years.

Fig.3: VESSEL 1, 2016 dry-dock, hull condition just after entering dry-dock

Fig.4: VESSEL 1, 2016 dry-dock, hull condition after 1 layer Hydrogel application

Vessel 2 was built in 2002. She was dry-docked in 2011 and conventional Self Polishing Hydrolyzing Silyl Acrylate hull coating was applied with spot blasting. Then she was dry-docked again in 2014, with poor hull condition, Fig.5. Her hull was fully blasted and Advanced Hydrogel Silicone Foul Release Coating applied. According to dry-docking performance, the average fuel oil consumption was 2.27 t/h in the reference period and 2.11 t/h in the evaluation period. Fuel consumption was decreased by 7.04%. Speed increased to 19.49 kn from 18.88 kn. Had the vessel kept speed at 18.88 kn, consumption would have been 1.86 t/h, i.e. decreased by 18.14%. Speed loss was calculated as -11.57% for the reference period and -7.09% with the application of new coating, i.e. 4.48% improvement on ship speed. Difference between average fuel consumptions and average speeds was statistically significant in the 95% confidence level. According to the In-Service Performance Indicator, speed was reduced to 19.33 kn from 19.49 kn, but fuel consumption remained same. Average consumptions in the reference period was 2.11 t/h and 2.12 t/h in the evaluation period.

Fig.5: VESSEL 2, 2014 dry-dock, hull condition after first wash, before Hydrogel Silicone application

Although speed reduced during the evaluation period, fuel consumption remained same. Had the vessel kept speed at 19.49 kn in the evaluation period, fuel consumption would have been 2.19 t/h, i.e. increased by 3.60%. Vessel 2 was dry-docked again in 2017. Hull and coating condition were checked visually. The hull was clean and coating condition was very good, Fig.6. Only a bit of slime was observed on the vertical side with a 0.5 m width on the loaded draft area where exposed to sunshine. Flat bottom was completely clean and no slime was observed. Just one layer of hydrogel silicone foul release coating was applied again to observe the performance of vessel for the next 5 years. The vessel used to be dry-docked every 2.5 years. With the performance of advanced hydrogel silicone technology, our company decided to dry-dock the vessel every 5 years.

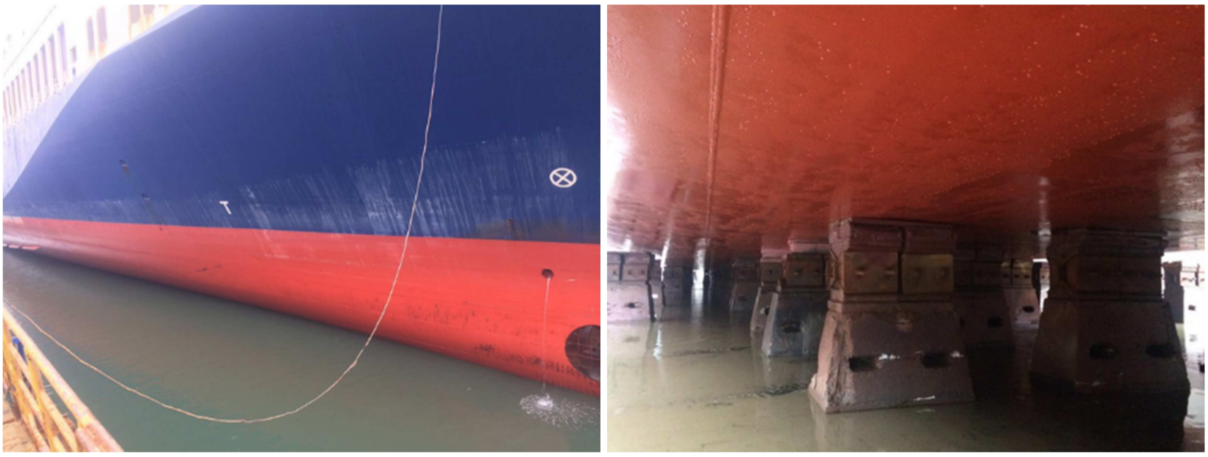

Fig.6: VESSEL 2, 2017 dry-dock, hull condition, just after entering dry-dock

Vessel 3 was built in 2005. She was dry-docked in 2010; conventional Self Polishing Hydrolyzing Silyl Acrylate hull coating was applied with spot blasting. Then she was dry-docked again in 2013. The hull condition was poor, Fig.7. Vessel 3 was spot blasted and the same technology self-polishing coating was applied again. Vessel 3 was used as control sample to evaluate results if same self-polishing coating was applied with spot blasting. According to dry-docking performance, average fuel oil consumption was 2.44 t/h in the reference period and 2.33 t/h in the evaluation period. Fuel consumption was decreased by 4.09%. However, speed was also reduced to 18.91 kn from 19.29 kn. Had the vessel kept speed at 19.29 kn, consumption would have been 2.53 t/h, i.e. increased by 3.57%. Speed loss was calculated as -8.80% for the reference period and -9.64% with the application of same coating which represents, i.e. decreased by 0.84%. The difference between average fuel consumptions and average speeds was statistically significant in the 95% confidence level. According to the In-Service Performance Indicator, the speed reduced to 18.19 kn from 18.91 kn, and fuel consumption to 2.27 t/h from 2.33 t/h.

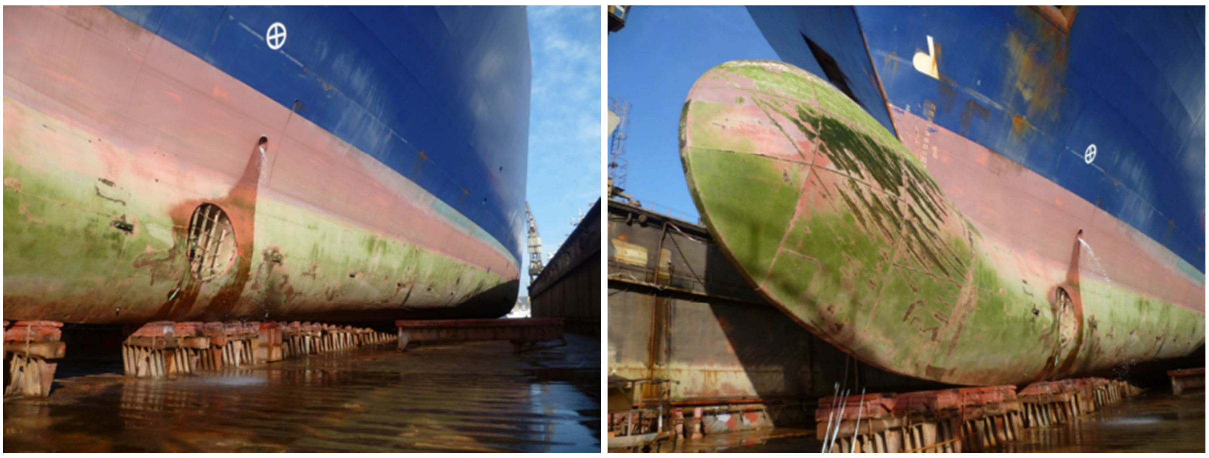

Fig.7: VESSEL 3, 2013 dry-dock, hull condition, just after entering dry-dock

By decreasing speed, vessel tried to keep fuel consumption under control which resulted in decreased schedule keeping due to increased sailing hours. Had the vessel kept speed as 18.91 kn, fuel consumption would have been 2.65 t/h, i.e. increased by 13.80%. Vessel 3 had been dry-docked every 2.5 years and her hull was not fully blasted at any dry-docking sequence since she was built. Results confirmed that if the vessel was not fully blasted and coated with same self-polishing technology as previously, hull performance decreases dramatically. Vessel 3 was dry-docked again in 2015. Hull and coating condition were checked visually. Hull and coating condition was very poor, Fig.8. The hull was fully blasted, an Advanced Fluoropolymer Silicone Foul Release coating applied. According to dry-docking performance, average fuel oil consumption was 2.26 t/h in the reference period and 2.30 t/h in the evaluation period, but speed also increased to 19.48 kn from 18.20 kn. Had the vessel kept speed as 18.20 kn, consumption would have been 1.75 t/h, i.e. reduced by 22.60%. Speed loss was -12.43% for the reference period and -6,64% in the evaluation period, i.e. improved by 5.79%. The difference between average fuel consumption in reference period (2.27 t/h) and in evaluation period (2.30 t/h) was statistically not significant in the 95% confidence level. But the speed difference (18.19 kn and 19.54 kn) was statistically significant in the 95% confidence level. According to the In-Service Performance Indicator, speed increased to 19.66 kn from 19.48 kn, fuel consumption to 2.36 t/h from 2.30 t/h. Had the vessel kept speed as 19.48 kn, fuel consumption would have been 2.27 t/h, i.e. decreased by 1.26%. Thus the results of Advanced Fluoropolymer Silicone Technology application test confirmed significant fuel savings.

Fig.8: VESSEL 3, 2015 dry-dock, hull condition, just after entering dry-dock

Vessel 4 was built in 2005. She was dry-docked in 2010 and again in 2013. Her hull and coating condition was very poor, Fig.9. The hull was fully blasted, a Biomimetic Super-Low Friction Technology Self Polishing Coating applied. Vessel 4 was a test vessel where self-polishing coating and foul release coating were applied with full blasting at consecutive dry-dockings in 2013 and 2015.

Fig.9: VESSEL 4, 2013 dry-dock, hull condition, just after entering dry-dock

According to dry-docking performance, average fuel oil consumption was 2.48 t/h in the reference period and 2.38 t/h in the evaluation period. Fuel consumption decreased by 4.03%, speed remained virtually the same (19.14 kn in the reference period and 19.16 kn in the evaluation period). The difference between average fuel consumptions was statistically significant in the 95% confidence level, the speed difference was not. According to the In-Service Performance Indicator, speed decreased to 18.84 kn from 19.16 kn, fuel consumption to 2.29 t/h from 2.38 t/h. By decreasing speed, vessel tried to keep fuel consumption under control which resulted in decreased schedule keeping. Had the vessel kept speed as 19.16 kn, fuel consumption would have been 2.46 t/h, i.e. increased by 2.98%. Vessel 4 was dry-docked again in 2015. Although her hull had been fully blasted in 2013, it was completely covered with fouling, Fig.10. The hull was fully blasted again and the Advanced Hydrogel Silicone Coating applied which had been used on Vessels 1 and 2. According to the dry-docking performance, average fuel oil consumption was 2.29 t/h in the reference period and 2.22 t/h in the evaluation period. Fuel consumption was decreased by 3.05%. Speed increased to 19.29 kn from 18.82 kn. Had the vessel kept speed as 18.82 kn, consumption would have been 2.01 t/h, i.e. decreased by 12.14%. Speed loss was -9.89% for the reference period and -6.96% for the evaluation period, i.e. improved by 2.93%. The difference between average fuel consumptions and average speeds were statistically significant in the 95% confidence level. In-service performance calculations were not performed as there were not enough samples.

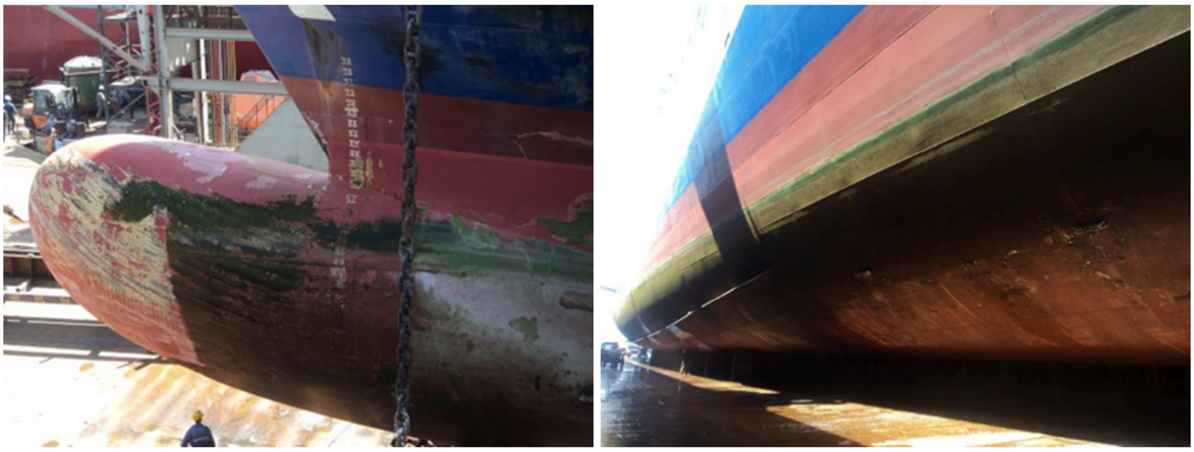

Fig.10: VESSEL 4, 2015 dry-dock, hull condition during high pressure wash

Vessel 5 was built in 2005. She was dry-docked in 2010 and again in 2013. Her hull and coating condition was poor, Fig.11. The flat bottom was fully blasted and vertical sides spot blasted. Then Hydrolyzing silyy methacrylate Copolymer Self-Polishing Coating was applied. According to the dry-docking performance, average fuel oil consumption was 2.42 t/h in the reference period and 2.28 t/h in the evaluation period. Fuel consumption decreased by 5.78%, but also speed to 19.18 kn from 19.44 kn. Had the vessel kept speed as 19.44 kn, consumption would have been 2.40 t/h, i.e. decreased by 0.75%. Speed loss was calculated as -8.27% for the reference period and -8.18% for the evaluation period. Despite fully blasting the flat bottom and using newer technology self-polishing coating, there was no significant improvement for fuel consumption or speed loss. According to the In-Service Performance Indicator, speed decreased to 18.80 kn from 19.18 kn and fuel consumption slightly increased to 2.33 t/h from 2.28 t/h. Had the vessel kept speed as 19.18 kn, fuel consumption would have been 2.52 t/h, i.e. increased by 10.70%. The speed loss was calculated as -8.18% for the reference period and -10.43% for the evaluation period, i.e. decreased by 2.25%. Vessel 5 was dry-docked again in 2015. The vertical sides were covered with heavy fouling, Fig.12, but the flat bottom area was better than the vertical sides. It is required to test this coating with a fully blasted hull in order to come to certain conclusions about its performance for high-speed Ro-Ro vessels. The hull was fully blasted and the Advanced Fluoropolymer Silicone Coating applied which had been applied to Vessel 3 before. According to the dry-docking performance, average fuel oil consumption was 2.31 t/h in the reference period and 2.35 t/h in the evaluation period. Fuel consumption increased by 1.73%, speed to 19.72 kn from 18.76 kn. Had the vessel kept speed as 18.76 kn, consumption would have been 1.92 t/h, i.e. decreased by 16.73%. Speed loss was -10.40% for the reference period and -

6.23% for the evaluation period, i.e. improved by 4.17%. The difference between average fuel consumption in the reference period (2.31 t/h) and in the evaluation period (2.35 t/h) was statistically not significant. The speed difference (18.76 kn and 19.92 kn) was statistically significant in the 95% confidence level. According to the In-Service Performance Indicator, speed decreased to 19.24 kn from 19.72 kn, while fuel consumption increased to 2.37 t/h from 2.35 t/h. Had the vessel kept speed as 19.72 kn, the fuel consumption would be 2.62 t/h, i.e. increased by 11.73%. The Advanced Fluoropolymer Silicone coating performed well during the first year after the dry-dock in 2015, but in-service performance was as not good as Vessel 3 which also had applied with same technology coating. The diver check carried out to understand why coating performance reduced dramatically after first year and why we could not observe similarly successful results as for Vessel 3. The hull was covered with slime. We think that there might have been an application problem for this vessel.

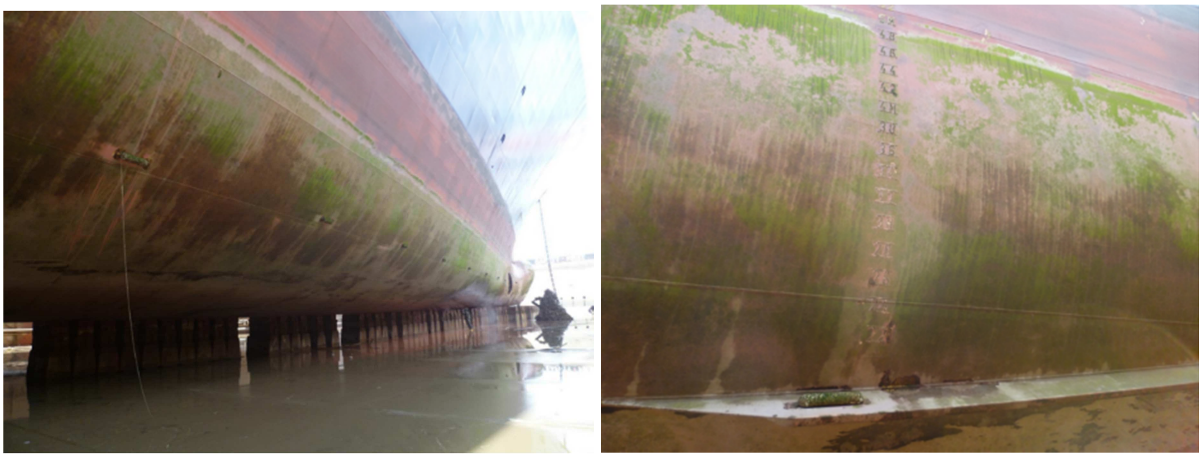

Fig.11: VESSEL 5, 2013 dry-dock, hull condition, just after entering dry-dock

Fig.12: VESSEL 5, 2015 dry-dock, hull condition before high-pressure water wash

Vessel 6 was built in 2006. She was dry-docked in 2010 and again in 2013. The hull was completely covered with heavy fouling, Fig.13. The hull was spot blasted and the same technology self-polishing coating applied again. This vessel was used as control sample like Vessel 3 to evaluate results if same self-polishing coating was applied with poor spot blasting. According to dry-docking performance, average fuel oil consumption was 2.39 t/h in the reference period and 2.31 t/h in the evaluation period. Fuel consumption was reduced by 3.34%, speed increased to 19.31 knot from 19.19 kn. Had the vessel kept speed as 19.19 kn, consumption would have been 2.25 t/h, i.e. decreased by 5.82%. Speed loss was calculated as -9.30% for the reference period and -7,97% in the evaluation period, i.e. improved by 1.33%. The difference between average fuel consumptions was statistically significant in the 95% confidence level, but nut the speed difference (19.19 kn and 19.31 kn). According to the In-Service Performance Indicator, speed decreased to 18.53 kn from 19.31 kn; fuel consumption remained same as 2.31 t/h. By decreasing speed, vessel tried to keep fuel consumption under control which resulted in decreased schedule keeping. Had the vessel kept speed as 19.31 kn, fuel consumption would have been 2.72 t/h, i.e. increased by 17.88%. Speed loss was -7.97% for the reference period and -11.67% for the evaluation period, i.e. a decrease by 3.70%. Applying the same self-polishing coating with spot blasting seems to work for maximum one year, sometimes less; hull performance becomes worst after the first year with dramatic speed loss. The observed heavily fouled hull explains why.

Fig.13: VESSEL 6, 2013 dry-dock, hull condition, just after entering dry-dock

Vessel 6 was dry-docked again in 2015. Her hull condition was poor. Hull was fully blasted and Advanced Hydrogel Silicone Foul Release coating applied. Also, the propellers of the vessel were changed with Alpha Kappel propellers to improve propeller efficiency. According to dry-docking performance, average fuel oil consumption was 2.34 t/h in the reference period and 2.33 t/h in the evaluation period; speed increased to 19.46 kn from 18.50 kn. Had vessel kept speed as 18.50 kn, consumption would have been 1.90 t/h, i.e. decreased by 18.85%. Speed loss was -12.16% for the reference period and -7,48% for the evaluation period, i.e. improved by 4.68%. There was no statistically significant difference for fuel consumption, but the speed difference (18.46 kn and 19.46 kn) was statistically significant in the 95% confidence level. In-service performance calculations could not be performed as there were not enough samples after the dry-docking in 2015.

Vessel 7 was another control sample where we tested applying the same self-polishing after spot blasting and different self-polishing coating applied with spot blasting again. The vessel was built in 2008 and had 2 dry-dockings until 2013 and only spot blasted at each dry-dockings. She was dry-docked in 2012. After applying spot blasting, conventional self-polishing hydrolyzing silyl acrylate coating was applied. Then she was dry-docked again in 2013, with spot blasting and same technology self-polishing coating applied again. Finally, she was dry-docked again in 2016. After spot blasting, different type of self-polishing coating, hydrolyzing antifouling based on Nano acrylate technology was applied. This vessel was not tested with any foul release technology since she was delivered from shipyard. When she was dry-docked in 2013, her hull was completely covered with fouling, especially the vertical sides, Fig.14. For the dry-docking performance of the dry-docking carried out in 2013, average fuel oil consumption was 2.26 t/h in the reference period and 2.19 t/h in the evaluation period. Fuel consumption decreased by 3.09%, speed to 19.25 kn from 19.37 kn. Had the vessel kept speed as 19.37 kn, consumption would have been 2.25 t/h, i.e. same as for the reference period. According to the In-Service Performance Indicator, speed decreased to 18.95 kn from 19.25 kn, fuel consumption increased to 2.37 t/h. Had the vessel kept speed as 19.25 kn, fuel consumption would have been 2.52 t/h, i.e. increased by 15.13%. Speed loss was -6.83% in the reference period and -9.94% in the evaluation period, i.e. decreased by 3.10%. Thus applying the same self-polishing coating with spot blasting causes increased speed loss and fuel consumption. Vessel 7 was dry-docked again in 2016. The hull was covered with heavy fouling, Fig.15. The hull was spot blasted, a different type of self-polishing coating, hydrolyzing antifouling based on Nano acrylate technology applied. According to dry-docking performance, the average fuel oil consumption was 2.50 t/h in the reference period and 2.36

t/h in the evaluation period. Fuel consumption was decreased by 5.6%, speed increased to 19.07 kn from 19.03 kn. Had the vessel kept speed as 19.03 kn, consumption would have been 2.34 t/h, i.e. decreased by 6.41%. Speed loss was -10.75% in the reference period and -9.35% in the evaluation period, i.e. increased by 1.40%. The difference between average fuel consumptions was statistically significant in the 95% confidence level, but the speed difference (19.03 kn and 19.07 kn) not. Thus, without full blasting, hull performance decreases each year and even newly coated hulls cannot perform well as previous coat layers increase the frictional resistance. In-service performance calculations could not be performed as there were not enough data after the dry-docking in 2016.

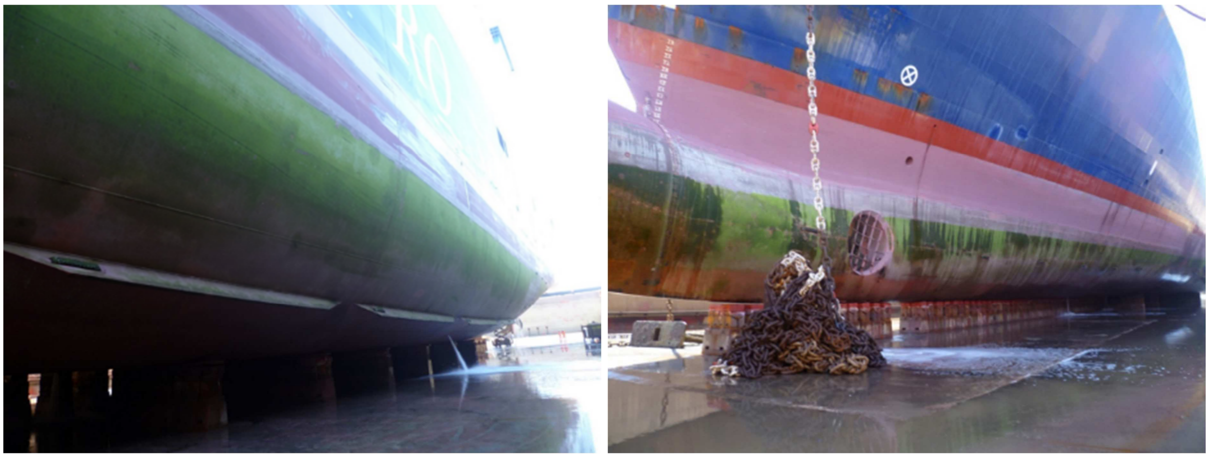

Fig.14: VESSEL 7, 2013 dry-dock, hull condition just after entering dry-dock

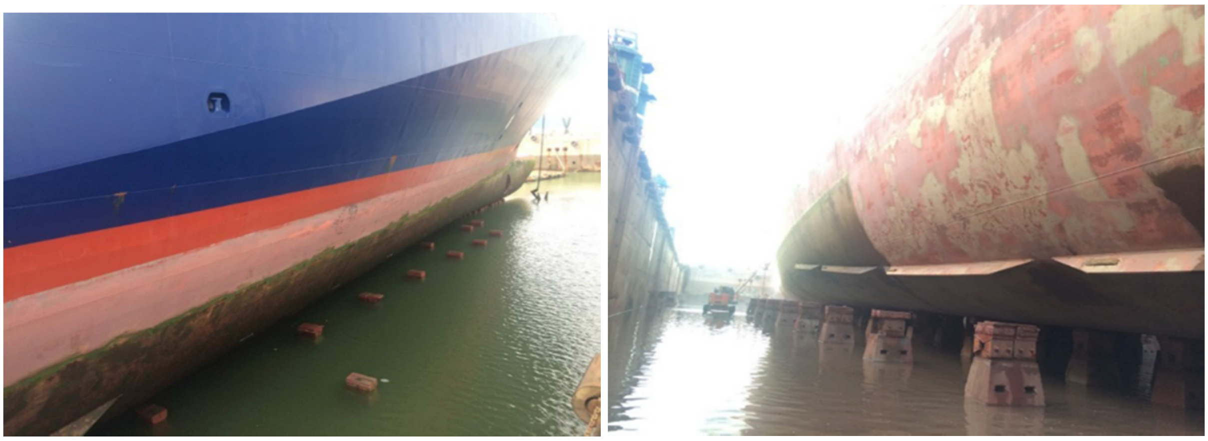

Fig.15: VESSEL 7, 2016 dry-dock, hull condition during high-pressure wash

Vessel 8 was built in 2008. She was dry-docked in 2011, a conventional self-polishing coating applied after a spot blasting like for the other sister vessels. Then she was dry-docked again in 2013, a different type of Self-polishing coating, Linear polishing polymer technology was applied after a spot blasting. According to dry-docking performance, average fuel oil consumption was 2.35 t/h in the reference period and 2.19 t/h in the evaluation period. Fuel consumption was decreased by 6.80%, speed decreased to 18.80 kn from 19.42 kn. Had the vessel kept speed as 19.42 kn, consumption would have been 2.50 t/h, i.e. increased by 6.38%. Speed loss was -7.38% for the reference period and -8.81% in the evaluation period, i.e. decreased by 1.42%. The difference between vessel's speed (19.42 kn and 18.80 kn) was statistically significant in the 95% confidence level. According to the In-Service Performance Indicator, speed was decreased to 18.66 kn from 18.80 kn, fuel consumption increased to 2.41 t/h. Had the vessel kept speed as 18.80 kn, fuel consumption would have been 2.48 t/h, i.e. increased by 13.13%. Speed loss was -8.81% for the reference period and -11.46% for the evaluation period, i.e. decreased by 2.65%. Thus the hull performance reduced dramatically. The vessel tried to keep her speed to keep the schedule accepting higher fuel consumption. As the hull performance decreased unexpectedly, a diver checked the hull finding heavy fouling, Fig.16. Vessel 8 was dry-docked again in 2016. The hull was completely covered with heavy fouling, Fig.17.

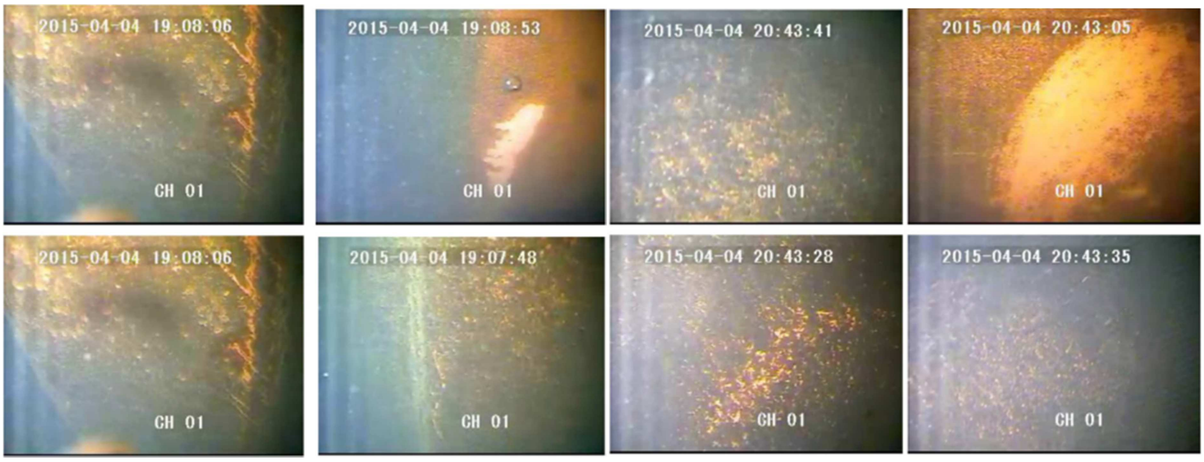

Fig.16: VESSEL 8, 2015 diver check, hull condition

Fig.17: VESSEL 8, 2016 dry-dock, hull condition just after entering the dry-dock

The hull was fully blasted, then an advanced hydrogel silicone technology was applied. Also the propeller was changed to SCHOTTEL CLT Blades to improve propeller efficiency. According to dry-docking performance, average fuel oil consumption was 2.44 t/h in the reference period and 2.21 t/h in the evaluation period. Speed increased to 19.14 kn from 18.67 kn. Had the vessel kept speed as 18.67 kn, consumption would have been 2.00 t/h, i.e. decreased by 17.82%. Speed loss was -11.72% for the reference period and -7.39% for the evaluation period, i.e. improved by 4.33%. The difference between average fuel consumption of reference period and evaluation period was statistically significant in the 95% confidence level. So was the difference in average speed. In-service performance calculations could not be performed as there were not enough data after the dry-docking in 2015.

Four vessels were used as control samples to evaluate what would be result if self-polishing coatings were applied to the spot blasted hull as in previous dry-dockings. Results of these vessels indicated that, if hull spot blasted and self-polishing coating applied, hull performance decreases even after the first year, Table VI. Fuel consumption increases dramatically and speed decreases. Therefore, full blasting is very critical for maintaining hull performance and avoiding increased fuel consumption. Vessel 4 was a control sample to evaluate full blasting applied to hull together with self-polishing coating. Results indicated that fuel consumption reduces for the 1st year, then increases until next dry-docking, but very limited compared to spot blasted vessels. Table VII shows results for Vessel 4. When we compare in service performance results of self-polished + spot blasted vessels and self-polished + full blasted vessels, the full blasted vessel's hull performance was better. Although Vessel 4 was completely covered with fouling, Fig.10, due to full blasting applied before self-polishing application, frictional resistance of surface was better than for spot blasted vessels. It is required to analyze results of more samples which are full blasted and different self-polishing coating technologies applied in order to have better evaluation.

Table VI: Performance of Self polishing coated and spot blasted vessels

SELF POLISHING COATING + SPOT BLASTING APPLIED VESSELS' PERFORMANCE				
	Dry-docking Performance		In-service Performance	
	Speed Loss %	*Fuel Consumption mt/hr*	*Speed Loss %*	*Fuel Consumption mt/hr*
VESSEL 3	-0,84%	3,57%	-2,87%	13,80%
VESSEL 6	1,33%	-5,82%	-3,70%	17,88%
VESSEL 7	0,12%	-0,54%	-3,10%	15,13%
VESSEL 8	-1,43%	6,38%	-2,65%	13,13%
VESSEL 7	1,40%	-6,41%		
Average	0,12%	-0,56%	-3,08%	14,99%

Table VII: Performance of Self polishing coated and full blasted vessel

SELF POLISHING COATING + FULL BLASTING APPLIED VESSELS' PERFORMANCE				
	Dry-docking Performance		In-service Performance	
	Speed Loss %	*Fuel Consumption mt/hr*	*Speed Loss %*	*Fuel Consumption mt/hr*
VESSEL 4	0,93%	-4,16%	-0,71%	2,98%

Two different technologies of foul release coatings were tested on 7 vessels. Results indicated that foul release coatings performed well. Fuel consumption of all vessels was reduced by ~17% in average regarding dry-docking performance results. Ships' speeds increased up to 4%. After the first year, fuel consumptions slightly increased together with a limited speed loss. Photos of Vessels 1 and 2, made during their docking cycle and dry-docked again in 2016 and 2017, confirm foul release coatings performed better than self-polishing coatings. There were not enough data to analyze in-service performance of Vessels 4, 6 and 8. Also, 5 of 7 vessels did not complete their docking cycle with foul release coating. It will be possible to evaluate results of completed docking cycles when all test vessels will be dry-docked again in 2018. Table VIII presents results of foul release coated vessels.

Table VIII: Performance of Foul Release coated vessels

FOUL RELEASE SILICONE COATING APPLIED VESSELS' PERFORMANCE				
	Dry-docking Performance		In-service Performance	
	Speed Loss %	*Fuel Consumption mt/hr*	*Speed Loss %*	*Fuel Consumption mt/hr*
VESSEL 1	2,67%	-11,27%	-1,77%	8,06%
VESSEL 2	4,48%	-18,14%	-0,82%	3,60%
VESSEL 3	5,79%	-22,60%	0,28%	-1,26%
VESSEL 4	2,93%	-12,07%		
VESSEL 5	4,17%	-16,73%	-2,55%	11,73%
VESSEL 6	4,68%	-18,85%		
VESSEL 8	4,33%	-17,82%		
Average	4,15%	-16,78%	-1,21%	5,53%

Table IX compares self-polishing and foul release coated vessel's dry-docking performances. Dry-docking performance results confirms that foul release coatings have positive effect on ship's speed and fuel saving.

Regarding In-service performance, foul release coated vessels performed better than self-polishing coated vessels in terms of speed loss and fuel consumption. Vessel 4 was the only sample where full blasting + self-polishing and full blasting + foul release coating applied in order to analyze effect of full blasting and coatings on the same ship. But there were not sufficient data to analyze in-service performance of foul release coating on this ship. Table X compares data of both coatings.

Table IX: Dry-docking performance comparison of self-polishing and foul release coatings

	Dry-Docking Performance Comparison			
	Speed Loss %		**Fuel Consumption mt/hr**	
	SELF POLISHING	***FOUL RELEASE***	***SELF POLISHING***	***FOUL RELEASE***
VESSEL 1		2,67%		-11,27%
VESSEL 2		4,48%		-18,14%
VESSEL 3	-0,84%	5,79%	3,57%	-22,60%
VESSEL 4	0,93%	2,93%	-4,16%	-12,07%
VESSEL 5	0,10%	4,17%	-0,75%	-16,73%
VESSEL 6	1,33%	4,68%	-5,82%	-18,85%
VESSEL 7	0,12%		-0,54%	
VESSEL 7	1,40%		-6,41%	
VESSEL 8	-1,43%	4,33%	6,38%	-17,82%
Average	0,23%	4,15%	-1,10%	-16,78%

Table X: In-service performance comparison of self-polishing and foul release coatings

	In-Service Performance Comparison			
	Speed Loss %		**Fuel Consumption mt/hr**	
	SELF POLISHING	***FOUL RELEASE***	***SELF POLISHING***	***FOUL RELEASE***
VESSEL 1		-1,77%		8,06%
VESSEL 2		-0,82%		3,60%
VESSEL 3	-2,87%	0,28%	13,80%	-1,26%
VESSEL 4	-0,71%		2,98%	
VESSEL 5	-2,25%	-2,55%	10,70%	11,73%
VESSEL 6	-3,70%		17,88%	
VESSEL 7	-3,10%		15,13%	
VESSEL 8	-2,65%		13,13%	
Average	-2,55%	-1,22%	12,27%	5,53%

For a better evaluation, we would need to standardize results of all vessels to the same speed level. Dry-docking and In-service performance results of self-polishing and foul release coated vessels were corrected and standardized to 18.74 kn which was average speed of foul release coated vessels before foul release application. Figy.18 and 19 present standardized results. Blue lines indicate required fuel consumption per hour (t/h) to create 18.74 kn speed in reference periods, red lines in evaluation periods. Fig.18 (left) proves that foul release coated vessels can make same speed 18.74 kn with 17% lower fuel consumption than before. Corrected and standardized results of in-service performance results confirmed that fuel consumptions can increase up to 14% in average during in-service period except Vessel 4 which was full blasted.

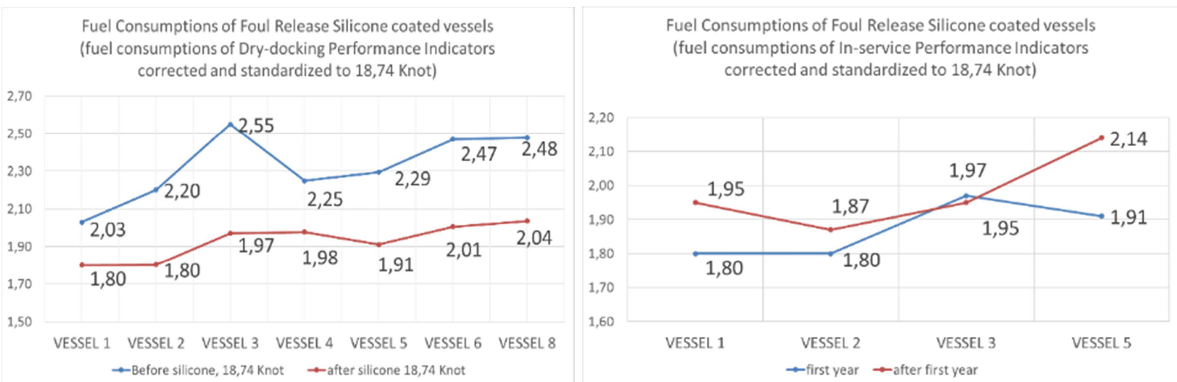

Fig.18: Corrected fuel consumptions of foul release coated vessels

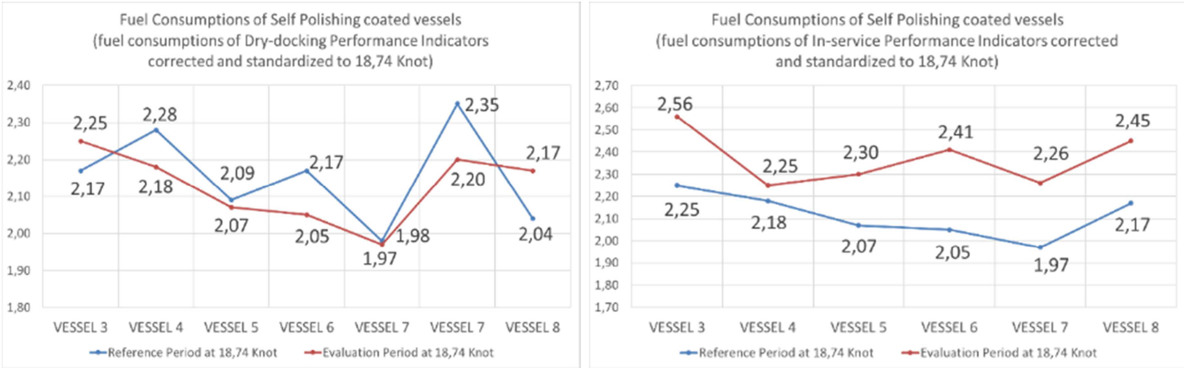

Fig.19: Corrected fuel consumptions of self-polishing coated vessels

In summary, key results were:

- Foul release silicone technologies performed better than self-polishing coatings for high-speed Ro-Ro vessels.
- Only one vessel was fully blasted and tested with Self-Polishing coating. More studies are needed to separate the effect of full blasting and coating, also for better comparison of self-polishing and foul release coatings.
- Advanced Hydrogel Silicone technology performed well on all tested vessels.
- Advanced Fluoropolymer Silicone technology performed well for both test vessels regarding dry-docking performance results. But for in-service performance, it performed well only on one vessel and not on the other.
- Full blasting is very critical and important for hull performance. If a ship's hull is only spot blasted, even if it is completely coated with self-polishing coating, the hull performance decreases dramatically. Most ship operators prefer spot blasting instead of full blasting for economic reasons. However, this approach increases fuel cost and reduces operational efficiency.
- Self-polishing coatings perform well for max 1 year for high-speed Ro-Ro vessels unless it is applied together with full blasting which increases this beneficial period. All self-polishing coated vessels arrived to next dry-dock with a fouled hull.
- Hull performance of foul release coated vessels also reduces during in-service period but reduction seems not dramatic like self-polishing coatings.
- Hull fouling occurs for the foul release coated vessels but not worse than self-polishing coated vessels. Photos taken just after entering the dry-dock confirms foul release coated vessels' hull were in good condition.

This study was about results of different hull coating applications to high-speed Ro-Ro vessels under different conditions. Result of same coating technologies may differ on different ship types and different operational conditions.

With the implementation of ISO 19030, we expect that more studies will be carried out to evaluate hull performance changes with field data. Uncertainty of field data will be always high unless they carried out according to ISO 19030 Part 2 which requires complete performance monitoring and logging system. Most vessels do not have performance monitoring and logging system. Therefore, real-life studies will be helpful for ship owners, paint producers, academia and other interested parties.

ISO 19030 declared four performance indicators as dry-docking performance, in-service performance, maintenance effect and maintenance trigger. However, in order to evaluate effect of coating, the standard could be strengthened with new indicators to evaluate performance of coating directly with comparing results of same periods after last dry-dock and recent dry-docks. For example, first year after previous dry-dock and first year after last dry-dock could be compared. This kind of comparison will result in better information regarding efficiency of coating under different conditions.

Also, the standard could be strengthened with adding a new method to Part 3 for liner vessels. Part 3 requires daily collected data to analyze. It would be more practical for liner vessels to compare results of each voyage or each leg if the vessel is trading on the same line for a period which covers required analysis duration.

References

CORBETT, J.J.; WINEBRAKE, J.J.; GREEN, E.; CORNER, B. (2010), *Energy and GHG Emissions Savings Analysis of Fluoropolymer Foul Release Hull Coating*, Energy and Environmental Research Associates

DEMIREL, Y.K.; KHORASANCHI, M.; TURAN, O.; INCECIK, A. (2013), *On the importance of antifouling coatings regarding ship resistance and powering*, Low Carbon Shipping Conf., pp.1-13

ISO (2016), *IS0 19030 Ships and Maritime Technology – Measurement of Changes in Hull and Propeller Performance*, Int. Organization for Standardization

LEJARS, M.; MARGAILLAN, A.; BRESSY, C. (2012) *Fouling release coatings: A nontoxic alternative to biocidal antifouling coatings*, Chemical Reviews, pp.4347-4390

MENG, Q.; DU, Y.Q.; WANG, Y., (2015), *Shipping log data based container ship fuel efficiency modeling*, Transportation Research Part B, pp.207-229

SØYLAND, S.; OFTEDAHL, G.A. (2016), *ISO 19030 – Motivation, scope and development*, 1st HullPIC Conf., Pavone, pp.292-297

Measurement of Speed Through Water

Eric Giesberg, NSWC-CD, Bethesda/USA, Eric.Giesberg@navy.mil

"This brief is provided for information only and does not constitute a commitment on behalf of the U.S. government to provide additional information on the program and/or sale of the equipment or system."

Abstract

The relevant issue with monitoring and measuring ship performance is the measurement of speed through water. In 2016 an Acoustic Doppler Current Profiler (ADCP) was mounted on a US Navy ship for the purposes of a hull monitoring program. At the onset of the program a baseline trial was completed to both determine the clean hull performance of the ship and the performance of the ADCP on a surface ship. The trial included completing reciprocals using standard calculations and 'triangles' using more advanced calculations to calculate speed through water. The results from the ADCP (Acoustic Doppler Current Profiler), maneuvers, ElectroMagnetic Log (EMLog), and surface based HFRadar (High Frequency Radar) corrections are compared in this report and examined for agreement and repeatability. The ADCP performed successfully showing strong agreement and repeatability though strong concerns still exist for long term viability. The EMLog was found to have issues beyond calibration offsets. The surface based HFRadar appears to be a passable correction method that may be of more benefit for measurement of ship maneuvers. The new method for analyzing GPS/INS (Global Positioning System/Inertial Navigation System) speed over the ground data presented in this report is shown to have good agreement with the ADCP with the added advantage over the classic calculation by generating an associated uncertainty with the speed.

1. Introduction

For comparison of ship performance, isolation of the ship's performance from its environment is critical. Once all the environmental factors are removed the ship's speed through water can be determined. There are three primary environmental factors that create drift: current, wind, and waves. Current, unlike the other two forces is a radially symmetric force when applied to the ship. The effect of wind and waves can be mitigated by only testing during 'calm' wind conditions (which are based on ship size). The effects can also be subtracted based on modeling using measured instruments. The wind and wave effects are outside the scope of this paper.

This paper compares various methods of measuring ship speed through water. Included is the most commonly accepted method based on reciprocal runs, Fig.1, to estimate the speed through water. A new method for calculating speed is also introduced in the paper that allows for calculation of speed uncertainty and allows non-reciprocal passes (reducing the time to execute) from purely GPS/ INS (Global Positioning System/Inertial Navigation System) data.

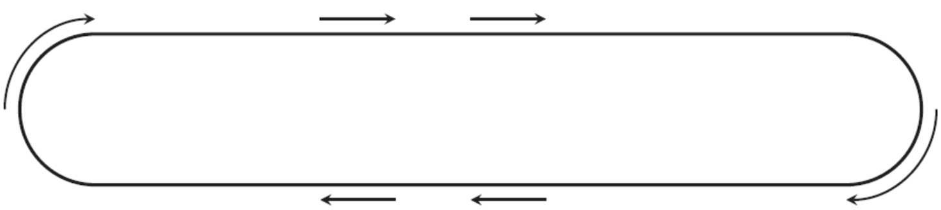

Fig.1: Typical racetrack maneuver used when estimating speed through water

2. Basic Theory and Nomenclature

Once the ship is at a fixed condition (i.e. constant power, pitch, rpm, etc.) without maneuvering the ship's speed through water should be constant. The ship's speed through water can be defined by two vectors:

- V_F – Forward velocity of the ship through the water
- V_L – Lateral velocity of the ship through the water

The drift due to current can be defined as such:

- D_Y – Drift in northings direction
- D_X – Drift in eastings direction

Though labeled here as single variables, drift is a function that varies continually across space *(x, y)* and time *(t).*

$$D_Y = f(t, x, y)$$
$$D_X = f(t, x, y) \tag{1}$$

The heading θ can be used to transfer the current vectors into the ship's reference frame

$$D_F = D_Y \sin\theta - D_X \cos\theta$$
$$D_L = D_X \cos\theta + D_Y \sin\theta \tag{2}$$

When added to the ship's speed through water the ship's speed over ground is given.

$$V'_F = V_F + D_F$$
$$V'_L = V_L + D_L \tag{3}$$

Commonly, of the above variables only the heading (θ) and the speed over ground (V'_F and V'_L) can be measured on a ship via INS and GPS.

3. Speed Through Water

Recently a ship was operated off the coast of San Diego equipped with various instruments for measuring the speed through water. These in combination with methods for deriving speed through water allowed for multiple points of comparison.

3.1. EM Log

An AN/WSN-8A Digital Electro-Magnetic Log (DEML) is currently installed and is the standard sensor for measuring speed through water on the ship when underway. The EM Log works by inducing a voltage in the water thus creating an electromagnetic field from coils at the bottom of the sensor, the voltage is then measured and is correlated to the speed of the water flow past the sensor.

3.2. ADCP

A Teledyne Workhorse Acoustic Doppler Current Profiler (ADCP), operating at 1200 kHz was mounted in the forward third of the ship adjacent to the EM Log. The ADCP works by transmitting a sound at a fixed frequency and measuring the frequency of the echoes due to backscatter. The Doppler shift in frequency can be used to measure the speed of the water in the component parallel to the beam. Using three sensors will give the speed in three directions, a fourth is used to supply the error velocity and measure agreement between the sensors, *NN (2011).*

3.3. New Comprehensive Calculation

When only using GPS (an SBG Ekinox during this trial) varying courses at constant conditions can be used to generate the data necessary to solve the above equations to solve for V_F and V_L. The data is recorded as discrete time series and the problem becomes determining the values of the speed through water V_F, V_L and drift (D_Y, D_X) that minimize the following equation:

$$\sum_{t=0}^{n} (V'_F - V_F - D_F)^2 + (V'_L - V_L - D_L)^2 \tag{4}$$

Where the speed over ground and heading is a time varying function and the drifts are both time and spatially varying. The currents are assumed to be only varying with time and a polynomial function can be used such as Eq.(5) for a constant current or Eq.(6) for a current varying linearly with time (t). (a,b,c,d are arbirtrary constants)

$$\begin{aligned} D_Y &= c \\ D_X &= d \end{aligned} \tag{5}$$

$$\begin{aligned} D_Y &= at + c \\ D_X &= bt + d \end{aligned} \tag{6}$$

For example, if Eq.(6) is substituted into Eq.(2), Eq.(4) becomes:

$$\sum_{t=0}^{n} \begin{matrix} (V'_F - V_F - (at + c)\sin\theta + (bt + d)\cos\ \theta)^2 + \\ (V'_L - V_L - (at + c)\cos\theta - (bt + d)\sin\theta\ )^2 \end{matrix} \tag{7}$$

When used with a recorded time series that might contain 3 passes of 5 minutes at a 10 Hz data rate, 9000 points may be generated. The minimization problem may be solved if polynomial functions are used employing linear algebra, computational minimization algorithms are often faster. An example of the analysis is given in Section 7.1. The equation also implies the possibility of non-reciprocal passes, such as doing triangles and maneuvers that allow testing of speed while still making positive headway to the next port. A few triangular maneuvers were completed and are discussed in the repeatability section.

To calculate the error associated with this method a 'stationary bootstrap', *Romano and Politis (1994)*, a type of block bootstrap that reduces issues with block size selection (though the average block size chosen is ~30 s), can be used. This bootstrapping in conjunction with the addition of random sampling from instrument uncertainty (correlated) will generate new data sets that can then be fit by the original method. The calculated forward velocities will create a distribution of points that can then be used to determine the uncertainties associated with the point.

3.4. Simplified

With the following assumptions, the above method can be simplified:

- Each pass can be described by a single velocity forward
- Each pass is perfectly reciprocal (180◦) to the previous pass
- The time between and the duration of each pass is the same

The derivation is given in Section 7.2. After derivation determining the velocity for two passes and a constant current is:

$$V = \frac{V_1 + V_2}{2} \tag{8}$$

and three passes and a changing current is:

$$V = \frac{V_1 + 2V_2 + V_3}{4} \tag{9}$$

This is the current standard practice for analysis of ship speed through water.

3.5. HFRadar

High frequency (HF) radar systems measure the speed and direction of ocean surface currents in near real time from the shore [3]. The HFRadar operates by sending radio waves and then measure the speed of the waves that bounce back. By changing the frequency of transmission, the length of the ocean wave that reflects the transmission back changes, a simple calculation estimates the speed of the wave in zero current. The current speed can be measured by removing the wave speed from the speed of the returned transmission. Combining two HFRadar sites will supply vectors in two directions. When used in conjunction with the ship's measured speed over ground from GPS/INS, it allows for calculation of the ship's speed over water.

4. Agreement of Methods

Validating all methods is difficult because no absolute truth exists to the measurements. The best that can be done is a direct comparison of each method and assume that the greater the overall agreement the better the method. Various methods given below are used to compare measurements taken during the trial.

- Average Bias - Magnitude of the average differences between each measurement
- Average Absolute Bias - Average of the absolute differences between each measurement
- Limits of Agreement - The 95% confidence interval of the differences between the two measurements, *Chambers (1983)*
- Maximum Bias - The maximum difference between each measurement over the course of the trial
- Scaled Pearson Correlation Coefficient
- Correlation of the two methods, discounts any bias effects
- Average Unaccounted Difference - Average of the differences not accounted for by overlap of the 95% uncertainty intervals
- Maximum Unaccounted Difference - The maximum difference between each measurement that can't be accounted for by the 95% uncertainty intervals

Table I to VII are colorized to help give a visual representation of the agreement where red indicates higher disagreement and green greater agreement. The values are given in knots except for the correlation coefficient where the range is from 0 to 1. Each cell is a comparison between the two methods. In Tables I through IV the bias errors associated with each method are compared. The first cell of the ADCP shows large errors which can be attributed to the fact the cell is measuring within the boundary layer of the ship. The EMLog has the largest errors overall (Table III) though which may indicate the lack of accuracy of the device. The simplified, comprehensive, and HFRadar methods give similar results while the HFRadar tends to have the greatest outliers when compared to the ADCP measurements out of all the three GPS methods.

Table V shows that the errors associated with the EMLog cannot be attributed purely to linear calibration errors as a Pearson Correlation Coefficient of 1 would indicate perfect linearity between the measurements.

Tables VI and VII show the accuracy or 'honesty' of the uncertainty measurements calculated from the instrument. All measurements except for the EMLog on average have a less than 0.08 kn of unaccounted difference. The HFRadar shows the maximum unaccounted for errors out of all the methods.

Table I: Average bias

	ADCP Cell 1	ADCP Cell 2	ADCP Cell 3	ADCP Cell 4	ADCP Cell 5	ADCP Cell 6	EMLog	Simplified	Comprehensive	HFRadar
ADCP Cell 1	0.000	0.293	0.296	0.276	0.249	0.237	0.100	0.172	0.149	0.150
ADCP Cell 2	0.293	0.000	0.003	0.017	0.044	0.056	0.393	0.103	0.107	0.121
ADCP Cell 3	0.296	0.003	0.000	0.021	0.047	0.059	0.396	0.117	0.114	0.122
ADCP Cell 4	0.276	0.017	0.021	0.000	0.027	0.039	0.376	0.104	0.093	0.100
ADCP Cell 5	0.249	0.044	0.047	0.027	0.000	0.012	0.349	0.083	0.066	0.071
ADCP Cell 6	0.237	0.056	0.059	0.039	0.012	0.000	0.337	0.075	0.052	0.058
EMLog	0.100	0.393	0.396	0.376	0.349	0.337	0.000	0.312	0.292	0.256
Simplified	0.172	0.103	0.117	0.104	0.083	0.075	0.312	0.000	0.026	0.013
Comprehensive	0.149	0.107	0.114	0.093	0.066	0.052	0.292	0.026	0.000	0.008
HFRadar	0.150	0.121	0.122	0.100	0.071	0.058	0.256	0.013	0.008	0.000

Table II: Average absolute bias

	ADCP Cell 1	ADCP Cell 2	ADCP Cell 3	ADCP Cell 4	ADCP Cell 5	ADCP Cell 6	EMLog	Simplified	Comprehensive	HFRadar
ADCP Cell 1	0.000	0.293	0.298	0.280	0.257	0.249	0.150	0.191	0.160	0.191
ADCP Cell 2	0.293	0.000	0.032	0.052	0.088	0.108	0.393	0.154	0.138	0.152
ADCP Cell 3	0.298	0.032	0.000	0.027	0.063	0.085	0.396	0.151	0.134	0.148
ADCP Cell 4	0.280	0.052	0.027	0.000	0.037	0.059	0.376	0.135	0.111	0.133
ADCP Cell 5	0.257	0.088	0.063	0.037	0.000	0.023	0.353	0.105	0.079	0.112
ADCP Cell 6	0.249	0.108	0.085	0.059	0.023	0.000	0.345	0.093	0.066	0.106
EMLog	0.150	0.393	0.396	0.376	0.353	0.345	0.000	0.312	0.292	0.273
Simplified	0.191	0.154	0.151	0.135	0.105	0.093	0.312	0.000	0.026	0.014
Comprehensive	0.160	0.138	0.134	0.111	0.079	0.066	0.292	0.026	0.000	0.026
HFRadar	0.191	0.152	0.148	0.133	0.112	0.106	0.273	0.014	0.026	0.000

Table III: Maximum bias

	ADCP Cell 1	ADCP Cell 2	ADCP Cell 3	ADCP Cell 4	ADCP Cell 5	ADCP Cell 6	EMLog	Simplified	Comprehensive	HFRadar
ADCP Cell 1	0.000	1.412	1.539	1.547	1.562	1.598	0.633	0.887	0.900	1.664
ADCP Cell 2	1.412	0.000	0.160	0.185	0.287	0.336	0.789	0.307	0.319	0.631
ADCP Cell 3	1.539	0.160	0.000	0.085	0.186	0.234	0.907	0.271	0.242	0.531
ADCP Cell 4	1.547	0.185	0.085	0.000	0.108	0.157	0.914	0.241	0.222	0.471
ADCP Cell 5	1.562	0.287	0.186	0.108	0.000	0.065	0.996	0.185	0.191	0.507
ADCP Cell 6	1.598	0.336	0.234	0.157	0.065	0.000	1.038	0.162	0.157	0.571
EMLog	0.633	0.789	0.907	0.914	0.996	1.038	0.000	1.070	1.082	1.032
Simplified	0.887	0.307	0.271	0.241	0.185	0.162	1.070	0.000	0.054	0.030
Comprehensive	0.900	0.319	0.242	0.222	0.191	0.157	1.082	0.054	0.000	0.092
HFRadar	1.664	0.631	0.531	0.471	0.507	0.571	1.032	0.030	0.092	0.000

Table IV: Limits of agreement

	ADCP Cell 1	ADCP Cell 2	ADCP Cell 3	ADCP Cell 4	ADCP Cell 5	ADCP Cell 6	EMLog	Simplified	Comprehensive	HFRadar
ADCP Cell 1	0.000	0.404	0.454	0.470	0.504	0.529	0.297	0.519	0.389	0.542
ADCP Cell 2	0.404	0.000	0.090	0.132	0.197	0.239	0.315	0.353	0.260	0.315
ADCP Cell 3	0.454	0.090	0.000	0.051	0.120	0.164	0.372	0.278	0.206	0.282
ADCP Cell 4	0.470	0.132	0.051	0.000	0.074	0.121	0.395	0.247	0.183	0.273
ADCP Cell 5	0.504	0.197	0.120	0.074	0.000	0.052	0.438	0.183	0.140	0.264
ADCP Cell 6	0.529	0.239	0.164	0.121	0.052	0.000	0.467	0.161	0.123	0.276
EMLog	0.297	0.315	0.372	0.395	0.438	0.467	0.000	0.572	0.427	0.411
Simplified	0.519	0.353	0.278	0.247	0.183	0.161	0.572	0.000	0.028	0.024
Comprehensive	0.389	0.260	0.206	0.183	0.140	0.123	0.427	0.028	0.000	0.070
HFRadar	0.542	0.315	0.282	0.273	0.264	0.276	0.411	0.024	0.070	0.000

Table V: Scaled Pearson correlation coefficient

	ADCP Cell 1	ADCP Cell 2	ADCP Cell 3	ADCP Cell 4	ADCP Cell 5	ADCP Cell 6	EMLog	Simplified	Comprehensive	HFRadar
ADCP Cell 1	1.000	0.968	0.954	0.948	0.937	0.928	0.965	0.931	0.944	0.870
ADCP Cell 2	0.968	1.000	0.997	0.993	0.985	0.978	0.983	0.955	0.962	0.951
ADCP Cell 3	0.954	0.997	1.000	0.999	0.994	0.990	0.971	0.972	0.976	0.960
ADCP Cell 4	0.948	0.993	0.999	1.000	0.998	0.994	0.964	0.978	0.981	0.963
ADCP Cell 5	0.937	0.985	0.994	0.998	1.000	0.999	0.951	0.988	0.989	0.965
ADCP Cell 6	0.928	0.978	0.990	0.994	0.999	1.000	0.941	0.991	0.991	0.961
EMLog	0.965	0.983	0.971	0.964	0.951	0.941	1.000	0.918	0.934	0.922
Simplified	0.931	0.955	0.972	0.978	0.988	0.991	0.918	1.000	1.000	1.000
Comprehensive	0.944	0.962	0.976	0.981	0.989	0.991	0.934	1.000	1.000	0.994
HFRadar	0.870	0.951	0.960	0.963	0.965	0.961	0.922	1.000	0.994	1.000

Table VI: Average unaccounted difference

	ADCP Cell 1	ADCP Cell 2	ADCP Cell 3	ADCP Cell 4	ADCP Cell 5	ADCP Cell 6	EMLog	Simplified	Comprehensive	HFRadar
ADCP Cell 1	0.000	0.164	0.185	0.173	0.158	0.099	0.004		0.091	0.072
ADCP Cell 2	0.164	0.000	0.003	0.009	0.033	0.035	0.178		0.076	0.057
ADCP Cell 3	0.185	0.003	0.000	0.001	0.019	0.026	0.193		0.070	0.049
ADCP Cell 4	0.173	0.009	0.001	0.000	0.003	0.011	0.181		0.050	0.042
ADCP Cell 5	0.158	0.033	0.019	0.003	0.000	0.000	0.166		0.030	0.031
ADCP Cell 6	0.099	0.035	0.026	0.011	0.000	0.000	0.112		0.016	0.030
EMLog	0.004	0.178	0.193	0.181	0.166	0.112	0.000		0.117	0.072
Simplified										
Comprehensive	0.091	0.076	0.070	0.050	0.030	0.016	0.117		0.000	0.000
HFRadar	0.072	0.057	0.049	0.042	0.031	0.030	0.072		0.000	0.000

Table VII: Maximum unaccounted difference

	ADCP Cell 1	ADCP Cell 2	ADCP Cell 3	ADCP Cell 4	ADCP Cell 5	ADCP Cell 6	EMLog	Simplified	Comprehensive	HFRadar
ADCP Cell 1		0.534	0.6584	0.6743	0.7868	0.4579	0.0769		0.7574	0.7263
ADCP Cell 2	0.534		0.0643	0.1014	0.1927	0.2408	0.4323		0.2254	0.4732
ADCP Cell 3	0.6584	0.0643		0.0334	0.1194	0.1739	0.5592		0.1784	0.4053
ADCP Cell 4	0.6743	0.1014	0.0334		0.0352	0.0897	0.5751		0.1583	0.3505
ADCP Cell 5	0.7868	0.1927	0.1194	0.0352		0.0219	0.6876		0.1242	0.3894
ADCP Cell 6	0.4579	0.2408	0.1739	0.0897	0.0219		0.5143		0.0862	0.4524
EMLog	0.0769	0.4323	0.5592	0.5751	0.6876	0.5143			0.7279	0.6246
Simplified										
Comprehensive	0.7574	0.2254	0.1784	0.1583	0.1242	0.0862	0.7279			0
HFRadar	0.7263	0.4732	0.4053	0.3505	0.3894	0.4524	0.6246		0	

5. Repeatability

Tables VIII to XI show the repeatability of the measurements during a few runs.

Table VIII: 15 knot racetrack three-pass

Run	Hdg	Wind	Dir	Usage					
A	-1.2	4.83	-30.2	•			•		•
B	178.4	3.97	-85.1		•		•	•	•
C	-1.2	4.88	-43.8			•		•	•
Instrument				**Measured Speed (kts)**					
Simplified							15.15	15.12	15.14
EMLog				14.75 ±0.15	14.64 ±0.15	14.80 ±0.15	14.69 ±0.15	14.71 ±0.15	14.72 ±0.15
Comprehensive							15.17 ±0.02	15.14 ±0.02	15.16 ±0.02
HFRadar				15.15 ±0.10	15.13 ±0.10	15.16 ±0.10	15.14 ±0.10	15.15 ±0.10	15.15 ±0.10
ADCP Depth Cell 1				14.89 ±0.03	14.85 ±0.03	14.95 ±0.03	14.87 ±0.02	14.90 ±0.02	14.89 ±0.02
ADCP Depth Cell 2				15.18 ±0.02	15.12 ±0.02	15.21 ±0.02	15.15 ±0.02	15.17 ±0.02	15.17 ±0.01
ADCP Depth Cell 3				15.22 ±0.02	15.18 ±0.02	15.23 ±0.02	15.20 ±0.01	15.20 ±0.02	15.21 ±0.01
ADCP Depth Cell 4				15.22 ±0.02	15.19 ±0.03	15.22 ±0.02	15.20 ±0.02	15.20 ±0.02	15.21 ±0.02
ADCP Depth Cell 5				15.21 ±0.03	15.19 ±0.03	15.22 ±0.03	15.20 ±0.02	15.20 ±0.02	15.20 ±0.02
ADCP Depth Cell 6				15.20 ±0.03	15.18 ±0.04	15.21 ±0.04	15.19 ±0.03	15.19 ±0.03	15.20 ±0.03

Table IX: 20 knot racetrack three-pass

Run	Hdg	Wind	Dir	Usage					
A	177.8	4.95	-86.2	•			•		•
B	-2.2	7.20	-49.3		•		•	•	•
C	179.3	6.09	-92.9			•		•	•
Instrument				Measured Speed (kts)					
Simplified							20.51	20.52	20.51
EMLog				20.30 ±0.20	20.31 ±0.20	20.29 ±0.20	20.31 ±0.20	20.30 ±0.20	20.30 ±0.20
Comprehensive							20.54 ±0.03	20.56 ±0.02	20.56 ±0.04
HFRadar				20.51 ±0.10	20.55 ±0.10	20.53 ±0.10	20.53 ±0.10	20.54 ±0.10	20.53 ±0.10
ADCP Depth Cell 1				20.38 ±0.07	20.46 ±0.09	20.40 ±0.09	20.41 ±0.08	20.43 ±0.09	20.42 ±0.08
ADCP Depth Cell 2				20.82 ±0.04	20.76 ±0.06	20.76 ±0.06	20.79 ±0.04	20.76 ±0.06	20.79 ±0.04
ADCP Depth Cell 3				20.82 ±0.04	20.72 ±0.04	20.77 ±0.04	20.78 ±0.04	20.75 ±0.04	20.78 ±0.04
ADCP Depth Cell 4				20.80 ±0.04	20.67 ±0.04	20.75 ±0.04	20.75 ±0.04	20.71 ±0.04	20.75 ±0.04
ADCP Depth Cell 5				20.74 ±0.03	20.60 ±0.03	20.70 ±0.04	20.68 ±0.02	20.65 ±0.03	20.70 ±0.02
ADCP Depth Cell 6				20.71 ±0.04	20.59 ±0.03	20.67 ±0.04	20.66 ±0.03	20.63 ±0.03	20.67 ±0.03

Tables VIII and IX are standard racetrack runs with three passes. Tables X and XI are an alternative maneuver that consists of one reciprocal followed by two 120° turns to create a triangle. In each table the measurements are shown for each possible combination of the runs. The heading, true wind speed in knots and wind direction (collected from the on-board ship's instrument) are shown for each pass.

In Table VIII the ADCP depth cells 1, 2, and 3 uncertainty estimates do not account for the difference between passes B and C. No environmental differences can be accounted for and depth cells 4 through 6 appear to be more consistent. In Table 9 Depth Cells 4 through 6 are the least consistent. Pass B in Table X seems to be unusually high across the measurements. Pass D also appears to be unusually high in Table 11. The final pass in Table 10 appears to skew the new calculation and HFRadar results towards a lower speed. Both use the GPS so some interesting skew may occur in results that may merit more observation. Comparison of the non-reciprocal portions of the maneuvers against the reciprocal portions shows good agreement.

Table X: 12 knot non-linear triangle multi-pass

Run	Hdg	Wind	Dir	Usage									
A	178.7	3.55	-116.6	•				•			•		•
B	-2.1	2.91	-62.6		•			•	•		•	•	•
C	-121.8	3.42	-99.4			•			•	•	•	•	•
D	118.5	1.20	-95.1				•			•		•	•
Instrument				**Measured Speed (kts)**									
Simplified								12.20					
EMLog				11.93 ±0.12	12.09 ±0.12	11.97 ±0.12	12.00 ±0.12	12.01 ±0.12	12.00 ±0.12	12.00 ±0.12	11.99 ±0.12	12.02 ±0.12	12.01 ±0.12
Comprehensive								12.23 ±0.02	12.21 ±0.09	12.12 ±0.04	12.23 ±0.05	12.16 ±0.03	12.16 ±0.05
HFRadar				12.29 ±0.10	12.15 ±0.10	12.29 ±0.14	12.05 ±0.04	12.22 ±0.10	12.20 ±0.11	12.12 ±0.07	12.25 ±0.11	12.16 ±0.09	12.19 ±0.09
ADCP Depth Cell 1				12.07 ±0.05	12.13 ±0.03	12.12 ±0.04	12.10 ±0.32	12.10 ±0.04	12.13 ±0.03	12.11 ±0.22	12.10 ±0.04	12.15 ±0.04	12.14 ±0.04
ADCP Depth Cell 2				12.24 ±0.03	12.33 ±0.62	12.32 ±0.03	12.31 ±0.03	12.29 ±0.33	12.33 ±0.02	12.31 ±0.03	12.29 ±0.02	12.35 ±0.02	12.34 ±0.02
ADCP Depth Cell 3				12.23 ±0.03	12.39 ±0.02	12.28 ±0.03	12.31 ±0.04	12.31 ±0.02	12.33 ±0.02	12.30 ±0.03	12.28 ±0.02	12.34 ±0.03	12.32 ±0.03
ADCP Depth Cell 4				12.22 ±0.03	12.44 ±0.02	12.23 ±0.03	12.27 ±0.04	12.33 ±0.02	12.33 ±0.03	12.26 ±0.03	12.25 ±0.03	12.30 ±0.03	12.29 ±0.03
ADCP Depth Cell 5				12.20 ±0.03	12.49 ±0.03	12.18 ±0.02	12.19 ±0.03	12.35 ±0.03	12.33 ±0.03	12.18 ±0.02	12.23 ±0.02	12.27 ±0.03	12.26 ±0.02
ADCP Depth Cell 6				12.16 ±0.04	12.55 ±0.02	12.15 ±0.03	12.19 ±0.02	12.36 ±0.03	12.34 ±0.03	12.18 ±0.02	12.21 ±0.03	12.26 ±0.03	12.25 ±0.03

6. Conclusion

The only absolute conclusions that can be made from this test is that the EMLog is only accurate at best to 0.3 knots and at worst off by 1 knots. The choice of the ADCP cell window should be made to make sure it is outside the boundary layer of the ship (at least 1 meter in this study).

Without testing in faster and changing currents, a limit exists to the rest of the conclusions that can be drawn. The new method agrees strongly with the classical calculation with the addition of the ability to handle non-reciprocal runs. Use of an HFRadar range may be a viable way to save time and money during future testing with the understanding of the limited accuracy (errors of up to 0.5 knots).

The repeatability section in this also tends to show that two passes are just as accurate as three passes during normal reciprocal runs. The non-reciprocal passes show the viability of the maneuver. The greater problem during testing is repeatability across large time frames.

Table XI: 16 knot non-linear triangle multi-pass

Run	Hdg	Wind	Dir	Usage									
A	-1.5	7.77	-62.7	•				•			•		•
B	177.6	5.28	-109.0		•			•	•		•	•	•
C	-61.4	8.16	-61.7			•			•	•	•	•	•
D	58.9	3.02	-90.0				•			•		•	•
Instrument				**Measured Speed (kts)**									
Simplified								16.28					
EMLog				16.01 ±0.16	15.95 ±0.16	15.91 ±0.16	16.14 ±0.16	15.99 ±0.16	15.95 ±0.16	16.04 ±0.16	15.97 ±0.16	16.02 ±0.16	16.02 ±0.16
Comprehensive								16.29 ±0.03	16.33 ±0.03	16.26 ±0.04	16.29 ±0.03	16.32 ±0.04	16.29 ±0.04
HFRadar				16.36 ±0.10	16.22 ±0.09	16.54 ±0.04	16.17 ±0.14	16.28 ±0.10	16.37 ±0.07	16.34 ±0.09	16.37 ±0.08	16.30 ±0.09	16.32 ±0.09
ADCP Depth Cell 1				16.17 ±0.04	16.17 ±0.04	16.05 ±0.04	16.27 ±0.03	16.17 ±0.04	16.13 ±0.04	16.18 ±0.03	16.14 ±0.03	16.19 ±0.03	16.18 ±0.03
ADCP Depth Cell 2				16.41 ±0.03	16.40 ±0.03	16.35 ±0.02	16.55 ±0.02	16.40 ±0.02	16.38 ±0.02	16.47 ±0.02	16.39 ±0.02	16.45 ±0.02	16.44 ±0.02
ADCP Depth Cell 3				16.42 ±0.04	16.40 ±0.03	16.39 ±0.03	16.56 ±0.45	16.41 ±0.03	16.40 ±0.02	16.49 ±0.27	16.41 ±0.03	16.46 ±0.02	16.45 ±0.03
ADCP Depth Cell 4				16.39 ±0.03	16.35 ±0.04	16.39 ±0.02	16.54 ±0.03	16.37 ±0.03	16.37 ±0.03	16.48 ±0.02	16.38 ±0.03	16.44 ±0.03	16.43 ±0.02
ADCP Depth Cell 5				16.39 ±0.03	16.26 ±0.04	16.40 ±0.03	16.48 ±0.03	16.31 ±0.03	16.32 ±0.03	16.45 ±0.03	16.35 ±0.03	16.39 ±0.03	16.39 ±0.03
ADCP Depth Cell 6				16.41 ±0.03	16.19 ±0.47	16.40 ±0.03	16.42 ±0.04	16.29 ±0.28	16.30 ±0.33	16.41 ±0.03	16.34 ±0.23	16.35 ±0.22	16.36 ±0.17

References

CHAMBERS, J.M. (1983), *Graphical methods for data analysis (Statistics)*, Springer

NN (2011), *Acoustic Doppler current profiler principles of operation a practical primer*, Teledyne RD Instruments.

NN (2017), *HF Radar Principles of Operation*, Coastal Observing Research and Development Center, http://cordc.ucsd.edu/projects/mapping/documents/principles.php

ROMANO, J.P.; POLITIS, D.N. (1994), *The stationary bootstrap*, J. American Statistical Association 89.428, pp.1303-1313, www.ssc.wisc.edu/~bhansen/718/Politis%20Romano.pdf

7. Supplemental Section

7.1. Example Calculation

The following is an example calculation of speed through water and uncertainty. An actual set of runs is taken from the test and is reduced from 10 Hz to 0.01 Hz.

Table XII: 0.01Hz Nominal 15 Knot 180◦ Reciprocal Two Pass

Pass 1				Pass 2			
t	V_{fwd}	V_{lat}	θ	t	V_{fwd}	V_{lat}	θ
[s]	[kn]	[kn]	[°]	[s]	[kn]	[kn]	[°]
0	15.144	0.047	359.62	1039	14.881	1.168	178.21
10	15.419	0.046	359.87	1049	14.955	0.894	178.84
20	15.144	0.121	359.50	1059	15.169	0.212	179.53
30	15.501	0.238	358.89	1069	15.100	0.495	179.48
40	15.324	0.024	358.25	1079	15.037	1.058	179.18
50	15.559	0.101	357.74	1089	14.925	1.129	178.84
60	14.999	-0.052	358.10	1099	15.041	0.819	178.07
70	15.404	0.112	358.30	1109	15.085	0.256	177.50
80	15.210	-0.318	358.99	1119	15.230	0.494	177.29
90	15.408	0.316	358.78	1129	14.984	0.885	177.07
100	15.088	0.106	358.65	1139	14.975	0.690	176.83
110	15.464	-0.105	358.23	1149	14.924	0.925	177.20
120	15.100	0.311	358.31	1159	14.889	0.881	178.15
130	15.219	0.115	358.86	1169	14.973	0.614	178.93
140	15.239	0.276	358.97	1179	15.023	0.511	179.35
150	15.223	0.465	359.21	1189	14.944	0.581	179.57
160	15.152	0.255	359.14	1199	15.102	0.420	179.16
170	15.403	0.049	358.81				

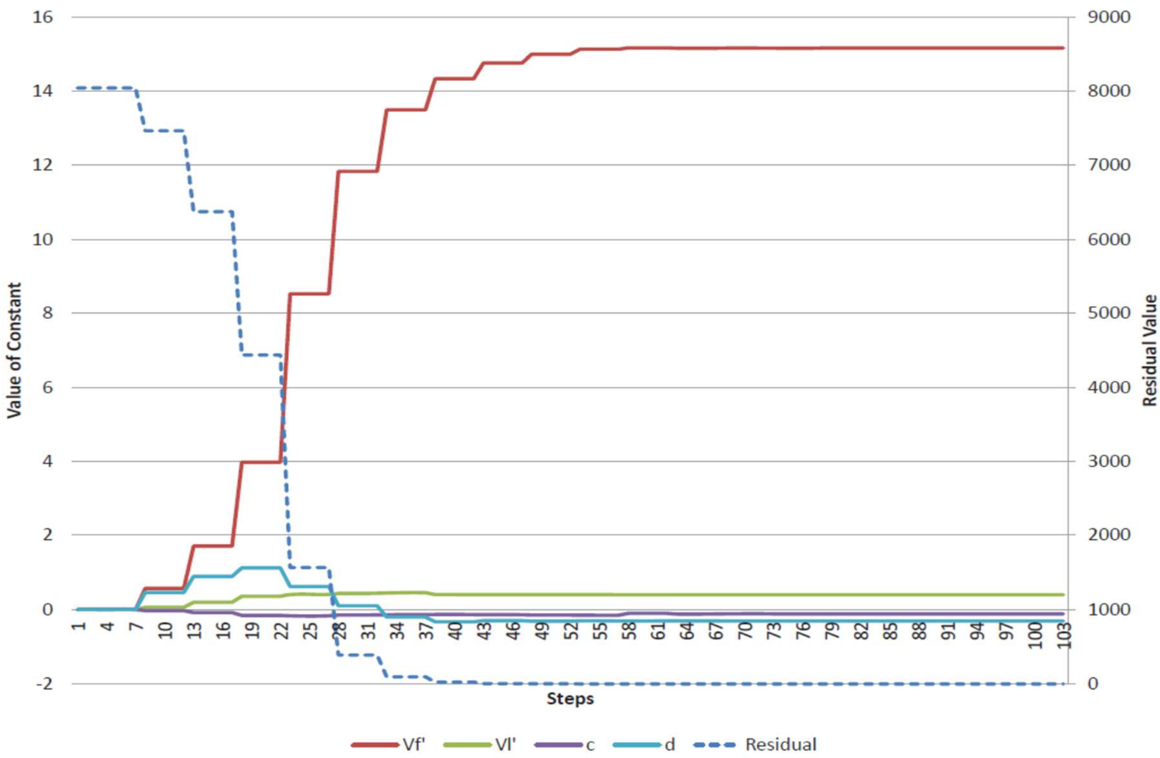

Fig.2: Convergence of minimization algorithm

Then for simplicity we will use a constant current model, the data can be given into a minimization algorithm that adjusts V'_F, V'_L, c and d to minimize the following objective equation (V'_F and V'_L can be set to the classic calculation and zero respectively to speed up convergence). The convergence over 103 steps of the chosen Levenberg-Marquardt algorithm is shown in Fig.2.

The values minimize to:

- $V'_F = 15.159$
- $V'_L = 0.399$
- $c = -0.1155$
- $d = -0.305$

$$\sum_{t=0}^{n} \begin{matrix} (V'_F - V_F - (c)\sin\theta + (d)\cos\ \theta)^2 + \\ (V'_L - V_L - (c)\cos\theta - (d)\sin\theta\ )^2 \end{matrix} \tag{10}$$

7.2. Derivation of simplified rule

First if we follow the assumption that each pass can be described by a single velocity forward Eq.(7) after transformation into a set of three equations to be solved becomes:

$$\begin{aligned} V'_{F1} &= V_F - (at_1 + c)\sin\theta_1 + (bt_1 + d)\cos\theta_1 \\ V'_{F2} &= V_F - (at_2 + c)\sin\theta_2 + (bt_2 + d)\cos\theta_2 \\ V'_{F3} &= V_F - (at_3 + c)\sin\theta_3 + (bt_3 + d)\cos\theta_3 \end{aligned} \tag{11}$$

Then if each pass is perfectly reciprocal we can substitute ±90° for each θ to simplify the equation (i.e. $\theta_1 = 90°$, $\theta_2 = -90°$). The equation becomes:

$$\begin{aligned} V'_{F1} &= V_F - (at_1 + c) \\ V'_{F2} &= V_F - (at_2 + c) \\ V'_{F3} &= V_F - (at_3 + c) \end{aligned} \tag{12}$$

If the time and duration between each pass are the same, we can describe t as being related to an arbitrary time t_{pass} which can then be divided by t to get simple time values.

$$\begin{aligned} t_1 &= -t_{pass} = -1 \\ t_2 &= 0 \qquad = 0 \\ t_3 &= +t_{pass} = 1 \end{aligned} \tag{13}$$

The previous equation becomes, which is three equations with three unknowns (V_F, a, c).

$$\begin{aligned} V'_{F1} &= V_F + a - c \\ V'_{F2} &= V_F + c \\ V'_{F3} &= V_F - a - c \end{aligned} \tag{14}$$

This can be solved algebraically to get:

$$V = \frac{V'_{F1} + 2V'_{F2} + V'_{F3}}{4} \tag{15}$$

Improving the Reality –
Paint Work in Dry Dock and Its Implication on Vessel Performance

Birk Fleischer, C.E.T., Hamburg/Germany, team@cet-hamburg.com

Abstract

Despite all theoretical analysis, preparation prior and in-depth monitoring after docking, the fate of vessel performance is determined by applying the appropriate coating system in dry dock correctly. The paper is highlighting major tripping stones prior and during a scheduled docking. The typical paint selection process of ship managers, skillset of decision makers and its influence on performance is explained. The relation of paint maker, shipyard and ship manager during the docking and its direct influence on the actual achieved result in dry dock is demonstrated. The paper further recalls some regular mistakes which are done in dock and their direct, irrevocable implication on the vessel performance. The paper closes with clear recommendations of how the shipping industry members can notably improve vessel performance prior and during the dry docking.

1. The zig-zag way to the dry dock

The typical paint selection process at an average ship manager starts with the recognition that the next docking for a vessel or series of vessels is upon them. While between 2005 and 2010 this might have been up to one year prior to the event, currently we have cases with head times of 7 days – for a regular planned docking. This can be mainly addressed to the changing economic environment, especially the involvement of more and more decision makers, which do not have maritime background. Banks, Trusts and Hedge funds are some of them.

Every ship manager – without exemption **-** is considering the fact of good anti-fouling performance in preparation of a docking. The starting point of paint selection usually is the best-for-money product the ship manager has knowledge of. That does not necessarily mean that this product performs well. But in the competitive environment of ship operation, the known is much more important than the possible better, which is unknown. Currently, a failure in ship performance is a severe commercial risk to any vessel intending to stay off the beaches of Alang.

It is this starting point of paint selection, which is already determining the path for paint selection. This starting point is set by budget and knowledge. While the budgets may be vastly different, the existing knowledge about paint within ship managers is quite equal among most of them – a topic touched later in this paper in more depth.

Once the ship manager has set the base product of choice, in most cases the already applied material they know, tenders from various makers are asked for. The procurement and technical people at the ship managers are consequently bombarded with offers and options. The given options are not only vast, but also conflicting. The "best" product in any given range can be procured with vast price differences. We have worked a case, where low friction Silyl SPC was offered in a range of 10,81 USD/L up to 52 USD/L [for a 2500 TEU container tender; German ship manager in personal communication in 2014] – with nearly identical performance description. The ship manager is fully aware that there is a difference in the products, but any person cannot avoid the question: Is the expensive stuff really some 5 times better?

The tender continues to run through the ship manager's corridors – the technical Superintendent, the commercial people, the procurement people and the management do favor a product – and certainly seldom the same. Recently, another factor comes into play – the ship owner. The paint selection process is made more complex by owners, which have ships by themselves but also give ships to other ship managers for technical operation, e.g. Maersk, Borealis or Delphis. These companies have their own ideas and experience about coating and can execute direct influence on the decision-making process of the ship managers. The result is often, a zig-zag course through the paint options in currently a very short time span. The result can seldom be predicted.

Although the starting point of all ship managers is good hull performance, the product finally selected for the upcoming docking may be very surprising for all involved parties. We reviewed systems with CDP/SPC/CDP coating combinations, CDP/Silyl coating combinations and even high quality Silyl applications on 10-year old, non-treated surfaces [for a 1700 TEU feeder tender; German ship manager in personal communication in 2013] – all the result of a compromise between the involved interests.

But there is one dominating factor in the selection process, which overshadows most other factors:

2. The paint maker's curse

The supply of paint material and all related works in dry dock are responsible for up to 30% of docking cost. The purchase of the paint material for a normal scheduled docking is usually the highest single expense in five years for any given vessel. Consequently, choosing the right paint material is strongly reviewed by ship managers and owners. Currently the biggest focus is on cost reduction while maintaining a bearable performance level.

But when it gets down to paint material knowledge the picture becomes blurry, very fast. Most ship managers or owners don't employ paint experts, who review the vessel needs and choose the required paint systems independently of the paint makers. As common practise, paint makers advise ship managers on paint material and to overcome shortcomings in paint knowledge the "usage" of competing paint makers to get a better picture is standard. Unfortunately, in most cases, this creates an even more fuzzy picture.

The performance of paint material as such but especially of anti-fouling paint is depending on a huge number of factors besides the material itself: On circumstances of application (winter/summer etc.), surface preparation (surface condition/blasting quality/etc.), sailing area of the vessel, idle times, damages in service, sailing speed and many more. Frustratingly, a paint maker having provided the "perfect" material can find disastrous conditions after five years of service while a "poor" paint material may enjoy a much – better – than – expected docking result after its service life.

It is a curse for the paint makers that their influence on final paint performance is limited. As the final product performance cannot be fully influenced, paint makers have put sales efforts on changing product names, ever changing vocabulary and serious statements of non-comparability of products among paint makers. This creates an extremely confusing view on paint for ship managers. Furthermore, considering the enormous commercial pressure on paint makers, the tendency to influence paint decisions with facts is low, while the tendency to influence decisions through other ways, be it commercial or through personal relations is very high. But is it the obligation of the paint maker, which after all needs to sell paint, to provide sufficient knowledge? Or is it:

3. The ship manager's obligation

Most decision makers for paint in shipping companies have technical background. Most common background is either a technical position on board, technical study at university or combination thereof. A non-representative review of internal CET records show some 60% engine related background, 20% nautical background and 20% other background of known decision makers. In a CET market review, of 1200 shipping people making paint decisions in Germany, namely fleet managers, Superintendents and Procurement positions, no decision maker could be identified with a straight paint job title or position (e.g. Paint Superintendent) and less than 1% of the shipping companies interviewed were stating to use maker independent knowledge on paint decisions.

It remains a mystery for the time being, why ship managers do not employ maker independent knowledge more aggressively, while the stakes for wrong decisions are high – commercially and in terms of vessel performance.

4. The paint equation

Once a paint system is chosen and the vessel is high and dry on the blocks in the shipyard, the actual paint work is starting – washing, scraping, blasting, air blowing and painting is keeping ship manager, shipyard and paint maker very busy.

But it is an uphill battle for any ship manager and one which is mostly lost by them.

Two parties in the paint equation are there to earn money: shipyard and paint maker and both have a huge advantage. It is nearly impossible for both to be attributed to a paint failure, especially after five years of vessels service – too many factors are not influenced by the yard and maker hence any commercial pressure by the ship managers can be fended off.

Based on the vast number of applications done by any given yard, they have an intimate knowledge of how to prepare the surface and apply coating fast and effectively. At the end of a docking, all shipyards need to earn money, so it is their full right and obligation to be swift and as good as required. To balance the quality of work with time and cost at a shipyard, ship managers rely to a notable extent on paint maker's representatives, be it local or from the home country of the ship manager. The reasoning of the ship managers is simple: the paint maker gives a performance guarantee for the paint, so it is in the sole interest of the paint maker to supervise the shipyard correctly. But is that really the case? After all, the paint maker can almost never be held responsible for paint failures – again due to the vast number of things that can go wrong outside of the paint makers influence in a five-year docking interval.

And the paint maker is a money receiving company in the paint equation. The interests of shipyard and paint maker are similar – to earn money, they need to blast and paint. The paint maker's representative is therefore wedged between the desire to fulfil his company's main topic – selling paint, while at the same time keeping a good relation with the ship manager. Many good paint representatives in the field are great diplomats, focusing on basic ship yard errors while still making sure that the ship manager's paint budget is fully used. And like the shipyard's needs there is nothing wrong with this, as the paint maker at the end of the day needs to sell paint for a living.

That leaves the ship manager being the only paying party in the paint equation – and big money it is with budgets (material + work) of over 300.000 USD for bigger vessels, [average cost for 7500 TEU vessel, with 15% SA2 blasting, full topside coating, full antifouling coating employing standard SPC 5-year paint system].

While shipyard and paint maker have in-depth knowledge of paint material and paint procedures, as well as several dedicated people on site with a high motivation to earn money, the ship manager's representatives are normally stretched between steel work, engine work, outfitting and painting – an extremely demanding task, even for teams of two or three people.

Limited time available, limited information on paint procedure options and limited information about paint material options on the part of the ship manager are eventually tipping the paint equation balance notably towards the receiving end.

It must be blatantly clear that in such a setup hull performance, although in the focus of the ship manager, is generally victim of the circumstances.

Two examples shall underline the living and breathing reality in docks:

5. The more the better - blasting

It is evidenced by various research that the more surface of a vessel is blasted, the smoother the hull hence the better the performance is expected. If standard spot blasting of 10% surface is increased to 50% full blasting, the hull resistance may drop by another 12%, *Kane (2013)*. It is a logic conclusion that a more blasted hull is resulting in better performance.

This is widely advertised and especially shipyards, looking rightly for good income, advertise this fact. Especially in recent years, the vessels condition is seldom in line with the expectations of the ship managers, usually worse. This is highly related to idling and vastly changed operating profiles in comparison to the assumptions made for the docking 5 or more years ago.

To realize the maximum result out of the available budget, blasting to SA1 standard becomes more common, being notable cheaper than SA2 and much faster executed. And blasting more surface is considered the right way to get better performance. Recalling the paint equation, we can also determine that shipyards and makers will mainly promote additional blasted surface to do more work and apply more paint.

Unfortunately, the achieved results executing SA1 blasting are very seldom in line with proper hull performance. The results of a research, *Fleischer (2011)*, executed in 2009 and 2010 speak a clear language. Fig.1 show typical examples, where SA1 blasting - also called grid sweeping - is considered. Fig.2 shows typical results achieved in most cases.

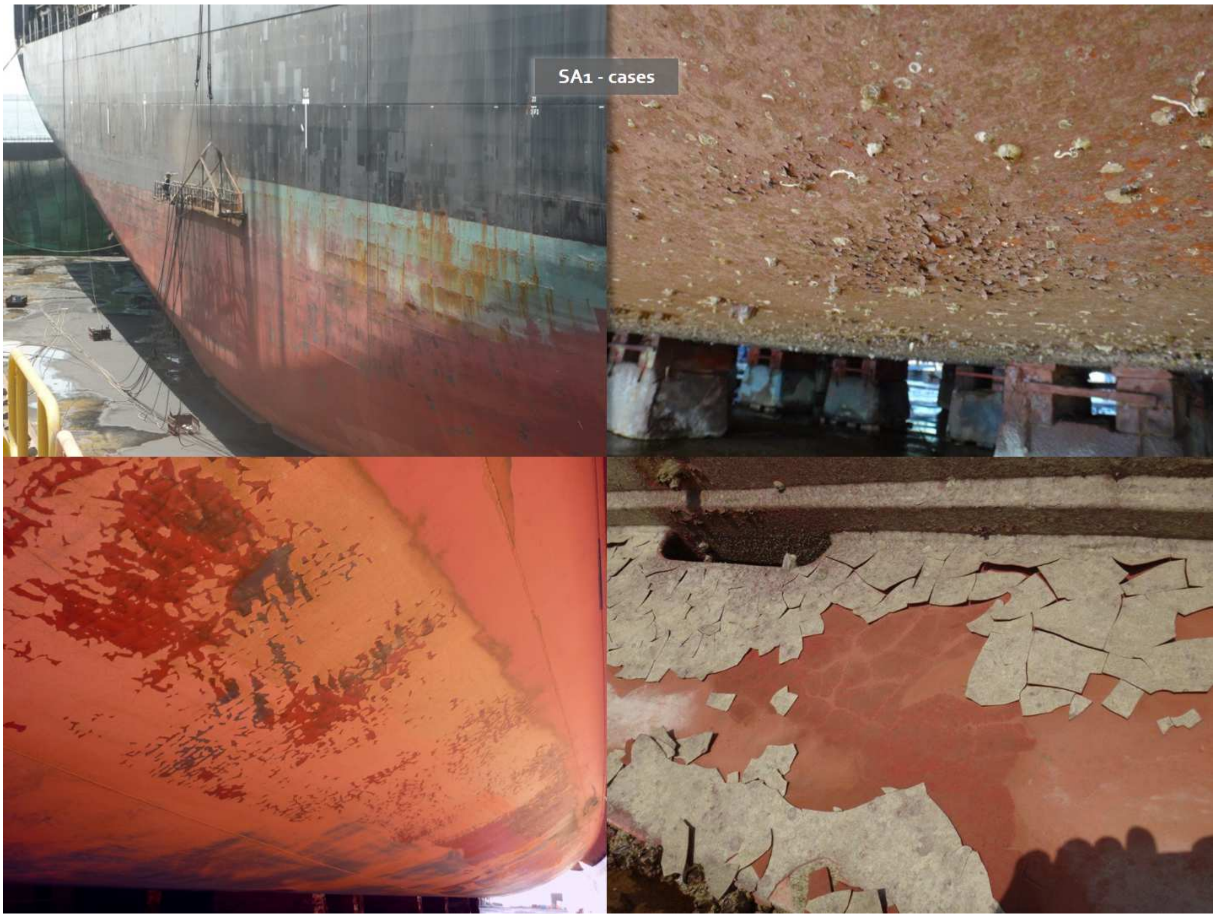

Fig.1: Typical examples of SA1 blasting

Two SA1 blasting tests were executed on a yard in Romania and one in Singapore. Fig.3 shows the results in various detail of such SA1 blasting performance. Various grits were used in patches next to each other and the best, meaning most equal patch, is shown in close detail.

Fig.2: Typical blasting results in most cases

Fig.3: Details of SA1 blasting

The Singaporean yard is well reputed and considered among the top yards in South East Asia. Fig.4 compares SA2 and SA1 at a Romanian shipyard. The test patch of SA2 in the upper left area shows the available skill of the blasting crew – fine bare metal surface is achieved while a clear feathering of all previous coats is perfectly visible on the edges. We have asked the same crew to do various test patches in SA1 quality and the result is visible on the lower center picture.

Fig.4: SA2 and SA1 blasting at a Romanian shipyard

Although hull roughness of the test patches was not measured, it is obvious that the hull roughness prior coating is exceeding 500µm. The surface is varying between bare metal and nearly original coating thickness. It is not a skill problem as demonstrated but rather a systematic problem of uneven adhesion of the existing coating and external circumstances of wind, grit sweeping motion, fluctuation of air pressure, movement of cherry picker basket and so on.

Having the images shown in Figs.1 to 4 in mind it must be clear that SA1 blasting should be banned when hull performance shall be improved. But contrary to that, it is, per CET data from past 50 dockings attended by CET Paint Superintendents, more common now than before.

We have a recorded case of the application of a high performance, low friction SPC (Meth-Silyl Acrylate SPC) last summer on a big tanker, where the full SA2 blasting was downgraded to a full SA1 blasting while maintaining (to our knowledge) the performance guarantee by the paint maker.

6. Just wash it away

Most paint people will agree that hull washing prior to any further surface preparation is an important part of the paint works. Some people state that washing is the most important part when related to anti-fouling paint, as it removes, properly done, the leached layer and embedded salts, impeding and disturbing any proper further paint application.

Regretfully the paint equation is taking its toll in a drastic way. As the shipyards are focusing on fast and efficient work flow, hull washing is focusing on removal of visible debris. When the hull is visibly clean from debris, most attending ship manager representatives will accept this as a good result and in practice, most paint makers will agree. It is uncommon, to test external hull surfaces after washing for salt and leached layer thickness. And it is very difficult for any paint representative who is doing it to explain to shipyard and ship manager that a nearly invisible leach layer and invisible salt may require another day of washing and therefore day in dry dock. Eventually, the paint equation is at work: The paint knowledge of the ship manager is insufficient for the situation or commercial pressure prevails, the shipyard is keen on effectivity and the paint maker will eventually not be addressable for the possible paint failure thus tacitly accepts the situation.

Fig.5 (left) shows a good result of a high-pressure hull wash with about 250 bar and proper nozzle guidance. A visible result like this is considered sufficient proof of cleaning efforts. However, the washing was supervised by a dedicated Paint Superintendent and close control of washing pump pressure and nozzle guidance. The normal washing result without intervention, according to our data, looks more like Fig.6 and is still widely accepted as sufficient. Fig.5 (right) shows what should happen. The test patch shows a 300 bar close surface wash, as shown during execution in the right lower picture. The difference is clearly visible.

Fig.5: High-pressure washing results

Lack of proper adhesion is a major reason for paint failure and hull performance reduction. The best available anti-fouling or foul-release system is useless when it has left the vessel. Above examples show the inherent difficulties that come with docking. The relation between shipyard, paint maker and ship manager is an unequal one to date and it directly influences the performance of the vessels, far beyond physical paint properties. The inherit flaw of the current situation is frustrating for most involved parties. Understanding and accepting the interests of the involved parties for painting in dry dock is the first, biggest and most important step towards a better paint condition and performance.

Fig.6: Normal washing results

7. The silver lining on the horizon

Such a set layout of ship manager, paint maker and shipyard cannot be overcome by a single party, nor can it be overcome overnight. First and foremost, we emphasize the need for ship managers to realize the lack of knowledge and act accordingly. Well informed ship managers (the “paying people”) are good for all involved, as it levels the playing field, gives way to more fact-based decision making and thus will eventually lead to higher coating quality and therefore better performance – at any given budget.

This can be achieved through employment or by arrangement of paint maker independent dry dock supervision – thus equalizing the paint equation by putting more knowledge and attendance on the ship managers’ side.

But also the paint makers can improve the situation by commonly defining paint vocabulary and using it appropriately. The labels CDP/SPC/Silyl anti-fouling could be tied to a certain set of binder/ingredient ranges thus allowing at least a rough classification by material base and expected performance. This could be achieved through voluntary tests, agreed by an industry panel or through regulatory bodies.

Ship managers could insist in the future that paint makers are also awarded the surface preparation and paint application work, thus reducing the “blame game” in dock and giving the paint makers more power to control all works directly, which will eventually lead to better results and higher performance.

Well informed ship managers will pay closer attention to ship yard performance on painting, which implies the chance for shipyards to increase revenue and quality levels.

Dry docking a vessel has always a direct impact to the hull performance. Despite all efforts while the vessel is in service, the actual work execution in dock is a major factor influencing hull performance. Improving the reality of surface preparation and paint application in dry dock will greatly increase the overall hull performance of every vessel.

References

FLEISCHER, B. (2011), *Review of practically achievable blasting results*, Internal Review, CET, Hamburg

KANE, D. (2013), *Developing a more Fuel Efficient Tonnage through Hull and Propeller Performance Monitoring*, Ship Efficiency Conference, Hamburg

Experience with and Achieved Benefits of a Low-Budget Plug-and-Play Logging Device

Søren A. Hattel, FORCE Technology, Lyngby/Denmark, shl@force.dk
Jimmie S. Beckerlee, FORCE Technology, Lyngby/Denmark, jib@force.dk
Giannis P.S. Papageorgiou, FORCE Technology, Lyngby/Denmark, gpp@force.dk

Abstract

Data collected by a simple low cost plug and play device for automatic logging is used to supplement data collected in noon reports for analysis of vessel performance. The quality of the performance analysis for the cases with and without the automatically logged data are compared. We observe that the scatter in the performance analysis is better than expected when using the automatically logged data. The extra metadata produced by the device is used to identify data of highest quality and data that are compatible with the method of analysis. We find that both the higher amount of data and the metadata provide opportunities that are not available with noon report data alone. Finally, we illustrate that the higher amount of data can be utilized to increase confidence in the performance analysis.

1. Motivation

Performance monitoring and analysis of ships' hull and propeller are essential tools for documenting the effect of energy saving efforts and to prove their return of investment in real life, *Kariranta (2014)* and *IMO's (2012)* SEEMP. In many cases the actual effect of the energy saving efforts have only been proven under laboratory conditions and under these conditions the actual amount of energy savings are often limited to only a few percent of the total energy consumption *Politis (2004), Larsen et al. (2012), Gougoulidis and Vasileiadis (2015), Schneekluth and Bertram (1998).* Only a few percent of energy reduction are nevertheless relevant from a commercial point of view and hence many investments in energy saving efforts are based on these relatively low numbers predicted by laboratory conditions which are difficult to detect in real operations or under realistic conditions *Pedersen (2014)*. The need for better and more accurate vessel performance analysis is well described in the newly formed ISO standard, *ISO19030*.

In real-life operations, the performance analysis must incorporate the effects of external influences that can easily be controlled in the laboratory but cannot be controlled in real operations. Some of these external influences are created by Nature such as wind conditions, sea state, swell and changing water depths during sea passage. Other influences originate from navigational, operational, commercial, regulatory or safety concerns such as ship draught and trim, ship maneuvering, changing speeds, changing courses, rudder movements. Whenever these external influences change it will affect the performance analysis as the influence must be corrected to have comparable data. The range of frequencies for changes in these external influences ranges from few minutes to several days.

Often performance analysis is based on manually recorded data from noon reports or from dedicated performance reports, *Kariranta (2014)*. Noon reports contain either average values for the day or snap shot values and the sampling frequency for the noon report approach is roughly one sample per day or less, which contrasts the much higher frequencies of the changing external conditions as stated above. Neither average values nor snapshot values can describe the external influences satisfactory. Hence, in general the noon report approach cannot comply with the increased accuracy requirements unless the noon approach is refined to report data recorded at higher frequency than the noon report itself. In one case, a ship operator decided to record manually entered performance data three times per day to improve on the sampling problem. Even in this rather extreme case the noon report approach also depends on the crew's ability – as well as motivation and willingness – to reliably record and report the average values and snap shot values. The human factor can seriously skew the manually recorded data and will often require careful training and motivation schemes to reduce or avoid.

The approach using dedicated performance reports is reminiscent of the laboratory tests aiming at making a controlled test of the vessels performance. The crew is informed to perform a test when external conditions are within certain limits to ensure that the external influences have reduced effect on analysis. This is a healthy approach but relies on the external influences being within the required limits which may be very rare for many vessels, and the approach rules out studying effects on a time scale shorter than the frequency that the crew is performing the controlled test. The frequency of the controlled tests is limited by commercial concerns as the crew will potentially have to deviate from the optimal commercial navigation resulting in extra costs. Hence, the frequency of data points is one order of magnitude lower than for noon reports. Again, the data quality depends on human factors.

For any approach based on manually collected data the human factor limits the obtainable accuracies. For instance, it is not feasible to ask the crew to amend the primary data values – whether averages or snap short values – with elaborate extra metadata describing the conditions for the primary data. Hence, even with the best of abilities of the crew – obtained e.g. from expensive and continuous training sessions - then they will not be able to provide the amounts of data that the modern world is used to. We consider this a serious limitation of the manual approaches.

Only recently within the last decade have dedicated systems for automated collection of high frequency data – casually referred to as “autologging systems” - become widely available for ship performance analysis. To install sensors and automated data collection systems onboard a vessel in operation is, however, usually an expensive operation and the expenses must be related to the potential benefits and cost reductions enabled by the system.

The benefits of the autologging systems should be obvious: High rates of data and not affected by human factors. From an academic point of view this should be ideal while not necessarily sufficient from a commercial point of view. Nevertheless, the skepticism towards autologging systems seem to persist even in academic circles. As an example, *Beiersdorf (2017),* carefully lists four serious reasons why autologging is not a solution. Although we agree that the article raises four relevant complications of autologging we do not agree they constitute sufficient arguments for ruling out autologging as part of a solution. Interestingly one of the issues raised is that autologging data is often compiled and reported on a frequency of only every 15 minutes which is – according to the article – not sufficient to give any new insight and new performance indicators. This statement is especially interesting when contrasted to the preferred methods described in the ISO 19030 standard where high frequency autologging is required for extracting performance indicators on a time scale of quarters of a year to several years.

Presumably the ISO 19030 standard requirements are motivated by the desire for higher accuracy of the performance indicators. We find it difficult to comprehend that a data frequency of at least five orders of magnitude higher than the frequency of the relevant performance indicators is required.

Our study is motivated by the search for pragmatic solutions that are simple and affordable. We believe, that the obvious shortcomings of manual approaches can be partially compensated by exploiting the obvious benefits of autologging systems while respecting the complications introduced by autologging.

In this study, we set out to explore the usage of a simple device and if possible quantify the benefits of the device and the data it provides. In this way, we aim to contribute to the debate about and understanding of how to obtain higher accuracy in performance analysis from autologging data and how to obtain higher confidence in the conclusions from performance analysis.

2. The settings

The central device in our study is a box sized 12 cm x 12 cm x 9 cm containing a few sensors and some electronic devices enabling collection of data from different external signals. (The device is manufactured by FORCE Technology and sold under the name of SeaLogger®). The box will record several parameters without being connected to any sensors. In most cases, though, external signals from existing sensors onboard the vessel will be connected to the device through external terminals on the cabinet.

The device is very simple to install. The data used in this study were collected by devices installed successfully by the crew onboard fourteen vessels while in their normal operation. Hence, no docking or idle time was required, and no third-party personnel was sent to the vessel.

For each vessel, the signals from sensors already available onboard the vessel were connected to the device when possible. Most of the connected signals were recognized and recorded immediately by the device while some needed uncomplicated configuration with the supervision from onshore system supporters to be recognized and recorded.

Evidently, due to this "plug & play" approach the data collected by the device will usually not be sufficient for a complete performance analysis. Therefore, the recorded data must be complemented by manually collected data from e.g. noon reports. Furthermore, the performance analysis system will have to automatically adjust to whatever data are available from autologging and in a smart way combine the data with the manually reported data. This is an obvious complication introduced by the "plug and play" approach.

Onboard the vessel the data from the device is processed automatically and aggregated into packages of statistical data and metadata. In this study data were collected and processed for every one hour. This choice was a balanced compromise between the cost of data transfer from the vessels and the timescales that the analysis would require. Although this sampling frequency is lower than time scales of some of the external influences the statistical nature of the data and the collected metadata enable better analysis than the sampling frequency seems to indicate.

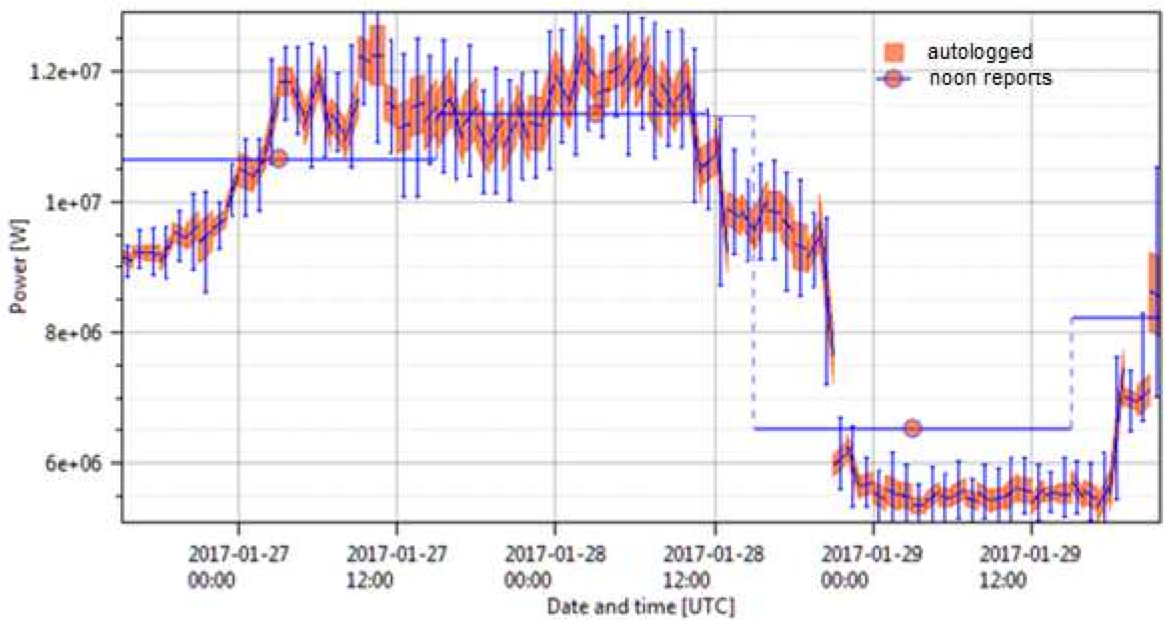

Fig.1: Extract of autologged data packages (parallelograms and error bars) of torsion meter power for one hour intervals and their corresponding manually reported average values (circles and full lines). Autologged data packages are represented by their recorded max and min values, average values, standard deviation, linear trend.

Fig.1 shows a typical example of data packages of torsion meter power recorded by the device accompanied by the corresponding reported average values from manual reporting. The graph readily illustrates the richness of detail from the autologged data and the rich metadata available. This contrasts with the simple manually reported average values. The qualitative benefits of the extra information are obvious as for instance the autologged data can be used as a means for evaluating the data quality of the manually reported data.

In this example one could easily deduce that the quality of the first and the third noon report data is not as good as the data quality of the second report, as the power was only reasonably stable for the entire period of the second noon report. Even if this was the only autologged signals we had the we would be able to point out specifically the noon reports with stable power data. In this way, as we are aware that our analysis techniques are only valid for stable conditions, we can improve the reliability of our analysis based on first principles about the nature of our system. We simply know much more about the data that we use for our analysis and we can improve the reliability of the analysis. In the end, confidence in the conclusions we may extract from the analysis is raised.

In cases where we have more complete sets of autologged data from various signals we can use each individual autologged data package directly for the analysis instead of only looking at the data on noon report time scale. Also in this case are the data packages superior to simple average values as we can readily decide from the collected metadata which data sets represent stable periods and which data sets represent transient periods. Since we have an abundance of data it is likely that there is a good number of stable periods within the span of one noon report. We end up with a higher number of data sets than can be achieved with noon reports, and each individual data set will be of better quality than the noon reports offer.

The same story applies to the information one can extract from the autologged packages for position and heading. Fig.2 shows an extract of the positions and headings recorded during a sea passage. Obviously, the crew has occasionally made significant course changes for some reasons. Data recorded during the course changes should not be used for performance analysis, as we are aware that our analysis techniques are based on assumptions of stable conditions and cannot correctly handle for instance rudder activity and wind and waves affecting the ship in different headings.

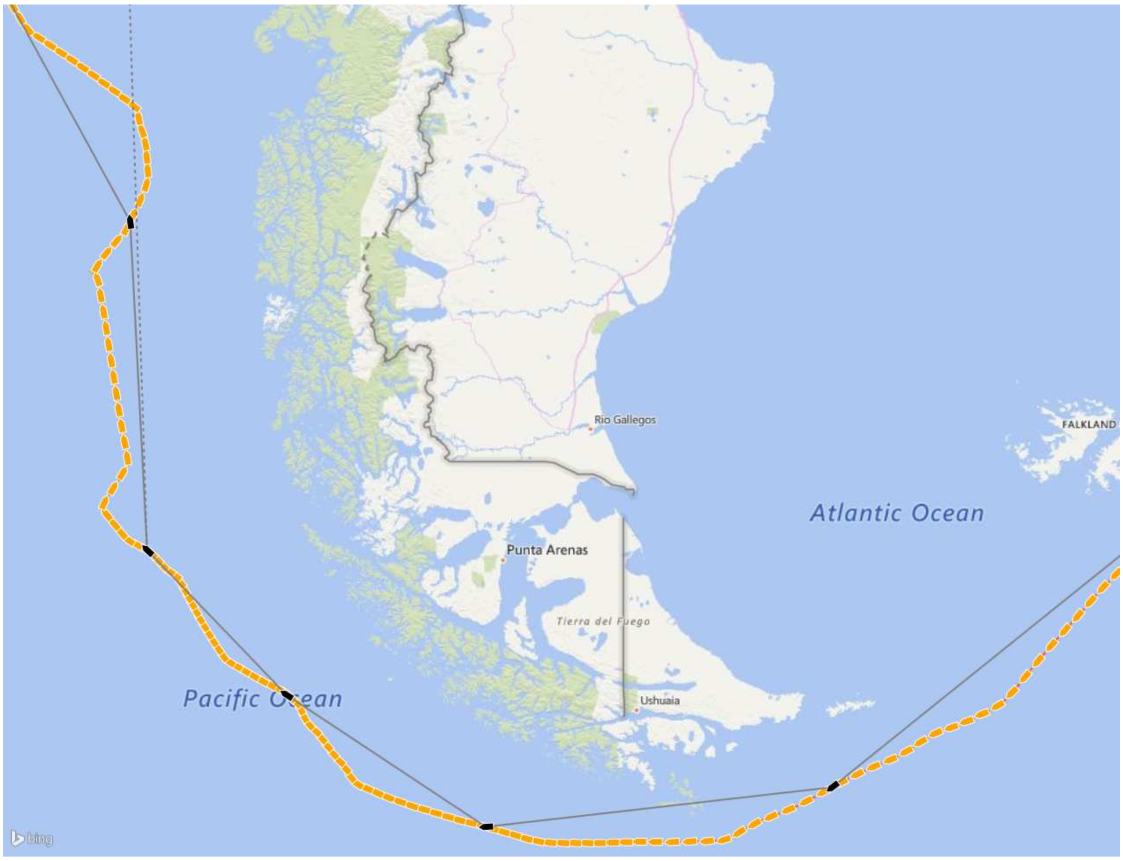

Fig.2: Position and heading data for a vessel compared to same data given in noon reports.

For this study, we had noon report data and autologged data packages available from fifteen different vessels (tankers, bulk carriers and one reefer container vessel). The vessels had different sensors onboard and had different signals autologged. Some vessels had speed log signal (speed through water) autologged, some had no torsion meter, some had torsion meter readings reported in noon reports, some had torsion meter data autologged, some had rudder angle autologged, some had anemometer autologged, some had echo sounder autologged. The variety of vessels and the impact on the quality of the performance analysis has not been considered in this study, but may be the subject of a future study.

3. Performance analysis method

In this paper, we study how the presence of the autologged data can improve the quality of the performance analysis. Hence, the primary goal is not to describe the specific performance analysis method applied to each individual dataset and to each individual vessel. Nevertheless, we will briefly outline the underlying analysis being studied.

The method for calculation of performance indicators in this study is based on detailed mathematical vessel models describing the expected performance of the vessels from first principles, see e.g. *Pedersen (2014), Kariranta (2014)* and *Beckerlee (2016)*. The quality of the vessel models depends on the available data for each vessel. For instance, in some cases a complete set of calm water resistance data was available from model tests, in some cases sea trial data was available, and other cases no data was available. The agreement between the measured performance and the expected performance will depend on the quality of the mathematical model and consequently the intrinsic accuracy of the analysis is different between the studied vessels. Consequently, we also expect that the presence of autologged data have different impacts depending on the quality of the vessel model.

For this paper, a power index was studied. The power index is defined as:

$$PI = \frac{P_{normalised}}{P_{expected}} * 100\%$$

$P_{normalised}$ is the propeller power estimated to be required at a fixed reference condition (operational and environmental conditions) given the data that was recorded and reported from the vessel. $P_{normalised}$ is the result of a complicated correction of the reported (autologged or manually) propeller power from the vessel - or estimated from the fuel consumption if torsion meter readings are not available. The corrections include effects of wind, sea state, off reference draught, off reference trim, off reference speed, shallow water etc. All corrections are estimated by use of the mathematical vessel model. The procedure is basically a refinement of the procedures recommended by *ITTC (2005,2011)*.

The normalization factor $P_{expected}$ is the propeller power predicted by the mathematical model at the reference condition. $PI < 100\%$ indicates exceptionally good hull and propeller performance and $PI > 100\%$ poor performance. This performance indicator is designed to study long-term trends in performance of hull and propeller and highlight the impact of hull and propeller maintenance. For periods between hull and propeller maintenance PI will be fitted using simple linear regression methods to look for significant trends, https://en.wikipedia.org/wiki/Statistical_hypothesis_testing. In our study, the goodness of the linear fit is characterized by the parameter, σ, calculated from root mean square of the residuals of the fit:

$$\sigma = \sqrt{\frac{1}{n}\sum\left(PI_{fit}(t_i) - PI(t_i)\right)^2}$$

$PI_{fit}(t_i) - PI(t_i) = E(t_i)$ is the deviation (residual) of the calculated PI at time t_i and the fit prediction at the same time. σ can be roughly interpreted as an estimate of the standard deviation of the distribution of the residuals and is thus a measure of the scatter of the data points.

Assume for a moment that the residuals $E(t_i)$ are independent stochastic variables that belong to a normal distribution. Furthermore, assume that the performance indicator for a full noon report could be calculated simply as the average of the performance indicators from the autologged data. Based on these assumptions the scatter, σ_{noon}, for PI from noon report based data will be reduced compared to the scatter, $\sigma_{autologged}$, for PI from autologged data:

$$\sigma_{noon} \approx \sigma_{autologged}/\sqrt{N}$$

where N is the number of autologged observations per noon report. This relationship is also known as the "standard error of the mean". From this formula we may expect the scatter for autologged data to be worse than the scatter for noon report data by a factor of 2 – 5 depending on the amount of autologged data per noon report.

Fig.3 shows an example of performance indicators. Both noon report data and autologged data are plotted. Light blue (greyed out) symbols indicate data excluded from the analysis according to methods described in section 4. Filtering method.

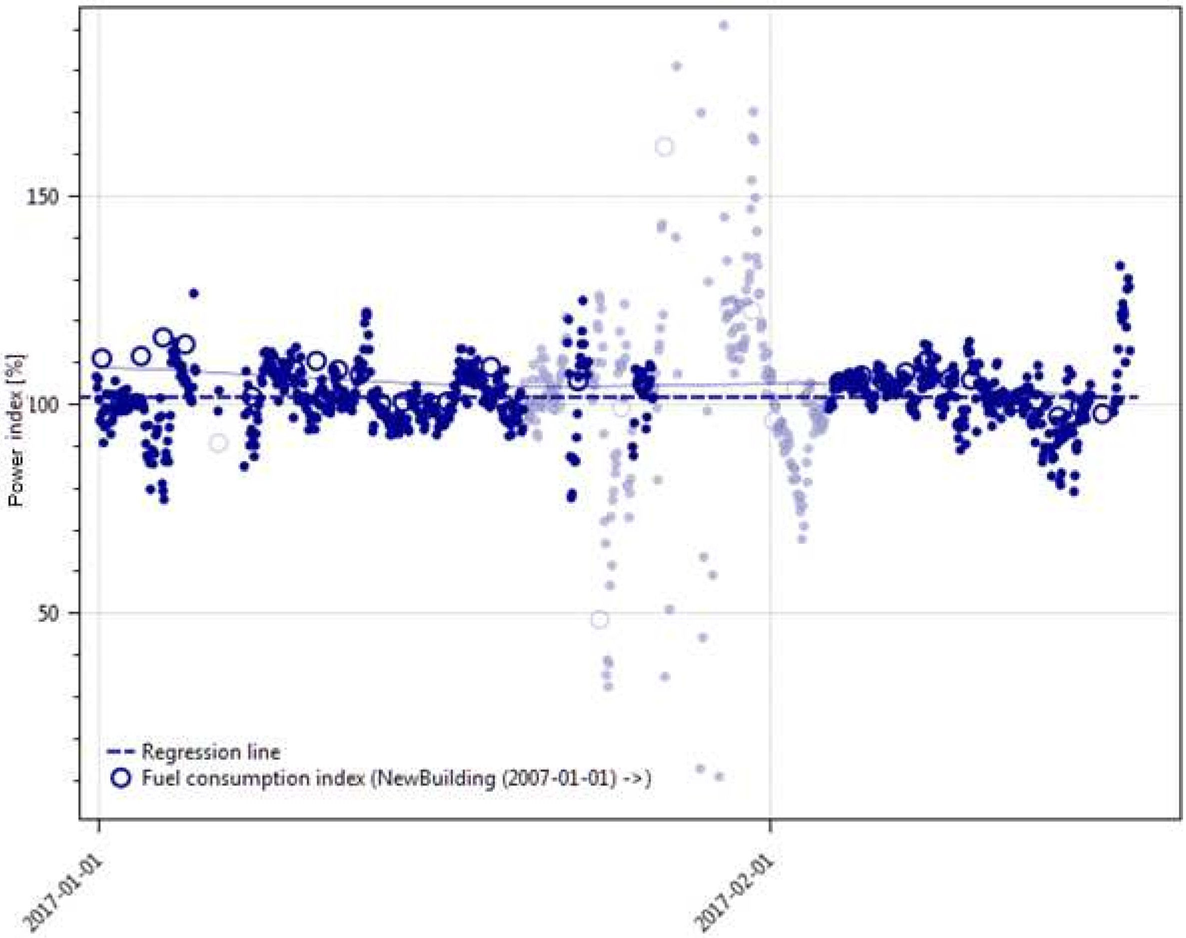

Fig.3: Power index trend analysis. Circles represent noon reports. Dots represent autologged data sets. Greyed out symbols represent data not included in the analysis (see 4. Filtering methods). The regression line has no significant trend. The average level is $\overline{\boldsymbol{PI}} = \mathbf{101.82}\%$ with $\boldsymbol{\sigma} = \mathbf{7.3}\%$ based on 890 data points. Same analysis for only noon reports gives $\overline{\boldsymbol{PI}} = \mathbf{105.4}\%$ with $\boldsymbol{\sigma} = \mathbf{4.8}\%$ based on 31 noon reports.

In this sample the calculated performance using autologged data is close to the expected 100% whereas the calculated performance from noon reports alone is somewhat higher. This tendency is not unique for this sample since our analyses show a general tendency that performance indicators calculated from noon reports on average indicate a poorer performance than performance indicators calculated from autologged data. This bias contradicts the assumption that the performance indicators from noon reports can be viewed as simple averages of the performance indicators from autologged data. σ is about 50% higher than for noon reports alone which on the other hand is much lower than the 400% predicted by the formula above. This contradiction again indicates that in the general case the performance indicator for a noon report is not simply the average of the performance indicators for autologged data. On the contrary, we believe that performance indicators from noon reports are heavily polluted by changes and periods over the day that the analysis will fail to handle. This influence is expected to be less severe for the autologged data which may explain why the scatter for the autologged data in Fig.3 is at a similar level as for the noon reports.

While the benefit of the autologged data is not so much to decrease scatter then we find that the benefit is in the confidence in the obtained analysis. Since σ is an estimate of the distribution of residuals we can have more confidence in the fit based on the larger population (autologged data) even if the scatter is not reduced. The significance of confidence will be discussed in section 6. Interpretation.

4. Filtering methods

As mentioned earlier, the recorded data – whether noon report data or autologged data – is more or less suitable for use in the analysis and it is necessary to filter out some of the data before using it in the performance analysis. The purpose of filtering is to reduce the amount of poor quality data that enter the analysis and affect the confidence of the performance indicators. Evidently, the filtering methods must be based on first principles about what is good quality and what is poor quality data. It is not allowed to define poor quality data as the data that is transformed into a poor performance! In other words, filtering of data based on performance indicators is not allowed. Filtering may only be based on the data fed into the performance analysis.

Some data may clearly be faulty data – outliers - that are in some sense outside the acceptable regions of the data. This could be due to human errors or faulty sensors. These data are filtered out using standard outlier detection methods, *Rousseeuw and Leroy. (1996).*

Other data are not faulty but nevertheless fall outside the range of validity or range of confidence of the mathematical model describing the vessels physics. This is typically the case for high sea state or swell and for very shallow water. The limits for validity are typically determined by the operator of the vessel or the draught of the vessel. Data sets beyond these limits are excluded from the analysis.

The above described filter techniques are equally applicable for noon reports and for autologged data sets and were applied for the data in Fig.3. If only noon reports are available, then they are virtually the only filtering techniques that can be applied. In the presence of autologged data other filtering techniques are available, as the autologged data sets provide so much more information than the mere mean values as was exemplified and discussed in Fig.1. Simply by inspection of the autologged data it is possible to filter out data that are not suitable for analysis.

Since we have an abundance of data we can afford to exclude a lot of data without loss of accuracy. Hence, we apply a method we named “decimation” where for each type of logged signal we exclude the data sets with the least stability. This procedure is repeated until we have decimated the dataset by at least 50%. In this way, we are confident that the most obviously instable data are excluded and only the best and most stable data enter our analysis.

The sample from Fig.3 is displayed in Fig.4 with decimation applied. Now, $\sigma = 5.2\%$ based on 294 data points. In this sample the filtering mechanism reduces scatter significantly (~28%) by reducing analysed data by approximately 67%. If the filtering method was based on irrelevant principles that selected the excluded datasets at random then the scatter would on average not be reduced. If the scatter is systematically reduced by the filtering method then it is a sign that the method is based on relevant criteria. Randomly removing data points would not reduce the scatter.

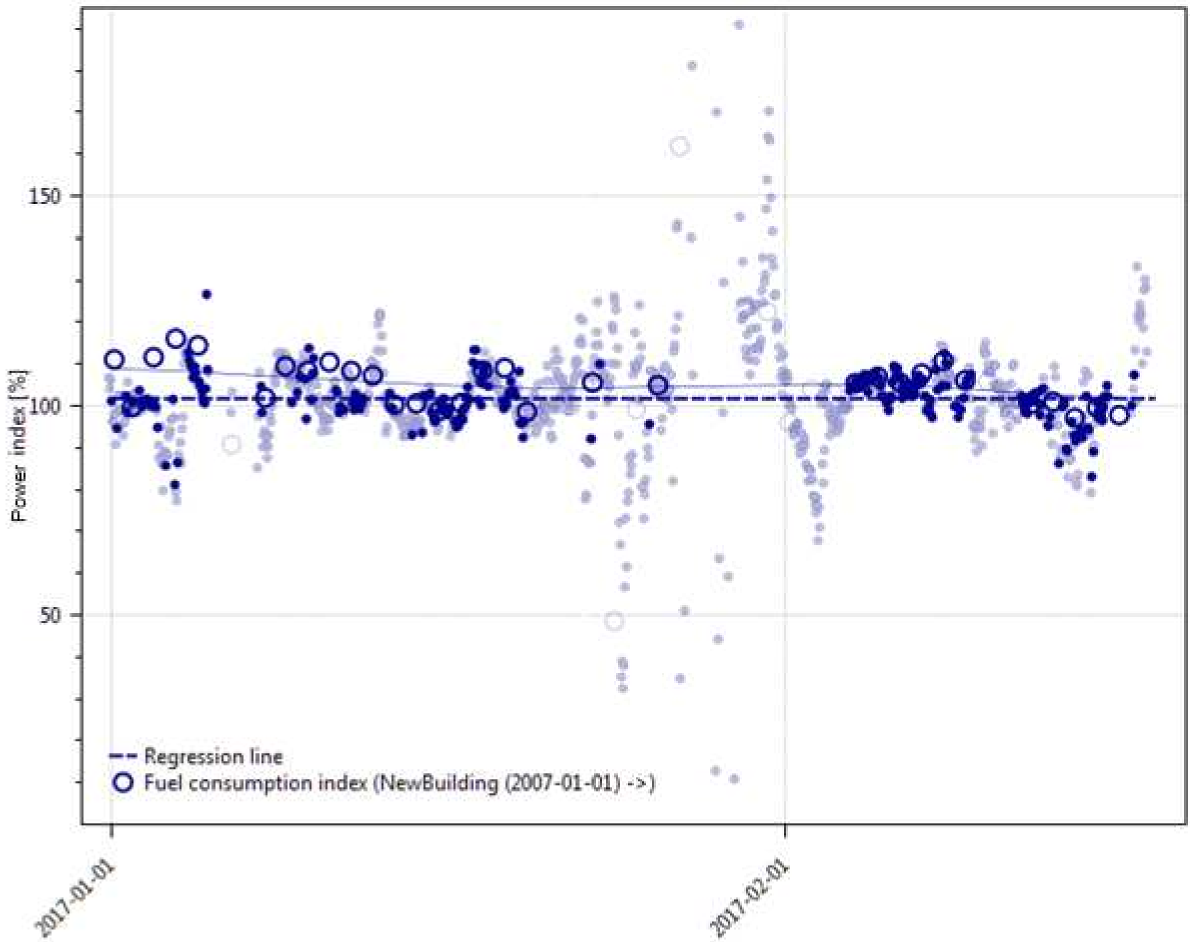

Fig.4: As in Fig.3, but with decimation methods applied. The average level is $\overline{\boldsymbol{PI}} = \mathbf{101.79}\%$ with $\boldsymbol{\sigma} = \mathbf{5.2}\%$ based on 294 data points. Scatter of the data used for analysis is considerably reduced by the decimation procedure and matches the scatter of the noon report data.

5. Meta-analysis

To study the influence of the presence of autologged data on the outcome of the performance analysis we collected the σ values from the analysis of all fifteen vessels with the autologging device installed. The performance analysis provides σ values for all periods of data between hull and/or propeller maintenance giving a total number of 32 σ values. The duration of the analysed periods various a from less than a month to one year. The upper limit of duration of the autologged data is 18 months which is the duration that the first vessel had the device installed. Due to these very different durations, the number of data sets N, used for the calculation of σ values, also varies a lot which causes a large variation in the actual σ values.

Remember that the vessels are very differently equipped providing very different types of datasets. For some vessels, no sensors were available, and we would expect only limited improvement from the autologged data. Some vessels were fully equipped with autologged signals from torsion meters and speed logs, and we should expect better accuracy of the analysis for these vessels.

We compared three different analyses:

- Full analysis with autologged data and advanced filtering (decimation)
- Full analysis with autologged data without advanced filtering (no decimation)
- Analysis based only on noon reports

Fig.5 shows the results from the meta-analysis. On the x-axis is the σ value for each analysis based only on noon reports. On the y-axis is the σ value for analyses based on autologged data. Triangles represent full autologged dataset analyses without decimation and circles represent full autologged dataset with decimation. Points above diagonal have worse scatter than for noon reports alone and below have better scatter than for noon reports alone. Dotted line is the trend line for autologged analysis without decimation. Dashed line is the trend line for autologged analysis with decimation enabled. Tendency is that with decimation the scatter is slightly better than noon reports only and without decimation the scatter is slightly worse than noon reports only. For none of the cases we observe scatter which is as poor as predicted by the formula for σ_{noon} introduced in section 3. Performance analysis method. For most cases the decimation technique improves the scatter. In one case, scatter was reduced by 92%. However, the decimation technique does not improve the scatter for all cases. In 24 of the analyses the scatter was improved by decimation while in 8 cases the scatter got slightly worse by decimation. In all 8 cases the scatter without decimation is already as good as for the noon reports indicating that scatter is already very low. In these cases, the decimation technique will not be better than randomly reducing the dataset and the technique cannot improve the scatter while the reduction of the number of data points lead to a worse estimate of the scatter.

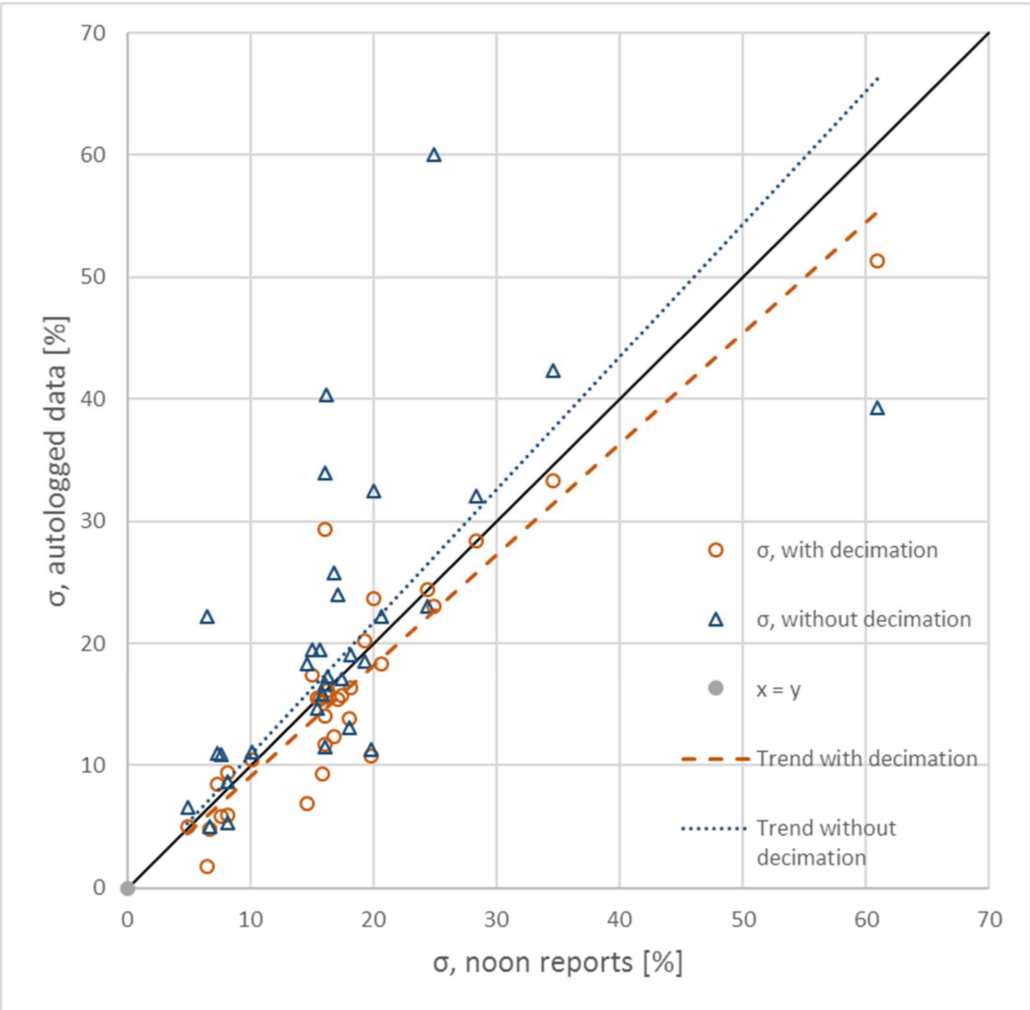

Fig.5: $\boldsymbol{\sigma}$ values from noon reports only analyses compared to $\boldsymbol{\sigma}$ values from analyses including autologged data. Triangles represent analyses with no decimation of data. Circles represent analyses using decimation of autologged data.

6. Interpretation

At this point we conclude that the major contribution from the autologging of data is to radically increase the number of data points for analysis purposes rather than reducing the scatter. Nevertheless, we argue that this is indeed an important achievement in itself as it increases confidence in the analyses.

We will use the sample of data presented in Fig.3 and Fig.4 to illustrate the point. The data is summarized in Table I. The data represent a period of 45 days. What kind of questions can we answer with this sample of data? Remembering that the output from the analyses are estimates of the average performance of the vessel over the period, then a very relevant question is: What is the real value of the performance indicator? If e.g. the vessel had a propeller and hull cleaning just before the auto-logging started, then it is relevant to know if the performance indicator could be at the optimal 100%. Also, if the performance indicator was believed to be 106% before the hull and propeller cleaning, then it is relevant to know if the cleaning caused the expected reduction of the performance indicator.

To answer this kind of questions we will apply statistical hypothesis testing. In this case, it is relevant to apply a simple *t*-test , https://en.wikipedia.org/wiki/Statistical_hypothesis_testing. (For the t-test to be strictly applicable the stochastic variables – in this case the PI - should be statistically independent and should belong to a normal distribution. These criteria have not been rigorously tested in this study. Presumably, the independence criteria is violated. Hence, the results of the test should be considered as informational and not conclusive) The null hypothesis we will test is:

$$H_0\colon PI_{real} = \gamma$$

PI_{real} is understood as the actual underlying mean value of the probability distribution of performance indicators. γ is the value we wish to have tested for. Statistical hypothesis testing verifies (accepts) or falsifies (rejects) the hypothesis by answering the question: Is the data sample consistent with PI_{real} being equal to the value γ? In other words: How likely is our observed $\overline{PI}$ given the null hypothesis? If it is very unlikely we must reject the hypothesis.

The alternative hypothesis – which must be accepted if H_0 is rejected – is:

$$H_1\colon PI_{real} \neq \gamma$$

For hypothesis testing we select a confidence level, α. In this case, we have selected the value $\alpha = 99.9\%$. Thus, we reject the null hypothesis, H_0, in case the data we have would only occur in 0.1% of datasets consistent with the null hypothesis. Hence, if we reject H_0 then we can with very high confidence accept the alternative hypothesis H_1.

In Table II**:**, the result of applying the hypothesis testing is presented for the different analyses and for different values of γ. Green cells indicate that the null hypothesis was accepted, and red cells that the null hypothesis was rejected. The green cells roughly correspond to what is known as the “confidence intervals” for the PI_{real}.

We observe that all three types of analysis reject that $PI_{real} = 100\%$. Since the average level for the performance indicators from noon reports is ~105% this is not surprising. On the other hand, it is very convincing that the two other methods can also rule out $PI_{real} = 100\%$ as these methods come out with an average level of only ~102% with a standard deviation of more than 5%. It shows that despite the similar standard deviations it is possible to resolve questions at a much more detailed level when more data is available.

More interestingly, Table II**:** shows that the autologging data clearly rejects that $PI_{real} = 106\%$ whereas the pure noon report data cannot reject it. Hence, in this example the noon reports alone would not be able to resolve the question whether the performance had improved from the 106% after the docking.

The most striking in Table II**:** is that hypothesis $PI_{real} = 102\%$ is rejected by the noon report data while it is accepted by the autologged data. Hence, with high confidence the noon report data rejects that the performance is at the level that the two autologged methods accept. This contradiction indicates that the PI calculated from noon reports do not have the same underlying stochastic mechanisms causing the scatter as for the autologged data. This is consistent with the argument that the averages reported during the time of the noon report do not reflect stable conditions and as such are not appropriate for the performance analysis which requires steady state conditions. This agrees with our previous observation that performance analyses based purely on noon report data tend to exaggerate the performance deterioration.

Table I: Summary of analysis output from data presented in Fig.3 and Fig.4

	Average level	Estimated σ	Population, N
Noon reports only	105.35%	4.8%	31
Autologged data, no decimation	101.82%	7.3%	890
Autologged data, with decimation	101.79%	5.2%	294

Table II: Test of the null hypothesis, $\boldsymbol{H_0}$, for different values of $\boldsymbol{\gamma}$. Red cells indicate $\boldsymbol{H_0}$ was rejected, and green cells indicate $\boldsymbol{H_0}$ was accepted.

Γ	100%	102%	104%	106%	108%	110%
Noon reports only						
Autologged data, no decimation						
Autologged data, with decimation						

What this sample illustrates is that although the set of performance indicators from noon reports show the lowest σ then the performance indicators from autologged data facilitate stricter conclusions about the actual performance and even contradicts the conclusions from noon reports. Evidently, this example is not representative of all cases, but we find it probable that the increased population of data and the increased population of high quality data from autologging in general will provide stricter conclusions and higher confidence in the performance analysis output.

7. Conclusion

We have demonstrated that the presence of data collected by a simple “plug and play” device can supplement noon report data and enhance the quality of the performance analysis. We observed a bias towards worse performance when comparing performance indicators based on noon reports data with those based on autologged data. Hence, a performance analysis based purely on noon report data tend to exaggerate the deterioration of performance of the vessel. Performance analysis based on autologged data basically produce a fairer view of the actual performance of the vessel.

We conjectured that the scatter in performance indicators should increase with the frequency of the automatically logged data. Analysis of the collected data does indeed show an increase but the increase is consistently lower than predicted. We argued that both this discrepancy and the bias of noon report based analyses are due to the intrinsically better quality of the higher frequency data in contrast to the noon report data which for many cases is an average covering varying conditions that cannot be captured and compensated for in the analysis.
A method for selecting the most suitable and reliable datasets was presented. The method utilizes the

metadata collected by the device. Application of this technique can reduce the scatter significantly.

Finally, it is demonstrated how the increased amount of data provided by the automatic logging device improves confidence in the analysis and enables more strict conclusions about the performance of the vessel.

Acknowledgements

This project is partly funded by the Danish government through the performance contract program managed by "Styrelsen for Forskning og Innovation".

References

BECKERLEE, J. (2016), *Ship Performance Monitoring and Analysis,* Master Thesis, Technical University of Denmark, Lyngby

BEIERSDORF, C. (2017), *4 reasons why autologging is not the solution to onboard data collection*, http://blogs.dnvgl.com/performance/4-reasons-autologging-not-solution-onboard-data-collection/

GOUGOULIDIS, G.; VASILEIADIS, N. (2015), *An overview of hydrodynamic energy efficiency improvement measures,* 5th Symp. Ship Operations Management & Economics, Athens

IMO (2012), *Resolution MEPC 213(63)*, Int. Mar. Org., London

ISO 19030, *Ships and marine technology -- Measurement of changes in hull and propeller performance*, ISO, Geneva

ITTC (2005), *Analysis of Speed/Power Trial Data*, Recommended Procedure 7.5-04-01-01.2

ITTC (2011), *1978 ITTC Performance Prediction Method*, Recommended Procedure 7.5-02-03-01.4

KARIRANTA, R.J. (2014), *Integrating performance monitoring and other onboard software*, 13th COMPIT Conf., Redworth

LARSEN, N.L.; SIMONSEN, C.D.; NIELSEN, C.K.; HOLM, C.R. (2012), *Understanding the physics of trim*, 9th Green Ship Technology Conf., Copenhagen

PEDERSEN, B.J. (2014), *Data-driven Vessel Performance Monitoring*, PhD Thesis, Technical University of Denmark, Lyngby, DCAMM Special Report No. S180.

POLITIS, G. (2004), *Modern unconventional propulsion systems for energy efficiency*, NTUA course notes, Athens

ROUSSEEUW, P.; LEROY, A. (1996), *Robust Regression and Outlier Detection*, John Wiley & Sons

SCHNEEKLUTH, H.; BERTRAM, V. (1998), *Ship Design for Efficiency and Economy*, Butterworth-Heinemann

Numerical and Experimental Investigation of Roughness Due to Different Type of Coating

Anders Östman, SINTEF Ocean[1], Trondheim/Norway, anders.ostman@sintef.no
Kourosh Koushan, SINTEF Ocean[1], Trondheim/Norway, Kourosh.Koushan@sintef.no
Luca Savio, SINTEF Ocean[1], Trondheim/Norway, luca.savio@sintef.no

[1] Formerly MARINTEK

Abstract

Effect of roughness on frictional resistance is investigated experimentally and numerically. Resistance tests are performed with several plates coated with different paints, which have different roughness. Front plate is 4 m long and aft plates are 6 m long resulting in a total hydrodynamic length of 10 m. Tests are conducted at different speeds up to 9 m/s covering a large range of Reynolds numbers. Numerical calculation of frictional resistance is performed for the same roughness as tested in the towing tank. Special wall function and numerical procedure is implemented for this purpose. Plates are 3D scanned and their roughness is categorized by several parameters, not only traditional roughness height. Numerical and experimental results are compared and discussed.

1. Introduction

Resistance due to fouling and poorly applied antifouling coating can have a significant contribution to the total resistance of a ship. This is especially true for ships operating at low Froude numbers, where skin friction resistance is the dominating component of the hydrodynamic resistance and could account for 60% or more of the total resistance. The present study is part of the BYEFOULING project, which was initiated within the European Union's Seventh Framework Programme. The main objective of the project is to find effective and environmentally friendly antifouling coatings for maritime applications. A part of the project is also to study the skin friction drag due to the applied antifouling coating. The work presented in the present paper is part of that sub-task.

An experimental test program was previously performed in the SINTEF Ocean (formerly MARINTEK) towing tank facilities, *Savio et al. (2015)*. Flat plates with various surface roughness were towed at constant speed. The roughness levels of the different plates were related to typical real applications processes used in the marine industry. The final quality and finish of the coated surface depends on the underlying surface preparation prior to applying the coating.

The most common numerical approach to model flow over rough surfaces is to modify the wall function formulation used for flow over smooth solid walls, by introducing the downward shift in the velocity profile that occurs in the boundary layer in vicinity to the rough surface. The model used in engineering applications are usually based roughness functions which originates from *Nikuradse (1933)* pipe flow experiments with roughness due to sand grain of various sizing. Appropriate equivalent roughness heights are then identified which matches the skin friction drag found in the Nikuradse experiments. This approach was recently used by *Vargas and Shan (2016)*, who implemented a modified k-ω turbulence model formulation based on work done by *Durbin et al. (2000)*. The model is based on experimentally estimates of the equivalent sand grain height. Vargas and Shan received good comparison against experiments for flat plate flow in fully rough flow regime. *Demirel et al. (2014)* instead used a Colebrook-type roughness function with an experimentally estimated roughness height that fits the Colebrook roughness function of *Grigson (1992)*.

In the present paper, an alternative, and more direct approach, is implemented in a customized wall function in the OpenFOAM simpleFOAM flow solver. Instead of trying to find a formulation for the roughness that matches Nikuradse or Colebrook experimental results, the roughness function is directly found based on the towing tank experiments. A logarithmic curve fit is found that describes the velocity shift in the logarithmic region of the boundary layer. The customized roughness function in the flow solver is directly based on the given expression for the velocity shift.

2. Experimental setup and results

The experimental test program was conducted in the SINTEF Ocean (formerly MARINTEK) towing tank facilities, *Savio et al. (2015)*. Flat plates with various surface roughness were towed at constant speed while resistance was recorded. The roughness on the plates was due to paint applied on the surface of the plates with various quality of application process. Three roughness levels (denoted A, B and C with increasing order of roughness) were considered. Roughness level A represents an optimal new build or full blast dry docking application of the paint. Roughness level B corresponds to dry dock situation with some underlying spot repair roughness and poor coating application of the paint. Finally, the plate with the most severe roughness was denoted level C, which could simulate an extreme case with severe underlying roughness accumulated from several dry dockings and very poor application of the paint. In addition, a set of smooth blank plates were used in order to have a reference to the theoretical smooth boundary layer friction drag.

The plates were towed in pairs, with one plate in front with a length of 4m and one plate behind with a length of 6 m, Fig.1. The plates were mounted with a gap of about 3 to 5mm between the plates. The front plate was of roughness level A during all runs. Different plates were considered in the aft in order to investigate the skin friction resistance for all roughness levels (A, B and C). The drag was recorded on each plate (both front and aft) independently. However, in the following analysis, only the measurement on the aft plate is considered. The purpose of front plate is to develop a boundary layer profile as inlet condition to the aft plate and to avoid undesired stagnation and minor wave making effects of front edge on the measurement of main plate. By doing this way, the drag recorded on the aft plate is less sensitive to boundary layer transition from laminar to turbulent, which will occur on the front plate.

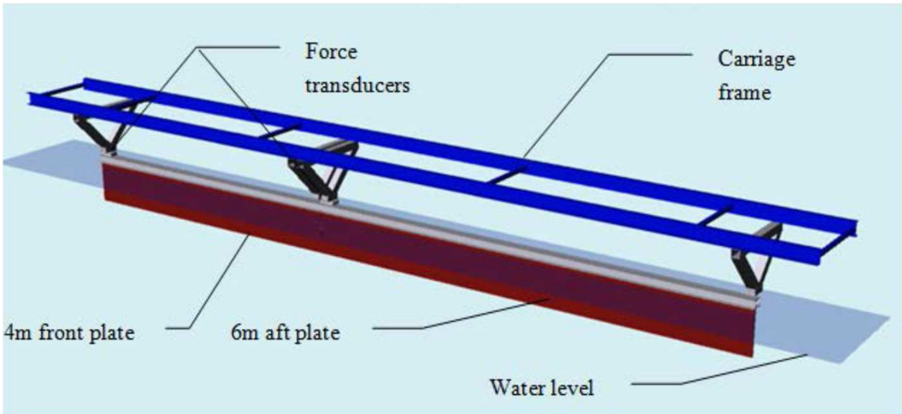

Fig.1: Setup of the plates under the carriage, from *Savio et al. (2015)*

The plates were towed at speeds ranging from 3 m/s to 9 m/s. The resulting friction drag coefficient on the aft plate is presented in Fig.2. The frictional drag coefficient is defined by:

$$C_F = \frac{F}{\frac{1}{2}\rho V^2 A}$$

F is the measured drag, V the towing velocity and A the wetted area, which is twice the submerged area of the plate.

As part of the post processing procedure, the value of the measured drag has been shifted such that the measurements of the blank plate matches the theoretical Schoenherr friction line. For details of the post-processing method, see *Savio et al. (2015)*.

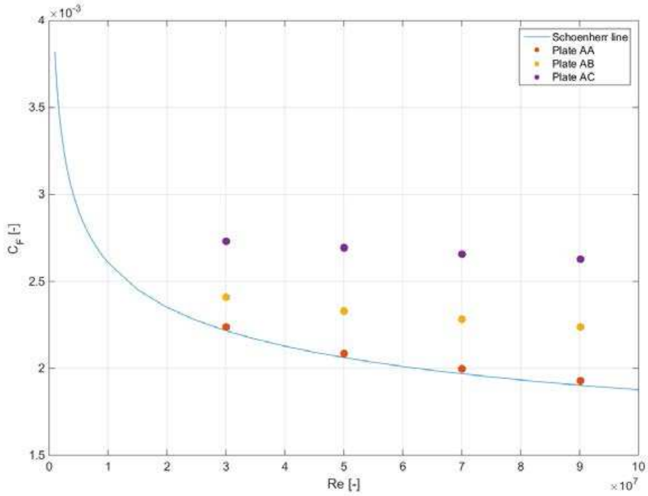

Fig.2: Friction drag coefficient of the aft plate, from *Savio et al. (2015)*

The measured drag was further post-processed following methods proposed by *Granville (1987)* and presented in terms of inner variables, Fig.4. The graph shows the shift ΔU^+ of the velocity profile in the logarithmic part of the boundary layer as a function of the non-dimensional roughness height, k^+, where k^+ is defined by $k^+ = kU_\tau/\nu$. The height, k [m] is a typical roughness height of the rough surface, U_τ is the friction velocity and ν is the fluid kinematic viscosity. The variable, k^+, can be interpreted as a local Reynolds number for the surface roughness in the boundary layer. The value of typical roughness height, *k,* is found from a statistical analysis of the actual rough surface, and defined as the rms (root mean square) of absolute heights of the surface. In the experimental procedure, a high-resolution laser scanning of imprints of the surface was conducted. The surfaces of the various plates can be characterized by means of the statistics of the surface found from the laser scans. In the following *Sq* is used to denote the root mean square of absolute heights of the surface. The skewness is denoted *Ssk* and describes the asymmetry of roughness deviations from the mean plane. The measured rms roughness height and skewness of the plates is presented in Table I:. Visualizations of the surface from the laser scan is shown in Fig.3.

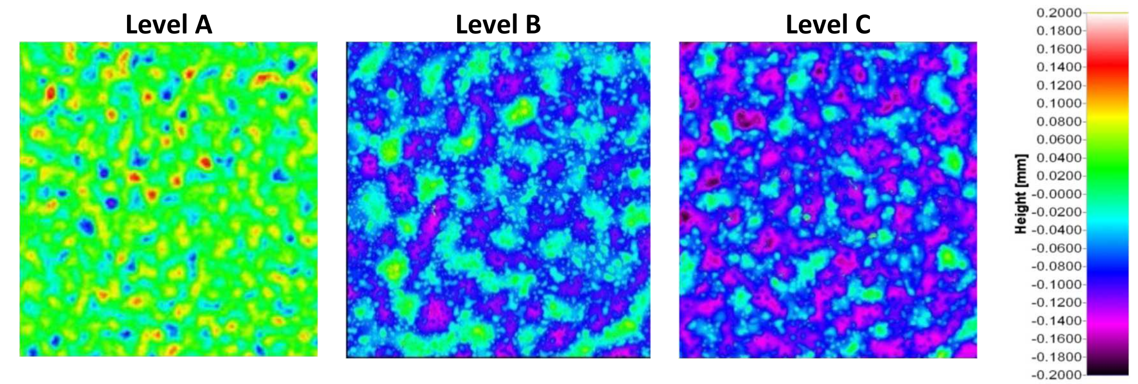

Fig.3: Visualization of surface scans of the plates

Fig.4 shows the results in terms of inner variable along with the data from Nikuradse sand for reference. Note that the parameter k^+ is dependent on which statistical parameter is used to describe the surface roughness and hence to same extent on the surface scanning technique; therefore, care should be used when comparing results that are relative to experiments carried out using different methods of measuring roughness. In fact, changing roughness parameter results in shifting the curves along the x-axis, making relative comparison of experiments obtained with different scanning techniques hardly valid. On the other hand, slopes can be compared, to check whether the tests have been carried either smooth, transitional or fully rough regime; this last fact allows for collapsing the experimental curves on the Nikuradse curve and introduce an equivalent sand roughness k_s. We show in this paper how that can be avoided when the results from model scale are to be used in CFD.

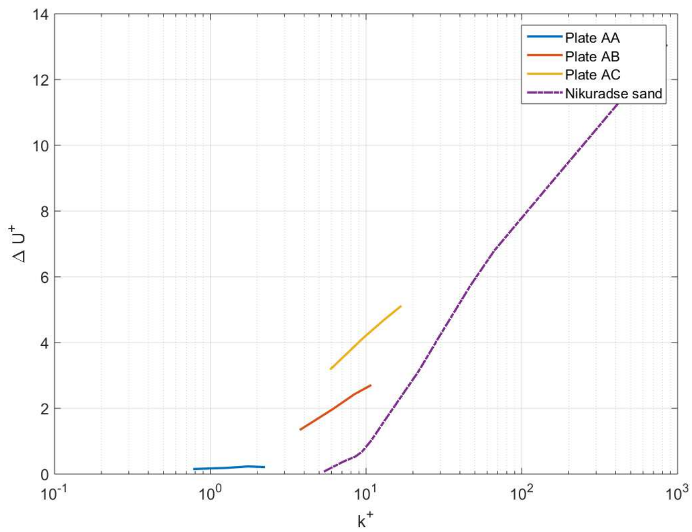

Fig.4: Presentation of the experimental data in terms of inner variables

Table I: Measured root mean square of absolute heights of the surface (*Sq*) and skewness (*Ssk*) of the surface roughness of the plates

Plate	***Sq[µm]***	***Ssk[-]***
PlateA	8.51	-0.14
PlateB	41.15	0.65
PlateC	64.44	0.43

3. Formulation of wall functions for smooth and rough surfaces

The most common method to resolve turbulent boundary layer flow in a CFD simulation is to apply a wall function formulation of the turbulence model. Wall functions rely on the fact that the boundary layer velocity profile has a logarithmic behavior within the log law region of the boundary layer, illustrated in Fig.5.

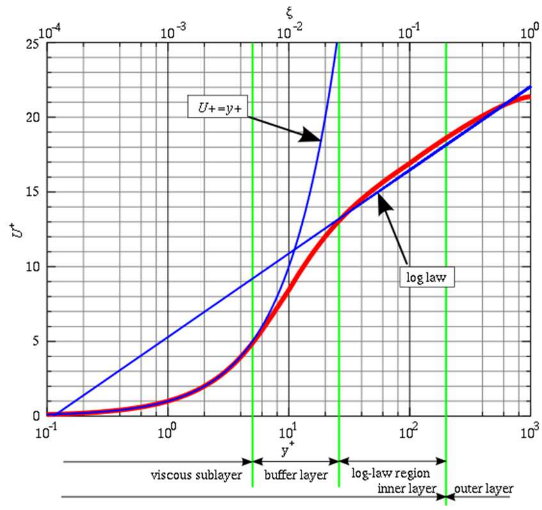

Fig.5: Boundary layer velocity profile plotted against a logarithmic scale of the non-dimensional wall distance coordinate y^+

The velocity profile in the log law region is described by the equation

$$U^+ = \frac{1}{\kappa}\ln(E\,y^+) \tag{1}$$

κ=0.41 is the von Karman constant and E is a constant which equals 9.8 for smooth walls. For rough walls the velocity profile is switched downward in the logarithmic region. This can mathematically be expressed by substituting E with a modified variable E' defined as

$$E' = \frac{E}{f} \tag{2}$$

f is the roughness function ($f=1$ for smooth walls). Usually, the effect of roughness in terms of downward shift of the velocity profile, is related to experiments performed by Nikuradse on additional drag in pipes coated with various size of sand grains. The flow over rough surfaces can be divided into three flow regimes: (i) *smooth*, for $k^+ \leq k^+_{smooth}$, (ii) *transitional region* when $k^+_{smooth} \leq k^+ \leq k^+_{rough}$ and (iii) *fully rough* for $k^+ > k^+_{rough}$. Commonly used values for k^+_{smooth} and k^+_{rough} are $k^+_{smooth} = 2.25$ and $k^+_{rough} = 90$. *Ioselevich and Pilipenko (1974)* found an analytical fit to the *Nikuradse (1933)* data. The fit is also presented in *Cebeci and Bradshaw (1977)*. The default roughness function implemented in OpenFOAM is based on this theory and reads:

$$\begin{aligned}
f &= 1 && \text{for} \quad k^+ \leq 2.25 \\
f &= \left[\frac{k^+ - 2.25}{87.75} + C_s k^+\right]^{\sin(0.4258\, ln(k^+) - 0.811)} && \text{for} \quad 2.25 < k^+ < 90 \\
f &= 1.0 + C_s k^+ && \text{for} \quad k^+ \geq 90
\end{aligned} \tag{3}$$

The constant C_s is normally chosen as 0.253 or 0.5. Note that the formula refers to the sand grain roughness as used in the Nikuradse experiments. The approach to use the formula is normally to relate the measured height of the actual roughness of interest to a sand grain height of the Nikuradse experiments that gives the best match in terms of roughness drag. This match must be done based on experimental results on the actual surface of interest and comparing the results against Nikuradse friction drag. The sand grain that best matches is called equivalent sand grain height, usually denoted k_s. *Flack and Schultz (2010)* compared several experimental results against Nikuradse and found an expression for k_s based on statistical parameters of the rough surface. The authors found that the root means square of the roughness heights (k_{rms}) and skewness of the roughness surface elevation probability density function (s_k) could be used to find a fit to k_s:

$$k_s \approx 4.43\, k_{rms}(1 + s_k)^{1.37} \tag{4}$$

The typical roughness heights used in this correlation are significantly larger than the typical roughness of paint coating roughness. Most surfaces tested had typical heights larger than 100 µm. The flow regime of these surfaces is believed to be in the fully rough region. In addition, the fit is biased towards best fitting the experiments with the largest surface roughness. It will therefore not be surprising if the fit as proposed in Eq. (3) is unsuitable for the paint coating in the present study.

It is strictly not necessary to relate the roughness to an equivalent sand grain roughness height. Instead, the roughness function f can be found directly based on experimental results of the velocity shift (ΔU^+). The procedure on how to estimate f directly from measurements are described in the following. Inserting the expression given in Eq. (2) into Eq. (1) gives:

$$U^+ = \frac{1}{\kappa}\ln\left(\frac{E}{f}\, y^+\right) = \frac{1}{\kappa}\ln(E\, y^+) - \frac{1}{\kappa}\ln(f\, y^+) \tag{5}$$

The last term in the equation is the velocity shift, ΔU^+

$$\Delta U^{+} = \frac{1}{\kappa}\ln(f\, y^{+}) \tag{6}$$

ΔU^+ is defined to be positive when the velocity profile is shifted downwards. The roughness function f can now be found directly from Eq. (6):

$$f = e^{(\kappa\, \Delta U^{+})} \tag{7}$$

The experimental results for the velocity shift are presented in Fig.4 as a function of k^+. It is evident that a logarithmic fit can be found for each plate. An expression of the velocity shift can be formulated as:

$$\Delta U^{+} = a_0 + a_1 \log_{10}(k^{+}) \tag{8}$$

where a_0 and a_1 are constants of the curve fit. The best fit for different plates are shown in Fig.6.

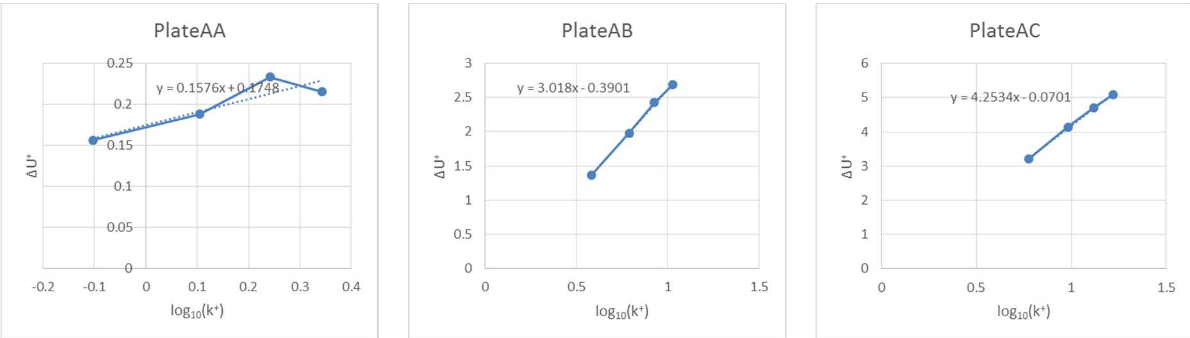

Fig.6: Curve fit of measured velocity shift for the plates

4. CFD setup

The problem is simplified in the CFD analysis by neglecting wave generation and end-effects of the towed plates. This is one by solving the equations for a mono-fluid flow field in a 2D dimensional flow domain. The flow solver that is used is the simpleFOAM flow solver that is included in the OpenFOAM CFD package. The solver solves the steady-state fluid flow using the SIMPLE algorithm, *Ferziger and Peric (2002)*. The k-omega SST turbulence model is used to model turbulence in the flow field. The freestream turbulence level is very low in the towing tank during experiments since each new run starts after waiting sufficiently long for the flow to come at rest. In the simulations the turbulence intensity is set to 0.1% and the turbulent length scale to 1 mm. This gives a turbulent viscosity ratio ν_{turb}/ν of about 10 in the freestream, which is considered to be very low.

The flow over the rough surfaces is modeled by means of modifying the smooth wall function as described in the previous section. Simulation are performed using both the default OpenFOAM implementation of the roughness function, Eq.(3), and the "direct roughness formulation" in Eq.(7). A customized rough wall function was implemented in OpenFOAM based on Eq. (7) and Eq.(8) where the coefficients a_0 and a_1 in Eq.(8) are found from the curve fit shown in Fig.6.

Separate meshes were generated for each speed using a blockMesh script. blockMesh is the simple mesh generator that comes with OpenFOAM and is easy to script for simple geometries. The meshes were generated with a target for the near wall mesh spacing that results in $y^+ \approx 60$ for the cell center of the wall adjacent cells. An illustration of the mesh and flow domain is shown in Fig.7. The boundary conditions are also indicated in the figure, with velocity inlet at the upstream boundary, pressure outlet downstream and slip wall at the far field side. The boundary condition for the forward and aft plates is no slip walls (with or without wall roughness depending on the simulated case).

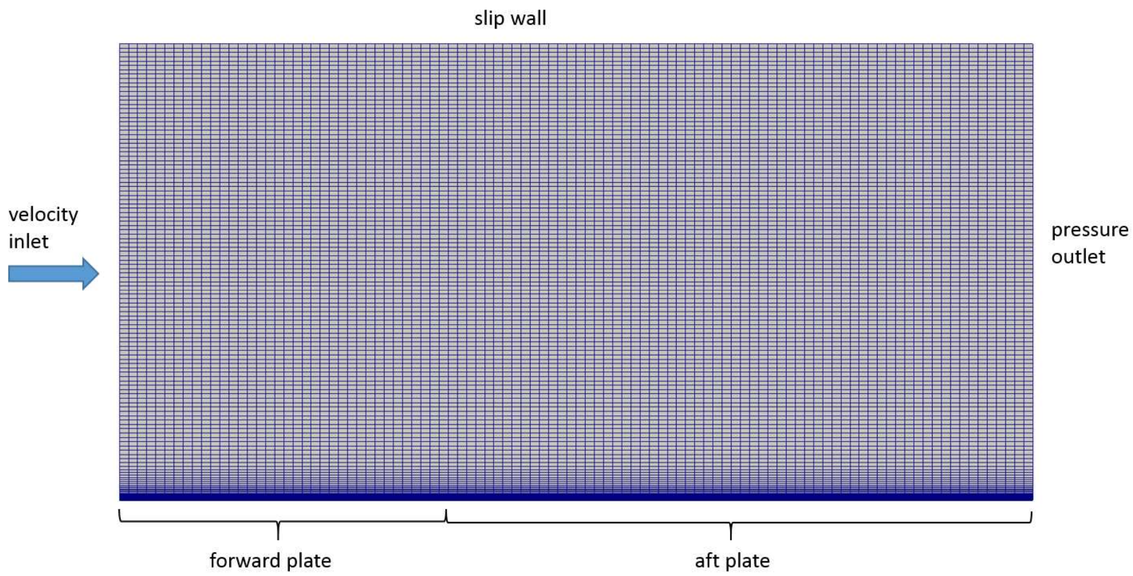

Fig.7: Mesh in the flow domain and boundary conditions

5. CFD simulation results

The simulations were performed for the same speeds as tested in the towing tank, U=3, 5, 7 and 9m/s. Two different approaches for modeling the roughness were studied. Simulations using the "direct roughness function" formulation, Eq.(7), was compared against more standard engineering approaches using the default roughness function implemented in OpenFOAM, Eq.(3), where the value for the roughness height is found from engineering considerations.

The simulations using the "direct roughness function" formulation, Eq. (7), are presented in Fig.8. The computed skin friction resistance coefficient is compared against the resistance coefficient found experimentally from the towing tests. The comparison against experiments is very good for PlateAB and PlateAC (the comparison is especially good for PlateAB). For PlateAC the resistance is slightly higher than experiments for the lowest and heights speeds. The simulated resistance of PlateAA is consistently smaller than the experimental results, but still very close.

Fig.9 compares the results using the direct roughness function against standard roughness formulations, which are usually used in engineering applications. The simulation was performed using the Ioselevich&Pilipenko roughness function formulation, Eq.(3). This is the default roughness function implemented in OpenFOAM. The roughness heights are selected in two different ways: The simplest method is by choosing the value for the roughness height to be equal to the root mean square of the measured roughness heights of the surface ($k=Sq$). This choice is compared against the Flack and Schultz proposal for the equivalent roughness height, Eq.(4), where $k_{rms}=Sq$ and $s_k=Ssk$ is used to compute the equivalent sand grain height k_s which is used as the value for the roughness height in Eq.(3). The value for the constant C_s in Eq.(3) is chosen as 0.253. Computations using the Flack and Schultz proposal for the roughness height results in a considerable overestimation of the skin friction resistance except for the smoothest plate (PlateAA), where the resistance is slightly lower than experiments for the lowest speeds and slightly higher than experiments for the highest speeds. The choice $k=Sq$ results in a significantly smaller resistance than experiments for all plates except for the smoothest plate, where the simulated results are almost identical to the results using the direct roughness function formulation.

The results using the direct roughness function are very promising. In the present study, separate curve fits were made for each plate with different level of roughness. For practical and engineering purposes, it is tempting to find a function that matches the velocity shift ΔU^+ in one single expression, which is valid for all surfaces where the roughness is related to paint coating on hull surfaces. *Savio et* *al. (2015)* found indications that such an expression could be obtained, where ΔU^+ depends on both k^+ and *Sq*. However, more experimental tests are necessary, before the hypothesis that such an expression exist can be confirmed.

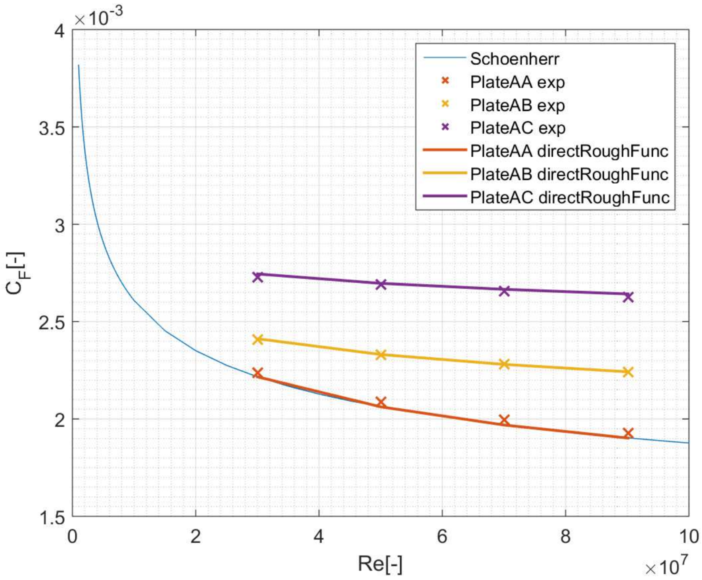

Fig.8: Skin friction resistance coefficient. Comparison of CFD results using the direct roughness function formulation Eq.(7) against experimental results.

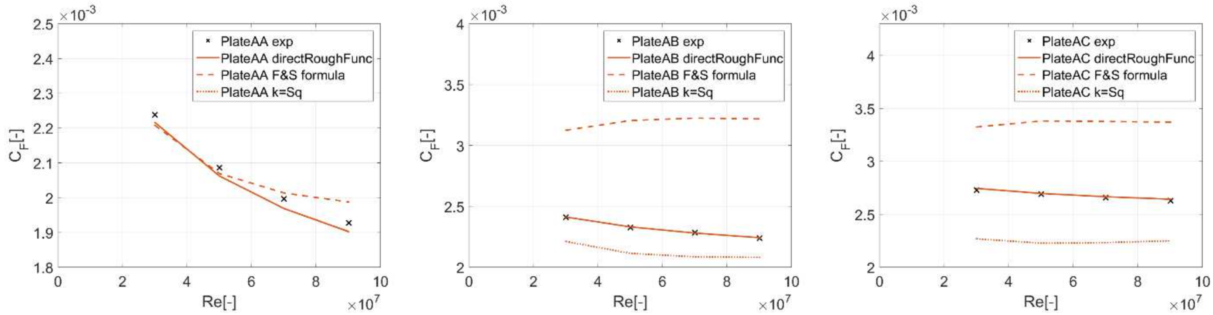

a) PlateAA b) PlateAB c) PlateAC

Fig.9: Skin friction resistance coefficient of the plates. Comparison of experimental results against CFD simulations using (i) the direct roughness function formulation Eq.(7), (ii) the formula for equivalent sand grain height proposed by Flack and Schultz and (iii) using *k=Sq* for the roughness height. Both (ii) and (iii) use the standard roughness formulation implemented in OpenFOAM, Eq.(3), where C_s=0.253.

6. Conclusions

In the present paper, a technique to apply directly results from model scale experiments on rough plate to CFD has been presented. The technique does not require defining an equivalent sand grain height to be then used to match a statistical regression of data obtained in the experiments from Nikuradse, which date back almost 100 years. The method proved to be working and therefore the idea promising; however, the next challenge is how to extend the technique to predict the effect of roughness in full scale starting from model scale data.

Acknowledgements

This work has been supported by the EU FP7 Project "Low-toxic cost-efficient environment-friendly antifouling materials" (BYEFOULING) under Grant Agreement no. 612717.

References

CEBECI, T.; BRADSHAW, P. (1977), *Momentum Transfer in Boundary Layers*, Hemisphere Publishing/McGraw-Hill, pp.176-180

DEMIREL, Y.K.; KHORASANCHI, M.; TURAN, O.; INCECIK, A. (2014), *A CFD model for the frictional resistance prediction for antifouling coatings*, Ocean Eng. 89, pp.21-31

DURBIN, P.A.; MEDIC, G.; SEO, J.M.; EATON, J.K.; SONG, S. (2000), *Rough wall modification of two-layer k-ε*, J. Fluids Eng. 123, pp.16-21

FERZIGER, J. H.; PERIC, M. (2002), *Computational Methods for Fluid Dynamics*, Springer

FLACK, K.A.; SCHULTZ, M.P. (2010), *Review of hydraulic roughness scales in the fully rough regime*, ASME J. Fluids Eng. 132/4, pp.041203-1–041203-10

GRANVILLE, P.S. (1987), *Three indirect methods for the drag characterization of arbitrarily rough surfaces on flat plates*, J. Ship Research 31, pp.70-77

GRIGSON, C.W.B. (1992), *Drag losses of new ships caused by hull finish*, J. Ship Research 36, pp.182-196

IOSELEVICH, V.A.; PILIPENKO, V.N. (1974), *Logarithmic velocity profile for flow of a weak polymer solution near a rough surface*, Soviet Physics Doklady 18, p.790

NIKURADSE, J. (1933), *Laws of flow in rough pipes*, NACA Technical Memorandum 1292

SAVIO, L.; BERGE, B.O.; KOUSHAN, K.; AXELSSON, M. (2015), *Measurements of added resistance due to increased roughness on flat plates*, 4th Int. Conf. Advanced Model Measurement Technology for the Maritime Industry, Istanbul

VARGAS, A.; SHAN, H. (2016), *A numerical approach for modeling roughness for marine applications*, ASME 2016 Fluids Eng. Division Summer Meeting, Washington

Vessel Performance Model and its Utilization in Shipping Company

Ryo Kakuta, Monohakobi Technology Institute, Tokyo/Japan, ryo_kakuta@monohakobi.com
Hideyuki Ando, Monohakobi Technology Institute, Tokyo/Japan, hideyuki_ando@monohakobi.com
Takashi Yonezawa, Monohakobi Technology Institute, Tokyo/Japan, takashi_yonezawa@monohakobi.com

Abstract

This paper presents how shipping company build vessel performance model and utilize it for improving its business. For shipping company, understanding vessel performance in actual service condition is crucial, because vessels are not always navigating in calm sea and fixed loading condition. To understand vessel performance in service, NYK/MTI has developed vessel performance model based on ship design information and collected data by VPMS (Vessel Performance Management System). Developed model has been utilized in several cases and showed its effectiveness on improving business performance of shipping company.

1. Introduction

The concern over IoT and big data utilization has risen in any industries. For example, digital twin is regarded as best way of utilizing IoT and big data. General Electric develops virtual simulation model of wind turbine as a digital twin and use it for optimization of wind turbine operation and maintenance. Data from IoT sensors on the turbine is used for developing digital twin and optimization. Same concept can be applied to any physical assets with sensors and IoT.

In the field of maritime business, shipping companies has started to utilize the data from vessel performance management system (VPMS) over the few years. Main reason for the spread of VPMS is increased interest in fuel and cost saving. In order to save fuel consumption, each shipping company tries to utilize it in different ways, but most of them do not focus on development of digital twin.

Obtaining the accurate picture of own fleet performance is important task of shipping company for managing operational cost and improving business performance. Digital twin for estimating vessel performance is expected to be most beneficial application of VPMS for optimizing operation in actual service. Based on the above understanding, NYK/MTI has started developing vessel performance model as digital twin based on collected data from VPMS since 2012. In this paper, how NYK/MTI builds vessel performance model and utilize it for improving their business.

2. Vessel performance management system

2.1. VPMS (Vessel Performance Management System)

VPMS (Vessel Performance Management System) is system for supporting vessel performance management. Recently, installation of VPMS has attracted some ship operators or charterers who would like to save fuel consumption and manage their fleet. In general, VPMS consists of two systems, auto-logging system on board and data viewer or dashboard for shore office. Auto-logging system collects vessel performance data and sends it to shore data server. VPMS users at shore office monitor the collected data or analysis result by using of data viewer or dashboard.

From a shipping company's point of view, clear understanding of vessel performance in service is one of the most expected fields of utilizing data collected from VPMS. Speed trial result or charter party performance do not give enough information for estimating actual fuel consumption, because vessels are not always operated in calm sea and design draft condition. Most of existing VPMS do not focus on vessel performance model and its utilization, but dashboard for visualizing voyage or trim optimization.

2.2. SIMS (Ship Information Management System)

SIMS (Ship Information Management System) is one of VPMS developed by NYK and MTI, *Ando et al. (2009)*. Fig.1 shows the overview of SIMS. SIMS collects data from onboard equipment such as VDR (Voyage Data Recorder) and AMS (Alarm Monitoring System). Collected data is processed in onboard computer and sent to shore server via vessel's satellite communication. The data output from SIMS is basically statistical data, such as average, maximum, minimum and standard deviation. Time interval of data processing in SIMS onboard unit is normally one hour, but configurable depending on the intended use. One motion sensor is added to onboard unit to estimate encountered weather based on roll, pitch and acceleration.

NYK has installed SIMS on more than 180 vessels including container vessels, PCCs, bulk carriers, tankers and LNG vessels. How NYK utilizes VPMS for vessel performance model is described in the following sections.

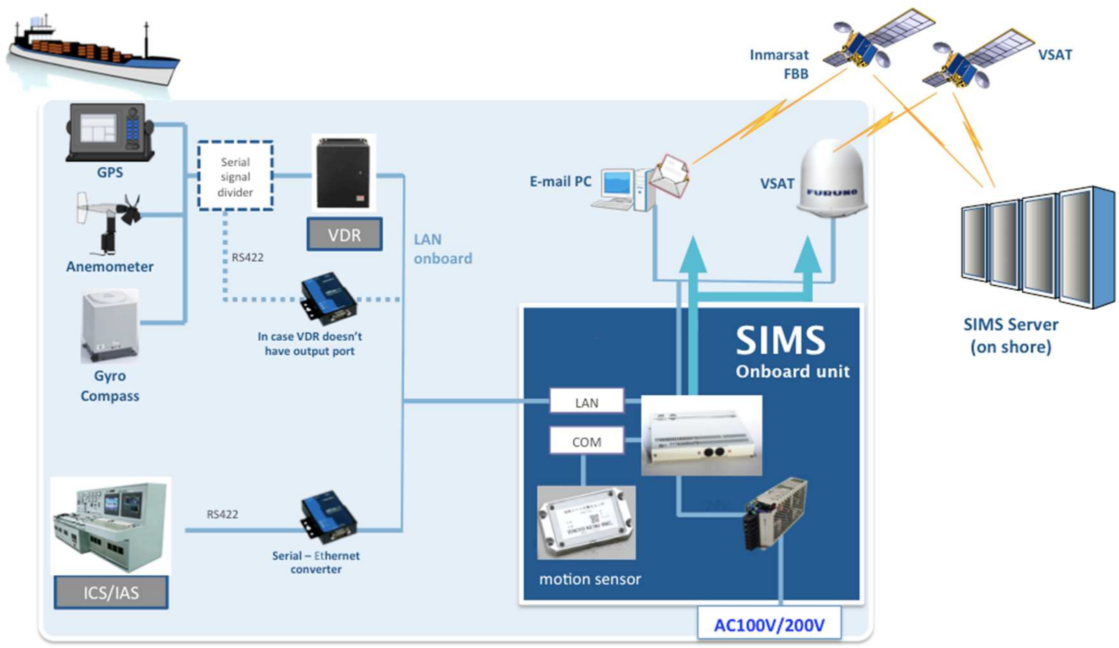

Fig.1: Overview of SIMS

3. Vessel performance model

3.1. Vessel performance in service

There are several types of vessel performance model. Most popular way is expressing speed-fuel consumption relation as one equation. If vessel's loading condition and encountered weather condition is almost same, this model may be able to give enough information to vessel operators. But in many cases, they are not satisfied with this model, because ship propulsive performance is affected by several factors, such as wind, wave, draft, displacement, trim, and conditions of the hull and propeller.

Fig.2 shows variation of draft, speed and weather condition during one round voyage for two container vessels. Those two vessels are similar in loading capacity, but deployed in different services. This means that difference of such operational profile must be considered for optimizing vessel deployment. If vessel performance in actual service can be estimated by using of the model, accuracy of operation cost estimation including fuel cost improves and it has a large impact on various decision making in shipping company.

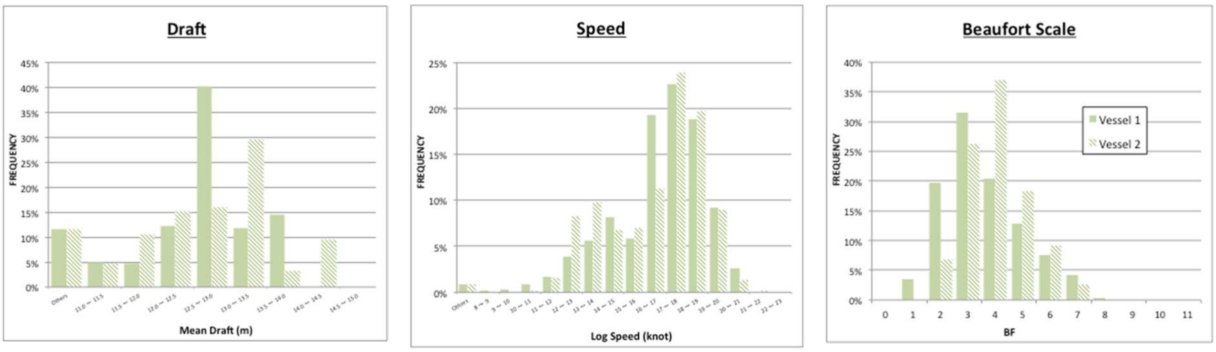

Fig.2: Operational profile of same size vessels deployed in different services

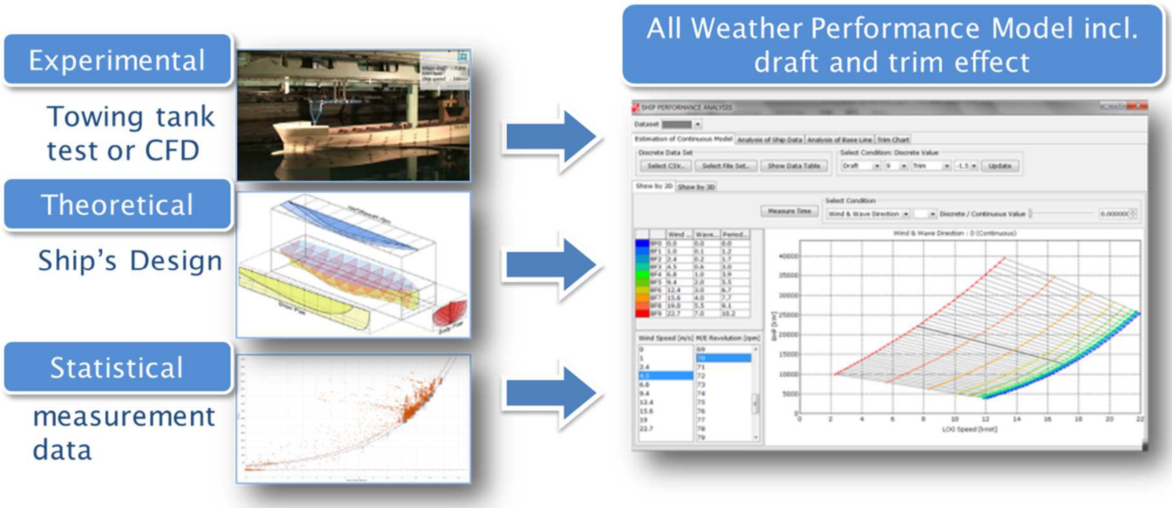

Fig.3: Vessel performance model development in SIMS

3.2. Vessel performance modelling

Fig.3 shows how vessel performance model is developed based on data from SIMS and other information. Three methods such as experimental, theoretical and statistical are combined to develop it. Effect of draft and trim is estimated from experimental method, performance in weather is estimated from theoretical method and difference between model and actual performance is calibrated based on measurement data.

3.2.1 Experimental method

To understand how trim and draft condition affect each ship, conducting towing tank test is the best way. It is well proven in long history of ship design and helpful to quantitatively identify the elements affecting vessel performance by draft and trim change. Trim tank test result is usually visualized by 2D chart shown in the left of Fig.4. Because test conditions are limited due to time and cost constraint, obtained chart from the test is discrete. For estimating vessel performance in any trim, draft and speed, the discrete model is converted to a continuous model by using of B-Spline interpolation.

3.2.2 Theoretical estimation

Theoretical estimation is useful for estimating wind and wave effect. It is not realistic to collect vessel performance data in all the possible wind and wave condition. Instead of that, we utilize the performance estimation method developed by National Maritime Research Institute, *Tsujimoto et al. (2013)*. It takes into account five elements relating to weather:

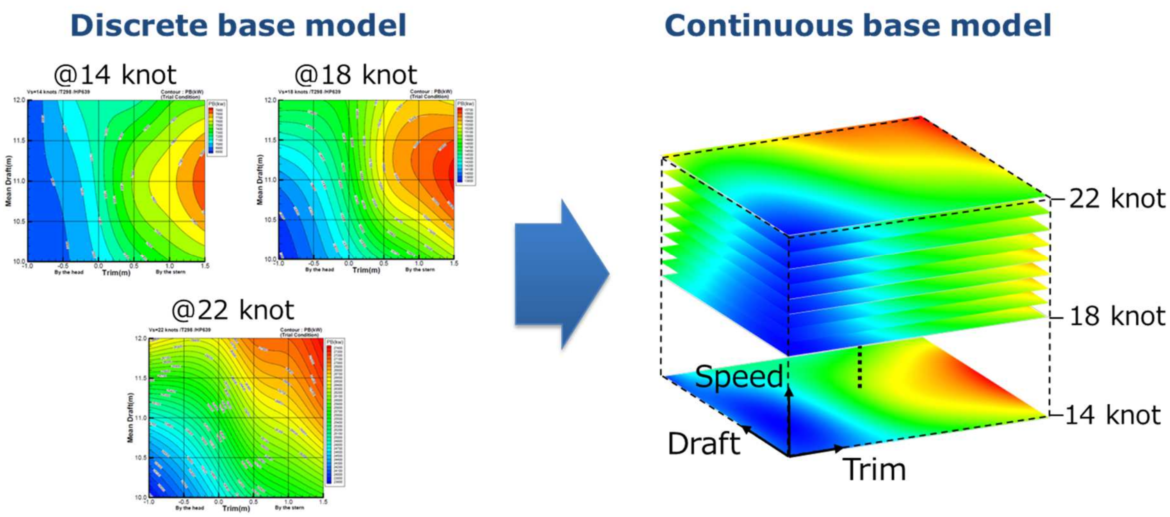

Fig.4: Conversion from discrete model to continuous model

1. Resistance in still water
2. Hydrodynamic forces and moment due to drift motion
3. Rudder forces and moment
4. Wind resistance
5. Added resistance in short-crested irregular waves

By using of the method, vessel performance model for all-weather condition can be estimated. Fig.5 shows an example that visualizes speed-power curves for various wind and wave direction from Beaufort scale 0 to 9.

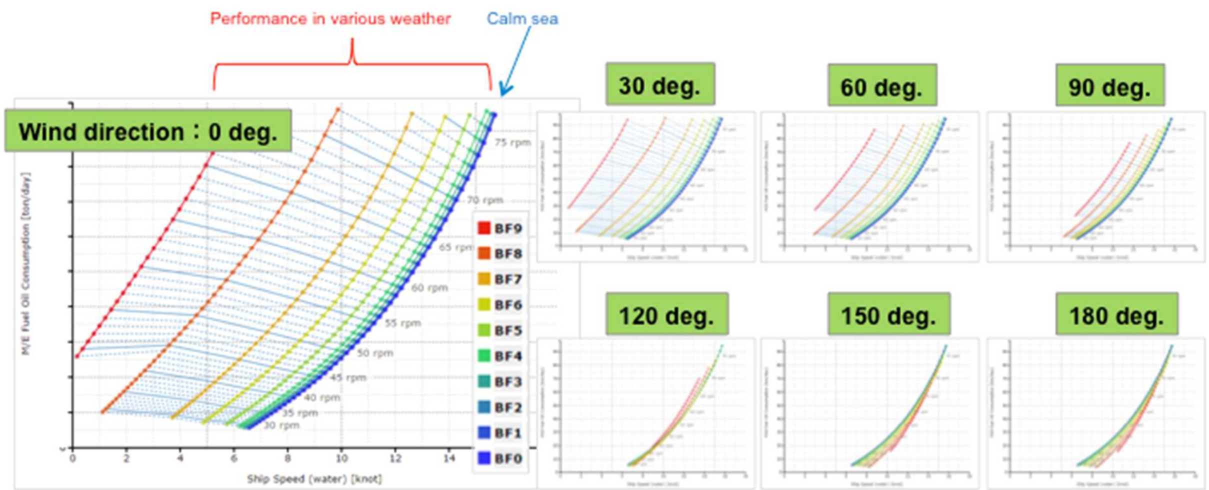

Fig.5: Vessel performance model for all-weather condition

3.2.3 Statistical approach

There are two main reasons for combining statistical approach with above two approaches. One of the reasons is vessel performance degradation due to hull or propeller fouling and engine performance change. Change of baseline performance affects all-weather performance of the vessel and calibration of the model based on measured data is required when performance changes. Another reason is existence of scale effect. Even if model test result is accurate, small difference possibly exists between full and model scale. Calibration of vessel performance model based on measurement data is required to fill a gap and improve accuracy of the model. For both calibrations, good data should be carefully selected among a lot of data collected by SIMS. In case of SIMS, the following data filter is applied for extracting good data.

- Beaufort scale is below 2
- RPM change is less than 0.5 rpm
- Max pitch angle is less than 1 degree
- Max rudder angle is less than 3 degree
- Difference between SOG (Speed over ground) and STW (Speed through water) is less than 0.5 kn

Fig.6 shows an example of vessel performance model calibration. In this case, required power in some draft and trim condition is calibrated based on measured data.

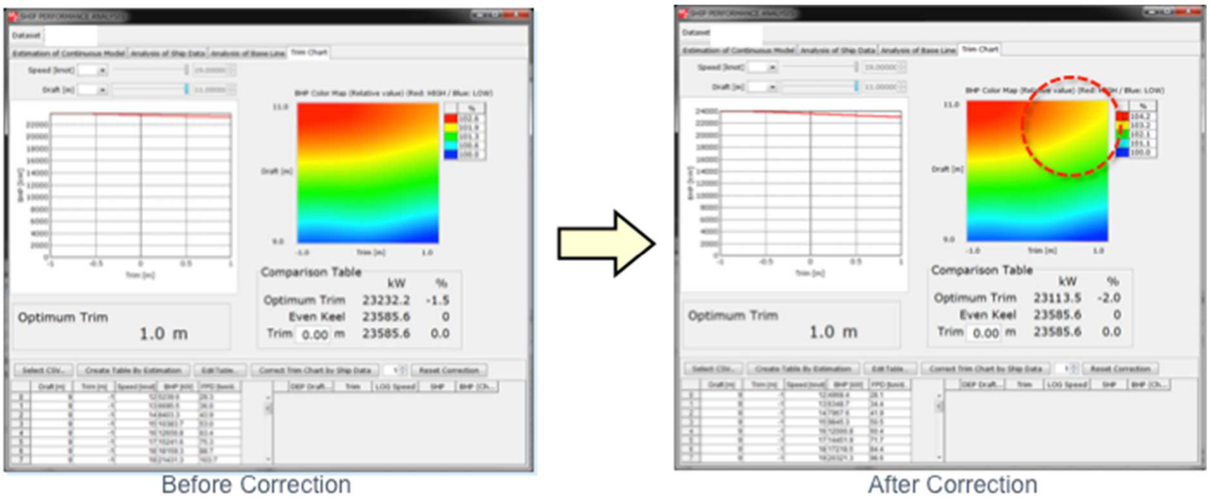

Fig.6: Vessel performance model calibration based on SIMS data (left: before, right: after)

4. Utilization of vessel performance model in shipping company

Estimation of sea margin is one of common task in shipping company. Typical example is the case of bulk carrier. Vessel operators of bulk carrier estimate sea margin of one voyage and order bunker fuel at discharging port. If estimation is much higher than actually required, it will cause reduction of cargo at loading port and profit loss.

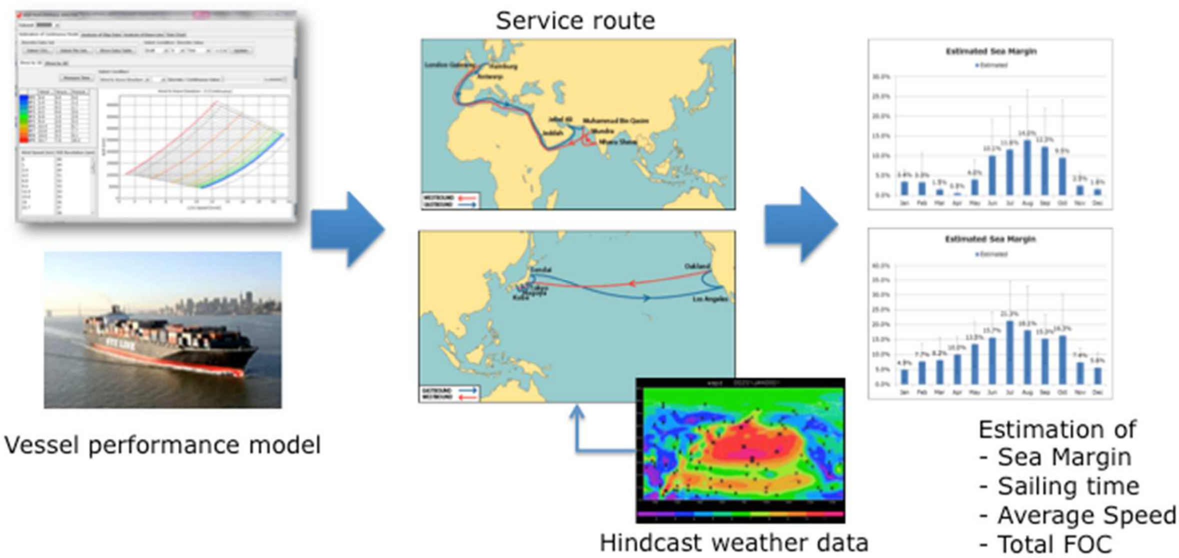

Fig.7: Process of sea margin estimation for target route

Fig.7 shows the process of sea margin estimation based on vessel performance model. At first, vessel performance model is developed as described in chapter 3. Secondly, service route is defined for target departure port to arrival port or one round voyage. Finally, many times of voyages are simulated at fixed speed or fixed engine load by combining vessel performance model, loading condition data and historical weather data. By this way, sailing time, average speed and total fuel oil consumption can be estimated, too.

Table I shows the result of seasonal sea margin estimation for one type of bulk carrier in different sea areas. 500 times of ballast and laden voyage simulation is conducted based on vessel performance model, historical weather and basic voyage route. Same simulation is conducted for more than sea 20 routes and it helps vessel operator's decision making in bunker order.

Table I: Sea margin estimation result - statistics (unit:%)

Route		Spring	Summer	Autumn	Winter
A	+3σ (99.7%)	27.4	27.6	23.7	23.8
	Average	17.9	19.0	16.3	15.9
B	+3σ (99.7%)	26.1	21.6	36.7	44.9
	Average	12.2	10.1	18.9	24.6
C	+3σ (99.7%)	10.3	14.3	16.2	17.7
	Average	4.8	6.3	7.4	8.8
D	+3σ (99.7%)	14.3	17.2	16.4	17.1
	Average	7.6	8.3	8.1	9.2
E	+3σ (99.7%)	11.2	16.8	17.4	15.8
	Average	5.1	7.1	7.3	7.9

5. Conclusion

To obtain the accurate picture of own fleet performance, vessel performance model in service is expected in shipping company. Collected data from VPMS is utilized for building and maintaining accurate vessel performance model. Vessel performance model is utilized for sea margin estimation by simulating voyage with various data including historical weather and route. Result of voyage simulation based on vessel performance model contributes to better decision making in daily operation of shipping company.

References

ANDO, H.; KAKUTA, R. (2009), *Development of Ship Performance Monitoring System for Fleet Operation*, ISSDC2009

KAKUTA, R.; ANDO, H.; YONEZAWA, T. (2016), *Utilization of Vessel Performance Management System in Shipping Company*, 1st Hullpic Conf., Pavone

TSUJIMOTO, M.; KURODA, M.; SOGIHARA, N. (2013): *Development of a Calculation Method for Fuel Consumption of Ships in Actual Seas with Performance Evaluation*, OMAE2013-11297 pp.1-10

So, Your Ship is Not Operating Efficiently (Because of Biofouling) – Now What?

Eric Holm, **Elizabeth Haslbeck**, **Dominic Cusanelli,** Naval Surface Warfare Center, Carderock Division, West Bethesda/USA, elizabeth.haslbeck@navy.mil

Abstract

Quantification of vessel fuel efficiency as a function of hull and propeller roughness, and in particular, roughness associated with biofouling, is a major focus of the HullPIC conferences. Once a ship owner is made aware their vessels are operating inefficiently (due to biofouling), they are then faced with solving the problem. The most effective technologies must, by definition, result in ships going to sea with reduced amounts of adherent biofouling on both propellers and hulls. The most common and obvious solutions are likely to come in the form of coatings (materials), cleanings (maintenance), or both. The potential for these solutions to affect ship powering efficiency in a meaningful and positive way is tied to a set of interdependent variables that, when not taken into consideration, or not considered comprehensively, can render quantifying their benefit difficult, thus making it challenging for the ship owner to formulate the correct business decision for their fleet. For instance, efficacy of both antifouling and fouling release biofouling control coating systems is closely tied to ship operational parameters such as operational tempo and speed/time profile. Additionally cleanings may be required and, depending on the coating and the cleaning tool, may cause damage, shorten or extend coating system service life, or reactivate a failing coating. The efficacy of hull and propeller cleanings is also linked closely with ship operations. The benefit of hull and propeller cleanings is a function of time spent pierside following cleaning, and the risk can vary temporally and spatially. In addition, the ability to detect and quantify improvements in ship operational efficiency specifically associated with improved biofouling condition is linked to the monitoring technique itself, biofouling control technology (including maintenance or cleaning), and ship operations. This paper will explore these and other important and interdependent variables, explore lessons learned from past US Navy biofouling and coatings research, and present recommendations for a way ahead.

Distribution Statement A – Approved for public release; distribution is unlimited. This brief is provided for information only and does not constitute a commitment on behalf of the U.S. government to provide additional information on the program and/or sale of the equipment or system.

1. Introduction

Accumulation of biofouling on hull and propeller(s) significantly impacts ship performance; see *WHOI (1952)*, *Townsin (2003)*, for reviews. Due to its effects on surface roughness, biofouling increases the power required to move a ship through the water, resulting in increased fuel use to maintain speed and decreased operating range or endurance, *Townsin et al. (1985)*, *Hundley and Tsai (1992)*, *Abbott et al. (2000)*, *Schultz (2007)*. Increased emission of greenhouse gases accompanies the increased fuel use; shipping is already a significant contributor to these emissions, *Eyring et al. (2010)*. Methods designed to assess or monitor the powering condition of a ship can indicate when performance may be impaired by the presence of biofouling, and can also be used to quantify that impairment. These methods may include various sorts of power trials, continuous or intermittent logging of ship performance and engineering data during operations, or modeling and prediction approaches, *Hundley and Tsai (1992)*, *Munk et al. (2004)*, *Lutkenhouse et al. (2016)*. When impaired performance is detected, an inspection of the hull and propellers can be carried out to determine if accumulation of biofouling is the cause of the impairment (as opposed to, e.g., wear on the power plant or other components of the propulsion system).

If biofouling is found to be the cause of impaired ship performance, the vessel owner or operator is faced with a decision as to how to correct the problem. The most common and obvious solutions come in the form of hull or propeller coatings to prevent the accumulation of the biofouling, or cleaning of the hull or propeller(s) to remove existing accumulations. The correct or best decision(s), however, may not necessarily be so obvious or simple, and potentially depend on a number of interrelated factors. We term these factors the "Four M's," and are currently using them as a framework within which to better understand biofouling and biofouling control as it affects United States (US) Navy vessels.

2. Defining the "Four M's"

The "Four M's", Fig.1, encompass a suite of several considerations or constraints that can affect choices as to how to manage biofouling on a ship's hull or propeller(s). These considerations can be divided into four factors or broad categories – Materials, Maintenance, Movement, and Monitoring – the "M's" of the "Four M's." The categories interact with each other strongly. Decisions made in isolation, for example, choosing a coating based strictly on criteria associated with the Materials category, may not result in improvement in ship performance or operating costs, if those decisions result in adverse outcomes in one of the other categories.

3. Materials

The Materials factor or category primarily concerns the coatings that might be employed to control the accumulation of biofouling. Multiple options are available including various antifouling formulations, fouling-release coating systems, hybrid coatings combining antifouling and fouling-release functionality, and even barrier coatings. These coatings represent different approaches to biofouling control, *Yebra et al. (2004), Dafforn et al. (2011), Lejars et al. (2012).*

Antifouling coatings employ biocides, typically copper or organic biocides, sometimes together *Lejars et al. (2012)*, to repel the attachment stages of macrofouling organisms or to kill any biofouling that may have attached. Formulations differ in the mechanism by which biocides are released into the environment, *Yebra et al. (2004), Lejars et al. (2012).* In ablative or soluble matrix paints, or controlled depletion polymers, biocides are mixed freely in a water-soluble matrix. The biocides are released or "leached" to the environment as the matrix dissolves, *Lejars et al. (2012).* With time, and as a characteristic "leached layer" develops which is free of biocides, biocide release decreases and dips below an effective rate, *Howell and Behrends (2005),* allowing biofouling to develop. Ship movement or cleaning will erode (ablate) or remove this leached layer and re-activate or restore antifouling performance. In contrast, the matrix of self-polishing paints is hydrolytically unstable and the release of the biocide is controlled primarily by hydrolysis rather than dissolution and erosion, *Yebra et al. (2004), Lejars et al. (2012)*. The rate of hydrolysis can be adjusted chemically to effect variable "polishing" rates and/or rates of biocide release and coating loss, which can be matched to ship activity levels (see Movement, below; *Yebra et al. (2004)*).

A number of biocides have been incorporated into ablative or self-polishing paints. Copper (cuprous oxide) is perhaps the most commonly used, either alone or with organic booster biocides. Organic biocides such as copper or zinc pyrithione, DCOIT, Tralopyril, Irgarol, Diuron, dichlofluanid, chorothalonil, and recently, medetomidine, may also be incorporated into copper-free antifouling formulations, *Pérez et al. (2009), Lejars et al. (2012)*.

Fouling-release coatings employ no biocidal compounds to prevent attachment of organisms, and thus biofouling readily attaches and grows on the coating surface. These paints are instead designed to reduce the adhesion strength of any accumulated biofouling, such that the organisms (including biofilms) are sloughed (released) from the hull or propeller(s) as the painted surface moves through the water ("hydrodynamic self-cleaning", *Schultz et al. (1999)*). Reduced adhesion strength is obtained through the surface and bulk properties of the cured paint, including low surface energy and elastic modulus (for reviews see *Brady and Singer (2000), Lejars et al. (2012)*). These coatings are typically soft silicone [poly(dimethylsiloxane)] rubber potentially with silicone or other types of oils added (for example, *Kavanagh et al. (2003)*). Recently hybrid coatings have been developed, which include both fouling-release and antifouling properties.

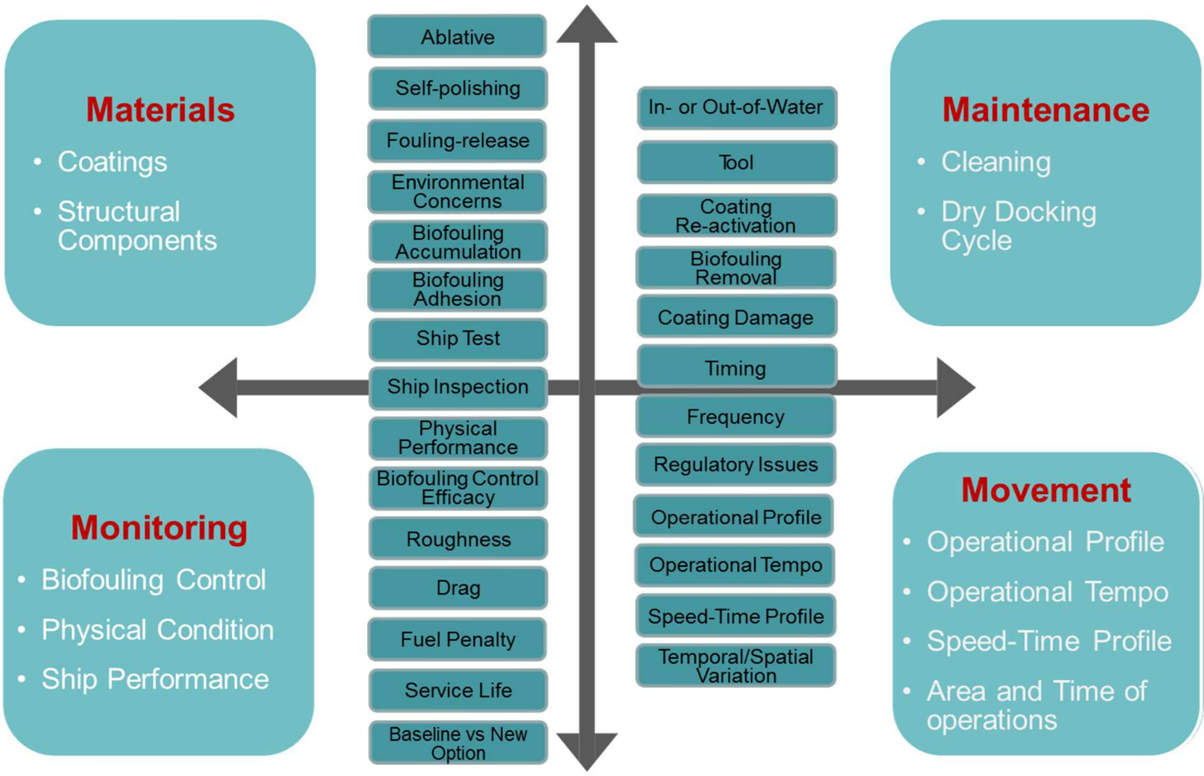

Fig.1: The "Four M's", showing each category (Materials, Maintenance, Movement, and Monitoring), a selection of their components, and the interactions among these components.

Barrier coatings represent epoxy anticorrosive paints or other extremely durable formulations that may possess no inherent biofouling-control properties beyond their ability to endure regular cleaning (see Maintenance, below).

Environmental regulations can limit coating choices available to ship owners or operators. These regulations may be associated with either the biocide suite (for antifouling coatings) or other components of the paint formulation (for any type of coating). Globally the continued widespread use of copper-containing antifouling coatings faces hurdles primarily tied to water quality, European Chemicals Agency Biocidal Products Regulation, https://echa.europa.eu/regulations/biocidal-products-regulation. A relatively large proportion of hull paint systems that are otherwise suitable for use outside the US may not be available for application in the US either because they contain biocides not registered for use in the US, or are not themselves registered by the US Environmental Protection Agency (EPA). Solvents in traditional antifouling paints often contain high quantities of volatile organic compounds and are thus subject to air quality restrictions during application, *IMO MEPC.203(62)*.

The selection and use of biofouling-control coating systems is also impacted by regulatory drivers that extend beyond release of biocides or air pollutants. For example, the underwater hulls and propellers of ships represent a risk for transport and introduction of non-indigenous species, *Gollasch (2002), Godwin (2003), Drake and Lodge (2007), Davidson et al. (2009); IMO MEPC.207(62)*. The degree to which a coating system can reliably control the accumulation of biofouling is directly tied to vessel fuel efficiency, *IMO MEPC.213(63)* – Ship Energy Efficiency Management Plan, and the design of energy efficient ships, *IMO MEPC.215(63)* - Energy Efficiency Design Index.

Finally, compatibility with ship hull and propeller structural materials also limits the choice of coatings. For example, in order to avoid galvanic corrosion, ship owners or operators are directed by the American Bureau of Shipping (ABS) to refrain from using antifouling coatings containing copper as a biocide, on aluminum-hulled vessels, *ABS (1975)*, and product data sheets for copper-containing antifouling paints may warn against use on aluminum.

4. Maintenance

For ship hulls, maintenance, in the form of cleaning (either in-water or out-of-water), is the primary alternative to application of coatings for controlling biofouling. For propellers, where coatings may be inappropriate for use due to the incidence of cavitation erosion or other phenomena that affect wear or service life of the material, cleaning may be the sole means of mitigating the impact of biofouling on ship performance. Three aspects of cleaning may affect the efficacy of the process, or its utility to the ship owner or operator – timing, frequency, and the type of cleaning tool used. Timing concerns the length of time the ship spends alongside the pier between cleaning and the next period of operations. The longer this period, the greater the opportunity for biofouling to attach and grow on the formerly clean surface. This concern may be particularly important for propeller surfaces unprotected by any fouling-control coating. Frequent cleaning may result in consistently smooth hulls or propellers and thus more efficient ship operations, but at the cost of damage to any applied coatings, and corresponding reduction in coating service life, and may be ineffectual if carried out too far in advance of the underway period. Cleaning of ablative antifouling coatings (and presumably self-polishing coatings as well) with rotating brush-type tools removes a thin layer of paint, *Wimmer (1997)*. Depending on the thickness of the coating, frequent cleaning may remove all antifouling paint, leaving the ship unprotected (E. Holm personal observation). Similarly, rotating brush tools can scratch the surface of comparatively soft fouling-release coatings, *Christiaen (1998)*. Scratches may degrade the performance of the coating by providing a rougher surface for adhesion, or exposing undercoats that possess no fouling-release properties.

A variety of tools are available to carry out hull or propeller cleaning, *McClay et al. (2015), Morrisey and Woods (2015),* and these may have differing impacts on coatings. Hulls of large US Navy vessels are routinely cleaned in the water using diver-operated vehicles mounting multiple brushes. The brush material can be chosen to match the observed level or type of biofouling, or the paint, *Morrisey and Woods (2015)*. Smaller patches of fouling, or the surfaces of propeller blades, may be cleaned with hand-held, single brush units. These tools require contact with the coated surface in order to remove any attached biofouling; this contact can result in damage to the coating surface (see above; E. Haslbeck personal observation). Water jets and cavitating water jets have also been developed for in-water removal of biofouling, *Morrisey and Woods (2015)*. Although these devices may be reported as being less damaging to the coating, if applied incorrectly (for example, improper stand-off distance or angle, improper residence time) significant damage can occur, including removal of entire layers of the coating system (E. Holm, personal observation). Various non-contact approaches have also been developed (for example, heat treatment or shrouding methods), but while these may result in the death of any biofouling, they do not remove the organisms, *McClay et al. (2015), Morrisey and Woods (2015)*. Thus, application of these treatments would not immediately improve vessel performance. The impact of these methods on the integrity or function of hull coatings has not been carefully researched, *Morrisey and Woods (2015)*.

Regulatory considerations will have a strong influence on the decision as to whether to execute an in-water hull or propeller cleaning. In the US, west coast ports are increasingly limiting in-water hull cleaning of antifouling paints in order to control release of biocides, *McClay et al. (2015)*. Washington and Oregon prohibit cleaning of antifouling coatings, while in California cleaning of such coatings is permitted only in areas that are not "pollution impaired", *McClay et al. (2015)*. Cleaning of fouling-release coatings or uncoated propellers may be allowed. Australia and New Zealand permit in-water cleaning under certain conditions, including capture, to the greatest extent possible, of biological components of any effluent > 50 µm in size, *McClay et al. (2015)*. No in-water cleaning of ship hulls and propellers is allowed in France. Ships must be dry docked before they are cleaned (C. Hubert, Direction Générale de l'Armement, personal communication). Regulations in some areas may increase the cost of hull cleaning, either by pushing in-water cleaning offshore or to remote locations, or requiring any cleaning to be conducted out of the water, in a dry dock, *McClay et al. (2015)*.

Dry docking presents an opportunity for maintaining the hull or propeller free of biofouling (see above). More importantly, however, a ship's dry docking cycle also impacts the choice of coatings used to protect the hull as it defines the coating service life that will be required. Although paints exist that can be applied underwater, these materials are typically used for spot repairs, are characterized by a limited service life, and may not possess any biofouling-control properties. Application of antifouling or fouling-release coatings is always carried out in dry dock or otherwise out of the water. If the service life of the paint chosen for application is shorter than the ship's dry docking interval, the hull or propellers may need to be cleaned more frequently in order to operate the vessel efficiently. Ship owners or operators relying primarily on cleaning to obtain improved operating efficiency may take on substantial risk of incurring a fuel penalty if it is not possible to time these cleanings appropriately, or carry them out whenever/wherever they are needed. Finally, the dry-docking interval will also determine the timing and rate of implementation of new biofouling-control coatings, and thus the rate at which improvements to performance, due to coating application, can be realized.

5. Movement

The movement factor comprises several aspects of ship operations, including both active and inactive periods, that may impact the occurrence of biofouling and the choices made to control it. That movement, in particular the frequency of movement and the location or environment wherein operations takes place, affects the accumulation of biofouling has been understood for many decades, e.g. *Visscher (1927)*. The development over the last 30 to 40 years of paint formulations whose function is strongly dependent on ship movement suggests that this factor continues to require close consideration. The components making up the movement factor comprise A) the operational profile or operational tempo, the distribution of operational periods within a given span of time, including the length of individual periods of time spent moving or at the pier; B) the speed-time profile, the frequency with which a ship operates at a given speed; and C) the time and area of operations, including inactive periods, which determine the rate at which biofouling may accumulate and grow, and the types of organisms within those accumulations.

Paint manufacturers design antifouling and fouling-release coatings to be used under variable yet specific operational scenarios. For ablative or controlled depletion polymer coatings, ship movement helps to erode away the leached layer which develops at the paint surface over time. Erosion (or ablation) exposes a "fresh" coating surface to ensure continuous biocide release at effective rates. Self-polishing coating formulations are designed to hydrolyze at varying rates, which are a function also of the activity level of the vessel. Finally, fouling-release paints depend on ship movement to generate the hydrodynamic shear and normal forces necessary to cause sloughing of attached bio-fouling, *Schultz et al. (1999). Lejars et al. (2012)* provide recommended activity levels, including operational tempo and speed-time profile, for several fouling-release coatings that were commercially available at the time. Although the speed-time profile would seem to be the most important aspect of movement affecting the efficacy of fouling-release coatings, as speed through the water generates the hydrodynamic forces on attached biofouling, the operational profile and operational tempo are also important as they affect the size of the attached biofouling and thus the magnitude of forces that must be applied in order to break the adhesive bond between the organism and the coating surface, *Kavanagh et al. (2001)*.

The efficacy of biofouling control coatings can vary with the time and area of operations, as the intensity of biofouling and the species composition of the resulting communities can be specific to particular regions of the planet, e.g. *DePalma (1972)*, and the dynamics of biofouling within those regions can vary with time (for example, seasonal patterns in biofouling attachment and growth). Harbors may contain biofouling species that are more or less sensitive to biocides employed in antifouling coatings, e.g. *Piola and Johnston (2006), Gall et al. (2013)*, or exhibit growth forms or strengths of adhesion that render them more or less likely to be sloughed from fouling-release coatings, e.g. *Holm et al. (2006)*.

6. Monitoring

The final "M," Monitoring, comprises metrics associated with the degree to which a particular technology, process, or strategy controls biofouling, and the benefits and costs of the approach including changes in ship performance, operating efficiency, or operating costs incorporating materials and maintenance costs if applicable.

The degree to which a biofouling control strategy, for either hulls or propellers, may be deemed successful depends on the extent to which the strategy actually reduces the presence of biofouling (efficacy), and the length of time that strategy remains efficacious. Coatings will be seen as effective when they reliably mitigate biofouling without the need for in-water cleaning, and retain their physical integrity, for the entire period between dry dockings. Efficacy in control of biofouling, for hulls or propellers, can be readily assessed visually during dedicated inspections, using either divers or remotely-operated vehicles. Inspections can also be carried out in dry dock. The accumulation of biofouling is generally described using various sorts of ranking or rating scales incorporating the type of organisms found (for example, “slime”, “weed”, “shell”, *Townsin (2003)*, or descriptors associated with particular growth forms – barnacles, tubeworms) and their coverage (*Swain and Lund (2016), Naval Ships’ Technical Manual* Chapter 081). Similar rating scales exist for coating physical condition (for example, *Naval Ships’ Technical Manual* Chapter 081). These assessments represent a snapshot in time, and their proper interpretation requires an understanding of coating type and age (if the control strategy incorporates a coating), and ship activity and maintenance history. Fouling-release paints may require more frequent monitoring than antifouling coatings, especially in cases where the ship’s operational tempo or speed-time profile do not meet the manufacturer’s recommendations.

Monitoring of gross changes in coating physical condition, for example, significant erosion, polish-through, or delamination, can also be carried out through visual inspections. However, quantification of changes in small-scale roughness of hull or propeller coatings or the surface of uncoated propellers, as may result from cleaning, and measurement of coating loss from operations and cleaning that does not result in any obvious visual cue, requires specialized equipment. Such assessments are as necessary to determining coating service life as evaluation of efficacy.

A meaningful metric of vessel operating efficiency as a function of the extent of biofouling present on the hull or propeller(s), as it is affected by a given control strategy or technology, is critical to justifying broader implementation of that strategy or technology. Improved procedures or approaches to obtain these data remain under development. Existing approaches range from full-scale evaluation of speed and power, to lab-scale characterization and modeling.

Dedicated power or towing trials, combined with inspections of hulls and propellers, have significantly advanced our understanding of the relationship between ship performance or powering condition and roughness due to biofouling. These studies have a long history, e.g. *Visscher (1927), Davis (1930), Izubuchi (1934), Kan et al. (1958),* and continue to be extremely valuable today, e.g. *Townsin et al. (1981), Hundley and Tsai (1992),* D. Cusanelli personal observation). Recently a standard method for collection and processing of full-scale speed/power data from ships was published, *ISO 19030*. Continuous, *Hagestuen (2016), Jonsson and Fridriksson (2016),* or intermittent, *Gundermann and Kirksen (2016)*, monitoring or logging of shipboard data streams (with or without data filtering algorithms for removing variability due to environmental conditions) is now being offered by a larger number of commercial entities than ever, *Hasselaar (2011)*.

Data from trials or monitoring systems may not always be available. In these cases, drag data collected from smaller towed objects (plates, pontoons) or flow channel testing, have been used to provide information for modeling impacts to powering. *Schultz (2007), Schultz et al. (2015), Monty et al. (2016)* have predicted performance impacts of biofouling by scaling (to full scale) laboratory measurements of drag on biofouled surfaces using similarity law procedures. The data may also be incorporated into Reynolds Averaged Navier-Stokes (RANS) models capturing the details of particular hull forms, and the complex flows around them (A. Vargas, Naval Surface Warfare Center Carderock Division, personal communication). These predictions (and to a certain extent, those from full-scale trials as well), while tremendously illuminating, are currently limited to a small range of biofouling conditions, and assume that the associated roughness is homogeneously distributed over the modeled surface. Unfortunately, the hydrodynamic characteristics of the diversity of biofouling conditions that might be observed on a ship hull or propeller are not necessarily amenable to derivation strictly from direct measurement of physical roughness, *Leer-Andersen and Larssen (2003)*.

Finally, monitoring includes an important historical component. Ultimately the ship owner or operator can only determine if newly implemented technologies or practices are improving vessel operating efficiency or reducing operating costs if data are available regarding the baseline ship performance and operating costs, that is, performance and costs during such time as the original coatings or cleaning practices or technologies were employed. Arguably, many vessel owners or operators have not well-characterized the baseline biofouling or fuel penalty condition of their ships, and thus the potential benefits that could be realized by a change in approach to biofouling control remain largely unknown. At a minimum data on vessel performance should be collected before any changes to current practices are made. Alternatively, baseline data can be collected on vessels that have not been subjected to these changes, while they are operating concurrently with any vessels for which new coatings have been applied, or new cleaning schedules or tools adopted.

7. Knowledge Gaps Associated with the "Four M's"

Considering biofouling control in the context of the "Four M's" also enables us to identify significant knowledge gaps that may lead to imperfect application of the framework. These knowledge gaps are associated with each of the "M's". Some of these have been identified above; however, there are additional needs in each area. The following discussion is by no means comprehensive. With regard to Materials, we are currently lacking screening tests that accurately predict coating performance at full scale. A large number of both published, standardized screening tests and unpublished proprietary tests are available. Despite the availability of these methods, full-scale testing still gives the best indication of how a coating will perform. No standardized test exists to evaluate the impact of cleaning tools on coating efficacy or physical performance, although efforts in this area have been made, e.g. *Christiaen (1998), Holm et al. (2003), Oliveira and Granhag (2016)*. Only recently have there been attempts to rigorously relate operational tempo, speed-time profile, and area of operations to ship hull roughness and performance, coating efficacy and service life (see International Paint's Intertrac® Vision program, http://www.international-marine.com/intertracvision/pages/home.html). In the absence of power trials carried out under a broad array of biofouling conditions, additional laboratory-scale work is needed to determine the range of drag values that might be observed in cases where biofouling is patchily distributed, or consists of individual organisms of differing size and shape. Performance monitoring programs may help to fill this gap, but only if the monitoring is combined with regular assessments of hulls and propellers for the presence of biofouling, so that the cause of any given impact to powering can be clearly identified.

8. Conclusions

For the past several decades, the US Navy has, in effect, utilized one type of underwater hull coating technology, and has combined that technology with an in-water inspection and cleaning program which together reduce the likelihood that a ship will go to sea with heavy biofouling on hulls or propellers. This strategy takes into account the US Navy's unusual operational tempo and speed-time profiles (relative to commercial vessels). Evidence suggests this approach could be improved. In the relatively recent past, as we tested advanced biofouling control technologies, we have been able to identify weaknesses as well as knowledge gaps that potentially interfere with evaluation or implementation of new technologies or processes. Our experiences led us to develop the framework described in this paper, that will allow us to better understand biofouling as it affects US Navy vessels, and biofouling control solutions and their benefit to our Fleet.

All vessels, from military and commercial ships to pleasure craft, are susceptible to the deleterious effects of biofouling. Choosing among the many options available to reduce these effects requires careful consideration. The performance of a control strategy and the characterization of its ability to mitigate biofouling will be closely tied to the interdependent factors outlined above – Materials, Maintenance, Monitoring, and Movement. The correct or best decisions will depend on a number of variables, the subset of which is unlikely to lead to a one-size-fits-all solution.

References

ABBOTT, A.; ABEL, P.D.; ARNOLD, D.W.; MILNE, A. (2000), *Cost-benefit analysis of the use of TBT: the case for a treatment approach*, Science of the Total Environment 258, pp.5-19

ABS (1975), *ABS Rules for Building and Classing Aluminum Vessels. Section 26.3.2*, American Buerau of Shipping

BRADY, R.F.; SINGER, I.L. (2000), *Mechanical factors favoring release from fouling release coatings*, Biofouling 15, pp.73-81

CHRISTIAEN, A.C. (1998), *Evaluation of the durability of elastomeric easy-release coatings*, PhD thesis, Virginia Polytechnic Institute and State University, Blacksburg

DAFFORN, K.A.; LEWIS, J.A.; JOHNSTON, E.L. (2011), *Antifouling strategies: history and regulation, ecological impacts and mitigation*, Marine Pollution Bulletin 62, pp.453-465

DAVIDSON, I.C.; BROWN, C.W.; SYTSMA, M.D.; RUIZ, G.M. (2009), *The role of containerships as transfer mechanisms of marine biofouling species*, Biofouling 25, pp.645-655

DAVIS, H.F.D. (1930), *The increase in S.H.P. and R.P.M. due to fouling*, J. American Society of Naval Engineers 42, pp.155-166

DEPALMA, J.R. (1972), *Fearless fouling forecasting*, 3rd Int. Congr. Marine Corrosion and Fouling, Gaithersburg, pp.865-879

DRAKE, J.M.; LODGE, D.M. (2007), *Hull fouling is a risk factor for intercontinental species exchange in aquatic ecosystems*, Aquatic Invasions 2, pp.121-131

EYRING, V.; ISAKSEN, I.S.A.; BERNTSEN, T.; COLLINS, W.J.; CORBETT, J.J.; ENDRESEN, O.; GRAINGER, R.G.; MOLDANOVA, J.; SCHLAGER, H.; STEVENSON, D.S. (2010), *Transport impacts on atmosphere and climate: shipping*, Atmospheric Environment 44, pp.4735-4771

GALL, M.L.; HOLMES, S.P.; DAFFORN, K.A.; JOHNSTON, E.L. (2013), *Differential tolerance to copper, but no evidence of population-level genetic differences in a widely-dispersing native barnacle*, Ecotoxicology 22, pp.929-937

GODWIN, L.S. (2003), *Hull fouling of maritime vessels as a pathway for marine species invasions to the Hawaiian Islands*, Biofouling 19(Supplement), pp.123-131

GOLLASCH, S. (2002), *The importance of ship hull fouling as a vector of species introductions into the North Sea*, Biofouling 18, pp.105-121

GUNDERMANN, D.; DIRKSEN, T. (2016), *A statistical study of propulsion performance of ships and the effect of drydockings, hull cleanings, and propeller polishes on performance*, 1st Hull Performance and Insight Conference (HullPIC), Pavone, p.282

HAGESTUEN, E.; LUND, B.; GONZALEZ, C. (2016). *Continuous performance monitoring – a practical approach to the ISO 19030 standard*, 1st Hull Performance and Insight Conference (HullPIC), Pavone, p.49

HASSELAAR, T.W.F. (2011), *An investigation into the development of an advanced ship performance monitoring and analysis system*, PhD thesis, University of Newcastle

HOLM, E.R.; HASLBECK, E.G.; HORINEK, A.A. (2003), *Evaluation of brushes for removal of fouling from fouling-release surfaces, using a hydraulic cleaning device*, Biofouling 19, pp.297-305

HOLM, E.R.; KAVANAGH, C.J.; MEYER, A.E.; WIEBE, D.; NEDVED, B.T.; WENDT, D.; SMITH, C.M.; HADFIELD, M.G.; SWAIN, G.; DARKANGELO WOOD, C.; TRUBY, K.; STEIN, J.; MONTEMARANO, J. (2006), *Interspecific variation in patterns of adhesion of marine fouling to silicone surfaces*, Biofouling 22, pp.233-243

HOWELL, D.; BEHRENDS, B. (2005), *An optical, non-intrusive method for measuring surface roughness of antifouling coatings*, 3rd Int. Conf. Marine Science and Technology for Environmental Sustainability (ENSUS), Newcastle

HUNDLEY, L.L.; TSAI, S.-J. (1992), *The use of propulsion shaft torque and speed measurements to improve the life cycle performance of U.S. naval ships*, Naval Engineers J. 104(6), pp.43-57

ISO 19030, *Ships and marine technology – Measurement of changes in hull and propeller performance – Parts 1, 2, and 3*, International Organization for Standardization

IZUBUCHI, T. (1934), *Increase in hull resistance through ship bottom fouling*, Zosen Kiokai 55, pp.57-100

JONSSON, S.; FRIDRIKSSON, H. (2016), *Continuous estimate of hull and propeller performance using auto-logged data*, 1st Hull Performance and Insight Conf. (HullPIC), Pavone, p.332

KAN, S.; SHIBA, H.; TSUCHIDA, K.; YOKOO, K. (1958), *Effect of fouling of a ship's hull and propeller upon propulsive performance*, Int. Shipbuilding Progress 5, pp.15-34

KAVANAGH, C.J.; SCHULTZ, M.P.; SWAIN, G.W.; STEIN, J.; TRUBY, K.; DARKANGELO WOOD, C. (2001), *Variation in adhesion strength of* Balanus eburneus, Crassostrea virginica, *and* Hydroides dianthus *to fouling-release coatings*, Biofouling 17, pp.155-167

KAVANAGH, C.J.; SWAIN, G.W.; KOVACH, B.S.; STEIN, J.; DARKANGELO WOOD, C.; TRUBY, K.; HOLM, E.; MONTEMARANO, J.; MEYER, A.; WIEBE, D. (2003), *The effects of silicone fluid additives and silicone elastomer matrices on barnacle adhesion strength*, Biofouling 19, pp.381-390

LEER-ANDERSEN, M.; LARSSEN, L. (2003), *An experimental/numerical approach for evaluating skin friction on full-scale ships with surface roughness*, J. Marine Science & Technology 8, pp.26-36

LEJARS, M.; MARGAILLAN, A.; BRESSY, C. (2012), *Fouling release coatings: a nontoxic alternative to biocidal antifouling coatings*, Chemical Reviews 112, pp.4347-4390

LUTKENHOUSE, C.; BRADY, B.; DELBRIDGE, J.; HASLBECK, E.; HOLM, E.; LYNN, D.; MICHAEL, T.; ROSS, A.; STAMPER, D.; TSENG, C.; WEBB, A. (2016), *Baseline propeller roughness condition assessment and its impact on fuel efficiency*, 1st Hull Performance and Insight Conf. (HullPIC), Pavone

McCLAY, T.; ZABIN, C.; DAVIDSON, I.; YOUNG, R.; ELAM, D. (2015), *Vessel biofouling prevention and management options report*, CG-D-15-15. U.S. Coast Guard Research & Development Center, New London

MONTY, J.P.; DOGAN, E.; HANSON, R.; SCARDINO, A.J.; GANAPATHISUBRAMANI, B.;

HUTCHINS, N. (2016), *An assessment of the ship drag penalty arising from light calcareous tubeworm fouling*, Biofouling 32, pp.451-464

MORRISEY, D.; WOODS, C. (2015), *In-water cleaning technologies: review of information*, MPI Technical Paper No. 2015/38, New Zealand Ministry for Primary Industries, Wellington

MUNK, T.; KANE, D.; YEBRA, D. (2009), *The effects of corrosion and fouling on the performance of ocean-going vessels: a naval architectural perspective*, Advances in Marine Antifouling Coatings and Technologies, Woodhead Publ., Cambridge, pp.148-176

NAVAL SHIPS' TECHNICAL MANUAL CHAPTER 081 (2006), *Underwater hull cleaning of Navy ships*, https://www.maritime.org/doc/nstm/ch081.pdf

OLIVEIRA, D.; GRANHAG, L. (2016), *Matching forces applied in underwater hull cleaning with adhesion strength of marine organisms*, J. Marine Science and Eng. 4/66

OMAE, E. (2003), *Organotin antifouling paints and their alternatives*, Applied Organometallic Chemistry 17, pp.81-105

PÉREZ, M.C.; STUPAK, M.E.; GLUSTEIN, G.; GARCIA, M.; MÅRTENSSON LINDBLAD, L. (2009), *Organic alternatives to copper in the control of marine biofouling*, Advances in Marine Antifouling Coatings and Technologies, Woodhead Publ., pp.554-571

PIOLA, R.F.; JOHNSTON, E.L. (2006), *Differential tolerance to metals among populations of the introduced bryozoan* Bugula neritina, Marine Biology 148, pp.997-1010

SCHULTZ, M.P. (2007), *Effects of coating roughness and biofouling on ship resistance and powering*, Biofouling 23, pp.331-341

SCHULTZ, M.P.; KAVANAGH, C.J.; SWAIN, G.W. (1999), *Hydrodynamic forces on barnacles: implications on detachment from fouling-release surfaces*, Biofouling 13, pp.323-335

SCHULTZ, M.P.; WALKER, J.M.; STEPPE, C.N.; FLACK, K.A. (2015), *Impact of diatomaceous biofilms on the frictional drag of fouling-release coatings*, Biofouling 31, pp.759-773

SWAIN, G.; LUND, G. (2016), *Dry-dock inspection methods for improved fouling control coating performance*, J. Ship Production and Design 32(3), pp.186-193

THOMAS, K. (2009), *The use of broad-spectrum organic biocides in marine antifouling paints*, Advances in Marine Antifouling Coatings and Technologies. Woodhead Publ., pp.522-553

TOWNSIN, R.L. (2003), *The ship hull fouling penalty*, Biofouling 19(Supplement), pp.9-15

TOWNSIN, R.L.; BYRNE, D.; SVENSEN, T.E.; MILNE, A. (1981), *Estimating the technical and economic penalties of hull and propeller roughness*, SNAME Trans. 89, pp.295-318

TOWNSIN, R.L.; SPENCER, D.S.; MOSAAD, M.; PATIENCE, G. (1985), *Rough propeller penalties*, SNAME Trans. 93, pp.165-187

VISSCHER, J.P. (1927), *Nature and extent of fouling of ships' bottoms*, Bulletin US Bureau of Fisheries 43, pp.193-252

WALKER, J.M.; SCHULTZ, M.P.; FLACK, K.A.; STEPPE, C.N. (2014), *Skin-friction drag measurements on ship hull coating systems*, 30th Symposium on Naval Hydrodynamics, Hobart

WIMMER, J.R. (1997), *Analyzing and predicting underwater hull coating system wear*, PhD thesis, Naval Postgraduate School, Monterey

WHOI (1952), *Marine fouling and its prevention*, Woods Hole Oceanographic Institution, United States Naval Institute, Annapolis

YEBRA, D.M.; KIIL, S.; DAM-JOHANSEN, K. (2004), *Antifouling technology – past, present and future steps towards efficient and environmentally friendly antifouling coatings*, Progress in Organic Coatings 50, pp.75-104

Estimating Added Power in Waves for Ships Through Analysis of Operational Data

P. Arun Lakshmynarayanana, University of Southampton, Southampton/UK, pl6g12@soton.ac.uk
Dominic A. Hudson, University of Southampton, Southampton/UK dominic@soton.ac.uk

Abstract

The accuracy of added power estimation using full scale operational data is directly related to the accuracy of determining the calm water power. Firstly, this paper focuses on a detailed analysis of the calm water powering, using voyage (operation) data supported by and compared to standard estimation techniques and model test data. Further, a method to quantify the added power in weather is developed. The added power due to the influence of waves and wind is treated as the difference between measured shaft power and calm water power requirement. It is shown that both quality and quantity of data is important to model calm water power accurately. The operational data suggests that trim by stern is favorable at lower speeds and has little effect with increase in speed. The added power in waves for most operational speeds considered is less than 10%.

1. Introduction

Increasing pressure on the marine industry from the global community to reduce Greenhouse Gas emissions from shipping has resulted in regulations governing fuel consumption, efficient operation and emissions from ships entering into force (e.g. EEDI, SEEMP). To improve the performance and efficiency of ship operations, it is first important to quantify accurately a vessel's performance, which can be carried out using in-service monitoring data. Traditionally, in-service monitoring is carried out using noon-report data (sampling frequency of approximately 24 hours) which is categorized as a medium precision method. This gives a limited number of data points to evaluate the performance of a vessel and also introduces significant uncertainties and potential for human error, *Aldous et al. (2013), Pedersen and Larsen (2009).* Automatic high-frequency data recording not only offers the possibility for analysis of ship performance in a shorter time, but also decreases errors arising from manual recording, *Aldous et al. (2015).* However, in continuous data recording both data frequency and quality are important; in fact the data quality are even more significant than data frequency for accurate performance prediction models, *Duckert et al. (2016)*. The data precision can be improved significantly by linking the automatic data acquisition to the MetOcean datasets to allow corrections to be made for current, wind and waves.

The hydrodynamic optimization of a ship is primarily carried out considering its calm water 'design' condition. In contrast, ships mostly operate in varying weather conditions which have a direct influence on their powering requirements. A ship operating in waves experiences an added power to maintain speed, or a lower speed to maintain constant power, when compared to calm water. An accurate estimation of the added power in waves is useful to improve operating efficiency and decrease fuel consumption. It is vital for accurate weather routing and should inform design and ship selection. Semi-empirical approaches such as *Townsin and Kwon (1983)*, derived from model tests, and updated by *Kwon (2000, 2008)* based on noon reports and sea state observations from the bridge are commonly used to calculate speed loss and added power in weather. Potentially more accurate estimations using 3-D potential flow, *Liu et al. (2011)*, and CFD techniques *Tezdogan et al. (2015)* have also been implemented but remain computationally intensive. A few attempts using Artificial Neural Networks (ANN) trained using data recorded at high frequency are promising, but require further validation, Parkes et al. (2017), *Grado and Bertram (2016).* Nevertheless, quantifying added power remains challenging and requires a deeper understanding of the capabilities and limitations involved, *Bertram (2016)*, but is an area where operational data could prove to be very useful, *Dinham-Peren and Dand (2010).*

This paper presents a method of quantifying the added power in weather developed using in-service data recorded from three merchant ships and the associated MetOcean data. The added power due to the influence of waves and wind is treated as a difference between the recorded shaft power and the calm-water power, *Webb and Hudson (2015).* The accuracy of the added power estimation from the operational data is thus directly related to the accuracy of determining the calm water power. In this study, we focus on the analysis of calm water powering, using voyage (operational) data supported by and compared to, standard estimation techniques and model tests. Data is filtered with respect to significant wave height and true wind speed criteria to generate a calm-water model from on-board measurements. The effect on calm water power of changes in draught and trim is investigated. The investigations provide some important insights into the sensitivity and accuracy of the filtering criteria used in modelling the calm water power.

2. Methodology

The methodologies used to analyse calm water and added powers from continuously monitored data are detailed in this section. Firstly, a summary of the data acquired from the ships are described with some insights into their operating profile. Furthermore, the data filtering applied to arrive at the calm water and added power model is explained.

2.1. Operational data acquisition

In-service data recorded using continuous monitoring was obtained for three sister merchant ships. ISO 19030-2 prescribes a minimum data acquisition rate of 15 seconds for the operating parameters of the vessel that shall be averaged over a relevant time interval. The present data was recorded at a sampling frequency of 1 Hz and averaged over 5 min intervals. The data contained 244833 data points (three ships combined) which also included the weather data from a MetOcean model. Data manipulation was performed using the open source programming language Python and its associated data science libraries. Fig.1 shows the number of data points for the various operating speeds, drafts and trim of the vessel for the original data set. The speed histogram of the ships indicates that they spend more time at higher speeds (>15.0 knots), which amounts to about 98000 data points (about 40% of the total data recorded). The ships mainly sail at two draft intervals (9-10 m and 10.5-11.5 m) as indicated by the draft profile of the original data. Trim is calculated as a difference between the forward and aft drafts, and hence, negative values indicate trim by stern. The speed, trim and draft show a narrow range of operational conditions.

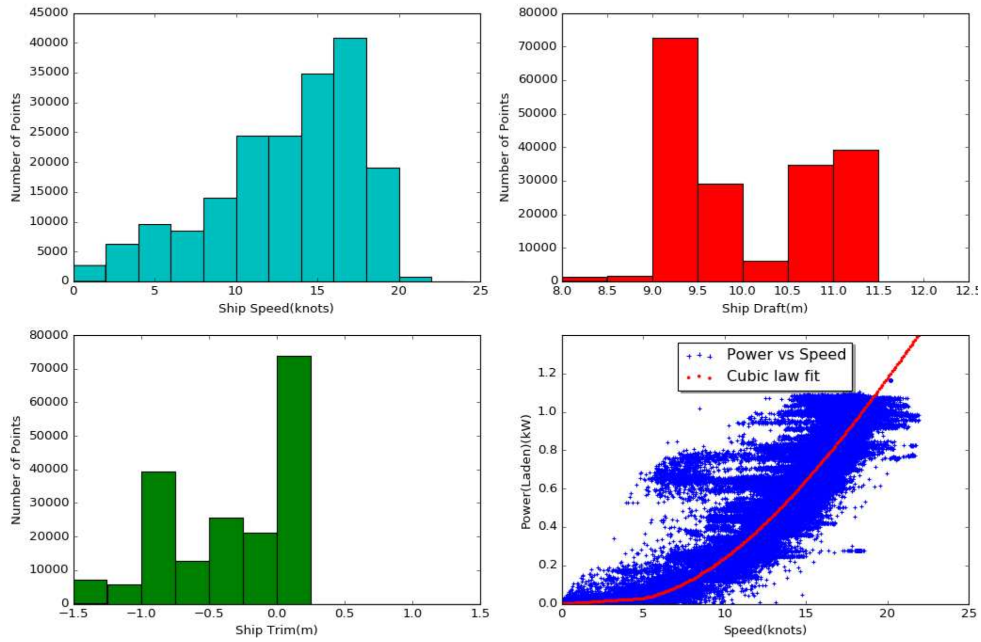

Fig.1**:** Ship speed, draft, trim and power vs speed recorded during the analysis period

Fig.2 shows the significant wave heights encountered by the vessels, which mainly fall in the range of 1-3 m. When calculating the calm water power it would be ideal to have a number of data points for very small wave heights. In this case, however, it appears to be difficult to use a very small wave height, for example less than 0.5 m, since it filters the data too severely. The polar plots in the figure show the apparent wind direction and the ship heading relative to the waves.

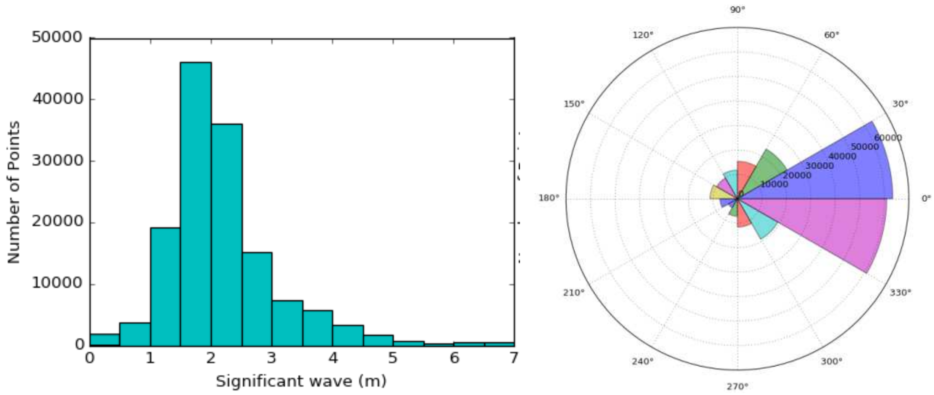

(a) (b)

Fig.2: (a) Encountered wave heights, (b) apparent wind by the ships.

2.2. Calm-water powering

The voyage data is used to estimate calm water power by appropriately filtering the data and further binning them into draft and trim intervals. The calm water power is considered to be a function of the ship speed, trim and draft. Before generating the shaft power variations with respect to these parameters the data required for analysis is filtered based on a minimum wave height condition. Looking at the wave height histogram it was decided to use the data by omitting significant wave heights of greater than 1.5m and true wind speed more than 10 knots. True wind speed and direction were calculated to eliminate the relative velocity of the ship from the apparent wind measurements, *Bertram (2012).* Additionally, a few other constraints were also applied to ensure that the quality of data and scatter used for the calm water model is acceptable, *Dinham-Peren and Dand (2010).* To calculate the calm water powering characteristics the original data was filtered by applying the following constraints:

- True wind speed less than 10 knots
- Significant wave height less than 1.5 m
- The difference between the over ground speed and the speed through water less than 1 knot. This constraint is to ensure that the effect of 'current' is small in the calm water model.
- Engine RPM is greater than zero, hence astern running is not included.
- Change in speed over ground between successive samples does not exceed 0.5 knots. In this case, only data points that represent the ship moving at a reasonably steady speed will be considered.

The above constraints to model the calm water condition produced a data set with 21756 data points which retains about 9 % of the original data recorded. This demonstrates the difficulty of estimating accurate calm water behaviour using full scale data. The data were then separated into four bins to remove the influence of ship speed. The four bins considered were: 16-17, 17-18, 18-19 and 19-20 knots since most data points lie within these speeds. Subsequently, the shaft power recorded was plotted for individual speed bins with respect to average draft and trim. Finally, a regression analysis was performed to fit the data as a linear function of draft and trim changes. The calm-water power is compared with predictions using *Holtrop and Mennen (1982)* and model test results.

Filtering the original data using a smaller wave height (<1.5m) will yield fewer data points for calm water investigations and vice versa when filtered using a larger wave height. In the present study two additional wave heights, 1.0 m and 2.0 m, are also applied to manipulate the data for the calm water model.

2.3. Added power estimation

The added power in waves at various speed intervals is considered as a difference between the total shaft power and the calm water power estimated for the corresponding speed intervals. The data mining is done in such a way that the total shaft power at a particular draft and the calm water power at the same draft are used to calculate the additional power (given in equation below). The added power calculated is considered as a function of the significant wave height.

$$P_{added} = P_{Total} - P_{calm} \qquad \textit{for the same draft conditions}$$

3. Results and Discussion

3.1 Original dataset

Fig.3 shows the plot of shaft power vs ship speed and ship speed vs the shaft rpm of the original data set measured using the continuous data acquisition i.e., before any filtering is applied. It should be noted that the power is normalised by design shaft power. From the plots one might be able to notice the quality of data recorded and the scatter in data. We expect the ship speed to be roughly linear with the shaft rpm and the plots indicate the same. Nevertheless, there is considerable spread in the trend with a wide range of shaft speeds for a particular speed or range of shaft rpm for a constant ship speed. This can partly be attributed to the time delay in the acceleration and deceleration of the ship with change in shaft rpm. For instance, the captain would have decreased the fuel throttle resulting in lowering of the shaft rpm but the ship speed takes a while to decrease. The power vs speed relation does reveal some scatter in the data with some relatively high shaft power for lower ship speeds, however, a cubic relation is clearly visible in the plot. It is expected that the filtering of this original dataset to remove some of the outliers would produce well-defined relationships between these operating parameters.

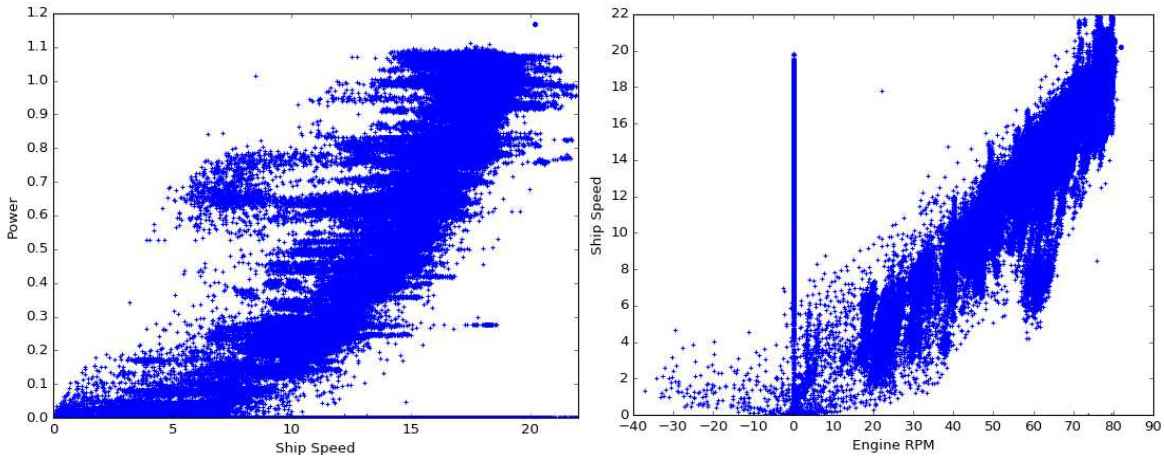

(a) (b)

Fig.3: (a) Power vs Ship speed, (b) Ship speed vs RPM plots for the original data

3.2 Calm water power

The power, speed and shaft rpm scatter plots for the data filtered for the calm water model by applying the constraints described in section 2.2 are shown in Fig.4. The filtering produces much better trends and decreases the spread of data. It is seen from the plots that we can obtain a cubic fit that represents the shaft power against the ship speed very well. Similarly, the variation is ship speed against the shaft rpm is also quite linear in Fig.4.

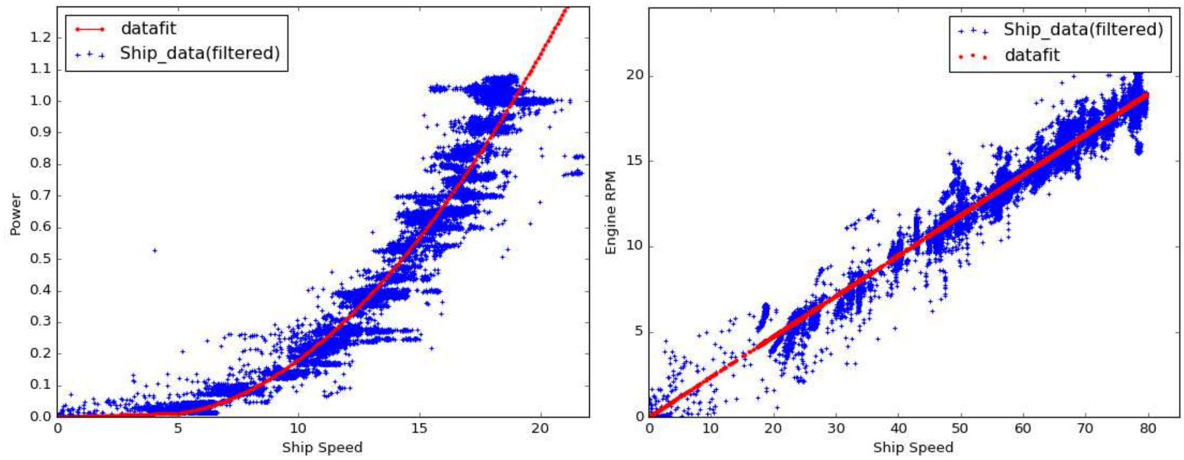

(a) (b)

Fig.4: (a) Power vs Ship speed, (b) Ship speed vs RPM for the filtered dataset

Table I: Percentage difference in calm-water power for increase in draft (9.0-11.0m). Positive value indicates an increase in shaft power.

Speed [kn]	16-17	17-18	18-19	19-20
difference	-10%	5%	7%	3%

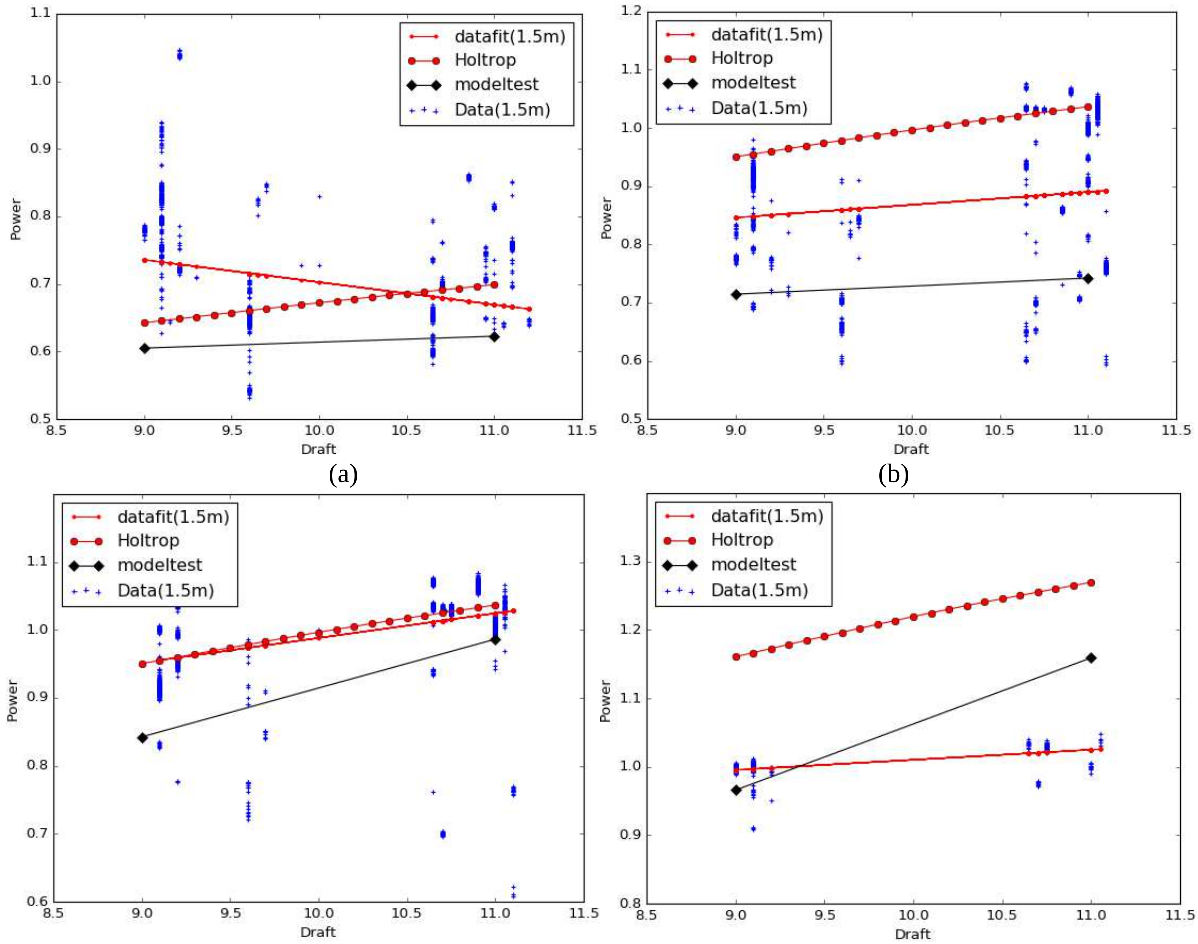

(a) (b) (c) (d)

Fig.5: Calm water power vs draft (a) 16-17 knots (b) 17-18 knots (c) 18-19 knots (d) 19-20 knots

Fig.5 shows the calm water powering for four speed bins plotted against the variation in draft. The data in all speed bins is mainly concentrated at two or three draft levels. The effective power obtained using Holtrop and model tests are divided by propulsive efficiency (η_D) to make a reasonable comparison with the recorded shaft power. The value of propulsive efficiency is assumed as 0.74 in this case. It should be noted that in the present investigations the draft and trim effects are not decoupled since this would require a much larger data set for every recorded draft and trim condition. For the speed bins 17-18, 18-19 and 19-20 knots the shaft power increases with increase in draft. The calm water power is proportional to the displacement raised to the power of 2/3 and hence the trends reflect a reasonable performance (Molland et al. 2011). **Error! Reference source not found.** shows the percentage difference in calm water power estimated from 9 m to 11m draft. For the speed interval 16-17 knots there is a decrease in shaft power about 10% for a change of draft from 9 m to 11 m. For speed bins other than 16-17 knots the shaft power increases with increase in draft so for the sake of understanding the power vs speed trends two speed bins (16-17 knots and 18-19 knots) were considered. The operational data for 16-17 knot bin suggest that there could be favorable operational drafts which could result in lower shaft power. For instance, the shaft power recorded at 9.2 m draft is on an average about 12-13% higher than those recorded at drafts greater than 9.6 m, whereas this is not the case for the 18-19 knot speed bin. Fig.6 shows the plot of engine rpm vs draft for two bins with a linear curve fitting the data. It is apparent from the trends that there is a slight decrease in shaft rpm for the 16-17 knot bin. There could be several other operational parameters (wave height, wind speed and direction, trim etc.) that could be influencing this behavior, nevertheless even for similar operational and weather parameters the shaft power were higher at around 9-9.2 m draft and decreased with increase in draft.

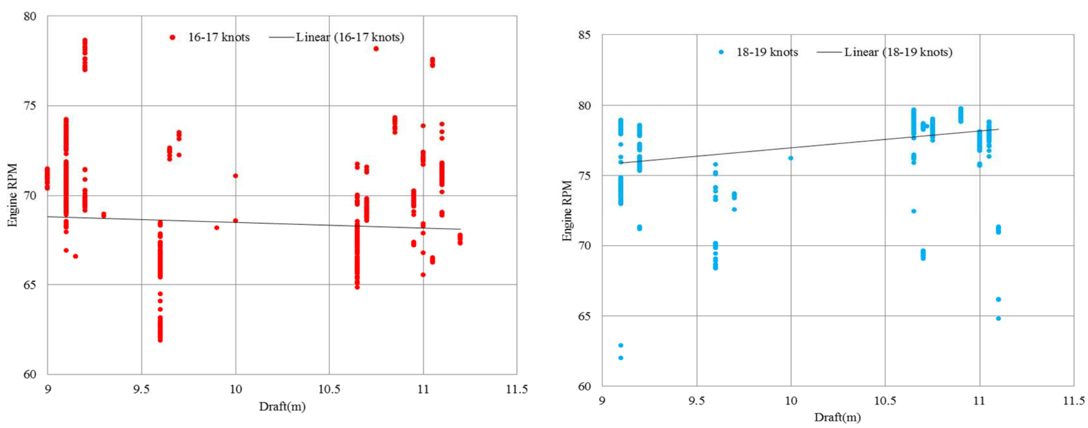

(a) (b)

Fig.6: Engine RPM vs Draft for ship speed of (a) 16-17 knots (b) 18-19 knots

Results in Fig.7 show that in general there is a benefit for trim by stern at all speeds, apart from 18-19 knots. The first two speed bins exhibits an obvious improvement in shaft power with the ship trimmed by the stern by about 4-5%. The benefit is marginal in the case of 19-20 knots, at about 0.6 % decrease with trim by stern. At 18-19 knots, moderate trim has little effect on the calm water shaft power and is approximately a constant (0.4% difference between even keel and 1.4 m trim by stern). For the vessels in this study moderate trim by stern seems to be beneficial for the calm water powering at the operational speeds investigated.

To study the effect of the significant wave height on the calm water model of power two additional wave heights (1.0m and 2.0m) were used to calculate the calm water power with respect to change in draft for the four speed bins. **Error! Reference source not found.** shows the number of data points obtained for the three significant wave height conditions and the power vs draft plots are shown in Fig.8. Firstly, the behaviour of the calm water power with change in draft is similar; however, there are changes in the slope of the fit for certain speed bins. The linear fit is very similar for 17-18 and 19-20 knots speed bins which is not the case for the 16-17 and 18-19 knots. In the case of 16-17 knots, the MetOcean data largely consisted of wave heights lower than 1.0 m, especially at lower drafts. This is demonstrated in Fig.9 where it is seen that more data points are retained in the lower draft interval (9-10m) than the higher.

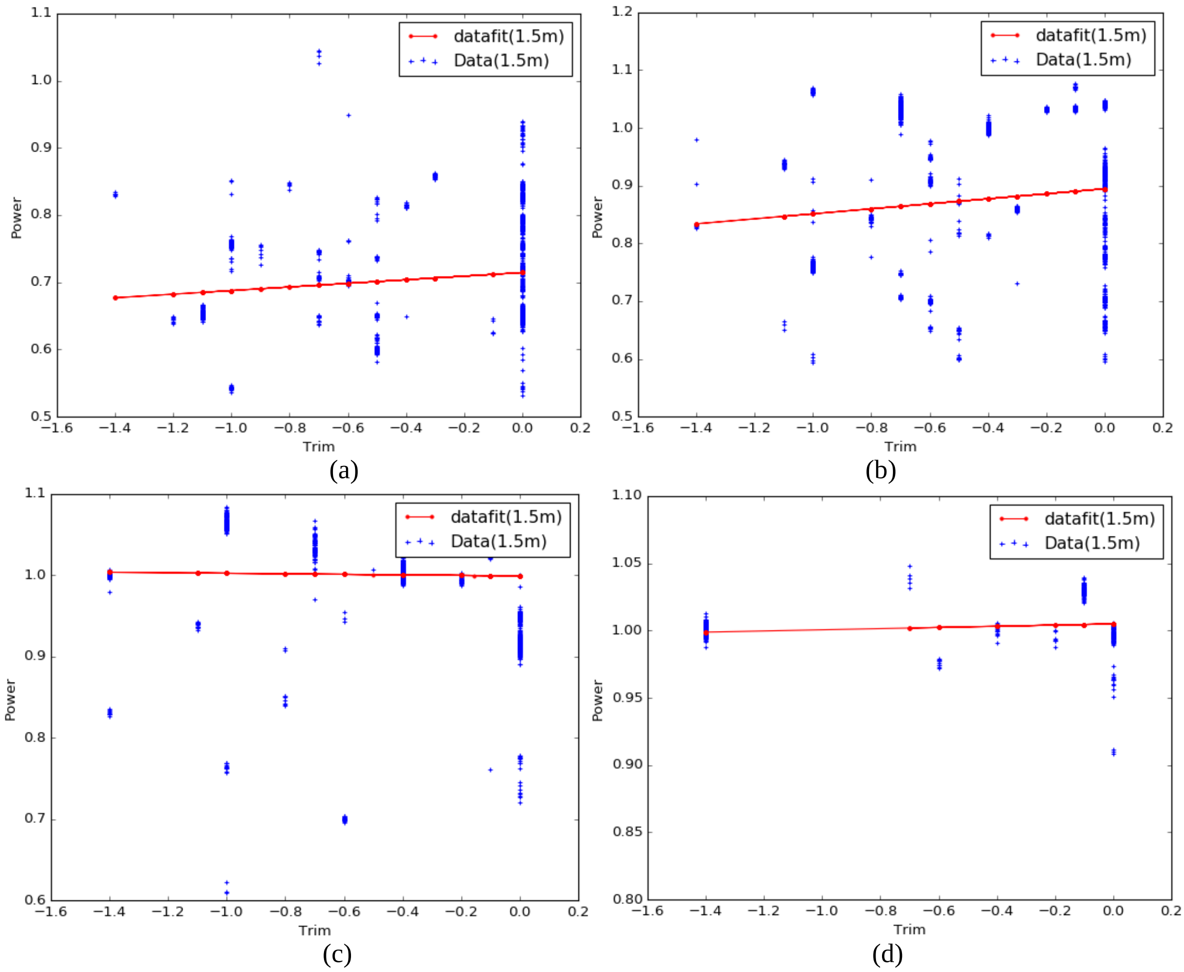

Fig.7: Calm water power vs trim (a) 16-17 knots (b) 17-18 knots (c) 18-19 knots (d) 19-20 knots.

For this speed bin the shaft power recorded were higher at the lower drafts even when the wave heights were very small. When using a higher wave height criteria the effect averages out and the slope of the linear fit decreases. At 18-19 knots speed bin the ship at lower draft operates predominately in the wave height of 1.0-1.4 m and using a lower wave height filters out these data points resulting in a steeper slope. This exercise illustrates that it is not always the number of data points that reflects the accuracy of estimations of the calm water model, but also how well that data is spread in the region of interest. In this case after using different wave heights, when the filtered data has enough quality data points spread evenly within the region, there are negligible changes in the power predictions using a curve fit. Nevertheless, if there is a bias in the data due to the filtering applied which results in a change in trend then the reason for such variations should be investigated to ascertain the relative accuracy between them. For example, in this case the variation in slope in 16-17 knots for 1.0 m wave height is due to the omission of some data points in the higher draft resulting in even fewer recordings. Although, it is appropriate to estimate the calm water resistance for the smallest wave height possible, it is also important to make the judgement if there are sufficient data points to generate a fit through the data points with minimum uncertainty.

Table II: Number of data points in four speed bins for three wave heights.

Wave Height	16-17 knots	17-18 knots	18-19 knots	19-20 knots
1.0 m	705	640	927	270
1.5 m	1976	1481	1794	555
2.0 m	3157	2723	2914	652

Finally, the effect of calm-water power vs draft for 16-17 knots speed bin is investigated by increasing and decreasing the sampling frequency of the original data set to 1 min and 15 min, respectively. The data is up sampled to 1 min frequency by duplicating the original dataset. The results of investigation shown in Fig.10 displays that there is minimal effect changing the sampling frequency and the relative accuracy remain unchanged in this case.

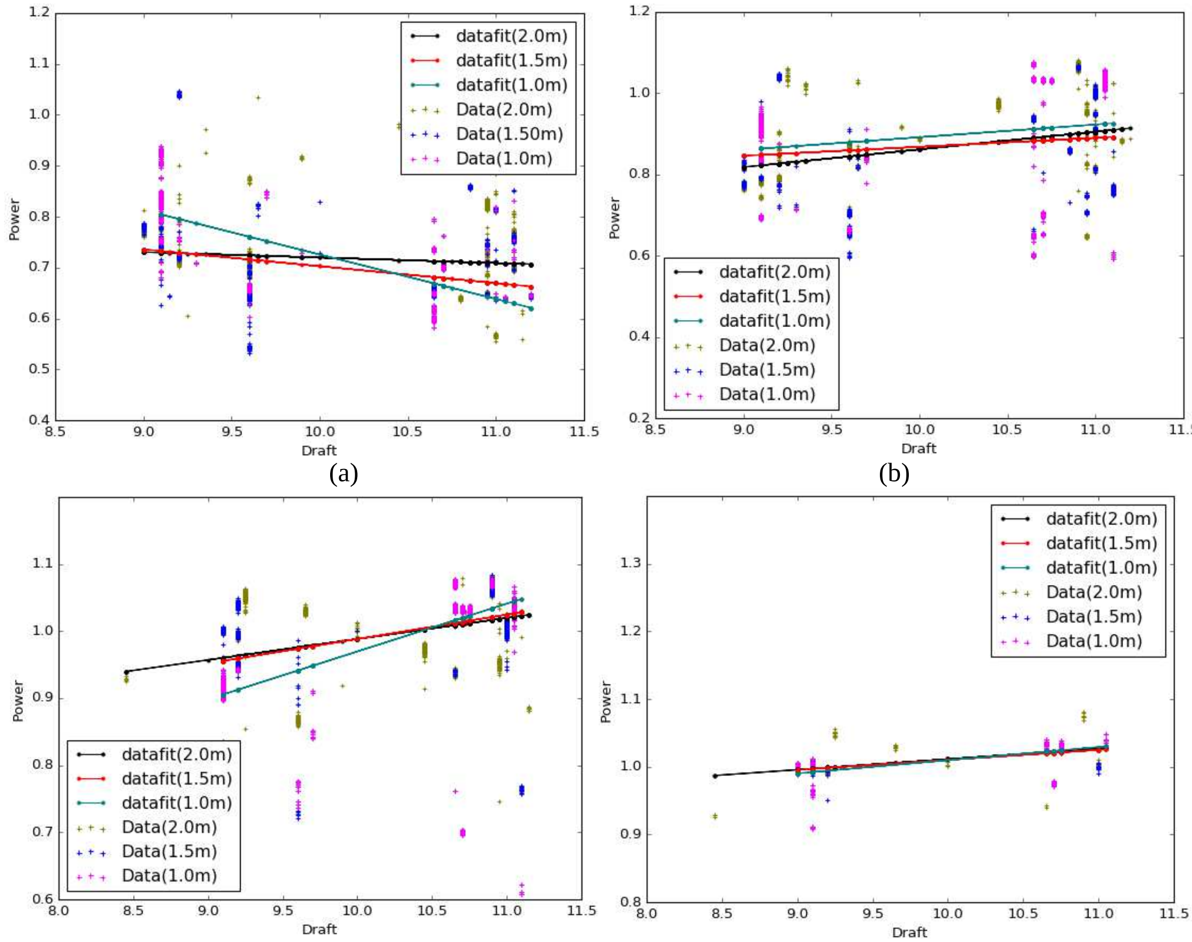

(a) (b)

(c) (d)

Fig.8: Calm-water power vs draft calculated for a constrained data set using 2 wave heights (a) 16-17 knots (b) 17-18 knots (c) 18-19 knots (d) 19-20 knots.

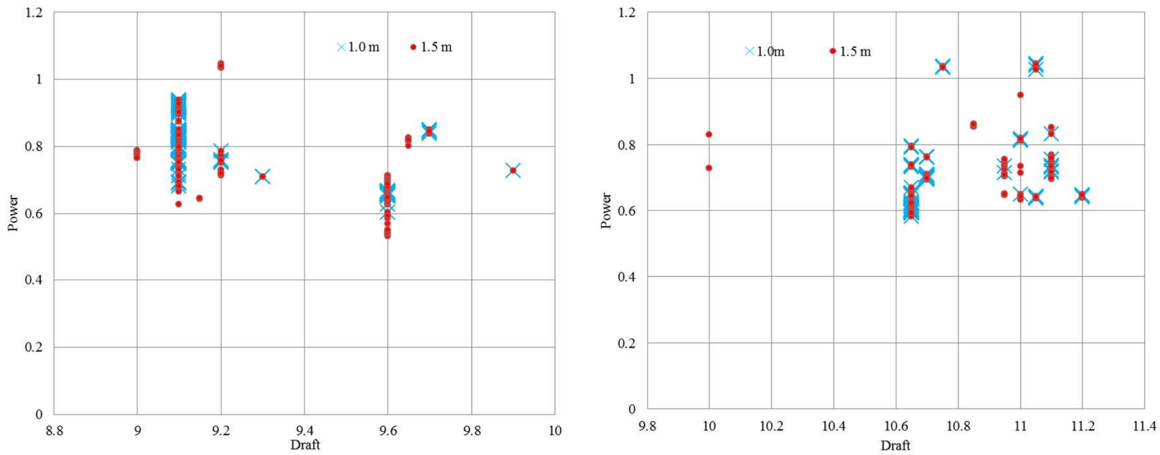

(a) (b)

Fig.9: Power vs draft for wave height (16-17 knots) of 1.0 and 1.5 m for (a) 9-10m and (b) 10-11 m draft interval.

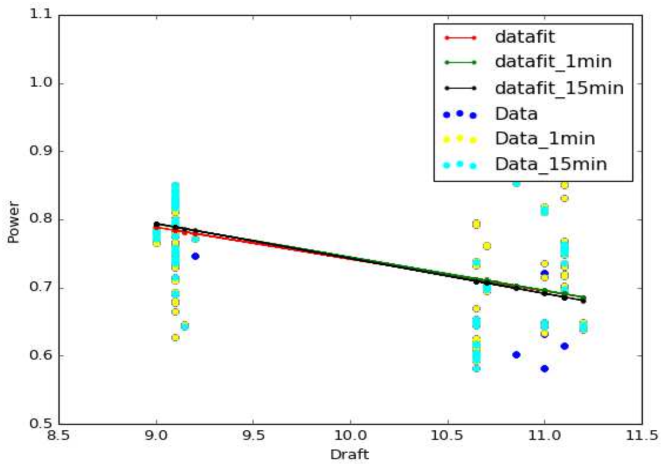

Fig.10: Calm-water power vs draft for original dataset sampling frequency increased and decreased

3.3 Added power in waves

The added power for the speed bins are estimated as per the equation in section 2.2. The original data set is filtered using a few constraints before subtracting the calm water power calculated. The constraints applied were:

- Draft greater than 8.0 m.
- Average shaft speed greater than 0.0, so no astern running.

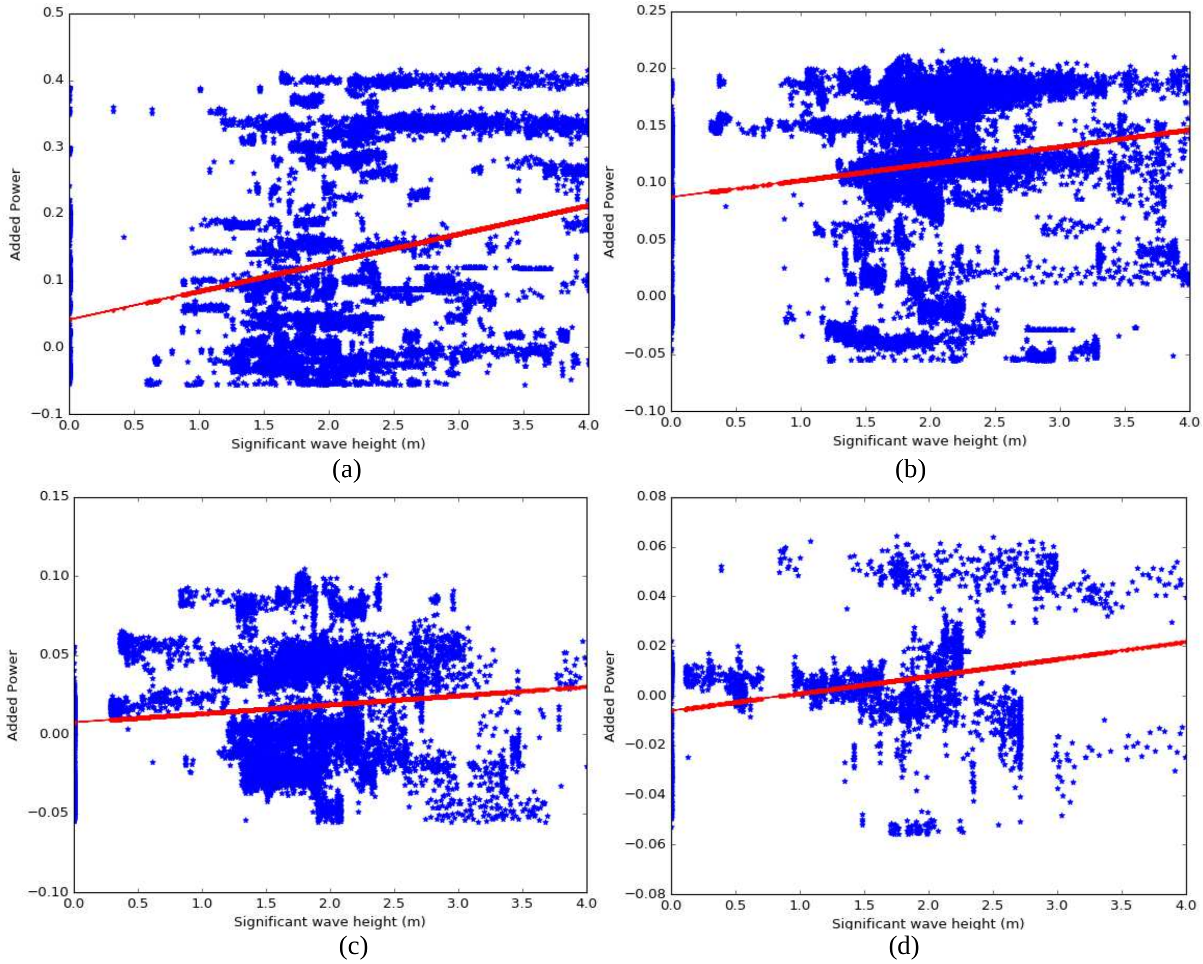

Fig.11: Added power in waves for (a) 16-17 knots (b) 17-18 knots (c) 18-19 knots (d) 19-20 knots

The data is then segregated into the four speed bins and the added power is calculated by subtracting the shaft power from the calm water predicted using the linear fit. It is ensured that the calm water power used to calculate the additional power is for the same draft conditions. The added power is only plotted as a function of significant wave height. The effect of ship heading relative to the wave is not considered since filtering the data points for each speed bin into heading bins (0-45, 45-90, 90-135 and 135-180 degrees) resulted in few data points. This results in considerable scatter in the data for the various speed bins in Fig.11 when compared to previous investigations by *Webb and Hudson (2015)*. A linear fit is also shown in the plots and although, this may not be the best fit possible, it will produce an overall trend of the added power due to the weather effect. Fig.11 displays a clear increase in added power with respect to increase in wave height. It is also encouraging that the added power in waves converges to a very small value for zero significant wave height. The maximum power increase is seen in the case of 16-17 knots where for 0.0 m to 4.0 m increase in wave height the added power increases by about 20%. At the other three speed intervals the weather effect increases the shaft power by a maximum of about 5-7%.

4. Conclusions

A method to calculate the calm water and added power in waves is investigated through data recorded using continuous in-service monitoring. The original data set is filtered by applying constraints to obtain a calm water model. The data quantity is reduced to approximately 10 % of the original dataset which can still provide valuable insights into calm water power variations with draft and trim for various operating speed bins. Three wave heights were used to model the calm water power for various speed bins. It was seen that if the filtered data represents the operating conditions well (vs draft) then the changes in the calm water power fit are modest even when the quantity of data is reduced. Hence, the quality of data is equally important as the quantity of data. The required calm water power showed an increase with increase in draft, except at one speed bin. Trim by stern seems to be marginally beneficial (about 5%) in calm water at lower operating speeds and has little effect with an increase in speed. The effect of weather on the shaft power had a considerable effect in the lower speed, however, for the other speeds investigated the added power requirements increased by a maximum of about 7 % due to the effect of waves. The power variation is only presented with respect to the wave heights and to investigate effect of ship headings more data points will be required. In the present approach, the accuracy of calm water model has a significant effect on the added power in waves. Numerical data and model tests should be considered to better understand calm water model using in-service data and make appropriate improvements to it.

References

ALDOUS, L.; SMITH, T.; BUCKNALL, R. (2013), *Noon report data uncertainty,* Low Carbon Shipping Conf., London

ALDOUS, L.; SMITH, T.; BUCKNALL, R. (2015), *Uncertainty analysis in ship performance modelling*, Ocean Eng. 110, pp.29-38

BERTRAM, V. (2012), *Practical Ship Hydrodynamics*, Butterworth-Heinemann

BERTRAM, V. (2016), Added power in waves-time to stop lying (to ourselves), Hull Performance & Insight Conf., Pavone, pp. 5-13

DINHAM-PEREN, T.A.; DAND, I.W. (2010), *The need for full scale measurements*, William Froude Conf.: Advances in Theoretical and applied Hydrodynamics-Past and Future, Portsmouth, pp. 1-13

DUCKERT, T.; SCHMODE, D.; TULLBERG, M. (2016), *Computing hull and propeller performance: Ship model alternatives and data acquisition methods,* Hull Performance & Insight Conf., Pavone, pp. 23-28

GRADO, D.H.; BERTRAM, V. (2016), *Predicting added resistance in wind and waves employing artificial neural nets*, Hull Performance and Insight Conf., Pavone, pp.14-22

HOLTROP, J.; MENNEN, G.G.J. (1982), *An approximate power prediction method,* Int. Shipbuilding Progress 29, pp.166-170

KWON, Y.J. (2000), *Estimating the effect of wind and waves on ship speed and performance*, The Naval Architect

LIU, S.; PAPANIKOLAOU, A.; ZARAPHONITIS, G. (2011), *Prediction of added resistance of ship in waves*, Ocean Eng. 38, pp.641-650

MOLLAND, A.F.; TURNOCK, S.R.; HUDSON, D.A. (2011), *Ship Resistance and Propulsion: Practical Estimation of Ship Propulsive Power*, Cambridge University Press

PARKES, A.I.; SOBEY, A.J.; HUDSON, D.A. (2017), *Physics-based shaft power prediction for large merchant ships using Neural Networks*, Applied Soft Computing (Under Review)

PEDERSEN, B.P.; LARSEN, J. (2009), *Modeling of ship propulsion performance,* World Maritime Technology Conf., Mumbai

TEZDOGAN, T.; DEMIREL, Y.K.; KHORANSANCHI, M.; INCECIK, A.; TURAN, O. (2015), *Full scale unsteady RANS CFD simulations of ship behaviour and perforamnce in head seas due to slow steaming*, Ocean Eng. 97, pp.186-206

TOWNSIN, R.L.; KWON, Y.J. (1983), *Approximate formulae for the speed loss due to added resistance in wind and waves,* Trans. RINA 125, pp.199-207

WEBB, A.; HUDSON, D.A. (2015), *Identifying added shaft power in weather from voyage analysis of RORO carrier, 18th Int. Conf. on Ships and Shipping Research*, Milan

`

Modeling of Ship Resistance as a Function of Biofouling Type, Coverage, and Spatial Variation

Abel Vargas, Hua Shan, Naval Surface Warfare Center Carderock Division,
West Bethesda/USA, abel.vargas@navy.mil

Abstract

A roughness wall model based on the equivalent sandgrain roughness approach that accounts for the log-law solution for turbulent boundary layer over biofouled surfaces is implemented into a viscous flow solver called NavyFOAM. The rough wall model is implemented as a wall function and is used in conjunction with the k-ω turbulence model. Two-phase unsteady Reynolds-Averaged Navier-Stokes (RANS) calculations were conducted on rough plates towed in a channel and validated against experimental data. The overall frictional resistance predicted for the rough plates towed in a water channel is within 2% of the experimentally obtained results. The current roughness model was then applied to a typical Navy destroyer covered by homogenous fouling ranging from light slime to heavy calcareous fouling. These simulations are the first steps in understanding the relationship between hull roughness, drag, and ship performance, and how that relationship changes with size, shape, distribution, and abundance of biofouling.

This paper is provided for information only and does not constitute a commitment on behalf of the U.S. government to provide additional information on the program and/or sale of the equipment or system.

1. Introduction

Biofouling is a constant problem in the marine industry whereby the buildup of microorganisms, plants and animals occurs on wet surfaces. Biofouling can range from soft fouling which includes biofilm slime, algae, and seaweed to hard fouling such as barnacles, tubeworms, and mollusks. Even the best antifouling paint cannot inhibit the accumulation of biofouling on a ship. On ship hulls, biofouling can impact the ships performance by increasing its frictional drag causing an increase in shaft power just to maintain a given speed, *Towsin (2003), Towsin (1981), Leer-Andersen and Larsson (2003), Schultz (2007), Schultz et al. (2011).* This increase in frictional drag adds an additional burden to the total ownership of a ship. For example, *Schultz et al. (2011)* estimates that the overall cost to the entire Arleigh Burk-class (DDG 51) destroyer fleet could be $56M a year which accounts for an increase in fuel consumption attributed to an increase in frictional drag plus the cost of hull cleaning and painting. The majority of the cost is attributed to the excess consumption of fuel to overcome the additional increase in frictional drag due to biofouling.

The full-scale predictions on the drag penalty and the decrease in efficiency performance are based on laboratory-scale tow tank measurements and Granville's, *Granville (1958), Granville (1987*) boundary layer similarity law analysis, as real sea trail data is difficult to obtain because it would interrupt the ship's service evolutions. Also, a ship is seldom available for a comprehensive test on biofouling as they are usually in service. A better approach in quantifying biofouling that can reduce the assumptions made in the full-scale predictions is using Computational Fluid Dynamics (CFD), where viscous and free-surface effects are taken into account.

Reynolds-Averaged Navier-Stokes (RANS) methods, typically used for modeling flow features around ship hulls, can potentially provide quantitative estimates of the resistance changes due to roughness. The application of RANS roughness modeling on ship hulls has not been adequately explored.

Recent numerical studies that incorporate roughness in their simulations include those by *Demirel et al. (2014), Khor and Xiao (2001), Izaguirre-Alza et al. (2010), Knopp et al.* (2009), *Leer-Andersen and Larson (2003)*. These studies, except for *Knopp et al*. (2009), focused on understanding the

`

roughness caused by antifouling (ATF) coatings with the aid of commercial CFD software, STAR-CCM+, *Demirel et al. (2014), Izaguirre-Alza et al. (2010)*, ANSYS Fluent *Khor and Xiao (2001)*, and SHIPFLOW *Leer-Andersen and Larsson (2003)*, with each software having a different built-in roughness model. *Knopp et al*. (2009) sought to develop a generalized roughness model by modifying two-equation k-ω turbulence model which imposes finite wall values to the turbulent kinetic energy and specific dissipation rate. This concept stems from the strategy presented by *Aupoix and Spalart (2003)* and *Durbin et al. (2000)* and the model is validated against experiments of *Ligrani and Moffat (1986).*

Although there are numerous experimental studies on roughness dating to *Nikuradse's (1933)* experiments on uniform, closely-packed sand, numerical work on biofouling is limited. The present paper implements the k-ω turbulence model with roughness modifications proposed by *Knopp et al*. (2009) into NavyFOAM, *Shan et al. (2011)* - an integrated Computational Fluid Dynamics package based on OpenFOAM, *Weller et al.(1998)*, developed at the Naval Surface Warfare Center Carderock Division funded by the Department of Defense High Performance Computing Modernization Program (HPCMP) under the CREATE Ship's Hydrodynamics Program. NavyFOAM includes a number of new features and advanced capabilities such as discretization schemes, advanced turbulence models, single-phase and multi-phase flow solvers and customized post-processing utilities not included in OpenFOAM. The functionalities of NavyFOAM are specifically tailored to naval applications ranging from surface ships, *Gorski et al. (2014), Kim et al. (2010)*, to submarine, *Kim et al. (2014)*, cavitation, *Kim and Brewton (2008), Kim and Schroeder (2010)* and propeller flow analysis, *Kim et al. (2010).* Both Reynolds-Average Navier-Stokes and Large Eddy Simulations (LES) capabilities also part of NavyFOAM's capabilities.

The roughness model has been validated against experiments conducted on rough plates in a water tunnel, *Schultz and Flack (2007), Flack et al. (2007)* and towed in a channel, *Schultz (2004)* and the results are found in *Vargas and Shan (2016)*. The roughness wall model is based on the equivalent sand grain roughness approach and accounts for theoretical considerations on the log-layer solution for fully rough surfaces; as a result, it is not constrained by extremely fine near wall resolution as required in the Wilcox roughness model. This alleviates the grid resolution issue when modeling high Reynolds number flows. The rough wall model is implemented as a wall function and can be used in conjunction with either the Wilcox k-ω model, *Wilcox (2006)* or the Menter's SST k-ω model, *Menter et al. (2003)*.

The roughness validation simulations, *Vargas and Shan (2016)* which accounted for roughness in the fully rough regime showed good agreement with the roughness functions (ΔU^+) and is within 1.5% of the experimental results. The overall frictional resistance predicted for the rough plates towed in a water channel was within 2% of the experimentally obtained results. With these promising results, the aim is to modify the roughness model to take into account biofouling that lies in the transitional regime and also have the capability to simulate the effect of antifouling coatings on ship hulls with low equivalent sandgrain roughness (k_s) values.

2. Governing Equations

The multi-phase solvers in NavyFOAM, as described in detail in *Shan et al. (2011)* were used in the current investigation. In addition to this reference, further details regarding the numerical methods can be found in *Shan and Kim (2011)* and *Gorski et al. (2014).* Here we provide a brief overview of the current method. In NavyFOAM, the free-surface is resolved by a two-phase, single-fluid Volume-Of-Fluid (VOF) method, *Hirt and Nichols (1981)*. The governing equations consist of the continuity equation, the momentum equation, the convection equation for volume fraction, and the turbulence transport equations. The continuity and momentum equation are written as:

$$\nabla \cdot \boldsymbol{u} = 0 \tag{1}$$

$$\frac{\partial(\rho \boldsymbol{u})}{\partial t} + \nabla \cdot (\rho \boldsymbol{u}\boldsymbol{u}) = -\nabla p + \nabla \cdot \left\{\mu_{eff}(\nabla \mathbf{u} + \nabla \boldsymbol{u}^T)\right\} + \rho \boldsymbol{g} + \Gamma \kappa \nabla \alpha, \tag{2}$$

`

$\boldsymbol{u}$ is the velocity vector, p the hydrodynamic pressure, , α the volume fraction, $\boldsymbol{g}$ the gravitational acceleration vector, Γ the surface tension coefficient, and κ the interface curvature, $\mu_{eff} = \mu + \mu_t$ the effective viscosity, μ the dynamic viscosity, and μ_t the turbulent eddy viscosity. The mixture properties such as density and dynamic viscosity are computed as functions of α from:

$$\rho = \alpha\rho_w + (1-\alpha)\rho_a, \tag{3}$$

$$\mu = \alpha\mu_w + (1-\alpha)\mu_a, \tag{4}$$

where the subscripts "w" and "a" denote water and air, respectively. The phase composition is represented by volume-fraction. The volume-fraction is obtained by solving its advection equation:

$$\frac{\partial\alpha}{\partial t} + \nabla\cdot(\boldsymbol{u}\alpha) = 0. \tag{5}$$

3. Turbulence Model

NavyFOAM contains a suite of turbulence models for incompressible flows, such as the *k*-ω model, *Wilcox (2006)*, and the SST *k*-ω model, *Menter et al. (2003)*. For the sake of briefness, the equations for the *k*-ω model are presented as follows:

$$\frac{\partial k}{\partial t} + \nabla\cdot(\boldsymbol{u}k) - \nabla\cdot[(\alpha_k\nu_t + \nu)\nabla k] = G - c_\mu\omega k, \tag{6}$$

$$\frac{\partial\omega}{\partial t} + \nabla\cdot(\boldsymbol{u}\omega) - \nabla\cdot[(\alpha_\omega\nu_t + \nu)\nabla\omega] = \gamma\frac{\omega}{k}G - \beta\omega^2 + \frac{\sigma_d}{\omega}\nabla \mathrm{k}\cdot\nabla\omega, \tag{7}$$

with k the turbulent kinetic energy, ω the specific dissipation rate of turbulent kinetic energy, G the production of turbulent kinetic energy, and model parameters c_μ, β, α_k, α_ω, γ, and σ_d are model parameters.

The wall function approach is widely utilized in engineering CFD applications. By placing the first grid point in the log-law region of the boundary layer, a relatively coarse mesh can be used for high Reynold number flows. The log-law a for turbulent boundary layer can be written as:

$$U^+ = \frac{1}{\kappa} ln\, y^+ + C, \tag{8}$$

$y^+ = y\,u_\tau/\nu$, κ = 0.41, C = 5.1, and $U^+ = u/u_\tau$, where u_τ is the friction velocity. Assuming equilibrium between the production and dissipation rate of turbulent kinetic energy, the following wall functions can be obtained:

$$\omega = \frac{k^{1/2}}{c_\mu^{1/4}\kappa y_{\Delta/2}}, \tag{9}$$

$$\nu_t = \nu\left(\frac{\kappa y^+_{\Delta/2}}{\ln(E\,y^+_{\Delta/2})} - 1\right), \tag{10}$$

$y_{\Delta/2}$ represents the wall-normal distance of the first cell center next to the wall, and E = 9.8441.

4. Roughness Model

For a turbulent boundary layer over rough surfaces, the log-law can be written as:

`

$$U^+ = \frac{1}{\kappa} ln\left(\frac{y}{k_s}\right) + B \text{,} \tag{11}$$

k_s is the equivalent sandgrain roughness height. *Nikuradse (1933)* found experimentally that B = 8.5 for turbulent pipe flow in the fully rough regime with sandgrain roughness and this constant was also confirmed by the experiments of *Ligrani and Moffat (198*6). For a more general case, B may depend on k_s and the nature of roughness, *Knopp et al. (2009), Ligrani and Moffat (1986),* and the following curve fit for B is proposed:

$$B = \left[C + \frac{1}{\kappa} ln\left(k_s^+\right)\right](1 - sin(\pi h/2) + 8.5\, sin(\pi h/2) \text{,} \tag{12}$$

with interpolation function h for the transitional rough regime

$$h = \begin{cases} \dfrac{ln\left(k_r^+ / k_{r,S}^+\right)}{ln\left(k_{r,R}^+ / k_{r,S}^+\right)}, & k_{s,S}^+ < k_s^+ < k_{s,R}^+ \\ 1, & k_s^+ > k_{s,R}^+ \\ 0, & k_s^+ < k_{s,S}^+ \end{cases} \tag{13}$$

where $k_s^+ = k_s u_\tau / \nu$, $k_{s,S}^+ = k_{s,S} u_\tau / \nu$, and $k_{s,R}^+ = k_{s,R} u_\tau / \nu$. The value of $k_{s,S}^+$ is the upper limit where the surface is considered hydraulically smooth and $k_{s,R}^+$ is lower threshold of the fully rough regime. Both $k_{s,S}^+$ and $k_{s,R}^+$ will depend on the roughness-geometry characteristics of the surface.

Note that (11) can be written as:

$$U^+ = \frac{1}{\kappa} \ln\left(\frac{y + d_0}{d_0}\right). \tag{14}$$

The variable d_0 is a hydrodynamic roughness length which represents the effective origin for turbulence where the turbulent kinetic energy can be properly implemented at the wall. As stated in *Durbin et al. (2000)*, d_0 is not a physical length but a way to produce suitable mean velocity and can be represented by:

$$d_0 \approx k_s e^{-\kappa B}. \tag{15}$$

As shown in *Knopp et al. (2009)*, utilizing the roughness log-law (15) and assuming equilibrium between the production and dissipation of the turbulent kinetic energy, the following wall functions can be obtained:

$$\omega = \frac{k^{1/2}}{c_\mu^{\ 1/4} \kappa (y_{\Delta/2} + d_0)}, \tag{16}$$

$$\nu_t = \nu \left(\frac{\kappa y_{\Delta/2}^+}{ln[(y_{\Delta/2} + d_0)/d_0]} - 1 \right). \tag{17}$$

5. Numerical Methods

The above roughness wall function has been integrated into NavyFOAM. The spatial discretization of the flow equations is based on the cell-centered finite-volume method for unstructured polyhedral meshes. The Navier-Stokes equations are solved implicitly in a segregated manner, making use of Pressure-Implicit with Splitting of Operators (PISO) type methods for velocity-pressure coupling. The solution gradients at cell centers are evaluated by applying the Green-Gauss theorem. The linear system of equations resultant from the pressure Poisson equation are solved using the preconditioned conjugate gradient (PCG) method. The linear system of equations resulting from the momentum equations is solved using the preconditioned bi-conjugate gradient (PBiCG) method. The spatial schemes are of second-order accuracy.

In the two-phase simulations, the modified high resolution interface capturing (MHRIC), *Park (2009)* scheme was used for the discretization of the advection term in the volume-fraction equation. MHRIC offers a sharper interface to capture the free-surface and is the scheme of choice when an air-water interface is present. The two-phase simulations employ an implicit time-advancement scheme with second-order accuracy for the volume-fraction equation.

Based on validations by *Vargas and Shan (2016)* on rough flat plates, it was determined that the results using the SST k-ω turbulence model as opposed to the High-Re k-ω model yield a smaller percentage difference when compared against the experimental results. Based on this finding, the simulations presented here employ the SST k-ω turbulence model with the adaptive roughness model.

6. Computational Geometries

6.1 Computational Domain: Towed 3-D Flat Plate

The grid and the computational domain for the plate towed in the water channel is seen in Fig.1. The plate is 1.52 m long, 0.76 m wide, and 3.2 mm thick with rounded leading and trailing edges with a 1.6 mm radius. The dimensions of the tow tank as described by *Schultz (2004)* are incorporated in the model. The bottom boundary which represents the floor of the tow tank is 4.9 m from the free-surface, and the lateral walls are 3.95 m from the center of the plate. A no-slip boundary condition was applied to all solid walls.

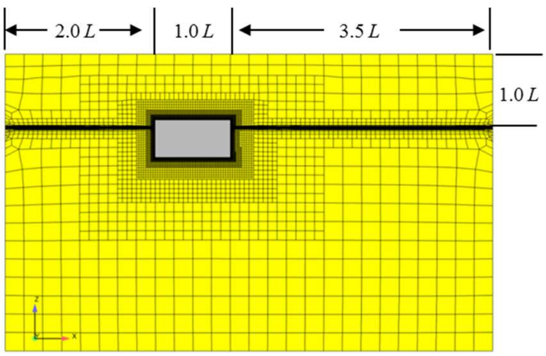

Fig.1: Computational domain for a towed plate

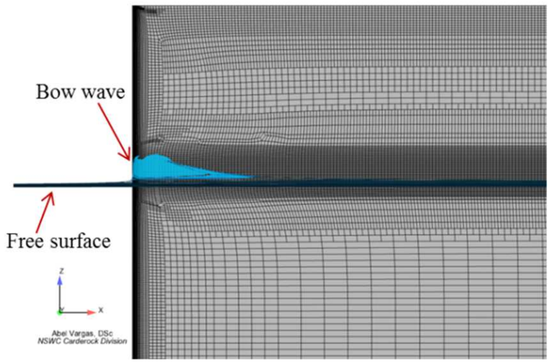

Fig.2: Surface grid at the leading edge of the vertically towed plate for the fine mesh case

The top boundary is 1.0 body length (L) above the undisturbed free-surface and incorporates a slip boundary condition. The leading edge of the plate is positioned 2.0 body lengths from the inlet boundary and the outlet boundary is 3.5 body lengths from the trailing edge. A constant inflow velocity normal to the boundary was imposed on the inlet boundary, and the outlet boundary was set to an outflow boundary, where the velocity gradient values are set to zero.

`

A non-conformal body-fitted full hexahedral unstructured grid was generated using HEXPRESS™, which allows for clustering near the free-surface and around the body thus reducing the overall cell count when compared to a block-to-block structured mesh. Several computational meshes were generated to arrive at a grid with sufficient resolution to resolve the free-surface and the wave at the leading edge as seen in Fig.2. HEXPRESS™ also provides smoothing capability to produce high-quality boundary layer grids. A wall function mesh with the first wall-adjacent cell at $y^+ \sim 60$ grown with a stretching ratio of 1.10 has twelve layers to resolve the boundary layer. The final grid of 8 million cells includes a thick band near the free-surface and tight spacing in the vertical direction to capture the subtle changes in the free-surface.

6.2 Flow Conditions: Three-Dimensional Towed Flat Plate

In the towed experiments of *Schultz (2004)*, different antifouling paints, 220-grit, and 60-grit sandpapers were tested at a Reynolds Number based on length (Re_L) ranging from 2.8×10^6 to 5.5×10^6. Among all the rough surfaces tested, the antifouling coatings have very low k^+ values, and thus the reason for modifying the roughness model in order to take into account the wide spectrum of roughness heights. The flat plates were simulated with a coverage of 60-grit sandpaper, which is in the fully rough regime and the ablative copper antifouling coating. Three Reynolds numbers, 2.8×10^6, 4.2×10^6 and 5.5×10^6 based on length were evaluated. The uniform sandgrain roughness for the 60-grit sandpaper was calculated from the following expression found in *Schultz (2004)*:

$$k_s = 0.75R_t, \tag{18}$$

where R_t is the maximum peak to trough height. The R_t value reported in the experiment for the 60-grit sandpaper was 983±89μm. For the simulation, the mean value of R_t = 983μm was used to compute the sandgrain roughness.

The expression to compute the uniform sandgrain roughness for ablative copper antifouling coating as proposed by *Schultz (2004)* is:

$$k_s = 0.17R_a, \tag{19}$$

where R_a is the centerline roughness height. The R_a value reported in the experiment for the copper antifouling coating was 13±1μm. For the simulation, the mean value of R_a = 13μm was used to compute the sandgrain roughness.

6.3 Computational Domain: DTMB 5415

The DTMB 5415 model, Fig.3, was selected for the hull roughness calculations as it represents a US Navy Surface Combatant. The flow conditions from case 3.1a were selected from "A Workshop on Numerical Ship Hydrodynamics" held in Gothenburg on 2010, *Larsson et al. (2014)*. Experimental tow tank data was performed at INSEAN by *Olivieri et al. (2001)* for a model with a length between perpendiculars *Lpp* = 5.72 m at Reynolds Number *Re* = 1.19×10^7 and Froude Number *Fr* = 0.28. The model was tested at a fixed sinkage and trim of -1.82×10^{-3}*Lpp* and -0.108° respectively.

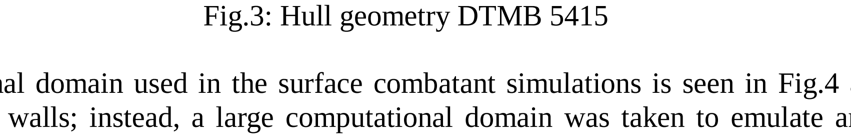

Fig.3: Hull geometry DTMB 5415

The computational domain used in the surface combatant simulations is seen in Fig.4 and does not contain the tank walls; instead, a large computational domain was taken to emulate an unbounded domain. Only one half of the ship was computed with the plane of (port-starboard) symmetry with the top boundary being 1.0 ship lengths above the undisturbed free-surface and incorporates a slip boundary condition. The other far-field boundaries, side and bottom, were placed at 1.5 and 2.0 ship lengths respectively. The bow of the ship is positioned 1.75 ship lengths from the inlet boundary and the outlet boundary is 2.0 ship lengths from the transom edge. A constant inflow velocity normal to the boundary was imposed on the inlet boundary, and the outlet boundary was set to an outflow boundary, where the velocity gradient values are set to zero.

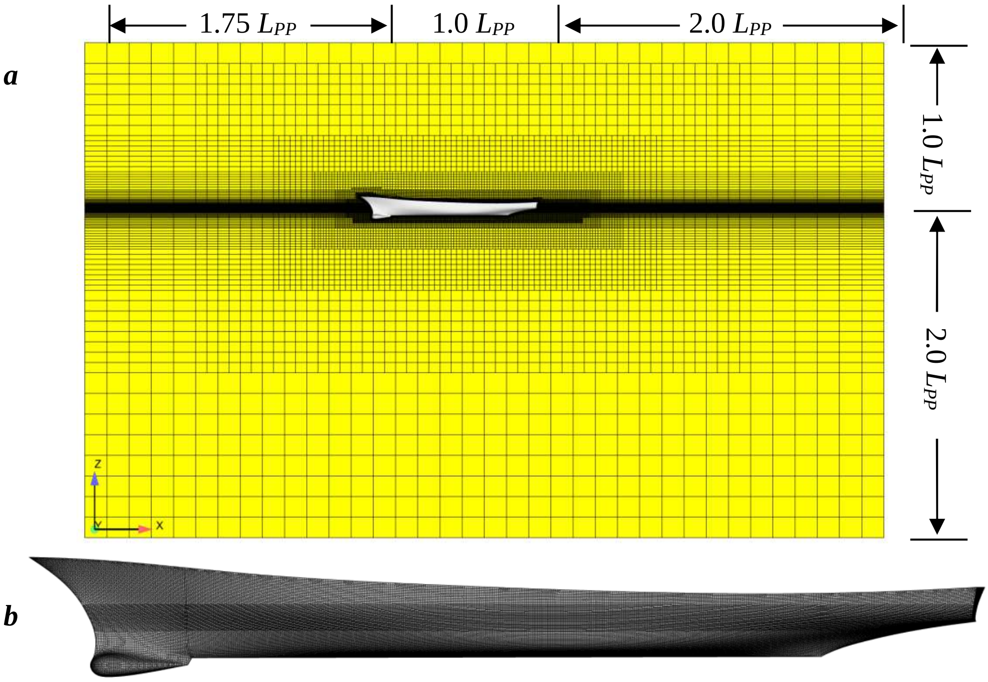

Fig.4: a) Computational domain and b) surface grid on the for DTMB 5415

As with the towed flat plate simulations, a non-conformal body-fitted full hexahedral unstructured grid was generated using HEXPRESS™. The final grid consisted of approximately 30 grid points used to resolve the free-surface having a thickness of 0.03 L_{pp}, which is more than adequate to properly capture the bow wave and the elevation changes of the free-surface near the hull. Also, a refinement zone near the hull was incorporated to produce a final grid consisting of 3 million cells. A grid refinement study was performed using three grid densities ranging from 1.5 million to a final grid used in the simulation of 3 million. As show in Table , the percent difference in the total resistance coefficient (C_F) drops as the grid increases in size, but the most important factor in driving the difference down is the resolution at the free-surface and the correct placement of the refinement zones near the hull.

Table I: Grid study comparing the total resistance of DTMB 5415

Grid Size	C_{F_CFD}	C_{F_Exp}	*% Difference*
1.5 M	0.004429	0.00423	4.60%
2.5 M	0.004102		3.08%
3.0 M	0.004227		0.06%

7. Results

7.1 Three-Dimensional Towed Plate Results

The objective of the 3D simulations was to predict the total resistance of a towed plate by inputting the experimentally obtained equivalent sandgrain roughness values for the 60-grit sandpaper and the antifouling coating into the RANS roughness model. Given that the roughness model is applied to a wall function mesh, the smooth wall analysis was carried out at a y^+ ~ 60. Fig.5 shows the iso-surface of the free-surface at $Re_L = 5.5 \times 10^6$ for a smooth plate. A leading edge bow wave is observed and there is minimal disturbance of the free-surface in the lateral direction.

Table II compares the total resistance coefficient C_F, defined as the total frictional force normalized by the dynamic pressure and wetted surface area for the smooth plate. The computational results obtained using the wall function grid has an average of 0.52% difference compared to the experimental results.

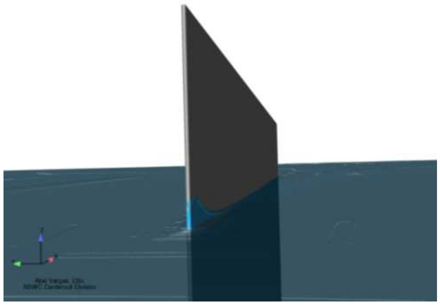

Fig.5: Iso-surface of the free-surface at $Re_L = 5.5 \times 10^6$

Table II: Total resistance for a smooth towed flat plate with $y^+ \sim 60$

Re_L	C_{F_CFD}	C_{F_Exp}	*% Difference*
5.5×10^6	0.0032405	0.0032260	0.45%
4.2×10^6	0.0033801	0.0034180	1.12%
2.8×10^6	0.0036048	0.0036050	0.01%

These results indicate that a wall function grid is sufficient to obtain the integrated values of resistance which are in excellent agreement to the experimental results. The usage of wall function grids is a practical method when applying the roughness model to surface ships operating at full scale Reynolds numbers in the order of 1×10^8. At these high Reynolds numbers, trying to generate a wall resolved grid will create a near-wall mesh having extremely high aspect ratios. In contrast, a wall function mesh relaxes the first cell off the wall, thus generating a smaller mesh, and still being able to predict the correct values of C_F.

The contours of skin friction C_f, defined as the wall shear stress normalized by the dynamic pressure, for the plate painted with the copper antifouling coating at the three Reynolds numbers are shown in Fig.6. The plate experiences a higher skin friction at the leading edge and then monotonically decreases in streamwise direction with an increase in C_f as it approaches the rounded trailing edge. This behavior is also seen in the profile of skin friction coefficient at mid-depth, $z/L = -0.194$, Fig.7. The slight increase in skin friction at the trailing edge occurs as the flow accelerates around the convex curvature. From the contour plots, the extent of the high C_f downstream of the leading-edge region is greater at a $Re_L = 2.8 \times 10^6$.

Similar to the plates with a copper antifouling coating, the skin friction is the highest at the leading edge of the 60-grit sandpaper plates as seen in Fig.8. Unlike the plate with the copper coating, there is minimal change in C_f near the leading edge for all Re_L evaluated, and the observable change in skin friction is detected at the free-surface at the formation of the bow wave. As seen in Fig.8, an increase in Reynolds number causes the skin friction at the leading edge of the plate to extend further downstream at the waterline which is attributed to the bow wave. Unlike the results shown in *Vargas and Shan (2016)* where a drop in C_f followed by a recovery was observed for all Reynolds numbers, the new roughness model eliminates this transition mainly due to the computing of the interpolation variable h and adjusting the B variable in (12) to fall under the correct roughness regime.

`

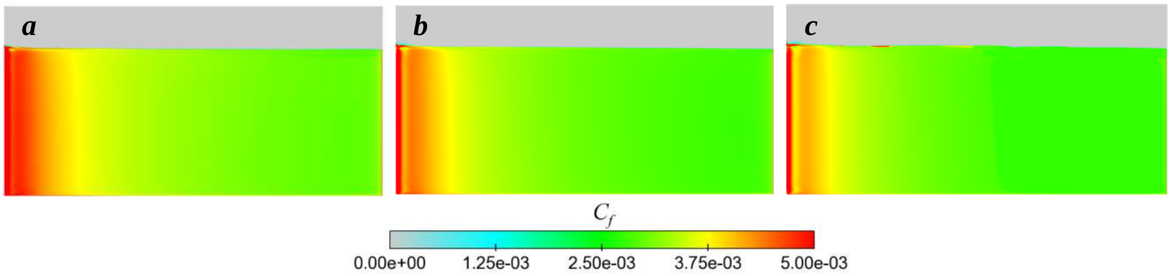

Fig.6: Contours of skin friction along a plate with ablative cooper antifouling coating *a*. $Re_L = 2.8 \times 10^6$ *b*. $Re_L = 4.2 \times 10^6$ *c*. $Re_L = 5.5 \times 10^6$.

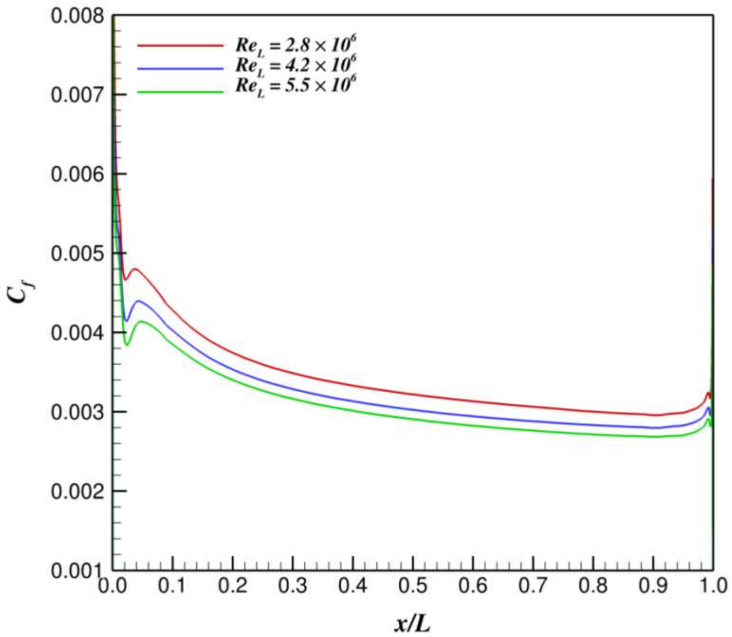

Fig.7: Skin friction distribution along the plate at three Re_L at mid-depth, z/L = -0.194, for the ablative copper antifouling coating.

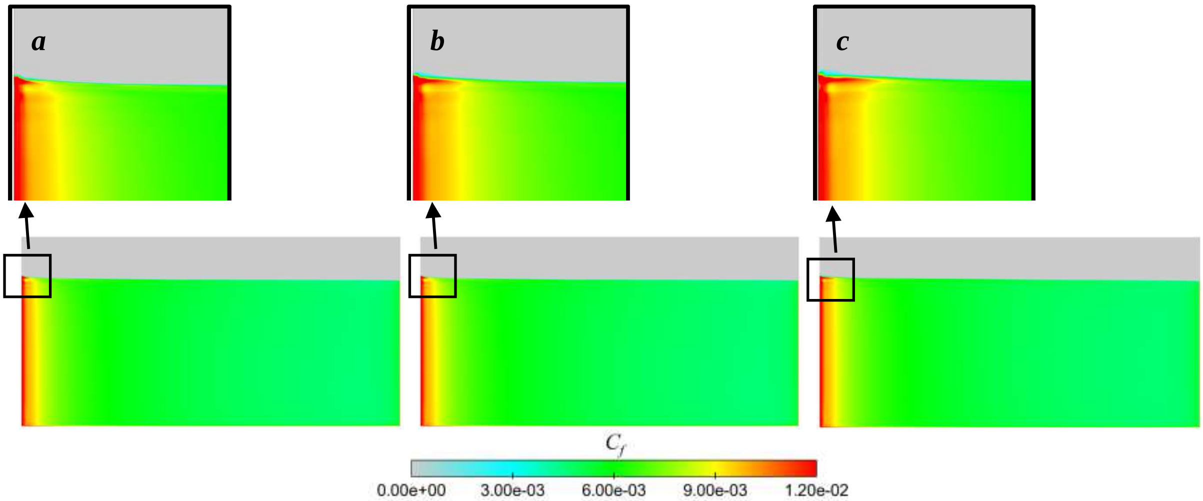

Fig.8: Contours of skin friction along a plate with 60-grit sandpaper *a*. $Re_L = 2.8 \times 10^6$, *b*. $Re_L = 4.2 \times 10^6$ *c*. $Re_L = 5.5 \times 10^6$.

The total resistance coefficients for both smooth and rough plates obtain through the simulations are plotted against the experimental results in Fig.9. The numerical results are within the uncertainty of the experimental data, i.e. ±2% at the highest Re_L and ±5% at the lowest Re_L. This plot also shows

`

that for the 60-grit plate, the total resistance varies slightly and then reaches a constant C_F value of approximately 0.006 beyond $Re_L > 4.0\times10^6$. The minimal change in total resistance confirms the skin friction distribution contours, all appearing the same at the Re_L simulated. The ablative copper coating plates show a detectable decrease in C_F as Reynolds number increases. The copper coating adds additional drag on a smooth plate and will definitely have an impact on the resistance of a ship. The C_F values at the three different Re_L for the three conditions are summarized in Table III. The results closely match the experimental results with a percent difference of no more than 1.41% and 2.76% for the 60-grit and copper coating respectively. When comparing to the smooth plate, the total resistance increases by about a factor of 2.0 due to the 60-grit sandpaper, whereas a smaller increase is detected with the copper coating.

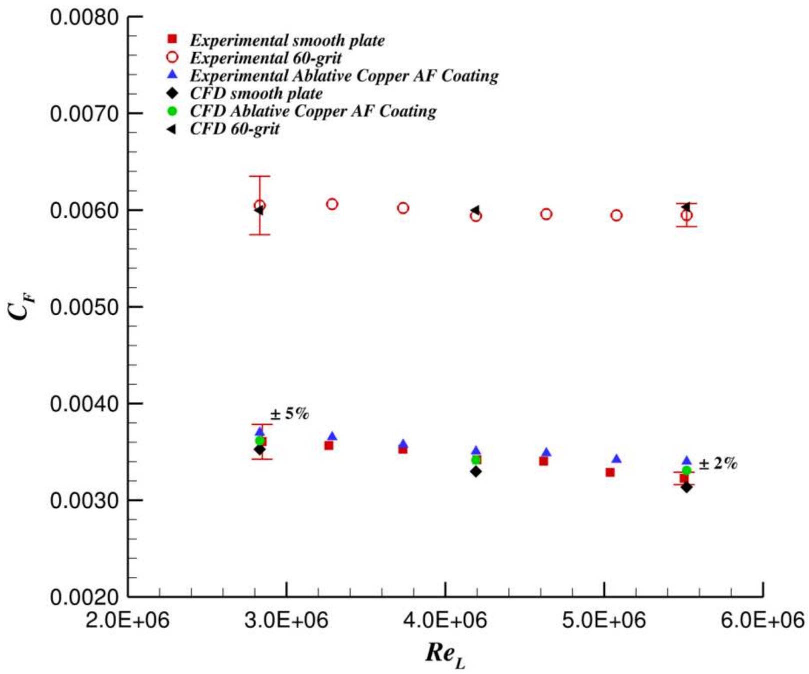

Fig.9: Total resistance comparison for the towed plate

Table III: Comparison of total resistance for towed rough plates at three Re_L

	60-grit Sandpaper			Ablative Copper Antifouling Coating		
Re_L	C_{F_Exp}	C_{F_CFD}	% Difference	C_{F_Exp}	C_{F_CFD}	% Difference
5.5×10^6	0.005949	0.0060325	1.39%	0.003401	0.003308	2.76%
4.2×10^6	0.005941	0.0060253	1.41%	0.003507	0.003416	2.62%
2.8×10^6	0.006048	0.0060074	0.67%	0.003701	0.003616	2.32%

7.2 DTMB 5415 Results

Having shown that the wall function roughness model can predict resistance within 2% of the measured data on a flat plate with roughness elements in the transitional and fully rough regime, the next step is to apply the model to a surface combatant ship model. The first step is to simulate DTMB 5415 in the hydraulically smooth condition and compare it with experimental data. As discussed in the "Computational Geometry" section, the percentage difference in total resistance is 0.06%. Having achieved a minimal difference in drag prediction, the next step is to model the ship with different levels of homogenous biofouling. Table IV, obtained from *Schultz (2007),* based on a fouled 1.52 m long flat plate, *Schultz (2004)*, describes the types of fouling and the associated k_s values that were applied to the numerical model scale ship hull. Also included in Table IV is the ablative copper antifouling coating with its corresponding k_s value obtained from the towed plate experiments from *Schultz (2004).*

`

Table IV: A range of hull conditions with its corresponding k_s values

Description of Fouling Condition	k_s (μm)
Hydraulically smooth surfaces	0
Ablative copper antifouling coating	2
Deteriorated coating or light slime	100
Heavy Slime	300
Small calcareous fouling or weed	1000
Medium calcareous fouling	3000

The skin friction contours of the DTMB 5415 at various fouling conditions are presented in Fig.10. A transition region near the bow extending to the end of the bulbous bow or sonar dome of low skin friction is followed by a region of high skin friction in the ideal smooth hull, as shown by Fig.10(*a*). No sudden change in skin friction occurs on the midship. A localized high skin friction zone is observed in the stern section by the keel. Applying an antifouling coating reduces the transition zone and moves the region of high C_f forward and covers about the first one-fourth of the ship, as shown by Fig.10(*b*). A comparison between Figs10(*b*) and (*c*) indicates that the hull covered with light slime retains similar C_f distribution, except that the skin friction is slightly higher, especially at the midship. Fig.10 (*d*) shows a large increase in C_f due to a homogenous coverage of heavy slime on the hull. The C_f distribution starts to show large differences compared to those in Fig.10(*a*)-(*c*), where the skin friction distribution is seen beyond the midship. At the point where the ship is covered by hard fouling represented by Fig.10(*e*) and (*f*), the impact the high C_f region extends all the way to the stern of the hull with an average C_f on the midship of about 0.006 and 0.007 for the small and medium calcareous fouling respectively. At these fouling conditions, the contour legend in Fig.10 is not appropriate to distinguish the skin friction distribution along the hull.

Fig.11 compares the two scenarios where hard fouling covers the hull at different upper bounds in skin friction. As observed in the fouling conditions with a low k_s, high levels of C_f are concentrated near the bow as seen in Fig.11(*a*). As the fouling transitions from small to medium calcareous fouling the impact of skin friction extends further along the hull. The fouling has minimal impact near the stern region downstream of the keel and this is observed for all fouling conditions presented in Fig.10. From the C_f contours one may infer that small gains are obtained by cleaning the stern part of the ship, and it is better to maintain the bow of the ship as clean as possible.

The C_f contours on the side of the hull have been shown in Figs.10 and 11, and they give an indication that C_f is changing at the keel with fouling level. To better examine the keel region, a view in Fig.12 compares three fouled scenarios. The keel also experiences a change in skin friction as the different homogeneous roughness levels increases. The longitudinal region of skin friction along the keel begins at the trailing edge of the sonar dome where the flow accelerating over the bow flows toward keel and merges with the flow from the sonar dome. The region of C_f widens as it approaches the end of the keel due to the weak counter-rotating vortices that convect downstream along the bottom of the hull bringing high momentum fluid to the keel which aids in the increase in C_f. As the roughness increases, the width of the longitudinal region of skin friction running along the keel increases from the ideal smooth scenario to the hull covered with the cooper antifouling coating. The values of the C_f distribution along the keel are much higher in the calcareous fouling case, Fig.12(*c*).

The region of the ship that also has a noticeable change in C_f besides that keel is the sonar dome. As seen in Fig.12, the transition region at the leading edge of the sonar dome, characterized by the light blue contours, decreases as the level of fouling increases and a band of higher C_f begins to increase at about mid length of the sonar dome. This increase in skin friction is attributed to the acceleration of flow over the sonar dome. As the fouling increases, there is a larger velocity gradient over the sonar dome due to the greater impedance of flow near the surface caused by the roughness elements that are modeled resulting in an increase in C_f.

The total resistance coefficient and the percentage change in C_F for all the fouling scenarios are summarized in Table V. A light slime coating on the hull cause a 10.82% increase in total drag, and a

`

26.84% increase in resistance occurs when the fouling reaches the stage of heavy slime coverage when compared to the hydraulically smooth hull. Once the ship is fully covered by hard fouling, the drag increase is greater than 50%. Table also computes the increase in C_F using the ablative copper antifouling coating as the reference condition. A slight drop in percentage change in C_F is observed in every fouling condition when compared to using the smooth hull as a reference; nevertheless, the impact of C_F is significant. The resistance penalty nearly doubles from the heavy slime condition to the small layer of calcareous fouling. The change in resistance as biofouling worsens closely matches the trends presented by *Schultz (2007)* where he analyzed the Oliver Hazard Perry class frigate (FFG 7) with the same fouling conditions.

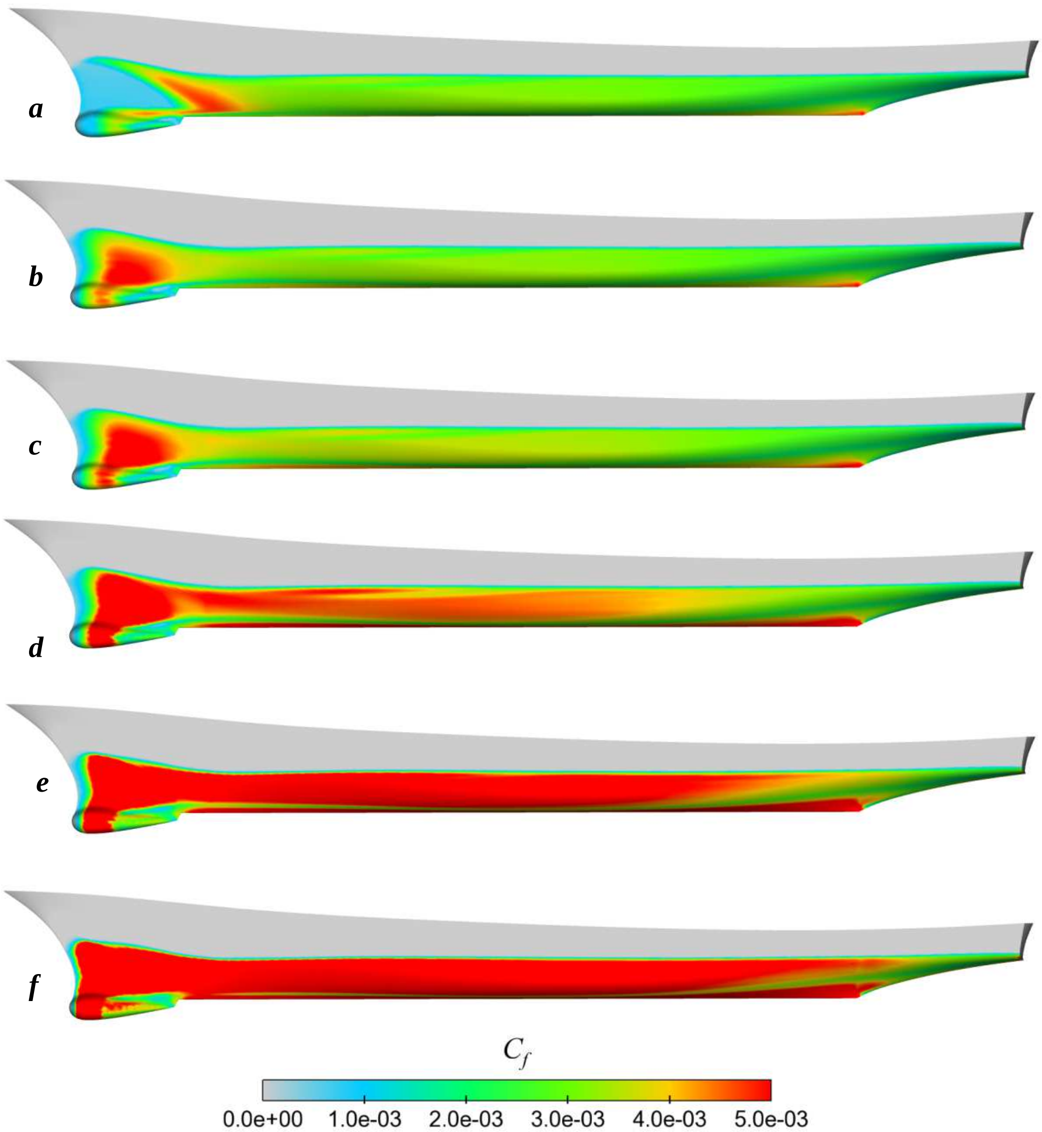

Fig.10: Skin friction contours on DTMB 5415 at various hull conditions. *a.* hydraulically smooth hull *b.* ablative copper coating *c.* light slime *d.* heavy slime *e.* small calcareous fouling *f.* medium calcareous fouling

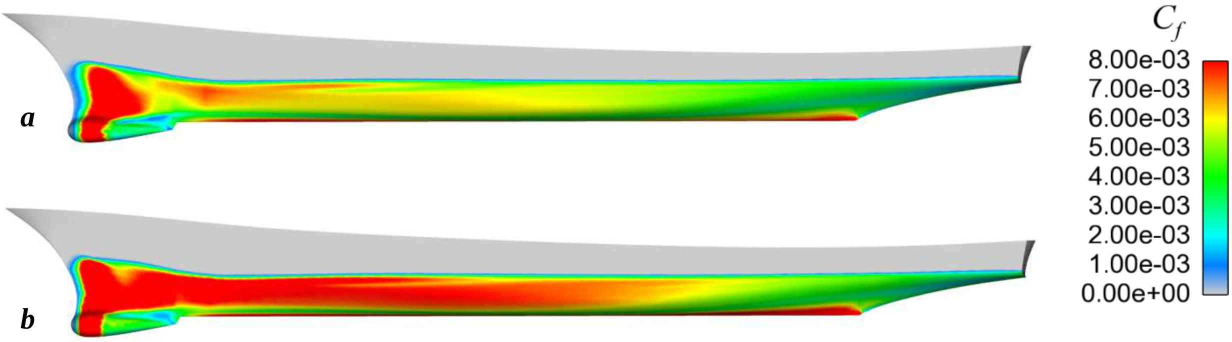

Fig.11: Skin friction contours on DTMB 5415 with *a*. small *b*. medium calcareous fouling

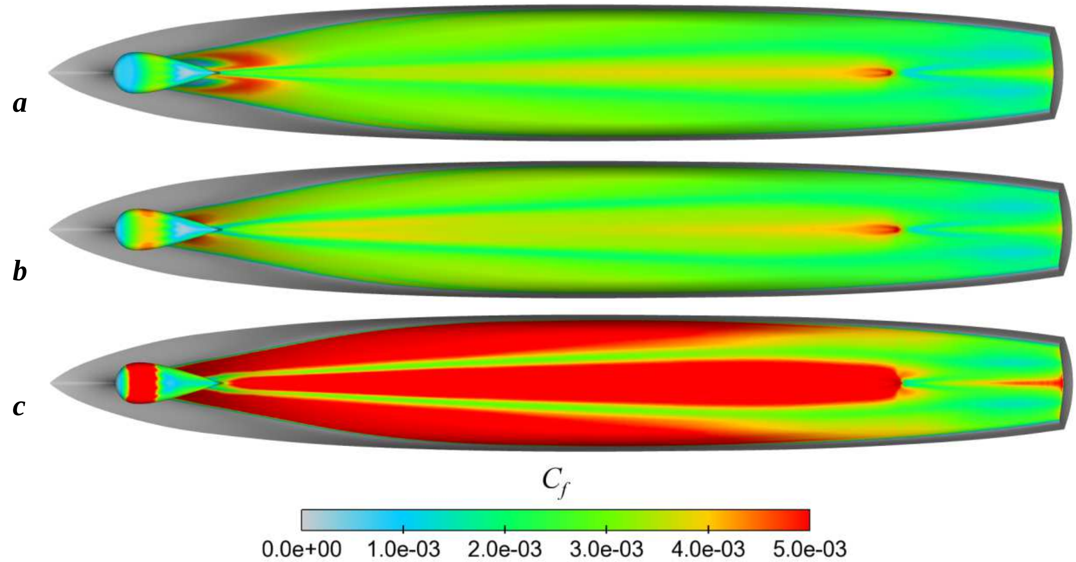

Fig.12: Skin friction contours on DTMB 5415 view from below at various hull conditions. *a*. hydraulically smooth hull *b*. ablative cooper coating *c*. small calcareous fouling

Table V: Percent change in total resistance due to fouling conditions measured from the hydraulically smooth hull and a hull with ablative copper antifouling coating

		Smooth Hull as Reference	*AF Coating as Reference*
Description of Fouling Condition	C_F	*% Change* C_F	*% Change* C_F
Hydraulically smooth surfaces	0.004227	–	–
Ablative copper antifouling coating	0.004488	6.17%	–
Deteriorated coating and light slime	0.004685	10.82%	4.38%
Heavy Slime	0.005362	26.84%	19.47%
Small calcareous fouling or weed	0.006634	56.93%	47.82%
Medium calcareous fouling	0.008080	91.14%	80.03%

Unlike experimental tests where only the total resistance is measured and the frictional resistance is computed using the ITTC-1957 formula, the numerical simulation allows direct calculation of the frictional F_v and pressure forces F_p. The frictional and pressure resistance coefficients are:

$$C_{F,p} = \frac{F_p}{.5*\rho U_\infty^2 A_{wet}}, \tag{20}$$

$$C_{F,v} = \frac{F_v}{.5*\rho U_\infty^2 A_{wet}}, \tag{21}$$

where U_∞ is the freestream velocity and A_{wet} is the wetted surface area.

`

The sum of both coefficients equals the total resistance coefficient: $C_F = C_{F,p} + C_{F,v}$. Fig.13 shows the contribution of the frictional and pressure resistance coefficient for each hull condition. For all hull conditions evaluated, the viscous force is the dominant drag force that amounts to more than 50% of the total resistance, whereas the pressure drag is constant making up about 30% of the total resistance. The ratio of $C_{F,v}$ and $C_{F,p}$ remains about the same up to the light slime conditions, but as the hull fouling transitions from heavy slime to hard fouling, a linear increase in $C_{F,v}$ is observed. Fig.14 shows the behavior of each resistance coefficient at the k_s values corresponding to each fouling condition starting with the hydraulically smooth hull. A constant $C_{F,p}$ with an average value of 1.43 × 10^{-3} is observed for all hull conditions. Fig.14 also indicates that both C_F and $C_{F,v}$ increase at roughly the same rate with increasing k_s values. Higher values of k_s need to be evaluated to determine whether C_F converges to a particular value.

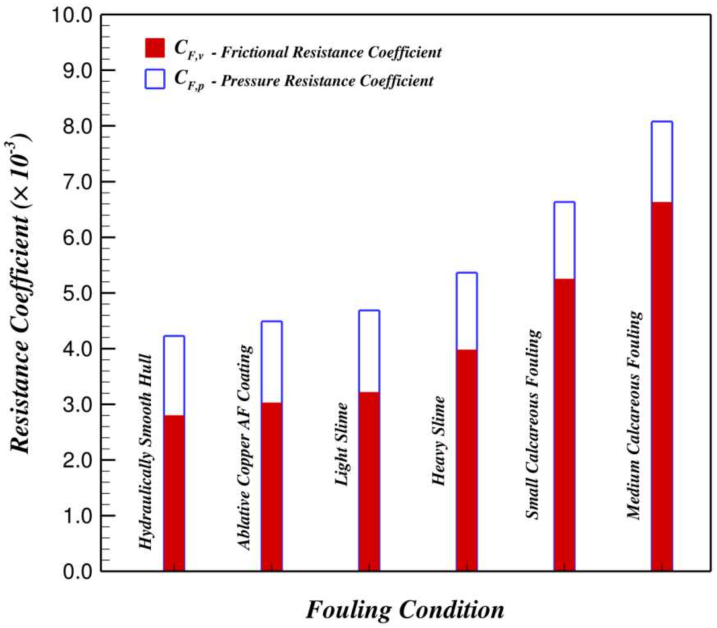

Fig.13: Breakdown of resistance coefficients for each hull condition

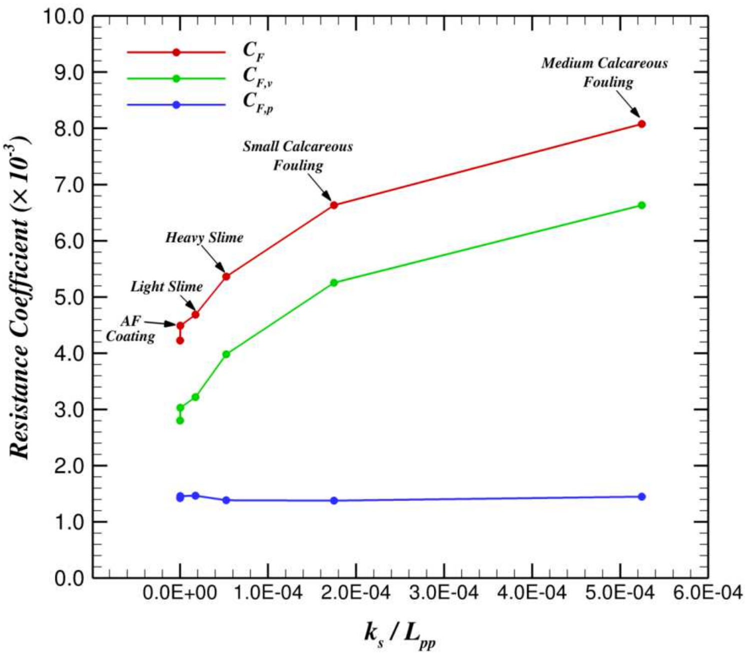

Fig.14: Resistance coefficients at different k_s values

To further understand which section of the ship generates the most drag, the hull was divided into three sections referred as the bow section, midship, and the stern section as seen in Fig.15. The border between the bow section and the midship is located at x/L_{pp}=0.12 from the forward perpendicular and the section break between the midship and the stern section is at x/L_{pp}=0.83. The percentage change in frictional resistance of each section of the hull is plotted in Fig.16. In Fig.16, the ablative copper antifouling coating is used as the reference hull to compute the percentage change as this scenario best represents a typical Navy ship. Isolating only the frictional resistance on the hull as it is the main contributor to the total resistance, the data shows that the higher percentage change occurs at the bow followed by the midship and then the stern region for fouling conditions beyond heavy slime. The bow and midship sections have approximately the same percent change when the fouling is classified as light slime. Fig.16 supports the observation provided by the C_f contours in that the bow is the region where frictional drag is most important.

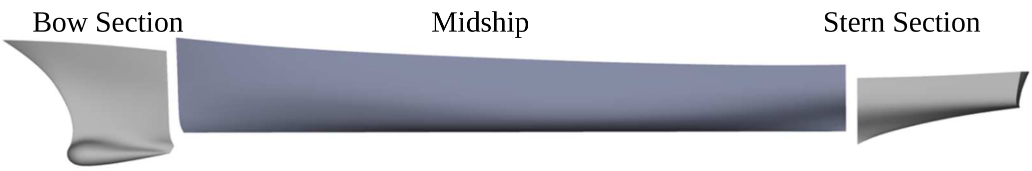

Fig.15: DTMB 5415 hull divided into 3 sections

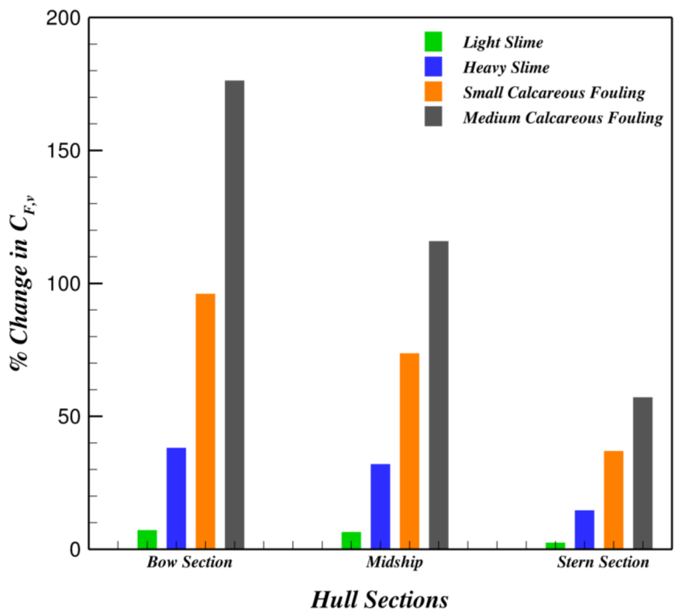

Fig.16: Percent change in frictional resistance at three different hull sections

8. Conclusions

The current roughness model implemented in NavyFOAM is able to capture the necessary physics that occurs on a rough plate for a range of k_s values. When the wall function roughness model was applied to towed plates, the overall frictional resistance predicted by the roughness model is within 2% of the experimental results. The modifications to the roughness model eliminated the unphysical transition region near the leading edge of the plate as seen in the previous version of our wall function roughness model. The main improvement to the roughness model was the constant B in the log-law that now depends on the nature of roughness and varies depending on the value of k_s^+ along the surface.

The simulations of different homogenous biofouling conditions on a hull provided useful insight into the resistance generated by each scenario. First, a concentration of high skin friction originates at the bow and intensifies with roughness. Second, the keel of the hull shows high levels of skin friction

`

which increases with increasing roughness. Third, the viscous force is the dominant drag force and amounts to more than 50% of the total resistance, whereas 30% of the total resistance originates from the pressure drag. A constant $C_{F,p}$ with an average value of 1.43×10^{-3} was observed for all hull conditions whereas $C_{F,v}$ kept increasing with increasing k_s. Higher values of k_s need to be evaluated to determine whether C_F converges to a particular value. Fourth, the data showed that fouling had minimal impact at the stern region downstream of the keel. Lastly, the data showed that the higher percentage change in frictional resistance occurred at the bow followed by the midship and then the stern region for fouling conditions beyond heavy slime. From the above observations, one can infer that maintaining the first one-fourth of the hull and the keel free from biofouling can lead to significant gains in reducing the total resistance on a ship.

These simulations have provided some insight into the resistance due to biofouling and are the first steps in quantifying their relationship with ship performance. The next step is to have certain parts of the hull free from biofouling, such as the bow section, and see how the resistance changes. This could emulate a hull cleaning procedure where cleaning is only done at strategic locations along the hull that may result in a lower drag. This type of evidence and data driven hull clean could be an efficient method of keeping a ship relatively clean without a significant drag penalty. Also, simulations of heterogeneous roughness applied at certain locations along the hull similar to what is observed on ships that are in service can further elucidate the relationship of drag and biofouling. Finally, full scale ship simulation with the same fouling conditions used in this paper will be conducted to determine the change in resistance and how it relates back to model scale.

Acknowledgements

This research was funded by the Naval Surface Warfare Center Carderock Division as part of the Naval Innovative Science and Engineering (NISE) program under the direction of Dr. J. Price. Many thanks to Dr. Eric Holm, Dr. Peter Chang, Dr. Joseph Gorski, and Dr. Shawn Aram for providing useful insight and technical support. Christina Dehn for her assistance in data reduction, and Prof. Michael Schultz from the U.S. Naval Academy for providing the experimental data is also thanked. The rest of the Hydrodynamic Modeling of Biofouling-associated Roughness and Drag team members are also acknowledged.

References

AUPOIX, B.; SPALART, P.R. (2003), *Extensions of the Spalart-Allmaras turbulence model to account for wall roughness,* Int. J. Heat and Fluid Flow 24, pp.454 – 462

CLAUSER, F.H. (1954), *Turbulent boundary layers in adverse pressure gradients,* J. Aeronaut. Sci. 21, pp.91-108

DEMIREL, Y. K.; KHORASANCHI; M.; TURAN, O.; INCECIK, A. (2014), *A CFD model for the frictional resistance prediction for antifouling coatings,* Ocean Eng. 89, pp.21-31

DURBIN, P.A.; MEDIC, G.; SEO, J.M.; EATON, J.K.; SONG, S. (2000), *Rough wall modification of two-layer k-ε,* J. Fluids Eng. 123, pp.16-21

FLACK, K.A.; SCHULTZ, M.P,; CONNELLY, J.S. (2007*), Examination of a critical roughness height for the outer layer similarity,* Phys. of Fluids 19, 095104

GORSKI J.; KIM, S.E.; ARAM; S.; RHEE B.J.; HUA, S. (2014), *Development of a CFD framework for prognoses of resistance, powering, maneuvering, and seakeeping of surface ships,* 30th Symp. Naval Hydrodynamics, Hobart

GRANVILLE, P.S. (1958) *The frictional resistance and turbulent boundary layer of rough surfaces,* J. Ship Reserach 2, pp.52-74

`

GRANVILLE, P.S. (1987), *Three indirect methods for the drag characterization of arbitrary rough surfaces on flat plates*, J. Ship Research 3/1, pp.70-77

HIRT, C.W.; NICHOLS, B.D. (1981), *Volume-of-fluid (VOF) method for dynamics of free boundaries,* J. Comp. Phys 39, pp.201–221

IZAGUIRRE-ALZA, P.; PÉREZ-ROJAS, L.; NÚÑEZ-BASÁÑEZ, J.F. (2010*), Drag reduction through special paint coated on the hull*, Int. Conf. Ship Drag Reduction SMOOTH-SHIP, Istanbul

KHOR, Y.S.; XIAO, Q. (2001), *CFD simulations of the effects of fouling and antifouling,* Ocean Eng. 38, pp.1065-1079

KIM, S.E.; BREWTON, S. (2008)*, A multiphase approach to turbulent cavitating flows,* 27th Int. Conf. Naval Ship Hydrodyn.,Seoul

KIM, S.E.; RHEE, B.J.; SHAN, H.; GORSKI, J.; PATERSON, E.; MAKI, K. (2010), *A scalable multiphase RANSE capability based on object-oriented programming and its applications to ship hydrodynamics,* Gothenburg 2010 Workshop on CFD in Ship Hydrodynamics, Gothenburg

KIM, S.E.; SCHROEDER, S. (2010), *Numerical study of thrust-breakdown due to cavitation on a hydrofoil, a propeller, and a waterjet,* 28th Symp. Naval Hydrodynamics, Pasadena

KIM, S.E.; SCHROEDER, S.; JASAK, H. (2010), *A multiphase CFD framework for predicting performance of marine propulsors,* 13th Int. Symp. Transport Phenomena and Dynamics of Rotating Machinery, Honolulu

KIM, S.E.; RHEE, B.J.; MILLER, R.W. (2014), *Anatomy of turbulent flow around DARPA SUBOFF body in a turning maneuver using high-fidelity RANS computations*, Int. Shipbuilding Progress 60/1, pp.207-231

KNOPP, T.; EISFELD, B.; CALVO, J.B. (2009), *A new extension for k-ω turbulence model to account for wall roughness,* Int. J. Heat and Fluid Flow 30, pp.54-65

LARSSON, L.; STERN, F.; VISONNEAU, M. (2014), *Numerical Ship Hydrodynamics, An assessment of the Gothenburg 2010 Workshop*, Springer

LEER-ANDERSEN, M.; LARSSON, L. (2003), *An experimental/numerical approach for evaluating skin friction on full-scale ships with surface roughness*, J. Mar. Sci. Technol. 8, pp.26-36

LIGRANI, P.M.; MOFFAT, R. J. (1986), *Structure of transitionally rough and fully rough turbulent boundary layers,* J. Fluid Mech. 162, pp.68-98

MENTER, F.R.; KUNTZ, M.; LANGTRY, R. (2003), *Ten Years of Industrial Experience with the SST*, Turbulence, Heat and Mass Transfer 4, Begell House, pp.625-632

NIKURADSE, J. (1933), *Laws of flow in rough pipes*, NACA Technical Memorandum 1292

OLIVIERI, A.; PISTANI, F.; AVANZINI, A.; STERN, F.; PENNA, R. (2001), *Towing tank experiments of resistance, sinkage and trim, boundary layer, wake, and free surface flow around a naval combatant INSEAN 2340 model,* IIHR Technical Report 421

PARK, I.R.; KIM, K.S.; KIM, J.; VAN, S.H. (2009), *A volume-of-fluid method for incompressible free surface flows,* Int. J. Numer. Meth. Fluids 61, pp.1331-1362

SCHULTZ, M.P.; MYERS, A. (2003), *Comparison of three roughness functions determination methods,* Exp. in Fluids 35, pp.372-379

`

SCHULTZ, M.P. (2004), *Frictional Resistance of Antifouling Coating Systems*, J. Fluid Engr. 126, pp.1039-1047

SCHULTZ, M.P. (2007), *Effect of coating roughness and biofouiling on ship resistance and powering,* Biofouling 25, pp.331-341

SCHULTZ, M.P.; FLACK, K.A. (2007), *The rough-wall turbulent boundary layer from the hydraulically smooth to the full rough regime*, J. Fluid Mech 580, pp.381-405

SCHULTZ, M.P.; BENDICK, J.A.; HOLM, E.R.; HERTEL, W.M. (2011), *Economic impact of biofouling on a naval surface ship,* Biofouling 27, pp.87-98

SHAN, H.; DELANEY, K.; KIM, S.E.; RHEE, B.; GORSKI, J.; EBERT, M. (2011), *Guide to Navy-FOAM V1.0.,* Naval Surface Warfare Center, NSWCCD-20-TR2011/25

SHAN, H.; KIM, S.E. (2011), *Numerical study of advection schemes for interface capturing in a volume of fluid method on unstructured meshes*, ASME-JSME-KSME Joint Fluids Engineering Conf., Hamamatsu

TOWSIN, R.L. (2003), *The ship fouling penalty*, Biofouling 19 (Supplement), pp.9-15

TOWSIN, R.L.; BRYNE, D; SVENSEN, T.E.; MILNE, A. (1981), *Estimating the technical and economic penalties of hull and propeller roughness* SNAME Trans. 89, pp.295-318

VARGAS, A.; SHAN, H. (2016), *A numerical approach for modeling roughness for marine applications*, ASME 2016 Fluids Engineering Division Summer Meeting, FEDSM2016-7791, Washington DC

WELLER, H.G.; TABOR, G.; JASAK, H.; FUREBY, C. (1998), *A tensorial approach to computational continuum mechanics using object-oriented techniques*, Comp. in Physics 12, pp.620-631

WILCOX, D.C. (2008), *Formulation of the k-omega turbulence model revisited,* AIAA J. 46/11, pp.2823-2838

WILCOX, D.C. (2006), *Turbulence Modeling for CFD,* DCW Industries

Hull and Propeller Performance … On an Absolute Scale?

Sergiu Paereli, Jotun A/S, Sandefjord/Norway, sergiu.paereli@jotun.no
Andreas Krapp, Jotun A/S, Sandefjord/Norway, andreas.krapp@jotun.no

Abstract

Knowing and managing the absolute level of the total performance of a vessel is one of the central tasks and interests of the technical manager of a vessel as this reflects directly in the fuel bill of the vessel. Hull and propeller performance is one of the components of vessel performance and thus the absolute level of hull and propeller performance is of interest. It is regularly topic of discussions when the questions of hull and propeller coating choice, hull and propeller surface maintenance alternatives or comparison of sister vessels are in focus. However, there are numerous challenges and pitfalls when discussing the absolute level of hull and propeller performance. The present contribution looks into the factors that influence hull and propeller performance indicators and questions if it is possible to measure hull and propeller performance on an absolute scale.

1. Introduction

Ship owners, yards, equipment suppliers, regulative bodies, academics … – all parties in the shipping ecosystem have an interest in knowing and managing the impact of the different components that together make up the total performance of a vessel. This is also true for the impact of the underwater hull and propeller. Common challenges in this area are how to judge if and how much the underwater hull and propeller deteriorate over a docking period, when to initiate maintenance and what the effect of the maintenance has been. All these challenges address relative performance; they all focus on changes of a vessel over time and can be answered by comparing a vessel with itself over time. Such a relative comparison reduces the complexity of the challenge considerably as not all factors influencing ship performance have to be resolved.

Other challenges, however, address the absolute performance. One example in this respect is the hull and propeller performance of a vessel that leaves the new building yard. How can one judge on the hull and propeller performance level of this newbuild? How can the impact of all work and efforts spent to optimize the surface condition of the underwater hull and propeller in a newbuild yard be quantified? Or, how should different vessels that leave a dry-dock be compared in terms of their hull and propeller performance, e.g. in order to establish quantified and transferable best practice?

The recently published ISO 19030 standard on Hull and Propeller performance measurement, *ISO (2016*), explicitly focusses on relative performance. The title "Measurement of Changes in Hull and Propeller Performance" is clear on that and the introduction and the scope statements make it explicit: "The aim of this document is to prescribe practical methods for measuring changes in ship specific hull and propeller performance … " and "… the objective is to compare the hull and propeller performance of the same ship to itself over time," *ISO (2016*).

Given that the ISO19030 standard in its current version does not give the answer if one is to state something on the absolute hull and propeller performance and that at the same time there is a need and therefore attempts to make such statements on absolute performance, this contribution shall shed light on what it takes to measure hull and propeller performance in service in absolute terms and if such an absolute scale is possible at all.

2. Total vessel performance

What one generally associates with vessel performance is closely related to the concept of energy efficiency. For engineers, efficiency equates to the ratio of energy put into a system and the useful work done by the system. For a vessel, the energy put into the vessel is equal to the energy content of the fuel to be burned and the work done is the movement of the vessel (and its cargo) over a distance and time. The absolute energy efficiency, or absolute vessel performance, can be quantified relatively easily, as fuel mass and calorific value, vessel mass and speed can be evaluated. This total efficiency is certainly what a vessel operator is really interested in, as it determines his cost competitiveness on the market place.

The total efficiency of a vessel measured in this way depends on the performance of the physical vessel as such in different environmental conditions ("tonnage performance"), the environmental conditions that the vessel encounters and the way the operator uses the vessel under the given conditions ("operational performance"). Engine performance and hull and propeller performance are examples of contributing elements that fall mainly under the heading of tonnage performance. But it is to be noted that the usage of the tonnage impacts its performance, meaning that there is a link between operational and tonnage performance. E.g. the quality of the engine maintenance or the level of activity have an impact on the performance of the engine or the hull and propeller.

If one leaves the influence of the vessel operation on the performance of the tonnage out of the discussion, the question to answer is "How can hull and propeller performance be isolated from the other components of tonnage performance and is this possible in an absolute manner?"

3. Hull and propeller performance – general reflections

As a starting point one could use the common definition of Hull and Propeller Efficiency η_{HP} as the ratio between the effective propulsive power P_E and the power delivered to the propeller P_D under given environmental, operational and loading conditions, Eq.(1).

$$\eta_{HP} = \frac{P_E}{P_D} = \frac{R_T \cdot v}{P_D} \qquad \text{(Eq.1)}$$

The effective power can be expressed as the product of vessel resistance R_T and its speed v.

Given that the total resistance of a vessel in-service is not directly measurable (at least not today), the ratio of vessel speed and power delivered appears as a sensible measurement for judging on performance, Eq.(2).

$$\frac{\eta_{HP}}{R_T} = \frac{v}{P_D} \qquad \text{(Eq.2)}$$

However, such a definition, while relatively easily measurable as the ratio of shaft power and vessel speed, does not really help for judging on hull and propeller performance as all effects that impact the total resistance are blended together. What one needs to do is to split the total resistance into its components. But this demands for a method for doing so, namely a vessel model that predicts how the environmental factors, the operational and loading conditions, etc. impact the resistance. Such a model would then be used to "eliminate" the corresponding resistance components. This would lead to a modified hull and propeller efficiency $\eta_{HP,mod}$ and the remaining resistance R_{Rem}, which – again – would not be measurable directly. The ratio of vessel speed and the corrected power $P_{D,corr}$ could be used.

$$\eta_{HP,mod} = \frac{R_{Rem} \cdot v}{P_D - P_{corr}} = \frac{R_{Rem} \cdot v}{P_{D,corr}} \qquad \text{(Eq.3)}$$

$$\frac{\eta_{HP,mod}}{R_{Rem}} = \frac{v}{P_{D,corr}} \qquad \text{(Eq.4)}$$

The first factor that is of importance for an absolute hull and propeller performance scale is therefore the accuracy of the vessel model. As the aim is an absolute scale, both the relative importance of the different effects and the absolute levels have to be predicted correctly by the model.

A second factor of importance is the accuracy of the measurements that are input to the vessel model, as e.g. the wind speed, the wave height or the shaft power. As the aim is an absolute scale, measurement bias is not acceptable.

A third factor that needs consideration is the uniqueness of vessels. Given that even sister vessels differ in their exact shape, the vessel model has to be able to adapt to e.g. structural differences, and these have to be measured.

If one assumes that one has a model that predicts the impact of environmental, loading and operational conditions 100% correctly, that the model is fitted to the specific vessel and that one measures the input parameters of the model and speed and power 100% correctly, will one then have access to an absolute scale for hull and propeller performance? Yes, one would, but one has to be clear on what this means. One would measure the absolute hull and propeller efficiency, meaning that one would measure the combined effect of the quality of the hull lines ("how good the hull design is"), the quality of the surface preparation and how effective the propeller is. Such an indicator would not help to judge e.g. on the quality of the surface preparation work in a newbuild yard for an isolated vessel.

If one aims to split the effect of the hull shape and the hull surface, one has to step into the territory of the "non-measurable". While the other mentioned resistance components are in principle measurable for a vessel in service, there is no way to measure the frictional resistance separated from the pressure resistance for a vessel in service. Theoretical models would need to be used, e.g. based on CFD simulations, to estimate the pressure resistance and to correct the remaining resistance (Equation 3) for that effect. But even this would not lead to a useful absolute scale for judging the hull surface quality as the importance of frictional resistance depends on the hull shape.

It seems as if there is no obvious way to measure hull and propeller performance in service in an absolute way and in a way that allows to distinguish between surface effects and shape effects of the hull. (For machine-learning approaches and alike the establishment of an absolute scale for e.g. a newbuild ves-sel would not be straightforward neither, as they would need variations in parameters to identify them and the frictional resistance of a newbuild vessel does not vary.)

4. Hull and propeller performance – pragmatic reflections

The obvious alternative is a relative performance index that compares the actual status to the ideal. The basic idea is to compare the measured power (or speed, or resistance) with an expected power (or speed, or resistance) for the measured environmental, operational and loading conditions and ideal hull and propeller conditions. Such an approach is often used, with variations in the details. One could mention as examples the "power index" as used by DNV GL in their ECOInsight or also the basic building block of the ISO19030 approach, namely the "speed loss values". It is noted here that the ISO19030 does not make use of the speed loss values as such for performance indication, but of <u>differences</u> between <u>averages</u> over speed loss values.

If one has to rely on relative performance indices to judge on the quality of surface treatment of a newbuild vessel or to establish best practice in terms of drydocking by comparing the absolute values of these performance indices after out-docking of different vessels, what does one have to be aware of? One has to be aware of the uncertainties that are linked to the values of the performance indicators.
The most important factors are

- the uncertainty of the vessel model that is used to correct for environmental factors, for loading conditions and to deal with the variations in speed and power
- the measurement uncertainty of the parameters used to compute the performance indicator
- the way in which the uniqueness of vessels is captured in the vessel model
- the variations in factors that are not covered by the vessel model

4.1. The uncertainty of the vessel model

Commonly used calm-water vessel models rely on the speed trial predictions from model tests, on speed trial results or on CFD simulations. The ISO19030 points to these types of models to resolve the speed-power relation and to allow for variations in loading conditions. Based on the speed value, which the model predicts for a measured power and loading condition, and the measured speed a “speed loss value” is computed.

If the model is off by 5%, then the absolute value of the “speed loss” is off. Model bias results in performance value bias. Such a constant bias is less of a problem if one compares the changes in the performance values of a ship over time, as is done in ISO19030. If one, however, relies on the absolute value of “speed loss” it is clear that the level of bias of the model is crucial. Fig.1 illustrates the model bias effect.

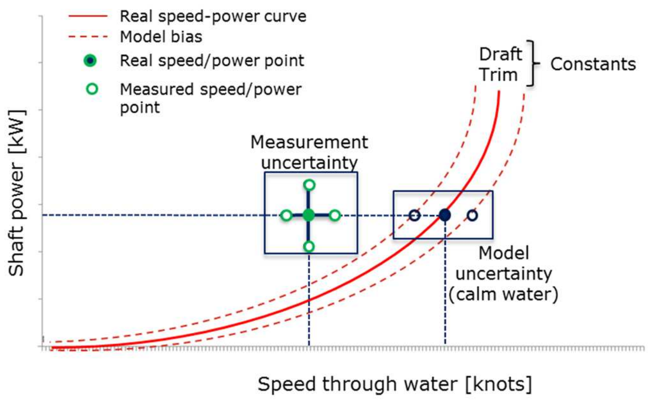

Fig.1: Illustration of the calm water vessel model uncertainty (at constant draft and trim) and the uncertainty of speed and power measurement.

The speed trial predictions by towing tank testing are known to differ between test institutes, even if the same physical model of the vessel is towed. The International Towing Tank Conference reported of a comparative test of 12 towing tank institutes where the variability of total resistance measured for the same physical vessel model is ±2% around the mean, when one outlier of +8% is neglected, *ITTC (2014)*. The repeatability for tests at single test institutes is reported to be in the range of 1-1.5% on average (in terms of standard deviation of the mean), while for some institutes repeated test could vary up to 3.6% among each other (measured as standard deviation of the mean).

These uncertainty estimates are for the resistance measurements on model scale. The methods to predict the speed-power relation for full scale at speed trial conditions will increase the uncertainty of the vessel models.

Simulations of the power-speed relation at different loading conditions using computational fluid dynamics are very powerful to build dense reference curves for use in the computation of hull and propeller performance indices, as e.g. “speed loss values”. It has been shown that the resolution of the impact of draft and trim on the speed-power relation is not trivial due to non-linearity effects and that dense CFD matrices are a good way to get control over the relative trends in the speed-power-draft-trim relation, *Krapp and Bertram (2016), Krapp and Schmode (2017)*. However, the absolute level of the predicted speed-power values from CFD simulations and the uncertainty of the predicted values is still an issue when such an approach is used. *ITTC (2014)* reports also on the uncertainty level of CFD simulations for speed-power predictions and points out that the difference in resistance coefficients between simulation and experimental model test shows a standard deviation of the mean of 2.1%. In a recent workshop on the capabilities of CFD simulation for ship scale predictions compared to speed trials, 17 CFD approaches from different workshop participants were applied using a 3D laser scan taken during a dry-docking prior to the speed trials as the basis geometry for both hull and propeller, *Ponkratov (2017).* The variation of the predicted total hull resistance varied between 11% and 16% depending on the vessel speed. Fig.2 illustrates the results for the self-propulsion prediction in comparison with the ISO15016 processed speed trial results.

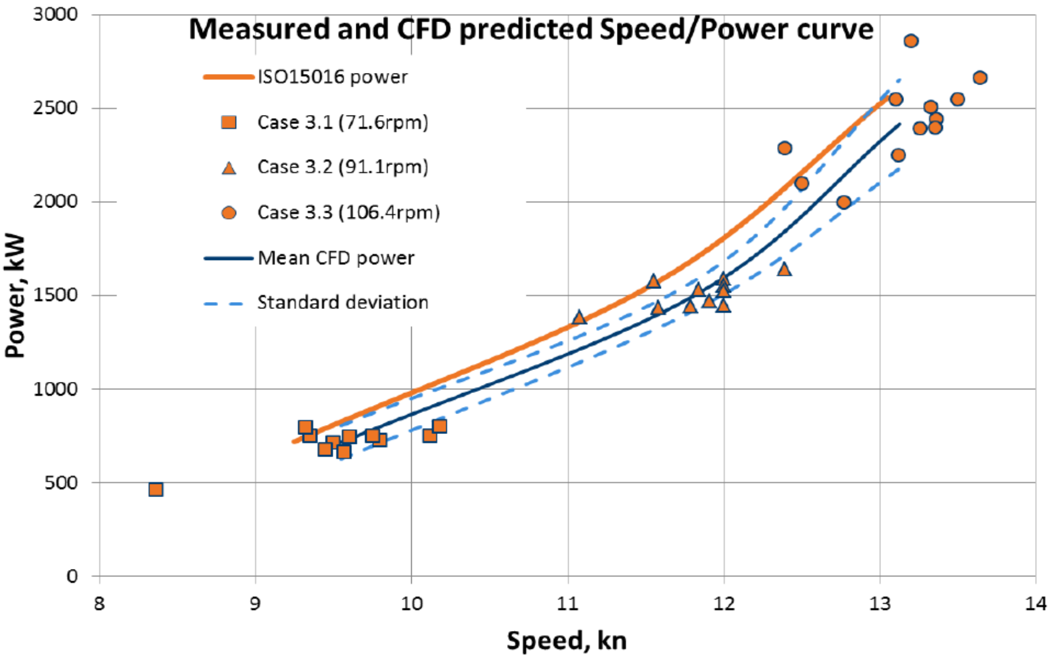

Fig.2: Measured and CFD predicted speed/power curves for full scale, *Ponkratov (2017)*

The uncertainty of the speed-power curves obtained from speed trials is influenced by both the uncertainty of the correction methods defined in the speed trial analysis procedures, as e.g. ISO15016, and the measurement uncertainty of the factors to correct for, as e.g. wave height and direction. Insel performed a detailed analysis of the uncertainty of speed trials, *Insel (2008),* and concluded with a bias limit of 3-5% and a precision limit of 7-9%. The relevant standard, ISO15016, was revised in 2015 and the uncertainty estimates have probably changed from Insel's study.

The vessel model that is at the base of any (relative) performance measurement approach has not only to deal with the variation in speed, power, draft and trim, for which above mentioned three sources can help – even if uncertain. The model also has to deal with variations in wind speed and direction, wave height and direction, sea water depth differences, sea water temperature and salinity variations, changes in loading conditions, currents and more. If there is an explicit correction for the factor in question, an uncertainty is linked to that correction which in turn leads to uncertainty in the Hull and Propeller Performance indicator values (e.g. single speed loss values). If the factor is not corrected for the uncertainty of the single performance value is increased. The ISO19030 method contains e.g. corrections for wind forces, whereas wave heights and direction are not corrected for. This is due to the difficulty to obtain reliable wave height and direction measurements on board for a vessel in service and due to the difficulty to obtain reliable response functions for specific vessels. The wind correction scheme used in ISO19030 relies as source for wind resistance coefficients on either explicit wind tunnel tests or tabulated coefficients from standard vessels as is also the case for ISO15016, the speed trial standard. As most ships do not undergo wind tunnel tests as part of the model test setup, the tabulated coefficients will be mostly used. The challenge with this approach is that the most appropriate type of the tabulated standard ships has to be chosen, without clear guidance on how to do that. For container ships the challenge is even more pronounced as the distribution of containers on board the vessel will have a significant impact on the wind load, while the standard models for wind correction consider only either empty or fully laden conditions. The uncertainty of the wind correction is thus significant. Such uncertainty is of less importance if one is interested in trends over time, but it will be very important if one is interested in the absolute level of Hull and Propeller performance values. Fig.3 illustrates the uncertainty of environmental effect corrections.

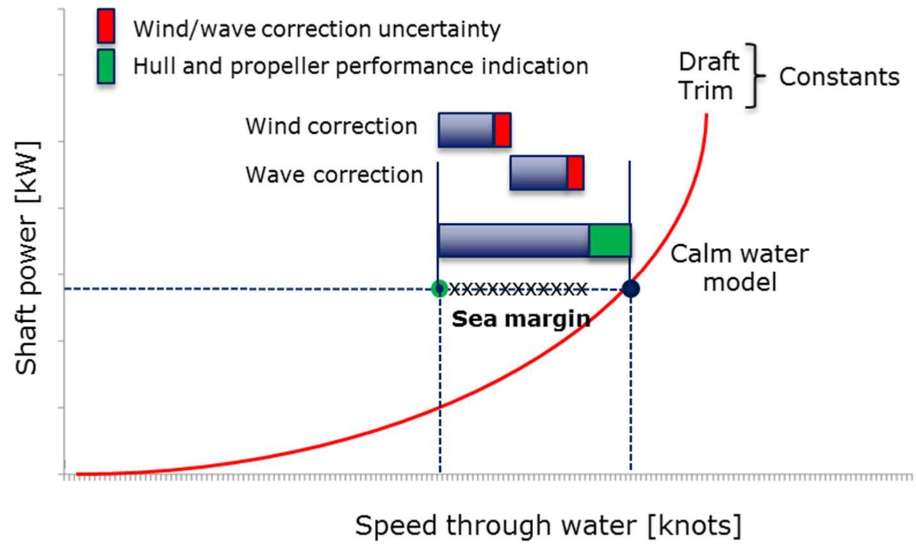

Fig.3: Illustration of the uncertainty of corrections for environmental factors that are part of the vessel model; only wind and wave corrections are given as examples. These uncertainties in turn result in uncertainty in Hull and Propeller Performance indications, as the reminder of the sea margin after all corrections have been made is commonly associated with Hull and Propeller Performance.

4.2. Measurement uncertainty

Correct measurement of a vessel operational parameters is crucial not only for establishing a correct model which fits a specific vessel but also for computation of hull and propeller performance indicators – speed deviation values.

Uncertainties in such measurements as wave height and direction might influence the precision of corrections made in speed trial analysis. On top of this, the model will suffer from uncertainties coming from measurement of speed through water, shaft power and draft. The measurement uncertainty has not only influence when building the vessel model (e.g. during speed trials), but it is central for the in-service performance indicator computations. The sensors that are installed on-board the vessel to measure speed, power, draft, trim, wind, etc. all have to be well calibrated at all time in order to exclude measurement bias which leads to bias in the performance indicator values. But even if the sensors are well calibrated, any measurement has an uncertainty which leads to uncertainty in the single performance indicator value. Unfortunately, it is not always the case that ship operators perform sensor calibrations frequently enough and/or properly. A good example in this sense is shown in Fig.4.

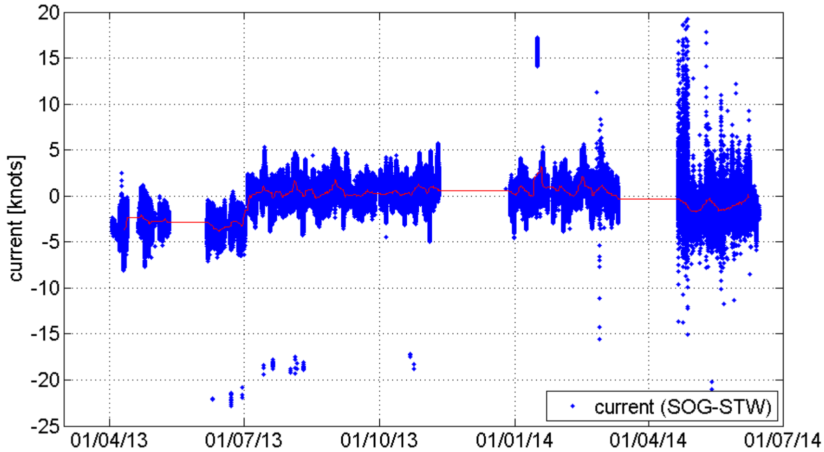

Fig.4: Time series of the difference between speed over ground and speed through water

Fig.4 shows that in the period April – July 2013 the difference between speed over ground and speed through water was significantly lower than in the period after July 2013. Within each of these periods some small variations can be observed, these being regular variations in currents that could be correlated with the trade of the vessel. A recalibration of the speed log was the reason for the sudden change.

When using measured speed through water for computing speed deviation values (as per ISO19030), the time series in Fig.5 is obtained. Clearly, an offset in the speed measurement leads to a significant offset in the single Hull and Propeller Performance indicator values. An offset of the speed sensor of about 3 knots led to an offset in speed loss of around 15-20%. This is of course an extreme example and most measurement sensors do not suffer from such big offsets. But it illustrates that sensor offsets are obviously not easily discovered during normal operations. Smaller offsets will be even more difficult to discover. Furthermore, offsets of the speed log are more easily identified as other sensor offsets, as speed through water and speed over ground are always measured and can be used to check for speed log offsets.

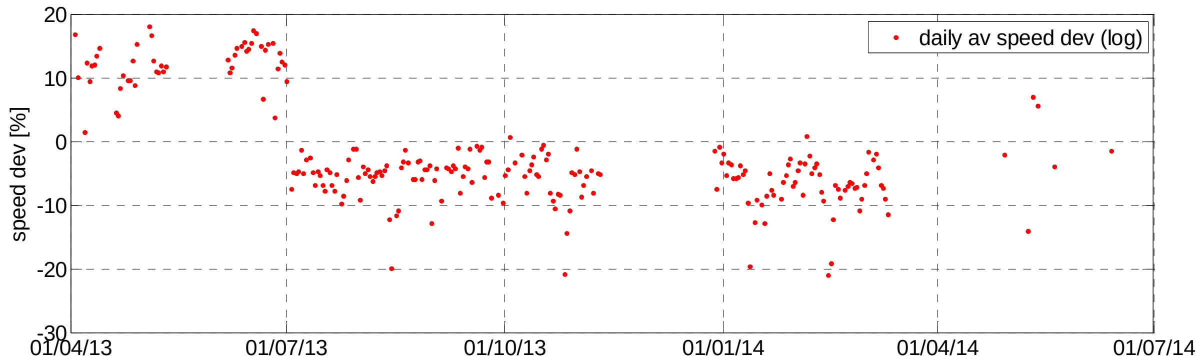

Fig.5: Time series of daily averaged speed deviation

For illustrating how big the influence of a sensor offset on the computed hull and propeller performance can be, a 0.1 knots offset in speed and 0.5% offset in shaft power has simulated for a 10000 TEU vessel. Results are presented in Fig.6.

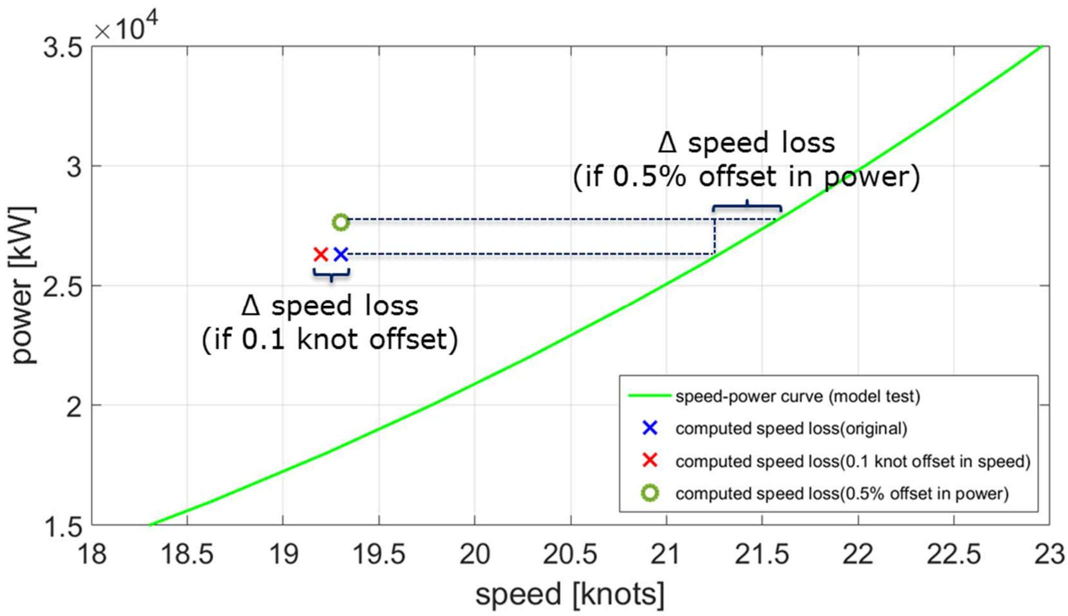

Fig.6: Illustration of sensor offset in speed and power (0.1 knot offset in speed; 0.5% offset in power) for a 10000 TEU vessel.

The offsets in speed and power lead to a significant difference in the absolute value of the single speed deviation values. If one assumes that sensors are properly calibrated, then the “correct” speed deviation value calculated from the provided model is found to be 9.9%. This means that compared to the ideal situation (vessel model), at a certain point in time, performance is lower by 9.9%.

If there were an offset of 0.1 knots in speed measurement, the computed speed deviation would be 10.4%, while an offset in shaft power measurement of 0.5% would lead to a speed deviation of 11.9%. This illustrates that even such small offsets lead to biases in speed deviation values of 0.5p.p and 1.0p.p.

When looking at changes in performance of a given vessel over time, a sensor offset would not make any difference since a constant bias is not a problem. The latter will, however, induce errors in analysis if one attempts to measure hull and propeller on absolute scale. If one wants to compare the absolute level of Hull and Propeller Performance indices e.g. between sister vessels, one has to be very careful, not the least due to the impact of even small sensor offsets.

4.3. Differences between sister vessels

Differences between sister vessels, even if built at the same yard with the same equipment and the same solutions for e.g. hull coatings and in the same period, can be significant already at the newbuild stage. Such differences can have their origin in differences in e.g. hull shape (small differences in hull dimensions, welding, alignment of bilge keel and other appendages, …), propeller, alignments of shaft or rudder, etc. Quantification of the differences is not straightforward as the procedures for measuring the tonnage performance at vessel delivery, namely the speed trial routines, are not free of uncertainties in themselves. An example of the differences between sister vessels at newbuild is given in Fig.7. It shows the model test prediction and the speed trial results for seven sister vessels (containerships). The speed trials are all corrected to standard conditions according to the same procedures. The ships generally required slightly higher power than predicted from model tests. Sister vessels showed a variation in power of up to 5% (respectively a variation in speed of up to 0.5 kn) in sea trial measurements.

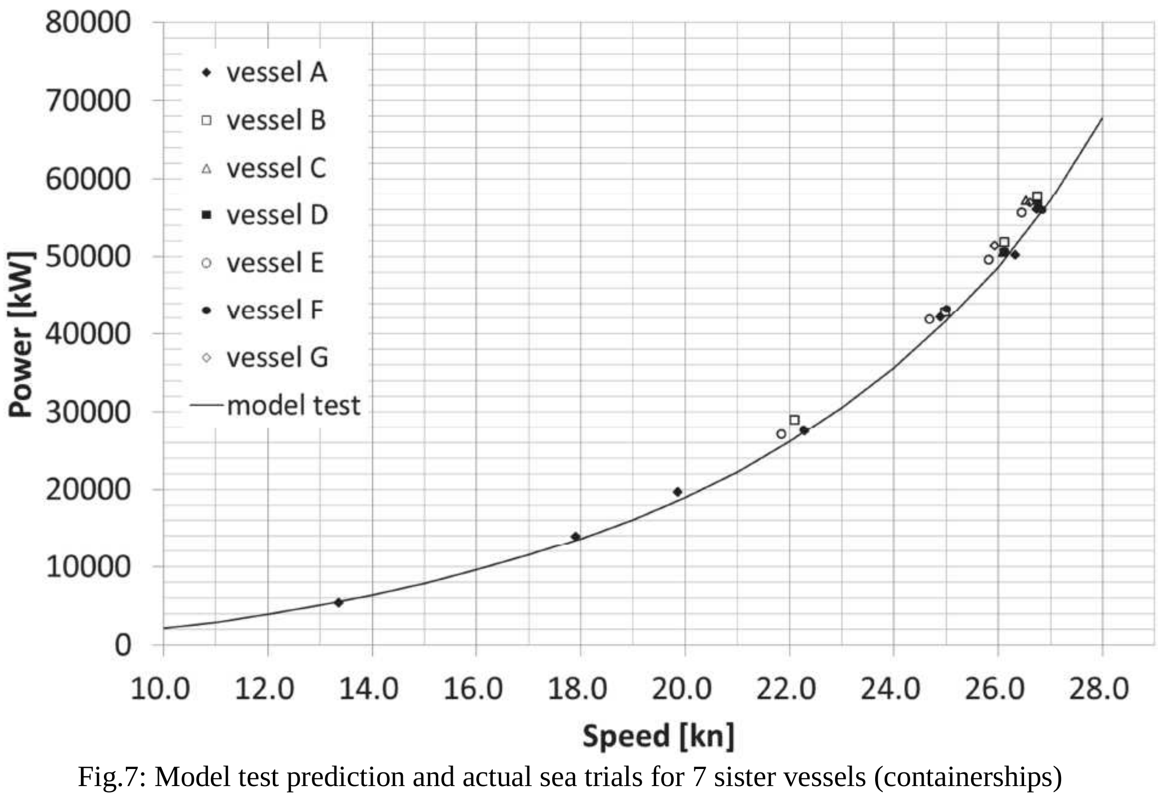

Fig.7: Model test prediction and actual sea trials for 7 sister vessels (containerships)

These initial differences will only increase over the lifetime of the vessels. Vessels will be exposed to impacts leading to individual deformations of hull and eventually propeller, vessel usage will differ and the wear and tear on propeller surface and hull surface will be different, vessel maintenance will not be identical, measurement equipment will not behave exactly the same on all vessels and also impact the measurability of differences.

Another example of comparative performance levels of two sister vessels is given in Fig.8. The two sister vessels are 388000 DWT bulk carriers which were built by the same yard, have the same age, are in the same trade and entered dry-dock in the same period. One year with data is available prior to dry-docking and about half a year with data after the dry-docking. Before the dry-docking the two vessels had different coating systems applied on their underwater hull. During the dry-docking the vessels underwent the same pre-treatment with full removal of the old coating system and the identical paint system has been applied in both cases. Very similar average hull roughness values have been measured for both vessels after coating application. Both vessels continued in the same trade after the dry-docking and have similar operational patterns. For the speed deviation computations, the same set of speed-power reference curves was used. Fig.8 shows that after dry-docking, the performance of the two sister vessels differs quite a bit. The difference between the averaged speed deviation of vessel 1 and 2 is about 2.5p.p.

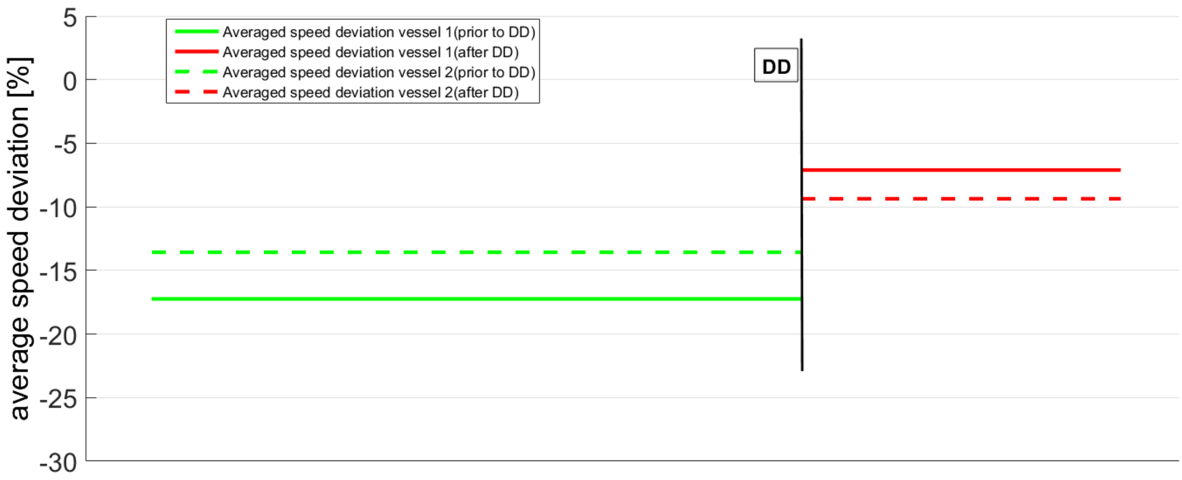

Fig.8: Averaged speed deviation prior to dry-docking (green) and after dry-docking (red) for two sister vessels.

Why is there a difference in the absolute level of hull and propeller performance in these two cases after dry-docking if all obvious factors are identical? Is it correct to say that vessel two performs worse after the dry-docking? As discussed before, there are many factors that influence the absolute value of the Hull and Propeller Performance indicator of a vessel. It is not clear whether the two vessels really have exactly the same hulls (differences from newbuild?, changes during the lifetime?) and there are no guarantees that the given vessel model (speed-power reference curves) fits perfectly both vessels and that it resolves correctly the slightly different environmental conditions that the vessels encounter. It is improbable that the sensors installed on-board each of the vessels are perfectly calibrated. The impact of these factors is considerable when looking at the absolute performance indication, but considerably lower when only looking at changes in performance of a vessel over time.

5. Summary and conclusion

Quantification of vessel performance (tonnage performance) is of big interest to the marine industry. It helps different parties to take right decisions and to reduce operational costs (reduce the fuel bill) and to save the environment (reduce emissions). One aspect of a ship performance is related to the hull and propeller efficiency. The commonly accepted approach for evaluating hull and propeller performance is based on capturing changes in “speed loss” of a vessel over time – this is the performance indicator discussed in ISO19030. Using this standard, one measures hull and propeller performance of a vessel in a relative way. This paper addresses the question whether it is possible to evaluate hull and propeller performance on an absolute scale. Such an evaluation on absolute scale would be of interest to judge e.g. on the quality of the surface treatment and hull coating of a newly built vessel or to compare the performance of sister vessels.

If one wants to measure the combined effect of hull design, propeller design and surface preparation, then, in theory, it is possible to do it on absolute scale. However, such an absolute indicator would only be reliable if a model for predicting reliably the impact of environmental and loading conditions on the speed-power relation were available, if the model fit perfectly the specific vessel and if all the measurements were 100% correct. If, however, one would like to judge e.g. on the quality of the surface treatment and hull coating of a newly built vessel or to compare the performance of hull coatings of two sister vessels, then frictional resistance would have to be measured separately from pressure resistance. Unfortunately, pressure and frictional resistance cannot be measured separately and thus it is not possible to judge e.g. on the surface treatment quality in an absolute way. As a pragmatic alternative, one compares the actual speed-power relation with an ideal speed-power relation. But this implies quite some uncertainties.

Several factors that influence the level of the values of hull and propeller performance indicators, e.g. the absolute level of speed loss, are discussed. Among these are accuracy of the vessel model, accuracy of the measurements of various parameters which are input to vessel model and the individuality of vessel hulls.

Commonly used vessel models rely on the speed trial predictions from model tests, on speed trial results or on CFD simulations. All these types of models are susceptible to prediction or measurement errors. The variability of speed trial predictions by towing tank testing could reach 2% with mean repeatability of the test of 1-1.5%. Models based on speed trials have been found to also suffer some uncertainties – 3-5%, while their precision limit varies between 7-9%. CFD simulations appear to be very powerful as vessel models when computing hull and propeller performance indices, as it is possible to resolve the speed-power-draft-trim relation in high detail. Nevertheless, CFD simulations also have a certain level of uncertainty and the uncertainty to predict the full scale speed-power curves on the absolute scale has been evaluated to be above 10%.

Quantification of absolute hull and propeller performance is also challenging considering the uncertainties in measuring the different parameters. If there is an offset in ship speed measurement, for instance, then this offset will reflect in the computed speed deviation point. In an example case, a small offset in speed measurement by 0.1 knot or in power measurement by 0.5%, led to a computed speed deviation that was 0.5p.p or 1.0p.p higher, respectively, than if there were no offset.

Differences in individual vessel hulls play an important role especially when comparing sister vessels. In speed trials after newbuild for 7 sister vessels differences in power of 5% have been seen. This can give an indication of such differences in the hull structure between sister vessels.

As an example for the challenges when comparing the absolute performance level of sister vessels, two sister vessels after dry-docking under identical conditions and with identical results of the hull surface quality and coating were compared. The performance indicators of the two vessels differ by 2.5p.p. in terms of speed loss. What the reason for this difference is, is unclear. But it illustrates that hull structure differences, sensor offsets or inaccuracies in the vessel model lead to uncertainties, and that one has to be very carefully when analyzing differences in the absolute hull and propeller performance indicators.

In conclusion, it appears that there is no reliable way to measure the hull and propeller performance on an absolute scale. One should be very carefully when comparing the level of speed loss values or similar performance indicators of different vessels given the numerous unquantifiable uncertainties.

On the other side, there is a real need for comparing the absolute hull and propeller performance of vessels or for judging on the quality of surface preparation work in a newbuild. Methods should thus be developed to cover that need by reducing todays' uncertainties.

References

ISO (2016), *Measurement of changes in hull and propeller performance - Part 1: General principles*, ISO 19030-1

ITTC (2014), *27th International Towing Tank Committee, Resistance Committee,* Final report

PONKRATOV, D. (2017), *2016 Workshop on Ship Scale Hydrodynamic Computer Simulation,* Lloyd's Register

INSEL, M. (2008), *Uncertainty in the analysis of speed and powering trials*, Ocean Engineering 35

KRAPP, A.; BERTRAM V. (2016), *Hull performance analysis – Aspects of speed-power reference curves*, 1st HullPIC, Pavone, pp.41-48

KRAPP, A.; SCHMODE D. (2017), *A Detailed Look at the Speed-Power Relation of Different Vessel Types at Different Loading Conditions*, 2nd HullPIC, Ulrichshusen, pp.50-56

Drag Performance Testing in Selection of Fuel Saving Hull Coatings

Job Klijnstra, Mark Bakker, Endures, Den Helder/The Netherlands, Job.Klijnstra@Endures.nl

Abstract

This paper describes some new test methods that, in addition to existing methodology, may help ship builders, operators and owners in selection of best performing fouling control coatings for different types of ships. Key element in the new methodology is measurement of friction drag properties of hull coatings that have been exposed to different types of static or dynamic ageing regimes and combinations thereof. The results of these tests are particularly useful for stakeholders that want to get relevant and independent test data for comparison of products from various suppliers.

1. Introduction

To safe fuel ships are provided with an antifouling coating that controls attachment and growth of marine fouling on a ship hull. This way increase in hull roughness can be diminished and lower hull roughness immediately results in lower fuel consumption and cost savings.

Selection of suitable products for different types of ships by ship builders or ship operators nowadays is merely based on information from suppliers on product characteristics and performance and on past practical experience. Information from suppliers may be (strongly) biased and moreover, different suppliers do not always give same type of product performance data, making it difficult to compare products from different suppliers in reliable way. Building decisions for product selection only upon past experience with coatings on operational ships means that more advanced products with possibly advantageous properties are not likely to be considered.

A widely used test method for product performance is a static raft test, in current terminology of *ECHA (2014)* called a simulated field test in coastal marine water with sufficient fouling pressure. In such tests, different products from different suppliers can be tested under exactly the same conditions. Next to the test facilities owned and used by the large coating manufacturers, there are worldwide several independent laboratories that can do these kinds of tests. Static raft tests are a worst-case test condition for ship hull coatings that, although of clear value in comparing products, do not provide accurate information on product performance under real-life conditions on a sailing ship.

Monitoring the performance of hull coatings on a sailing ship is not an easy task. Very much effort is being put last couple of years in development of a new ISO 19030 standard for such purpose. This paper will not go into any detail of this ISO standard, other presenters at this meeting can do that much better. The important thing we want to concentrate on in this paper is the step before the measures of ISO 19030 can be put in place: How to select a proper hull coating for a specific type of ship with special emphasis on friction drag properties. Some new methodology will be discussed that can measure friction drag properties of hull coatings in relation to simulated operational patterns of ships. With such methodology dedicated information on key performance of various hull coatings can be obtained independent from paint suppliers. Additional advantage is that both self-polishing coatings (SPC's) and fouling release coatings (FRC's) can be compared in similar way on key performance: reduction of drag penalties caused by marine fouling.

2. Test Methods

Three different test protocols that will help to characterize friction drag properties of hull coatings in relation to fouling development in static and/or dynamic ageing regimes are described in this paper.

2.1 Friction Drag Properties of Hull Coatings with Fouling

For the measurement of friction drag properties of hull coatings with and without fouling a dedicated test set up was built at our laboratory some years ago. This test set up (the FDM) was rebuilt from an old US Navy test set up that *Holm et al.* (2004) used for similar experiments. The basic principle of this set up is to measure the torque of rotating disks at various speeds in a container filled with seawater. Differential measurements on the same coated disk with and without marine fouling will reveal the difference in torque between both conditions, so will give the added drag or drag penalty that can be ascribed to a particular fouling condition. In the paper of *Holm et al*. (2004) results are shown on specific slime fouling conditions giving added friction drag between 9 and 29 %.

The FDM at Endures, Fig.1, consists of a variable speed motor that drives a shaft onto which disks are mounted. A torque sensor (Datum Electronics M420 Rotary Torque Transducer) installed on the shaft measures the torque produced when the disk rotates. Coated disks (23 cm diameter) mounted on the shaft are immersed in a cylindrical Perspex container (32 cm height and 30 cm diameter) completely filled with filtered natural seawater. Distance between disk and bottom of the container is 10 cm. Torque on the motor shaft is recorded as the disks are spun at increasing angular velocities from 500 rpm to 1500 rpm (in increments of 200 rpm) where each speed step is maintained for 2 minutes. The torque values measured during the last 60 s of each speed step are used in data analysis. The total test time of 6 x 2 minutes is called one experimental run. Depending on the type of test 2 or 3 consecutive runs were carried out in order to discriminate between drag effects of initial fouling and of so-called remaining fouling, i.e. the fouling that remains present on the coating surface when the disk has gone through the first experimental run. More details on the rotation protocol are described below and illustrated in Fig.4. Coated disks are first measured in clean, newly applied condition. After this the disks will be exposed for some time to marine fouling at the raft in the harbour of Den Helder, Fig.2. When retrieved from the raft the disks with fouling are measured again in the FDM and the added drag of the fouling condition is determined.

Fig.1: Overview of FDM (left) and detailed picture of disk in seawater container (right).

Fig.2: Raft exposure facility in Den Helder port

Fig.3: Dynamic ageing set up in natural seawater

Long-term rotation of coated disks in natural seawater is a suitable technique for dynamic ageing of hull coatings simulating real-life conditions on a sailing ship. Friction drag measurements on the coatings at various intervals during dynamic ageing may give further information on (change in) long term friction drag properties of coatings. The set up shown in Fig.3 is designed for dynamic ageing of hull coatings at various rotation speeds. Simulation of a full operational pattern of a ship can be achieved by combining the dynamic ageing process with intermittent short periods of static raft exposure comparable to specific idle times of the ship.

Disks with fouling were subjected to a dedicated rotation protocol consisting of at least two runs. This protocol is illustrated in Fig.4. Disk picture at left shows a disk with initial fouling prior to the first drag measurement. After completion of the 1st run (picture in the middle) the seawater in the container is refreshed and the disk is subjected again to a full run from 500 to 1500 rpm, each speed for 2 minutes. Photograph at right in Fig.4 shows the disk after completion of run 2. The blue lines in Fig.4 show the torque values that were measured at various rotation speeds (pink lines) in both experimental runs. In the torque curve of the first run it is clearly visible that at each change of speed the torque values go up to a higher level and after a couple of seconds gradually go down to a lower, rather stable value in the remaining time at that speed. This decrease in torque values after a few seconds can be ascribed to the release of fouling during the test.

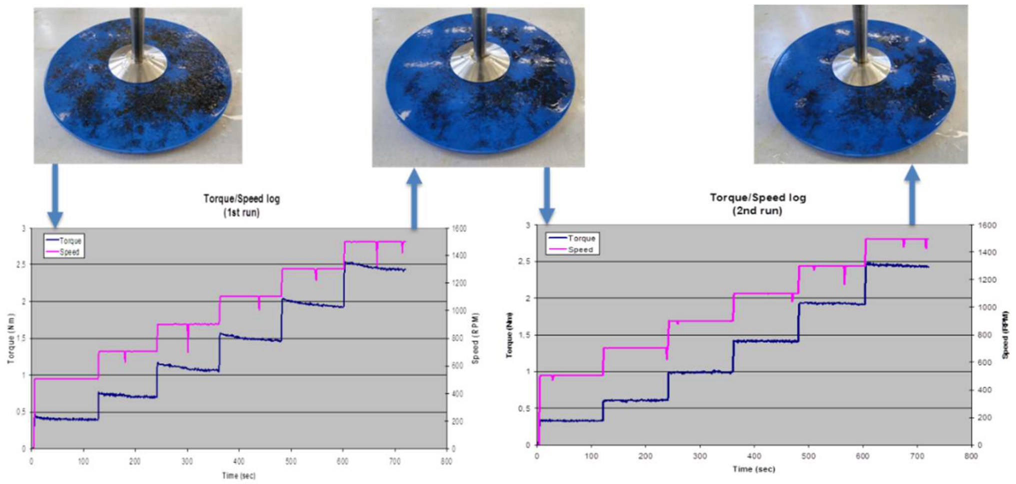

Fig.4. Schematic presentation of the rotation protocol used in drag measurements in the FDM.

Results of two different test series will be shown in this paper. In the first one two FRC products were investigated on added drag effects of slime fouling as it developed in different times of the season. In the second series a range of commercially available products (both SPC and FRC) is compared on friction drag properties after specific static exposure periods.

2.1.1 Added drag of slime fouling in different times of the year

Two commercially available FRC products (I and II) were exposed at the raft for 11 weeks in summer and for 10 weeks during autumn/winter. In the summer period the two products showed some difference in the build-up of slime fouling with a thin biofilm on product I and a more dense biofilm on product II. The drag measurements also revealed a clear difference: for product I a small added drag effect around 5% was found over the entire speed range whereas on product II a strong initial drag penalty (around 40 %) was observed that diminished with increasing speed to a value of 11 % added drag at 1500 rpm, still twice as high as on product I. Pictures of the disks and graphs of the results of drag measurements will be shown in the presentation. Other disks with the same products were compared on drag properties of a slime biofilm that had developed in autumn/ winter time. From visual perspective, the biofilms on the disks looked quite dense but when starting the drag tests at low speed it appeared that on both products the slime fouling showed very little adhesion and gave hardly any added drag (less than 2%).

Among other things these results give evidence that with regard to added drag effects of slime fouling, it is important to realize that even under the same exposure conditions biofilms may develop differently on different products. The data in this small set of test results clearly indicate that also for biofilms next to percentage cover also the adhesion of the organisms is an important factor to take into account when investigating added drag effects of slime fouling.

2.1.2 Comparison of commercially available products on friction drag properties

In large collaborative research project 9 commercially available products (6 SPC and 3 FRC) from 3 different suppliers were investigated among other things on friction drag properties. Coated disks were exposed for variable times at the raft, Fig.5, and retrieved from time to time for drag measurements in the FDM.

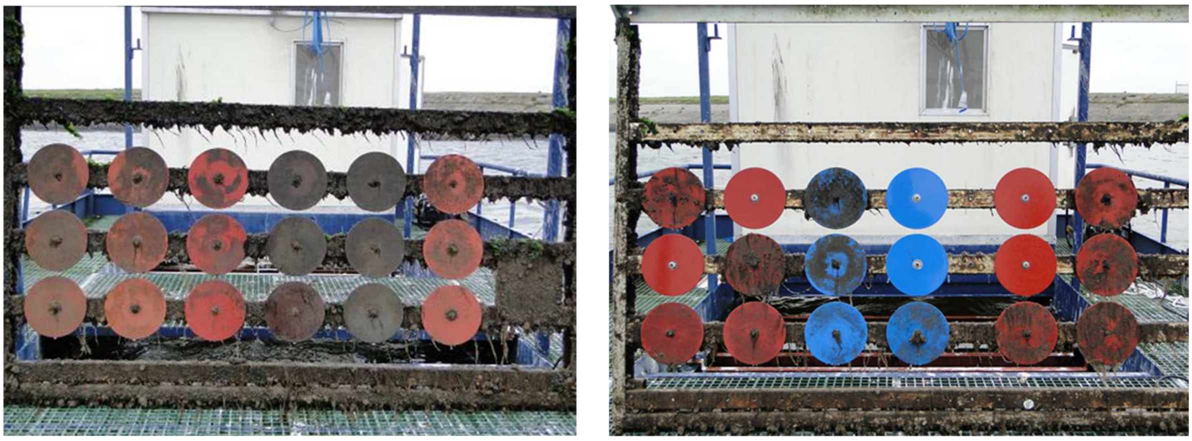

Fig.5. Exposure of 6 SPC products (left) and 3 FRC products (right) at the raft of Endures

Fouling condition of the disks was characterised using the scheme described in *NSTM (2006)* of US Navy. Fouling rates (FR) in this scheme are as follows: FR10: light slime; FR20: advanced slime; FR30: algal and soft animal fouling; FR40/FR50: small calcareous fouling.

Coated disks with fouling were subjected to the same test protocol, two consecutive runs in the FDM. The drag values measured at each speed were compared to the friction drag values of the same coating in pristine condition and the difference in friction drag is expressed as % added drag. This was done for each speed step and then an average % added drag over all speeds was calculated. This average % added drag is shown in Fig.6 and Fig.7. In these Figures also photographs of the disks are shown first prior to drag testing (top row) and secondly (bottom row) after completion of the 2nd run in the FDM. So the pictures in the bottom row of each Figure show the remaining fouling condition on each disk.

Results of friction drag measurements on a set of 6 SPC's are shown in Fig.6. These disks were exposed for 11 weeks during spring/ early summer. Fouling condition (FR type and % coverage) of each disk prior to drag testing is indicated in the yellow square and is visually shown in the first row of photographs. All disks had only slime fouling (FR20) except SPC6 that contained some barnacles next to thin slime. The red bars in Fig.6 give the drag penalty that can be ascribed to initial fouling and the blue bars show added drag of remaining fouling.

SPC6 with the barnacles showed much higher added drag than the other 5 products with only slime. Also after completion of the second run this disk had still some barnacles present and this is reflected in the % added drag of remaining fouling. The slime fouling on products 1 to 5 was all of category FR20 with percentage coverage varying from 50 to 90 % but the added drag due to this did not vary very much between the products. Added drag of remaining fouling (ranging from 10 – 18%, except SPC6) was always lower than that of initial fouling (20 – 30 %, except SPC6).

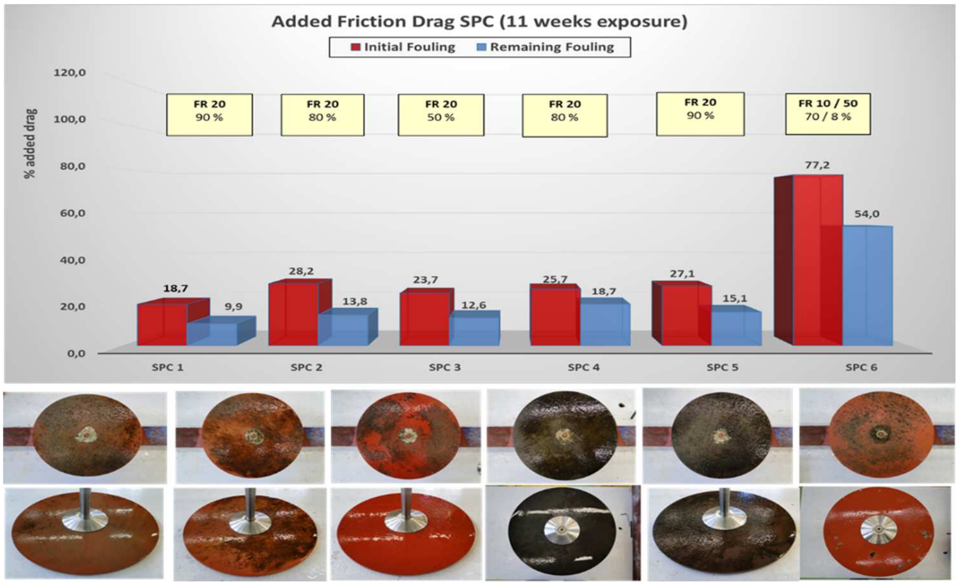

Fig.6: Added drag effects of fouling conditions after 11 weeks raft exposure of 6 SPC products.

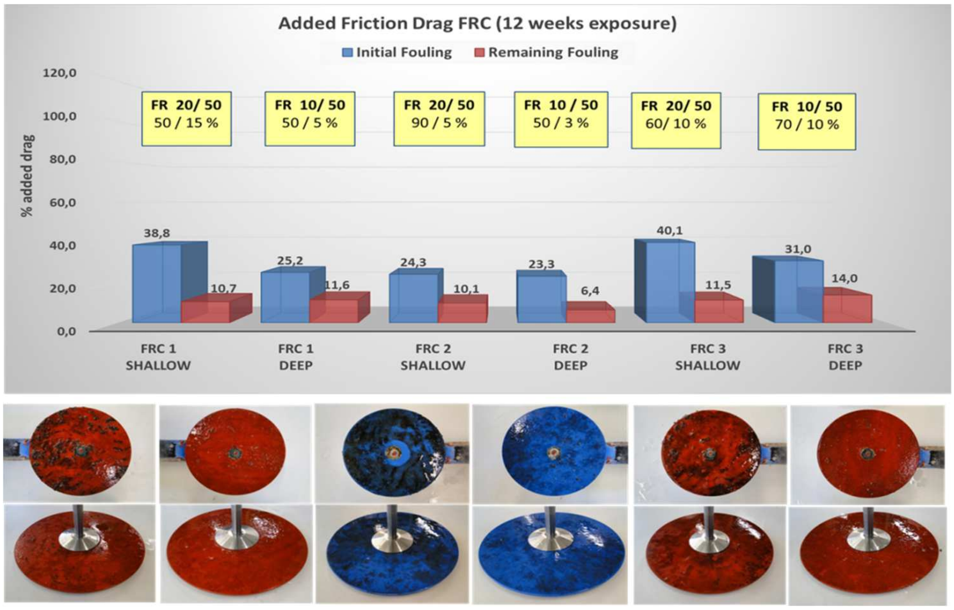

Fig.7: Added drag effects of fouling conditions after 12 weeks raft exposure of 3 FRC products.

A set of 3 FRC products was similarly investigated on friction drag properties after 12 weeks of static exposure in about the same time of the season. In this test two disks of each product were used, one exposed at shallow depth, just below the water level and the other one exposed at 1 m water depth. The results of these drag measurements are shown in Fig.7. All FRC disks contained slime fouling (FR10 or FR20) as well as some barnacles (FR50). The added drag of initial fouling varied between 23 and 40 %. Looking in more detail at the blue bars in Fig.7, it can be seen that the disks with higher barnacle coverage also have highest added drag (31 – 40 %). Added drag of remaining fouling ranged between 6 and 14 %, so was substantially lower. Fig.7 shows that the FRC's do not get fully clean after the 2 consecutive runs in the FDM. There is remaining fouling that still gives added drag. However, when comparing this with the SPC's in Fig.6, the latter give a higher drag penalty after similar period of static exposure.

In a third set of experiments, which will be shown in the presentation, the self-cleaning effect of fouling release coatings is much more evident. In this case the coatings were exposed (all at the same depth) for 5 months at the raft and all disks were strongly fouled with mainly barnacles and soft fouling on top of this. Percentage coverage of barnacles ranged from 40 to 80 %. The average drag penalty of this initial fouling was very high, at 3 disks more than 80 %. After the second run of these disks almost all fouling was washed off and except for one disk, that still contained a few barnacles, very little added drag was found, between 2.6 and 6.9 %.

Conclusions from these tests are:

- In static exposure periods of similar length FRC products may assemble more (barnacle) fouling than SPC's. Initially this will give higher added drag but due to better fouling release properties the FRC's give lower drag penalty.
- At long idle times FRC's usually get much more fouling than SPC's but also this (hard) fouling can easily be washed off with very low drag penalty as a result.

2.2. Minimal speed foul release test and antifouling performance in relation to idle time

Over the last 20 years coating manufacturers have invested a lot in getting fouling control coatings with better foul release properties. This has resulted in products that show improved release properties at lower speeds and this development will probably continue. However, for what could be called a minimal foul release speed, customers such as ship builders or operators are still dependent on product information and performance claims from the suppliers. Underbuilding of such claims is not standardized yet and comparison of product performance on this specific parameter can be difficult. With the test protocol described here I want to propose a test method that is suitable for product comparison, not only for FRC's but also for SPC's.

In this test a rotor drum setup is used, Fig.8. Slightly curved coated panels (size 15x8 cm) are mounted on the rotor drum in such a way that all panels fit neatly to each other on every row of the rotor drum. Each row may contain 10 panels and with 7 rows each rotor drum can accommodate 70 panels in total. The drum rotates in a 600 L tank containing filtered (5 µm) natural seawater. The temperature of the seawater is held constant, usually at 25°C but it can be adjusted between 15 and 30°C by a heating element. Cooling of the seawater in the tank is done by adjusting the refreshment rate in the tank. Maximum refreshment rate is 300 L/h.

Fig.8: Test set-up with rotor drum in seawater. Right: drum with coated panels when lifted

In order to investigate the speed at which fouling is released, we first need to get fouling on the coated panels. To that end we expose them for certain time at the raft in the harbour of Den Helder. Exposure time may vary from one or two weeks up to a few months, depending on what needs to be investigated.

Fouled panels retrieved from the raft are mounted on the rotor drum and initial fouling condition is characterized. Then a dedicated rotation protocol is carried out, starting at the minimum speed of 4 knots and for a short rotation time, for instance 5 minutes. After this step the panels are inspected again to look for changes in fouling condition. Next a longer rotation time at same speed or similar short rotation time at higher speed can be done, dependent on the type of results you want to get.

This way an experimental scheme can be drawn up that will reveal at what speed after certain time specific fouling patterns are diminished or removed. All kinds of variables in diverse combinations can be incorporated in such test schemes. Fouling condition can be described in % coverage and successive series of photographs of the panels will illustrate how the coatings perform. Foul release speed is usually associated with fouling release coatings (FRC), however, self-polishing coatings (SPC) can be characterized in similar way.

Preliminary tests with this protocol were done in the past, Fig.9 shows some results of such tests. The grey panels in Fig.9 are fouled panels of two different products (FRC in the top row and a hard epoxy coating in the bottom row) that were exposed to different combinations of rotation speed and time. The results are clear in the sense that the FRC gets rather clean when exposed to a speed of 25 knots for 30 minutes. From the fact that it does not get clean at a speed of 18 knots you can derive that this product does not belong to the latest generation of FRC's. On the protective coating at the bottom row a speed of 30 knots is able to remove the scales of barnacles but even at that speed the barnacle base plates remain present. These base plates give substantial increase in surface roughness and thus give added drag. The blue panels in Fig.9 are another FRC product with fouling that was successively exposed to various rotation speeds for one hour. This product already shows some fouling removal at 5 knots; at 10 knots the percentage fouling cover is strongly reduced and after 1 hour at 20 knots the panel is (almost) fully clean.

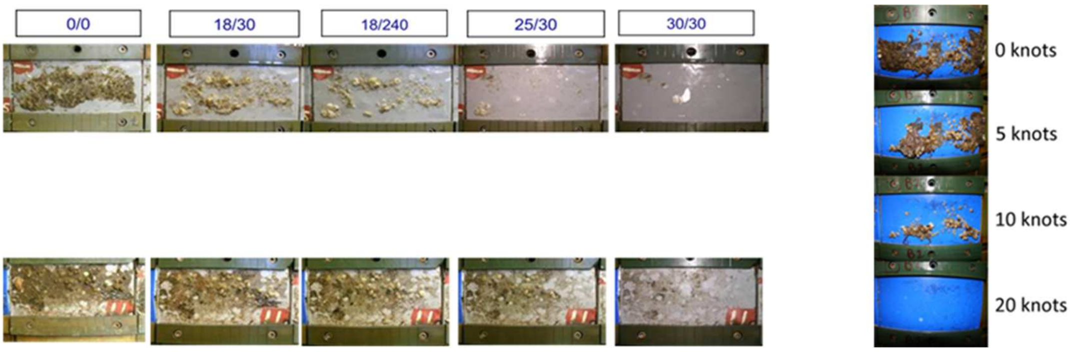

Fig.9: Results from rotor tests on foul release properties of hull coatings

The protocol described above is a simple rather straightforward method to investigate fouling control products on their foul release properties. Comparative testing of products from various suppliers will give quantitative data that may help to select hull coatings with optimal friction drag properties. The test protocol for determination of the minimal fouling release speed of a coating product can easily be extended with another or multiple cycles of static raft exposure and then give information on (changes in) foul release speed at longer term. To this end the panels need to be robust enough to survive long term and repetitive exposure cycles in seawater. To get away from the steel panels used in the past we adapted the test system for use of PVC panels. These PVC panels are curved, have the same radius as the rotor drum, do not need corrosion protection and paints under investigation are directly applied onto the panels. Such an extended test protocol can also be seen as a test method for establishing coating performance in relation to different idle times. This aspect is getting more and more attention in shipping, because for various reasons ships may spend (much) more time laying idle than in the past. If this is to be expected after a refit or dry-docking, it would be good to know if the coating product that will be applied in dry-dock will show good performance in a different operational profile. The test method could help to evaluate and discriminate coating products on such properties and when additionally extended with a dynamic ageing regime (which can easily be accomplished at the same rotor system), then coating performance could be studied under various simulated operational patterns.

In this paper, I can only give more information on the test method that we use for this. The data we have collected are confidential and cannot be made public at this stage. Fig.10 shows a set of rotor panels prior to raft exposure and the same panels after a few weeks' exposure in the sea. The fouled panels were brought back (in wet condition) to the lab for rotation testing at the rotor drum.

Fig.10: Raft rack with rotor panels prior to (left) and after certain raft exposure period (right). These panels were retrieved to the lab for rotation tests at the rotor drum.

Fig.11 (left) shows the rotor drum with fouled panels mounted. Fig.11 (right) shows 3 different paint systems before and after two rotation times at a speed of 8 knots. At this quite low speed not much fouling is released from the surface of paints A and B. Coating C had very little fouling already at the start; even that has disappeared after short rotation at low speed. Further details on the results of this test cannot be given because of confidentiality but hopefully the pictures give good impression on how the basic method looks like. Either at higher speeds or after longer rotation times you can imagine that more fouling will be washed off and this kind of data is very useful for getting better insight in friction drag properties and thus performance of hull coatings.

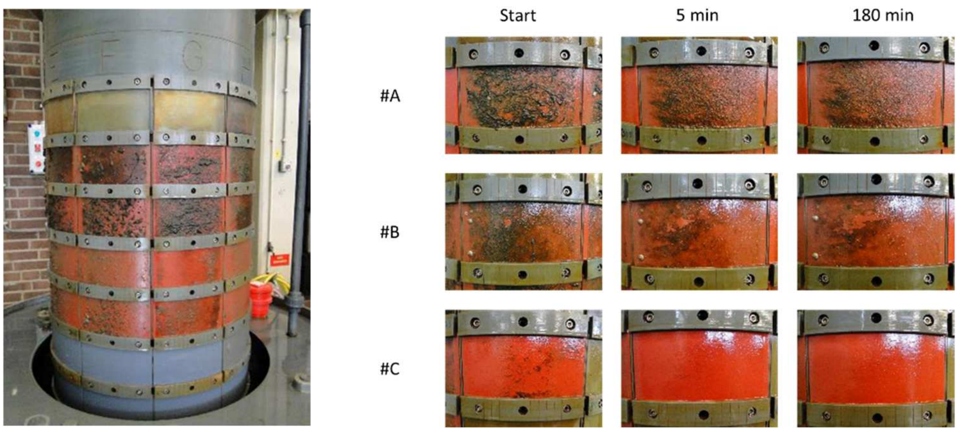

Fig.11: Left: Fouled panels mounted on the rotor drum prior to rotation; Right: Panels of 3 paint systems before and after rotation at 8 knots.

3. Conclusions

- The test method with the FDM allows product comparison on the key performance parameter of hull coatings: Friction Drag properties. The flat coated disks give an easy way to obtain replicate samples with fouling patterns that may develop under various operational conditions. Comparative measurements in the FDM of coatings with and without fouling will give quantitative data on the added drag of the fouling pattern.
- The test method with the rotor drum can determine two other aspects of friction drag properties of hull coatings:
  - What is the minimal speed at which (specific) fouling patterns are released?
  - How much fouling will accumulate on (dynamically aged) hull coatings after different periods of static immersion (idle times) in seawater and at what speed is this fouling removed again?
- The use of static and dynamic ageing procedures in variable combinations along with the above test protocols may help to unravel the long term friction drag properties of hull coatings.

References

ECHA (2014), *Transitional Guidance Document on Efficacy Assessment for Product Type 21 Antifouling Products*, European Chemicals Agency

HOLM, E.R.; SCHULTZ, M.P.; HASLBECK, E.G.; TALBOTT, W.J.; FIELD, F.J. (2004), Evaluation of hydrodynamic drag on experimental fouling release surfaces using rotating disks, Biofouling 20 (4/5), pp.219-226

NSTM (2006), Naval Ships Technical Manual Chpt.081: Waterborne underwater hull cleaning of Navy Ships, US Navy

Index by Authors

3rd Hull Performance & Insight Conference (HullPIC)

Redworth / UK, 12-14 March 2018

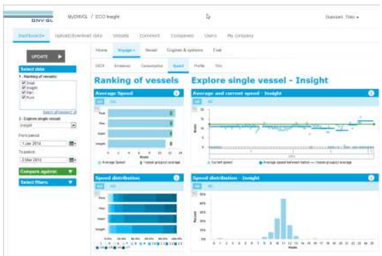


Topics: ISO 19030 and beyond / sensor technology / information fusion / big data / uncertainty analysis / hydrodynamic models / business models / cleaning technology / coating technology / ESDs

Organiser: Volker Bertram (Tutech Innovation (TU Hamburg))
Geir Axel Oftedahl (Jotun)

Advisory Committee:

Michael vom Baur	MVB Euroconsult	**Liz Haslbeck**	NSWC-CD	**Jussi Pyörre**	Eniram
Torsten Büssow	DNV GL	**Esa Henttinen**	NAPA	**Hideaki Saito**	JSTRA
Helgi Fridriksson	Marorka	**Tsuyoshi Ishiguro**	JMUC	**Svend Soyland**	Nordic Energy Research
Erik Hagestuen	Kyma	**Jeppe S. Juhl**	BIMCO	**Geoff Swain**	FIT
Simon Hayes	BMT Smart	**Andreas Krapp**	Jotun	**Diego M. Yebra**	Hempel

Venue: The conference will be held at the Redworth Hall Hotel near Darlington/UK

Format: Papers to the above topics are invited and will be selected by a selection committee. Papers may have up to 15 pages. The proceedings will be made freely available to the general public.

Deadlines:

anytime	Optional “early warning” of interest to submit paper
01.12.2017	Submission of abstracts
10.02.2018	Payment due for authors
10.02.2018	Final papers due

Fees: **600 €** – early registration (by 10.2.2018)
700 € – late registration

Fees are subject to VAT (reverse charge mechanism in Europe)
Fees include proceedings, lunches, coffee breaks and conference dinner

Sponsors: Jotun (further sponsors to be announced)

Information: www.HullPIC.info
volker.bertram@dnvgl.com